



**SELINUS UNIVERSITY**  
OF SCIENCES AND LITERATURE

**Analyzing the Challenges of Transition towards Sustainable  
100% Renewable Electrical Power and Energy System along  
with Power Quality Solutions on Stability, Security, and  
Interoperability of the IEEE 9 bus system**

**By Loai Ziad Hasan Al-Adim**

**A DISSERTATION**

Presented to the Department of  
**ELECTRICAL ENGINEERING**  
program at Selinus University

Faculty of **ENGINEERING & TECHNOLOGY**  
in fulfillment of the requirements  
for the degree of Doctor of Philosophy  
in **ELECTRICAL ENGINEERING**

2024

## **AUTHORIZATION**

I, Loai Zaid Al-Adim, authorize Selinus University to supply copies of my thesis to libraries or establishments or individuals on request, according to the University regulations.

## **DEDICATION**

To

My father, my mother, my wife, my son, my daughter  
my sisters, my brother and  
the rest of my family.

## **ACKNOWLEDGEMENT**

I would like to express my gratitude to both my contemporaries and my family members, who have provided me with an incredible amount of support over the whole of the research project. I am indebted to everyone for their support and guidance, and I would like to use this opportunity to express my appreciation to each and every one of you. I would like to express my gratitude to my professor, who has been there for me anytime I had questions or needed assistance while I was studying and has been an incredible resource for me.

## Table of Contents

<b>Subject</b>	<b>page</b>
Thesis Approval	iii
Authorization	iv
Dedication	v
Acknowledgment	vi
Bibliography	viii
List of Figures	xi
List of Tables	xvi
Acronyms	xvii
Nomenclatures	xix
Abstract	xxi

## Table of Contents

<b>1. PART ONE</b>	<b>1</b>
<b>1.1 CHAPTER ONE: INTRODUCITON</b>	<b>2</b>
1.1.1 RESEARCH BACKGROUND	2
1.1.2 RESEARCH PROBLEM	5
1.1.3 RESEARCH AIM	11
1.1.4 RESEARCH OBJECTIVES	12
1.1.5 RESEARCH QUESTION	12
1.1.6 THESIS STRUCTURE	12
<b>1.2 CHAPTER TWO: LITERATURE REVIEW</b>	<b>14</b>
1.2.1 RENEWABLE ENERGY	14
1.2.2 RENEWABLE AND NON-RENEWABLE ENERGY MIX	20
1.2.3 CARBON NEUTRALITY AND CO2 EMISSIONS REDUCTION	25
1.2.4 STABILITY, SECURITY AND INTEROPERABILITY OF RENEWABLE EPES	26
1.2.5 IEEE 9 BUS SYSTEM- POWER SYSTEM ANALYSIS	34
1.2.6 GRID IMPACT OF RENEWABLE ENERGY SOURCES INTEGRATED TO IEEE 9-BUS SYSTEM.	37
1.2.7 THE NEED OF POWER QUALITY SOLUTIONS FOR HIGH RENEWABLE PENETRATION AND GRID CODE COMPLIANCE	41
1.2.8 CHALLENGES IN TRANSITION TO 100% RENEWABLE ENERGY IEEE 9-BUS SYSTEM	46
1.2.9 RESEARCH GAP	52
<b>1.3 CHAPTER THREE: METHODOLOGY AND PHILOSOPHY</b>	<b>53</b>
1.3.1 INTRODUCTION	53
1.3.2 RESEARCH PROCESS	53
1.3.3 RESEARCH PHILOSOPHY	54
1.3.4 RESEARCH APPROACH.	55
1.3.5 RESEARCH STRATEGY	57
1.3.6 DATA COLLECTION METHOD	58
1.3.7 POPULATION AND SAMPLING	59
1.3.8 RESEARCH ONION	59
<b>2. PART TWO</b>	<b>60</b>

<b>2.1</b>	<b><u>CHAPTER FOUR: MAIN COMPONENTS OF A LARGE-SCALE GRID CONNECTED PV PLANT / WIND FARM.</u></b>	<b>60</b>
2.1.1	OVERVIEW	60
2.1.2	PHOTO VOLTAIC GENERATOR (PVG) – PV IRR UNIT	63
2.1.3	WIND TURBINE GENERATOR (WTG) – WTG IRR UNIT	83
2.1.4	COLLECTION MV/HV SUBSTATION	109
2.1.5	POWER QUALITY SOLUTIONS	113
<b>2.2</b>	<b><u>CHAPTER FIVE: CASE STUDY IEEE 9-BUS SYSTEM- POWER SYSTEM ANALYSIS AND ETAP SIMULATION</u></b>	<b>128</b>
2.2.1	IEEE 9 BUS SYSTEM – OVERVIEW	128
2.2.2	IEEE 9 BUS –SYSTEM PARAMETERS	131
2.2.3	PER UNIT ANALYSIS	133
2.2.4	POWER FLOW STUDIES	141
2.2.5	TIME DOMAIN POWER FLOW STUDIES	166
2.2.6	FAULT CALCULATIONS	169
2.2.7	STABILITY STUDY	182
2.2.8	POWER SYSTEM DIFFERENTIAL EQUATIONS	201
2.2.9	VOLTAGE STABILITY STUDY	216
2.2.10	HARMONIC ANALYSIS	230
2.2.11	CONTINGENCY ANALYSIS	238
<b>2.3</b>	<b><u>CHAPTER SIX: GRID CONNECTED SOLAR PV PLANT AND WIND FARM- GRID IMPACT STUDY AND ETAP SIMULATION FOR MODIFIED IEEE 9 BUS SYSTEM</u></b>	<b>242</b>
2.3.1	OVERVIEW AND GRID CODE COMPLIANCE	242
2.3.2	GRID CONNECTED PHOTO VOLTIC PLANT	246
2.3.3	GRID CONNECTED WIND FARM	277
<b>2.4</b>	<b><u>CHAPTER SEVEN: 100% RENEWABLES GRID INTEGRATED TO IEEE 9 BUS SYSTEM</u></b>	<b>308</b>
<b>3.</b>	<b><u>PART THREE</u></b>	<b>330</b>
<b>3.1</b>	<b><u>CHAPTER EIGHT: DATA COLLECTION AND ANALYSIS</u></b>	<b>330</b>
3.1.1	DATA COLLECTION:	331
3.1.2	DATA CLEANING:	336
3.1.3	EXPLORATORY DATA ANALYSIS (EDA):	338

3.1.4	DATA TRANSFORMATION:	342
3.1.5	MODEL BUILDING:	343
3.1.6	MODEL EVALUATION:	349
3.1.7	INTERPRETATION AND VISUALIZATION:	350
<b>3.2</b>	<b>CHAPTER NINE: CONCLUSIONS</b>	<b>370</b>
<hr/>		
3.2.1	TIME DOMAIN LOAD FLOW ANALYSIS	371
3.2.2	TRANSIENT STABILITY STUDY	373
3.2.3	POWER SYSTEM ANALYSIS	383
<b>3.3</b>	<b>CHAPTER TEN: RECOMMENDATIONS AND FUTURE WORKS</b>	<b>391</b>
<hr/>		
3.3.1	TIME DOMAIN LOAD FLOW	391
3.3.2	TRANSIENT STABILITY STUDY	392
3.3.3	POWER SYSTEM ANALYSIS	392

## List of Figures

<b>Figure 1.1-1</b>	IEA first 3 pillars of COP28.....	3
<b>Figure 1.1-2</b>	Carbon dioxide (CO <sub>2</sub> ) emissions from fossil fuels and industry from 1750 to 2022.....	6
<b>Figure 1.1-3</b>	Solar Radiation Journey.....	7
<b>Figure 1.1-4</b>	Natural Greenhouse Effect vs Human Enhanced Greenhouse Effect .....	8
<b>Figure 1.1-5</b>	Scope of Emissions .....	9
<b>Figure 1.2-1</b>	Renewable Energy Sources.....	15
<b>Figure 1.2-2</b>	Solar Panels for Photovoltaic (PV) plant.....	16
<b>Figure 1.2-3</b>	Wind Turbine Generators (WTG) in Wind Farm .....	16
<b>Figure 1.2-4</b>	Hydroelectric Power Plant Dam .....	17
<b>Figure 1.2-5</b>	Geo-Thermal Power Plant .....	18
<b>Figure 1.2-6</b>	Ocean Thermal Energy Plant .....	19
<b>Figure 1.2-7</b>	Ocean Mechanical Energy Plant.....	19
<b>Figure 1.2-8</b>	Biomass Power Plant .....	20
<b>Figure 1.2-9</b>	Generation of electricity worldwide 2022, by energy source.....	21
<b>Figure 1.2-10</b>	Global renewable generation capacity (GW) from 2014-2022 .....	23
<b>Figure 1.2-11</b>	Global installed renewable energy capacity by technology in GW for year 2022 .....	23
<b>Figure 1.2-12</b>	Renewable capacity growth from 2022 to 2030 and the gap to global tripling renewables.....	24
<b>Figure 1.2-13</b>	Electricity generation by technology, 2000-2028 .....	24

Figure 1.2-14: Carbon Neutrality Concept .....	25
Figure 1.2-15: Average Greenhouse Gas emission per Technology. ....	26
<b>Figure 1.2-16:</b> Classification of power system stability with CIG's .....	28
<b>Figure 1.2-17:</b> IoT in Energy and Industry.....	32
<b>Figure 1.2-18:</b> Smart Grid .....	33
<b>Figure 1.2-19:</b> Electrical Power System Structure and Energy Streams .....	34
<b>Figure 1.2-20:</b> IEEE 9-Bus System Single Line Diagram .....	35
<b>Figure 1.2-21:</b> Solar PV 243MW integrated at IEEE 9 Bus system. ....	38
<b>Figure 1.2-22:</b> 100MW WF grid integrated with Bus No.4 of IEEE 9 bus system .....	39
<b>Figure 1.2-23:</b> MATLAB Model for Gradual Penetration of WF to IEEE 9 Bus system.....	41
<b>Figure 1.2-24:</b> ETAP Model for 200MW PV Plant .....	43
<b>Figure 1.2-25:</b> Typical SVC configuration and V/I diagram. ....	45
<b>Figure 1.2-26:</b> Typical STATCOM configuration and V/I diagram. ....	46
<b>Figure 1.2-27:</b> Change in ROCOF with Inertia change. ....	48
<b>Figure 1.2-28:</b> Effect of SCR on Voltage Stability .....	49
<b>Figure 1.2-29:</b> Shift of harmonic resonances to lower order of harmonics. ....	49
<b>Figure 1.3-1:</b> Saunders Research Onion.....	53
<b>Figure 1.3-2:</b> Research Philosophies .....	54
<b>Figure 1.3-3:</b> Research Approach Paths.....	55
<b>Figure 1.3-4:</b> Research Onion .....	59
<b>Figure 2.1-1:</b> Generators for Renewable Generations .....	62
<b>Figure 2.1-2:</b> Block Diagram of a Large-Scale Grid Connected PV Plant.....	65
<b>Figure 2.1-3:</b> Basic Operating Principle of a Solar Cell.....	66
<b>Figure 2.1-4:</b> Diagram of the Possible Components of a Photovoltaic System .....	66
<b>Figure 2.1-5:</b> The equivalent Circuit for the Solar Cell.....	67
<b>Figure 2.1-6:</b> Current-Voltage Characteristic of Semiconductor Diode.....	68
<b>Figure 2.1-7:</b> Load Side of Solar Cell .....	69
Figure 2.1-8:Open Circuited Solar Cell .....	70
<b>Figure 2.1-9:</b> Short Circuited Solar Cell.....	72
<b>Figure 2.1-10:</b> Open circuited Solar Cell .....	73
<b>Figure 2.1-11:</b> Current - Voltage (I-V) characteristic for Solar Cell .....	74
<b>Figure 2.1-12:</b> Characteristic Impedance Equivalent Circuit .....	75
<b>Figure 2.1-13:</b> Current - Voltage & Power-Voltage Curve of Solar Panel at Different Irradiations .....	75
<b>Figure 2.1-14:</b> Central Inverter with Step-Up Transformer and RMU .....	77
<b>Figure 2.1-15:</b> Block Diagram of Two Central Inverters and MV step-up station.....	77
<b>Figure 2.1-16:</b> Two Central Inverters and Step-Up Solar Power Transformer with MV RMU.....	78
<b>Figure 2.1-17:</b> Basic Three Phase Bridge Inverter.....	78
<b>Figure 2.1-18:</b> Pulse-Width Modulated Waveform for a Three Phase Bridge Inverter[43] .....	80
<b>Figure 2.1-19:</b> 2000 kVA, 0.66/33 kV, Dy11 Two Winding Solar step-up Power Transformer .....	81
<b>Figure 2.1-20:</b> 2400 kVA, 0.4-0.4/33 kV, Dy11y11 Three Winding Solar Step-up Power Transformer .....	81
<b>Figure 2.1-21:</b> Central Inverter with Step Up Transformer and RMU .....	82
<b>Figure 2.1-22:</b> Ring Main Unit Three – Way .....	82

<b>Figure 2.1-23:</b> Block Diagram of a Large-Scale Grid Connected Wind Farm .....	85
<b>Figure 2.1-24:</b> Atmospheric Pressure Difference and Movement of Air .....	86
<b>Figure 2.1-25:</b> Stream of Air of mass $m$ and moving with velocity $v$ Facing Wind Turbine Rotor .....	87
<b>Figure 2.1-26:</b> HAWT vs VAWT .....	92
<b>Figure 2.1-27:</b> Upstream and Down-stream Wind. ....	93
<b>Figure 2.1-28:</b> Cp curve vs $V_0/V$ ratio .....	95
Figure 2.1-29: Important Parameters of an Airfoil .....	96
<b>Figure 2.1-30:</b> Lift and Drag Force due to Pressure difference.....	96
<b>Figure 2.1-31:</b> Main Components of Horizontal Axis Wind Turbine.....	101
Figure 2.1-32: Classification of Wind Turbines Technologies .....	102
Figure 2.1-33:Squirrel cage Induction Generator block diagram. ....	103
<b>Figure 2.1-34:</b> Power Flow for Squirrel Cage Induction Generator .....	104
Figure 2.1-35: Wound Rotor Induction Generator block diagram.....	105
<b>Figure 2.1-36:</b> Power Flow for Wound Rotor Induction Generator.....	105
<b>Figure 2.1-37:</b> Constructional Drawings of MV Power Cable .....	111
<b>Figure 2.1-38:</b> MV Switchgear ABB type UniGear ZS2 .....	111
<b>Figure 2.1-39:</b> Step-Up Transformer 3D drawing .....	112
<b>Figure 2.1-40:</b> HV AIS Substation .....	113
<b>Figure 2.1-41:</b> Active and Reactive Power Representation Example .....	114
<b>Figure 2.1-42:</b> AC Voltage and Current Phase Shift .....	115
<b>Figure 2.1-43:</b> Applications of Reactive Power Requirements .....	116
<b>Figure 2.1-44:</b> Power Triangle.....	117
<b>Figure 2.1-45:</b> Power Factor Correction .....	117
<b>Figure 2.1-46:</b> Parallel Plate Capacitor .....	118
<b>Figure 2.1-47:</b> Capacitor Bank Design and Building Block .....	121
<b>Figure 2.1-48:</b> Open Rack Capacitor Bank .....	122
<b>Figure 2.1-49:</b> SVC Single Line Diagram .....	123
<b>Figure 2.1-50:</b> 50 Mvar Inductive to 150 Mvar Capacitive SVC SLD .....	124
<b>Figure 2.1-51:</b> Layout for 50 Mvar Inductive to 150 Mvar Capacitive.....	125
<b>Figure 2.2-1:</b> IEEE 9 Bus system Single Line Diagram .....	129
<b>Figure 2.2-2:</b> Normalized PU equivalent impedance diagram.....	141
<b>Figure 2.2-3:</b> Two-Bus System with a Short Transmission Line .....	143
<b>Figure 2.2-4:</b> Load Bus (P-Q bus) .....	147
<b>Figure 2.2-5:</b> Generator Bus (PV Bus) .....	148
<b>Figure 2.2-6:</b> Flow Chart for Power Flow Solution Using N-R Method .....	152
Figure 2.2-7:Power Flow Equivalent Circuit.....	156
<b>Figure 2.2-8:</b> ETAP Power Flow Results .....	164
<b>Figure 2.2-9:</b> Bar Chart for ETAP Power Flow Results.....	165
<b>Figure 2.2-10:</b> Generation and Demand Variations.....	166
<b>Figure 2.2-11:</b> Time Domain Active Power Flow for Phase A for Loads A, B, and C .....	167
<b>Figure 2.2-12:</b> Time Domain Reactive Power Flow for Phase A for Loads A, B, and C .....	167
<b>Figure 2.2-13:</b> Time Domain Current Flow for Phase A for Loads A, B, and C.....	168

<b>Figure 2.2-14:</b> Time Domain Power Flow for Generators 1, 2, and 3.....	168
<b>Figure 2.2-15:</b> Total System Time Domain Load Flow (Source, Load, Losses P and Q) .....	169
<b>Figure 2.2-16:</b> Types of Faults in Electrical Power System .....	170
<b>Figure 2.2-17:</b> Simplified Equivalent Impedance Diagram .....	170
<b>Figure 2.2-18:</b> Total (DC and AC components) of a Symmetrical Short Circuit Current .....	172
<b>Figure 2.2-19:</b> Three Phase Device Duty IEC 60909 – Single Line Diagram .....	173
<b>Figure 2.2-20:</b> Bus No.1 - Transient Short Circuit Current .....	174
<b>Figure 2.2-21:</b> Bus No.2-Transient Short Circuit Current.....	174
<b>Figure 2.2-22:</b> Bus No.3-Transient Short Circuit Current.....	175
<b>Figure 2.2-23:</b> Bus No.4-Transient Short Circuit Current.....	175
<b>Figure 2.2-24:</b> Bus No.5-Transient Short Circuit Current.....	176
<b>Figure 2.2-25:</b> Bus No.6-Transient Short Circuit Current.....	176
<b>Figure 2.2-26:</b> Bus No.7-Transient Short Circuit Current.....	177
<b>Figure 2.2-27:</b> Bus No.8-Transient Short Circuit Current.....	177
<b>Figure 2.2-28:</b> Bus No.9-Transient Short Circuit Current.....	178
<b>Figure 2.2-29:</b> Singe Line to Ground Fault .....	179
<b>Figure 2.2-30:</b> Single Line to Ground Fault with ( $V_b$ and $3I_o$ ).....	179
<b>Figure 2.2-31:</b> Double Line Fault.....	180
<b>Figure 2.2-32:</b> Double Line Fault with ( $V_a$ and $3I_o$ ).....	180
<b>Figure 2.2-33:</b> Double Line to Ground Fault .....	181
<b>Figure 2.2-34:</b> Double Line to Ground Fault with ( $V_a$ and $3I_o$ ).....	181
<b>Figure 2.2-35:</b> Power System Stability Classifications .....	182
<b>Figure 2.2-36:</b> Three-Phase Fault at Beginning of Line 1 (connecting Bus 4 and Bus 5) .....	186
<b>Figure 2.2-37:</b> PU Equivalent Circuit in Pre-Fault Condition.....	187
<b>Figure 2.2-38:</b> Simplified Equivalent Circuit No.1 in Pre-Fault Condition.....	188
<b>Figure 2.2-39:</b> Internal Generated Voltage for Generator G1 in Pre-Fault Condition.....	188
<b>Figure 2.2-40:</b> Two Bus System with Transfer Reactance in Pre-Fault Condition .....	189
<b>Figure 2.2-41:</b> Power Angle Curve in Pre-Fault Condition .....	190
<b>Figure 2.2-42:</b> Power Angle Curve During Fault .....	190
<b>Figure 2.2-43:</b> Single Line Diagram with Line 1 Outage.....	191
<b>Figure 2.2-44:</b> PU Equivalent Circuit after Line 1 is out of Service. ....	192
<b>Figure 2.2-45:</b> Simplified Equivalent Circuit with Line 1 is out of Service. ....	192
<b>Figure 2.2-46:</b> Power Angle Curve in Pre, During, and Post-Fault Condition .....	193
<b>Figure 2.2-47:</b> Acceleration and Deceleration Areas.....	194
<b>Figure 2.2-48:</b> Generators Gen1, 2, and 3 dynamic Response for large disturbance - transient stability study.....	196
<b>Figure 2.2-49:</b> Generators Gen1, 2, and 3 dynamic Response for large disturbance - transient stability study BB No.5 fault .....	199
<b>Figure 2.2-50:</b> Grid Forming Principle .....	200
<b>Figure 2.2-51:</b> Line connecting between two buses i and j .....	201
<b>Figure 2.2-52:</b> IEEE 9 bus system with equivalent circuit. ....	202
<b>Figure 2.2-53:</b> MATLAB m.file Output.....	211

<b>Figure 2.2-54:</b> Equivalent circuit of the transmission link and its phasor diagram. ....	219
Figure 2.2-55: Nose Curve at different power factor angle (1) $\varphi=45^\circ$ lag , (2) $\varphi=30^\circ$ lag, (3) $\varphi=0^\circ$ lag, (4) $\varphi=30^\circ$ lead.....	224
<b>Figure 2.2-56:</b> P-V curve at different power factors.....	225
<b>Figure 2.2-57:</b> Voltage Stability Range for P-V curve.....	226
<b>Figure 2.2-58:</b> V-Q sensitivity for original IEEE 9 bus system ( with 0% renewable penetration ) .....	227
<b>Figure 2.2-59:</b> Bus No.2 P-V and Q-V results .....	227
Figure 2.2-60: P-V and Q-V Analysis ETAP simulation output.....	228
Figure 2.2-61: Bus No.2 P-V Curve .....	229
Figure 2.2-62: Voltage P-V and Q-V curves for all 9 buses of IEEE 9-Bus system .....	229
<b>Figure 2.2-63:</b> Voltage Stability Range for Q-V curve .....	230
<b>Figure 2.2-64:</b> Harmonic Waveform for fundamental, 3 <sup>rd</sup> , 5 <sup>th</sup> , 7 <sup>th</sup> order, and Resultant .....	232
<b>Figure 2.2-65:</b> Effect of 3 <sup>rd</sup> order harmonic (starting with positive cycle) on resultant distorted waveform .....	234
<b>Figure 2.2-66:</b> Effect of 3 <sup>rd</sup> Order harmonic (starting with negative cycle) on resultant distorted waveform .....	234
Figure 2.2-67: Several Harmonics waveforms and the composite waveform.....	235
Figure 2.2-68: ETAP Voltage THD (%) Harmonic Analysis for all IEEE 9 bus system without transformer harmonic model.....	236
Figure 2.2-69:ETAP Voltage THD (%) Harmonic Analysis for all IEEE 9 bus system with transformer harmonic model.....	237
Figure 2.2-70: ETAP Harmonic Impedance Scan Z magnitude and Z angle .....	237
<b>Figure 2.3-1:</b> Minimum P-Q Diagram to be fulfilled by IRR Plant [32].....	243
<b>Figure 2.3-2:</b> Definition and Control of PoCC Reactive Power .....	243
<b>Figure 2.3-3:</b> V-PF Characteristics at PoCC .....	244
<b>Figure 2.3-4:</b> Definition of Voltage Characteristic at the PCC for LVRT .....	245
<b>Figure 2.3-5:</b> Grid Connected PV plant with IEEE 9 Bus System (Bus No.7: POCC) .....	247
<b>Figure 2.3-6:</b> PV Plant Architecture drawing. ....	249
<b>Figure 2.3-7:</b> P-Q Capability Curve for PVS 980-2000 kVA.....	256
<b>Figure 2.3-8:</b> Load Capacity curve under different temperature conditions; 2066 kVA @ 45°C .....	256
<b>Figure 2.3-9:</b> Methods of Exporting Q from Solar Inverters [14].....	259
<b>Figure 2.3-10:</b> Capacitor Bank Implementation for Exporting Q to the Grid.....	259
<b>Figure 2.3-11:</b> Capacitor Bank Implementation for Exporting Q to the Grid.....	260
<b>Figure 2.3-12:</b> Proposed Open Rack Capacitor Bank .....	263
<b>Figure 2.3-13:</b> PV Plant Single Line Diagram Drawing with MV Capacitor Banks .....	264
<b>Figure 2.3-14:</b> Active and Reactive (P and Q) delivered by 200MW Grid Connected PV Plant.....	265
<b>Figure 2.3-15:</b> P and Q delivered by the 200MW PV plant at the MV/HV Station .....	266
<b>Figure 2.3-16:</b> ETAP - Run 3-Phase Device Duty using IEC 60909 at PoCC Bus No.7 IEEE 90 Bus.....	266
Figure 2.3-17:ETAP - Run 3-Phase Device Duty using IEC 60909 at HV Bus of Solar Step-Up station. ....	267
<b>Figure 2.3-18:</b> ETAP - Run Transient Short Circuit using IEC 61363.....	267
<b>Figure 2.3-19:</b> Three Phase Fault Current as Per IEC 61363 at PoCC (Bus 7 of IEEE 9 Bus system ).....	268
<b>Figure 2.3-20:</b> Voltage and Current Total Harmonic Distortion (THD) at PoCC of PV Plant .....	269

<b>Figure 2.3-21:</b> IEEE 12-Pulse Pre-defined Harmonic Model (Waveform and Spectrum) .....	269
Figure 2.3-22: Current THD (%) Cable Intertie for PV plant .....	269
Figure 2.3-23: Voltage THD (%) Bus 7 - PoCC for PV plant.....	270
Figure 2.3-24: Harmonic Frequency Scan Z magnitude and Z angle.....	270
<b>Figure 2.3-25:</b> Generator Gen 1 and Gen 3 dynamic response due to 3 Phase fault at BB No.7 without fault clearance.....	271
<b>Figure 2.3-26:</b> Generator Gen 1 and Gen 3 dynamic response due to 3 Phase fault at BB No.7 with fault clearance after 1 sec .....	271
Figure 2.3-27: Generator Gen 1 and Gen 3 dynamic response due to 3 Phase fault at BB No.7 with fault clearance after 0.5 sec .....	272
Figure 2.3-28:Generator Gen 1 and Gen 3 dynamic response due to 3 Phase fault at Line No.1 without fault clearance.....	272
Figure 2.3-29:Generator Gen 1 and Gen 3 dynamic response due to 3 Phase fault at Line No.1 with fault clearance .....	273
Figure 2.3-30:Generator Gen 1 and Gen 3 dynamic response due to loss of 200MW PV plant at t=5 sec	273
Figure 2.3-31:Generator Gen 1 and Gen 3 dynamic response due to Sudden Load Change .....	274
Figure 2.3-32: Generator Gen 1 and Gen 3 dynamic response due to Tripping of Line No.4 .....	274
Figure 2.3-33: V-Q Sensitivity for 9 Buses of IEEE 9 Bus system .....	275
Figure 2.3-34: V-Q Sensitivity Analysis for MV PV plant collection switchgear .....	275
Figure 2.3-35: P-V and Q-V for 9 Buses of IEEE 9 bus system .....	276
Figure 2.3-36: P-Q and Q-V curves for MV side main collection SWGR of PV plant .....	276
<b>Figure 2.3-37:</b> Wind Farm Architecture drawing.....	280
<b>Figure 2.3-38:</b> P-Q Capability Curve for WTG Converter .....	287
<b>Figure 2.3-39:</b> Capacitor Bank Implementation for Exporting Q to the Grid.....	289
<b>Figure 2.3-40:</b> Wind Farm Single Line Diagram Drawing with MV Capacitor Banks.....	293
<b>Figure 2.3-41:</b> Active and Reactive (P and Q) delivered by 100MW Grid Connected Wind Farm.....	294
<b>Figure 2.3-42:</b> P and Q delivered by the 100MW Wind Farm at the MV/HV Station.....	295
<b>Figure 2.3-43:</b> ETAP - Run 3-Phase Device Duty using IEC 60909 at PoCC Bus No.9 IEEE 9- Bus .....	296
<b>Figure 2.3-44:</b> ETAP-Run 3-Phase Device Duty using IEC 60909 at HV Bus of WF Step Up station.....	296
<b>Figure 2.3-45:</b> ETAP - Run Transient SC using IEC 61363 .....	297
<b>Figure 2.3-46:</b> Three Phase Fault Current as Per IEC 61363 at PoCC ( Bus 9 of IEEE 9 Bus system ).....	297
<b>Figure 2.3-47:</b> Voltage and Current Total Harmonic Distortion (THD) at PoCC of Wind farm. ....	298
<b>Figure 2.3-48:</b> IEEE 12 Pulse Pre-defined Harmonic Model (Waveform and Spectrum).....	298
Figure 2.3-49: Voltage (THD)% Harmonic Waveform and Spectrum at Wind Farm PoCC (Bus 9) .....	299
Figure 2.3-50:Current (THD)% Harmonic Waveform and Spectrum at Wind Farm PoCC (cable intertie ).	299
Figure 2.3-51: Harmonic Frequency Scan (Z magnitude and Z angle) .....	300
<b>Figure 2.3-52:</b> Generator Gen 1 and Gen 2 dynamic response due to 3 Phase fault at BB No.9 without fault clearance .....	300
<b>Figure 2.3-53:</b> Generator Gen 1 and Gen 2 dynamic response due to 3 Phase fault at BB No.9 with fault clearance after 1 sec .....	301
Figure 2.3-54:Generator Gen 1 and Gen 2 dynamic response due to 3 Phase fault at BB No.9 with fault	301

Figure 2.3-55:Generator Gen 1 and Gen 2 dynamic response due to 3 Phase fault at Line No.1 without fault clearance.....	302
Figure 2.3-56: Generator Gen-1 and Gen-2 dynamic response due to 3-Phase fault at Line No.1 with fault clearance.....	302
<b>Figure 2.3-57:</b> Generator Gen 1 and Gen 2 dynamic response due to loss of Wind farm at t=5 sec.....	303
<b>Figure 2.3-58:</b> Generator Gen 1 and Gen 2 dynamic response with the gradual penetration of Wind Farm .....	303
<b>Figure 2.3-59:</b> PoCC for Wind Farm (Bus No.9) dynamic response with the gradual penetration of Wind Farm .....	304
Figure 2.3-60: WTG's 1,2,3 and 4 dynamic responses for load change .....	304
Figure 2.3-61:Generator Gen 1 and Gen 2 dynamic response due to Disconnection of Line 4 .....	305
Figure 2.3-62:WTG's 1,2,3 and 4 dynamic responses for disconnection of Line 4 .....	305
Figure 2.3-63: Bus No.9 (WF PoCC) dynamic responses for disconnection of Line 4 .....	306
Figure 2.3-64: V-Q Sensitivity - transmission buses.....	306
Figure 2.3-65: P-V and Q-V for Transmission Buses.....	307
Figure 2.4-1:ETAP model for IEEE 9 bus system with 100% Renewable Energy Sources .....	310
<b>Figure 2.4-2:</b> Power Flow for IEEE 9 bus system with 100% Renewable generations.....	311
<b>Figure 2.4-3:</b> Load curve for Load A for one day (24 hour) .....	312
Figure 2.4-4: Irradiance in W/m <sup>2</sup> for Solar PV plant for one day .....	313
Figure 2.4-5: Wind Turbine Generator P and Q variation for one day .....	313
Figure 2.4-6: Loads A, B, and C variations over one month.....	314
Figure 2.4-7: Hydroelectric Generator No.1 time domain power flow main parameters.....	314
Figure 2.4-8: Total system performance over one complete month.....	314
Figure 2.4-9: Hydro Electric Generator Active Power Flow over one complete month. ....	315
Figure 2.4-10:Wind Turbine Generator Active Power Flow over one complete month. ....	315
Figure 2.4-11:PV Generator Active Power Flow over one complete month. ....	315
<b>Figure 2.4-12:</b> ETAP - Run 3-Phase Device Duty using IEC 60909 at Transmission Buses of IEEE 9 Bus system .....	316
<b>Figure 2.4-13:</b> ETAP - Run Transient SC using IEC 61363 .....	317
<b>Figure 2.4-14:</b> IEEE 12 Pulse Pre-defined Harmonic Model (Waveform and Spectrum).....	318
Figure 2.4-15: ETAP Harmonic Analysis output voltage and current THD (%) on Single Line Diagram .....	318
Figure 2.4-16: Distorted waveform and spectrum for main buses.....	319
Figure 2.4-17: Harmonic Impedance Scan (Z magnitude and Z angle) .....	319
<b>Figure 2.4-18:</b> Hydroelectric generator Gen1 dynamic response for a fault at PV plant PoCC with and without fault clearance.....	320
<b>Figure 2.4-19:</b> PV plant PoCC dynamic response for a fault at PV plant PoCC with and without fault clearance.....	320
<b>Figure 2.4-20:</b> PoCC bus voltage angle with and without fault clearance.....	321
<b>Figure 2.4-21:</b> Dynamic Response for HE Gen-1 Three Phase Balanced Fault at WF PoCC with 1 sec FCT	321
<b>Figure 2.4-22:</b> Dynamic Response for HE Gen-1 Three Phase Balanced Fault at WF PoCC with 0.5 sec FCT .....	322

Figure 2.4-23: generator Gen1 response due to Three Phase Balanced Fault at Line 6 with/without Fault Clearance .....	322
<b>Figure 2.4-24: Generator Gen1 response due to Loss of 200MW PV Plant at t=5 sec.....</b>	<b>323</b>
Figure 2.4-25: PV plant PoCC dynamic response due to Loss of 200MW PV Plant .....	323
Figure 2.4-26:Generator Gen1 response due to Loss of 100MW Wind Farm at t=5 sec.....	324
Figure 2.4-27:Wind farm PoCC dynamic response due to Loss of 100MW Wind farm.....	324
Figure 2.4-28: Generaroe G1 dynamic response due to Loads A, B, and C change.....	325
Figure 2.4-29:Generaroe G1 dynamic response due to Line 4 disconnection.....	325
Figure 2.4-30: V-Q Sensitivity Analysis.....	326
Figure 2.4-31: ETAP P-V and Q-V simulation output of Voltage Stability Study .....	326
Figure 2.4-32: P-V and Q-V curves for all transmission buses .....	327
Figure 2.4-33: Energy and Security Classification .....	328
Figure 2.4-34: Smart Grid Interoperability pillars .....	329
Figure 3.1-1: Eight (8) sustainable energy scenarios and contribution in (%) of MW per technology.....	332
Figure 3.1-2:Primary Energy Source Technology Contribution per Scenario .....	332
Figure 3.1-3:ETAP time domain load flow summary for 100% Renewable Energy Sources.....	337
Figure 3.1-4: Exploratory Data Analysis Chart .....	338
Figure 3.1-5:Linear regression for LCOE for PV.....	339
Figure 3.1-6:Exponential Smoothing for LCOE for PV.....	340
Figure 3.1-7:Linear regression for LCOE for Wind Energy .....	340
Figure 3.1-8:Linear regression for LCOE for Hydro Electric .....	340
Figure 3.1-9:Power Generation Cost per Technology ( 2010-2022) in USD/KWh .....	341
Figure 3.1-10: Electricity tariff USD/kWh.....	343
Figure 3.1-11: Summary of Time Domain load flow for 8 scenarios.....	351
Figure 3.1-12: Total system MVAh for each scenario and surplus of Energy .....	351
Figure 3.1-13: CO2 and LCOE for each Scenario for one complete month.....	352
Figure 3.1-14: Profit (%) for one complete month for each scenario.....	352
Figure 3.1-15: Losses in KWh for each scenario .....	353
Figure 3.1-16:PowerBI Dashboard for S1-0% Renewable Energy.....	354
Figure 3.1-17:PowerBI Dashboard for S2-15% Renewable Energy (Wind).....	354
Figure 3.1-18:PowerBI Dashboard for S3-30% Renewable Energy (Solar) .....	355
Figure 3.1-19:PowerBI Dashboard for S4-45% Renewable Energy (Wind + Solar).....	355
Figure 3.1-20:PowerBI Dashboard for S4-56% Renewable Energy (Hydro).....	356
Figure 3.1-21:PowerBI Dashboard for S6-75% Renewable Energy (Hydro+Wind) .....	356
Figure 3.1-22:PowerBI Dashboard for S7-85% Renewable Energy (Hydro+Solar) .....	357
Figure 3.1-23:PowerBI Dashboard for S6-100% Renewable Energy (Hydro+Wind+Solar).....	357
Figure 3.1-24: CO2 emissions per Scenario .....	358
Figure 3.1-25: LCOE per Scenario.....	358
Figure 3.1-26: Short Circuit Power (MVA <sub>sc</sub> ) for each scenario.....	359
Figure 3.1-27: Three phase short circuit current I <sup>sc</sup> (kA) for each 230kV bus per scenario .....	359
Figure 3.1-28:Gen1 - Degree - Generator Absolute Power Angle .....	360
Figure 3.1-29: Generator 1 frequency dynamic response for each scenario .....	361

Figure 3.1-30:Gen1 - Generator Mechanical Power ( in MW) .....	362
Figure 3.1-31:Gen_1 - MW - Generator Electrical Power .....	363
Figure 3.1-32:Gen1 - Mvar - Generator Reactive Power .....	363
Figure 3.1-33:Gen1 - Generator Terminal Current (Amp) .....	364
Figure 3.1-34:Gen_1- Generator Exciter Voltage (PU).....	364
Figure 3.1-35:Gen Exciter Current- Per Unit.....	365
Figure 3.1-36: Summary of Load Flow Study for 8 scenarios.....	366

## List of Tables

Table 1.2-1:Overview of IRENA 100% RE scenarios analyzed.....	51
<b>Table 2.1-1:</b> Power Terminologies .....	115
<b>Table 2.3-1:</b> Frequency Relaying Requirements .....	245
<b>Table 2.3-2:</b> Voltage Range for Normal Operation.....	246
<b>Table 2.3-3:</b> Voltage Relaying Requirements .....	246
<b>Table 2.3-4:</b> Proposed Grid Connected PV plant Parameters. ....	247
<b>Table 2.3-5:</b> Power Cables Voltage Drop at 0.85 PF .....	252
<b>Table 2.3-6:</b> Power Cables Voltage Drop at 0.95 PF .....	254
<b>Table 2.3-7:</b> P-Q Capability Assessment .....	257
<b>Table 2.3-8:</b> Inverter Characteristics at P.F = 0.867, $V_{inv} = 1 \times V_n$ , Design Temp =45°C, and $V_{PoCC} = 0.9 V_n$ .....	258
<b>Table 2.3-9</b> Technical Parameters of Open Rack Capacitor Bank.....	262
<b>Table 2.3-10:</b> Proposed Grid Connected Wind Farm Parameters .....	277
<b>Table 2.3-12:</b> Power Cables Voltage Drop at 0.85 PF .....	283
<b>Table 2.3-13:</b> Power Cables Voltage Drop at 0.95 PF .....	285
<b>Table 2.3-13:</b> P-Q Capability Assessment for WTG.....	288
<b>Table 2.3-14:</b> WTG Characteristics at P.F = 0.805, $V_{WTG} = 0.95 \times V_n$ .....	288
<b>Table 2.3-10</b> Technical Parameters of Open Rack Capacitor Bank.....	292

## ACRONYMS

AC	Alternating Current
AM	Air Mass
AVR	Automatic Voltage Regulator
BB	Bus Bar
CB	Circuit Breaker
CT	Current Transformer
DC	Direct Current
Dis	Disconnecter
GIS	Grid Impact Study or Gas Insulated Switchgear
HV	High Voltage
IAC	Internal Arc Classification
IGBT	Insulated Gate Bi-polar Transistor
KCL	Kirchhoff's Current Law
KVL	Kirchhoff's Voltage Law
LSC	Loss of Service Continuity
LV	Low Voltage
MV	Medium Voltage
TSO	Transmission System Operator
OLTC	On-load Tap Changer

PoCC	Point of Common Coupling
PV	Photo-Voltic
RMU	Ring Main Unit
RTCCP	Remote Tap Changer Control Panel
SA	Surge Arrester
SF <sub>6</sub>	Sulfur hexafluoride
SLD	Single Line Diagram
SPWM	Sinusoidal Pulse Width Modulation
SS	Switching Substation
STATCOM	Static Compensator
SVC	Static Var Compensator
SWGR	Switchgear
VT	Voltage Transformer
WTG	Wind Turbin Generator
WF	Wind Farm
SCIG	Squirrel Cage Induction Generator
WRIG	Wound Rotor Induction Generator
DFIG	Doubly Fed Induction Generator
PMSG	Permanent Magnet Synchronous Generator
RE	Renewable Energy
IRR	Intermittent Renewable Resources
ROCOF	Rate of Change of Frequency
ETAP	Electric Transient Analyzer Program

MATLAB	Matrix Laboratory
THD	Total Harmonic Distortion

## NOMENCLATURES

$S$	Apparent Power
$P$	Active Power
$Q$	Reactive Power
$PF$	Power Factor
$R$	Resistance Value
$L$	Inductance Value
$C$	Capacitance Value
$Z$	Impedance
$Y$	Admittance
$G$	Conductance
$B$	Susceptance
$i_{PU}$	Per Unit Current
$i_f$	Fault Current
$I_B$	Base Current
$\omega$	Angular Frequency
$J$	Total moment of inertia of the rotor mass (kg.m <sup>2</sup> )
$\theta_m$	Angular displacement of the rotor with respect to a stationary axis (rad)
$t$	Time (seconds)

$T_m$	Machinal torque supplied by the prime mover
$T_e$	Electrical or electromagnetic torque
$T_a$	Accelerating torque
$M$	Angular momentum
$W_k$	Stored kinetic energy
$H$	Stored kinetic energy for 1MVA
$\Delta V$	Voltage Drop
$I_{ph}$	Photo Current
$E_{ph}$	Photon Energy
$h$	Planck constant $6.62607015 \times 10^{-34}$ J·s
$c$	Light Speed 300,000 km/s
$\lambda$	Wavelength
$R_{sh}$	Shunt resistance
$R_{sr}$	Series resistance
$q$	Change of electron $1.6 \times 10^{-23}$ C
$I_o$	Reverse saturation current
$V_{o.c}$	Open circuit voltage (V-I <sub>sh</sub> )
$A$	Ideality factor where $A= 1$ for ideal diode and $A= 1 - 2$ for a practical diode
$K$	Boltzmann factor ( $1.38 \times 10^{-23}$ J/K)
$T$	Absolute temperature for solar cells
$J$	Current Density
$FF$	Fill Factor
$V_{mpp}$	Maximum Power Point Voltage

$I_{mpp}$	Maximum Power Point Current
$I_{sh.c}$	Short Circuit Current
$G$	Irradiation

### **ABSTRACT**

For over a century, the combustion of fossil fuels (coal, oil, natural gases) has been the primary energy source for driving our vehicles, fueling our industries, and maintaining the illumination in our residences. However, energy production, primarily through the combustion of fossil fuels, is responsible for approximately 75% of worldwide greenhouse gas emissions which is a primary catalyst for climate change, also incurs significant health risks, resulting in a minimum of five million fatalities annually due to air pollution.

In its latest Assessment Report (AR6), the UN Intergovernmental Panel on Climate Change emphasized the importance of this decade in limiting global temperature rise to 1.5°C above pre-industrial levels by the end of the century. Strong scientific consensus calls for immediate action by 2030 to halve global CO<sub>2</sub> emissions from 2019 levels. The 1.5°C pathway emphasizes electrification and energy efficiency as key drivers of the energy transition, supported by renewable energy, clean hydrogen, and sustainable biomass. The (COP28) also laid the framework for a rapid, fair, and equitable transition, signaling the beginning of the end of the fossil fuel era. Both increased funding and drastic cuts to emissions will lend credence to this shift.

However, this transition in the electrical power and energy system will be gradual until we reach to achieve 100% renewable energy, and for this to be achieved planning, optimization, and traceability are necessary to operate a power system with high penetration of renewable energy sources such as solar, wind, hydro, and biomass. This supports the transition to a net zero energy system and requires new tools and digital technologies.

The IEEE 9 bus system, which is regarded as a small-scale electrical power system, was chosen as the case study to validate the aforementioned. The system was deeply and thoroughly analyzed by performing a per-unit analysis, power flow study, time domain load flow, steady state and dynamic short circuit calculations, transient stability study, formulating a system of differential equations for currents and algebraic equations for bus voltages, voltage stability study, harmonic analysis, and contingency analysis. After that a grid impact study has been conducted for large scale Photovoltaic Plant and wind farm. This grid impact study includes a per-unit analysis, a power flow study, P-Q capability checks, steady state and dynamic short circuit calculations, a transient stability study, system of differential equations for currents, bus voltages, voltage stability study, harmonic analysis. It also uses power quality dynamic shunt compensators to ensure that PV/Wind/hydro plants are in compliance with grid code requirements.

This thesis analyzes the IEEE 9-Bus system's power system in eight (8) scenarios starting with 0% contribution of renewable and reaching up to 100% renewable IEEE 9 bus system. The findings will subsequently be applied to our large-scale power systems whereby increased renewables penetration and switching in and out of Inverter Based Resources (IBRs) will negatively impact the stability and reliability of the power system, it is no longer possible to do so without causing a significant impact on grid stability, and there are several challenges that expected to come with more renewables such as lower short circuit power and system strength, lower system inertia which causes increased rate of change of frequency (RoCoF), power imbalance results in reduced frequency, injection of more harmonics into the grid, voltage dips and post-fault voltage recovery profiles

Besides, a data analysis techniques and Artificial Intelligence tools to analyze the financial and sustainable impact of this gradual transitioning for electrical power and energy IEEE 9 bus system from fossil-fuel based primary energy sources to fossil-free based primary energy sources. Then, a comparative analysis for all the 8 scenarios was conducted.



# PART ONE



# 1.1 Chapter One: INTRODUCTON

## 1.1.1 Research Background

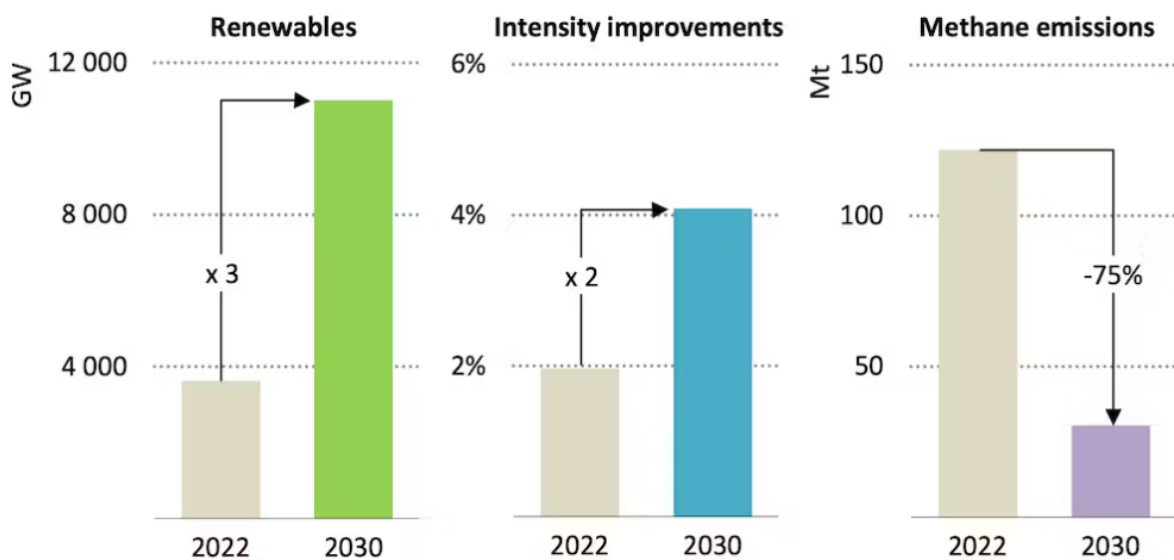
The United Nations Intergovernmental Panel on Climate Change, in its most recent Assessment Report (AR6), emphasized the importance of this decade in achieving the objective of restricting the rise in the average global temperature to 1.5°C above pre-industrial levels by the conclusion of this century. There is a prevailing scientific consensus that emphasizes the imperative of promptly and expeditiously implementing measures by the year 2030 to reduce global carbon dioxide (CO<sub>2</sub>) emissions by 50% compared to the levels recorded in 2019 (IPCC, 2023). The 1.5°C pathway emphasizes the significance of electrification and energy efficiency as crucial catalysts for the energy transition. This transition is facilitated by the utilization of renewable energy sources, clean hydrogen, and sustainable biomass.

The electrical energy industry should be moving towards a low-carbon pathway and aiming towards carbon neutrality, characterized by a growing proportion of renewable energy sources. Renewable Energy (RE) sources play a significant role in the provision of sustainable and environmentally friendly energy, therefore contributing to the mitigation of climate change. One of the primary objectives in the field of electricity generation is to eliminate the reliance on fossil fuels. However, in the interim, generation station facilities have the capacity to reduce emissions by integrating energy derived from renewable sources such as wind and solar with conventional coal or gas stations. The objective is to attain a significant degree of energy security that aligns with a sustainable trajectory, ensuring the continuation of progress towards carbon neutrality.

This will be accomplished through the allocation of resources towards low-carbon and climate-responsive initiatives, as well as the expansion of clean energy utilization and exportation within the domestic sphere. These efforts will drive the development of a green economy, benefiting all individuals, including those in vulnerable communities. The principles of inclusivity and fairness will guide these endeavors, while also contributing to the global endeavor of stabilizing the climate system.

In Conference of Parties (COP28) that was held in November 2023, it was agreed that It is imperative that the globe to make significant changes to the manner in which they generate and utilize energy to swiftly reduce emissions of greenhouse gases, the International Energy Agency (IEA) and International Renewable Energy Agency (IRENA) have called for the following pillars for action by year 2033, see **Figure 1.1-1** for the first 3 pillars :

1. Triple global renewable capacity
2. Double the rate of energy efficiency.
3. Commitments by the fossil fuel industry, and oil and gas companies in particular, to align activities with the Paris Agreement, starting by cutting methane emissions from operation by 75%.
4. Establish large-scale financing mechanisms to triple clean energy investment in emerging and developing economies.
5. Commit to measures that ensure an orderly decline in the use of fossil fuels, including an end to new approvals of unabated coal fire power plants.



Left: Global renewable energy capacity, gigawatts. Centre: Annual rate of improvement in the energy intensity of the global economy - the rate of energy use per unit of GDP. Right: Global energy sector methane emissions, million tonnes. Source: World Energy Outlook 2023.

**Figure 1.1-1**-IEA first 3 pillars of COP28.

Also, the (COP28) marked the beginning of the end of the age of fossil fuels by establishing the groundwork for a transition that is quick, fair, and equitable. This transition will be supported by significant reductions in emissions and increased financing.

Nevertheless, the shift towards a fully renewable energy system will occur gradually. To achieve this goal, it is imperative to implement planning, optimization, and traceability measures. These measures are essential for effectively operating a power system that relies heavily on renewable energy sources such as solar, wind, hydro, and biomass. This facilitates the shift towards a net zero energy system and necessitates the use of novel tools and digital technologies.

In this thesis, the IEEE 9 bus system was taken as the basis for the case study. This benchmark model includes three synchronous machines that have built-in automatic voltage regulation functionality and speed regulators via load frequency control, three generator-step up transformers with two windings each, six overhead transmission lines with constant parameters that interconnects between these generation stations and three constant power loads.

This thesis performs a detailed power system analysis and grid impact study for this IEEE 9-Bus system with two options: non-renewable and renewable energy source in eight (8) scenarios.

1. Option No.1: **Fossil fuel** (non-renewable) based primary energy sources driving the synchronous machines which are driven by steam turbines.
2. Option No.2: **Fossil Free** (renewable) based primary energy source through partial and full transition towards a 100% renewable and sustainable primary energy sources like solar, wind, hydroelectric power plants connected to IEEE 9 bus system as a replacement of the original synchronous machines driven by fossil fuel sources, and this was conducted by having eight (8) scenarios.

However, renewable energy generation installations have noted several different design and performance issues that have not always been properly addressed during the development of the projects. These issues include harmonic problems, transient over-voltages, transformer

saturation, lower short circuit power and system strength, lower system inertia which causes increased rate of change of frequency (RoCoF), power imbalance results in reduced frequency, injection of more harmonics in the grid, voltage dips and post-fault voltage recovery profiles and reactive power losses. That's why a grid impact study should be performed that covers the per unit analysis, power flow study,  $P$ - $Q$  capability checks, steady state and dynamic short circuit calculation, transient stability study, voltage stability study, harmonic analysis, voltage drop calculations, and system of differential equations for currents, sending and receiving-end bus voltages and fault voltage at Point of Common Coupling (PoCC). Also, it checks the PV/Wind/hydro plants compliance with the grid code requirements using the power quality dynamic shunt compensators.

The case study that was selected to verify the previously mentioned was IEEE 9 bus system which is considered a small-scale electrical power system, and the results that will be obtained will be implemented to the large-scale power systems. The actual system has been simulated using ETAP software.

### **1.1.2 Research Problem**

For over a century, the combustion of fossil fuels (coal, oil, natural gases) has been the primary energy source for driving our vehicles, fueling our industries, and maintaining the illumination in our residences. According to the U.S. Energy Information Administration, oil, coal, and gas continue to meet approximately 80% of our energy requirements in the present day. As a result, Energy production, primarily through the combustion of fossil fuels, is responsible for approximately 75% of worldwide greenhouse gas emissions which is a primary catalyst for climate change, also incurs significant health risks, resulting in a minimum of five million fatalities annually due to air pollution.

The combustion of fossil fuels in power plants results in the release of various pollutants, including sulfur dioxide ( $SO_2$ ), nitrogen oxides (NOX), particulate matter (PM), carbon dioxide ( $CO_2$ ), mercury (Hg), and other similar particles. The emissions of NOX and  $SO_2$  are responsible for the

creation of ground-level ozone and fine particulate matter (PM), which can result in respiratory and cardiovascular ailments. Additionally, exposure to mercury can heighten the likelihood of health problems, including cancer and immune system impairment. The presented chart **Figure 1.1-2** illustrates the progression of worldwide emissions from the mid-18th century to the present day. Prior to the Industrial Revolution, emissions were significantly minimal. The rate of increase in emissions remained relatively sluggish until the middle of the 20th century. The global carbon dioxide (CO<sub>2</sub>) emissions in 1950 amounted to 6 billion metric tons. By 1990, the quantity had nearly quadrupled, surpassing 20 billion tons. The rate of emissions has exhibited a persistent upward trend, with current annual emissions surpassing 35 billion tons. The rate of emissions growth has decelerated in recent years; however, it has not yet attained its zenith.

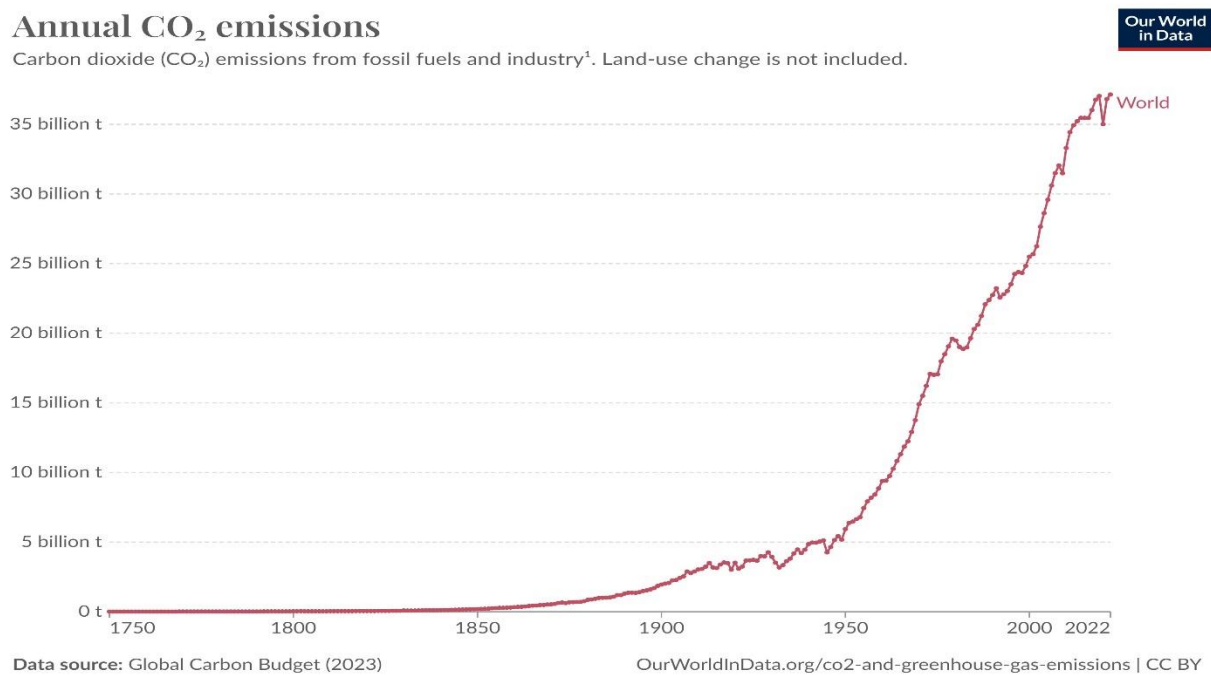


**Figure 1.1-2:** Carbon dioxide (CO<sub>2</sub>) emissions from fossil fuels and industry from 1750 to 2022

Climate change encompasses substantial changes in the climate system occurring across temporal scales ranging from decades to millions of years. The primary catalyst for climate change is the escalation in greenhouse gas emissions (effect), which subsequently induces global warming. Global warming refers to the sustained rise in the temperature of Earth's surface over an extended period, starting from the pre-industrial era (specifically, the time frame between 1850 and 1900).

This phenomenon may be attributed to human activity, mostly the combustion of fossil fuels, which leads to elevated amounts of greenhouse gases in the Earth's atmosphere, hence intensifying the retention of heat. The earth receives solar radiation in various forms, including visible light, radiation, infrared emissions, and others. When this solar radiation/sun's energy reaches the earth's atmosphere, a portion of it is reflected back into space, while the remainder is absorbed and re-radiated by greenhouse gases. Approximately 70% of the radiation is retained, while 30% is reflected. The ingested energy warms the Earth's atmosphere and surface. This process keeps the Earth's temperature approximately 33°C above what it would be otherwise, allowing life to exist on Earth.

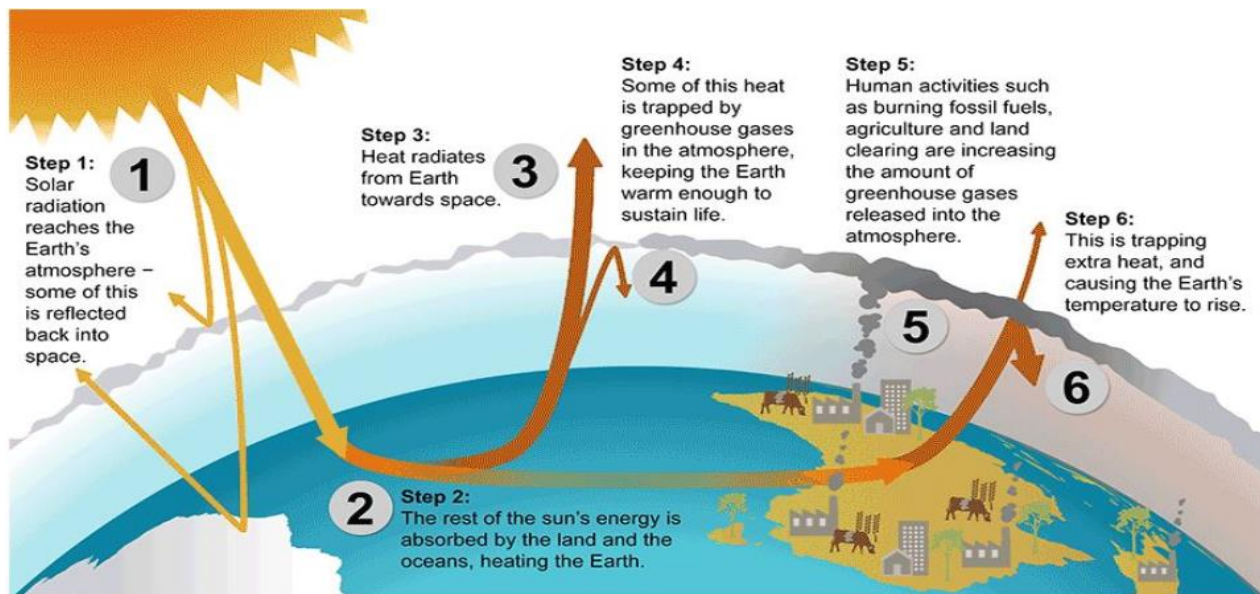


**Figure 1.1-3:** Solar Radiation Journey

Figure 1.1-3 shows the solar radiation journey starting from Step 1 where solar radiation reaches the Earth's atmosphere, then a portion of it is reflected back into space. Then, In Step 2: The remainder of the sun's energy is absorbed by the land and oceans, warming the planet. After this, Step 3: The Earth emits heat into space. Then in Step 4: Greenhouse gases in the atmosphere capture a portion of this heat, keeping the planet temperate enough to support life. Step 5: Human activities such as the combustion of fossil fuels, agriculture, and land clearance increase the quantity of greenhouse gases emitted into the atmosphere where the global emissions of greenhouse gases have seen a significant rise. According to recent statistics, the atmospheric concentration of carbon dioxide CO<sub>2</sub> is above the threshold of 400 parts per million. Finally, Step

6: This is capturing extra heat and causing the Earth's temperature to rise, and these anthropogenic factors contribute to the acceleration of global warming and subsequent climate change. However, increased concentrations of greenhouse gases in the Earth's atmosphere leads to an intensification of the natural greenhouse effect, resulting in a rise in global temperatures. This phenomenon is called "Enhanced Greenhouse Effect" which refers to the phenomenon whereby the Earth's temperature rises as a result of an increase in the concentration of greenhouse gases. The phenomenon of enhanced greenhouse effect (GHE) may be attributed to anthropogenic activities, However, a concern arises as human activities have begun to disrupt this natural equilibrium, leading to an intensified greenhouse effect, primarily attributed to the advent of industrialization, such as the unregulated combustion of fossil fuels (including coal, oil, and natural gas), as well as agricultural practices and land clearance. See **Figure 1.1-4**

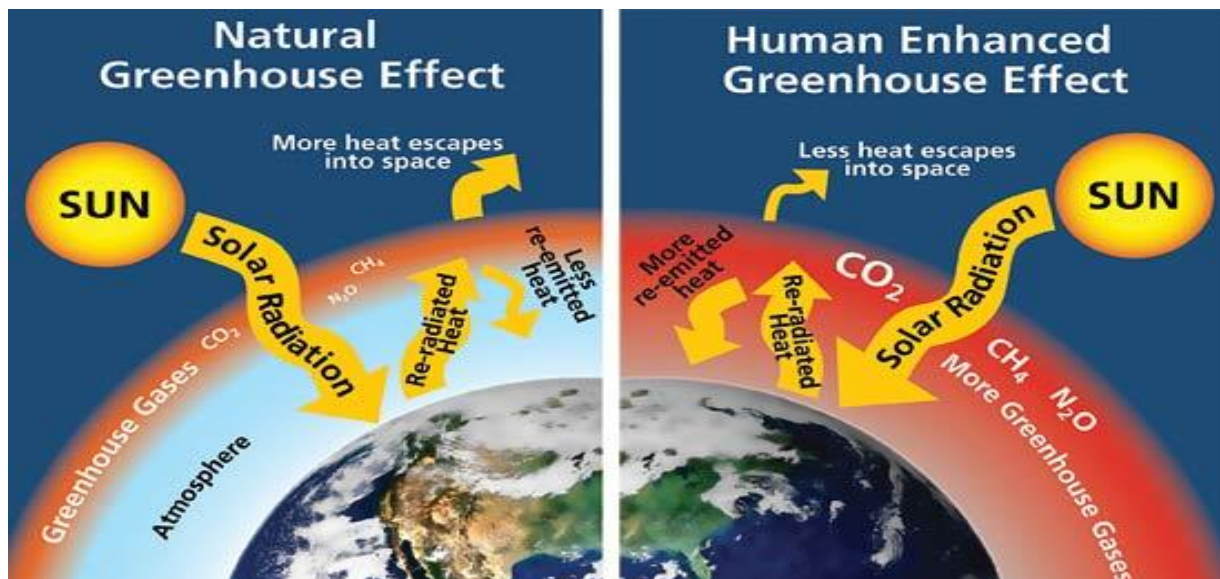


**Figure 1.1-4:** Natural Greenhouse Effect vs Human Enhanced Greenhouse Effect

Greenhouse gases may be classified into two categories: *direct emissions* and *indirect emissions*. Direct emissions refer to the emissions generated by the operational activities that are owned or controlled by the reporting organization and are categorized under Scope 1. Indirect emissions may be further classified into two distinct categories, namely Scope 2 and Scope 3, see *Figure 1.1-5* ; Scope 2 encompasses the emissions resulting from the production or procurement of purchased power, steam, heating, and cooling that are used by the reporting organization. All

residual indirect emissions that transpire inside the value chain of the reporting entity are categorized as Scope 3 emissions (Wiedmann, 2021).

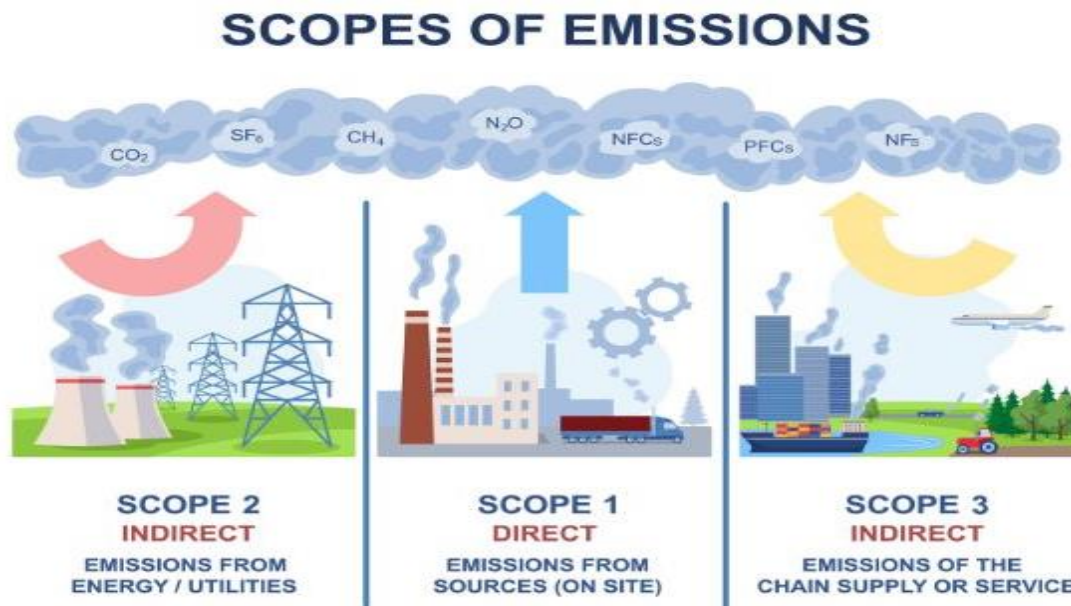


**Figure 1.1-5:** Scope of Emissions

Thus, it is imperative that we transition completely away from fossil fuels and exclusively rely on pollution-free, 100% clean energy to power our entire society and energy industry utilities should gradually reduce their dependability on fossil fuel primary energy source, slow global warming, and accelerate the energy transition towards sustainability transition to renewable generation that is entirely fossil-free in the long term such as solar, wind , and hydro.

However, critics in the energy sector (especially those who work in fossil fuel plants for long time) have doubt on energy transition to fossil free sustainable resources. For example, some of them raise these questions: what about the impact on the global economy? will renewable energy subsidies replace or eliminate high-paying employment in the fossil fuel industry specially that no indigenous energy sources available in most of the middle east countries? can the intermittent of the renewable energy sources meet the base load in each country especially with the high growth of electricity demand? can renewable energy provide low-cost power even without government handouts? All these issues should be of interest to citizens and governments alike. But continuing business as normal at any cost would be disastrous for our world.

The utilities claim that the switch to 100% of renewable energy presents a dilemma since, unless you live in an environmentally visible nation (hilly or sunny or geologically active), fossil-free energy or electricity will likely start to depend on the weather. For example, in wind energy, In the gust wind, if the wind speed is too high (more than around 25m/s) wind turbines must be shut down to prevent damage or if the wind speed is too low (less than about 2.5m/s) it is not viable to switch on the Turbines. As for the solar PV, the utilities justification is that after sunset, solar panels cannot produce electricity, and they are less efficient in cloudy conditions, also in high temperature or dusty weather, the efficiency of the solar panel goes steeply down.

Obviously; utilities globally need to modify their energy generation and consumption patterns if they are targeting to reduce their dependability on fossil fuel, slow global warming, and accelerate the energy transition toward sustainability which have changed dramatically over the last twenty to thirty years, from initial rejection to the elevation of sustainability as a major strategic organization objective due to the awareness that it is not only beneficial for the environment but financially lucrative.

Electric power energy systems (EPESs) structured into generation, transmission, and distribution (T&D), as well as the consumption is categorized into residential, commercial, and industrial loads. Electric power energy systems (EPESs) are now encountering a several restrictions, challenges, and limitations. These limitations include the need to effectively balance the fuel mix due to growing amount of grid integrated renewable energy sources such as solar and wind, electricity transmission losses, lack in providing reliable power supply with high power quality which leads to frequent power outages, power system instability problems, electromobility integrations, enhance asset level visibility and management, grid modernization, cyber-attacks threats, develop new sources of revenue, address the challenges posed by an aging workforce and knowledge capture, and integrate emerging technologies. For example, the diversity of primary energy sources and fuel mix used for power generation stations is becoming more varied and adaptable, including centralized (bulk) generation sources such as fossil fuels (coal, oil, natural gases), nuclear power plants, distributed renewables generating resources like (solar photovoltaic, wind), as well

as the integration of energy storage systems that further enhances the flexibility of the fuel mix. Achieving a proper optimized balance of this fuel mixture; by optimizing the flow of electric power throughout minimizing the amount of power drawn and absorbed from the fossil fuel based conventional power generations while simultaneously maximizing the amount of power generated from distributed renewable energy sources and energy storage systems is of utmost importance; to optimize the cost-effectiveness and energy yield of the Electric Power Energy System (EPES)

### **1.1.3 Research Aim**

The aim of this study is to analyze the effects and challenges of transitioning for electrical power and energy system from fossil-fuel primary energy sources to fossil-free (renewable energy) sources on the stability, security, and interoperability by taking as a small-scale sample electrical power system, the IEEE 9 bus system, first; conduct a comprehensive power system analysis and studies, and then model verification using ETAP and MATLAB. Second; the examination of transition for IEEE 9 bus from fossil fuel-based conventional synchronous machines to grid integrated and interconnected sustainable electric power energy systems (EPES) through the gradual utilization towards 100% renewable primary energy sources, including solar, wind, and hydro, along with the implementation of a power quality solution that optimizes stability, security, and interoperability. Third, conduct a grid impact study if all fossil fuel power plants (synchronous machines) within the IEEE-9 Bus system are substituted with renewable energy sources (solar, wind, and hydro) that have identical capacities of each replacement. Fourth, examine the power system analysis, stability, security, interoperability, and performance for the 100% renewable energy scenario. Fifth, perform a financial analysis and life cycle assessment for complete one month and use the data analysis methods, tools, and techniques to analyze and visualize the data. Finally, conduct a diagnostic analysis for the dynamic short circuit and transient stability for the IEEE 9 bus, then perform comparative analysis for all the 8 scenarios in terms of power flow, short circuit, harmonic analysis, transient and voltage stability studies.

#### **1.1.4 Research Objectives**

- 1.1.4.1 To perform steady state and dynamic power system analysis for the original IEEE-9 Bus system with fossil fuel based primary energy sources driven synchronous machines.
- 1.1.4.2 To replace the fossil fuel based primary energy sources driven synchronous machines by equivalent fossil free primary energy sources (solar/wind/hydro) in the IEEE 9 bus system and then perform the necessary grid impact studies.
- 1.1.4.3 To identify the challenges of partially and fully transitioning to 100% renewable electrical power and energy system for IEEE 9 Bus system in terms of stability, security, and interoperability.
- 1.1.4.4 To perform a financial analysis and sustainability assessment for the 8<sup>th</sup> scenario 100% renewable energy system.

#### **1.1.5 Research Question**

- 1.1.5.1 What are steady state and dynamic stability limits for the IEEE-9 Bus system with fossil fuel based primary energy sources driven synchronous machines?
- 1.1.5.2 What are the optimum and visible fossil free primary energy sources: solar/wind/hydro that could replace the fossil fuel based primary energy synchronous machines?
- 1.1.5.3 What are the challenges of partially and fully transitioning to 100% renewable electrical power and energy system for IEEE 9 Bus system?
- 1.1.5.4 What are the LCOE, LROE, and profit for each scenario, and perform life cycle assessment for all the scenarios, and specifically the 100% renewable energy scenario?

#### **1.1.6 Thesis Structure**

This thesis is based on three parts; First part contains of three chapters: introduction, literature review, and methodology and philosophy, second part contains of four chapters: Grid Connected PV/Wind main components, Case study & architecture plant, Power system analysis for IEEE 9-Bus system, grid impact studies for 100% renewables grid integrated to IEEE 9 bus system, third part contains: Data collection, conclusion, recommendation and Future works.

The first part, serving as both an introduction and background part, provides an overview of the research topic, elucidates the study's purpose and goals. Additionally, the literature review chapter provides two distinct frameworks, namely empirical and theoretical frameworks, for the analysis of the research issue. In the third chapter, the application of the approach and methods for gathering the necessary information is undertaken, accompanied by a rationale for the decision-making process. The outcome section has delineated the insights acquired from the used research methodology. The last chapter of this research has conducted a comparative analysis between the study's results and the existing literature in order to derive pertinent findings and draw conclusions for the whole study.



## 1.2 Chapter Two: Literature Review

### 1.2.1 Renewable Energy

Since the industrial revolution, fossil fuels (coal, oil, natural gases) which are basically called non-renewable primary energy sources have dominated the energy mix in most countries worldwide. This has tremendous consequences for both the global climate and human health. Three-quarters of worldwide greenhouse gas emissions come from the use of fossil fuels for energy. Fossil fuels contribute significantly to local air pollution by releasing CO<sub>2</sub>, which causes at least 5 million premature deaths each year. Renewable energy sources are clean sources of energy that have a much lower environmental impact than conventional energy technologies which are based on fossil fuels primary energy source. Hence, they become as attractive topic for the sustainable energy solutions developers, planners, authors, and researchers and many references and textbooks explored them in detail like in [1] - [4]. Renewable energy serves as a viable substitute for conventional energy sources which heavily depend on fossil fuels (oil, gas, coal), and have a significantly reduced environmental impact that's why it is of great importance for sustainable development consequently the use and consumption of renewable energy worldwide is regularly increasing. [5].

Renewable technologies are considered as clean sources of energy and optimal use of these resources minimize environmental impacts, produce minimum secondary wastes and are sustainable based on current and future economic and social societal needs [6]. Renewable energy refers to a clean, renewable, sustainable, or green kind of energy derived from naturally occurring resources that are neither limited or depletable, in other words that are regenerated at a rate equal to or greater than their use, such as wind, solar, hydro, etc. The phrases '*clean*', '*renewable*', '*sustainable*', or '*green energy*' are often used interchangeably, despite their distinct meanings. Below are concise explanations outlining the distinguishing characteristics of various energy type descriptions.

- Green energy refers to energy derived from natural sources.
- Clean energy refers to energy derived from sources that do not emit air pollutants.

- Renewable energy refers to energy derived from sources that possess the inherent capability for natural replenishment.

Besides, there are 6 main types of sustainable renewable primary energy sources, which are depicted in **Figure 1.2-1** and described in summary below:

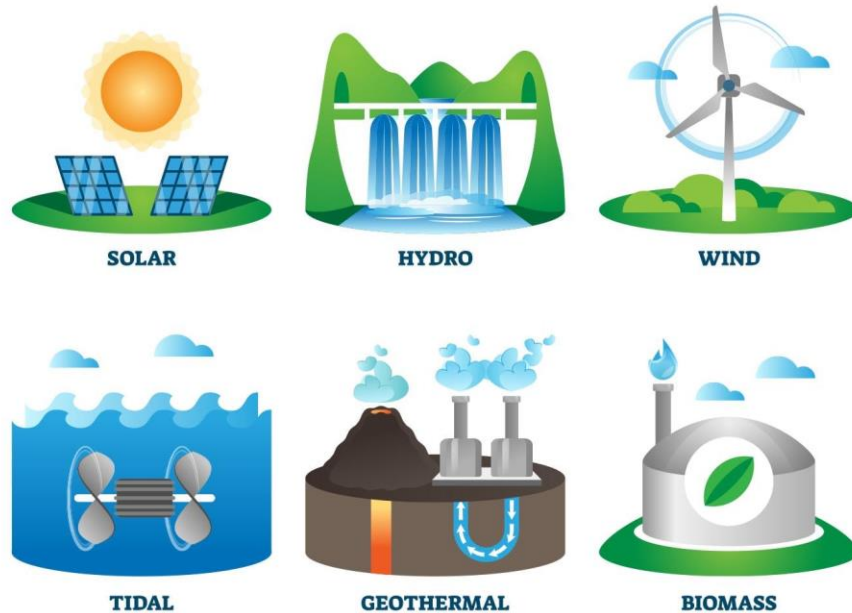


**Figure 1.2-1: Renewable Energy Sources**

#### 1.2.1.1 Solar Energy

Solar energy is a renewable source of power derived from the sun's radiation through harnessing radiant energy emitted by the sun and then transforming it into thermal energy, electrical energy, or heated water. One notable advantage associated with solar energy is the almost limitless availability of sunshine. The availability of solar energy, facilitated by advanced technological capabilities, has the potential to surpass the finite nature of fossil fuel resources, hence rendering the latter obsolete. The use of solar energy in lieu of fossil fuels contributes to the enhancement of public health and environmental circumstances. Solar energy has the potential to eliminate energy expenditures over an extended period of time, while also offering the immediate benefit of reducing energy bills. Numerous governmental entities at the federal, state, and municipal levels provide incentives such as rebates and tax credits to encourage investments in solar energy.



**Figure 1.2-2:** Solar Panels for Photovoltaic (PV) plant.

#### 1.2.1.2 Wind Energy

Wind energy is the natural movement of air streams, caused by the uneven heating of the Earth's surface whereby wind farms harness the kinetic energy of wind currents via the use of turbines, subsequently transforming it into electrical energy. The occurrence often referred to as "wind" may be attributed to the variances in atmospheric temperature, the rotational motion of the Earth, and the geographical characteristics of the planet. The advantages or positive outcomes that can be derived from a particular situation, action, or decision that a wind energy is classified as a sustainable and environmentally friendly energy source due to its inherent characteristic of producing little air pollution compared to other energy sources. Wind energy is characterized by its lack of carbon dioxide emissions and absence of toxic byproducts that might contribute to environmental deterioration or have adverse effects on human health, such as smog, acid rain, and other heat-trapping gases.



**Figure 1.2-3:** Wind Turbine Generators (WTG) in Wind Farm

### 1.2.1.3 *Hydroelectric Energy*

Hydroelectric energy is often associated with the use of dams. Pumped-storage hydropower involves the use of water passing through the turbines of a dam in order to generate energy. Run-of-river hydropower is a method that involves the use of a water channel to direct the flow of water, as opposed to relying on a dam for its generation. The advantages or positive outcomes that can be derived from a particular situation, action, or decision is that hydroelectric power exhibits remarkable versatility, since it may be harnessed via many means, including both huge undertakings such as the Hoover Dam, as well as more modest initiatives like underwater turbines and smaller dams situated along minor rivers and streams. Hydroelectric power is characterized by its lack of pollutant emissions, making it a very ecologically sustainable energy alternative for our natural surroundings.



**Figure 1.2-4:** *Hydroelectric Power Plant Dam*

### 1.2.1.4 *Geothermal energy*

Geothermal refers to the utilization of heat derived from the Earth's internal sources for various. Geothermal heat refers to the thermal energy that is contained under the Earth's crust, resulting from the Earth's creation around 4.5 billion years ago and subsequent radioactive decay processes. Occasionally, substantial quantities of thermal energy are spontaneously released, although in a sudden manner, leading to recognizable phenomena, such as volcanic eruptions and geysers. The thermal energy present in the form of heat may be harnessed and used for the generation of geothermal energy. This can be achieved by using steam derived from the heated water reservoirs located under the Earth's surface. The steam then ascends to the surface and can be effectively employed to drive a turbine, therefore facilitating the production of geothermal

energy. The advantages or positive outcomes that can be derived from a particular situation, action, or decision is that geothermal energy, although less prevalent compared to other forms of renewable energy, has substantial potential for meeting energy demands. Due of its potential for subterranean construction, this technology exhibits little land impact. Geothermal energy is inherently renewable and so does not pose a danger of depletion during the timeframe relevant to human activities.



**Figure 1.2-5: Geo-Thermal Power Plant**

#### **1.2.1.5 Ocean Energy**

Ocean has the capacity to generate two distinct forms of energy, namely thermal and mechanical. Ocean thermal energy is a method of harnessing energy that is contingent upon the presence of warm sea surface temperatures. This energy is generated via the use of various technologies. Ocean thermal energy conversion (OTEC) refers to a technique or technological approach that enables the generation of energy by capitalizing on the thermal gradients existing between the surface waters and the deeper regions of the ocean.

Solar radiation warms the surface water of the ocean. In tropical climates, it is observed that the temperature of surface water tends to be much higher compared to that of deep water. The temperature differential may be used for the purpose of generating power and facilitating the desalination of seawater. Ocean Thermal Energy Conversion (OTEC) systems harness the thermal gradient between different water temperatures, typically with a minimum difference of 20° Celsius or 36° Fahrenheit, in order to drive a turbine and generate electrical energy. The process involves the circulation of heated surface water through an evaporator that contains a working

fluid. The fluid in a vaporized state is used to propel a turbine/generator. The process involves the recondensation of the vaporized fluid, which is achieved by using a condenser that is cooled by the circulation of cold ocean water sourced from the deeper regions of the ocean. Ocean Thermal Energy Conversion (OTEC) systems that use seawater as the primary working fluid have the capability to utilize the condensed water byproduct for the production of desalinated water.

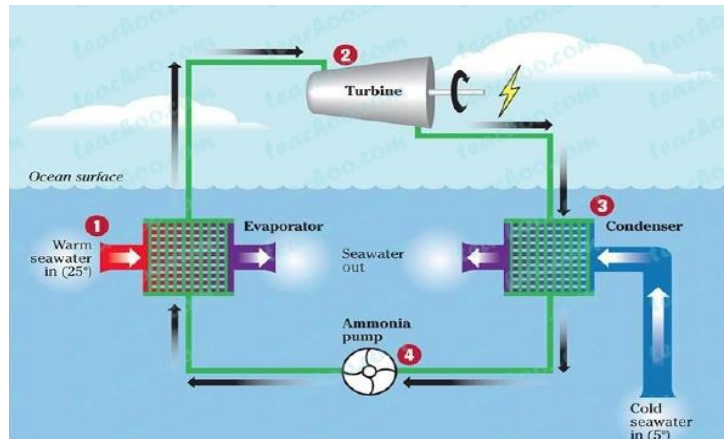


**Figure 1.2-6: Ocean Thermal Energy Plant**

Ocean mechanical energy harnesses the cyclical movements of tides to produce power, a phenomenon resulting from the gravitational forces exerted by the moon and the rotational motion of the Earth. The advantages or positive outcomes that can be derived from a particular situation, action, or decision is that wave energy which exhibits a high degree of predictability, enabling accurate estimation of the energy output. Wave energy has a higher degree of consistency compared to other renewable energy sources, such as solar and wind power, which are subject to fluctuations caused by diverse variables.

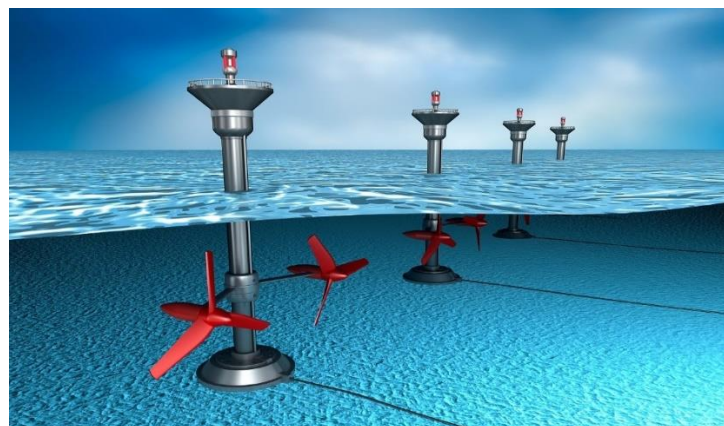


**Figure 1.2-7: Ocean Mechanical Energy Plant**

### 1.2.1.6 Biomass

Biomass is a source of sustainable energy that is obtained from organic matter, known as bioenergy. Biomass refers to the organic material derived from recently deceased plants and creatures. The use of wood as a fuel source in residential fireplaces serves as a well-recognized illustration of biomass. A range of techniques are used for the production of energy from biomass resources. The use of biomass combustion or the capture of methane gas generated via the organic decay process in bodies of water or landfills are potential methods for achieving this objective. The advantages or positive outcomes that can be derived from a particular situation, action, or decision the use of biomass for energy generation results in the emission of carbon dioxide into the atmosphere. However, the subsequent regrowth of plants facilitates the absorption of an equivalent quantity of carbon dioxide, so establishing an equilibrium within the atmospheric composition. Biomass has many applications in both personal and commercial contexts, therefore contributing significantly to several aspects of our everyday routines. The sources of this energy include wood, biofuels such as ethanol, and energy derived from methane obtained by landfill capture or the incineration of municipal trash.



**Figure 1.2-8:** Biomass Power Plant

### 1.2.2 Renewable and Non-Renewable Energy Mix

Even though, countries' aim is transition towards sustainable fossil-free primary energy sources and to reduce reliance on fossil fuel-based primary energy sources, as these sources are major contributors to the significant increase in greenhouse gas emissions, fossil fuels have the highest

share in primary energy consumption. Coal remained the dominant fuel for power generation in 2022, reaching 38% of global electricity production, 10% points ahead of renewables (28% = 15% Hydropower + 8% wind +5% Solar). Coal’s share of power production had been oscillating around 40% since the mid-2000s, before starting to slide in 2015 as renewables began to grow strongly. Renewables’ share of electricity production overcame that of natural gas in 2013 and the gap has kept growing. In 2019, renewables provided almost 28% of global electricity, eight points more than natural gas (20%). The share of nuclear has plateaued around 10% for eight years.

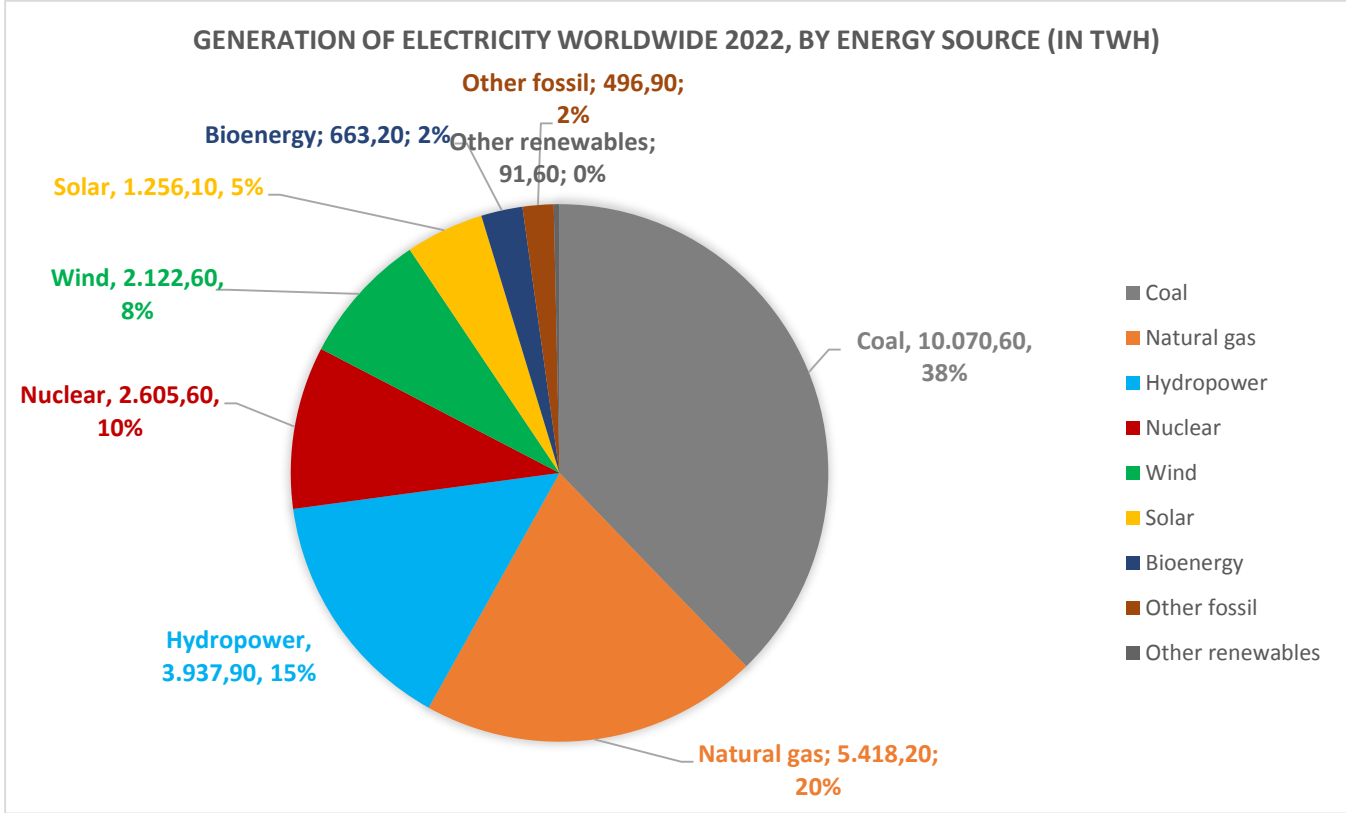
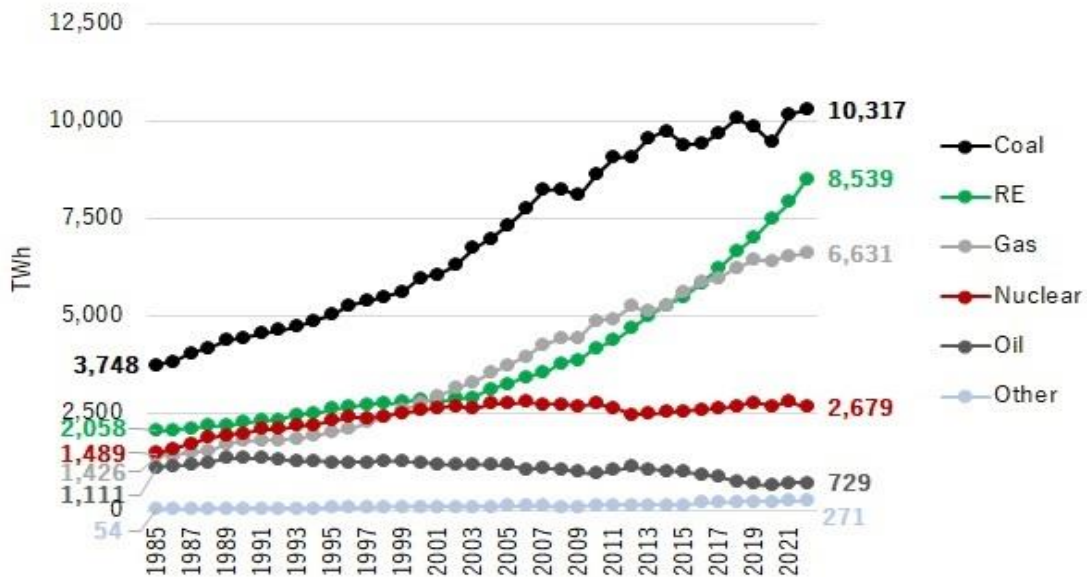


**Figure 1.2-9:** Generation of electricity worldwide 2022, by energy source.

< 1985-2022 >

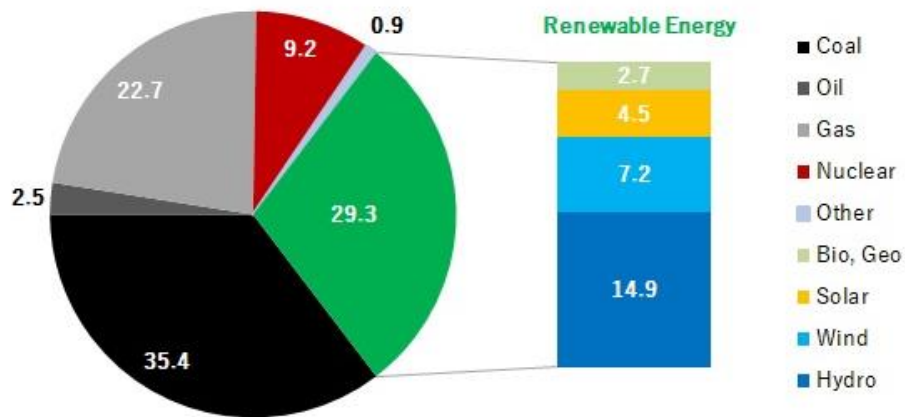
Updated: 27 June 2023



Notes: "RE" (renewable energy) includes hydro, wind, solar, bioenergy and geothermal. "Other" includes pumped hydro, other fossil generation, and statistical differences. Based on "gross" generation.

Source: Energy Institute, Statistical Review of World Energy 2023 (June 2023) (downloaded 27 June 2023).

Total: 29,165 TWh



Notes: "Other" includes pumped hydro, other fossil generation, and statistical differences. Based on "gross" generation.

Source: Energy Institute, Statistical Review of World Energy 2023 (June 2023) (downloaded 27 June 2023).

As per International Renewable Energy Agency (IRENA), Global renewable generation capacity as of year 2022 is **3,372 GW**, see **Figure 1.2-10** below.

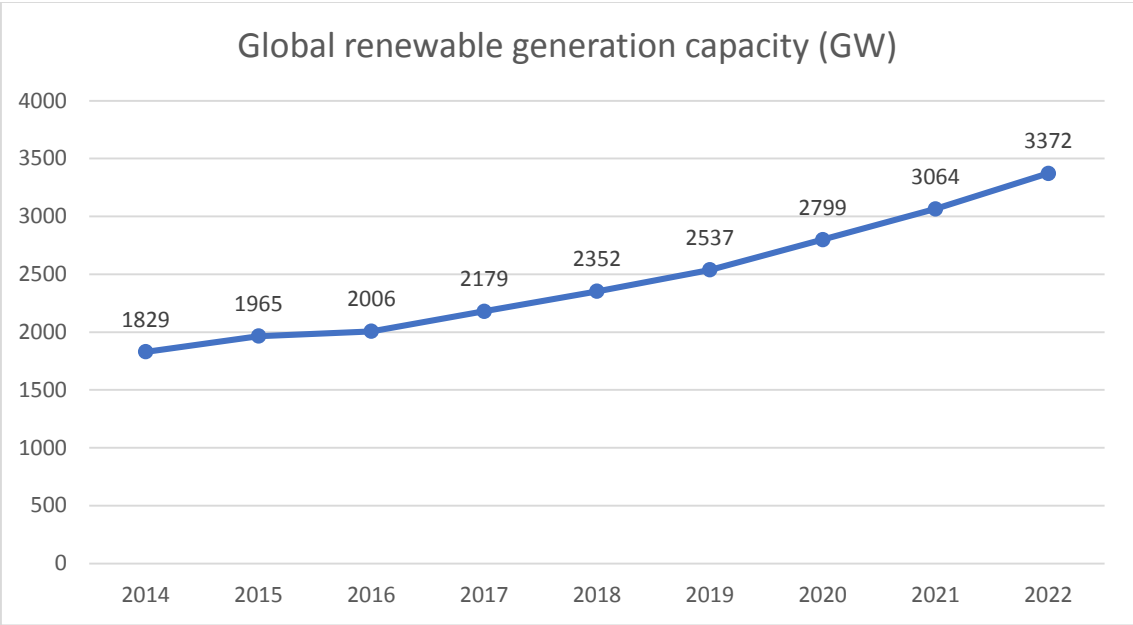


**Figure 1.2-10:** Global renewable generation capacity (GW) from 2014-2022

Below is the distribution of global installed renewable energy capacity by technology in GW for year 2022

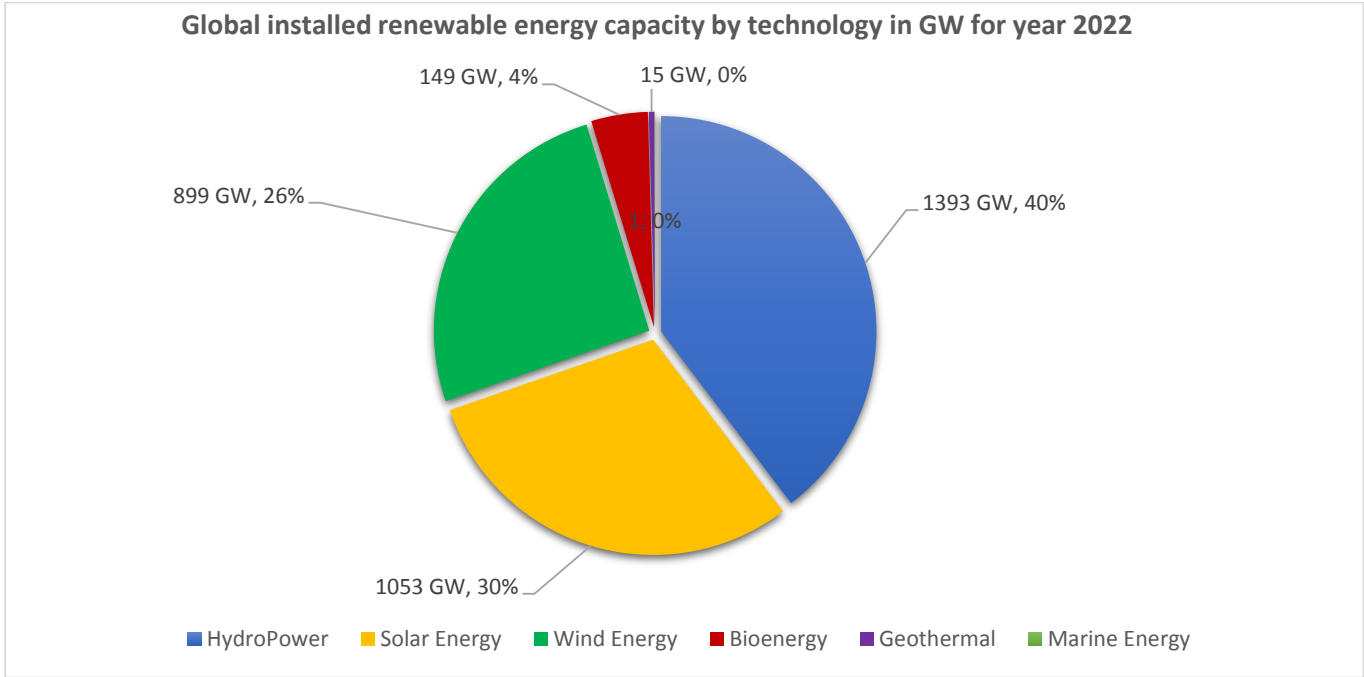


**Figure 1.2-11:** Global installed renewable energy capacity by technology in GW for year 2022

Under existing policies and market conditions, global renewable capacity is forecast to reach **7,300 GW** by 2028. This growth trajectory would see global capacity increase to 2.5 times its current level by 2030, falling short of the triple goal.

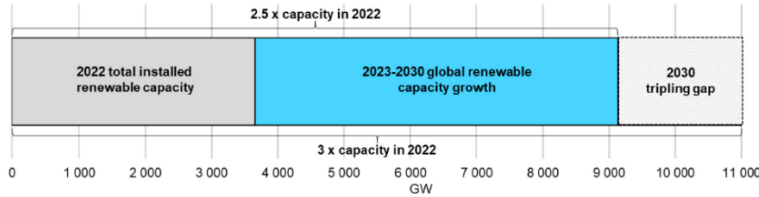


**Figure 1.2-12:** Renewable capacity growth from 2022 to 2030 and the gap to global tripling renewables.

Besides, as per International Energy Agency in their annual report “Renewables 2023, Analysis and forecast to 2028” Global annual renewable capacity additions increased by almost 50% to nearly 510 gigawatts (GW) in 2023, the fastest growth rate in the past two decades.

Over the coming five years, several renewable energy milestones are expected to be achieved:

- In 2024, wind and solar PV together generate more electricity than hydropower.
- In 2025, renewables surpass coal to become the largest source of electricity generation.
- Wind and solar PV each surpass nuclear electricity generation in 2025 and 2026 respectively.
- In 2028, renewable energy sources account for over 42% of global electricity generation, with the share of wind and solar PV doubling to 25%.

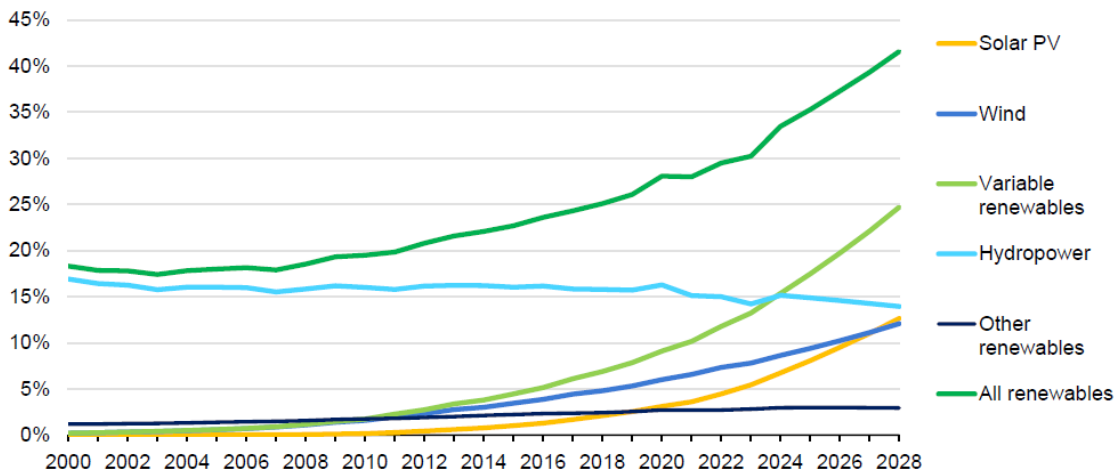


**Figure 1.2-13:** Electricity generation by technology, 2000-2028

### 1.2.3 Carbon Neutrality and CO<sub>2</sub> emissions reduction

To minimize CO<sub>2</sub> emissions and local air pollution, the world has to swiftly transition to low-carbon energy sources such as renewable technologies (solar, wind, hydro, biomass, geothermal, ocean, etc). In the next decades, renewable energy sources will be crucial in the effort to reduce carbon emissions and achieve the carbon neutrality from our energy systems.

Carbon neutrality refers to the goal of reducing net carbon dioxide (CO<sub>2</sub>) emissions to zero by effectively balancing the release of CO<sub>2</sub> with its removal. This is achieved by reaching a state of equilibrium between carbon emissions and carbon absorption in atmospheric carbon sinks. By preventing the accumulation of CO<sub>2</sub> in the atmosphere, carbon neutrality helps mitigate the adverse effects of global warming and limits it to a maximum increase of 1.5°C.

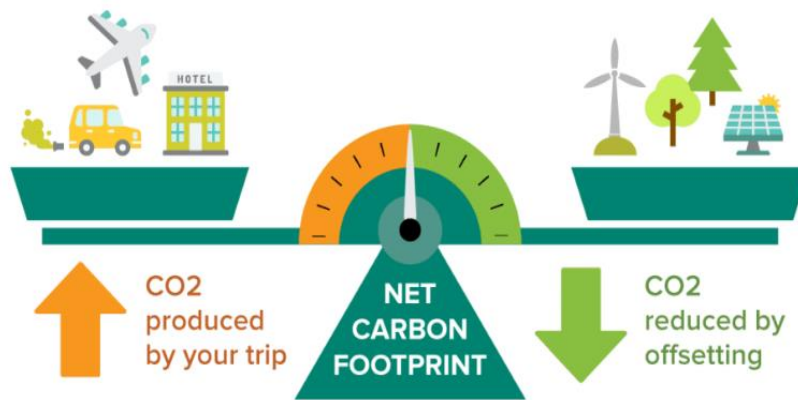
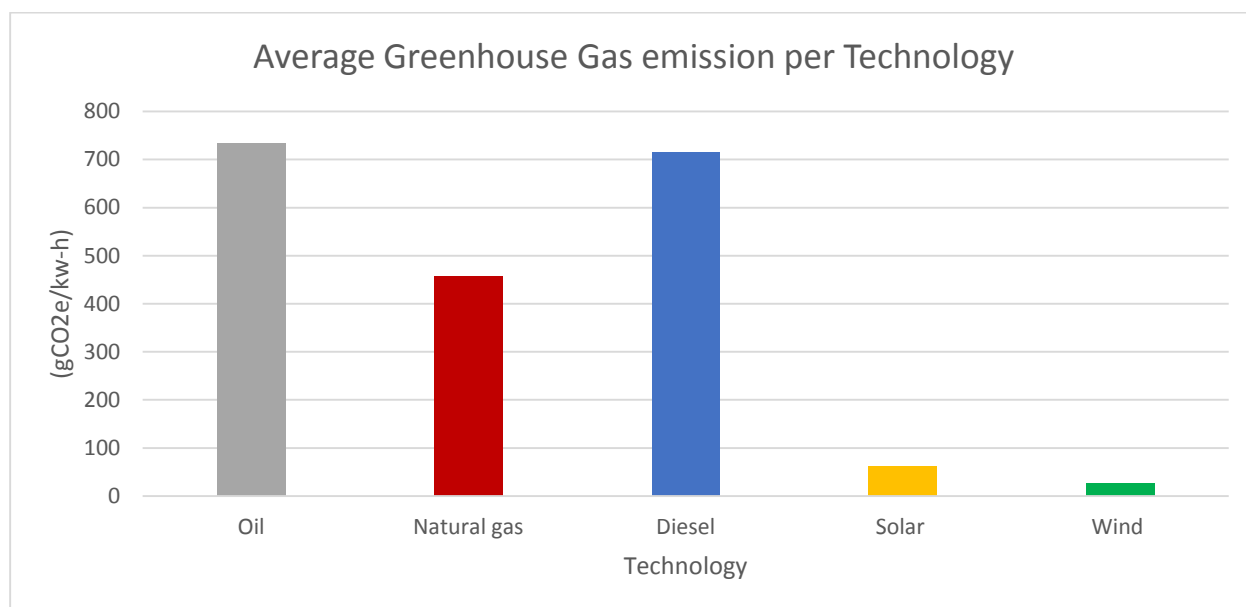


Figure 1.2-14: Carbon Neutrality Concept

As a result of integration of more renewable energy sources, in article that was published on Sep 2016 by Nidal Hussein, his research demonstrated that the solar and wind initiative would lead to a substantial decrease in the anticipated greenhouse gas (GHG) emissions of the country, estimated to range from 1.93 to 3.21 mega tons of CO<sub>2</sub>e per year. Moreover, Nidal in his paper [7] Various kinds of gases are released into the atmosphere, and the environmental effect of each method of power generation per kilowatt-hour generated is assessed by measuring the equivalent quantity of carbon dioxide emissions (expressed in gCO<sub>2</sub>e/kw-h). In this paper, there is a table presenting GHG emissions for the different electricity generation technology and how much of (gCO<sub>2</sub>e/kw-h) from each type of primary energy source will be emitted and the table clearly shows that the highest emissions come from the fossil fuel sources (oil, diesel, natural gases), while the lowest emissions come from the renewable energy sources (solar, wind) and nuclear.



*Figure 1.2-15: Average Greenhouse Gas emission per Technology.*

The introduction of additional energy generation capacity derived from a renewable and environmentally friendly source is expected to lead to a reduction in greenhouse gas (GHG) emissions as compared to the existing state of affairs.

#### **1.2.4 Stability, Security and Interoperability of Renewable EPES**

Power systems are transitioning towards a future that is low in carbon emissions or completely carbon-neutral, with a significant increase in the use of renewable energy sources. The replacement of traditional fossil-fueled synchronous generators in the transmission network with highly dispersed renewable energy production is giving rise to new issues in controlling and maintaining stability in large-scale power networks. Power systems need new analysis and control approaches in order to effectively manage the continuous revolution.

In [8] six prominent specialists were asked to offer keynote talks at the CSEE JPES event. The attending scholars and professionals engaged in comprehensive exchanges and debates about the control and stability of power systems. The presentation focused on the possible changes and problems that arise when power systems have a significant amount of renewable energy production. It also presented and described sophisticated control approaches that may be used

to increase the transient stability of power grids. The experts' main perspectives are summarized as follows.

- 1- In power systems with highly penetration renewable energy production, there will be a need for more coordination between the transmission and distribution networks, as well as greater automation of the power system control.
- 2- There is a need to create new theories and approaches to assess the dependability of power systems in order to handle the variability in demand and the widespread use of renewable energy sources in transmission and distribution networks.
- 3- Power electronic interfaces in renewable energy production offer significant potential to improve power system transient stability by enabling quick active power control. During the planning phase, it is preferable to provide sufficient space for inverters.
- 4- Power systems with strong renewable energy production would see significant changes in their operating characteristics. Power systems must face several operational obstacles, including stability issues.
- 5- Load damping control offers significant potential to enhance the main frequency regulation capabilities of power systems, which is becoming more necessary for future low-carbon or carbon-neutral scenarios.
- 6- It is necessary to create new techniques for controlling energy balance and coordinated control frameworks in order to protect future power systems from the risks to transitory stability. Anticipate the emergence of novel distributed stability control frameworks.

Power system stability analysis [9] and [10] is a method that evaluates system stability, which is the ability of the power system to remain in synchronism and regain its state of equilibrium after being subjected to some kind of disturbance. Stability analysis uses the results of state estimation and contingency analysis to determine the stability margin, which is the difference between the actual operating values and the critical values of system variables, such as angle, frequency (speed), or power, and voltage. Stability analysis helps to monitor the system dynamics, identify the stability problems, and propose stability improvement measures.

As Converter Interfaced Generation (CIGs) become more prevalent in power generation, additional stability issues arise. CIGs have different dynamic behavior than traditional synchronous generators, causing several issues. Authors in [11] introduced two new stability classes, namely “Converter-driven stability” and “Resonance stability”. Adding these two new classes was motivated by the increased use of CIGs see **Figure 1.2-16**:Classification of power system stability with CIG's

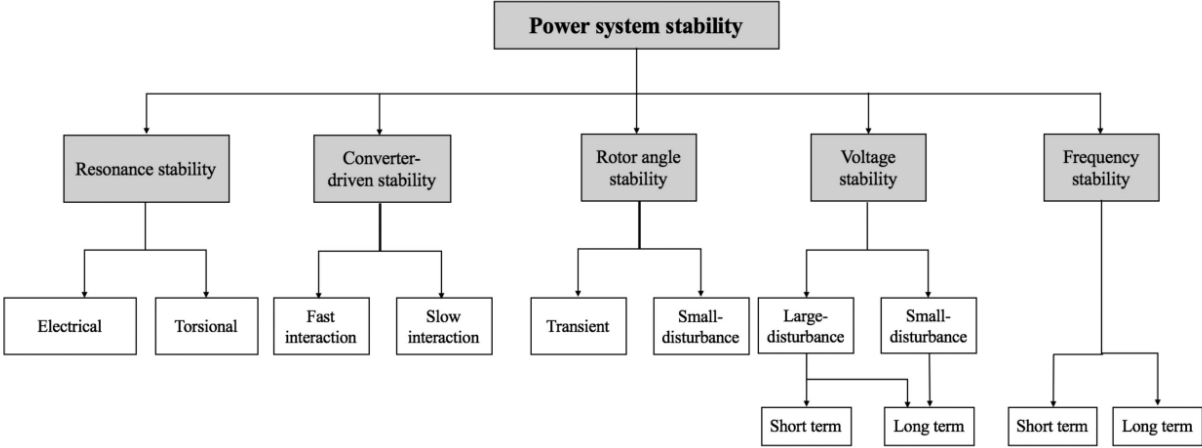


**Figure 1.2-16**:Classification of power system stability with CIG's

The work in [12] discussed that the intelligent renewable energy incorporates highly efficient, bidirectional, intelligent, automated, robust, flexible, cyber-enabled, grid integrated and interconnected sustainable electric and computational intelligence across the whole energy system, spanning from generation to the consumption ends. Although there are many advantages, this approach exposes renewable energy to security risks, providing hackers with a new opportunity to exploit weaknesses in smart renewable energy systems. In addition, wrongdoers specifically focus on smart renewable energy systems because to their dependence on public solutions and Internet-based protocols for monitoring and administration. These assaults have the potential to inflict both physical and financial effects, resulting in the disruption of the electrical system's functions. These factors have physical and economic impacts on the operation of the electrical power and energy system.

Based on above, a security assessment must be conducted in which system security is evaluated, by examining ability of the system to maintain its steady state operating limits and standards

under normal and abnormal conditions. Security assessment uses the results of contingency analysis and state estimation to determine the security margin, which is the difference between the actual and the maximum allowable values of system variables, such as voltage, frequency, or power. Security assessment helps to monitor the system performance, identify the security violations, and propose security enhancement measures.

In order for smart, digital grids to become a reality, it is essential to provide a sufficient degree of interoperability. This means that all devices, components, and applications involved in the smart grid must be able to operate together by sharing data and information.

Moreover, Bedi, G., Venayagamoorthy, G.K., Singh, R., Brooks, R.R. and Wang, K.C., in their article “Review of Internet of Things (IoT) in electric power and energy systems” [13] which was published in 2018 focused on enhancing operational efficiency and reliability of Electric Power and Energy Systems EPESs, promoting energy conservation, facilitating the use of renewable sources for distributed power production, and mitigating carbon emissions.

In contrast to the existing collection of scholarly literature, which often concentrates on a single subsector within the energy business or certain Internet of Things (IoT) technology, this research examines the implementation of IoT in the energy sector comprehensively in Jordan, including energy generation, transmission and distribution (T&D), as well as the best proposed renewable energy basket and their impact on enhancing the energy efficiency and reduction of wastages and their impact on the carbon footprint reduction, and ultimately achieving carbon neutrality in the country. Authors stated that electrical power energy systems are now undergoing a revolution in order to supply clean distributed energy for environmentally responsible economic expansion worldwide, the IoT is at the vanguard of this transition, which is imparting new possibilities. The primary contributions of this review work were: emphasizing the constraints inherent in the present electric power and energy systems, analysing the impact of the Internet of Things (IoT) on the evolution of conventional electric power networks into intelligent power networks, conducting a comprehensive examination of the various applications and services of IoT-based electric power and energy systems, this study aims to conduct a comprehensive survey and

technical evaluation of IoT sensors used in smart home applications, the research emphasized on the economic, societal, and environmental implications of implementing IoT in electric power and energy systems, extensive analysis have been provided on the topics of communications, networking, and security as they pertain to IoT-based electric power and energy systems, the study identified and discussed the limitations associated with deploying IoT in electric power and energy systems, and propose potential solutions to address these challenges. This work concluded that digitizing the electric power ecosystem using IoT helps to better account for distributed energy resources (DER) integration; reduce energy wastage; generate savings; and improve the efficiency, reliability, resiliency, security, and sustainability of the electric power networks. Also, this work ensures that the implementation of Internet of Things (IoT) in the context of Electric Power and Energy Systems (EPEs) is a highly promising domain that fosters novel advancements and exhibits substantial implications on various facets such as the economy, society, and environment. This integration of IoT in EPEs has demonstrated noteworthy outcomes including augmented revenue generation, decreased carbon dioxide (CO<sub>2</sub>) emissions, enhanced convenience in daily life, improved public safety, efficient energy utilization, reduced expenses, and the promotion of a sustainable and healthy living environment. there are also several obstacles that are closely linked to it. These issues include sensing, connection, power management, big data, computing, complexity, and security.

Abdul Salam in his article “Internet of Things in Sustainable Energy Systems” [13] published in 1-1-2020, tried to implement the IoT to get a sustainable energy system whereby he brought some important points such as our planet has abundant renewable energy sources and conventional energy resources, but technological capability and capacity gaps coupled with water-energy needs limit the benefits of these resources to citizens. Through IoT technology solutions and state-of-the-art IoT sensing and communications approaches, sustainable energy-related research and innovation can bring a revolution in this area.

Additionally, authors Ramiz Salama, Sinem Alturjman, and Fadi Al-Turjman published in their article “INTERNET OF THINGS AND AI in SMART GRID APPLICATIONS” [15] brought a nice

terminology whereby they said that the implementation of IoT technology, referred to as the Power Internet of Things (PIoT) in the energy industry, results in enhanced operational effectiveness. They also discussed the future Massive Internet of Things (MIoT) which is considered a fundamental element within the framework of the 5G/6G network infrastructure. They also examined the architectural aspects and associated difficulties pertaining to the next generation of intelligent power grids, specifically focusing on AI-driven smart grids and the incorporation of AI, IoT, and 5G technologies to enhance the functionality of smart grids.

Similarly, authors Ying Wu, Yanpeng Wu, Josep M. Guerrero, and Juan C. Vasquez in their article [16] published in 2021 brought another concept for the IoT applied in energy sector which is Energy Internet (EI) which entails the development of a future energy system that prioritizes sustainability, efficiency, economics, and environmental considerations. This is achieved by the establishment of a flexible physical space that integrates many energy sources, the digitalization of data-driven cyber space, and the creation of a customer-aware social space that encourages interaction.

Almost 80% of the world's ultimate energy comes from fossil fuels, which the energy industry is heavily reliant on today. Because of air pollution and climate change, excessive fossil fuel extraction and burning has a negative effect on the environment, human health, and the economy. However, climate change mitigation and sustainable energy transitions are largely made possible by the integration of renewable energy, energy usage optimization, building a robust, intelligent, and flexible transmission network, and integration of modern intelligent power quality solutions. It is evident from the energy and sustainability discourse that global energy access cannot be achieved without technology adoption. Using technology, robust solutions for reliable, low-cost energy access have been developed. There are innovations that can improve the functionality and efficacy of the existing power infrastructure, assisting enterprises in enhancing client value, minimizing costs, and finally augmenting profit margins. Hence, with the use of advanced sensing and communication technologies, it is possible to address the want for accessible energy within the community, and it is evident that a vast majority of progressive

organizations have now adopted Internet of Things (IoT) techniques which are important to effectively and affordably cater to the fundamental human need of energy services and foster commercial development. There are several uses for contemporary technology like the Internet of Things (IoT) in the energy industry, including energy generation, transmission, and distribution, as well as utilization (consumption). Using IoT may help increase energy efficiency boosting the proportion of renewable energy and minimizing the effects of energy consumption on the environment.

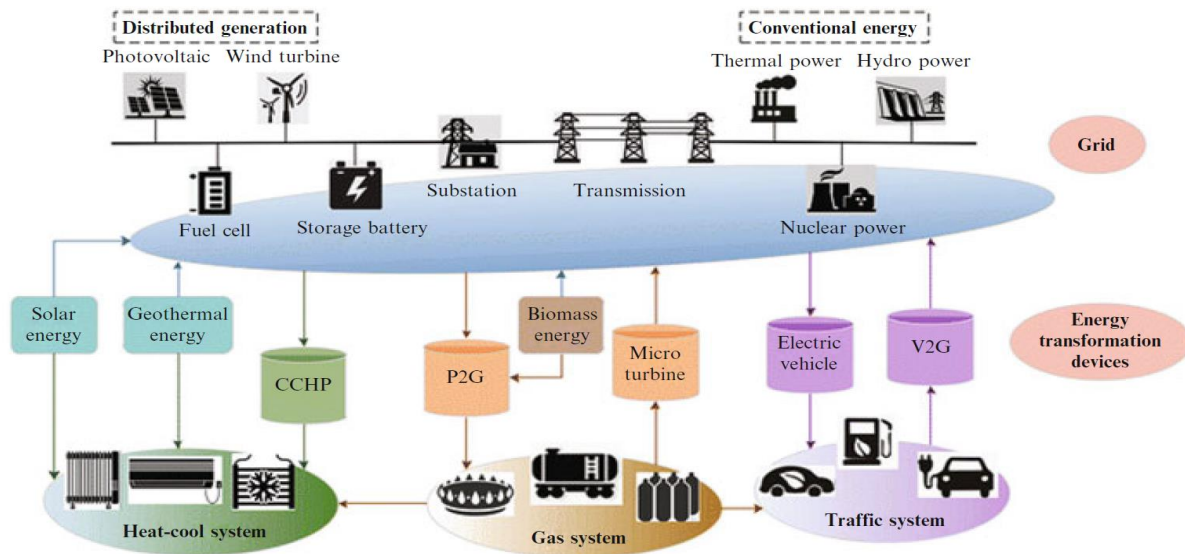


**Figure 1.2-17: IoT in Energy and Industry**

The elements of sustainability Internet of Things (IoT) are delineated as follows:

- Smart meters, net zero energy houses, green energy, and smart industry are all related to the use of advanced technology and sustainable practices in many sectors.
- The generation of energy may be achieved by several means such as natural gas, coal, and renewable sources like solar, wind, and water.
- Transmission, phasor measuring unit, and transmission SCADA (Supervisory Control and Data Acquisition) is a system used for controlling and monitoring many aspects of power distribution, including smart grids, microgrids, and voltage control. It also encompasses

functions like as billing, SAP integration, CRM (Customer Relationship Management), and work order management.

- The entities involved include customers, markets, retail energy providers, wholesale providers, and service providers.
- The areas of focus are plant management, electric cars, and distributed intelligence.
- Management of loading, bulk operations, and power outages.

See Figure 1.2-18: Smart Grid

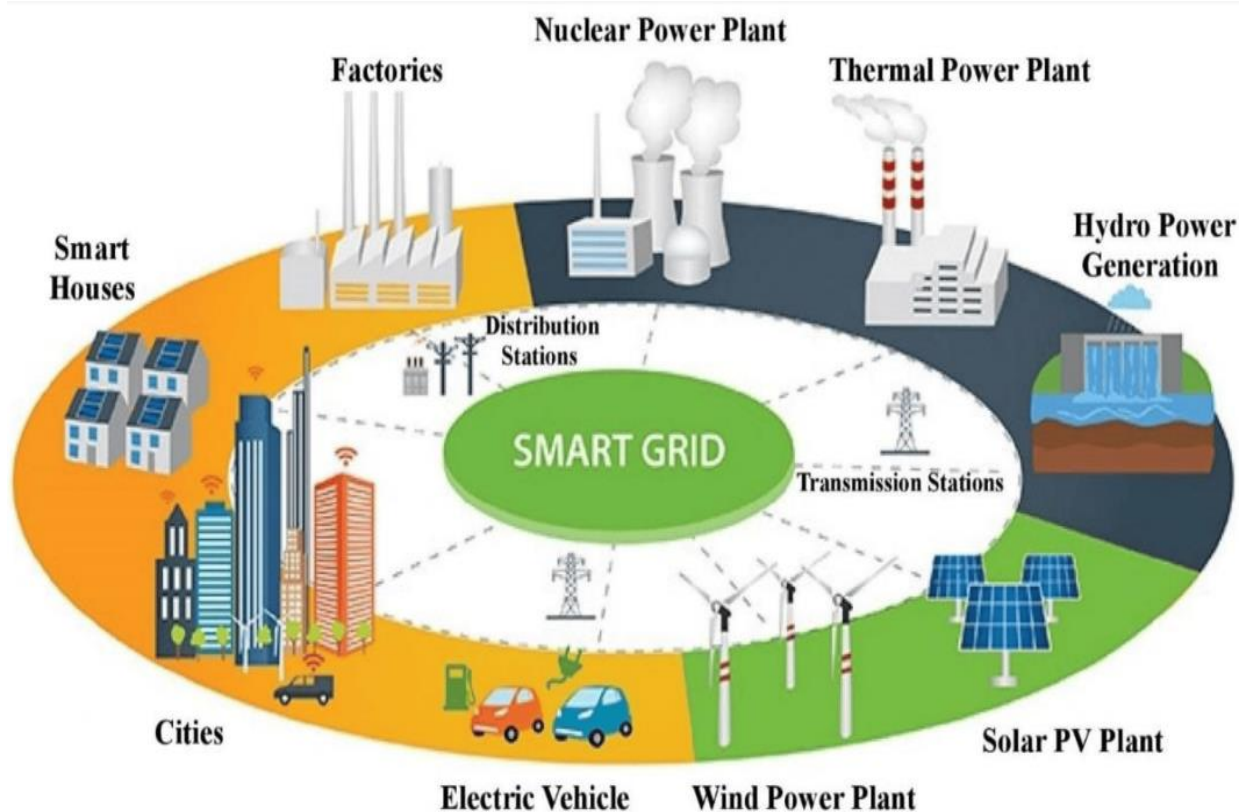


**Figure 1.2-18:** Smart Grid

The Internet of Things (IoT) is a growing technological field that leverages the power of the internet to establish communication among tangible objects, sometimes referred to as "things".

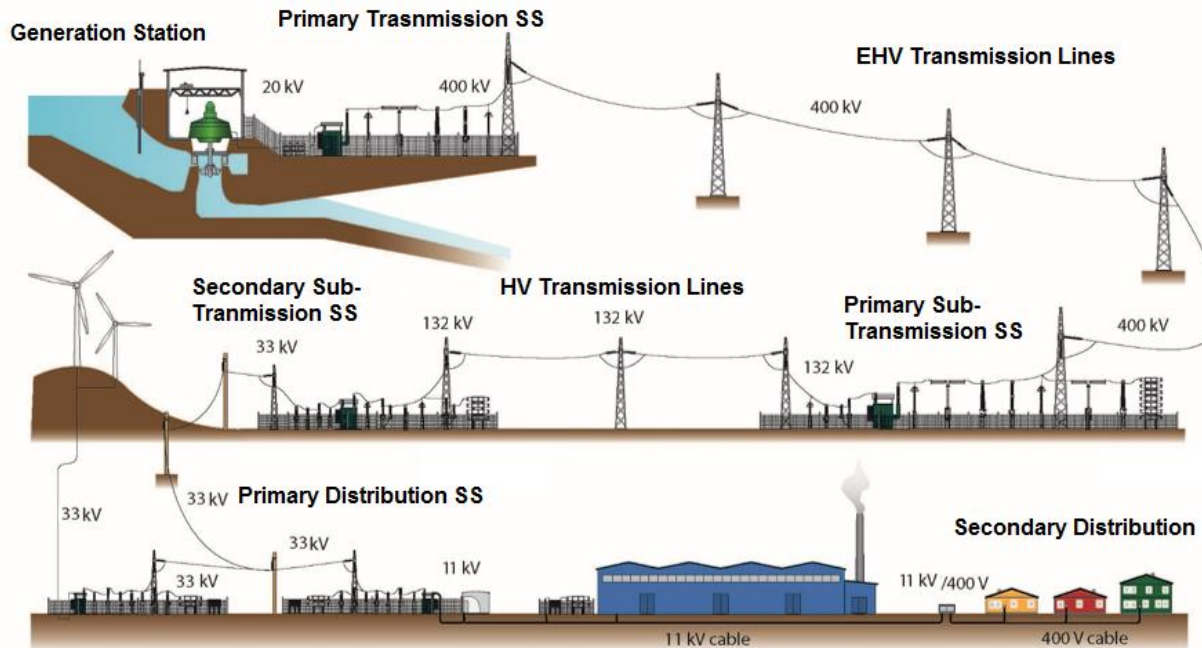


**Figure 1.2-19: Electrical Power System Structure and Energy Streams**

Electric power and energy systems (EPEs) are now undergoing a revolution in order to supply clean distributed energy for sustainable economic development on a worldwide scale. The Internet of Things (IoT) is at the forefront of this transformation, providing capabilities such as real-time monitoring, situational awareness and intelligence, control, cyber security, improved asset visibility, optimal management of distributed generation, elimination of energy waste, and cost savings through the digitization of the electric power ecosystem using IoT and transforming the existing unidirectional EPES's into bidirectional, intelligent, cyber-enabled electrical power networks which are automated, intelligent, adaptable, resilient, and customer-centric systems that facilitate the bidirectional movement of both energy and data.

### 1.2.5 IEEE 9 Bus System- Power System Analysis

In the field of power system analysis and research, the IEEE 9 bus system is a test network that is used to perform several power system studies. It is a simplified model of a power transmission network that is made up of 3 synchronous machines and their generator step-up transformers each 100MVA, nine buses ( one slack bus, 2 PG buses, and seven load buses) that are linked to

one another via overhead transmission lines, and three constant power loads as illustrated in **Figure 1.2-20** .

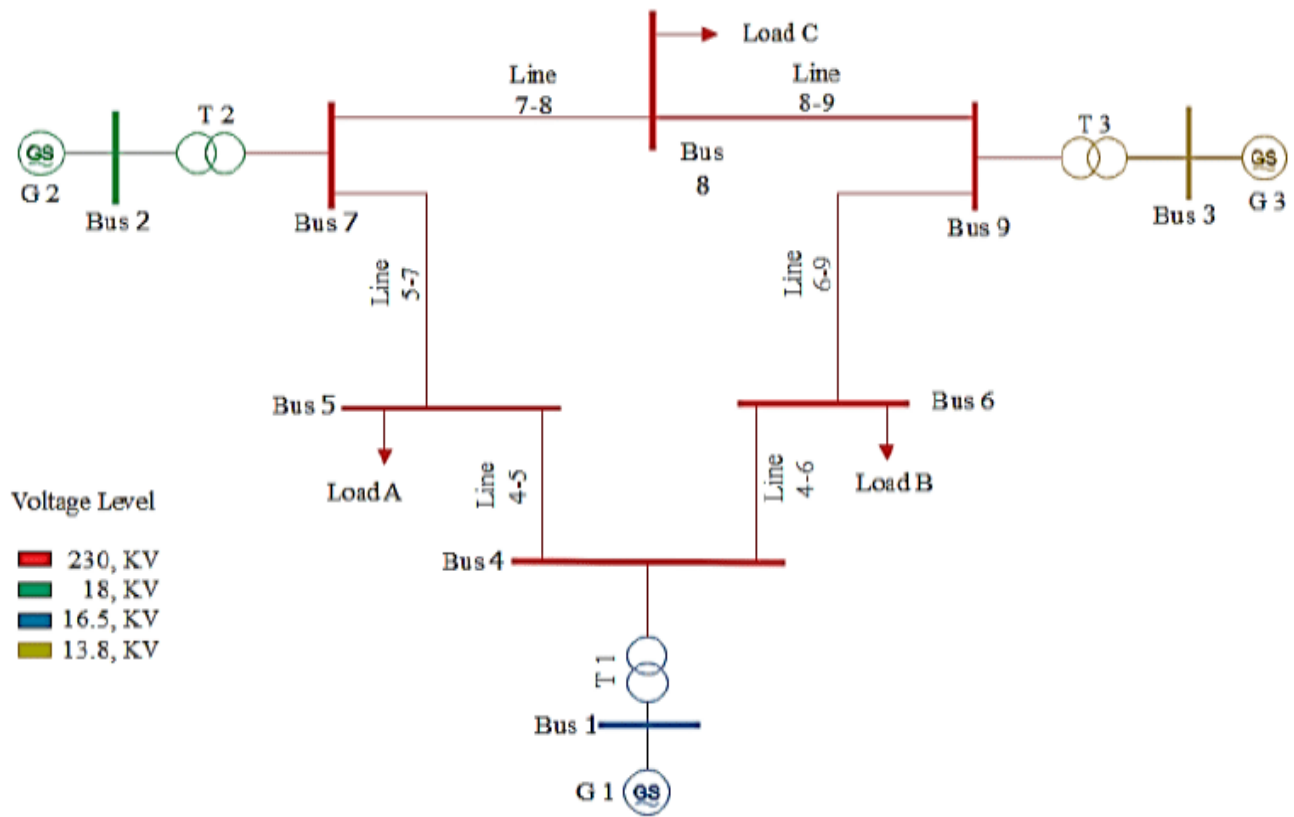


**Figure 1.2-20: IEEE 9-Bus System Single Line Diagram**

The system is often used for the purpose of conducting research on a variety of elements of power systems, including fault detection and classification, the effect of integrating renewable energy sources, system stability analysis, optimization of power flow, and load flow analysis. For the purpose of developing and testing new algorithms, methodologies, and technologies for power system analysis and control, researchers utilize the IEEE 9 bus system as a benchmark.

In this context, by the analysis conducted by Nallagalva, S.K., Kirar, M.K. and Agnihotri in [17], the IEEE 9 bus system has been modeled using ETAP software, and then a “large disturbance rotor angle stability” or “Transient stability” analysis for various faults on the test system was examined to check about the fast fault clearing and load shed to bring back the system to the stability. The rate of change of frequency ( $df/dt$ ) is used as indicator of the transient stability of the system

because it gives an indicator of overload as it is directly related to the real power and this ( $df/dt$ ) used to calculate the amount of load to be shed by adaptive load shedding and measures taken to maintain stability and frequency of the system. Also, in this paper conventional under frequency load shedding (ULFS) and adaptive load shedding methods are studied through IEEE 9 bus test system simulated on ETAP.

In the article that was published by authors [18] in 2015, Contingency analysis was used to calculate parameters violations of the Western System Coordinating Council 3 Machine, 9 Bus test system. Furthermore, the maximum loading parameter was calculated, and contingency status was done using Power System Analysis Toolbox (PSAT) toolbox in MATLAB by Step by Step removing each transmission line and simulate for the Power Flow and Continuation Power Flow for finding maximum loading parameter for each transmission line. PSAT is an open-source MATLAB toolbox used in simulation and analysis of small and medium sized electric power system.

Of equal importance, authors in [19] in their article “Short Circuit Analysis & Over current Relaying Coordination of IEEE 9-Bus System” that was published in 2018, short circuit analysis and protection relaying coordination of IEEE 9-Bus system was analyzed and designing of overcurrent relaying scheme to operate the relay quickly and disconnect the faulty section from healthy section. Load flow has been performed to obtain the electrical power systems steady-state voltages at fundamental frequency, besides, several three phase faults, and unbalanced types of faults such as L-G, L-L and L-L-G have been placed individually on Bus-7 and results have been recorded also. Furthermore, short circuit analysis of system is also included in this paper to determine the positive (+ve), negative (-ve) and zero (0) -sequence impedance of faults, Then main task of their work was on the sequence of operation of the protection relays connected on bus-7 and controlling on the relay having minimal effect should run first and so on.

Of equal importance of the work done in [17], authors in [20] has performed a transient stability of IEEE-9 bus system that is comprised of three generators. The software utilized to conduct the simulations was Power World Simulator (PWS). A load flow analysis is performed to ascertain the pre-fault conditions. In the second step, fault analysis was conducted to determine the stability of the system by examining post-fault conditions such as load switching and rapid fault clearance time. In order to analyze the fluctuations of a system under various fault conditions, the frequency and rotor angle of the system were utilized to compare and contrast the Euler and Runge methods for transient stability analysis.

S. Al-Jufout in [21]-[27] presented an overview for several electrical power systems and how to mathematically model them using differential equations, also he has presented both transient and steady-state conditions, fault simulation, load ignorance, immittance matrix partition by hypothetical capacitor. The same methodology of building a system differential equation will be used for the case study IEEE-9 Bus system.

#### **1.2.6 Grid Impact of Renewable Energy Sources integrated to IEEE 9-Bus system.**

If utility-scale solar PV and wind farms do not use a specific control system for grid support, they will simply be disconnected when there is a grid disruption, with catastrophic consequences when the solar/wind farm is enormous. Hence Several studies have been undertaken to address the varied wind and solar power generation. Therefore, in light of [28] Kumar, A. K., M. P. Selvan, and K. Rajapandiyam who have studied and analysed the impact of the large scale penetration ( from 0% to 100% penetration with 10% step of penetration ) of 243MW solar PV power into grid by simulating the IEEE 9-bus system into ETAP and grid integrate a solar PV plant at one of the system buses ( Bus No.5, then Bus No.6, then Bus No.8), they have also investigated the impact of large penetration of solar PV systems on steady state performance ( voltage profile at the buses, active and reactive power losses for the lines ) as well as transient stability for several types of

disturbances ( bus fault, load rejection, and transmission line faults), and the relative rotor angle for generator G2 has been plotted for several penetrations. Two major observations were taken on the PV plant model; first the output from the solar inverter should be at the LV voltage level not MV (11kV) besides, second for such a large-scale PV plant, the PV arrays and their associated solar inverters with their associated LV/MV step up transformer and ring main unit should form PV plant building block.

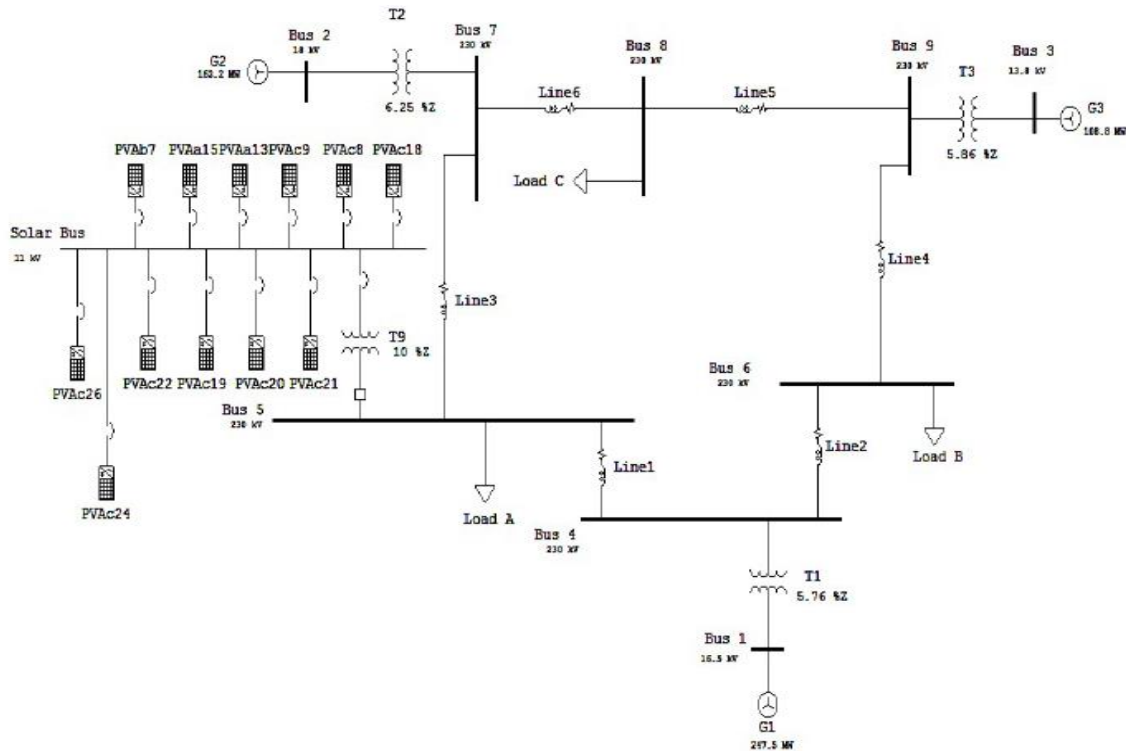


**Figure 1.2-21:** Solar PV 243MW integrated at IEEE 9 Bus system.

Moreover, the work done in [29] examined the stability of a power network when a wind turbine is integrated. The study utilized an open-source software to simulate the system. The OpenModelica program was used to mimic the IEEE 9 bus system. The system's steady-state stability analysis was conducted both with and without the use of Automatic Voltage Regulator (AVR) and Speed Governor (GOV) controllers. An analysis was conducted to examine the long-term effects of incorporating a wind turbine. Furthermore, an analysis was conducted on the correlation between the power output of the wind turbine and the voltage.

In article [30] that was published in 2020, a 100MW wind turbine generator (WTG) is integrated at the point of connections (PoC) which is Bus No.4 of IEEE 9 Bus system and transient stability is assessed through the a three-phase fault inserted at bus 8 at a period of 1 second in ETAP and there was no fault clearance, and it was found that at time  $t= 3$  sec, the generators come to a halted position losing all three generators synchronism

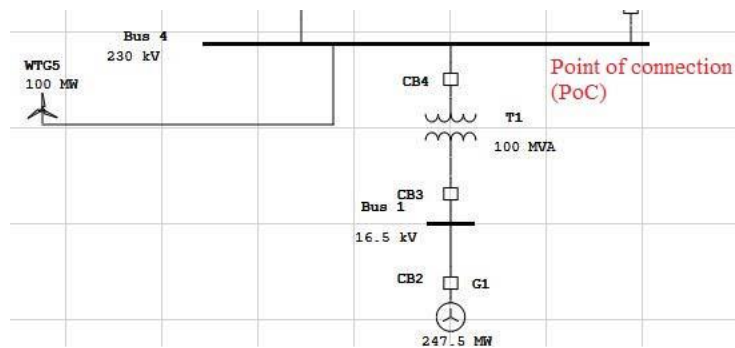


**Figure 1.2-22:** 100MW WF grid integrated with Bus No.4 of IEEE 9 bus system

First, the transient study of the generators is conducted without the presence of WTG (wind turbine generator) and no-fault clearing. The swing angle of the generator reaches its limit at  $\delta = \pm 180^\circ$  and then stops after a time period of 3 seconds. The increase in the maximum and minimum values of current may be attributed to the significant flow of current inside the generators. G1, a slack bus generator, supplies reactive power to the system, but is unable to maintain stable voltage levels across the buses. The wind turbine generator (WTG) maintains its connection to the power grid at the point of connection (PoC) even when a three-phase fault occurs at bus 8. During this fault, the WTG continues to produce a steady supply of reactive power to the power grid. Once the problem is resolved at 1.114s, the terminal voltage increases to 98% with minor fluctuations caused by the lingering transient currents inside the Point of Connection (PoC). The active power output stabilizes at 2.0 per unit (pu), which meets the parameters set after the fault operation, namely a 10% decrease from the pre-fault level. WTG effectively provided reactive power injection to provide voltage stability throughout the Low Voltage Ride Through (LVRT) procedure, especially for three-phase breakdowns. However, the wind farm model is no accurate,

where authors should have built a complete 100MW wind farm from a collection of WTG's connected in parallel

Similarly, a grid integrated 60MW wind farm was studied according to the work done in [2920] by Ramlochun, B., Vaithilingam, C.A., Alsakati, A.A. and Alnasseir, J., in their article that was published in 2021, a Wind Turbine (WT) is simulated using two distinct kinds of induction generators (IGs), the Doubly-Fed Induction Generator (DFIG) and the Squirrel-Cage Induction Generator (SCIG). These models are then applied to the IEEE 9-Bus system in order to evaluate its transient stability. The DC1A excitation system was used for both Synchronous Generators (SGs) and Power System Stabilizers (PSS). The transmission line 7-5 was discovered to have a very high peak value of the relative power angle, measuring roughly 130 degrees. Regarding the settling time, the settling time was 20.69 seconds without the Power System Stabilizer (PSS) and decreased to 6.23 seconds with the PSS. The system used a wind farm with a rated capacity of 60 MW. The combination of wind turbine (WT) combined with doubly-fed induction generator (DFIG) has the lowest peak value of 127 degrees at Bus locations 4 and 5. In contrast, for squirrel cage induction generator (SCIG), the peak value is somewhat higher at Bus 5, measuring 136 degrees. Therefore, it may be promoted as the ideal destination. Furthermore, this is attributed to the occurrence of a three-phase fault at transmission line 7-5, which is situated at a considerable distance from Buses 4 and 5. Ultimately, the integration of the Wind Turbine (WT) with Doubly Fed Induction Generator (DFIG) results in a decreased peak value of relative power angle compared to the Squirrel Cage Induction Generator (SCIG). However, the converse is true for the settling time. Authors in this paper only considered type 1 and 3 of WTG types while they could have considered the other 2 types; type 2 WRIG and Type 4 PMSG as well.

The work [32] Alsakati, A.A., Vaithilingam, C.A. and Alnasseir, J., 2021. Transient stability assessment of IEEE 9-bus system integrated wind farm. In MATEC Web of Conferences (Vol. 335, p. 02006). EDP Sciences. The use of wind energy in electrical networks may affect load flow and power system stability. The transient stability of the IEEE 9-Bus system with DFIG is examined in this study. Wind farm penetration levels are also examined. With 5% wind energy penetration,

the synchronous generator's maximum power angle is  $129^\circ$ , identical to the current technology. More wind turbines with 15% wind farm penetration raise the power angle to  $140^\circ$ . The system loses stability after 25% wind energy penetration. The findings show that substantial wind energy penetration destabilizes the network. Wind farm site also influences transient stability. This study will evaluate power system integrated DFIG stability. Thus, this research will promote wind energy in power systems over traditional power plants and assess the stability of alternative energy sources in the grid to improve grid dependability.

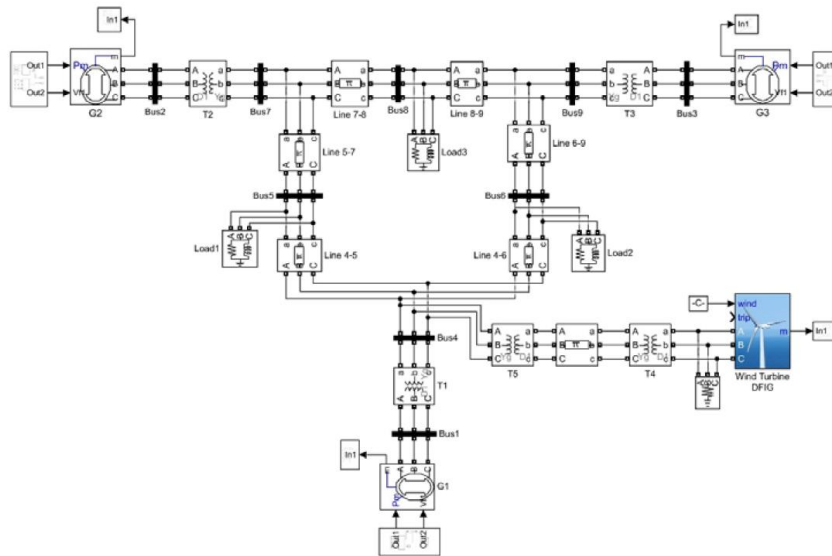


**Figure 1.2-23:** MATLAB Model for Gradual Penetration of WF to IEEE 9 Bus system.

### 1.2.7 The Need of Power Quality Solutions for High Renewable Penetration and Grid Code Compliance

It is important to recognize that there is a strong relationship between voltage levels in a power system and reactive power. Shunt compensation can be static and dynamic. Static shunt compensation, which includes the usage of shunt reactors and shunt capacitors, is used to provide voltage stability under steady-state conditions. While Dynamic shunt compensation, including SVCs, STATCOMs, synchronous condensers, and Enhanced STATCOMs, is used to provide voltage stability in both steady-state and dynamic situations. Additionally, it offers benefits such as enhancing system strength and inertia.

Large penetration of renewables in today's electric power grids will affect and change system characteristics; reduce the system strength (short circuit power) , reduce system inertia, shift harmonic resonances to lower frequencies and slow down voltage recovery after system faults. This will require Synchronous Condenser (SC) to be installed in many future grids and new type of devices (or control features) which enhance inertia, dynamic performance and improves stability of the grid. One of these devices is the Hybrid SC, a combination of SC and STATCOM technologies.

Dynamic shunt compensation devices are widely used in power systems, including many applications:

- close to power generating source: To meet the requirements of the grid code and optimize the amount of electricity produced.
- Transmission and distribution systems: To guarantee optimal functionality-
- close to industrial loads: To comply with grid regulations and maximize operational efficiency.

Based on all above, reactive power compensation in a grid connected PV plants/wind farms is an attractive topic for the researchers. A. Kalyuzhny, B. Reshef, G.Yehuda, G.David, P. Koulbekov, and T. Day in [33] showed how to design a capacitor bank in parallel to photovoltaic power plant in order to avoid any unacceptable voltage fluctuations due to the randomness in the output power of PV systems due to irregular solar radiation, The solution includes operation of PV with predetermined leading power factor and addition of a capacitor bank in parallel to PV plant to compensate the reactive power absorbed by the PV inverters, but they did not consider the reactive power losses in the Solar Transformers and MV cables in designing the capacitor bank.

The researchers Mr.Piyush M.Desai and Mr.S.S.Khule in [3334] studied the integration of solar PV with STATCOM for reactive power compensation as well as the active power sharing with grid. Control technique called  $I\cos\Phi$  algorithm has been implemented for the control of the STATCOM.

In [35] Al-Adim, Loai, Mehrdad Aliasgari, Mohammad Mozumdar, and Saleh Al Jufout. In their paper published in 2022 "Reducing the number of central inverters of a photovoltaic plant using medium-voltage capacitor banks." They have investigated the effect of Medium-Voltage (MV) capacitor banks on the number of central inverters of grid-connected Photovoltaic (PV) plants whereby 3 cases of a 200 MW grid connected Photo Voltic plant were investigated. These cases are with and without increasing the size or the number of the central inverters; while the third case is without increasing the number or the size of the central inverters but with adding Medium Voltage mechanically switched capacitor banks to meet the base reactive power load and comply with grid code requirements. The resistances of the system components were not ignored which led to more accurate calculations. Grid impact study (power flow, voltage drop calculation, fault analysis and transient stability calculations) have been performed using ETAP software for all possible cases: with and without increasing the number/size of the inverters and with capacitor banks. The active-reactive power capability curves have been discussed for the above cases as well.

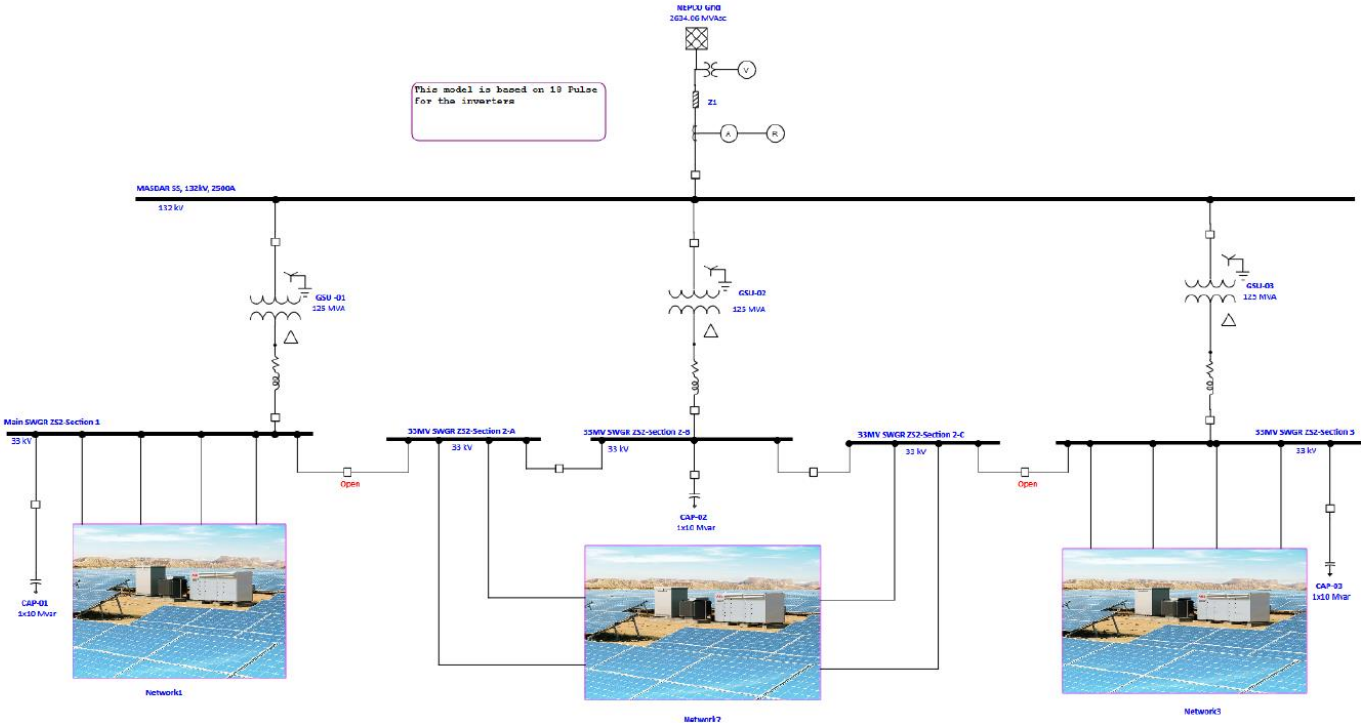


Figure 1.2-24: ETAP Model for 200MW PV Plant

After this, <sup>36</sup> same authors above, in [36] they have continued the year after and investigated the Harmonics Analysis of the same 200MW Photovoltaic Plant with a Reduced Number of Solar Central Inverters. In 2023 IEEE Green Energy and Smart Systems Conference (IGESSC) (pp. 1-4). IEEE. This analysis has been conducted for the photovoltaic plant with 120 and 138 number of central inverters without capacitor banks and with 120 number central inverters with 30 MVAR capacitor banks. Calculations have been performed using ETAP software for all three cases. Three harmonics models have been introduced for each solar inverter and these models are typical IEEE-6 pulse, IEEE-12 pulse, and IEEE-18 pulse models. And the total harmonic distribution (THD) for the voltage and current have been recorded for each of the 3 cases above, Results show that the lowest THD values for the voltage and the current are in the case of 120 solar inverters with 30MVAR capacitor banks. The harmonics analysis using the IEEE-18 pulse model confirms that the proposed solution in [35] is the best solution to comply with the transmission grid code.

The work above was based on mechanically switched capacitor, while there are other more dynamic shunt compensators solutions as presented in the work done by authors Stiger, A., Rivas, R.A. and Halonen, M. in their article [37] whereby they have examined the difficulties associated with modern power systems that have a significant integration of renewable energy sources. It emphasizes the significance of short circuit contribution and inertia. Another feature of the article is to emphasize the influence on power quality solution (such as SVC, STATCOM, HVDC, MSC, harmonic filters, etc.) when there are changes in system characteristics like harmonic resonances and Short Circuit Ratio (SCR). Authors have concluded that installing Synchronous Condensers may address the problem of decreasing fault levels on the system. These devices increase the grid's inertia, dynamic performance, and stability. The paper discussed a hybrid configuration as well that combines STATCOM and Synchronous Condenser technologies to maximize power system performance by using the best characteristics of each technology.

Additionally, the work in [38] have discussed dynamic reactive power compensation where Flexible AC Transmission (FACTS) devices are required because switching of reactive elements by means of circuit breakers is too slow. Besides, several factors will change the system's operation

in a dependable manner: extensive incorporation of renewable energy generation, expansion of the steel and automotive industries in certain areas, deployment of smart grid technology, introduction of a grid code, and enactment of a new electric industry law that enables private sector involvement in electricity generation and sales. Their paper covered some aspects of the new generation of dynamic shunt compensators and the system aspects to be considered for making the new challenges to the operation of the Mexican system less problematic and invisible to the electricity consumers.

A traditional Static Var Compensator (SVC) usually consists of many branches of fixed and switched reactive power banks (**Figure 1.2-25**), with at least one branch being regulated by thyristors. The selection of branch sizes and their configuration mostly relies on the operational and performance criteria for the SVC. An SVC typically consists of a minimum of two branches, which may comprise Thyristor Controlled Reactor (TCR), Thyristor Switched Reactor (TSR), Thyristor Switched Capacitor (TSC), Fixed Harmonic Filter Capacitor (FC), Mechanically Switched Capacitor bank (MSC), and/or Reactor bank (MSR).

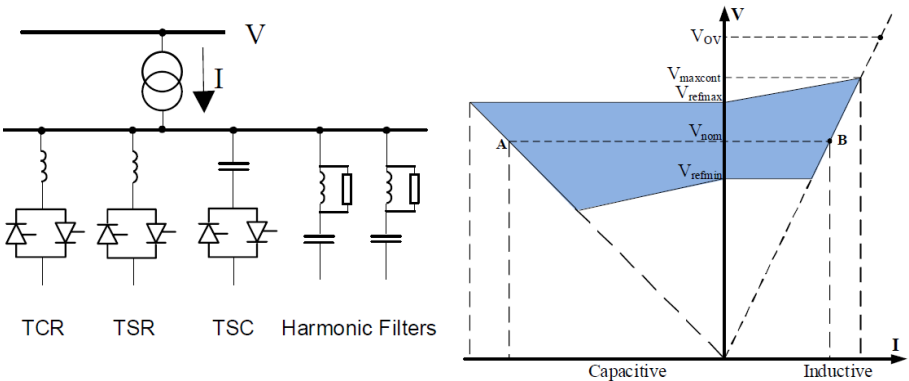


**Figure 1.2-25:** Typical SVC configuration and V/I diagram.

Static Synchronous Compensators (STATCOM) have gained competitiveness against traditional SVCs due to advancements in converter valve technology, lower losses, and a more compact physical footprint, as well as the development of semiconductor devices with turnoff capability (e.g., IGBT and IGCT). As illustrated in **Figure 1.2-26**, the Voltage-Source Converter (VSC) is the central component of a conventional STATCOM. Throughout its operational range, the VSC possesses symmetrical characteristics. From the high-voltage (HV) perspective, the VSC functions as a controllable current source that can be modified in an independent manner from the system voltage, facilitated by the closed-loop control.

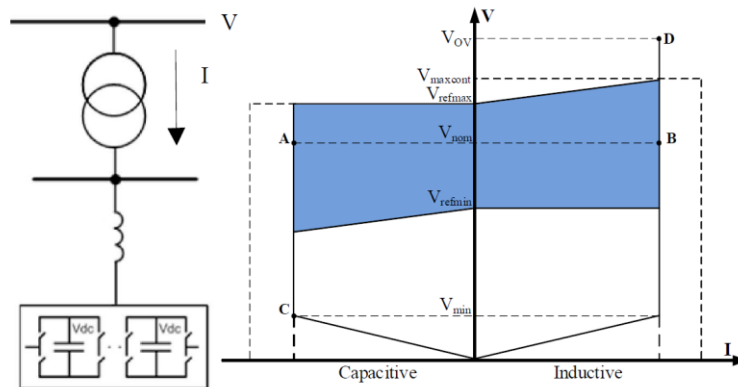


**Figure 1.2-26:** Typical STATCOM configuration and V/I diagram.

Modern STATCOMs with Grid Forming control not only provide assistance after contingencies, but also during real breakdowns. Their purpose is to avoid voltage collapses, often known as "blackouts," as well as harmful over-voltages.

Gómez-González, J. et. al. in [39] discussed Reactive power management in photovoltaic installations connected to low-voltage grids to avoid active power curtailment, where Photovoltaic (PV) inverters are traditionally designed to operate with unity power factors. In order to use reactive power capabilities of smart inverters, in this work two strategies are analyzed: limiting the amount of active power delivered or oversizing the inverter. The first of these options implies a reduction in the PV production and therefore, it would lead to reduced earnings for the PV system owner. On the other hand, oversizing the PV inverter allows having reactive power compensation capabilities, while delivering full power output from its PV field.

Researchers S. Balasubramanyan and M. Sasirekha in [40] proposed an optimized reactive power compensation method and evaluates the effect of reactive power compensation on grid interactive PV system with cascaded converter modules.

### 1.2.8 Challenges in Transition to 100% Renewable Energy IEEE 9-bus system

Several recent developments have changed the features and characteristics of the transmission power grid, which will have an impact on the future functioning of the system and the power market globally, such driving points are:

- 1- The retirement of traditional and conventional power generation stations (like thermal power plants with heavy rotating mass) aiming to gradually phase out fossil fuels and nuclear energy while mitigating sectoral impacts. However, some sectors may still require the use of fossil fuels and nuclear energy with carbon removal strategies due to technical challenges in decarbonizing and electrifying them.
- 2- Integration of more renewable energy sources, particularly solar/wind power plants cause a major shift in the generating mix, and this is being significantly enhanced by political support and cost reductions in renewable energy systems, resulting in a substantial increase in the use of renewable energy in distribution and transmission networks.
- 3- Industrial expansion in some areas, particularly in the steel and automotive sectors. These industrial loads have a considerable impact on the power quality at the grid connection, particularly in terms of power factor, voltage flicker, and harmonic levels. While the use of capacitor banks and filters may somewhat decrease harmonic levels and enhance power factor, it is advisable to use dynamic shunt compensation in industries with rapidly changing loads and when the plant is coupled to less robust systems.
- 4- The new electric industry legislation and new laws enables private sector participation in power generation and sales via joint ventures with state-owned entities. However, the system remains under TSO supervision.

Based on above, modern power systems are encountering difficulties and several challenges due to rapid fluctuations and changes in generation mix which has a negative impact on the dynamic stability of the power system. Renewable energy sources are replacing conventional generators, resulting in a substantial increase in the use of renewable energy in distribution and transmission networks.

- 1- When integrating renewable energy sources such as wind and solar power plants into power grids, it is important to ensure that system stability and reliability are not compromised, especially when there are no rotating masses involved. Hence, Transmission System Operators should establish and update their Grid Codes standards, particularly concerning reactive power, voltage and frequency regulation, and fault ride-through capabilities. Wind farms and solar PV plants of significant size often need the use of dynamic reactive power compensation in order to adhere to the regulations outlined in the Grid Code.
  
- 2- Solar and Wind farms are unlike thermal power plant are asynchronously integrated into the grid through inverters, hence they do not contribute to grid inertia, and will massively cause a reduction in system inertia, which will increase the steepness of the rate of change of frequency (ROCOF)

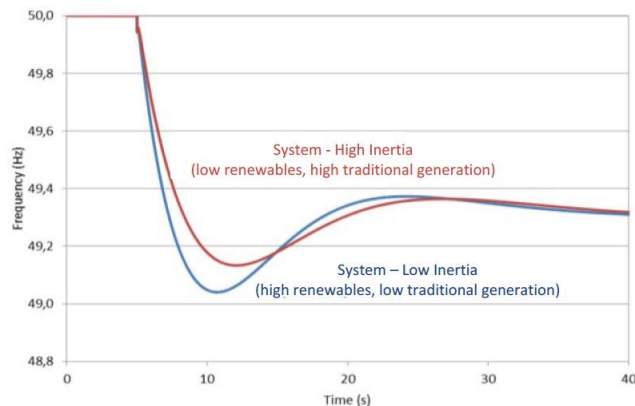


**Figure 1.2-27:** Change in ROCOF with Inertia change.

- 3- The significant incorporation of renewable energy sources into the power grids of today will result in a modification of system characteristics. This includes a decrease in system strength (fault level) MVA<sub>sc</sub>.

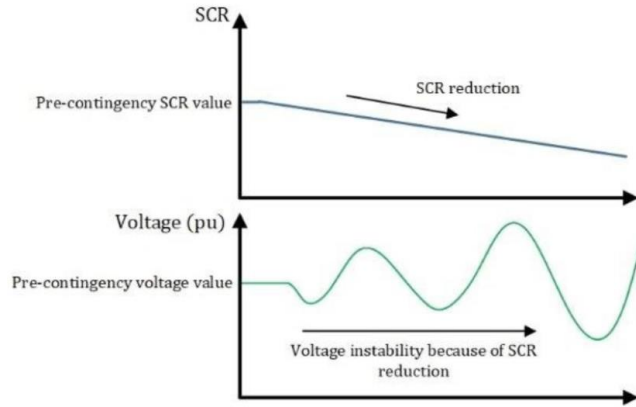


**Figure 1.2-28:** Effect of SCR on Voltage Stability

- 4- A shift in harmonic resonances to lower frequencies, and a slowdown in voltage recovery after system breakdowns.

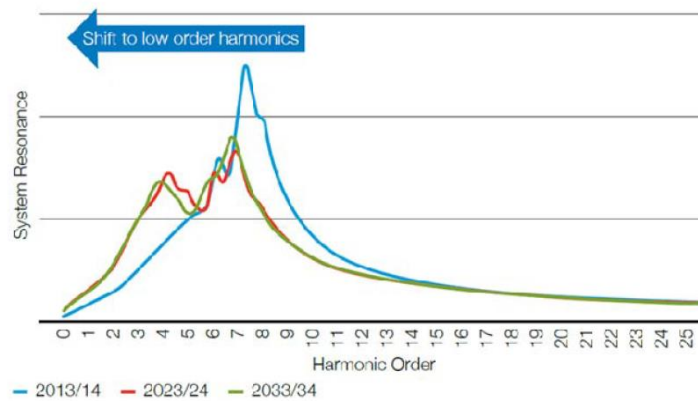


**Figure 1.2-29:** Shift of harmonic resonances to lower order of harmonics.

Net-zero energy system scenarios aim to limit global temperatures to 1.5°C by combining renewables, residual fossil and nuclear energy, and carbon removal strategies. This aligns with the Paris Agreement goals. In order to successfully restrict the global temperature, rise to 1.5°C. Over pre-industrial levels by the end of the century, it is imperative for the world to reach a state where the amount of greenhouse gas emissions being released into the atmosphere is completely offset by the amount being removed by 2050.

In accordance with the conclusions drawn from the Intergovernmental Panel on Climate Change's (IPCC) 1.5°C report of 2018 and the recent 6th Assessment Report, or AR6 (2023), the eradication

of all anthropogenic greenhouse gas emissions by 2050, or earlier, will be necessary to limit climate change to no more than 1.5°C above pre-industrial levels by the conclusion of this century (IPCC, 2019, 2023). To limit global warming to 1.5°C, the AR6 report additionally urges "rapid and substantial, and in the majority of cases, immediate reductions in greenhouse gas emissions across all sectors within this decade." Considering the fact that energy-related activities account for the majority of anthropogenic emissions, achieving these emission reductions will require the implementation of renewable energy technologies (solar, wind, hydro, geothermal, bioenergy, ocean, etc.) in conjunction with substantially increased energy efficiency measures (IPCC, 2023). These measures will additionally yield societal advantages, including enhanced local air quality. Furthermore, when accompanied by appropriate policies, they will promote energy accessibility and equity, bolster local economies, and facilitate progress.

As per [48], The significance of modelling scenarios that aim to utilize 100% renewable energy has increased over the last decade, according to a seminal article by Khalili and Breyer (2022). Numerous national, regional, and international 100% renewable energy scenario studies were assessed in their publications and found to have increasing credibility and dependability as data and methodologies advance.

IRENA in [41] examined three energy transformation scenarios that are committed to attaining 100% renewable energy by the year 2050. The following scenarios have been incorporated into The University of Technology Sydney's "Achieving the Paris Climate Goals" report: The University of Technology Lahti University of Technology (LUT) Global 100% RE Scenario [42]; Stanford University's 100% Wind-Water-Solar (WWS) Scenario [43], which encompasses 145 countries; and The University of Technology Sydney (UTS) 1.5°C Scenario [44]. The aforementioned scenarios were selected on the grounds that they are worldwide in reach, employ 100% renewable energy, and extend their analysis to the year 2050.

Table 1.2-1: Overview of IRENA 100% RE scenarios analyzed.

Energy System Model	Global 100% RE	100% Wind, Water, Solar (WWS)	Net Zero Emissions																																								
<b>Institution</b>	Lappeenranta-Lahti University of Technology-LUT (2021)	Stanford (2022)	International Energy Agency-IEA (2021)																																								
<b>Target(s)</b>	100% renewable energy system by 2050	80% WWS by 2030. 100% WWS by 2050 for 145 countries	Net zero by 2050																																								
<b>Renewable energy share in total energy supply (TES) by 2050</b>	100%	100%	67% in total energy supply (88% in electricity generation)																																								
<b>Energy sources included in 2050</b>	Solar photovoltaic (PV), concentrated solar power (CSP), wind, hydropower, geothermal and bioenergy	Generation: wind, solar PV, CSP, geothermal, hydro and ocean energy. Heat: solar thermal, geothermal heat	TES: solar, bioenergy, wind, hydropower, geothermal, other renewables, nuclear, natural gas, oil and coal.																																								
<b>2050 share of electricity (electrification level)</b>	89% (total primary energy demand)	Efficiency measures result in total energy demand decreasing by 56.4%, so that remaining energy is nearly all (~99.1%) electricity: 85% higher than 2018 actual levels (total installed capacity)	49% of electricity in total final energy consumption																																								
<b>Cumulative investment needed to 2050</b>	USD 72 trillion, noting net energetic yield per invested unit of capital in renewable electricity solutions far exceeds the one in upstream fossil fuels	Around USD 61.5 trillion Upfront costs are recovered through energy sales, covering WWS electricity; heat and green hydrogen generation; storage for electricity, heating, cooling and green hydrogen; district heating heat pumps; all- distance transmission; and distribution	Annual average capital invested is indicated for 2030-2040-2050: - 40-50 trillion USD, annual investments of 4-5 trillion per year by 2030. - Almost USD 5 trillion annually by 2040. - USD 4.5 trillion annually by 2050																																								
<ul style="list-style-type: none"> <li>● Solar</li> <li>● Solar PV</li> <li>● Solar CSP</li> <li>● Hydropower</li> <li>● Ocean energy</li> <li>● Bioenergy</li> <li>● Geothermal</li> <li>● Wind energy</li> <li>● Natural gas</li> <li>● Nuclear</li> <li>● Oil</li> <li>● Fossil</li> <li>● Coal</li> <li>● Other renewables</li> <li>● Other non-renewables</li> </ul>	<p><b>GLOBAL 100% RE (LUT)</b></p> <table border="1"> <caption>Global 100% RE (LUT) Composition</caption> <thead> <tr> <th>Source</th> <th>Percentage</th> </tr> </thead> <tbody> <tr> <td>Solar PV</td> <td>69%</td> </tr> <tr> <td>Wind energy</td> <td>18%</td> </tr> <tr> <td>Bioenergy</td> <td>6%</td> </tr> <tr> <td>Ocean energy</td> <td>3%</td> </tr> <tr> <td>Geothermal</td> <td>2%</td> </tr> <tr> <td>Other renewables</td> <td>2%</td> </tr> </tbody> </table>	Source	Percentage	Solar PV	69%	Wind energy	18%	Bioenergy	6%	Ocean energy	3%	Geothermal	2%	Other renewables	2%	<p><b>WWS (STANFORD)</b></p> <table border="1"> <caption>WWS (Stanford) Composition</caption> <thead> <tr> <th>Source</th> <th>Percentage</th> </tr> </thead> <tbody> <tr> <td>Solar PV</td> <td>45%</td> </tr> <tr> <td>Wind energy</td> <td>46%</td> </tr> <tr> <td>Ocean energy</td> <td>5%</td> </tr> <tr> <td>Geothermal</td> <td>3%</td> </tr> <tr> <td>Other renewables</td> <td>1%</td> </tr> </tbody> </table>	Source	Percentage	Solar PV	45%	Wind energy	46%	Ocean energy	5%	Geothermal	3%	Other renewables	1%	<p><b>NZE (IEA)</b></p> <table border="1"> <caption>Net Zero Emissions (IEA) Composition</caption> <thead> <tr> <th>Source</th> <th>Percentage</th> </tr> </thead> <tbody> <tr> <td>Solar PV</td> <td>20%</td> </tr> <tr> <td>Wind energy</td> <td>16%</td> </tr> <tr> <td>Bioenergy</td> <td>19%</td> </tr> <tr> <td>Ocean energy</td> <td>6%</td> </tr> <tr> <td>Geothermal</td> <td>11%</td> </tr> <tr> <td>Other renewables</td> <td>11%</td> </tr> </tbody> </table>	Source	Percentage	Solar PV	20%	Wind energy	16%	Bioenergy	19%	Ocean energy	6%	Geothermal	11%	Other renewables	11%
Source	Percentage																																										
Solar PV	69%																																										
Wind energy	18%																																										
Bioenergy	6%																																										
Ocean energy	3%																																										
Geothermal	2%																																										
Other renewables	2%																																										
Source	Percentage																																										
Solar PV	45%																																										
Wind energy	46%																																										
Ocean energy	5%																																										
Geothermal	3%																																										
Other renewables	1%																																										
Source	Percentage																																										
Solar PV	20%																																										
Wind energy	16%																																										
Bioenergy	19%																																										
Ocean energy	6%																																										
Geothermal	11%																																										
Other renewables	11%																																										

### 1.2.9 Research Gap

Unlike previous research's, which frequently focuses on partial integration of one or more renewable plant into IEEE 9 bus system, and address some of the integration complexities and challenges for such integrations, this thesis does examine the following:

- 1- Performed a detailed and comprehensive power system analysis for the traditional and conventional IEEE 9 bus system with 0% penetration of renewables (1<sup>st</sup> scenario), not like previous studies which performed a partial analysis.
- 2- The IEEE 9 bus system was partially and gradually integrated with renewable that replaces the conventional synchronous machines (scenarios: 2<sup>nd</sup> to 7<sup>th</sup>), and full transition and integration of 100% renewable in the 8<sup>th</sup> scenarios which replaces the conventional synchronous machines with an equivalent renewable energy source (solar/wind/hydro) with similar capacities.
- 3- Integrates an actual renewable solar PV plant /wind farm, starting from the IRR building blocks till the PoCC, not like previous studies that unrealistically integrate a large-scale wind farm with only one WTG.
- 4- Examines the challenges and solutions for the 100% renewable transitions in terms of stability, security, and interoperability on the IEEE 9 bus system.
- 5- Performs a time domain load flow for one complete month, and then conducted a financial analysis addressing the total levelized cost of energy (LCOE), levelized revenue of energy (LROE), and the profit for each scenario for one complete month.
- 6- Conducts a life cycle assessment and CO<sub>2</sub> emissions estimations for each scenario.
- 7- Implements the data analysis techniques and tools to analyse and visualize the data.

# 1.3 Chapter Three: Methodology and Philosophy

## 1.3.1 Introduction

This chapter is one of the most important ones in the research since it focuses on the tactics and procedures that were used in order to carry out the research. As an additional point of interest, the subsequent chapter has presented reasons that are supported by secondary sources to finish the research, analysis, and system investigation.

## 1.3.2 Research Process

A research method refers to a *systematic approach used to gather and analyse data*. The research methodology may include the use of a particular tool, such as a **self-completion questionnaire** or a **scheduled interview schedule**. Alternatively, it may entail participant observation, when the researcher actively listens to and observes individuals. A research methodology refers to a systematic strategy used in the research process, which encompasses a collection of methodologies utilized to gather and analyse data.

The research onion framework developed by Saunders has been used to guide the inquiry process, including several phases. The justification for adopting Saunders's onion lies in its ability to provide a methodical and organized approach to research, facilitating the collection of necessary data by progressing through many levels. See below **Figure 1.3-1**

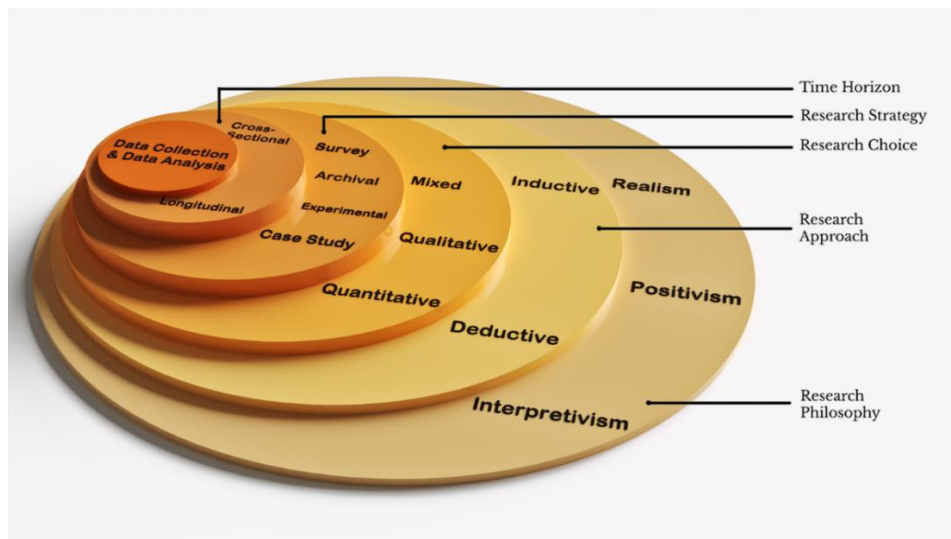


**Figure 1.3-1:** Saunders Research Onion

### 1.3.3 Research Philosophy

The research philosophy includes assumptions, knowledge, and the nature of the investigation. It is concerned with a certain method of acquiring information. All researchers may have various assumptions about the nature of truth and knowledge, and philosophy is the means by which these assumptions may be understood. It is a notion about the optimum method for gathering, analysing, and using data about a phenomenon.

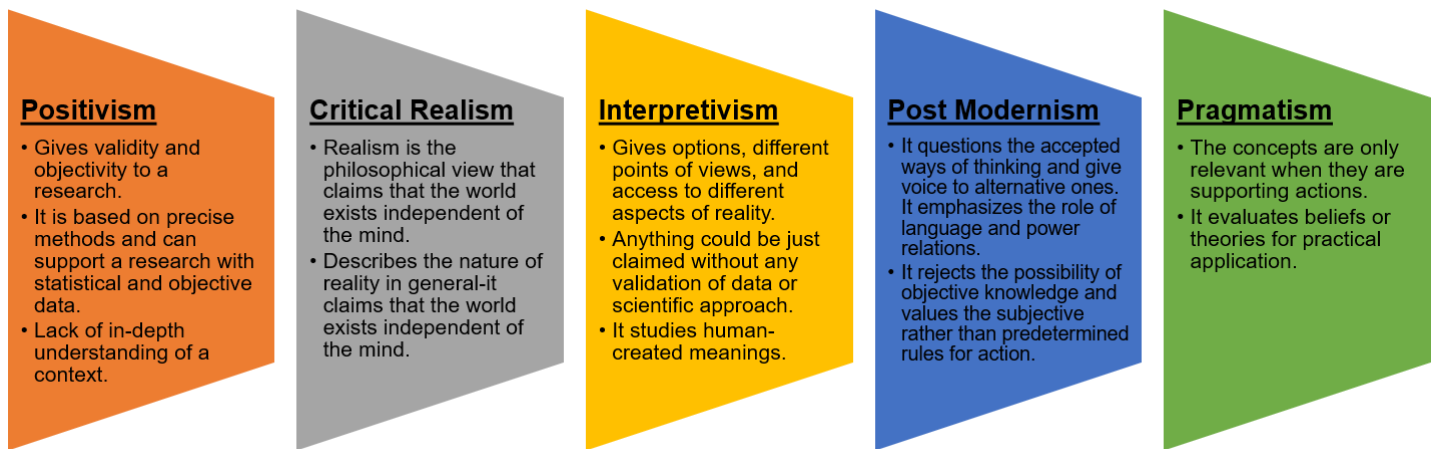


**Figure 1.3-2: Research Philosophies**

The chosen philosophy in this research is **post modernism** that challenges conventional modes of thought and amplifies alternative perspectives. It highlights the significance of language and the dynamics of power relations. It denies the existence of objective knowledge and prioritizes the subjective above fixed norms for analysing the challenges of transition to sustainable 100% renewable electrical power and energy system along with power quality solutions on stability, security, and interoperability of the IEEE 9 bus system. This approach relies on rigorous methodologies and has the capacity to bolster research endeavours via the utilization of statistical and objective data. Insufficient comprehension of a given situation. This approach is deemed essential for a thorough understanding of the subject matter. By adopting this methodology, in reflection of above, Kumar, A. K., M. P. Selvan, and K. Rajapandiyam who have studied and analysed the impact of the large scale penetration 243MW solar PV power into grid by simulating the IEEE 9-bus system into ETAP and grid integrate a solar PV plant at one

of the system buses ( Bus No.5, then Bus No.6, then Bus No.8), they have investigated the impact of large penetration of solar PV systems on steady state performance ( voltage profile at the buses, active and reactive power losses for the lines ) , and it was found that the voltage profile is affected by the fault locations.

By adopting post modernism methodology, Alsakati, A.A., Vaithilingam, C.A. and Alnasseir, J., 2021. concluded that with 5% wind energy penetration, the synchronous generator's maximum power angle is 129°, identical to the current technology. More wind turbines with 15% wind farm penetration raise the power angle to 140°. The system loses stability after 25% wind energy penetration. The findings show that substantial wind energy penetration destabilizes the network.

#### 1.3.4 Research approach.

Scientific research may follow one of two paths: inductive or deductive, see **Figure 1.3-3**. A researcher's purpose in inductive research is to infer theoretical notions and patterns from observable facts. However, researcher's purpose in deductive research is to examine ideas and patterns known from theory using fresh empirical evidence.



*Figure 1.3-3: Research Approach Paths*

The chosen approach in this research is **deductive** in which the goal is to test concepts and patterns known from theory using new empirical data. work done by authors Stiger, A., Rivas, R.A. and Halonen, M. in their article [37] whereby they have examined the difficulties associated with modern power systems that have a significant integration of renewable energy sources. It emphasizes the significance of short circuit contribution and inertia. Another feature of the article is to emphasize the influence on power quality solution (such as SVC, STATCOM, HVDC, MSC, harmonic filters, etc.) when there are changes in system characteristics like harmonic resonances and Short Circuit Ratio (SCR). Authors have concluded that installing Synchronous Condensers may address the problem of decreasing fault levels on the system.

Also, as per [35] the analysis conducted for the photovoltaic plant with 120 and 138 number of central inverters without capacitor banks and with 120 number central inverters with 30 MVAR capacitor banks. Calculations have been performed using ETAP software for all three cases. Three harmonics models have been introduced for each solar inverter and these models are typical IEEE-6 pulse, IEEE-12 pulse, and IEEE-18 pulse models. And the total harmonic distribution (THD) for the voltage and current have been recorded for each of the 3 cases above, Results show that the lowest THD values for the voltage and the current are in the case of 120 solar inverters with 30MVAR capacitor banks. Methodological Choice

Upon conducting ETAP simulation for each of the 8 scenarios below, all the system parameters will be recorded making it a **quantitative study**. Thus, the chosen method is **mono-quantitative** utilizing the case study which is IEEE 9 Bus system. In which explanation through numbers is used, it is an objective, deductive reasoning, predefined variables and measurement, data collection before analysis, and cause and effect relationships.

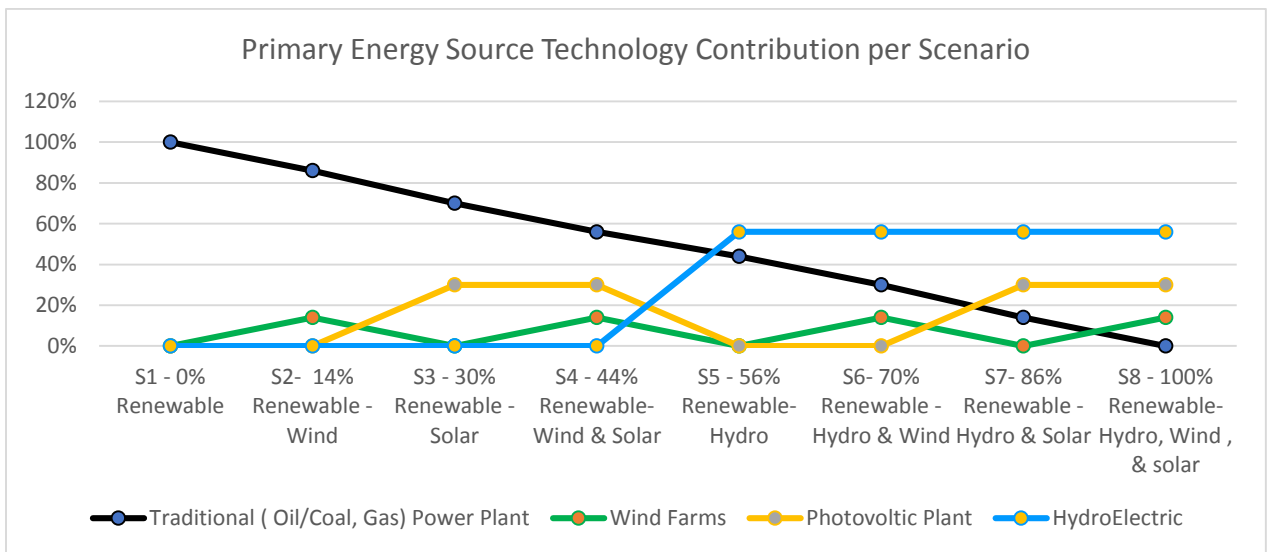
Reasoning based on deduction, variables and measurements that have been predefined, data gathering prior to analysis, and the investigation of cause-and-effect connections.

### 1.3.5 Research Strategy

The data collected for the research is mostly numerical and comes from IEEE 9-Bus system **case study** conducting ETAP simulation for 8 scenarios of the IEEE 9-Bus systems which are:

1. 0% Renewable contribution of IEEE 9 Bus System with Fossil Fuel Primary Energy Sources driven Synchronous Machines
2. 14% Renewable Contribution with IEEE 9 Bus System with Fossil Fuel Primary Energy Sources driven Synchronous Machines + 125MVA Wind Farm replaces SM3.
3. 30% Renewable Contribution with IEEE 9 Bus System with Fossil Fuel Primary Energy Sources driven Synchronous Machines + 270MVA PV plant replaces SM2.
4. 44% Renewable Contribution for IEEE 9 Bus System with Fossil Fuel Primary Energy Sources driven Synchronous Machines with 270MVA PV Plant Replacing SM2+ 125MVA Wind Farm replaces SM3.
5. 56% Renewable Contribution for IEEE 9 Bus System with Fossil Fuel Primary Energy Sources driven Synchronous Machines 512MVA Hydro Electric Power Plant replacing SM1.
6. 70% Renewable Contribution for IEEE 9 Bus System with Fossil Fuel Primary Energy Sources driven Synchronous Machines 512MVA Hydro Electric Power Plant replacing SM1 + 125MVA Wind farm replaces SM3.
7. 85% Renewable Contribution for IEEE 9 Bus System with Fossil Fuel Primary Energy Sources driven Synchronous Machines 512MVA Hydro Electric Power Plant replacing SM1 + 270MVA PV plant replaces SM2.
8. 100% Renewable for IEEE 9 Bus System with Fossil Free Primary Energy Sources (Solar / Wind / Hydro) with 512MVA Hydroelectric Power Plant replaces SM1+270MVA PV Plant Replacing SM2+ 125MVA Wind Farm replaces SM3.

Technology	S1 - 0% Renewable	S2- 14% Renewable - Wind	S3 - 30% Renewable - Solar	S4 - 44% Renewable- Wind & Solar	S5 - 56% Renewable- Hydro	S6- 70% Renewable - Hydro & Wind	S7- 86% Renewable - Hydro & Solar	S8 - 100% Renewable- Hydro, Wind , & solar
	100%	86%	70%	56%	44%	30%	14%	0%
	0%	14%	0%	14%	0%	14%	0%	14%
	0%	0%	30%	30%	0%	0%	30%	30%
	0%	0%	0%	0%	56%	56%	56%	56%



### 1.3.6 Data Collection Method

The data will be collected through primary and secondary sources within cross sectional time horizon.

Cross sectional time horizon commonly referred to as a one-shot study, this research design involves the collection of data on a single occasion. The study subject might potentially be addressed over an extended timeframe, spanning days, weeks, or even months.

A cross-sectional study is a research design that captures a snapshot of several variables at a certain moment in time, using a representative sample. The Primary Data Collection was done

through performing simulation for IEEE 9 Bus case study, while the secondary data collection was done through resources such as: the internet, reports, and articles. The data obtained from this analysis may be beneficial for policymakers and energy industry stakeholders seeking to make well-informed decisions about 100% transitioning to renewable in a large-scale power grid.

**1.3.7 Population and Sampling**

The objective of this study is to investigate challenges of transition to sustainable 100% renewable electrical power and energy system along with power quality solutions on stability, security, and interoperability of the IEEE 9 bus system as a small-scale power system, and the results and outcomes that will be obtained can be reflected on a larger scale power system

**1.3.8 Research Onion**

Based on all above, below **Figure 1.3-4** reflects the research onion for the subject research

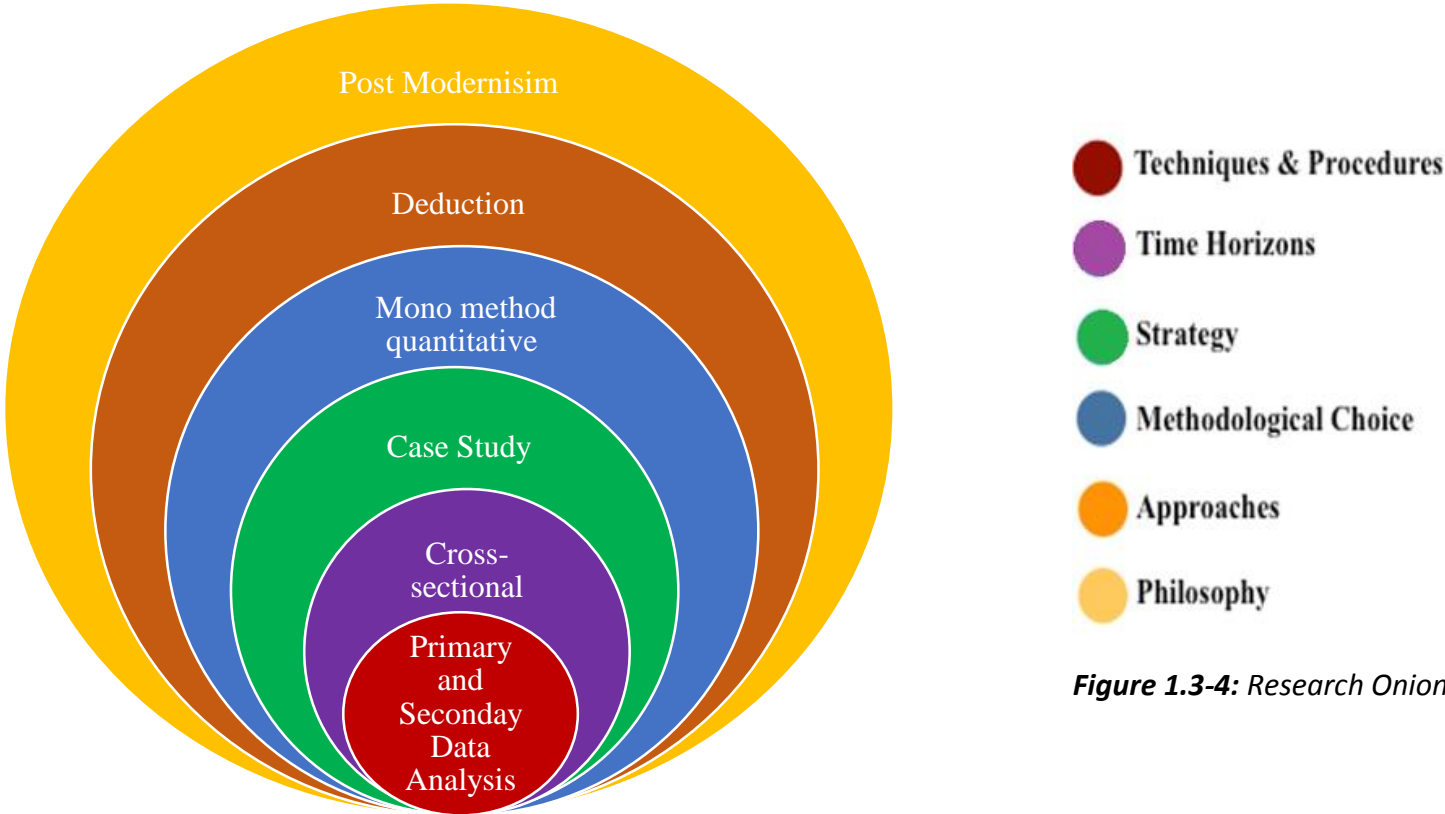


*Figure 1.3-4: Research Onion*

## PART TWO



### **2.1 Chapter Four: Main Components of a Large-Scale Grid Connected PV Plant / Wind Farm.**

#### **2.1.1 Overview**

All generators connected to the transmission system must be complied with Transmission System Operator (TSO) grid code which defines the technical interconnection rules. This transmission grid code was originally created and developed assuming synchronous generators driven by prime movers (steam turbines, gas turbines, etc....) that depends on primary energy sources such as natural gas and other petroleum products such as heavy fuel and diesel oil.

The renewable energy sectors globally acquired significant progress during the past years, by boosting the contribution of renewable energy sources (wind energy, solar energy, hydroelectric)

in the total energy mix in-line with the three proposed scenarios by IRENA in [41] new policies and cumulative investment needed to 2050 which is represented by expanding the renewable energy projects as a local source for sustainable alternative energy and as one of the most important solutions for reducing the dependency of electricity generation on the primary energy sources. Thus, Wind Turbine Generators (WTG) and Photovoltaic (PV) generators, both fall under the Intermittent Renewable Resources (IRR), deserve provisions of the transmission grid code specifically for them. This grid code establishes the technical interconnection code rules which IRRs must comply with in relation to their connection requirements to the Transmission System.

In this chapter, we will discuss in a more depth manner the following:

- 1- PV Generator – PV IRR Unit for Solar Plant [2.1.2]
- 2- WT Generator – WTG IRR Unit for Wind Farm [2.1.3]
- 3- Collection MV/HV Substation (common for PV plant and Wind Farm) [2.1.4]
- 4- Power Quality Solutions (common for PV plant and Wind Farm) [2.1.5]

The PV Generator is basically the “photovoltaic module and fully rated converter”, and it is classified under the “DC generator with inverter” type of generators for renewable generation. As illustrated in **Figure 2.1-1**

On the other hand, WT Generators are basically the “AC Generators”, and it is categorized into fixed and variable speed, which can be further classified into 4 types; Type-1: squirrel cage induction generator, Type-2: Wound Rotor Induction generator, Type-3: Doubly fed induction generator, and Type-4 permanent magnet synchronous generators under the “DC generator with inverter” type generators for renewable generation. As illustrated in **Figure 2.1-1**

Both the PV generators and WT generator are collectively called Inverter Based Resources (IBR) in which they are asynchronously interconnected to grid. Not like wise in the fixed speed AC generators which are directly connected synchronous generators which are electromagnetically

connected to the grid and can contribute to the inertial response, such are concentrated solar power, biomass and biogas, and hydro-electric power plants.

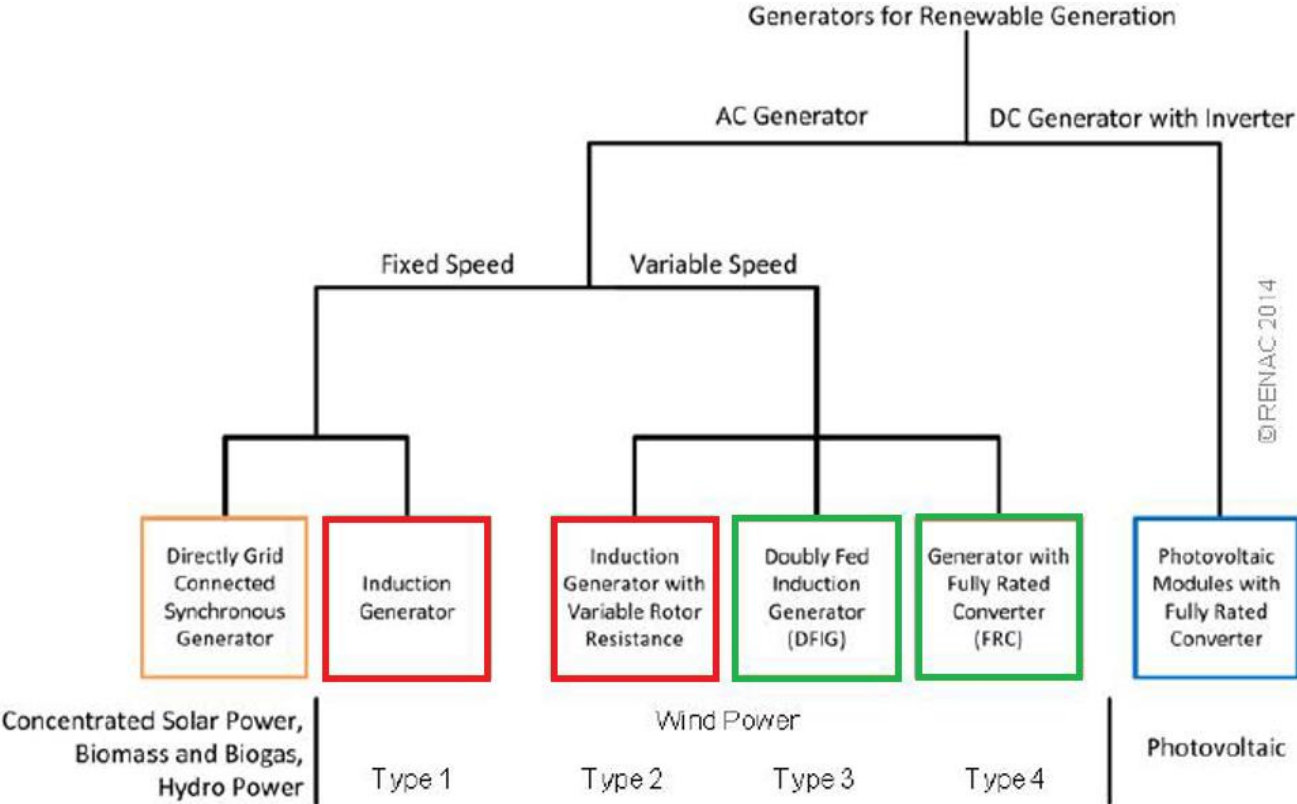


Figure 2.1-1: Generators for Renewable Generations

## 2.1.2 Photo Voltaic Generator (PVG) – PV IRR Unit



### 2.1.2.1 Large Scale Grid Connected Solar PV Plant – Overview

A grid connected Photo-Voltic (PV) plant consists of mainly the photovoltaic cells and associations that converts the electromagnetic solar radiation of solar energy directly into electricity through photovoltaic effect. Being exposed to the sunlight, photons with energy greater than the energy bandgap of the semiconductor create some pairs of electron-holes proportional to the incident irradiation.

A group of solar cells connected in series will create the solar module or panel, and a group of solar modules in series will form the string. Moreover, a group of strings in parallel will build up the PV solar array which sometimes is referred to as PV generator. This PV generator will have a certain amount of DC voltage depending on the number of solar modules connected in series (string voltage) and DC power depending on the total number of solar panels (modules).

As the voltage generated is a DC voltage and the grid which the PV plant is connected with is an AC grid, then a DC to AC converter should be used which are solar inverters. Directly after the solar inverters that converted the DC voltage into LV AC voltage, a solar step-up power transformer is used that step-up the voltage from the LV AC into MV AC voltage level.

In order to maximize the number of solar inverters connected in series then ring system will be used, however in some PV plants a radial system is used too. A medium voltage Ring Main Units (RMU's) are used, and they are connected together through MV power cables with cable terminations to develop the MV PV incoming feeder of the MV main switchgear. The MV switchgear will receive the power from the PV plant and evacuate this power through an MV/HV Step-Up power transformers, besides, the power flow can be controlled in case of emergency using the MV circuit breakers of Bus Tie circuits at the MV Switchgear. Also, the MV switchgear will connect the MV capacitor banks or STATCOMS (if any). Right after the MV/HV power transformer, the HV primary transmission substation comes which is considered as point of common coupling (PoCC). Summarizing the main components of a grid connected PV plant. A PV plant consists of mainly the following, and they can be visualized in Figure 2.1-2

1. Photovoltaic Cells and Associations
2. (DC/AC) Solar Central Inverters
3. Step-Up (LV/MV) Solar Power Transformer Station and MV Ring Main Units
4. Medium Voltage (MV) Switchgear
5. Medium Voltage (MV) Capacitor Banks
6. Step-Up (MV/HV) Power Transformer
7. HV Primary Transmission Substation

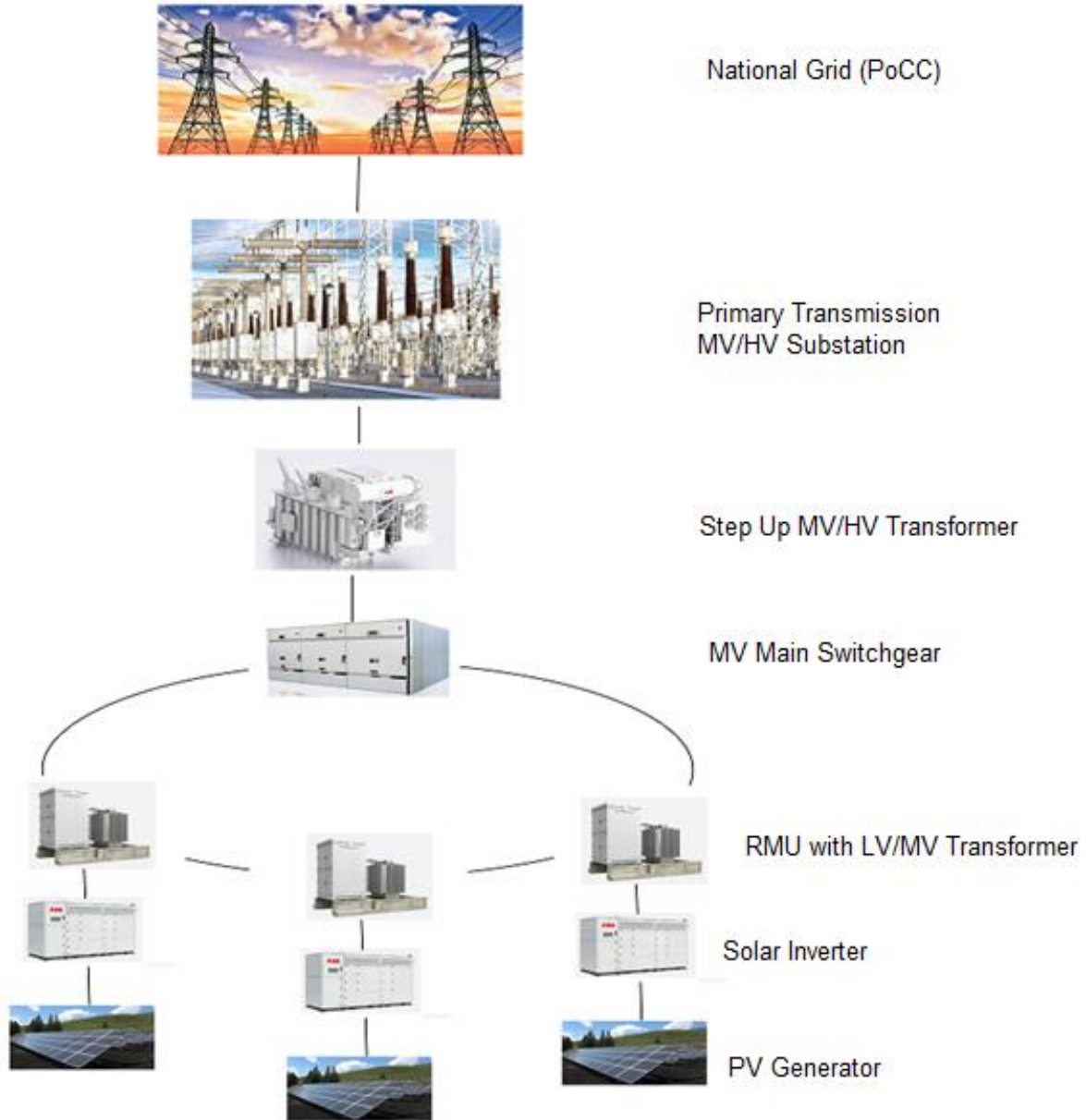


**Figure 2.1-2:**Block Diagram of a Large-Scale Grid Connected PV Plant

**2.1.2.2 Components of a Grid Connected PV Plant**

**2.1.2.2.1 Photovoltaic Solar Cells and Association**

A solar cell is basically a P-N junction fabricated in a thin wafer of semiconductor. The electromagnetic solar radiation of solar energy can be directly converted into electricity through photovoltaic effect. Being exposed to the sunlight, photons with energy greater than the band-

gap energy of the semiconductor create some electron-hole pairs proportional to the incident irradiation. Figure 2.1-3 shows the basic operating principle of a solar cell [11].

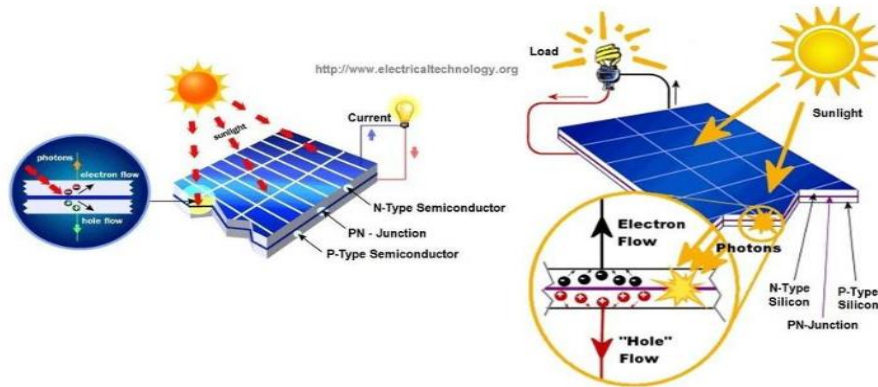


**Figure 2.1-3:** Basic Operating Principle of a Solar Cell

PV cells are grouped in larger units called PV modules which are further interconnected in a parallel-series configuration to form PV arrays. The basic element in a photovoltaic system is the solar cell. Group of solar cells in series are called a solar module, and a group of solar modules in series are called solar panels or string. Moreover, a group of solar panels in parallel are called solar array which sometimes it is referred to as PV generator. Figure 2.1-4 shows the Diagram of the possible components of a photovoltaic system.

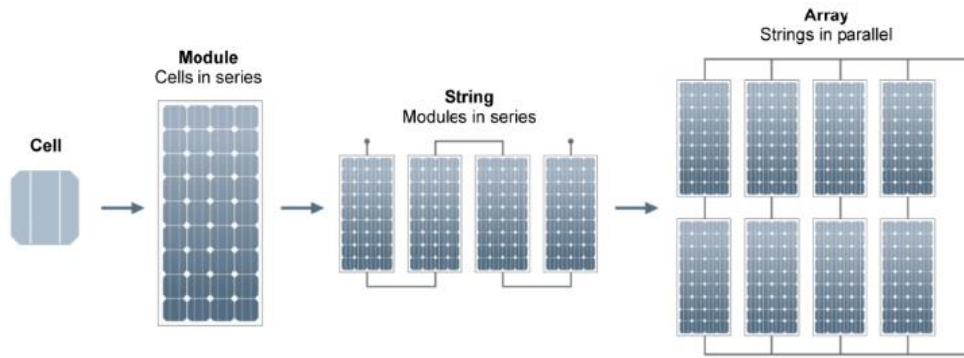


**Figure 2.1-4:** Diagram of the Possible Components of a Photovoltaic System

### 2.1.2.2.2 Solar Cell Equivalent Circuit

#### 2.1.2.2.2.1 Electrical Parameters for Solar Cell

The equivalent circuit of a PV cell is as shown in Figure 2.1-5. The current source  $I_{ph}$  represents the cell photocurrent, whereby each photon carries an energy that depends on the wavelength.

$$E_{ph} = \frac{hc}{\lambda}$$

When this photon strikes the solar cell, then consequently it will generate a pair of electron-hole (e<sup>-</sup>hole) which will generate the photo current  $I_{ph}$ .

The resistances  $R_{sh}$  and  $R_{sr}$  are the intrinsic shunt and series resistances of the cell, respectively. Usually, the value of  $R_{sh}$  is very large and that of  $R_{sr}$  is very small, hence they may be neglected to simplify the analysis.

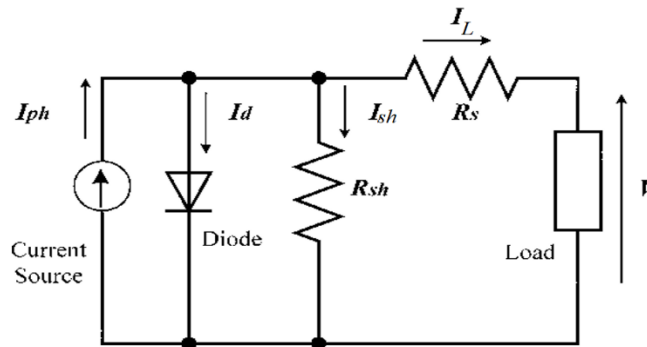


**Figure 2.1-5:** The equivalent Circuit for the Solar Cell

From the above equivalent circuit, and applying Kirchhoff's Current Law (KCL)

$$I_{ph} = I_d + I_{sh} + I_L$$

Where;

$I_{ph}$ : Photo current.

$D$ : P-N junction and it is a representation for the ideal diode.

$R_{sh}$ : Shunt resistance due either the leakage at edges of P-N junction or defects on the P-N junction.

$R_{sr}$ : Series resistance

$$R_{sr} = R_{front\ contact} + R_{Back\ contact} + R_{Semi-conductor} + R_{N-type}$$

$R_{Front\ contact}$ : Resistance of the front contacts of the metal mask.

$R_{Back\ contact}$ : Resistance of the front contacts of the Back contact.

$R_{\text{Semi-conductor}}$ : Resistance with the  $e^-$  faces during crossing from the semi-conductor to the contact.

$R_{N\text{-type}}$ : Resistance due to the depth of N-layer in the P-N junction.

$I_D$ : Ideal diode current and it is given by the equation.

Figure 2.1-6 shows current-voltage characteristic of semiconductor diode

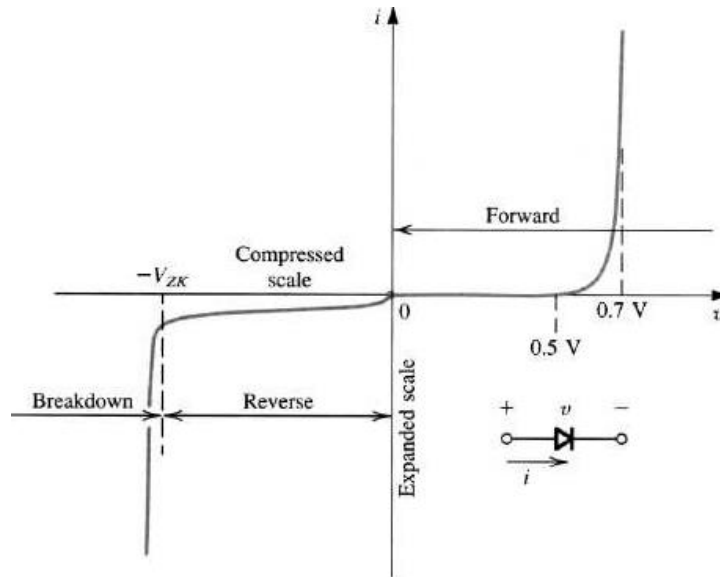


**Figure 2.1-6:** Current-Voltage Characteristic of Semiconductor Diode

The current equation of the diode is given in below.

$$I_D = I_0 e^{\frac{qV_{oc}}{AKT}} - 1$$

Where

$I_0$ : Reverse saturation current

$q$ : Charge of electron  $1.6 \times 10^{-23} \text{ C}$

$V_{o.c}$ : Open circuit voltage ( $V-I_{sh}$ )

$A$ : Ideality factor, where  $A= 1$  for an ideal diode and  $A= 1 - 2$  for a practical diode

$K$ : Boltzmann factor

$T$ : Absolute temperature for solar cells

Shunt Current  $I_{sh}$  is the current which flows in  $R_{sh}$

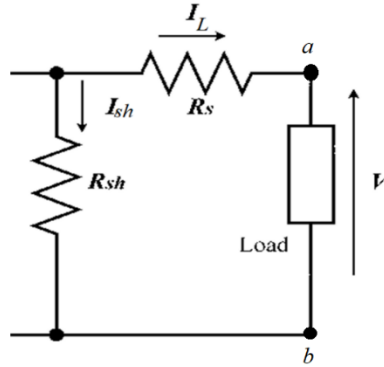


**Figure 2.1-7: Load Side of Solar Cell**

Figure 2.1-7 shows the load side of solar cell. Applying Kirchhoff's Voltage Law (KVL) at the load side of the solar cell

$$V_{ab} = \sum E - \sum IR$$

$$V_{ab} = V = 0 - (-I_{sh}R_{sh} + I_L R_{sr})$$

$$V = I_{sh}R_{sh} - I_L R_{sr}$$

$$I_{sh} = \frac{V + I_L R_{sr}}{R_{sh}}$$

For ideal solar cells, then the shunt resistance will be assumed as an open circuit  $R_{sh} = \infty$ , and the series resistance will be assumed as short circuit  $R_s = 0$

As per Kirchhoff's Current Law (KCL)

$$\sum I_{in} = \sum I_{out}$$

$$I_L = I_{ph} - I_D - I_{sh}$$

Substituting equations 2.4 and 2.8 in equation 2.10, [11]

$$I_L = I_{ph} - \left( I_o e^{\frac{qV_{o.c}}{AKT} - 1} \right) - \frac{V + I_L R_{sr}}{R_{sh}}$$

But the open circuit voltage is given in equation 2.12

$$V_{o.c} = V - I_L R_{sr}$$

Substituting equation No. (2.12) in equation 2.11

$$I_L = I_{Ph} - \left( I_o e^{\frac{q(V - I_L R_{sr})}{AKT} - 1} \right) - \frac{V + I_L R_{sr}}{R_{sh}}$$

I-V characteristics depends on  $I_{sh}$  and  $V_{o.c}$ :

1.  $I_{ph} = I_{sh.c}$  It depends on number of generated  $e^-$  holes
2.  $V_{o.c}$  depends on the width of the depletion region, the wider the depletion region the higher the  $V_{o.c}$  and vice versa.

The open circuit voltage can be found by assuming that  $I_L = 0$  and  $R_{sh}$  is very high which means that the solar cell will look like an open circuit

If we assume  $I_L = 0$ ,  $R_{sh}$  is very high = Open circuit

$$I_L = I_{Ph} - \left( I_o e^{\frac{qV_{o.c}}{AKT} - 1} \right) - \frac{V + I_L R_{sr}}{R_{sh}}$$

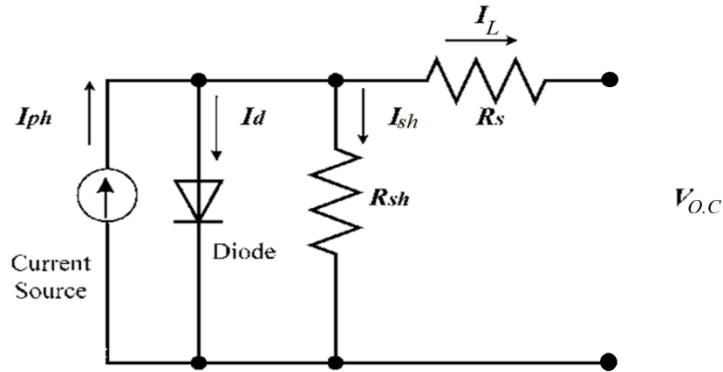


Figure 2.1-8: Open Circuited Solar Cell

$$0 = I_{Ph} - \left( I_o e^{\frac{qV_{o.c}}{AKT} - 1} \right) - \frac{V + 0}{R_{sh}}$$

$$0 = I_{Ph} - \left( I_o e^{\frac{qV_{o.c}}{AKT} - 1} \right) - \frac{V}{R_{sh}}, \quad R_{sh} \text{ is very high thus } \frac{V}{R_{sh}} \approx 0$$

$$I_{Ph} = \left( I_o e^{\frac{qV_{o.c}}{AKT} - 1} \right)$$

$$\frac{I_{ph}}{I_o} = \left( e^{\frac{qV_{o.c}}{AKT}} - 1 \right)$$

$$\ln\left(\frac{I_{ph}}{I_o}\right) = \left(\frac{qV_{oc}}{AKT}\right) - 1$$

$$\ln\left(\frac{I_{ph}}{I_o}\right) + 1 = \left(\frac{qV_{oc}}{AKT}\right)$$

$$V_{o.c} = \left(\frac{AKT}{q}\right) \left\{ \ln\left(\frac{I_{ph}}{I_o}\right) + 1 \right\}$$

As  $R_{sh}$  decreases and  $R_{sr}$  increases the shape will be close to a triangle; However, as  $R_{sh}$  increases and  $R_{sr}$  decreases the shape will be close to square.

The output voltage for the solar module (solar panel) will be given as below.

$$V_{out-module} = V_{Solar\ cell} \times N_{solar\ cell}$$

However, the total current from the solar module (solar panel) will be given as below

$$I_{total} = I_{ph} \times M - \left( I_o M e^{\frac{qV_{oc}}{AKT}} \right)$$

Where

M: Number of parallel cells per module

N: Number of series cell

The conclusion from above is that the parallel cells increase the current, and series cells increases the voltage.

#### 2.1.2.2.2.2 Short Circuit Current for Solar Cells

Taking the equivalent circuit of the solar cell in Figure 2.1-5, the short circuit current of the solar cell is achieved when the solar cell voltage is zero, which means the solar cell terminals are short circuited as indicated in Figure 2.1-9.

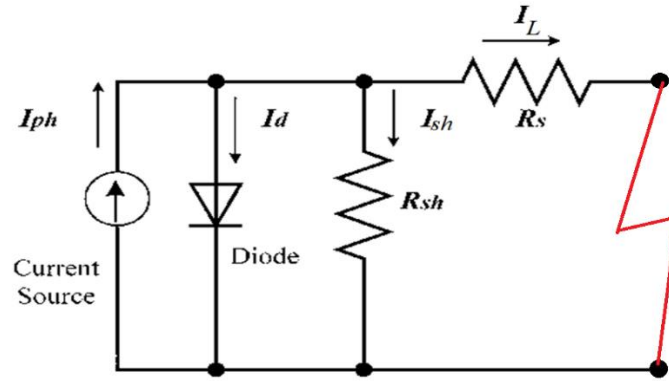


**Figure 2.1-9: Short Circuited Solar Cell**

$$I_{sh.c} = I|_{V=0}, \text{ as } R=0$$

The short circuit current of the solar cells depends on the following:

1. Number of the solar cell, however in order to differentiate between solar cells, ideally, the current density is used, where best solar cell at standard conditions gives a current density  $J=45 \text{ mA/cm}^2$ , while practically  $J= 25\sim 35\text{mA/cm}^2$ .

The current density is given in below equation 2.20

$$J = \frac{I}{A}$$

2. Number of photons, whereby the greater number of photons absorbed by solar cell, the more electron-hole are generated in the cell.
3. Spectrum of solar radiation. Light spectrum depends on the wavelength ( $\lambda$ ), where

$$E = \frac{hc}{\lambda} = \frac{1.24}{\lambda}$$

Thus obviously different wave length would give different (E). However, to utilize the energy generated at different wave lengths a cascaded solar cell is used with different  $E_{gap}$ .

4. Collection probability for charge carrier, which is the probability to collect free electrons before their recombination with their holes.
5. Material properties (lifetime of electron), where it is the period that starts from the time of generation electron-hole to the time of the recombination for the electron to its hole again. The lifetime of electron depends on ideality factor, doping ratio, defects in PN-junction and the quality of the PN-junction.

### 2.1.2.2.3 Open Circuit Voltage for Solar Cell

Taking the equivalent circuit of the solar cell in Figure 2.1-5, the open circuit voltage of the solar cell is achieved when the solar cell current is zero, which means the solar cell terminals are open circuited as indicated in Figure 2.1-10.

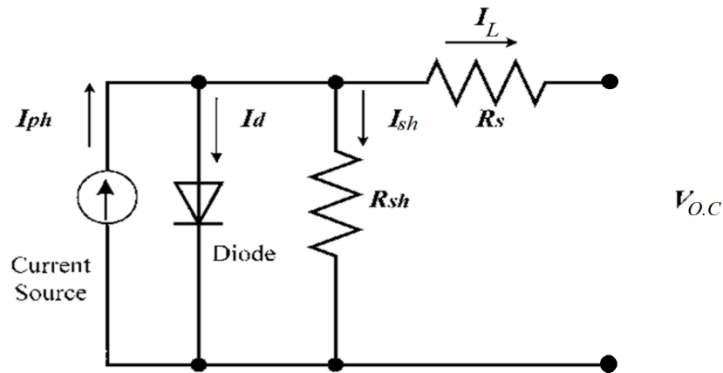


**Figure 2.1-10:** Open circuited Solar Cell

$$V_{o.c} = V|_{I=0}, \text{ as } R=\infty$$

It is the voltage of the solar cell when the current is equal to zero.

$$V_{o.c} = \left( \ln \left( \frac{I_{ph}}{I_o} \right) + 1 \right) \left( \frac{AKT}{q} \right)$$

$V_{o.c}$  is slightly affected by changes of  $I_{ph}$ ; however, it mainly depends on  $I_o$

1.  $I_o$  depends on the following:

- The type of re-combination in the solar cell (p-n junction) between the generated  $e^-$  and the holes.
- Also,  $I_o$  depends on the doping.

In ideal solar cells the  $V_{o.c}$  could reach up to 750 mV (Si), however for Gallium Arsenide the  $V_{o.c}$  could reach up to 800 mV.

### 2.1.2.2.4 Fill Factor (FF)

The fill factor is essentially a measure of quality of the solar cell. It is calculated by comparing the maximum power  $P_{MAX}$  to the theoretical power  $P_T$  that would be output at both the open circuit voltage and short circuit current together. The FF is given in equation 2.23, and Figure 2.1-11 shows the current-voltage characteristics of the solar cell.

$$FF = \frac{V_{mpp} \times I_{mpp}}{V_{o.c} \times I_{sh.c}}$$

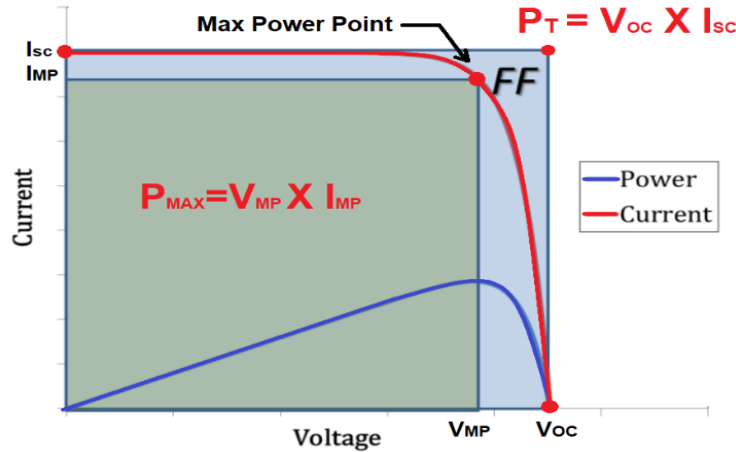


**Figure 2.1-11:** Current - Voltage (I-V) characteristic for Solar Cell

The fill factor for ideal solar cell reaches up to 0.85, however in reality it reaches up to 0.45. Fill factor mainly depends on the ideality factor (A) of the solar cells. And it determines the following:

- Quality of the P-N junction (no defects). Defect states that there a leakage in the structure of the P-N junction.
- Re-combination between free  $e^-$  and the holes.

#### 2.1.2.2.2.5 Efficiency of the Solar Cell $\eta$

Efficiency of the solar cell is ratio of the output maximum power and input power, which can be given in equation below

$$\eta = \frac{(\text{Max power point I})(\text{Max power point for V})}{(\text{Radiation})(\text{Area of the solar cell})} \times 100\%$$

$$\eta = \frac{P_{out}}{P_{in}} \times 100\% = \frac{I_{mpp} \times V_{mpp}}{G \times A} \times 100\% = \frac{I_{sh.c} \times V_{o.c} \times FF}{G \times A} \times 100\%$$

Efficiency of the solar cell depends on the Air mass (AM), Temperature (T), and Radiation (G).

#### 2.1.2.2.2.6 Maximum Output Power of Solar Cell

Maximum output power depends on the characteristic impedance  $R_{ch}$ , where the  $R_{ch}$  is the value of  $R$  which gives  $I_{sh.c}$  and  $V_{o.c}$ .

$$R_{ch} = \frac{V_{o.c}}{I_{sh.c}} \approx \frac{V_{mpp}}{I_{mpp}}$$

Figure 2.1-12 shows the characteristic impedance equivalent circuit. Figure 2.1-13 shows the current - voltage & power-voltage curve of solar panel at different irradianations.

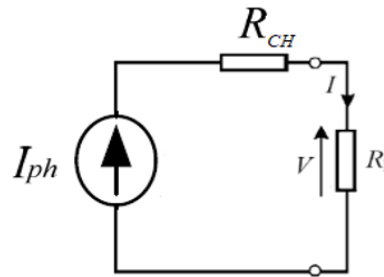


**Figure 2.1-12:** Characteristic Impedance Equivalent Circuit

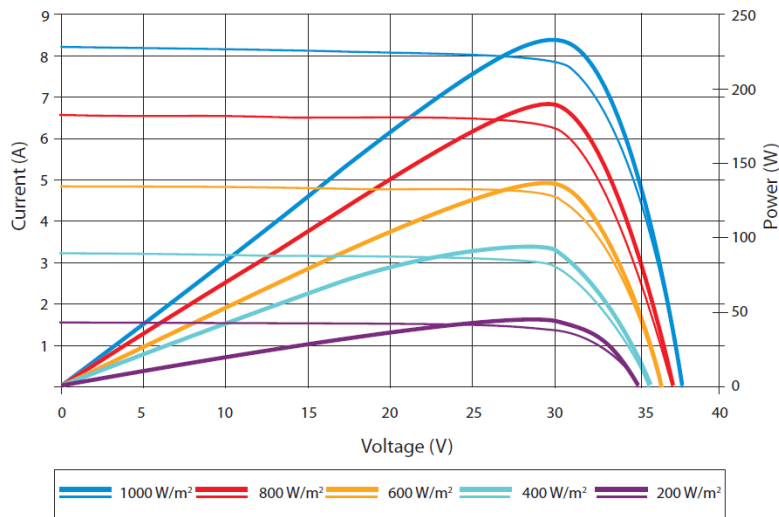


**Figure 2.1-13:** Current - Voltage & Power-Voltage Curve of Solar Panel at Different Irradianations

#### 2.1.2.2.2.7 Effect of Temperature on Solar Cell

Maximum Temperature affects both short circuit current of the solar cell  $I_{sh.c}$  and open circuit voltage of the solar cell  $V_{o.c}$ , and consequently the output power  $P_{out}$

1. Effect of temperature on  $I_{sh.c}$

In semiconductors as the Temp increases, the resistance decreases, leading to increase of

current which results a decrease in the energy gap. As the  $E_{gap}$  decreases less energy would be needed to transfer  $e^-$  from the covalence band to the conduction band.

Each (1 kelvin) increase in Temperature, the short circuit current  $I_{sh.c}$  would increase by ( 0.05~0.07%)

$$I_{sh.c} = I_o (1+ \alpha\Delta T)$$

## 2. Effect of Temperature on $V_{o.c}$

As the temp increases the open circuit voltage  $V_{o.c}$  would decrease.

Each increment of temperature by  $1^\circ\text{C}$  , lead to a decrease in voltage by 0.0032 V

$$V_{o.c} = V_o (1-\beta\Delta T)$$

## 3. Effect of Temperature on $P_{out}$

Each increment of temperature by  $1^\circ\text{C}$  , lead to a decrease in Power by 0.5%

$$I_{sh.c} = I_o (1+ \alpha\Delta T)$$

$$V_{o.c} = V_o (1- \beta\Delta T)$$

$I_o$  and  $V_o$  are the initial value of both the current and voltage at a standard Temp ( $25^\circ\text{C}$ ) respectively.

$\alpha$  and  $\beta$  are the thermal expansion coefficient of Si

$$P_{out} = P_o (1 - 0.005 \Delta T )$$

The output power decreases by this amount due to temperature increment.

### 2.1.2.2.3 Solar Inverters

#### 2.1.2.2.3.1 Solar Inverter Definition

Solar inverters, also called grid-tied inverters, convert the direct current (DC) electricity produced by the solar PV panels to alternating current (AC) electricity that can be exported back to the grid. Figure 2.1-14 shows a central solar inverter along with its associated solar step-up transformer and MV Ring main Unit (RMU)



**Figure 2.1-14:** Central Inverter with Step-Up Transformer and RMU

**2.1.2.2.3.2 Solar Inverter Single Line Diagram (SLD)**

As shown in Figure 2.1-15, two central inverters are evacuating the power through a three winding solar transformer which is connected with a MV Ring Main Unit

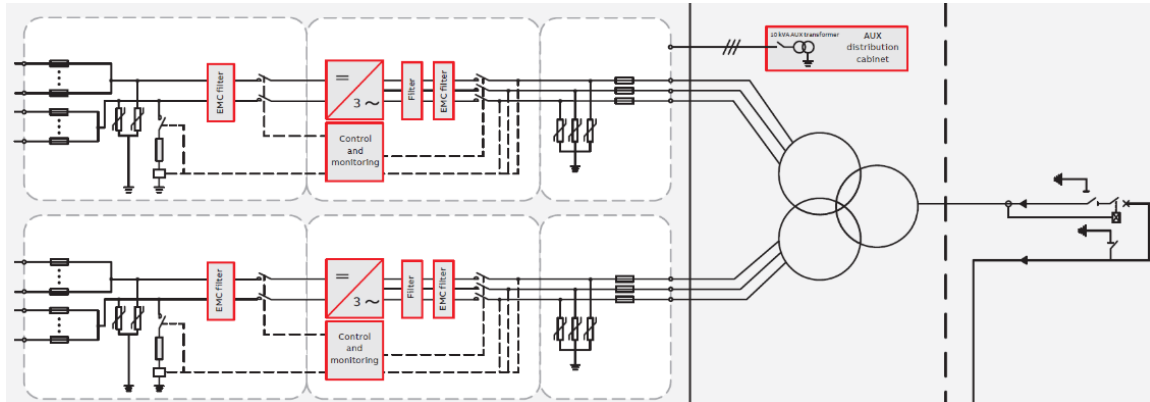


**Figure 2.1-15:** Block Diagram of Two Central Inverters and MV step-up station

The same can be visualized in Figure 2.1-16. shows the general layout drawings for PVS 980-2000 kVA



**Figure 2.1-16:** Two Central Inverters and Step-Up Solar Power Transformer with MV RMU

### 2.1.2.2.3.3 Three-phase Sinusoidal Pulse Width Modulation SPWM Inverter

Three-phase SPWM inverters are controlled by having three reference sinusoidal modulating signals at the frequency of the desired output frequency but displaced from each other by  $120^\circ$  modulate the high frequency triangular wave to determine the firing instants of each IGBT. The resulting switching signals from each comparator are used to drive the inverter switches of the corresponding leg. The switching signals for each inverter leg are complementary. These are shown in Figure 2.1-17.

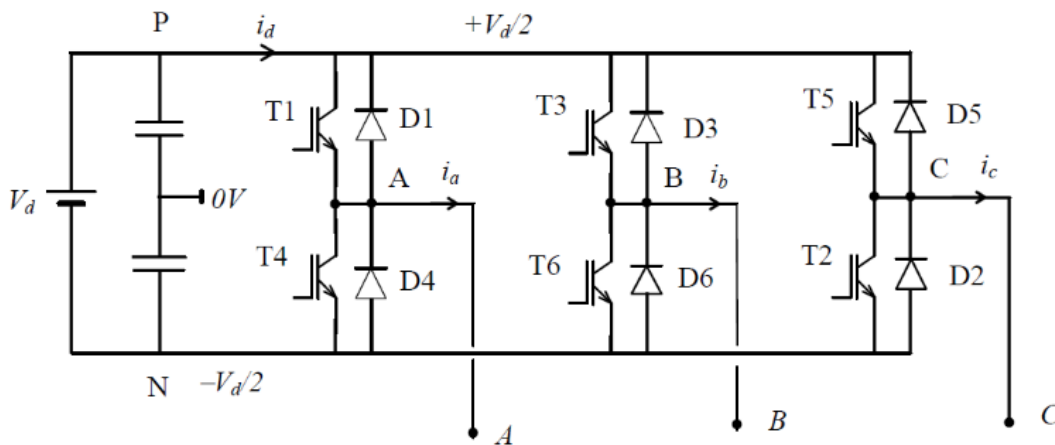


**Figure 2.1-17:** Basic Three Phase Bridge Inverter

One or other of the devices in each arm is conducting at all times, connecting the load line to either the positive or negative of the d.c. source. Taking, for example, the arm to phase A with

devices numbered 1 and 4 in Figure 2.1-17, if  $i_a$  is positive, IGBT T1 conducting, then when IGBT T4 is fired, T1 turns off and the load current transfers to diode D4. If, however,  $i_a$  were negative, diode D1 would have been conducting and when IGBT T4 fired, it would have taken up the load current immediately; in this condition, IGBT T1 did not require turning off, as it was in any case not on.

Referring to Figure 2.1-18, the firing pulses must be continuous into the gate of the IGBT when current is required from that arm, so that the IGBT can take up the load current when it reverses under inductive loading. If the instantaneous load current is reversed to the voltage, then the diode on is that in parallel with IGBT receiving firing pulses. Hence, in the period shown when (say)  $i_{g1}$  present either IGBT T1 or diode D1 is on. [43]

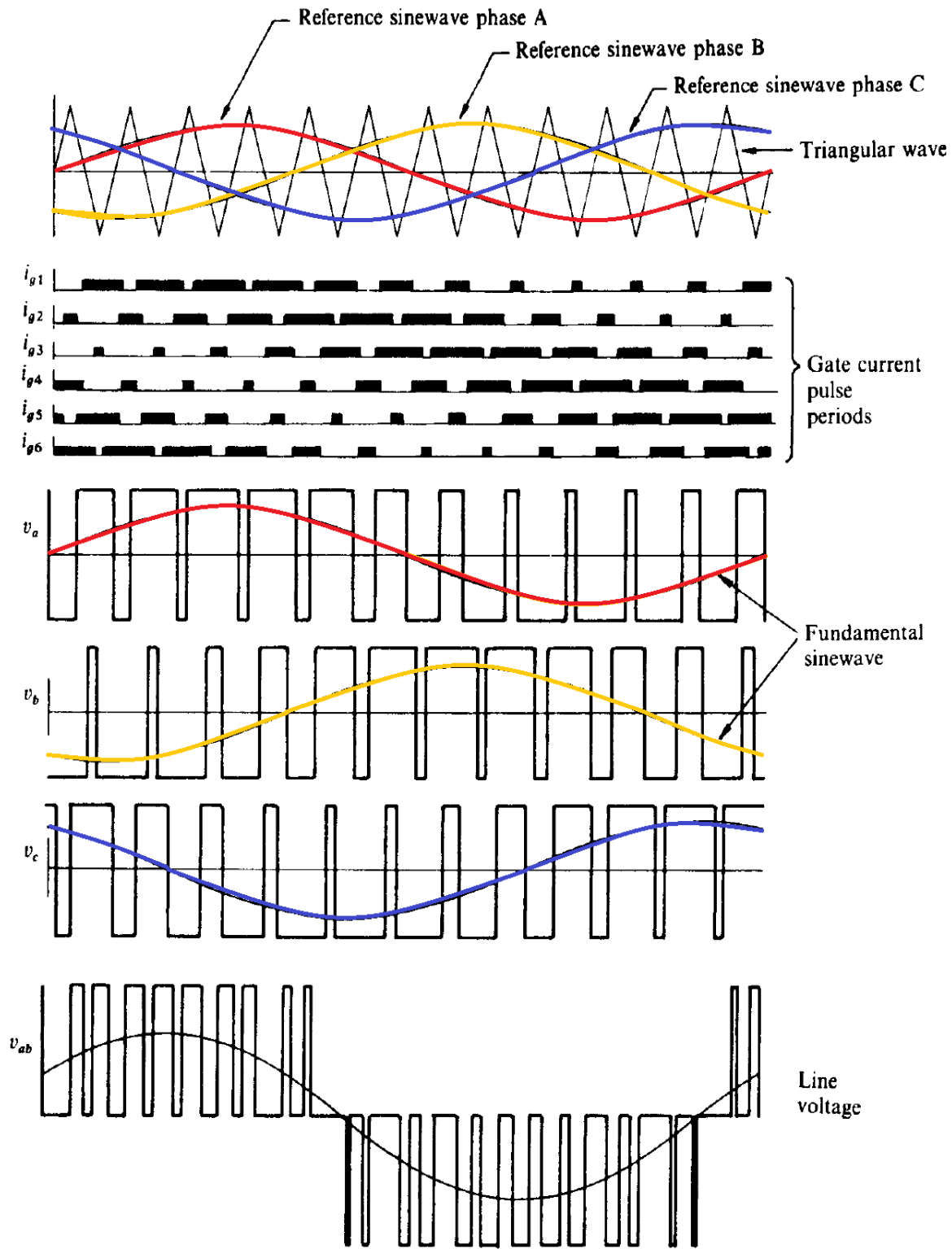


Figure 2.1-18: Pulse-Width Modulated Waveform for a Three Phase Bridge Inverter[43]

**2.1.2.2.4 Step-Up (LV/MV) Solar Power Transformer Station and Ring Main Units**

**2.1.2.2.4.1 Solar Power Transformer**

solar power transformers are used to step up the output low voltage AC received from the central inverters (400 V, 480 V, 690 V, 1000 V, etc..) into the medium voltage AV (11 kV, 20 kV, 33 kV, etc.). Solar Power Transformers differ than another normal transformer by the following:

- An electrostatic screen between HV and LV windings is applied.
- Transformer is designed to limit DC components occur in core, as appropriate to solar application.
- Basic Insulation level for the LV is higher than the normal transformer.

**2.1.2.2.4.2 Solar Power Transformer Types**

solar transformer can be either two windings' transformers as shown in Figure 2.1-19

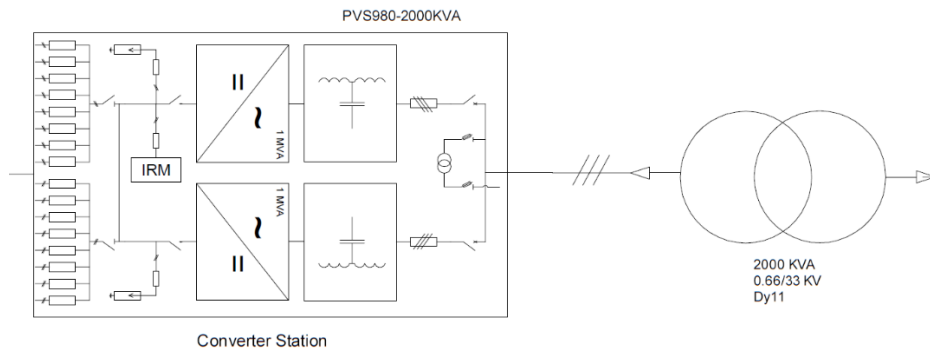


**Figure 2.1-19: 2000 kVA, 0.66/33 kV, Dy11 Two Winding Solar step-up Power Transformer**

or three winding transformers (transformer with two secondaries) as shown in Figure 2.1-20

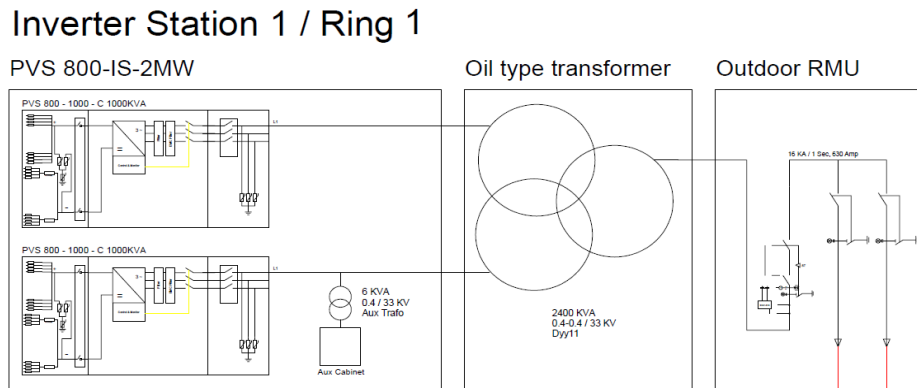


**Figure 2.1-20: 2400 kVA, 0.4-0.4/33 kV, Dy11y11 Three Winding Solar Step-up Power Transformer**

Below Figure 2.1-21 is a photo showing a central inverter (right) is connected with the step-up solar transformer (middle), and from this transformer to the MV Ring Main Unit (left)



**Figure 2.1-21:** Central Inverter with Step Up Transformer and RMU

#### 2.1.2.2.4.3 *MV Ring Main Unit*

Medium Voltage Ring Main Unit (RMU) is a compact switchgear for applications in medium voltage distribution networks, Solar PV plants, and Wind Farms. They can be used as 2-, 3- or 4-way standard configurations with additional equipment according to the system requirement. Below Figure 2.1-22 shows a photo for a typical RMU.



**Figure 2.1-22:** Ring Main Unit Three – Way

### 2.1.3 Wind Turbine Generator (WTG) – WTG IRR Unit



#### 2.1.3.1 Large Scale Grid Connected Wind Farm-Overview

A grid connected Wind Farm (WF) consists of mainly the Wind Turbine Generator (WTG) which captures the wind's kinetic energy in a rotor consisting of two or more blades mechanically coupled to an electrical generator via speed step-up gear box. The turbine is mounted on a tall tower to enhance the energy capture. Numerous wind turbines are installed at one site to build a wind farm of the desired power generation capacity.

The Generators convert the mechanical energy supplied by the WTG rotor through the gear box into electrical power energy, and this electrical power energy is tied with the grid either directly or through converters. Traditionally, there are **two (2) main types** of wind turbine generators (WTGs) which can be considered for the various wind turbine systems, these types are:

- 1- *Induction (Asynchronous) generators.*
- 2- *Synchronous generator*

In principle, each can be run at fixed or variable speed. However, due to the fluctuating nature of wind power, it is advantageous to operate the WTG at variable speed which reduces the physical

stress on the turbine blades and drive train, and which improves system aerodynamic efficiency and torque transient behaviors.

The turbine is mounted on a tall tower to enhance the energy capture. Numerous wind turbines are installed at one site to build a wind farm of the desired power generation capacity. In order to maximize the number of WTG's connected in series then ring system will be used, however in some Wind Farms a radial system is used too. A medium voltage Ring Main Units (RMU's) inside the base of the WT tower are used, and they are connected together through MV power cables with cable terminations to develop the MV WTG incoming feeder of the MV main switchgear. The MV switchgear will receive the power from the Wind farm and evacuate this power through an MV/HV Step-Up power transformers, besides, the power flow can be controlled in case of emergency using the MV circuit breakers of Bus Tie circuits at the MV Switchgear. Also, the MV switchgear will connect the MV capacitor banks or STATCOMS (if any). Right after the MV/HV power transformer, the HV primary transmission substation comes which is considered as point of common coupling (PoCC). Summarizing the main components of a grid connected to a Wind Farm. A Wind Farm consists of mainly the following, and they can be visualized in Figure 2.1-23

1. Wind Turbine Generator. Each turbine is made of the following basic components:

- 1.1. *Tower structure.*
- 1.2. *Rotor with two or three blades attached to the hub.*
- 1.3. *High speed and low speed shaft.*
- 1.4. *Mechanical gear box.*
- 1.5. *Electrical generator.*
- 1.6. *Yaw mechanism, such as the tail vane.*
- 1.7. *Sensors and control.*
- 1.8. *Converters (in the case of Type 3 and 4 WTG's).*
- 1.9. *Step-Up (LV/MV) Solar Power Transformer Station.*
- 1.10. *MV Ring Main Units*

2. Medium Voltage (MV) Switchgear
3. Medium Voltage (MV) Capacitor Banks
4. Step-Up (MV/HV) Power Transformer
5. HV Primary Transmission Substation

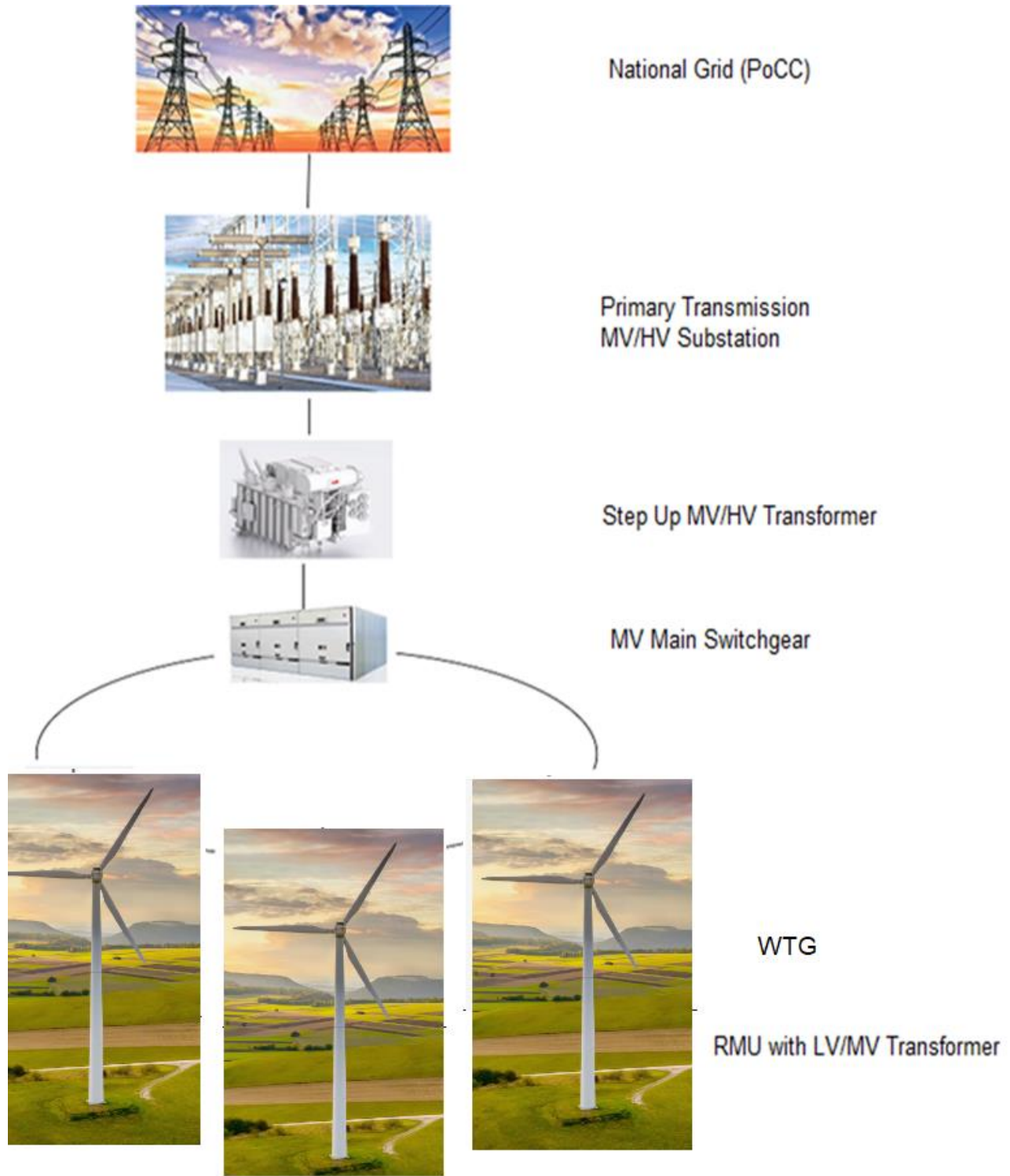


**Figure 2.1-23:**Block Diagram of a Large-Scale Grid Connected Wind Farm

### 2.1.3.2 What Causes Wind?

Wind is simply the movement of air, and this movement of air is created due to pressure differences within the atmosphere. When we have low-pressure; it is because the air is being heated up by the sun, so it gets warmer and less dense, and this causes the air to rise through the atmosphere, on the other hand, when we have a high pressure, the air gets cooler, denser and this will cause the air to descend in the atmosphere. Whenever we have a pressure difference within the system, these pressures will try and equalize, as the pressure equalizes, we will get the high-pressure area moving into the low-pressure area, and the process is continuous.

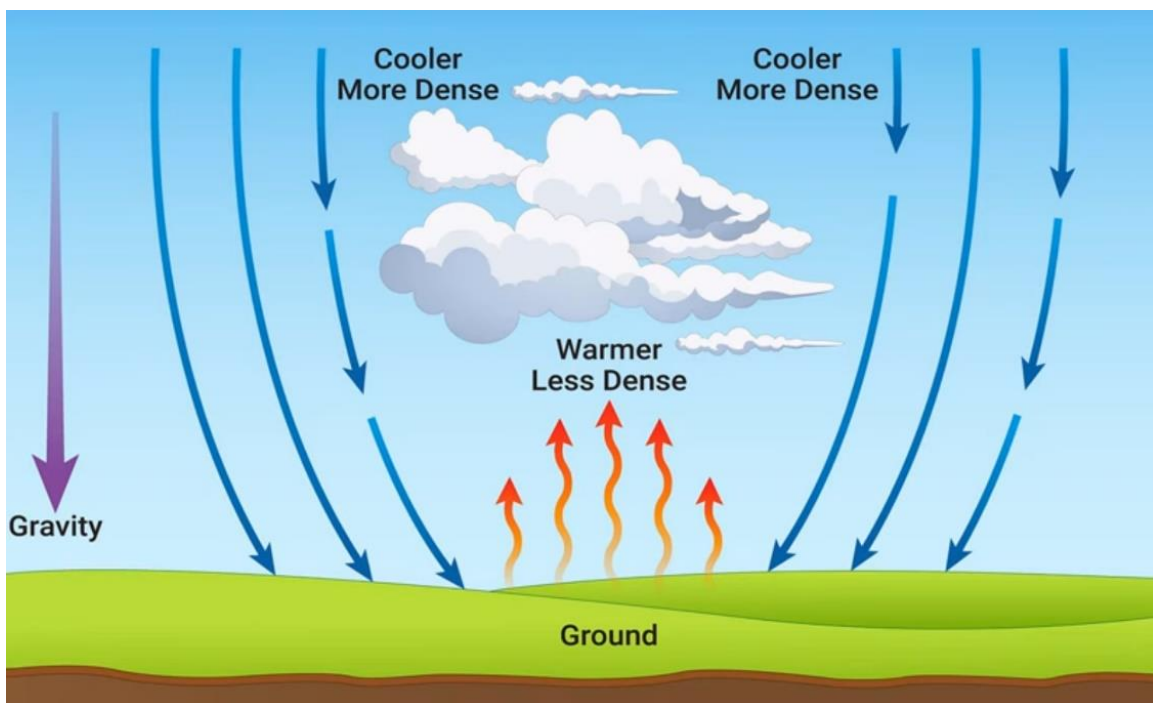


**Figure 2.1-24:** Atmospheric Pressure Difference and Movement of Air

Depending on the pressure difference will get either rapid movement of air from the high-pressure area to the low-pressure area or perhaps will have more gradually, the larger the pressure difference the more movement will be going to get and as a result more wind we will get.

The earth receives around  $1.7 \times 10^{14}$  kW of power from the sun in the form of solar radiation. This radiation heats up the atmospheric air. The intensity of this heating will be more at the equator ( $0^\circ$  latitude) as the sun is directly overhead.

Air around the poles gets less warm, as the angle at which the radiation reaches the surface is more acute. The density of air decreases with an increase in temperature. Thus, lighter air from the equator rises up into the atmosphere to a certain altitude and then spreads around. This causes a pressure drop around this region, which attracts the cooler air from the poles to the equator. This movement of air causes the wind.

Air moves from high-pressure areas to low-pressure areas. And the bigger the difference between the pressures, the faster the air will move from the high to the low pressure. That rush of air is the wind we experience.

Wind results from a horizontal difference in air pressure and since the sun heats different parts of the Earth differently, causing pressure differences, the Sun is the driving force for most winds.

The wind turbine captures the wind’s kinetic energy in a rotor consisting of two or more blades mechanically coupled to the hub and driving an electrical generator via speed step-up gear box.

**2.1.3.3 Power Available in the Wind**

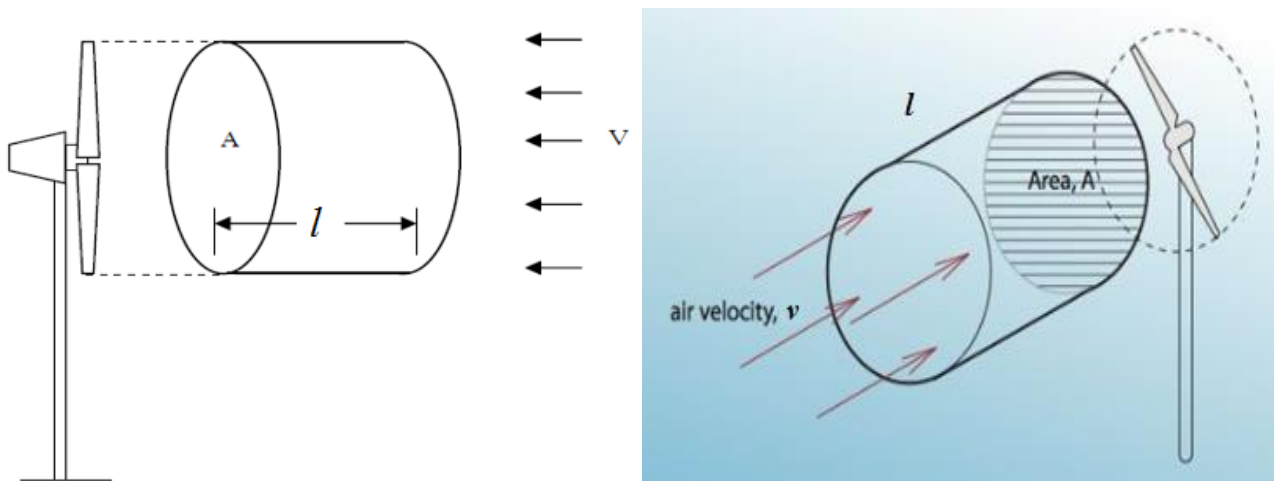


**Figure 2.1-25:** Stream of Air of mass **m** and moving with velocity **v** Facing Wind Turbine Rotor

The kinetic energy in a stream of air of mass **m** moving with speed **V** is given by the following (in joules):

$$E = \frac{1}{2}mV^2$$

The power in moving air is the flow rate of kinetic energy per second (in watts):

$$P = \frac{dE}{dt} = \dot{E} = \frac{1}{2} \dot{m} V^2$$

But the mass  $m$  equals the product of air density  $\rho$  and its volume  $v$

$$m = \rho_a \times v$$

The volume  $v$  of stream of air equals to  $A \times l$

$$m = \rho_a \times (A_T \times l)$$

The mass flow rate

$$\dot{m} = \frac{dm}{dt} = \frac{d}{dt} \{ \rho_a \times (A_T \times l) \}$$

$$\dot{m} = \frac{dm}{dt} = \rho_a A_T \frac{dl}{dt}$$

But the rate of change for the distance  $\frac{dl}{dt}$  is the velocity  $V$ .

$$\dot{m} = \rho_a A_T V$$

$$P = \frac{dE}{dt} = \frac{1}{2} \dot{m} V^2 = \frac{1}{2} (\rho_a A_T V) V^2 = \frac{1}{2} \rho_a A_T V^3$$

$$P = \frac{1}{2} \rho_a A_T V^3$$

$P$  = mechanical power in the moving air (watts),

$\rho_a$  = air density (kg/m<sup>3</sup>),

$A_T$  = area swept by the rotor blades (m<sup>2</sup>), and

$V$  = velocity of the air (m/sec)

The factors influencing the power available in the wind stream:

1. The air density.
2. Area of the wind rotor
3. The wind velocity.

#### 2.1.3.4 Wind Velocity

The effect of the **wind velocity** is more prominent owing to its cubic relationship with the power. The following are calculations for power available in the wind at three different velocities for one of the wind turbines. The calculations will show what happens when you double, then triple the velocity. Take a moment to think about how much available power will increase if you double and triple the velocity:

The standard density of air is  $1.225 \text{ kg/m}^3$

The turbine has a **24 m diameter**, which means the **radius is 12 m**. Thus, the swept area of the turbine is:  $\pi r^2 = 3.14159(12^2) = 452.4 \text{ m}^2$

At 6 m/s:

The power in the wind at 6 m/s is

$$P = \frac{1}{2} \rho_a A_T V^3 = \frac{1}{2} \times 1.225 \times 452.4 \times 6^3 = 59,851 \text{ W} = 59.85 \text{ kW}$$

At 12 m/s:

The power in the wind at 12 m/s is (8 times as large)

$$P = \frac{1}{2} \rho_a A_T V^3 = \frac{1}{2} \times 1.225 \times 452.4 \times 12^3 = 478,808 \text{ W} = 478.8 \text{ kW}$$

At 18 m/s:

The power in the wind at 18 m/s is (27 times as large)

$$P = \frac{1}{2} \rho_a A_T V^3 = \frac{1}{2} \times 1.225 \times 452.4 \times 18^3 = 1,615,979 \text{ W} = 1,615 \text{ kW}$$

As you can see, when the velocity doubles, the power increased by a factor of 8 and when the velocity triples, it increases by a factor of 27. This is because the velocity is cubed:

$$2^3 = 8 \text{ and } 3^3 = 27.$$

#### 2.1.3.5 AIR DENSITY

Wind power also varies linearly with the air density sweeping the blades. The air density  $\rho$  varies with pressure and temperature in accordance with the gas law:

$$P V = n R T$$

Where

**P** is the pressure

**V** is the volume of the gas

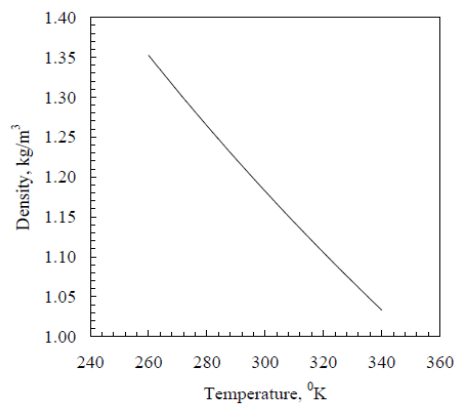
**n** is the number of kilo moles of the gas

**R** is the universal gas constant **T** is the temperature

The air density at sea level at 1 atm (14.7 psi) and **60°F** is **1.225 kg/m<sup>3</sup>**.

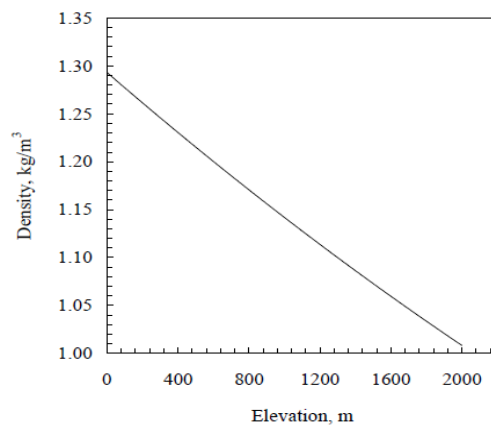
$$C^{\circ} = \frac{5}{9}(F^{\circ} - 32) = \frac{5}{9}(60 - 32) = 15.55^{\circ}\text{C}$$

$$\rho = \rho_o - (1.194 \times 10^{-4} H_m)$$



The temperature varies with the elevation as follows in °C:

$$T = 15.5 - \frac{19.83 H_m}{3048}$$



The density of air decreases with the increase in site elevation and temperature as the air density may be taken as 1.225 kg/m<sup>3</sup> for most of the practical cases.

Due to this relatively low density, wind is rather a diffused source of energy.

Hence large sized systems are often required for substantial power production.

#### **2.1.3.6 ROTOR-SWEPT AREA**

As seen in the preceding power equation, the output power of the wind turbine varies linearly with the rotor-swept area. For the **horizontal-axis turbine**, the rotor-swept area is

$$A = \frac{\pi}{4} D^2$$

Where  $D$  is the rotor diameter

For the Darrieus **vertical-axis machine**, determination of the swept area is complex as it involves elliptical integrals. However, approximating the blade shape as a parabola leads to the following simple expression for the swept area:

$A = \frac{2}{3}$  (maximum rotor width at the center) x (height of the rotor)

$$A = \frac{2}{3} (W \times H)$$

The most prominent factor deciding the power available in the wind spectra is its **velocity**.

When the wind velocity is doubled, the available power increases by 8 times. In other words, for the same power, rotor area can be reduced by a factor of 8, if the system is placed at a site with double the wind velocity. The advantages are obvious. Hence, selecting the right site play a major role in the success of a wind power projects.

That's why two potential wind sites are compared in terms of the specific wind power expressed in watts per square meter of area swept by the rotating blades. It is also referred to as the power density of the site, and is given by the following expression in watts per square meter of the rotor-swept area:

$$\text{Specific Power at Site} = \frac{1}{2} \rho_a V^3$$

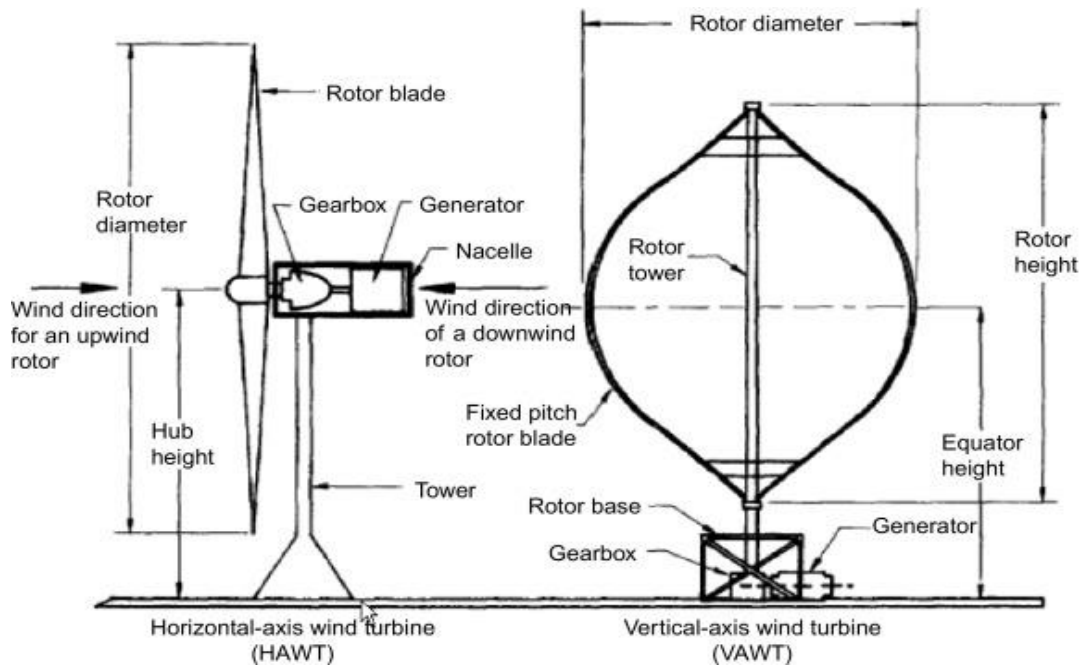


**Figure 2.1-26: HAWT vs VAWT**

Two distinctly different configurations are available for turbine design, the **horizontal-axis** configuration and the **vertical-axis** configuration. The horizontal-axis machine has been the standard in Denmark from the beginning of the wind power industry. Therefore, it is often called the *Danish wind turbine*. The vertical-axis machine has the shape of an egg beater and is often called the *Darrieus rotor* after its inventor. It has been used in the past because of its specific structural advantage. However, most modern wind turbines use a horizontal-axis design. Except for the rotor, most other components are the same in both designs, with some differences in their placements.

### 2.1.3.7 POWER EXTRACTED FROM THE WIND

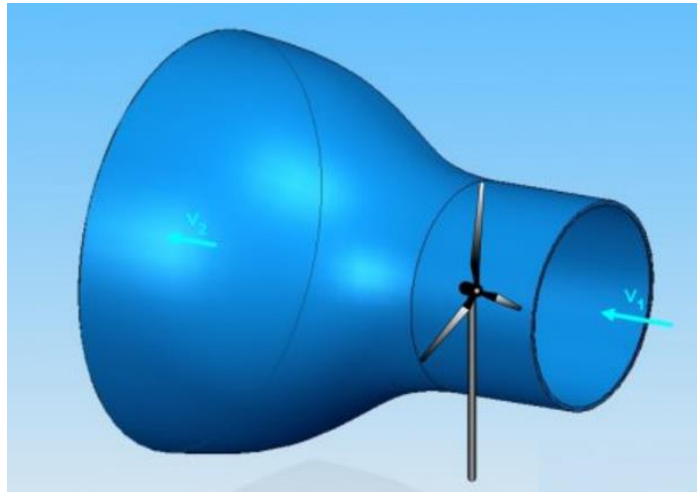


**Figure 2.1-27:** Upstream and Down-stream Wind.

The actual power extracted by the rotor blades is the difference between the upstream and downstream wind powers:

$$P_o = \frac{1}{2} \dot{m} V_1^2 - \frac{1}{2} \dot{m} V_2^2$$

$$P_o = \frac{1}{2} \dot{m} (V_1^2 - V_2^2)$$

Where:

$P_o$  = mechanical power extracted by the rotor, i.e., the turbine output power,

$V_1$  = upstream wind velocity at the entrance of the rotor blades, and

$V_2$  = downstream wind velocity at the exit of the rotor blades.

The air velocity is discontinuous from  $V_1$  to  $V_2$ , at the “plane” of the rotor blades, with an “average” of  $\frac{1}{2}(V_1 + V_2)$ . Multiplying the air density by the average velocity, therefore, gives the mass flow rate of air through the rotating blades, which is as follows:

$$\dot{m} = \rho_a A_T V_{ave} = \rho_a A_T \left\{ \frac{V_1 + V_2}{2} \right\}$$

The mechanical power extracted by the rotor, which drives the electrical generator, is therefore.

$$P_o = \frac{1}{2} \dot{m} (V_1^2 - V_2^2)$$

$$P_o = \frac{1}{2} \left[ \rho_a A_T \frac{V_1 + V_2}{2} \right] (V_1^2 - V_2^2)$$

The preceding expression is algebraically rearranged in the following form:

$$P_o = \frac{1}{2} \rho_a A_T V_1^3 \left[ \frac{1}{2} \left( 1 + \frac{V_2}{V_1} \right) \right] \left( 1 - \frac{V_2^2}{V_1^2} \right)$$

Changing the velocities subscripts as below

$V_1 = V$  = upstream wind velocity at the entrance of the rotor blades, and

$V_2 = V_o$  = downstream wind velocity at the exit of the rotor blades.

$$P_o = \frac{1}{2} \rho_a A_T V^3 \left\{ \left[ \frac{1}{2} \left( 1 + \frac{V_o}{V} \right) \right] \left( 1 - \frac{V_o^2}{V^2} \right) \right\}$$

$$P_o = \frac{1}{2} \rho_a A_T V^3 \frac{\left( 1 + \frac{V_o}{V} \right) \left( 1 - \frac{V_o^2}{V^2} \right)}{2}$$

The power extracted by the blades is customarily expressed as a fraction of the upstream wind power in watts as follows:

$$P_o = \frac{1}{2} \rho_a A_T V^3 C_p$$

Where  $C_p$

$$C_p = \frac{\left( 1 + \frac{V_o}{V} \right) \left( 1 - \frac{V_o^2}{V^2} \right)}{2}$$

$$C_p = \frac{P_T}{\frac{1}{2} \rho_a A_T V^3} = \frac{2 \times P_T}{\rho_a A_T V^3}$$

We can say that  $C_p$  is the fraction of the upstream wind power that is extracted by the rotor blades and fed to the electrical generator. The remaining power is dissipated in the downstream wind. The factor  $C_p$  is called the **power coefficient** of the rotor or the **rotor efficiency**.

For a given upstream wind speed, above Equation clearly shows that the value of  $C_p$  depends on the ratio of the downstream to the upstream wind speeds ( $V_o/V$ ). A plot of power vs. ( $V_o/V$ ) shows that  $C_p$  is a single-maximum-value function. It has the maximum value of 0.59 when the  $V_o/V$  ratio is one third. The maximum power is extracted from the wind at that speed ratio, i.e., when the downstream wind speed equals one third of the upstream speed. Under this condition (in watts):

$$P_{max} = \frac{1}{2} \rho_a A_T V^3 \times 0.59$$

The theoretical maximum value of  $C_p$  is **0.59**.

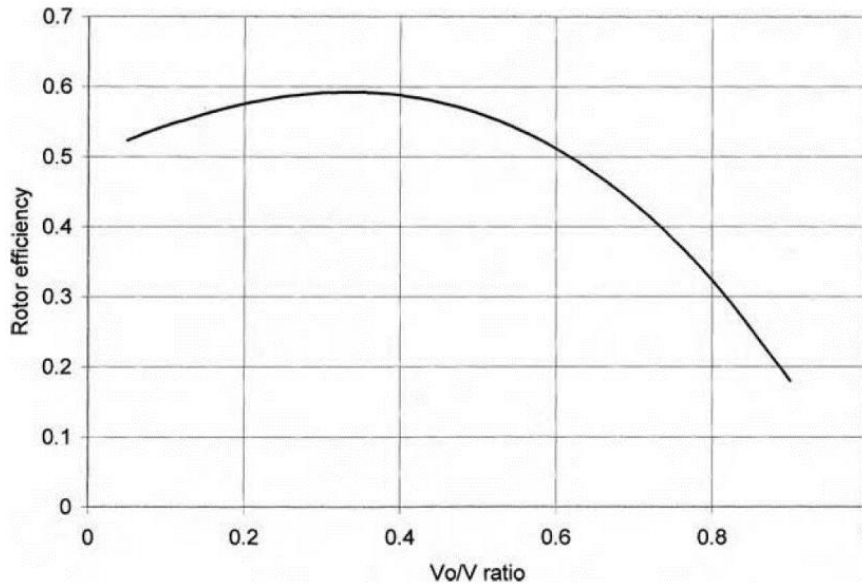


**Figure 2.1-28:** Cp curve vs Vo/V ratio

$C_p$  is often expressed as a function of the rotor tip-speed ratio (TSR) as shown in Figure 3.4. TSR is defined as the linear speed of the rotor's outermost tip to the upstream wind speed.

In practical designs, the maximum achievable  $C_p$  ranges between 0.4 and 0.5 for modern high speed two-blade turbines, and between 0.2 and 0.4 for slow-speed turbines with more blades. If we take **0.5** as the practical maximum rotor efficiency, the maximum power output of the wind turbine becomes a simple expression (in watts per square meter of swept area):

$$P_{max} = \frac{1}{4} \rho_a V^3$$

### 2.1.3.8 AERODYNAMICS OF WIND TURBINE, THRUST FORCE AND TORQUE COEFFICIENT

Aerodynamics deals with the motion of air or other gaseous fluids and the forces acting on bodies moving through them.

Earlier initiatives in this direction relied more on the aviation industry. Aerodynamic theories developed for airplanes and helicopters were adopted for defining the performance of wind turbines. However, now, theories are specifically formulated for wind turbines which are further refined and reinforced with the help of experimental techniques.

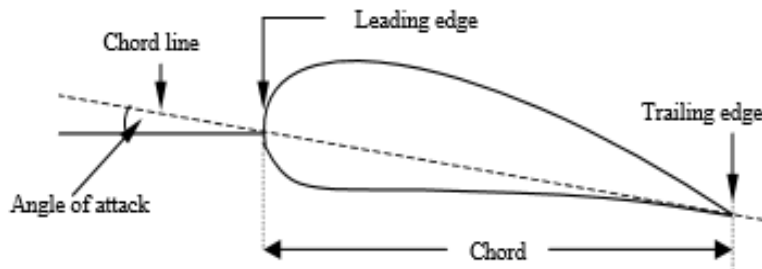


Figure 2.1-29: Important Parameters of an Airfoil

When an airfoil is placed in a wind stream, air passes through both upper and lower surfaces of the blade.

Due to the typical curvature of the blade, air passing over the upper side has to travel more distance per unit time than that passing through the lower side. Thus, the air particles at the upper layer move faster than those at the lower. According to Bernoulli's theorem, this should create a low-pressure region at the top of the airfoil. This pressure difference between the upper and lower surfaces of the airfoil will result in a force  $F$ .

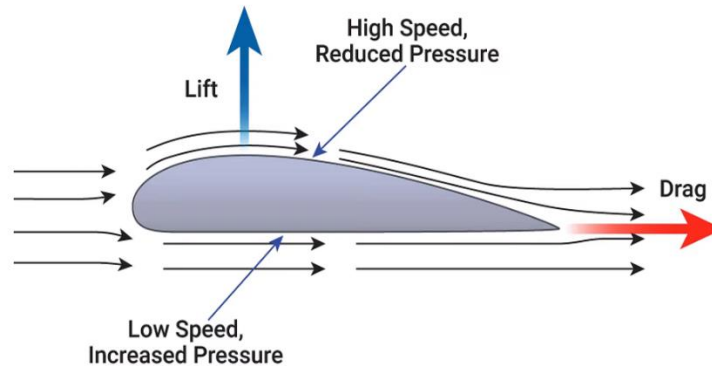


Figure 2.1-30: Lift and Drag Force due to Pressure difference.

The thrust force experienced by the rotor (F) can be expressed as

$$F = \frac{1}{2} \rho_a A_T V^2$$

The component of this force perpendicular to the direction of the undisturbed flow is called the lift force L, while, the force in the direction of the undisturbed flow is called the drag force D.

The lift force (L) is given by:

$$L = C_L \times \frac{1}{2} \rho_a A_T V^2$$

And the drag force (D) by

$$D = C_D \times \frac{1}{2} \rho_a A_T V^2$$

Hence, we can represent the rotor torque (T) as

$$T = F \times R = \frac{1}{2} \rho_a A_T V^2 \times R$$

Where  $R$  is the radius of the rotor. This is the maximum theoretical torque and in practice the rotor shaft can develop only a fraction of this maximum limit.

The ratio between the actual torque developed by the rotor and the theoretical torque is termed as the torque coefficient ( $C_T$ ). Thus, the torque coefficient is given by:

$$C_T = \frac{T_T}{\frac{1}{2} \rho_a A_T V^2 \times R} = \frac{2 \times T_T}{\rho_a A_T V^2 \times R}$$

Where  $T_T$  is the actual torque developed by the rotor.

The power developed by a rotor at a certain wind speed greatly depends on the relative velocity between the rotor tip and the wind.

For example, consider a situation in which the rotor is rotating at a very low speed and the wind is approaching the rotor with a very high velocity. Under this condition, as the blades are moving slow, a portion of the air stream approaching the rotor may pass through it without interacting

with the blades and thus without energy transfer. Similarly, if the rotor is rotating fast and the wind velocity is low, the wind stream may be deflected from the turbine and the energy may be lost due to turbulence and vortex shedding. In both the above cases, the interaction between the rotor and the wind stream is not efficient and thus would result in poor power coefficient.

The ratio between the velocity of the rotor tip and the wind velocity is termed as the tip speed ratio (TSR or  $\lambda$ ). Thus,

$$\lambda = \frac{\omega R}{V}$$

The power coefficient and torque coefficient of a rotor vary with the tip speed ratio. There is an optimum  $\lambda$  for a given rotor at which the energy transfer is most efficient and thus the power coefficient is the maximum ( $C_{P \max}$ ).

Let us consider the relationship between the power coefficient and the tip speed ratio.

The power developed in the rotor  $P_T$  can be expressed as

$$P_T = T_T \times \omega$$

$$C_p = \frac{2 P_T}{\rho_a A_T V^3} = \frac{2 \times T_T \times \omega}{\rho_a A_T V^3}$$

$C_p$  can be re-written as below.

$$C_p = \frac{2 P_T}{\rho_a A_T V^3} = \frac{2 T_T \times \omega}{\rho_a A_T V^2 \times V} = \frac{2 T_T}{\rho_a A_T V^2} \times \frac{\omega}{V}$$

But we know that TSR can be expressed as below.

$$\lambda = \frac{\omega R}{V} \Rightarrow \frac{\omega}{V} = \frac{\lambda}{R}$$

Substituting in  $C_p$

$$C_p = \frac{2 T_T}{\rho_a A_T V^2} \times \frac{\lambda}{R}$$

$$C_p = \frac{2 T_T}{\rho_a A_T V^2 R} \times \lambda$$

But we know that torque coefficient  $C_T$  is expressed as below:

$$C_T = \frac{2 \times T_T}{\rho_a A_T V^2 \times R}$$

Substituting in  $C_p$

$$C_p = \frac{2 T_T}{\rho_a A_T V^2 R} \times \lambda \Rightarrow C_p = C_T \times \lambda$$

$$\lambda = \frac{C_p}{C_T}$$

Thus, the tip speed ratio is given by the ratio between the power coefficient  $C_p$  and torque coefficient  $C_T$  of the rotor.

The pressure difference between the upper and lower surfaces of the airfoil will result in a force **F**. The reason of using **air foil** shape is that we want to generate lift. Lift is a force that occurs when a fluid flows over an airfoil, we convert the kinetic energy into lift. And lift acts perpendicular to the flow directions, and we use different shapes of the airfoil depending on the fluid and fluid velocity.

#### **2.1.3.9 SYSTEM COMPONENTS**

The wind power system (wind farm) comprises one or more wind turbine units operating electrically in parallel.

Each turbine is made of the following basic components:

- Tower structure
- Rotor with two or three blades attached to the hub
- High speed and low speed shaft
- Mechanical gear box
- Electrical generator
- Yaw mechanism, such as the tail vane
- Sensors and control
- Anemometers, which measure the wind speed and transmit the data to the controller.
- Numerous sensors to monitor and regulate various mechanical and electrical parameters. A 1-MW turbine may have several hundred sensors.
- Stall controller, which starts the machine at set wind speeds of 8 to 15 mph and shuts off at 50 to 70 mph to protect the blades from overstressing and the generator from overheating.
- Power electronics to convert and condition power to the required standards.

- Control electronics, usually incorporating a computer.
- Battery for improving load availability in a stand-alone plant.
- Transmission link for connecting the plant to the area grid.

The following are commonly used terms and terminology in the wind power industry:

**Tower:** It is where wind turbine, nacelle and rotor sit upon

**Nacelle:** The rotor attaches to the nacelle, which sits atop the tower and includes a gearbox, low- and high-speed shafts, generator, controller, and a brake. A cover protects the components inside the nacelle. Some nacelles are large enough for technicians to stand inside while working.

**Rotor:** consists of the blades and rotor hub

**Blade:** Manufactured from fiber glass, some from wood (small turbine ) some from epoxy resin mixture and this depends on the size of the blades and the conditions which they will be operating

**Pitch:** Blades are turned, or pitched, out of the wind to keep the rotor from turning in winds that have speeds too high or too low to produce electricity.

**Low-speed shaft:** The rotor turns the low-speed shaft at 30 to 60 rotations per minute (rpm), however for very big (large) turbine 5-12 RPM

**Gearbox:** Gears connect the low-speed shaft to the high-speed shaft and increase the turbine speed from 30 to 60 rpm to the 1200 to 1800 rpm required by most generators to produce electricity in an efficient manner.

Because the gearbox is a costly and heavy part, design engineers are exploring slow-speed, direct-drive generators that need no gearbox.

**High-speed shaft:** It drives the generator via a speed step-up gear.

**Brake:** A disc brake, which stops the rotor in emergencies. It can be applied mechanically, electrically, or hydraulically.

**Generator:** It is usually an off-the-shelf induction generator that produces 50- or 60-Hz AC power.

**Upwind and downwind:** The upwind turbine operates facing into the wind in front of the tower, whereas the downwind runs facing away from the wind after the tower.

**Vane:** It measures the wind direction and communicates with the yaw drive to orient the turbine properly with respect to the wind.

**Yaw drive:** It keeps the upwind turbine facing into the wind as the wind direction changes. A yaw motor powers the yaw drive. Downwind turbines do not require a yaw drive, as the wind blows the rotor downwind.

The design and operating features of various system components are described in the following subsections.

To summarize, the main components constituting horizontal axis wind turbines are (see **Figure 2.1-31**):

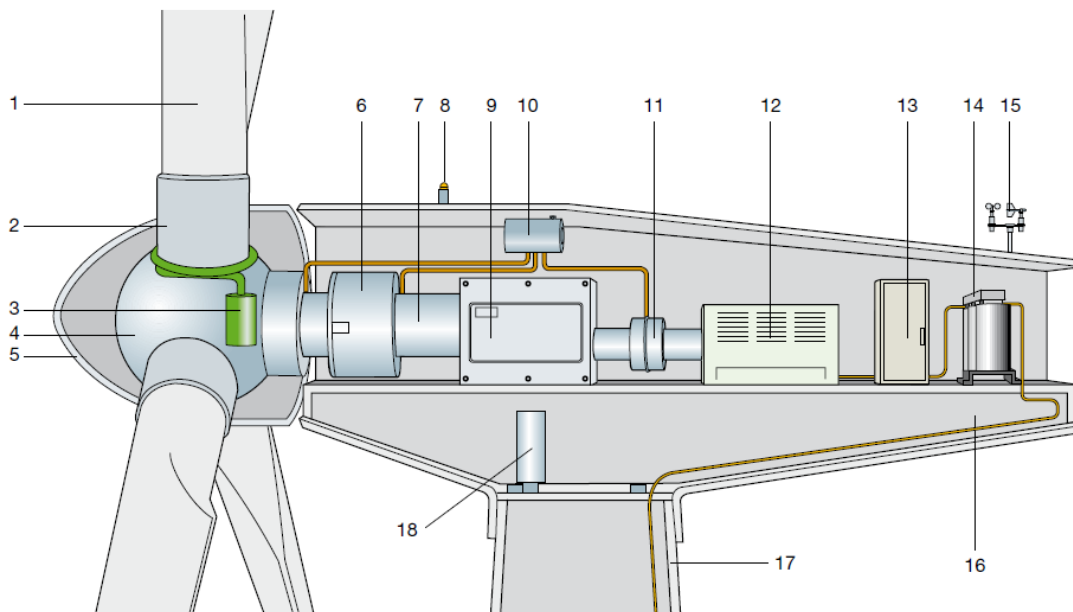


**Figure 2.1-31:** Main Components of Horizontal Axis Wind Turbine

1. Blade
2. Blade support
3. Pitch angle actuator
4. Hub
5. Spinner
6. Main support
7. Main shaft
8. Aircraft warning lights

- 9. Gearbox
- 10. Hydraulic cooling devices
- 11. Mechanical brakes
- 12. Generator
- 13. Power converter and electrical control, protection and disconnection devices
- 14. Transformer
- 15. Anemometers
- 16. Frame of the nacelle
- 17. Supporting tower
- 18. Yaw driving device

**2.1.3.10 Classification of Generators for Wind Turbines**

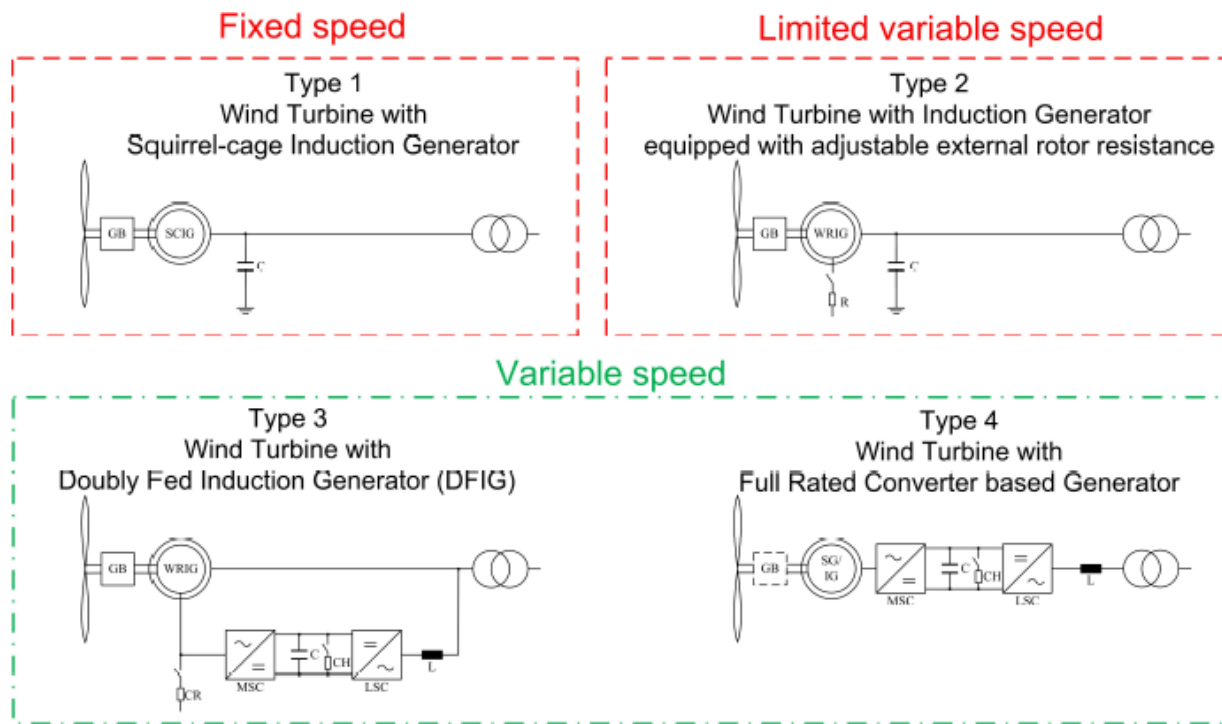


Figure 2.1-32: Classification of Wind Turbines Technologies

### 2.1.3.11 AC Generator Technologies

#### 2.1.3.11.1 Type 1: Direct-Connected Induction (Asynchronous) Generator: Squirrel Cage Induction Generator

Sometimes referred to as fixed-speed wind turbines employ stall-regulated (fixed-pitch) blades connected to a hub, which is coupled via a gearbox to a conventional squirrel-cage induction generator ( $N_m > N_s$ ). The generator is directly connected to the line (grid) and it injects active power  $P$  and absorbs reactive power  $Q$  (in other words, it does not have reactive power support), and may have automatically switched shunt capacitors for reactive power compensation and possibly a soft-start mechanism which is bypassed after the machine has been energized, where if we don't compensate for the reactive power consumption we may experience problem with the voltage stability at the terminal of the wind turbine.

The speed range of the turbine is fixed by the torque vs. speed characteristics of the induction generator. Some of these turbines do not have blade-pitching capability. Although simple, relatively robust and reliable, there are significant disadvantages of this technology, namely that energy capture from the wind is sub-optimal and reactive power compensation is required.

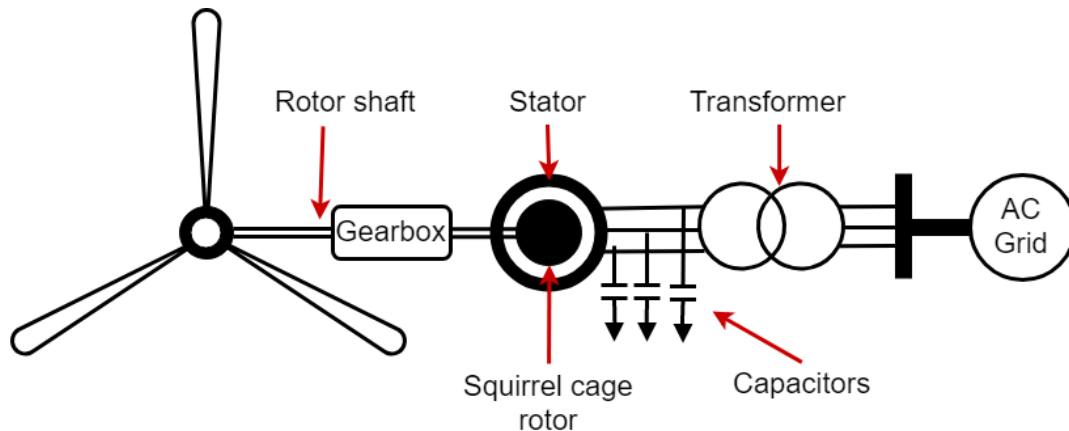
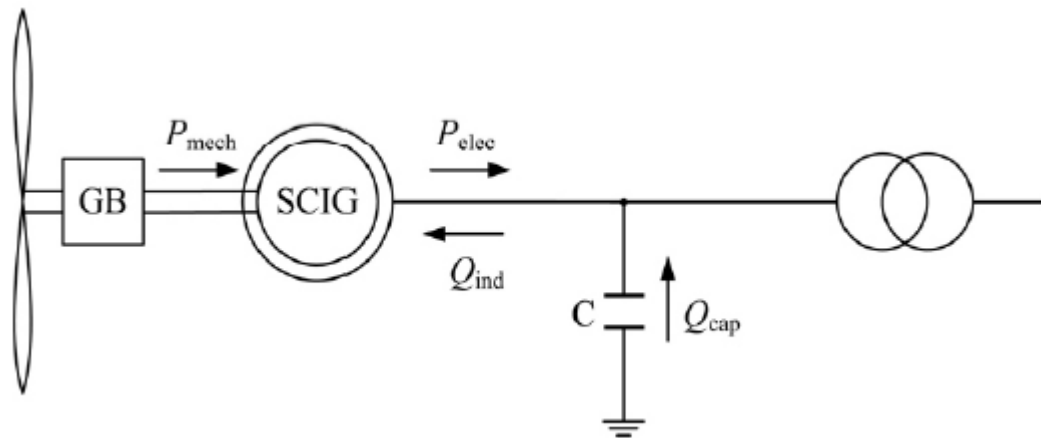


Figure 2.1-33:Squirrel cage Induction Generator block diagram.

### Sequence of Operation:



**Figure 2.1-34:** Power Flow for Squirrel Cage Induction Generator

- 1- Rotor and magnetic field rotate at the same speed in asynchronous generator.
- 2- Initially it draws current from the grid as in the case of a motor.
- 3- The speed picks up and the rotation of the wind turbine causes the system to exceed the synchronous limit  $N_s$ .
- 4- Thus, rotor moves faster than the rotating magnetic field. At speeds higher than ( $N_s$ ), the torque is negative. Thus, current flows in the opposite direction, that is from the system to the grid.
- 5- Thus, the machine functions as a generator when it is driven by an external prime mover, like the wind turbine in our case.

The generator speed depends on the torque applied by the turbine.

External excitation is essential for an induction generator before it is put to work. However, in standalone mode, external devices like capacitors or batteries are required to provide the necessary excitation current to the generator.

A wind turbine can be designed to run at fixed or variable speeds. In fixed speed turbines, the rotor is coupled with an induction generator via speed increasing gears. The stator winding of the generator is directly wired to the grid. Induction generators require excitation power from

the grid. This may result in undesirable voltage variations. To avoid this problem, capacitors are provided in the circuit.

**2.1.3.11.2 Type 2: Wound-Rotor Induction Generator with External Resistance Control**

Sometimes referred to as variable-slip wind turbines (not much + 10~20% speed) employ a wound rotor induction generator with a mechanism for controlling the magnitude of the rotor current through adjustable external rotor circuit resistors, and pitch regulation of the turbine blades to assist in controlling speed. The speed range of the turbine is widened because of the external resistors.

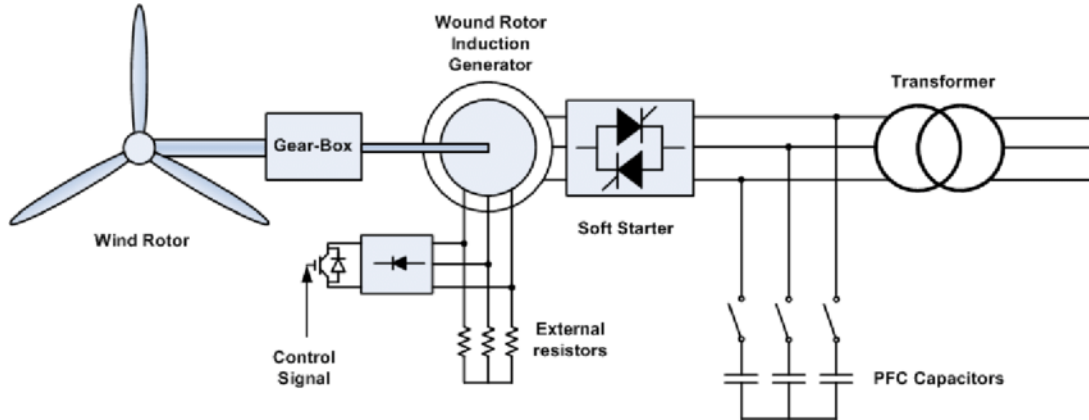


Figure 2.1-35: Wound Rotor Induction Generator block diagram.

**Sequence of Operation:**

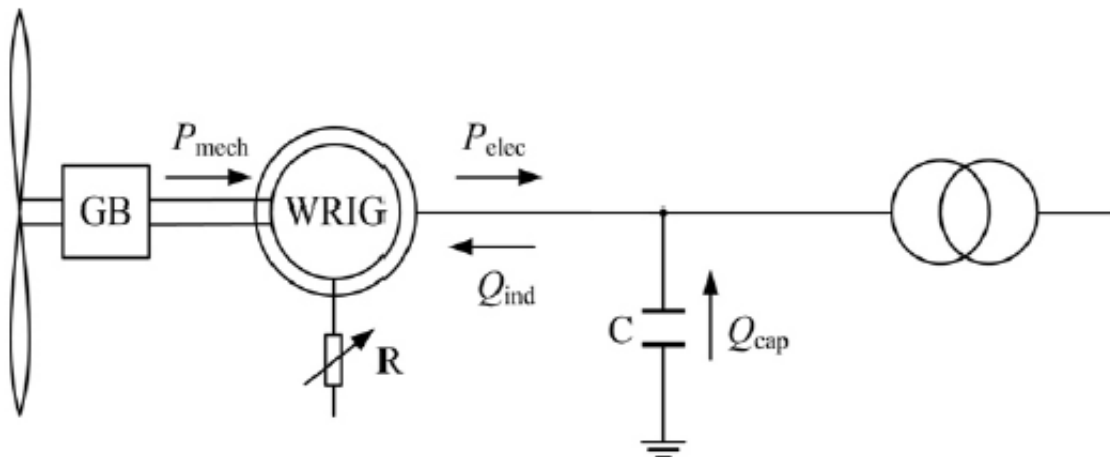


Figure 2.1-36: Power Flow for Wound Rotor Induction Generator

- 1- In WRIG slight improvement in speed range by increasing the rotor resistance, such arrangements tend to increase the speed range by about 2–10%

- 2- Increased losses in the external rotor resistance
- 3- wind fluctuations increase the mechanical stress on the turbine shaft.
- 4- In the case of a weak grid, severe voltage fluctuations might be caused by WRIG.
- 5- Inductive reactive power demand by the generator requires compensation devices, such as capacitor banks.
- 6- Gearbox necessary.

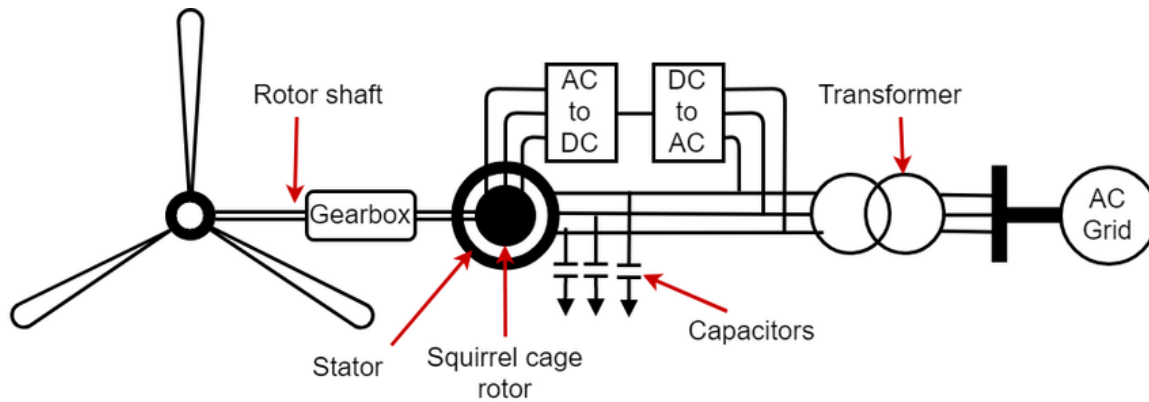
In above types 1 and 2, we have less control in speed (frequency) is available ...but if we take 2 MW WTG connected with 20,000 GW grids ...it will never have this much impact. In type 1 and 2, we need to provide additional reactive power support, and they need to be excited from the grid, and they don't have LVRT capabilities.

#### **2.1.3.11.3 Type 3: Doubly-fed Asynchronous Generator – DFAG: Doubly-fed Induction Generator - DFIG**

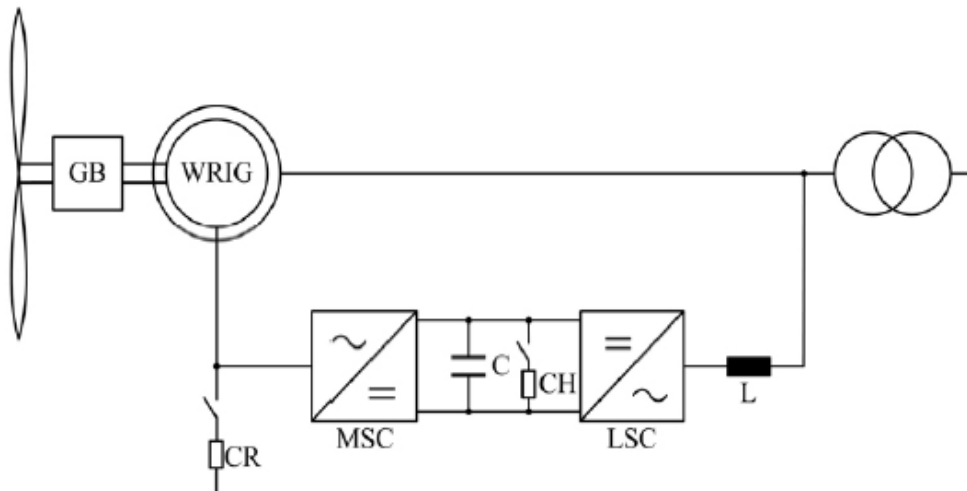
Sometimes referred to as doubly fed induction generator (DFIG) wind turbines employ a wound rotor induction generator where the rotor circuit is coupled to the line terminals through a **four-quadrant power converter** that's why it is called **IBR (Inverter-Based Resource)** which have capability to inject reactive power.

The converter provides for vector (magnitude and phase angle) control of the rotor circuit current, even under dynamic conditions, and substantially widens the operating speed range of the turbine.

Flux-vector control of rotor currents allows decoupled real and reactive power output, as well as maximized wind power extraction and lowering of mechanical stresses. Since the converter is only handling the power in the rotor circuit, it does not need to be rated at the machine's full output. Turbine speed is primarily controlled by actively adjusting the pitch of the turbine blades. 70% of power directly taken from stator, and 30% from the rotor



**Sequence of Operation:**

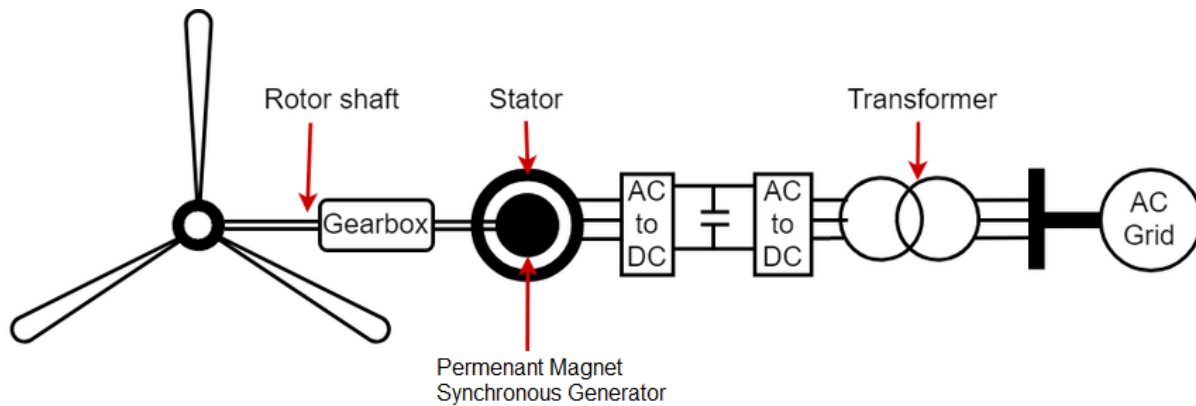


- 1- The stator of the machine is connected directly to the grid at system frequency while the rotor is fed from a power converter at slip frequency.
- 2- The Machine Side Converter (MSC) or sometime Rotor Side Converter (RSC), is connected to the rotor via slip rings and the second, the Line Side Converter (LSC), is connected to the grid.
- 3- The MSC injects voltage into the slip rings at slip frequency that is controlled in both magnitude and phase and allows both the torque (active power "P" control) and the power factor of the machine to be controlled (reactive power "Q" control) over a large speed range (typically +/- 30%).
- 4- LSC injects a voltage into the grid at grid frequency and is typically controlled to maintain a constant DC link voltage.
- 5- Between grid and LSC there is an inductance in order to improve the power quality provided from the converter.

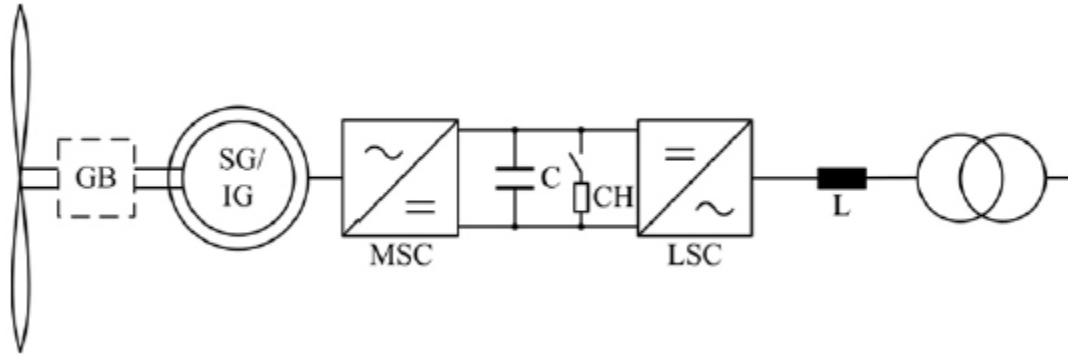
- 6- The capacitor connected in the DC-link acts as a constant, ripple free DC voltage source.
- 7- Rotor crowbar is designed to bypass the machine side converter, i.e. to short-circuit the rotor, in order to avoid overcurrent on the MSC as well as overvoltage on the DC-link capacitor.
- 8- DC-link chopper is provided in the DC-link bus to dissipate excess energy in the DC-link capacitor during a grid fault.

**2.1.3.11.4 Type 4: Variable Speed Turbine with Full-Rated Power Converter: Permanent Magnet Synchronous Generator**

Sometimes referred to as full-converter wind turbines employ a variable-speed wind turbine with a full-rated **power converter** between the electrical generator and the grid that’s why it is called **IBR (Inverter-Based Resource)** which have capability to inject reactive power. The power converter provides substantial decoupling of the electrical generator dynamics from the grid, such that the portion of the converter connected directly to the electrical system defines most of the characteristics and behavior important for power system studies. These turbines may employ synchronous or induction generators and offer independent real and reactive power control.



**Sequence of Operation**



1. The generator is completely decoupled from the power system, so the output frequency of the generator is different from the grid frequency.
2. a synchronous generator can have either an electrically excited rotor with salient poles or a rotor equipped with permanent magnets to provide the rotating magnetic field.
3. One attraction of the permanent magnet machine is its high efficiency since no magnetizing or field current is necessary to provide the magnetic field.
4. The induction generator can have a squirrel-cage induction generator in which the magnetization has to be provided by the machine side converter.

Type 3 and 4 are mostly used these days, and the higher capacities are type 4 specially in offshore wind. LVRT are majorly required for Type 3 and 4

#### 2.1.4 Collection MV/HV Substation



The collection MV/HV Substation collects the power from the PV plant/Wind farm. A ring system is utilized to maximize the number of PV/WTG IRR Units connected in series; however, radial systems are also employed in some PV/WF plants. MV power cables with cable terminations are utilized to connect medium voltage Ring Main Units (RMUs) in order to construct the MV PV/WF incoming feeder of the MV main switchgear.

The power supplied to the MV collecting switchgear will originate from the solar/wind farm and will be evacuated via MV/HV step-up power transformers. Additionally, the MV circuit breakers of Bus Tie circuits located at the MV Switchgear will enable emergency control of the power flow. Furthermore, if present, the MV capacitor banks, SVC's, and STATCOMS will be connected via the MV switchgear. Immediately following the MV/HV power transformer is the HV primary transmission substation, which serves as the PoCC (point of common coupling).

#### *2.1.4.1 Medium Voltage (MV) Power Cables*

To connect between the inverter stations and RMU's distributed all over the PV plant, MV power cables are used. Figure 2.1-37 shows constructional drawings for one example of MV power cables.

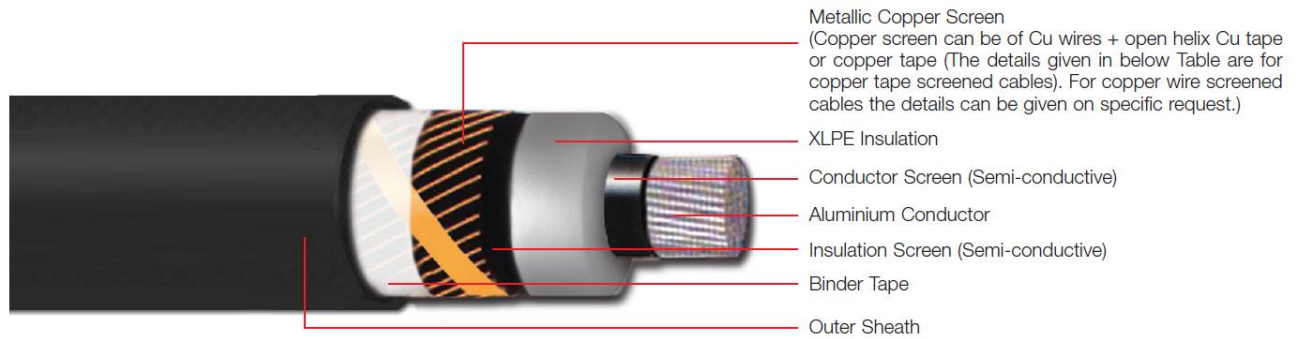


**Figure 2.1-37:** Constructional Drawings of MV Power Cable

#### 2.1.4.2 Medium Voltage (MV) Switchgear

MV switchgear collects the power generated from the inverter stations and evacuate it through the grid, The MV switchgear is also used to switch on/off circuits (PV Feeders, bus sections, step-up transformer feeders) in and out of the system.

There are two main types of the MV Switchgear:

- Air Insulated Switchgear (AIS)
- Gas Insulated Switchgear (GIS)

In this thesis the AIS switchgear will be discussed. Figure 2.1-38 shows an AIS switchgear ABB type UniGear ZS2.



**Figure 2.1-38:** MV Switchgear ABB type UniGear ZS2

#### 2.1.4.3 Step-Up (MV/HV) Power Transformer

After the MV switchgear comes the step-up transformer that steps up the AC voltage from the MV to the HV voltage level to be ready for grid connection. power transformers do not change power or frequency. Figure 2.1-39 shows a step-up transformer 3D drawing.

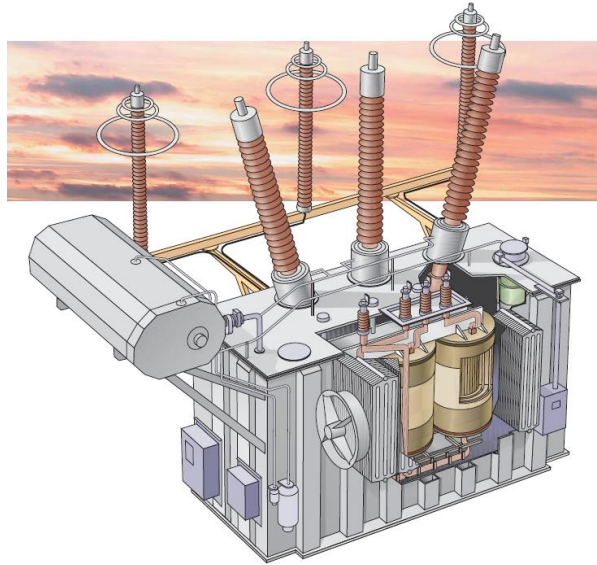


**Figure 2.1-39:** Step-Up Transformer 3D drawing

#### 2.1.4.4 Primary Transmission (MV/HV) Substation

A substation (Figure 2.1-40) high-voltage electric system facility which is made by an assemblage of electrical components including busbars, switchgears, power transformers, auxiliaries, etc. where the power flow of electrical energy takes place through electrical substation by switching on/off Generators, Substation equipment, and incoming /outgoing circuits or lines in and out of a system where each circuit has certain electrical components such as circuit breakers, isolators, current and voltage transformers, surge arresters ,etc. Also, Electrical substation used to change AC voltages from one level to another, and/or change alternating current (AC) to direct current (DC) or direct current (DC) to alternating current (AC).



**Figure 2.1-40: HV AIS Substation**

### **2.1.5 Power Quality Solutions**

Power quality refers to a quantitative measurement that quantifies the effectiveness with which power is used and delivered in terms of its levels of consistency, reliability, quality, stability, availability, and efficiency. Maintaining a high level of power quality is essential across the whole energy value chain. The substantial demand for power quality is triggered by multiple factors that are dispersed throughout the entire energy value chain, encompassing generation, transmission, and distribution. On the generation side, increased distributed generation, integration of more renewable energy sources (solar, wind), and increased energy production are all aspects to consider. On the transmission side, factors such as infrastructure deterioration, evolving regulations and grid code compliance, interregional energy trading, and reversible power flow are significant concerns. Increasing power consumption, new infrastructure in emerging markets, and more robust and rapid transportation systems comprise the distribution side. There is a strong correlation between voltage levels in a power system and reactive power.

Benefits of Power quality solutions:

1. Regulation and control of a defined voltage to the required set point under normal and contingency conditions.
2. Provides fast response reactive power following contingencies.
3. Preventing and reducing risk for voltage collapses in the grid.

4. Preventing over voltages at loss of load.
5. Boosting voltage during undervoltage disturbances such as faults.
6. Detecting and damping of active power oscillations.
7. Increased power transfer capability, by stabilizing voltage in weak points (heavy loads) in the grid.
8. Load balancing.

### 2.1.5.1 Reactive Power

Reactive power builds up magnetic fields and controls the voltage in an AC system. The reactive power needs space in transmission- and power lines, gives rise to losses in electric machines and apparatus and limits the utilization of the electrical energy in the equipment.

One way of describing reactive power in a simpler way is to liken it to a barge being towed along a canal, see picture in Figure 2.1-41. The barge is towed by means of the rope  $S$ , which therefore forms an angle,  $\Phi$ , to the direction of movement. The tensile stress in the rope may be divided into a force in the direction of movement  $P$  and a transverse force towards the canal bank  $Q$ . The force acting in the direction of movement is the useful active work. It is the work driving the barge forward. The force at right angles creates only a lateral pressure that contributes nothing to the movement of the barge and actually represents the loss of some of the energy from the horse.

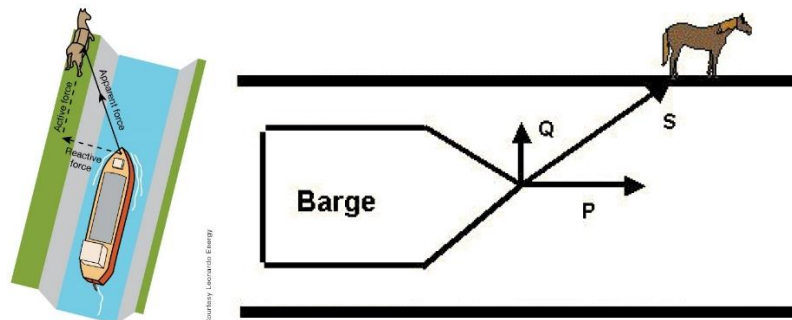


**Figure 2.1-41:** Active and Reactive Power Representation Example

Reactive power is present when the voltage and current are **not** in phase.

- One waveform leads the other.

- Phase angle not equal to 0°
- Power factor less than unity

Measured in volt-ampere reactive (var)

Produced when the current waveform leads voltage waveform (Leading power factor) or vice versa, consumed when the current waveform lags voltage (lagging power factor)

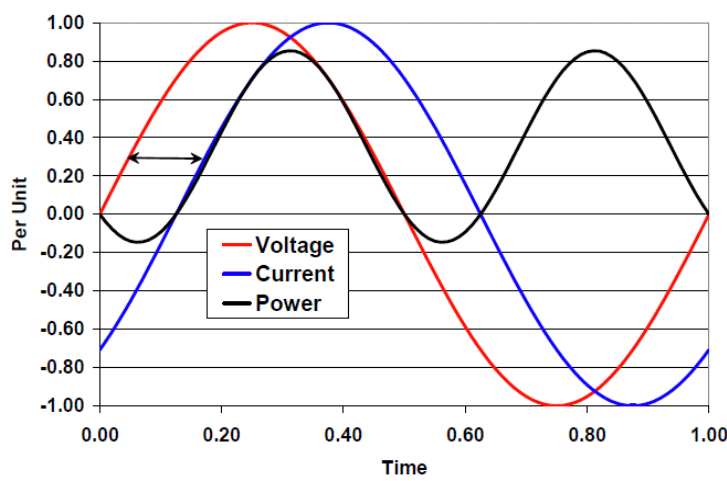


**Figure 2.1-42:** AC Voltage and Current Phase Shift

Below Table 2.1-1 shows the types of power, the description of each type, the formula, and phasor diagram

**Table 2.1-1:** Power Terminologies

Type	Description	Formula	Phasor Diagram
Active power (P)	It is the useful power that is doing the actual work. It is measured in W, kW, MW.	$P = S \times \cos \varphi$	
Reactive power (Q)	It is a consequence of an AC system. Reactive power is used to build up magnetic fields. It is measured in var, kvar, Mvar.	$Q = S \times \sin \varphi$ $Q = P \times \tan \varphi$	
Apparent power (S)	Or total power (S) is the combination of active and reactive power. Apparent power is measured in VA, kVA, MVA	$S = \sqrt{P^2 + Q^2}$	

### 2.1.5.2 Importance of Reactive Power

The voltage profile of the power transmission networks is significantly influenced by the reactive power control. Control of reactive power sufficiently improves power factor, transmission efficiency, system stability, and flat voltage profile maintenance at all power transmission levels. The intrinsic electrical properties of an electric power system are modified by means of the Series and Shunt Capacitor compensation methods.

Dynamic loads require reactive power to convert the input power into useful work. It is utilized to produce magnetic fields for their operations. All loads that need magnetic field to operate need a reactive power like power transformers, fluorescent lamps, electric arc furnace. Reactive power is required to maintain the voltage to deliver active power through transmission lines, and it needs to be supplied along with active power. Figure 2.1-43 shows the applications of reactive power requirements.

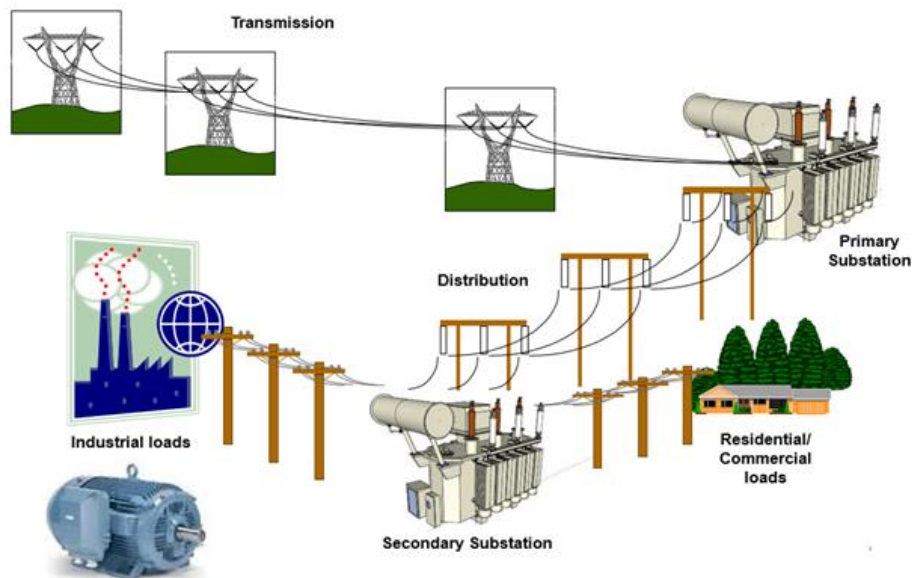
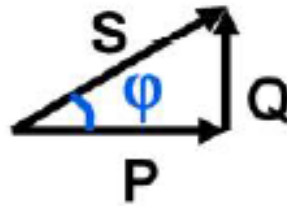


Figure 2.1-43: Applications of Reactive Power Requirements

#### 2.1.5.2.1 Power Factor Correction

It is a measurement of the efficiency in a system. Power factor describes the relationship between active  $P$  and apparent Power  $S$ . The power triangle is indicated in Figure 2.1-44



**Figure 2.1-44:** Power Triangle

The horizontal axis is the active power  $P$  and the vertical axis is the Reactive Power  $Q$ . The arc is the apparent power,  $S$ , which is the geometrical sum of  $P$  and  $Q$ . The vector is always on the arc and will give a different ratio of  $P$  and  $Q$  at different phase angles  $\varphi$ . If reactive power  $Q$  is injected from AC source outside the system, for instance by use of a capacitor bank, the phase angle  $\varphi_1$  is reduced to  $\varphi_2$  and the active Power drawn from the system is increased from  $P_1$  to  $P_2$ , but with the same apparent power (Total Power). The power factor, the ratio of active power compared to the apparent power has been increased from  $\cos\varphi_1$  to  $\cos\varphi_2$ .

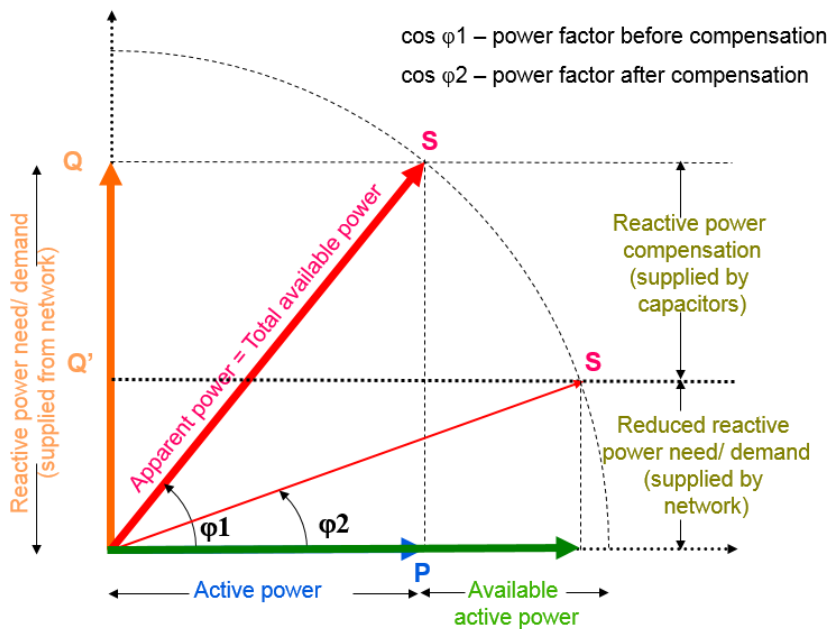


**Figure 2.1-45:** Power Factor Correction

Reactive power demand for the loads is catered by the generation/ grid, and the system capacity is often limited to the transformer capacity, besides, Reactive power gives rise to losses in

transformers, transmission lines & loads. Also, reactive power influences the voltage in transmission lines.

### 2.1.5.3 Static Shunt Compensator (Mechanically Switched Capacitor Bank)

On Medium Voltage side the shunt capacitor is used as a fixed or automatically switched compensation. The use of shunt capacitors will improve the power factor and stabilize the voltage as well as reduce the network losses. Capacitor bank in parallel to PV plant/Wind farm to compensate the reactive power absorbed by the solar/wind step up power transformers.

#### 2.1.5.3.1 Capacitor Theoretical Principle

A capacitor consists of two plates (electrodes) insulated from each other by a medium, dielectric. The features of a capacitor are dependent on the capacitance and the voltage.

The capacitance is dependent on three factors, the area of the electrodes, the distance between them and the dielectric constant for the insulating material. The picture below shows the area,  $A$ , as the width,  $w$ , times the depth,  $d$ . The distance between the electrodes is  $h$  and the dielectric constant is  $\mu$ . In modern power capacitors, the dielectric constant commonly is between 2.2 and 2.7. Figure 2.1-46 shows a parallel plate capacitor.

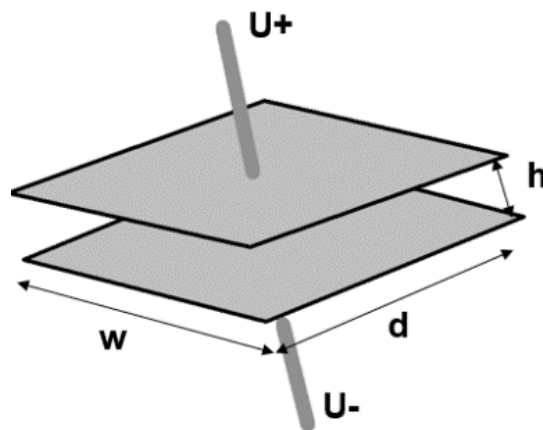


Figure 2.1-46: Parallel Plate Capacitor

- Capacitance  $C$

$$C = \varepsilon \frac{A}{h}$$

- Reactive power  $Q$

$$Q = \frac{V^2}{X_c} = \frac{V^2}{\frac{1}{\omega C}} = 2\pi f \times V^2 \times C$$

- $\varepsilon$  – the permittivity of the insulating material, the dielectric, (other name: dielectric constant)
- $A$  – the area of the plates ( $w*d$ ).
- $h$  – the distance btw plates/thickness of dielectric

Increasing the area of the electrodes means increasing the capacitance. This is what happens when capacitors are connected in parallel. Increasing the distance between the electrodes means decreasing the capacitance and increasing the voltage strength. The principle is the same as connecting capacitors in series.

Capacitance in parallel

$$C_p = C_1 + C_2 + C_3 + \dots + C_n$$

Capacitance in series

$$C_s = \frac{1}{\frac{1}{C_1} + \frac{1}{C_2} + \frac{1}{C_2} + \dots + \frac{1}{C_n}}$$

Capacitor development until present days usually has meant developing new insulation materials in order to increase the dielectric constant,  $\mu$ , or to reduce the distance between the electrodes by using thinner dielectrics. This way the voltage stress on the dielectric system will increase and so the power density of the capacitor. A capacitor works as a short circuit for AC currents and as an interruption for DC current. This is explained by the capacitor impedance formula:

$$X_c = \frac{1}{\omega \times C} = \frac{1}{2\pi f \times C}$$

Where:

$X_c$  = capacitor impedance

$f$  = system frequency

$C$  = capacitance

The higher the frequency  $f$ , the lower the impedance of the capacitor  $X_c$ . This means that for very high frequencies, the capacitor will appear as a short circuit for the current, since ( $X_c = 0$ ). For a DC current, since the frequency is 0, the capacitor appears as an interruption ( $X_c = \infty$ ). These are the electrical features for a capacitor most often used in electronics applications

#### **2.1.5.3.1.1 Applications of Capacitor Banks**

In the electrical power systems, the capacitor is more commonly used for:

- Storing electric energy
- Producing reactive power

#### **Storing Energy**

Capacitors are connected in the DC-link in HVDC-systems and frequency converters to keep the voltage steady. The DC capacitors will also work as a buffer to reduce voltage variations.

#### **Producing Reactive Power**

The most common application for power capacitors is in a power factor correction system or, as it sometimes is called, reactive power compensation equipment.

#### **2.1.5.3.1.2 Benefits of Using Capacitor Banks**

1. Power factor is improved.
2. Voltage is stabilized.
3. Reduces harmonic content in the network which further reduces disturbances in telecommunication network, misbehavior in control equipment's and relay protections, measuring errors in metering system.
4. Reduces network losses.
5. Reduces equipment overloading & stress on insulation.
6. Reduces cost and generates higher revenue for the customer.

7. Reduces unplanned outages and increases power availability.

### 2.1.5.3.2 Capacitor Bank Design

Bank design means transforming the requested reactive power into a physical structure with all environmental aspects. A capacitor consists of two plates, electrodes, insulated from each other by an insulating material, the dielectric system. The capacitor element is the smallest part of the capacitor. The element is a winding of aluminum foil and plastic film. The elements are connected in a matrix in series and in parallel to form a capacitor unit, with the wanted voltage and power rating. On an average, a capacitor unit consists of 40 elements. The elements are connected in series to build the voltage and in parallel to build the power in the unit. The units are mounted in hot-dip galvanized steel racks, to build up the capacitor bank. The minimum number of capacitor units in a three-phase bank is three, one per phase. For more power and higher voltage, capacitor units are connected in series for voltage and parallel for power. below Figure 2.1-47 shows the capacitor bank design and building blocks and Figure 2.1-48 shows an open rack capacitor bank.

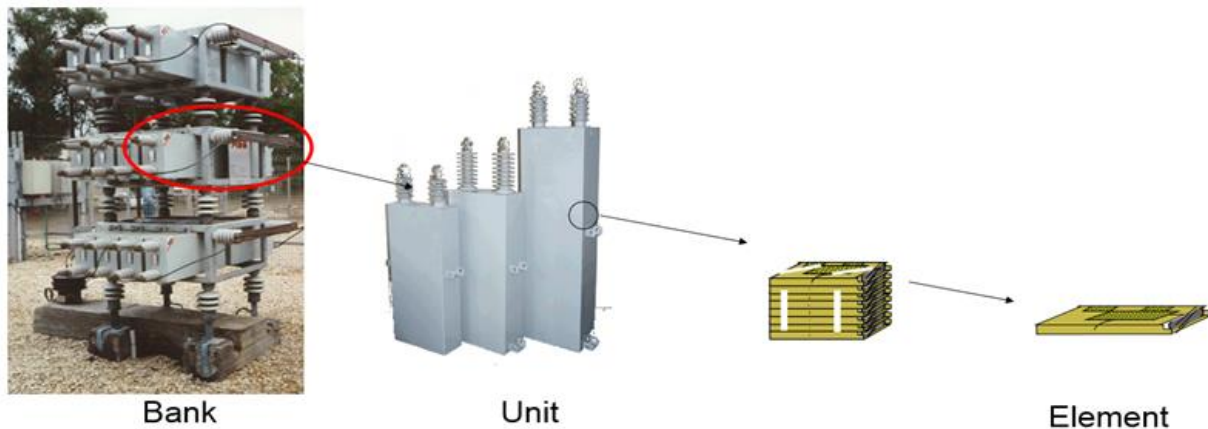


**Figure 2.1-47:** Capacitor Bank Design and Building Block

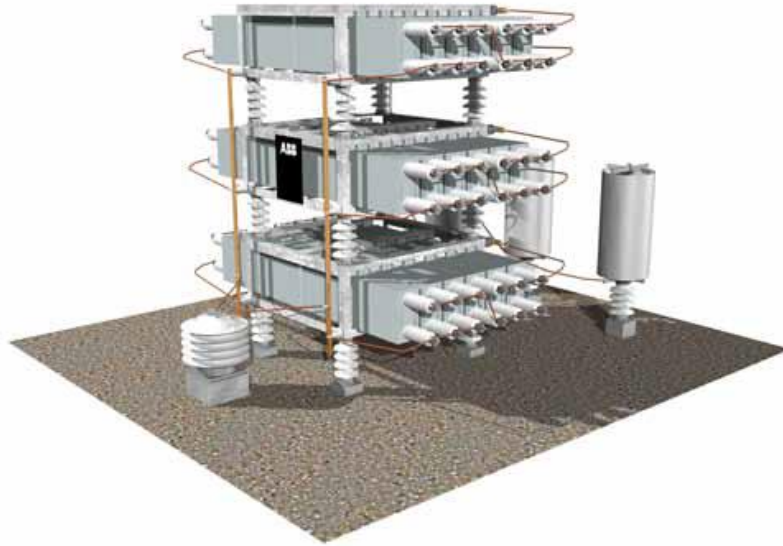


**Figure 2.1-48: Open Rack Capacitor Bank**

#### **2.1.5.4 *Dynamic Shunt Compensator***

One of the most significant uses of dynamic shunt compensators power quality solutions is in the integration of renewable energy sources, such as wind and solar power, which are variable and unpredictable energy sources that can cause voltage swings and instability. In addition, the grid code's increasing needs for preserving reactive power balance are the reason for the Reactive Power Balance. The dynamic shunt compensators can ride through voltage in the event of a grid fault, but there are disadvantages. Specifically, using converters causes harmonics to be produced.

Dynamic shunt compensation, including SVCs, STATCOMs, synchronous condensers, and Enhanced STATCOMs, is used to provide voltage stability in both steady-state and dynamic scenarios. Additionally, these systems offer additional benefits such as enhancing system strength and inertia. There are two distinct techniques available for dynamic voltage support. Both systems, SVC and STATCOM, are actively maintained and continuously updated.

##### **2.1.5.4.1 SVC – Static Var Compensator**

The Static Var Compensator (SVC) was first developed during the 1970s. SVC utilizes a thyristor-controlled shunt regulator for dynamic compensation of reactive power. This is achieved through the use of Line commutated 6 pulse or 12 pulse converters, which produce odd harmonics such as 3<sup>rd</sup>, 5<sup>th</sup>, 7<sup>th</sup>, 9<sup>th</sup>, 11<sup>th</sup>, etc. Consequently, the TCR generates harmonics that necessitate the use of Harmonic filters to mitigate their impact. See below typical diagram for the SVC system

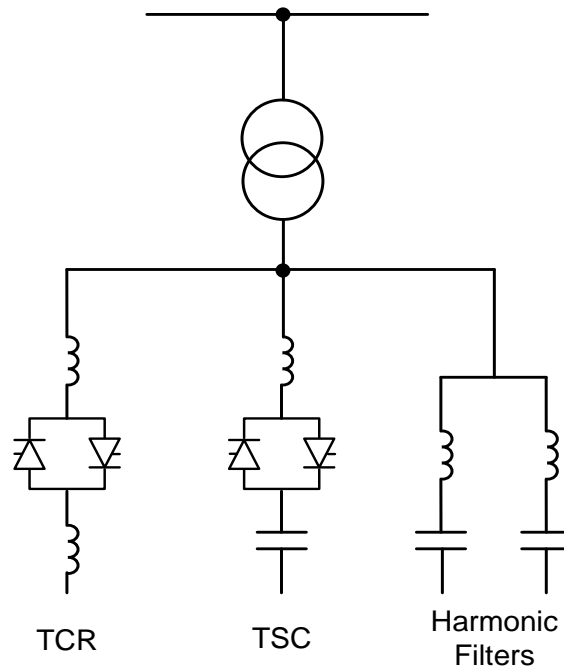


**Figure 2.1-49:** SVC Single Line Diagram

The primary components of the SVC system, as shown by the Single Line Diagram (SLD), begin with the Power Transformer. This transformer connects the SVC main components to the High Voltage (HV) bus, also known as the Point of Common Coupling (PoCC). Next in line is the TCR, or Thyristor Controlled Reactor, which supplies reactive power in the form of inductive power  $Q_L$ . The current of the system may be adjusted continuously from zero to the maximum inductive current,  $I_L$ . However, this adjustment process generates harmonics that have the potential to be transferred to the power grid. Harmonic filter capacitors are used to mitigate the harmonics produced by the TCR and provide capacitive power  $Q_c$ . These capacitors are consistently linked. Following this, a TSC (Thyristor Switched Capacitor) is introduced, which supplies capacitive power by either

enabling a full capacitive current or disabling it completely. A dedicated SVC control system will be implemented to govern and manage the operation and reactions of the whole SVC system.

As an example for the SVC system, below is a 50 MVAR Inductive to 150 MVAR Capacitive

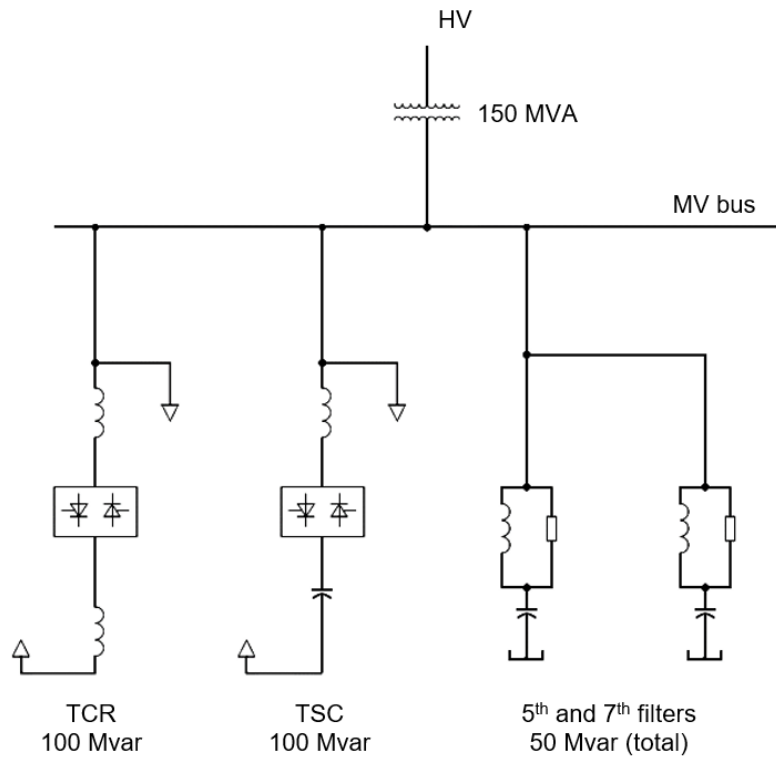


**Figure 2.1-50:** 50 Mvar Inductive to 150 Mvar Capacitive SVC SLD

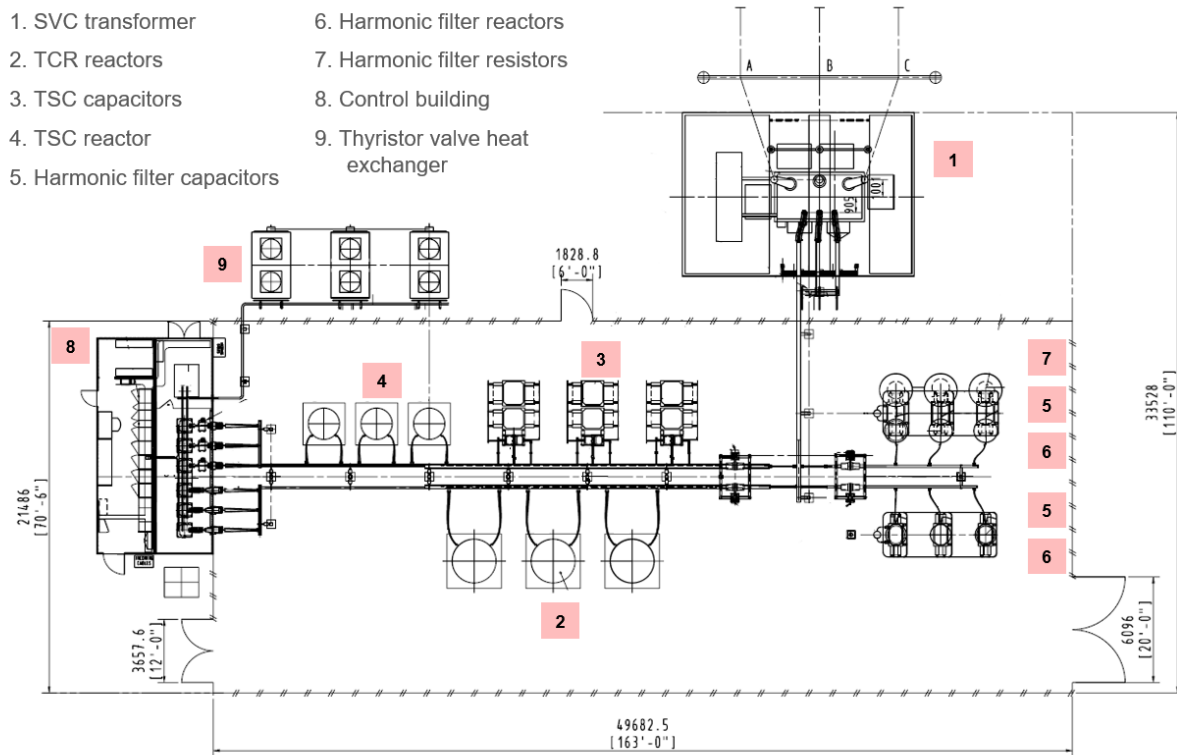
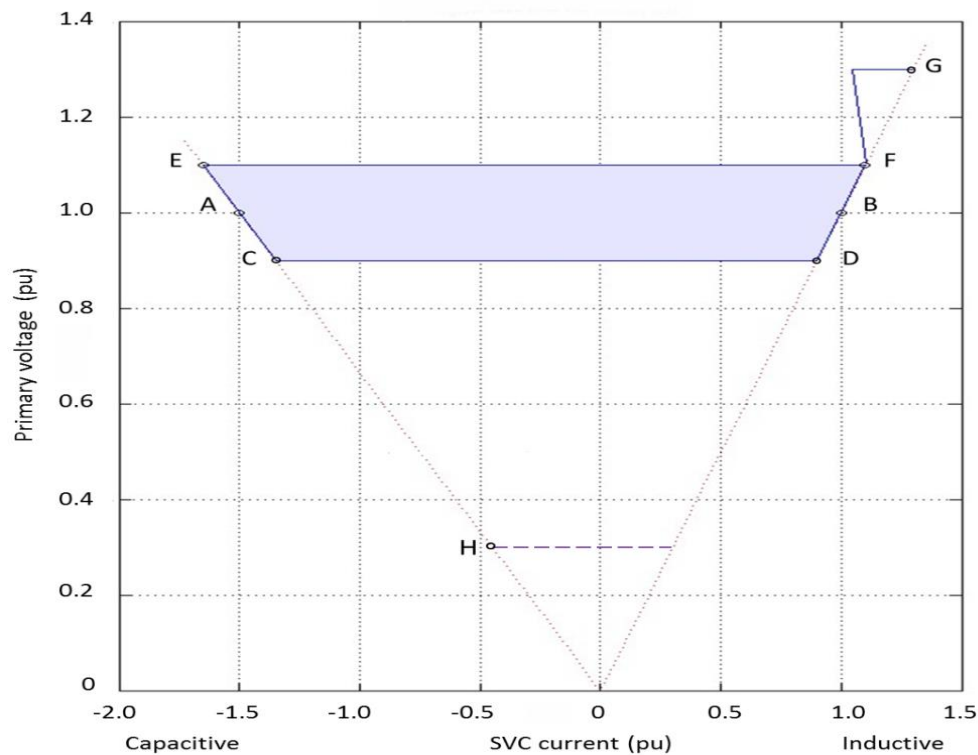


**Figure 2.1-51: Layout for 50 Mvar Inductive to 150 Mvar Capacitive**



At 1.0 p.u. primary voltage

- Point A, Capacitive continuous output, 150Mvar
- Point B, Inductive continuous output, 100 Mvar

At 0.9 p.u. primary voltage

- Point C, Capacitive continuous output, 121Mvar
- Point D, Inductive continuous output, 81Mvar

At 1.1 p.u. primary voltage

- Point E, Capacitive continuous output, 181Mvar
- Point F, Inductive continuous output, 121Mvar

At 1.3 p.u. primary voltage during 1 second

- Point G, Inductive output, 169Mvar

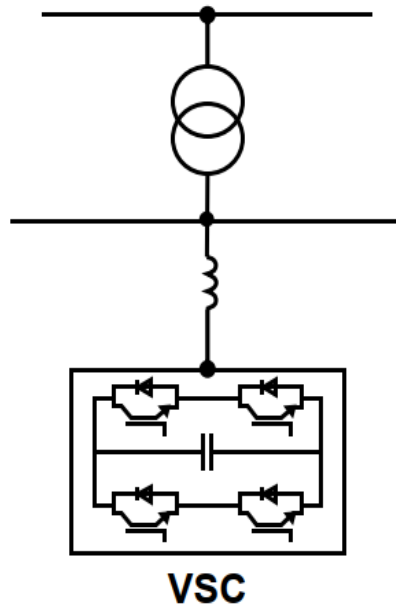
At 0.3 p.u. primary voltage

- Point H, Capacitive continuous output

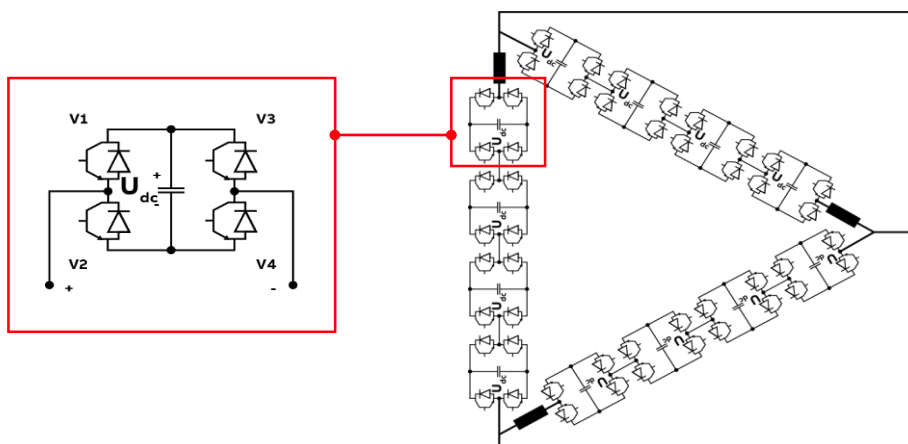
#### 2.1.5.4.2 STATCOM

The two- and three-level STATCOM, which use IGCT and IGBT technologies, were released in the late 1990s. STATCOM: STATic COMpensator is based on VSC (Voltage Sourced Converter) technology that has Electrical similarities with synchronous compensators (controllable voltage behind a reactance). However, no moving parts., where a new concept of IGBT and IGCT based

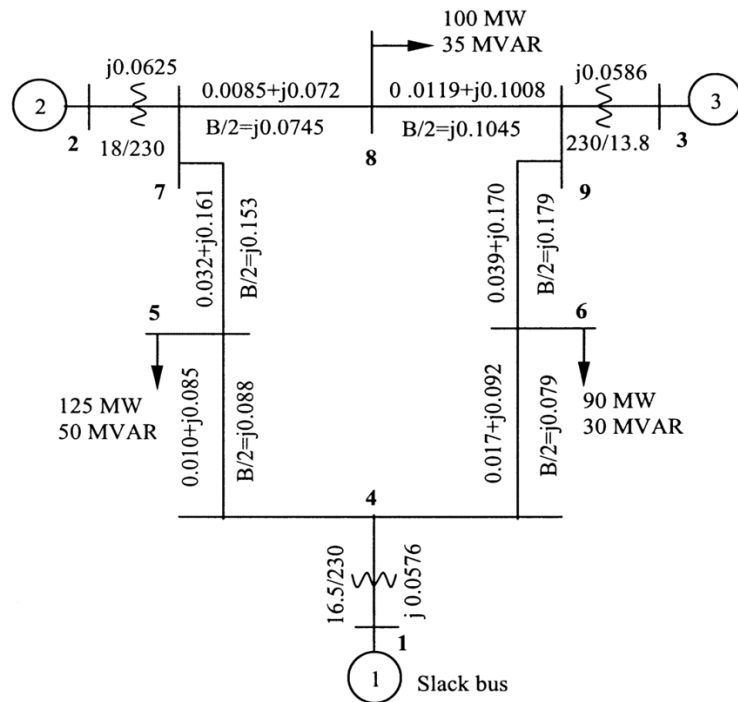
MMC VSC is state of the art with low harmonic generation, this technology is superior for under-voltage performance, and STATCOM used in both utility and industrial applications.



- Multilevel cascaded H-bridges, modular design.
- Modular in # of cells:  
1 cell = 4 semiconductors (V1 – V4)
- Valve Modules connected in series. Number depends on required output.
- Distributed dc-link
- The sum of all valve module output voltages form the terminal voltage
- Low switching frequency



## 2.2 Chapter Five: Case Study IEEE 9-bus system- Power System Analysis and ETAP Simulation



### 2.2.1 IEEE 9 Bus system – Overview

The IEEE 9 bus system serves as a test electrical power network for many applications, and the system is often used for the aim of performing research on many aspects of power systems, including fault detection and classification, the impact of integrating renewable energy sources, study of system stability, optimization of power flow, and load flow analysis. Researchers use the IEEE 9 bus system as a benchmark to develop and evaluate novel algorithms, techniques, and technologies for power system analysis and control. The model consists of three (3) synchronous machines and their generator step-up transformers, each with a capacity of 100MVA. It also includes nine (9) buses (one (1) slack bus, two (2) PV buses, and six (6) load buses) that are interconnected through overhead transmission lines. Additionally, there are three (3) constant power loads with overall load demand is 315MW and 115 MVAR, as depicted in the diagram **Figure 2.2-1: IEEE 9 Bus system Single Line Diagram.**

The modified IEEE 9-bus system is same as the original one described above, however made up of three (3) synchronous machines that are equipped with IEEE type-1 exciters, and three generators step up transformers with modified capacity to evacuate the synchronous machines full capacity.

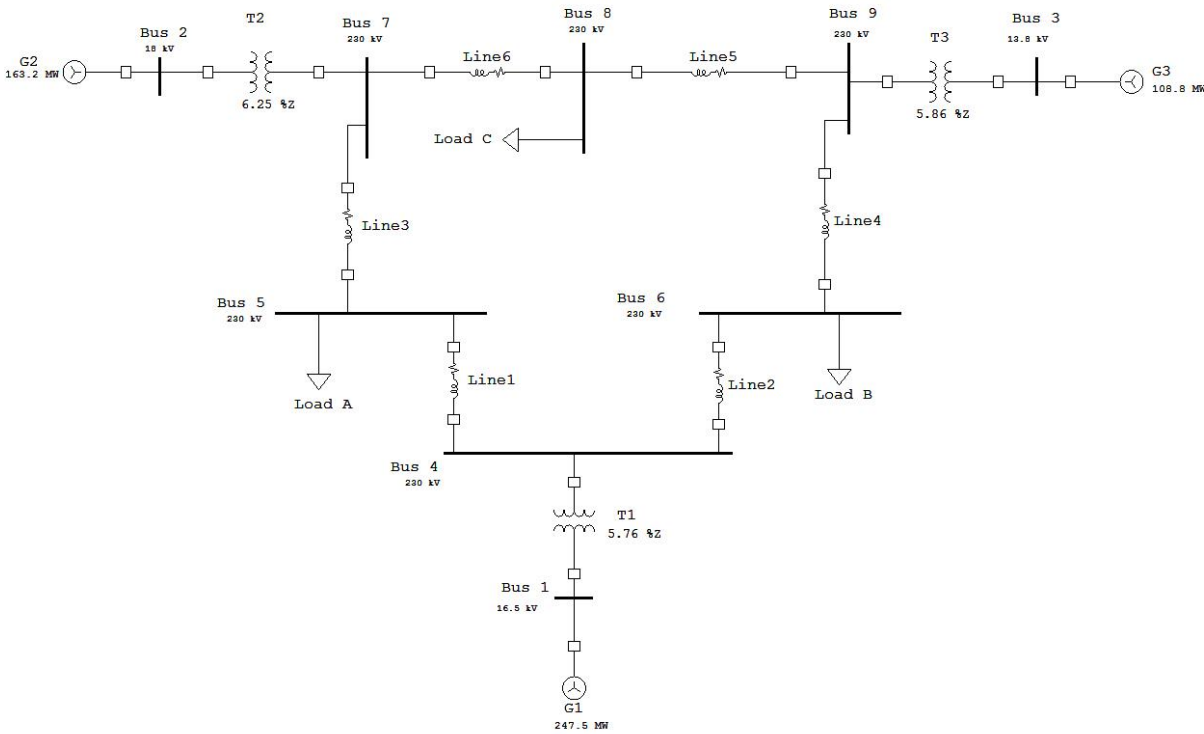


**Figure 2.2-1:** IEEE 9 Bus system Single Line Diagram

Model validation and verification of the IEEE 9 bus electrical power system and planning the operation for the original model requires several power system analysis studies, such as power flow studies, fault calculations, harmonic analysis, transient stability studies, voltage stability, and contingency analysis, study of the system. Here is a concise overview of the significance of each of these studies. For example, Power flow analysis is performed to reveal the performance of electric power system, provide information about the equipment loading conditions, to calculate the magnitude and phase angle of voltages at the buses and the active power and reactive voltamperes flow for the given terminal or bus conditions. The variables associated with each bus or node are: voltage magnitude  $|V|$ , phase angle of voltage  $\delta$ , active (real) power,  $P$ , and the reactive power,  $Q$ .

Short circuit studies or fault calculations are essential to design the power system protection schemes for various parts of the system. The protective scheme consists of current and voltage sensing devices, protective relays, and circuit breakers. The selection of these devices mainly depends on various currents that may flow in the fault conditions and the system must be protected against the flow of heaving short circuit current by isolating the faulty part from the healthy part of the system by means of circuit breakers and protection relays.

Harmonic Analysis is a mathematical way for simulating or predicting harmonic distortion levels and protentional resonance, it can affect the power quality and operation of equipment. High levels of Harmonics in the system may lead to overheating component thus causing shorten the life of the equipment, reduced power factors. The ideal power source for power systems is a pure sinusoidal wave. These pure waves can be distorted from a sinusoidal form due to the presence of harmonics.

Transient stability study is performed to check of the ability of the electrical power system to return to its normal stable operating condition after being subjected to some kind of disturbance, in other words we will study the ability to regain the equilibrium state after the disturbance.

Voltage stability has emerged as a significant issue in modern power system networks, particularly in systems with extensive transmission lines. Moreover, it has become a matter of worry in networks under heightened strain due to increased load. Voltage Stability conducting Continuation Load Flow (CLF) studies on power systems, namely for P-V and Q-V studies. Additionally, it enables V-Q sensitivity studies to analyze the static voltage stability of power systems.

Contingency analysis is a tool that use a simulated model of the power system to assess the impacts and determine any overloads caused by each loss occurrence. Contingency Analysis is mostly a technique used for preliminary analysis.

## 2.2.2 IEEE 9 Bus –System Parameters

Below are the IEEE 9 bus system main components parameters.

### 2.2.2.1 Synchronous machines



Parameter	SM1	SM2	SM3
Nominal Power (MVA)	512	270	125
Nominal Voltage (kV RMS)	16.5	18	13.8
$X_d$ (pu)	1.70	1.70	1.22
$X'_d$ (pu)	0.27	0.256	0.174
$X''_d$ (pu)	0.2	0.185	0.134
$T'_{do}$ (s)	3.8	4.8	8.97
$T''_{do}$ (s)	0.01	0.01	0.033
$X_q$ (pu)	1.65	1.62	1.16
$X'_q$ (pu)	0.47	0.245	0.25
$X''_q$ (pu)	0.2	0.185	0.134
$T'_{qo}$ (s)	0.48	0.50	0.50
$T''_{qo}$ (s)	0.0007	0.0007	0.07
$R_a$ (pu)	0.004	0.0016	0.004
$X_l$ (pu)	0.16	0.155	0.0078
$S(1.0)$	0.09	0.125	0.1026
$S(1.2)$	0.4	0.45	0.432
$H$ (s)	9.95	4.1296	4.768
$D$ (pu)	2	2	2
Parameter for Exciter	SM1	SM2	SM3
$K_p$	5.3	5.3	5.3
$K_a$	200	30	25
$K_f$	0.0635	0.05	0.108
$T_r$ (s)	0	0	0.06
$T_a$ (s)	0.395	0.4	0.2
$T_f$ (s)	1	1.3	0.35
$V_t$ min (pu)	0.1	0.1	0.1
$V_t$ max (pu)	100	100	100
$V_r$ min (pu)	-3.84	-4.59	-3
$V_r$ max (pu)	3.84	4.59	3

### 2.2.2.2 Power Transformers



Transformer parameters	T1	T2	T3
Apparent Power (MVA)	600	300	150
Nominal primary voltage (kV RMS L-L)	24	18	15.5
Nominal secondary voltage (kV RMS L-L)	230	230	230
R1 (pu)	1E-10	1E-10	1E-10
L1 (pu)	0.0288	0.0313	0.0293
R2 (pu)	1E-10	1E-10	1E-10
L2 (pu)	0.0288	0.0313	0.0293
Rm (pu)	5000	5000	5000
Lm (pu)	5000	5000	5000

### 2.2.2.3 Transmission Lines



Transmission Line		Length	R1	L1	C1	R0	L0	C0
From	To	(km)	( $\Omega$ /km)	(H/km)	(F/km)	( $\Omega$ /km)	(H/km)	(F/km)
4	5	89.93	0.0588	0.00133	9.81E-09	0.588	0.00398	5.89E-09
4	6	97.336	0.0924	0.00133	8.14E-09	0.924	0.00398	4.88E-09

5	7	170.338	0.0994	0.00133	9.01E-09	0.994	0.00398	5.41E-09
6	9	179.86	0.115	0.00133	9.98E-09	1.15	0.00398	5.99E-09
7	8	76.176	0.059	0.00133	9.81E-09	0.59	0.00398	5.89E-09
8	9	106.646	0.059	0.00133	9.83E-09	0.59	0.00398	5.9E-09

#### 2.2.2.4 Loads

Capacity	Load A	Load B	Load C
Nominal Active Power (MW)	125	90	100
Nominal Reactive Power (MVAR)	50	30	35

#### 2.2.3 Per Unit Analysis

In the per unit analysis for electrical power system, two base values should be selected which are:

1. The base apparent power  $S_B$  or  $(MVA)_B$  which will be common for the whole electrical power system, and it is recommended to be the highest MVA of the study case power system, however as per IEC it is recommended to be equal to 100.
2. The base voltage  $V_B$  or  $(KV)_B$  at a selected section that should be before or after of a transformer.

From the above base values, we can derive the other base values as below.

$$\text{Base Current } I_B = \frac{1000 \times (MVA)_B}{\sqrt{3} \times (kV)_B} = \frac{1000 \times S_B}{\sqrt{3} \times V_B}$$

$$\text{Base Impedance } Z_B = \frac{1000 \times (kV)_B}{\sqrt{3} \times I_B} = \frac{1000 \times V_B}{\sqrt{3} \times I_B}$$

Substituting  $I_B$  value in  $Z_B$  equation

$$Z_B = \frac{1000 \times (kV)_B}{\sqrt{3} \times \left( \frac{1000 \times (MVA)_B}{\sqrt{3} \times (kV)_B} \right)} = \frac{(kV)_B^2}{(MVA)_B} = \frac{V_B^2}{S_B}$$

Normally the generators, transformers, and motors impedances are described using their nominal values.

$$Z_{pu} = \frac{Z_{actual}}{Z_B} = \frac{Z_{actual}}{\left( \frac{(kV)_B^2}{(MVA)_B} \right)} = \frac{Z_{actual} \times (MVA)_B}{(kV)_B^2}$$

If base values are changed which is assumed it to be as a reference

$$Z_{pu-new} = Z_{pu-old} \times \left( \frac{(MVA)_{B-new}}{(MVA)_{B-old}} \right) \times \left( \frac{(kV)_{B-old}}{(kV)_{B-new}} \right)^2$$

Steps that should be followed to perform the normalization or per unit analysis.

1. Choose the **(MVA)<sub>B</sub>** and **(KV)<sub>B</sub>** at a certain section of the power system.
2. Calculate the normalized per unit impedance for the components at that section which have the same voltage level.
3. For the generators or motors, we use below equation

$$X''_{G-new} = X''_{G-old} \times \left( \frac{(MVA)_{B-G-new}}{(MVA)_{B-G-old}} \right) \times \left( \frac{(KV)_{B-G-old}}{(KV)_{B-G-new}} \right)^2$$

$$X''_{M-new} = X''_{M-old} \times \left( \frac{(MVA)_{B-M-new}}{(MVA)_{B-M-old}} \right) \times \left( \frac{(KV)_{B-M-old}}{(KV)_{B-M-new}} \right)^2$$

4. Calculate the new **(KV)<sub>B</sub>** for the new section (before or after) the transformer.

$$X_{T-new} = X_{T-old} \times \left( \frac{(MVA)_{B-T-new}}{(MVA)_{B-T-old}} \right) \times \left( \frac{(KV)_{B-T-old}}{(KV)_{B-T-new}} \right)^2$$

5. For the overhead transmission lines or cables, we calculate the PU impedance as below.

$$Z_{Line-Actual} = Z_L (\Omega/Km) \times l_L (km)$$

$$Z_{B-Lines} = \frac{(KV)_B^2}{(MVA)_B}$$

$$Z_{PU-Line} = \frac{Z_{actual-Line}}{Z_B}$$

Choosing **(MVA)<sub>B</sub>=100** and **(KV)<sub>B</sub>=20** at G1 section side (Bus No.1)

**For Generator G1 section (Bus No.1)**

G<sub>1</sub>=512 MVA, 16.5kV, X''<sub>d</sub> = X''<sub>q</sub> =20%, PF=0.9

### **Generator G1**

$$X''_{G1-new} = X''_{G1-old} \times \left( \frac{(MVA)_{B-G1-new}}{(MVA)_{B-G1-old}} \right) \times \left( \frac{(KV)_{B-G1-old}}{(KV)_{B-G1-new}} \right)^2$$

$$X''_{G1-new} = 20\% \times \left( \frac{100}{512} \right) \times \left( \frac{16.5}{20} \right)^2 = \mathbf{0.0266 PU}$$

### **Transformer T1**

T<sub>1</sub>=600 MVA, (16.5/230) kV, X% = 2 X 2.88 X 10<sup>-2</sup> =5.76%

$$X_{T1-new} = X_{T1-old} \times \left( \frac{(MVA)_{B-T1-new}}{(MVA)_{B-T1-old}} \right) \times \left( \frac{(KV)_{B-T1-old}}{(KV)_{B-T1-new}} \right)^2$$

$$X_{T1-new} = 5.76\% \times \left( \frac{100}{600} \right) \times \left( \frac{16.5}{20} \right)^2 = \mathbf{0.00653 PU}$$

$$K_{T1} = \frac{V_1}{V_2} = \frac{(KV)_{B-BB1}}{(KV)_{B-BB4}} = \frac{16.5}{230} = \frac{20}{(KV)_{B-BB4}} \Rightarrow (KV)_{B-BB4} = \frac{20 \times 230}{16.5} = 278.8kV$$

Or we can find the new normalized PU impedance for the transformer at the secondary side.

$$X_{T1-new} = 5.76\% \times \left( \frac{100}{600} \right) \times \left( \frac{230}{278.8} \right)^2 = \mathbf{0.00653 PU}$$

### **For Generator G2 section (Bus No.2)**

We should find the new (KV)<sub>B</sub> for at side of Generator G2 (at Bus No.2)

$$K_{T2} = \frac{V_1}{V_2} = \frac{(KV)_{B-BB2}}{(KV)_{B-BB7}} = \frac{18}{230} = \frac{(KV)_{B-BB2}}{278.788} \Rightarrow (KV)_{B-BB2} = \frac{18 \times 278.788}{230} = 21.82 kV$$

### **Generator G2**

G<sub>2</sub>=270 MVA, 18kV, X''<sub>d</sub> = X''<sub>q</sub> =18.5%, PF=0.85

$$X''_{G2-new} = X''_{G2-old} \times \left( \frac{(MVA)_{B-G2-new}}{(MVA)_{B-G2-old}} \right) \times \left( \frac{(KV)_{B-G2-old}}{(KV)_{B-G2-new}} \right)^2$$

$$X''_{G2-new} = 18.5\% \times \left(\frac{100}{270}\right) \times \left(\frac{18}{21.82}\right)^2 = \mathbf{0.04663 PU}$$

### **Transformer T2**

$T_2=300 \text{ MVA, (18/230) kV, } X\% = 2 \times 3.13 \times 10^{-2}=6.26\%$

$$X_{T2-new} \text{ primary side} = X_{T2-old} \times \left(\frac{(MVA)_{B-T2\_new}}{(MVA)_{B-T2\_old}}\right) \times \left(\frac{(KV)_{B-T2\_old}}{(KV)_{B-T2\_new}}\right)^2$$

$$X_{T2-new} = 6.26\% \times \left(\frac{100}{300}\right) \times \left(\frac{18}{21.82}\right)^2 = \mathbf{0.01420 PU}$$

Or we can find the new normalized PU impedance for the transformer at the secondary side.

$$X_{T2-new} \text{ secondary side} = 6.26\% \times \left(\frac{100}{300}\right) \times \left(\frac{230}{278.8}\right)^2 = \mathbf{0.01420 PU}$$

### **For Generator G3 section (Bus No.3)**

We should find the new  $(KV)_B$  for at side of Generator G3 (at Bus No.3)

$$K_{T3} = \frac{V_1}{V_2} = \frac{(KV)_{B-BB3}}{(KV)_{B-BB9}} = \frac{13.8}{230} = \frac{(KV)_{B-BB3}}{278.788} \Rightarrow (KV)_{B-BB3} = \frac{13.8 \times 278.788}{230} = 16.727 \text{ kV}$$

### **Generator G3**

$G_3=125 \text{ MVA, } 13.8\text{kV, } X''_d = X''_q =13.4\%, \text{ PF}=0.85$

$$X''_{G3-new} = X''_{G3-old} \times \left(\frac{(MVA)_{B-G3\_new}}{(MVA)_{B-G3\_old}}\right) \times \left(\frac{(KV)_{B-G3\_old}}{(KV)_{B-G3\_new}}\right)^2$$

$$X''_{G3-new} = 13.4\% \times \left(\frac{100}{125}\right) \times \left(\frac{13.8}{16.727}\right)^2 = \mathbf{0.07296 PU}$$

### **Transformer T3**

$T_3=150 \text{ MVA, (13.8/230) kV, } X\% = 2 \times 2.93 \times 10^{-2}=5.86\%$

$$X_{T3-new} \text{ primary side} = X_{T3-old} \times \left(\frac{(MVA)_{B-T3\_new}}{(MVA)_{B-T3\_old}}\right) \times \left(\frac{(KV)_{B-T3\_old}}{(KV)_{B-T3\_new}}\right)^2$$

$$X_{T3-new} = 5.86\% \times \left(\frac{100}{150}\right) \times \left(\frac{13.8}{16.727}\right)^2 = \mathbf{0.02659 PU}$$

Or we can find the new normalized PU impedance for the transformer at the secondary side.

$$X_{T3-new \text{ secondary side}} = 5.86\% \times \left(\frac{100}{150}\right) \times \left(\frac{230}{278.8}\right)^2 = \mathbf{0.02659 PU}$$

**For Lines 1, 2, 3, 4, 5, and 6 Section.**

The base impedance for lines

$$Z_{B-Lines} = \frac{(KV)_B^2}{(MVA)_B} = \frac{(278.8)^2}{100} = 777.23 \Omega$$

Taking the positive +ve sequence impedance parameters R(1), L(1), C(1) of each line, we can calculate the actual +ve sequence impedance. The actual line impedances can be calculated below.

$$\begin{aligned} Z_{Line1-Actual}^{4 \rightarrow 5} &= Z_{L1}(\Omega/Km) \times l_{L1}(km) = [5.88 \times 10^{-2} + j(2\pi \times 50 \times 1.33 \times 10^{-3})] \times 89.93 \\ &= 5.287 + j37.576 \Omega \end{aligned}$$

$$\begin{aligned} Z_{Line2-Actual}^{4 \rightarrow 6} &= Z_{L2}(\Omega/Km) \times l_{L2}(km) \\ &= [9.24 \times 10^{-2} + j(2\pi \times 50 \times 1.33 \times 10^{-3})] \times 97.336 = 8.994 + j40.67 \Omega \end{aligned}$$

$$\begin{aligned} Z_{Line3-Actual}^{5 \rightarrow 7} &= Z_{L3}(\Omega/Km) \times l_{L3}(km) \\ &= [9.94 \times 10^{-2} + j(2\pi \times 50 \times 1.33 \times 10^{-3})] \times 170.338 = 16.931 + j71.17 \Omega \end{aligned}$$

$$\begin{aligned} Z_{Line4-Actual}^{6 \rightarrow 9} &= Z_{L4}(\Omega/Km) \times l_{L4}(km) \\ &= [1.15 \times 10^{-1} + j(2\pi \times 50 \times 1.33 \times 10^{-3})] \times 179.86 = 20.68 + j75.151 \Omega \end{aligned}$$

$$Z_{Line5-Actual} = Z_{L5}(\Omega/Km) \times l_{L5}(km) \\ = [5.9 \times 10^{-2} + j(2\pi \times 50 \times 1.33 \times 10^{-3})] \times 106.646 = 6.292 + j44.56 \Omega$$

$$Z_{Line6-Actual} = Z_{L6}(\Omega/Km) \times l_{L6}(km) = [5.9 \times 10^{-2} + j(2\pi \times 50 \times 1.33 \times 10^{-3})] \times 76.167 \\ = 4.494 + j31.83 \Omega$$

After this, the per unit impedance of each line can be calculated, noting that the resistance of the lines can be ignored for fault and stability study calculations, however for the load flow study the resistance should be taken into account.

$$Z_{PU-Lines} = \frac{Z_{actual-Lines}}{Z_{B-Lines}}$$

$$Z_{PU-Line1} = \frac{Z_{actual-Line1}}{Z_B} = \frac{5.287 + j37.576}{777.23} = \mathbf{0.0068 + j 0.048346 PU}$$

$$Z_{PU-Line2} = \frac{Z_{actual-Line2}}{Z_B} = \frac{8.994 + j40.67}{777.23} = \mathbf{0.01157 + j 0.0523 PU}$$

$$Z_{PU-Line3} = \frac{Z_{actual-Line3}}{Z_B} = \frac{16.931 + j71.17}{777.23} = \mathbf{0.0218 + j 0.0915 PU}$$

$$Z_{PU-Line4} = \frac{Z_{actual-Line4}}{Z_B} = \frac{20.68 + j75.151}{777.23} = \mathbf{0.0266 + j 0.0967 PU}$$

$$Z_{PU-Line5} = \frac{Z_{actual-Line5}}{Z_B} = \frac{6.292 + j44.56}{777.23} = \mathbf{0.0081 + j 0.0573 PU}$$

$$Z_{PU-Line6} = \frac{Z_{actual-Line6}}{Z_B} = \frac{4.494 + j31.83}{777.23} = \mathbf{0.0058 + j 0.0409 PU}$$

### For Loads Section

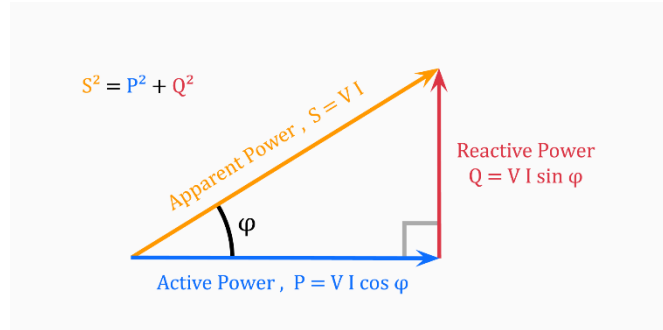
Each load is specified by the active and reactive power (P and Q) drawn from the bus where it is connected with.

$$I_L = \frac{S}{\sqrt{3} \times V} = \frac{\sqrt{P^2 + Q^2}}{\sqrt{3} \times V}, \varphi = \tan^{-1} \left( \frac{Q}{P} \right)$$

$$Z_{Load\ Actual} = \frac{V \angle 0^\circ}{\sqrt{3} \times I_L \angle -\varphi}$$

$$Z_{Load-B} = \frac{(kV)_B^2}{(MVA)_B}$$

$$Z_{PU-Load} = \frac{Z_{actual-Load}}{Z_{Load-B}}$$



### **For Load A**

125MW+j50MVAr, V=230kV

$$\varphi = \tan^{-1} \left( \frac{50}{125} \right) = 21.8^\circ$$

$$I_{L-A} = \frac{S}{\sqrt{3} \times V} = \frac{\sqrt{P^2 + Q^2}}{\sqrt{3} \times V} = \frac{\sqrt{125^2 + 50^2}}{\sqrt{3} \times 230} \times 1000 = 337.948 \text{ A}$$

$$Z_{Load-A\ Actual} = \frac{230 \times 10^3 \angle 0^\circ}{\sqrt{3} \times 337.948 \angle -21.8^\circ} = 364.831 + j145.922 \ \Omega$$

$$Z_{Base-Load} = \frac{(KV)_B^2}{(MVA)_B} = \frac{(278.8)^2}{100} = 777.23 \ \Omega$$

$$Z_{PU-Load\ A} = \frac{364.831 + j145.922}{777.23} = \mathbf{0.469 + j0.1877 \text{ PU}}$$

**For Load B**

90MW+j30MVA<sub>r</sub>, V=230kV

$$\varphi = \tan^{-1}\left(\frac{30}{90}\right) = 18.435^\circ$$

$$I_{L-B} = \frac{S}{\sqrt{3} \times V} = \frac{\sqrt{P^2 + Q^2}}{\sqrt{3} \times V} = \frac{\sqrt{90^2 + 30^2}}{\sqrt{3} \times 230} \times 1000 = 238.14 \text{ A}$$

$$Z_{\text{Load-B}}^{\text{Actual}} = \frac{230 \times 10^3 \angle 0^\circ}{\sqrt{3} \times 238.14 \angle -18.435^\circ} = 529 + j176.334 \ \Omega$$

$$Z_{\text{Base-Load}} = \frac{(KV)_B^2}{(MVA)_B} = \frac{(278.8)^2}{100} = 777.23 \ \Omega$$

$$Z_{\text{PU-Load B}} = \frac{529 + j176.334}{777.23} = \mathbf{0.6806 + j0.2268 \text{ PU}}$$

**For Load C**

100MW+j35MVA<sub>r</sub>, V=230kV

$$\varphi = \tan^{-1}\left(\frac{35}{100}\right) = 19.29^\circ$$

$$I_{L-C} = \frac{S}{\sqrt{3} \times V} = \frac{\sqrt{P^2 + Q^2}}{\sqrt{3} \times V} = \frac{\sqrt{100^2 + 35^2}}{\sqrt{3} \times 230} \times 1000 = 238.14 \text{ A}$$

$$Z_{\text{Load-C}}^{\text{Actual}} = \frac{230 \times 10^3 \angle 0^\circ}{\sqrt{3} \times 238.14 \angle -19.29^\circ} = 471.27 + j164.945 \ \Omega$$

$$Z_{\text{Base-Load}} = \frac{(KV)_B^2}{(MVA)_B} = \frac{(278.8)^2}{100} = 777.23 \ \Omega$$

$$Z_{\text{PU-Load C}} = \frac{471.27 + j164.945}{777.23} = \mathbf{0.606 + j0.2122 \text{ PU}}$$

Based on the normalization and per unit analysis above, we can draw the PU equivalent impedance diagram as per **Figure 2.2-2** below

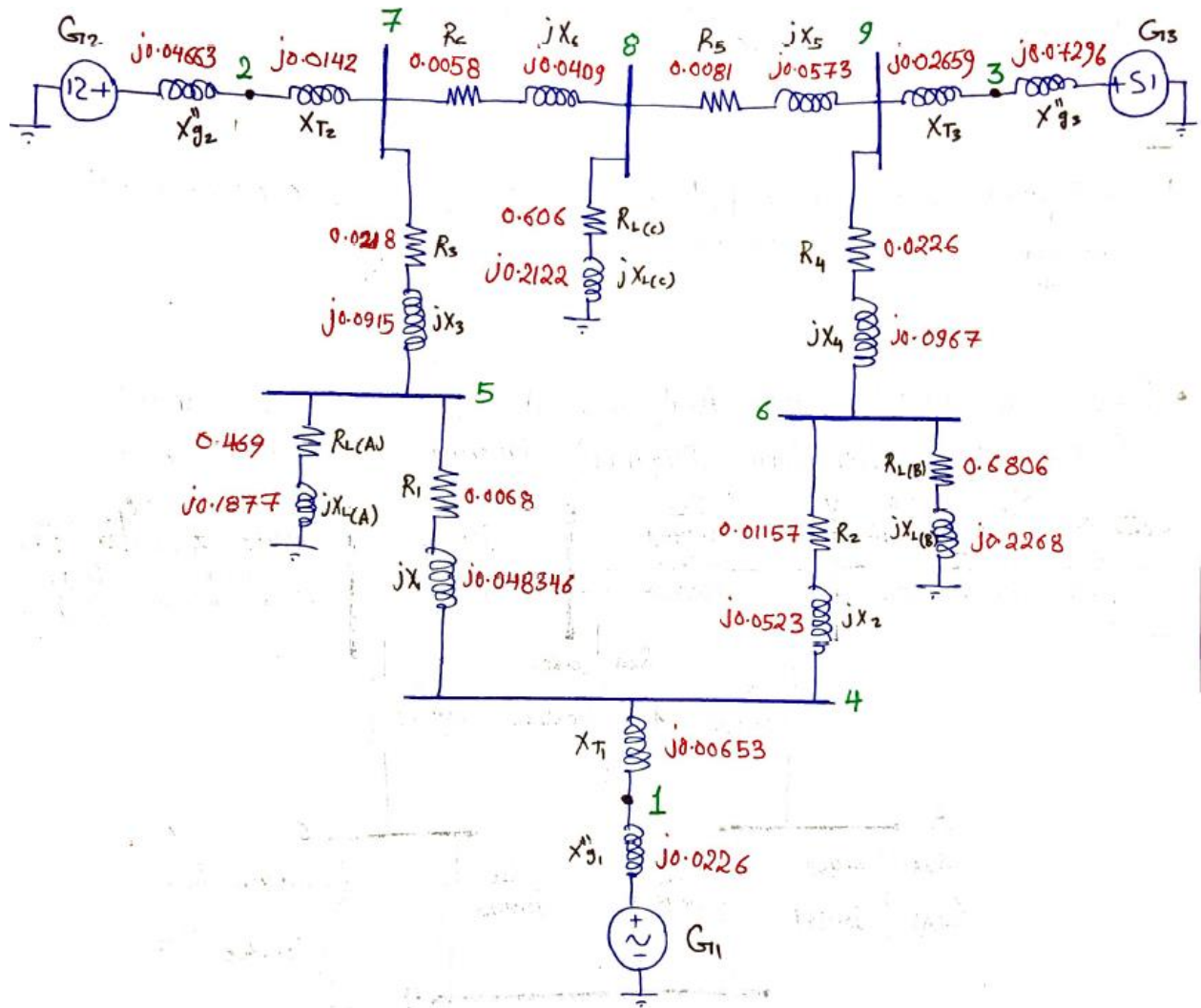


**Figure 2.2-2:** Normalized PU equivalent impedance diagram.

## 2.2.4 POWER FLOW STUDIES

A power flow study (load-flow study) is a steady-state analysis whose target is to reveal the performance of the electrical power system through determining the voltages, currents, and real and reactive power flows in a system under a given load conditions and ultimately determine the system steady state stability. The purpose of power flow studies is to plan ahead and account for various hypothetical situations. For example, if a transmission line is to be taken off for

maintenance, can the remaining lines in the system handle the required loads without exceeding their rated values.

Based on the above, power flow study is one of the most important aspects of power system planning and operation. The power flow gives the sinusoidal steady state of the entire system – voltages, real (active) and reactive power generated and absorbed and line losses. Since the load is a static quantity and it is the power that flows through transmission lines, it is preferred to call this power flow study rather than load flow studies.

Through the power flow study, the voltage magnitudes, and angles at each bus in the steady state can be obtained and thus the voltage profile for all the buses can be determined. This is important as the magnitudes of the bus voltages are required to be held within a specified limit and we utilize this to find the on-load tap changer range for all the transformers.

Once the bus voltage magnitudes and their angles are computed using the power flow, the current flow can be calculated and this gives clear indication about equipment loading for each branch like line/cable/transformer/ducts in the power system, besides, based on bus voltage and angle determination, the real and reactive power flow through each branch can be computed. Also based on the difference between power flow in the sending and receiving ends, the branch losses in a particular line can also be computed. Furthermore, from the line power flow the over and under load conditions can be determined.

Another important outcome of the power flow studies, is to determine the power factor at all the buses and to calculate the power factor correction capacitor rating or any dynamic hunt compensator (SVC/STATCOM) reactive power capability.

The steady state active and reactive powers supplied by a bus in a power network are expressed in terms of nonlinear algebraic equations. Therefore, iterative methods are used for solving these equations.

### 2.2.4.1 Power Flow Between Two Buses for Short Transmission Line

Assuming a two-bus system as shown in **Figure 2.2-3**

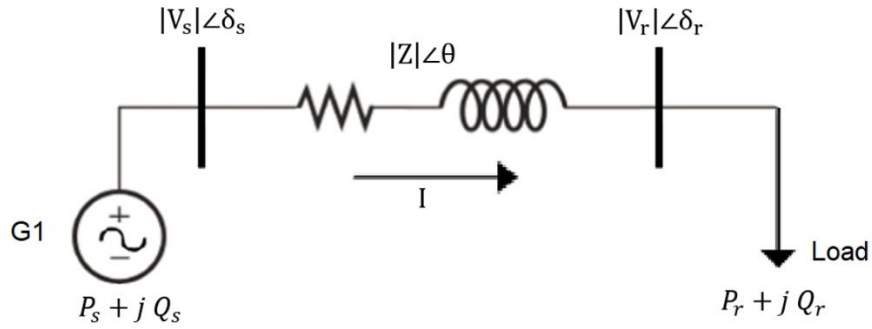


**Figure 2.2-3:** Two-Bus System with a Short Transmission Line

The apparent power is given by:

$$S = V \times I^* = P + j Q = \sqrt{P^2 + Q^2} \angle \tan^{-1} \left( \frac{Q}{P} \right) = |S| \angle \alpha; \quad \alpha = \widehat{V, I} \quad (4.26)$$

The current flows between the two buses is given by:

$$I = \frac{|V_s| \angle \delta_s - |V_r| \angle \delta_r}{|Z| \angle \theta} = \frac{|V_s| \angle \delta_s}{|Z| \angle \theta} - \frac{|V_r| \angle \delta_r}{|Z| \angle \theta} = \frac{|V_s|}{|Z|} \angle (\delta_s - \theta) - \frac{|V_r|}{|Z|} \angle (\delta_r - \theta) \quad (4.27)$$

The conjugated current will be as:

$$I^* = \frac{|V_s|}{|Z|} \angle (\theta - \delta_s) - \frac{|V_r|}{|Z|} \angle (\theta - \delta_r) \quad (4.28)$$

Then both the sending and receiving end power can be found.

### 2.2.4.2 Sending-End Power

Substituting the conjugated current in the sending-end apparent power  $S_s$

$$S_s = V_s \times I^* = P_s + j Q_s = V_s \angle \delta_s \times \left( \frac{|V_s|}{|Z|} \angle (\theta - \delta_s) - \frac{|V_r|}{|Z|} \angle (\theta - \delta_r) \right)$$

$$S_s = V_s \times I^* = P_s + j Q_s = \left( \frac{V_s^2}{Z} \angle (\theta) - \frac{V_s \times V_r}{Z} \angle (\theta - \delta_r + \delta_s) \right)$$

$$P_s = \frac{V_s^2}{Z} \cos(\theta) - \frac{V_s \times V_r}{Z} \cos(\theta - \delta_r + \delta_s)$$

$$Q_s = \frac{V_s^2}{Z} \sin(\theta) - \frac{V_s \times V_r}{Z} \sin(\theta - \delta_r + \delta_s)$$

If the resistance of the transmission line is neglected, then  $\theta=90^\circ$

$$P_s = \frac{V_s^2}{Z} \cos(90^\circ) - \frac{V_s \times V_r}{Z} \cos(90^\circ - (\delta_r - \delta_s)) = -\frac{V_s \times V_r}{Z} \sin(\delta_r - \delta_s)$$

$$Q_s = \frac{V_s^2}{Z} \sin(90^\circ) - \frac{V_s \times V_r}{Z} \sin(90^\circ - (\delta_r - \delta_s)) = \frac{V_s^2}{Z} - \frac{V_s \times V_r}{Z} \cos(\delta_r - \delta_s)$$

### 2.2.4.3 Receiving-End Power

Substituting the conjugated current in the receiving-end apparent power  $S_r$

$$S_r = V_r \times I^* = P_r + j Q_r = V_r \angle \delta_r \times \left( \frac{V_s}{Z} \angle (\theta - \delta_s) - \frac{V_r}{Z} \angle (\theta - \delta_r) \right)$$

$$S_r = V_r \times I^* = P_r + j Q_r = \left( \frac{V_s \times V_r}{Z} \angle (\theta - \delta_s + \delta_r) - \frac{V_r^2}{Z} \angle (\theta) \right)$$

$$P_r = \frac{V_s \times V_r}{Z} \cos(\theta - \delta_s + \delta_r) - \frac{V_r^2}{Z} \cos(\theta)$$

$$Q_r = \frac{V_s \times V_r}{Z} \sin(\theta - \delta_s + \delta_r) - \frac{V_r^2}{Z} \sin(\theta)$$

If the resistance of the transmission line is neglected, then  $\vartheta=90^\circ$

$$P_r = \frac{V_s \times V_r}{Z} \cos(90^\circ - (\delta_s - \delta_r)) - \frac{V_r^2}{Z} \cos(90^\circ) = \frac{V_s \times V_r}{Z} \sin(\delta_s - \delta_r)$$

$$Q_r = \frac{V_s \times V_r}{Z} \sin(90^\circ - (\delta_s - \delta_r)) - \frac{V_r^2}{Z} \sin(90^\circ) = \frac{V_s \times V_r}{Z} \cos(\delta_s - \delta_r) - \frac{V_r^2}{Z}$$

#### 2.2.4.4 REAL (ACTIVE) AND REACTIVE POWER INJECTED IN A BUS

For the formulation of the real and reactive power entering a bus, the following quantities needed to be defined. Let the voltage at the  $i^{\text{th}}$  bus be denoted by:

$$V_i = |V_i| \angle \delta_i = |V_i| (\cos \delta_i + j \sin \delta_i)$$

Also let us define the self-admittance at bus- $i$  as

$$Y_{ii} = |Y_{ii}| \angle \theta_{ii} = |Y_{ii}| (\cos \theta_{ii} + j \sin \theta_{ii}) = G_{ii} + jB_{ii}$$

Similarly, the mutual admittance between the buses  $i$  and  $j$  can be written as

$$Y_{ij} = |Y_{ij}| \angle \theta_{ij} = |Y_{ij}| (\cos \theta_{ij} + j \sin \theta_{ij}) = G_{ij} + jB_{ij}$$

The apparent power at  $i^{\text{th}}$  bus

$$S_i = V_i * I_i^* = P_i + jQ_i$$

$$S_i^* = V_i^* * I_i = P_i - jQ_i$$

Let the power system contains a total number of  $n$  buses.

$$\begin{bmatrix} Y_{11} & Y_{12} & Y_{13} & \dots & Y_{1i} & \dots & Y_{1n} \\ Y_{21} & Y_{22} & Y_{23} & \dots & Y_{2i} & \dots & Y_{2n} \\ Y_{31} & Y_{32} & Y_{33} & \dots & Y_{3i} & \dots & Y_{3n} \\ \vdots & \vdots & \vdots & \vdots & \vdots & \vdots & \vdots \\ Y_{i1} & Y_{i2} & Y_{i3} & \dots & Y_{ii} & \dots & Y_{in} \\ \vdots & \vdots & \vdots & \vdots & \vdots & \vdots & \vdots \\ Y_{n1} & Y_{n2} & Y_{n3} & \dots & Y_{ni} & \dots & Y_{nn} \end{bmatrix} \begin{bmatrix} V_1 \\ V_2 \\ V_3 \\ \vdots \\ V_i \\ \vdots \\ V_n \end{bmatrix} = \begin{bmatrix} I_1 \\ I_2 \\ I_3 \\ \vdots \\ I_i \\ \vdots \\ I_n \end{bmatrix}$$

The current at bus  $i$

$$I_i = Y_{i1}V_1 + Y_{i2}V_2 + \dots + Y_{ii}V_i + \dots + Y_{in}V_n$$

Rewriting above equation using summation symbol

$$I_i = \sum_{k=1}^n Y_{ik} V_k$$

Substituting equation  $I_i$  in  $S_i^*$  equation

$$S_i^* = V_i^* \cdot \sum_{k=1}^n Y_{ik} V_k$$

But  $V_i = |V_i| \angle \delta_i$ ,  $V_k = |V_k| \angle \delta_k$ ,  $Y_{ik} = |Y_{ik}| \angle \theta_{ik}$

$$S_i^* = |V_i| \cdot \sum_{k=1}^n |Y_{ik}| \cdot |V_k| \angle (\theta_{ik} + \delta_k - \delta_i) = P_i - jQ_i$$

$$P_i = |V_i| \cdot \sum_{k=1}^n |Y_{ik}| \cdot |V_k| \cos(\theta_{ik} + \delta_k - \delta_i)$$

$$Q_i = -|V_i| \cdot \sum_{k=1}^n |Y_{ik}| \cdot |V_k| \sin(\theta_{ik} + \delta_k - \delta_i)$$

#### 2.2.4.5 CLASSIFICATION OF BUSES

For power flow studies it is assumed that the loads are constant, and they are defined by their active and reactive power consumption. It is further assumed that the generator terminal voltages are tightly regulated and therefore are constant. The main objective of the power flow is to find the voltage magnitude of each bus and its angle when the powers generated, and loads are pre-specified. To facilitate this, the different buses of the power system are listed below.

##### 2.2.4.5.1 Slack or Swing or Reference Bus $1 \angle 0^\circ$

Usually this bus is numbered "1" for the power flow studies. This bus sets the angular reference for all the other buses. Since it is the angle difference between two voltage sources that dictates the active and reactive power flow between them, the particular angle of the slack bus is not important. However, it sets the reference against which angles of all the other

bus voltages are measured. For this reason, the angle of this bus is usually chosen as  $0^\circ$ . Furthermore, it is assumed that the magnitude of the voltage of this bus is known.

#### 2.2.4.5.2 Load Buses (P-Q Buses)

In these buses, no generators are connected and hence the generated active power  $P_{Gi}$  and reactive power  $Q_{Gi}$  are taken as zero. The load drawn by these buses are defined by active power  $-P_{Li}$  and reactive power  $-Q_{Li}$  in which the negative sign accommodates for the power flowing out of the bus. This is why these buses are sometimes referred to as P-Q bus. The objective of the load flow is to find the bus voltage magnitude  $|V_i|$  and its angle  $\delta_i$ . **Errore. L'origine riferimento non è stata trovata.** shows the load bus (P-Q bus).

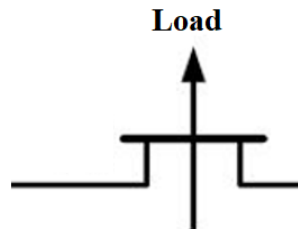
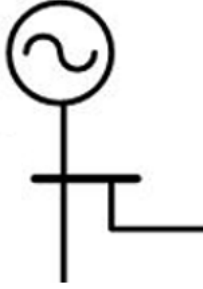


Figure 2.2-4: Load Bus (P-Q bus)

#### 2.2.4.5.3 Voltage Controlled Buses (P-V Buses)

These are the buses where generators are connected. Therefore, the power generation in such buses is controlled through a prime mover while the terminal voltage is controlled through the generator excitation. Keeping the input power constant through turbine-governor control and keeping the bus voltage constant using automatic voltage regulator, constant  $P_{Gi}$  and  $|V_i|$  for these buses can be specified. This is why such buses are also referred to as P-V buses. The objective of the load flow is to find the reactive power supplied by the generator  $Q_{Gi}$  which depends on the system configuration and cannot be specified in advance. Furthermore, the unknown angle  $\delta_i$  of the bus voltage have to be found. **Figure 2.2-5** shows the generator bus (PV bus).



**Figure 2.2-5:** Generator Bus (PV Bus)

#### 2.2.4.6 LOAD FLOW BY NEWTON-RAPHSON (N-R) METHOD

In this study, the Newton-Raphson method is used for the power flow calculation. Assuming an  $n$ -bus power system contains a total number of  $n_p$  load buses while the number of generator buses is  $n_g$  such that  $n = n_p + n_g + 1$ . Bus-1 is assumed to be the slack bus which will be the PoCC bus in this case study. The mismatch equations of  $\Delta P_i$  and  $\Delta Q_i$  given in (4.9) and (4.10) respectively will be used.

Let real (active) and reactive power generated at bus- $i$  be denoted by  $P_{Gi}$  and  $Q_{Gi}$  respectively. Also let us denote the real and reactive power consumed at the  $i^{\text{th}}$  bus by  $P_{Li}$  and  $Q_{Li}$  respectively. Then the net real (active) power injected in bus- $i$  is

$$P_{i,inj} = P_{Gi} - P_{Li}$$

Let the injected power calculated by the load flow program be  $P_{i,calc}$ . Then the mismatch between the actual injected and calculated values is given by

$$\Delta P_i = P_{i,inj} - P_{i,calc} = P_{Gi} - P_{Li} - P_{i,calc}$$

In a similar way the mismatch between the reactive power injected and calculated values is given by

$$\Delta Q_i = Q_{i,inj} - Q_{i,calc} = Q_{Gi} - Q_{Li} - Q_{i,calc}$$

The purpose of the power flow is to minimize the above two mismatches

The mismatch can be rewritten as:

$$\Delta P_i = \sum_{K=2}^n \frac{\partial P_i}{\partial \delta_k} \Delta \delta_k + \sum_{K=2}^n \frac{\partial P_i}{\partial |V_k|} \Delta |V_k|$$

$$\Delta Q_i = \sum_{K=2}^n \frac{\partial Q_i}{\partial \delta_k} \Delta \delta_k + \sum_{K=2}^n \frac{\partial Q_i}{\partial |V_k|} \Delta |V_k|$$

It is more convenient to re-write the term which is partially differentiated with respect to  $V_k$  as:

$$\Delta P_i = \sum_{K=2}^n \frac{\partial P_i}{\partial \delta_k} \Delta \delta_k + \sum_{K=2}^n \frac{\partial P_i}{\partial |V_k|} |V_k| \frac{\Delta |V_k|}{|V_k|}$$

$$\Delta Q_i = \sum_{K=2}^n \frac{\partial Q_i}{\partial \delta_k} \Delta \delta_k + \sum_{K=2}^n \frac{\partial Q_i}{\partial |V_k|} |V_k| \frac{\Delta |V_k|}{|V_k|}$$

We can rewrite (4-53) and (4-54) in matrix form

$$\begin{bmatrix} \Delta P_i \\ \Delta Q_i \end{bmatrix} = \begin{bmatrix} \sum_{K=2}^n \frac{\partial P_i}{\partial \delta_k} & \sum_{K=2}^n \frac{\partial P_i}{\partial |V_k|} |V_k| \\ \sum_{K=2}^n \frac{\partial Q_i}{\partial \delta_k} & \sum_{K=2}^n \frac{\partial Q_i}{\partial |V_k|} |V_k| \end{bmatrix} \begin{bmatrix} \Delta \delta_k \\ \frac{\Delta |V_k|}{|V_k|} \end{bmatrix}$$

$$J \begin{bmatrix} \Delta \delta_2 \\ \vdots \\ \Delta \delta_n \\ \frac{\Delta |V_2|}{|V_2|} \\ \vdots \\ \frac{\Delta |V_{1+n_p}|}{|V_{1+n_p}|} \end{bmatrix} = \begin{bmatrix} \Delta P_2 \\ \vdots \\ \Delta P_n \\ \Delta Q_2 \\ \vdots \\ \Delta Q_{1+n_p} \end{bmatrix}$$

where the Jacobian matrix is divided into submatrices as

$$J = \begin{bmatrix} J_{11} & J_{12} \\ J_{21} & J_{22} \end{bmatrix}$$

It can be seen that the size of the Jacobian matrix is  $(n + n_p - 1) \times (n + n_p - 1)$ . The dimensions of the submatrices are as follows:

$$J_{11}: (n - 1) \times (n - 1), J_{12}: (n - 1) \times n_p, J_{21}: n_p \times (n - 1) \text{ and } J_{22}: n_p \times n_p$$

The submatrices are

$$J_{11} = \begin{bmatrix} \frac{\partial P_2}{\partial \delta_2} & \dots & \frac{\partial P_2}{\partial \delta_n} \\ \vdots & \ddots & \vdots \\ \frac{\partial P_n}{\partial \delta_2} & \dots & \frac{\partial P_n}{\partial \delta_n} \end{bmatrix}$$

$$J_{12} = \begin{bmatrix} |V_2| \frac{\partial P_2}{\partial |V_2|} & \dots & |V_{1+n_p}| \frac{\partial P_2}{\partial |V_{1+n_p}|} \\ \vdots & \ddots & \vdots \\ |V_2| \frac{\partial P_n}{\partial |V_2|} & \dots & |V_{1+n_p}| \frac{\partial P_n}{\partial |V_{1+n_p}|} \end{bmatrix}$$

$$J_{21} = \begin{bmatrix} \frac{\partial Q_2}{\partial \delta_2} & \dots & \frac{\partial Q_2}{\partial \delta_n} \\ \vdots & \ddots & \vdots \\ \frac{\partial Q_{1+n_p}}{\partial \delta_2} & \dots & \frac{\partial Q_{1+n_p}}{\partial \delta_n} \end{bmatrix}$$

$$J_{22} = \begin{bmatrix} |V_2| \frac{\partial Q_2}{\partial |V_2|} & \dots & |V_{1+n_p}| \frac{\partial Q_2}{\partial |V_{1+n_p}|} \\ \vdots & \ddots & \vdots \\ |V_2| \frac{\partial Q_{1+n_p}}{\partial |V_2|} & \dots & |V_{1+n_p}| \frac{\partial Q_{1+n_p}}{\partial |V_{1+n_p}|} \end{bmatrix}$$

#### 2.2.4.7 Load Flow Algorithm

The Newton-Raphson procedure shown in **Figure 2.2-6** is as follows:

**Step-1:** Choose the initial values of the voltage magnitudes  $|V|^{(0)}$  of all  $n_p$  load buses and  $n - 1$  angle  $\delta^{(0)}$  of the voltages of all the buses except the slack bus.

Step-2: Use the estimated  $|V|^{(0)}$  and  $\delta^{(0)}$  to calculate a total  $n - 1$  number of injected real power  $P_{calc}^{(0)}$  and equal number of real power mismatch  $\Delta P^{(0)}$ .

Step-3: Use the estimated  $|V|^{(0)}$  and  $\delta^{(0)}$  to calculate a total  $n_p$  number of injected reactive power  $Q_{calc}^{(0)}$  and equal number of reactive power mismatch  $\Delta Q^{(0)}$ .

Step-3: Use the estimated  $|V|^{(0)}$  and  $\delta^{(0)}$  to formulate the Jacobian matrix  $J^{(0)}$ .

Step-4: Solve (4.30) for  $\Delta\delta^{(0)}$  and  $\Delta|V|^{(0)}/|V|^{(0)}$ .

Step-5: Obtain the updates from

$$\delta^{(1)} = \delta^{(0)} + \Delta\delta^{(0)}$$

$$|V|^{(1)} = |V|^{(0)} \left[ 1 + \frac{\Delta|V|^{(0)}}{|V|^{(0)}} \right]$$

Step-6: Check if all the mismatches are below a small number. Terminate the process if yes. Otherwise go back to step one to start the next iteration with the updates given by (4.36) and (4.37).

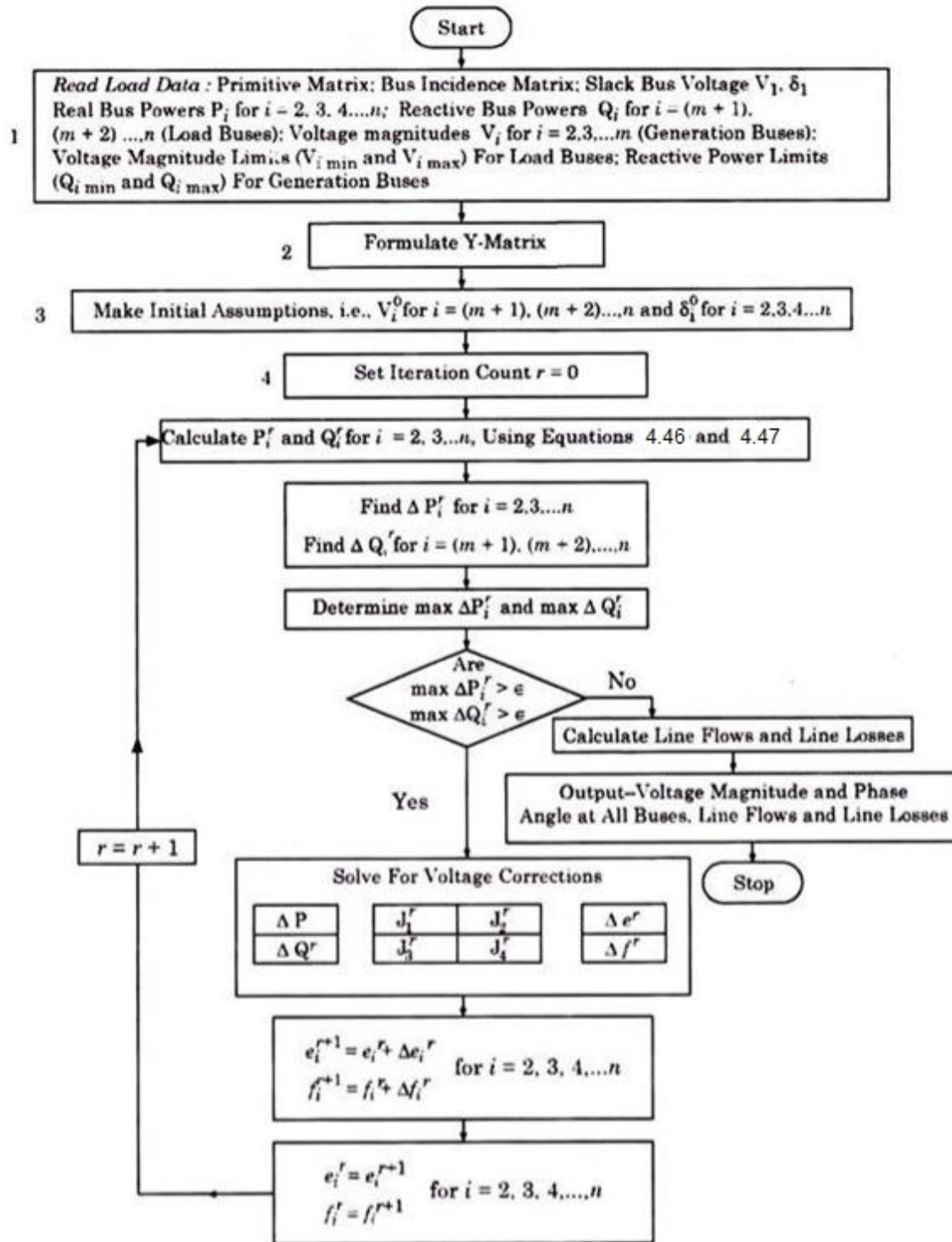


Figure 2.2-6: Flow Chart for Power Flow Solution Using N-R Method

### 2.2.4.8 Formation of the Jacobian Matrix

In order to format the submatrices of the Jacobian matrix. The real and reactive power equations of (4-46) and (4-47) shall be used. Let us rewrite them with the help of (4.38) as

$$P_i = |V_i|^2 G_{ii} + \sum_{\substack{k=1 \\ k \neq i}}^n |Y_{ik} V_i V_k| \cos(\theta_{ik} + \delta_k - \delta_i) \quad (4.64)$$

$$Q_i = -|V_i|^2 B_{ii} - \sum_{\substack{k=1 \\ k \neq i}}^n |Y_{ik} V_i V_k| \sin(\theta_{ik} + \delta_k - \delta_i) \quad (4.65)$$

#### 2.2.4.8.1 Formation of $J_{11}$

Let us define  $J_{11}$  as

$$J_{11} = \begin{bmatrix} L_{22} & \cdots & L_{2n} \\ \vdots & \ddots & \vdots \\ L_{n2} & \cdots & L_{nn} \end{bmatrix}$$

It can be seen from (4-58) that  $M_{ik}$ 's are the partial derivatives of  $P_i$  with respect to  $\delta_k$ . The derivative  $P_i$  (4-64) with respect to  $k$  for  $i \neq k$  is given by

$$L_{ik} = \frac{\partial P_i}{\partial \delta_k} = -|Y_{ik} V_i V_k| \sin(\theta_{ik} + \delta_k - \delta_i), \quad i \neq k$$

Similarly, the derivative  $P_i$  with respect to  $k$  for  $i = k$  is given by

$$L_{ii} = \frac{\partial P_i}{\partial \delta_i} = \sum_{\substack{k=1 \\ k \neq i}}^n |Y_{ik} V_i V_k| \sin(\theta_{ik} + \delta_k - \delta_i)$$

Comparing the above equation with (4-65)  $L_{ii}$  can be written as below

$$L_{ii} = \frac{\partial P_i}{\partial \delta_i} = -Q_i - |V_i|^2 B_{ii}$$

#### 2.2.4.8.2 Formation of $J_{21}$

Let us define  $J_{21}$  as

$$J_{21} = \begin{bmatrix} M_{22} & \cdots & M_{2n} \\ \vdots & \ddots & \vdots \\ M_{n_p 2} & \cdots & M_{n_p n} \end{bmatrix}$$

From (4.60), it is evident that the elements of  $J_{21}$  are the partial derivative of  $Q$  with respect to  $\delta$ .

From (4.65),  $M_{ik}$  can be derived as below.

$$M_{ik} = \frac{\partial Q_i}{\partial \delta_k} = -|Y_{ik} V_i V_k| \cos(\theta_{ik} + \delta_k - \delta_i), \quad i \neq k$$

Similarly, for  $i = k$ ,  $M_{ii}$  can be derived as below

$$M_{ii} = \frac{\partial Q_i}{\partial \delta_i} = \sum_{\substack{k=1 \\ k \neq i}}^n |Y_{ik} V_i V_k| \cos(\theta_{ik} + \delta_k - \delta_i) = P_i - |V_i|^2 G_{ii}$$

#### 2.2.4.8.3 Formation of $J_{12}$

Let us define  $J_{12}$  as

$$J_{12} = \begin{bmatrix} N_{22} & \cdots & N_{2n_p} \\ \vdots & \ddots & \vdots \\ N_{n 2} & \cdots & N_{nn_p} \end{bmatrix}$$

As evident from (4.59), the elements of  $J_{21}$  involve the derivatives of real power  $P$  with respect to magnitude of bus voltage  $|V|$ . For  $i \neq k$ ,  $N_{ik}$  can be derived from (4-64) as below

$$N_{ik} = |V_k| \frac{\partial P_i}{\partial |V_k|} = |Y_{ik} V_i V_k| \cos(\theta_{ik} + \delta_k - \delta_i) = -M_{ik} \quad i \neq k$$

For  $i = k$ ,  $N_{ii}$  can be derived from (4-64) as below

$$\begin{aligned} N_{ii} &= |V_i| \frac{\partial P_i}{\partial |V_i|} = |V_i| \left[ 2|V_i| G_{ii} + \sum_{\substack{k=1 \\ k \neq i}}^n |Y_{ik} V_k| \cos(\theta_{ik} + \delta_k - \delta_i) \right] \\ &= 2|V_i|^2 G_{ii} + \sum_{\substack{k=1 \\ k \neq i}}^n |Y_{ik} V_i V_k| \cos(\theta_{ik} + \delta_k - \delta_i) = 2|V_i|^2 G_{ii} + M_{ii} \end{aligned}$$

#### 2.2.4.8.4 Formation of $J_{22}$

For the formation of  $J_{22}$  let us define

$$J_{22} = \begin{bmatrix} O_{22} & \cdots & O_{2n_p} \\ \vdots & \ddots & \vdots \\ O_{n_p 2} & \cdots & O_{n_p n_p} \end{bmatrix}$$

For  $i \neq k$ ,  $Q_{ik}$  can be derived from (4.65)

$$O_{ik} = |V_i| \frac{\partial Q_i}{\partial |V_k|} = -|V_i| |Y_{ik} V_i V_k| \sin(\theta_{ik} + \delta_k - \delta_i) = L_{ik}, \quad i \neq k$$

Finally, for  $i = k$ ,  $Q_{ii}$  can be derived from (4.65)

$$\begin{aligned} O_{ii} &= |V_i| \frac{\partial Q_i}{\partial |V_k|} = |V_i| \left[ -2|V_i| B_{ii} - \sum_{\substack{k=1 \\ k \neq i}}^n |Y_{ik} V_k| \sin(\theta_{ik} + \delta_k - \delta_i) \right] \\ &= -2|V_i|^2 B_{ii} - \sum_{\substack{k=1 \\ k \neq i}}^n |Y_{ik} V_i V_k| \sin(\theta_{ik} + \delta_k - \delta_i) = -2|V_i|^2 B_{ii} - L_{ii} \end{aligned}$$

We therefore see that once the submatrices  $J_{11}$  and  $J_{21}$  are computed, the formation of the submatrices  $J_{12}$  and  $J_{22}$  is straightforward. For large system this will result in considerable saving in the computation time.

#### 2.2.4.9 Buses Classification for the IEEE 9 Bus system

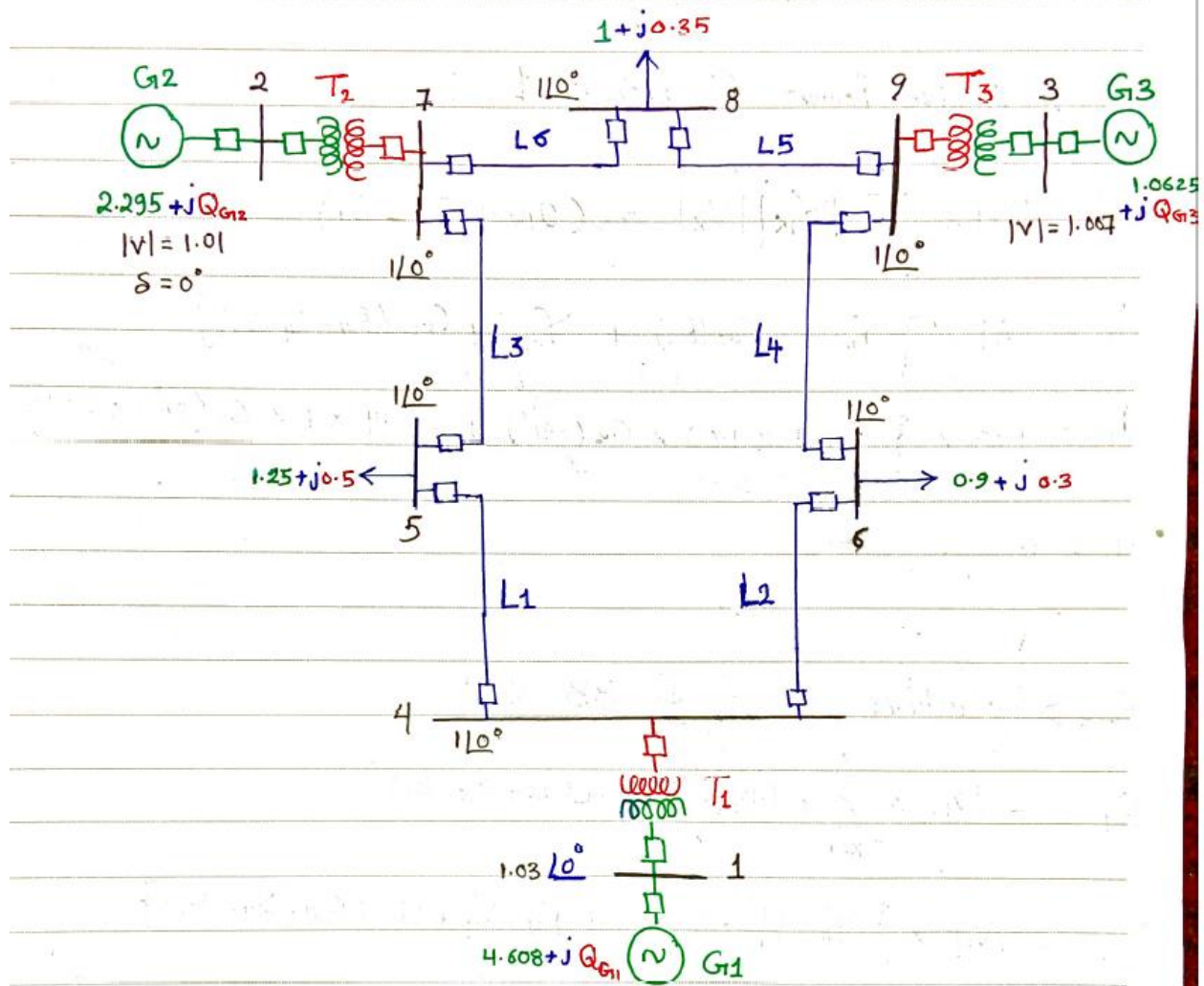
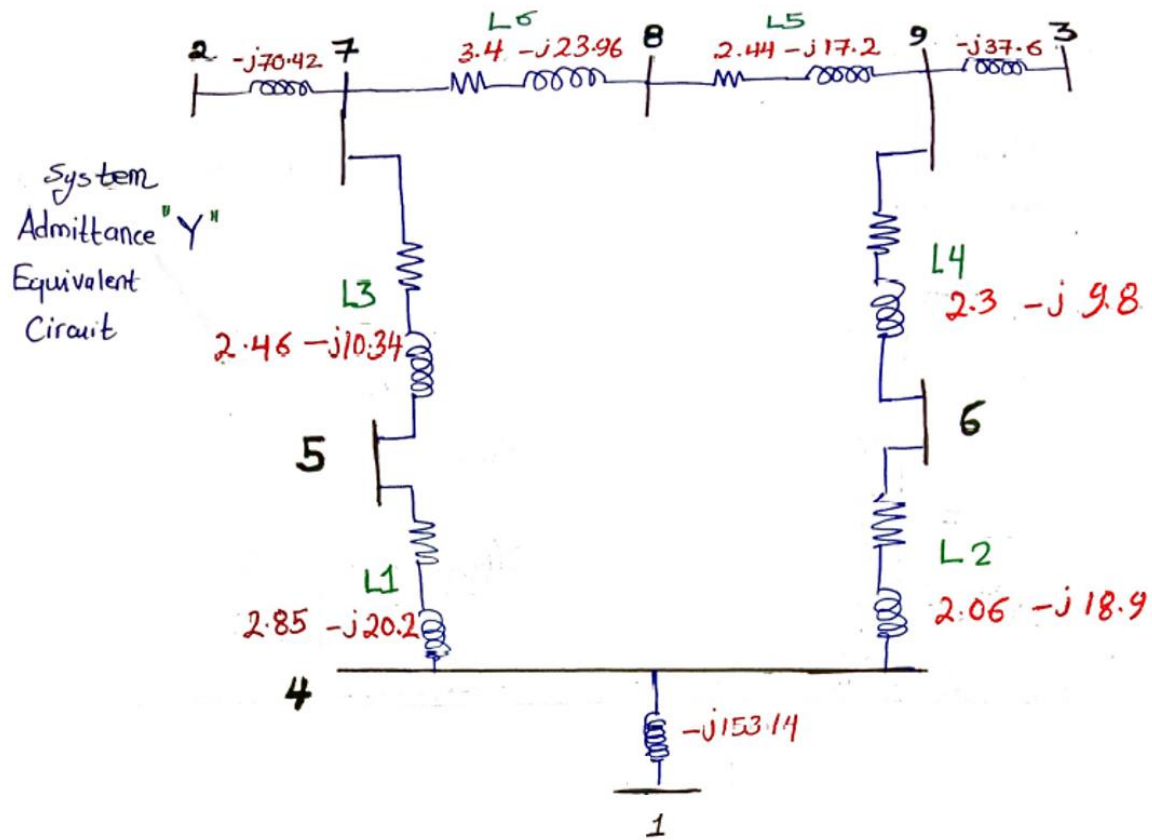


Figure 2.2-7: Power Flow Equivalent Circuit

Bus No	Bus Type	Specified Quantity	Assumed Parameter	Calculated Power
1	Slack	$1.03\angle 0^\circ$	N/A	
2	PV Bus	$P=2.295,  V =1.01$	$\delta=0^\circ$	$P_2$
3	PV Bus	$P=1.0625,  V =1.007$	$\delta=0^\circ$	$P_3$
4	Load Bus	$P=0, Q=0$	$ V \angle\delta = 1\angle 0^\circ$	$P_4, Q_4$
5	Load Bus	$P=1.25, Q=0.5$	$ V \angle\delta = 1\angle 0^\circ$	$P_5, Q_5$
6	Load Bus	$P=0.9, Q=0.3$	$ V \angle\delta = 1\angle 0^\circ$	$P_6, Q_6$
7	Load Bus	$P=0, Q=0$	$ V \angle\delta = 1\angle 0^\circ$	$P_7, Q_7$
8	Load Bus	$P=1, Q=0.35$	$ V \angle\delta = 1\angle 0^\circ$	$P_8, Q_8$
9	Load Bus	$P=0, Q=0$	$ V \angle\delta = 1\angle 0^\circ$	$P_9, Q_9$

### 2.2.4.10 FORMULATION OF Y BUS



$Y_{BUS} =$

	1	2	3	4	5	6	7	8	9
1	$153.4 \angle -90^\circ$	0	0	$153.4 \angle -90^\circ$	0	0	0	0	0
2	0	$70.42 \angle -90^\circ$	0	0	0	0	$70.42 \angle -90^\circ$	0	0
3	0	0	$37.6 \angle -90^\circ$	0	0	0	0	0	$37.6 \angle -90^\circ$
4	$153.4 \angle 90^\circ$	0	0	$153.3 \angle -165^\circ$	$20.4 \angle 98^\circ$	$19.01 \angle 96^\circ$	0	0	0
5	0	0	0	$20.4 \angle 98^\circ$	$31 \angle 80^\circ$	0	$10.6 \angle 103^\circ$	0	0
6	0	0	0	$19.01 \angle 96^\circ$	0	$29 \angle -81^\circ$	0	0	$10.6 \angle 103^\circ$
7	0	$70.42 \angle 90^\circ$	0	0	$10.6 \angle 103^\circ$	0	$73.1 \angle -152^\circ$	$24.2 \angle 98^\circ$	0
8	0	0	0	0	0	0	$24.2 \angle 98^\circ$	$41.6 \angle -82^\circ$	$17.4 \angle 98^\circ$
9	0	0	$37.6 \angle 90^\circ$	0	0	$10.6 \angle 103^\circ$	0	$17.4 \angle 98^\circ$	$64.8 \angle -86^\circ$

### 2.2.4.11 Calculation of Active (Real) Power and Reactive Power for each of the buses

#### 2.2.4.11.1 Active/Reactive Power injected in/delivered by Bus No.1

P1 => Active power at Bus No.1

$$P_1 = |V_1| \cdot \sum_{k=1}^9 |Y_{1k}| \cdot |V_k| \cos(\theta_{1k} + \delta_k - \delta_1)$$

$$P_1 = |V_1| \cdot \{|Y_{11}| \cdot |V_1| \cos(\theta_{11} + \delta_1 - \delta_1) + |Y_{14}| \cdot |V_4| \cos(\theta_{14} + \delta_4 - \delta_1)\}$$

$$P_1 = |1.03| \cdot \{|153.4| \cdot |1.03| \cos(-90^\circ + 0^\circ - 0^\circ) + |153.4| \cdot |1| \cos(90^\circ + 0^\circ - 0^\circ)\}$$

$$P_1 = 0$$

Q1 => Reactive power at Bus No.1

$$Q_1 = -|V_1| \cdot \sum_{k=1}^9 |Y_{1k}| \cdot |V_k| \sin(\theta_{1k} + \delta_k - \delta_1)$$

$$Q_1 = -|V_1| \cdot \{|Y_{11}| \cdot |V_1| \sin(\theta_{11} + \delta_1 - \delta_1) + |Y_{14}| \cdot |V_4| \sin(\theta_{14} + \delta_4 - \delta_1)\}$$

$$Q_1 = -|1.03| \cdot \{|153.4| \cdot |1.03| \sin(-90^\circ + 0^\circ - 0^\circ) + |153.4| \cdot |1| \sin(90^\circ + 0^\circ - 0^\circ)\}$$

$$Q_1 = 4.74 \text{ PU}$$

#### 2.2.4.11.2 Active/Reactive Power injected in/delivered by Bus No.2

P2 => Active power at Bus No.2

$$P_2 = |V_2| \cdot \sum_{k=1}^9 |Y_{2k}| \cdot |V_k| \cos(\theta_{2k} + \delta_k - \delta_2)$$

$$P_2 = |V_2| \cdot \{|Y_{22}| \cdot |V_2| \cos(\theta_{22} + \delta_2 - \delta_2) + |Y_{27}| \cdot |V_7| \cos(\theta_{27} + \delta_7 - \delta_2)\}$$

$$P_2 = |1.01| \cdot \{|70.42| \cdot |1.01| \cos(-90^\circ + 0^\circ - 0^\circ) + |70.42| \cdot |1| \cos(90^\circ + 0^\circ - 0^\circ)\}$$

$$P_2 = 0$$

Q2 => Reactive power at Bus No.2

$$Q_2 = -|V_2| \cdot \sum_{k=1}^9 |Y_{2k}| \cdot |V_k| \sin(\theta_{2k} + \delta_k - \delta_2)$$

$$Q_2 = -|V_2| \cdot \{|Y_{22}| \cdot |V_2| \sin(\theta_{22} + \delta_2 - \delta_2) + |Y_{27}| \cdot |V_7| \sin(\theta_{27} + \delta_7 - \delta_2)\}$$

$$Q_2 = -|1.01| \cdot \{|70.42| \cdot |1.01| \sin(-90^\circ + 0^\circ - 0^\circ) + |70.42| \cdot |1| \sin(90^\circ + 0^\circ - 0^\circ)\}$$

$$Q_2 = 0.711242 \text{ PU}$$

#### 2.2.4.11.3 Active/Reactive Power injected in/delivered by Bus No.3

P3 => Active power at Bus No.3

$$P_3 = |V_3| \cdot \sum_{k=1}^9 |Y_{3k}| \cdot |V_k| \cos(\theta_{3k} + \delta_k - \delta_3)$$

$$P_3 = |V_3| \cdot \{|Y_{33}| \cdot |V_3| \cos(\theta_{33} + \delta_3 - \delta_3) + |Y_{39}| \cdot |V_9| \cos(\theta_{39} + \delta_9 - \delta_3)\}$$

$$P_3 = |1.007| \cdot \{|37.6| \cdot |1.007| \cos(-90^\circ + 0^\circ - 0^\circ) + |37.6| \cdot |1| \cos(90^\circ + 0^\circ - 0^\circ)\}$$

$$P_3 = 0$$

Q3 => Reactive power at Bus No.3

$$Q_3 = -|V_3| \cdot \sum_{k=1}^9 |Y_{3k}| \cdot |V_k| \sin(\theta_{3k} + \delta_k - \delta_3)$$

$$Q_3 = -|V_3| \cdot \{|Y_{33}| \cdot |V_3| \sin(\theta_{33} + \delta_3 - \delta_3) + |Y_{39}| \cdot |V_9| \sin(\theta_{39} + \delta_9 - \delta_3)\}$$

$$Q_3 = -|1.007| \cdot \{|37.6| \cdot |1.007| \sin(-90^\circ + 0^\circ - 0^\circ) + |37.6| \cdot |1| \sin(90^\circ + 0^\circ - 0^\circ)\}$$

$$Q_3 = 0.265 \text{ PU}$$

#### 2.2.4.11.4 Active/Reactive Power injected in/delivered by Bus No.4

P4 => Active power at Bus No.4

$$P_4 = |V_4| \cdot \sum_{k=1}^9 |Y_{4k}| \cdot |V_k| \cos(\theta_{4k} + \delta_k - \delta_4)$$

$$P_4 = |V_4| \cdot \{|Y_{41}| \cdot |V_1| \cos(\theta_{41} + \delta_1 - \delta_4) + |Y_{44}| \cdot |V_4| \cos(\theta_{44} + \delta_4 - \delta_4) + |Y_{45}|$$

$$\cdot |V_5| \cos(\theta_{45} + \delta_5 - \delta_4) + |Y_{46}| \cdot |V_6| \cos(\theta_{46} + \delta_6 - \delta_4)\}$$

$$P_4 = |1| \cdot \{|153.4| \cdot |1.03| \cos(90^\circ + 0^\circ - 0^\circ) + |153.4| \cdot |1| \cos(-165^\circ + 0^\circ - 0^\circ) + |20.4|$$

$$\cdot |1| \cos(98^\circ + 0^\circ - 0^\circ) + |19.01| \cdot |1| \cos(96^\circ + 0^\circ - 0^\circ)\}$$

$$P_4 = -153.08 \text{ PU}$$

Q4 => Reactive power at Bus No.4

$$Q_4 = -|V_4| \cdot \sum_{k=1}^9 |Y_{4k}| \cdot |V_k| \sin(\theta_{4k} + \delta_k - \delta_4)$$

$$Q_4 = -|V_4| \cdot \{|Y_{41}| \cdot |V_1| \sin(\theta_{41} + \delta_1 - \delta_4) + |Y_{44}| \cdot |V_4| \sin(\theta_{44} + \delta_4 - \delta_4) + |Y_{45}|$$

$$\cdot |V_5| \sin(\theta_{45} + \delta_5 - \delta_4) + |Y_{46}| \cdot |V_6| \sin(\theta_{46} + \delta_6 - \delta_4)\}$$

$$Q_4 = -|1| \cdot \{|153.4| \cdot |1.03| \sin(90^\circ + 0^\circ - 0^\circ) + |153.4| \cdot |1| \sin(-165^\circ + 0^\circ - 0^\circ) + |20.4|$$

$$\cdot |1| \sin(98^\circ + 0^\circ - 0^\circ) + |19.01| \cdot |1| \sin(96^\circ + 0^\circ - 0^\circ)\}$$

$$Q_4 = -157.43 \text{ PU}$$

#### 2.2.4.11.5 Active/Reactive Power injected in/delivered by Bus No.5

P5 => Active power at Bus No.5

$$P_5 = |V_5| \cdot \sum_{k=1}^9 |Y_{5k}| \cdot |V_k| \cos(\theta_{5k} + \delta_k - \delta_5)$$

$$P_5 = |V_5| \cdot \{|Y_{54}| \cdot |V_4| \cos(\theta_{54} + \delta_4 - \delta_5) + |Y_{55}| \cdot |V_5| \cos(\theta_{55} + \delta_5 - \delta_5) + |Y_{57}|$$

$$\cdot |V_7| \cos(\theta_{57} + \delta_7 - \delta_5)\}$$

$$P_5 = |1| \cdot \{|20.4| \cdot |1| \cos(90^\circ + 0^\circ - 0^\circ) + |31| \cdot |1| \cos(-80^\circ + 0^\circ - 0^\circ) + |10.6| \cdot |1| \cos(103^\circ + 0^\circ - 0^\circ)\}$$

$$P_5 = -153.08 \text{ PU}$$

Q5 => Reactive power at Bus No.5

$$Q_5 = -|V_5| \cdot \sum_{k=1}^9 |Y_{5k}| \cdot |V_k| \sin(\theta_{5k} + \delta_k - \delta_5)$$

$$Q_5 = -|V_5| \cdot \{|Y_{54}| \cdot |V_4| \sin(\theta_{54} + \delta_4 - \delta_5) + |Y_{55}| \cdot |V_5| \sin(\theta_{55} + \delta_5 - \delta_5) + |Y_{57}| \cdot |V_7| \sin(\theta_{57} + \delta_7 - \delta_5)\}$$

$$Q_5 = -|1| \cdot \{|20.4| \cdot |1| \sin(90^\circ + 0^\circ - 0^\circ) + |31| \cdot |1| \sin(-80^\circ + 0^\circ - 0^\circ) + |10.6| \cdot |1| \sin(103^\circ + 0^\circ - 0^\circ)\}$$

$$Q_5 = -157.43 \text{ PU}$$

#### 2.2.4.11.6 Active/Reactive Power injected in/delivered by Bus No.6

P6 => Active power at Bus No.6

$$P_6 = |V_6| \cdot \sum_{k=1}^9 |Y_{6k}| \cdot |V_k| \cos(\theta_{6k} + \delta_k - \delta_6)$$

$$P_6 = |V_6| \cdot \{|Y_{64}| \cdot |V_4| \cos(\theta_{64} + \delta_4 - \delta_6) + |Y_{66}| \cdot |V_6| \cos(\theta_{66} + \delta_6 - \delta_6) + |Y_{69}| \cdot |V_9| \cos(\theta_{69} + \delta_9 - \delta_6)\}$$

$$P_6 = |1| \cdot \{|19.01| \cdot |1| \cos(96^\circ + 0^\circ - 0^\circ) + |29| \cdot |1| \cos(-81^\circ + 0^\circ - 0^\circ) + |10.06| \cdot |1| \cos(103^\circ + 0^\circ - 0^\circ)\}$$

$$P_5 = 0.286505 \text{ PU}$$

Q6 => Reactive power at Bus No.6

$$Q_6 = -|V_6| \cdot \sum_{k=1}^9 |Y_{6k}| \cdot |V_k| \sin(\theta_{6k} + \delta_k - \delta_6)$$

$$Q_6 = -|V_6| \cdot \{|Y_{64}| \cdot |V_4| \sin(\theta_{64} + \delta_4 - \delta_6) + |Y_{66}| \cdot |V_6| \sin(\theta_{66} + \delta_6 - \delta_6) + |Y_{69}| \cdot |V_9| \sin(\theta_{69} + \delta_9 - \delta_6)\}$$

$$Q_6 = -|1| \cdot \{|19.01| \cdot |1| \sin(96^\circ + 0^\circ - 0^\circ) + |29| \cdot |1| \sin(-81^\circ + 0^\circ - 0^\circ) + |10.06| \cdot |1| \sin(103^\circ + 0^\circ - 0^\circ)\}$$

$$Q_6 = -0.065062 \text{ PU}$$

#### 2.2.4.11.7 Active/Reactive Power injected in/delivered by Bus No.7

P7 => Active power at Bus No.7

$$P_7 = |V_7| \cdot \sum_{k=1}^9 |Y_{7k}| \cdot |V_k| \cos(\theta_{7k} + \delta_k - \delta_7)$$

$$P_7 = |V_7| \cdot \{|Y_{72}| \cdot |V_2| \cos(\theta_{72} + \delta_2 - \delta_7) + |Y_{75}| \cdot |V_5| \cos(\theta_{75} + \delta_5 - \delta_7) + |Y_{77}| \cdot |V_7| \cos(\theta_{77} + \delta_7 - \delta_7) + |Y_{78}| \cdot |V_8| \cos(\theta_{78} + \delta_8 - \delta_7)\}$$

$$P_6 = |1| \cdot \{|70.42| \cdot |1.01| \cos(90^\circ + 0^\circ - 0^\circ) + |10.6| \cdot |1| \cos(103^\circ + 0^\circ - 0^\circ) + |73.1| \cdot |1| \cos(-152^\circ + 0^\circ - 0^\circ) + |24.2| \cdot |1| \cos(98^\circ + 0^\circ - 0^\circ)\}$$

$$P_5 = -70.3 \text{ PU}$$

Q7 => Reactive power at Bus No.7

$$Q_7 = -|V_7| \cdot \sum_{k=1}^9 |Y_{7k}| \cdot |V_k| \sin(\theta_{7k} + \delta_k - \delta_7)$$

$$Q_7 = -|V_7| \cdot \{|Y_{72}| \cdot |V_2| \sin(\theta_{72} + \delta_2 - \delta_7) + |Y_{75}| \cdot |V_5| \sin(\theta_{75} + \delta_5 - \delta_7) + |Y_{77}| \cdot |V_7| \sin(\theta_{77} + \delta_7 - \delta_7) + |Y_{78}| \cdot |V_8| \sin(\theta_{78} + \delta_8 - \delta_7)\}$$

$$Q_7 = -|1| \cdot \{|70.42| \cdot |1.01| \sin(90^\circ + 0^\circ - 0^\circ) + |10.6| \cdot |1| \sin(103^\circ + 0^\circ - 0^\circ) + |73.1| \cdot |1| \sin(-152^\circ + 0^\circ - 0^\circ) + |24.2| \cdot |1| \sin(98^\circ + 0^\circ - 0^\circ)\}$$

$$Q_7 = -71.1 \text{ PU}$$

#### 2.2.4.11.8 Active/Reactive Power injected in/delivered by Bus No.8

P8 => Active power at Bus No.8

$$P_8 = |V_8| \cdot \sum_{k=1}^9 |Y_{8k}| \cdot |V_k| \cos(\theta_{8k} + \delta_k - \delta_8)$$

$$P_8 = |V_8| \cdot \{|Y_{82}| \cdot |V_2| \cos(\theta_{72} + \delta_2 - \delta_7) + |Y_{75}| \cdot |V_5| \cos(\theta_{75} + \delta_5 - \delta_7) + |Y_{77}| \cdot |V_7| \cos(\theta_{77} + \delta_7 - \delta_7) + |Y_{78}| \cdot |V_8| \cos(\theta_{78} + \delta_8 - \delta_7)\}$$

$$P_6 = |1| \cdot \{|70.42| \cdot |1.01| \cos(90^\circ + 0^\circ - 0^\circ) + |10.6| \cdot |1| \cos(103^\circ + 0^\circ - 0^\circ) + |73.1| \cdot |1| \cos(-152^\circ + 0^\circ - 0^\circ) + |24.2| \cdot |1| \cos(98^\circ + 0^\circ - 0^\circ)\}$$

$$P_5 = -70.3 \text{ PU}$$

Q7 => Reactive power at Bus No.7

$$Q_7 = -|V_7| \cdot \sum_{k=1}^9 |Y_{7k}| \cdot |V_k| \sin(\theta_{7k} + \delta_k - \delta_7)$$

$$Q_7 = -|V_7| \cdot \{|Y_{72}| \cdot |V_2| \sin(\theta_{72} + \delta_2 - \delta_7) + |Y_{75}| \cdot |V_5| \sin(\theta_{75} + \delta_5 - \delta_7) + |Y_{77}| \cdot |V_7| \sin(\theta_{77} + \delta_7 - \delta_7) + |Y_{78}| \cdot |V_8| \sin(\theta_{78} + \delta_8 - \delta_7)\}$$

$$Q_7 = -|1| \cdot \{|70.42| \cdot |1.01| \sin(90^\circ + 0^\circ - 0^\circ) + |10.6| \cdot |1| \sin(103^\circ + 0^\circ - 0^\circ) + |73.1| \cdot |1| \sin(-152^\circ + 0^\circ - 0^\circ) + |24.2| \cdot |1| \sin(98^\circ + 0^\circ - 0^\circ)\}$$

$$Q_7 = -71.1 \text{ PU}$$

### 2.2.4.12 ETAP Simulation – Power Flow

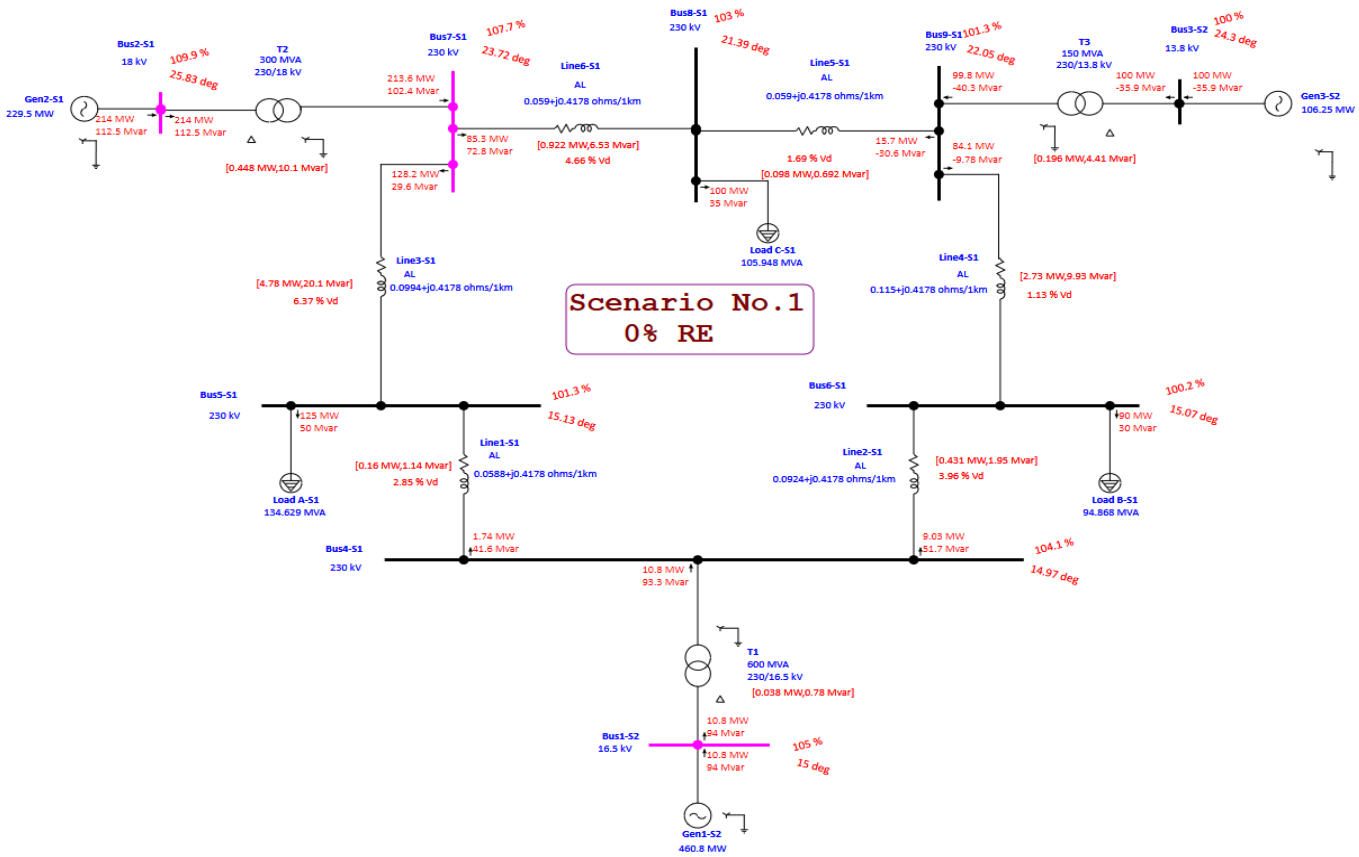


**Figure 2.2-8: ETAP Power Flow Results**

Study ID	Load Flow Analysis
Study Case ID	LF
Data Revision	Base
Configuration	Normal
Loading Cat	Design
Generation Cat	Design
Diversity Factor	Normal Loading
Buses	9
Branches	9
Generators	3
Power Grids	0
Loads	3
Load-MW	315
Load-Mvar	115
Generation-MW	324.807
Generation-Mvar	170.61
Loss-MW	9.807
Loss-Mvar	55.61
Mismatch-MW	0
Mismatch-Mvar	0

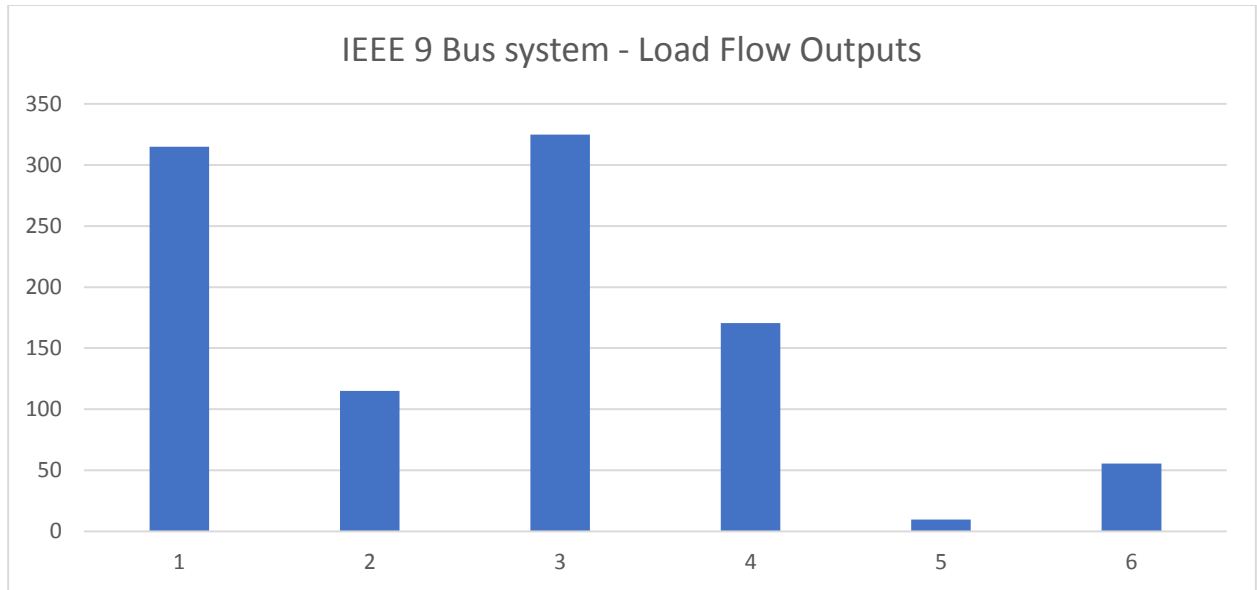


Figure 2.2-9: Bar Chart for ETAP Power Flow Results

Bus ID	Nominal kV	Amp Rating	Type	Voltage	MW Loading	Mvar Loading	Amp Loading	% Loading
Bus1-S2	16.5	0	SWNG	105	10.807	94.048	3155	0
Bus2-S1	18	0	Load	109.9	214	112.5	7056	0
Bus3-S2	13.8	0	Gen.	100	100	35.938	4446	0
Bus4-S1	230	0	Load	104.14	10.769	93.267	226.3	0
Bus5-S1	230	0	Load	101.28	125	50	333.7	0
Bus6-S1	230	0	Load	100.17	90	49.707	257.6	0
Bus7-S1	230	0	Load	107.66	213.552	102.417	552.2	0
Bus8-S1	230	0	Load	103	100	66.264	292.4	0
Bus9-S1	230	0	Load	101.31	99.804	40.35	266.7	0
ID	Bus 1	Bus 2	Type	Rating 1	Rating 2	Allowable		
Line1-S1	Bus5-S1	Bus4-S1	Line	89930 m	587	0 A		
Line2-S1	Bus6-S1	Bus4-S1	Line	97336 m	587	0 A		
Line3-S1	Bus7-S1	Bus5-S1	Line	170330 m	587	0 A		
Line4-S1	Bus9-S1	Bus6-S1	Line	179860 m	587	0 A		
Line5-S1	Bus8-S1	Bus9-S1	Line	76176 m	587	0 A		
Line6-S1	Bus7-S1	Bus8-S1	Line	76176 m	587	0 A		
T1	Bus4-S1	Bus1-S2	Transf. 2W	230 / 16.5 kV	600 MVA	600 MVA		
T2	Bus7-S1	Bus2-S1	Transf. 2W	230 / 18 kV	300 MVA	300 MVA		
T3	Bus9-S1	Bus3-S2	Transf. 2W	230 / 13.8 kV	150 MVA	150 MVA		
ID	MW Flow	Mvar Flow	Amp Flow	% PF	% Loading	% Voltage Drop	kW Losses	kvar Losses
Line1-S1	1.579	40.475	100.4	3.9		2.85	159.9	1136.1
Line2-S1	8.599	49.707	126.4	17.05		3.96	431.1	1949.4
Line3-S1	123.421	9.525	306.8	99.7		6.37	4781.1	20095.8
Line4-S1	84.134	-9.777	209.9	-99.33		1.13	2733.1	9929.4
Line5-S1	15.67	-30.572	85.12	-45.61		1.69	97.7	691.8
Line6-S1	84.427	66.264	261.6	78.66		4.66	922.5	6532.4

T1	10.807	94.048	3155	11.42	15.8	0.86	37.63	780.4
T2	214	112.5	7056	88.51	80.6	2.24	448.1	10082.9
T3	99.804	-40.35	266.7	-92.71	71.8	1.31	195.8	4411.4
ID	Rating/Limit	Rated kV	kW	kvar	Amp	% PF	% Loading	V terminal
Load A-S1	134629 kVA	230	125000	50000	333.7	92.85	98.7	101.28
Load B-S1	94868.3 kVA	230	90000	30000	237.7	94.87	99.8	100.17
Load C-S1	105948 kVA	230	100000	35000	258.2	94.39	97.1	103
ID	Rating/Limit	Rated kV	MW	Mvar	Amp	% PF	% Generation	
Gen1-S1	460.8 MW	16.5	10.807	94.048	3155	11.42	2.3	
Gen2-S1	229.5 MW	18	214	112.5	7056	88.51	93.2	
Gen3-S1	106.25 MW	13.8	100	-35.938	4446	-94.11	94.1	

## 2.2.5 TIME DOMAIN POWER FLOW STUDIES

The load in the power plants fluctuates periodically as a result of unpredictable demands in the electrical power system. The energy consumption of an individual consumer (industrial, commercial, or residential) at a certain moment is unique from the energy consumption of another consumer. Hence, for the aim of varying load and generation in the system and solving the steady state power flows in the system as a function of time, time domain imbalanced power flow or time series distribution load flow simulation is used.

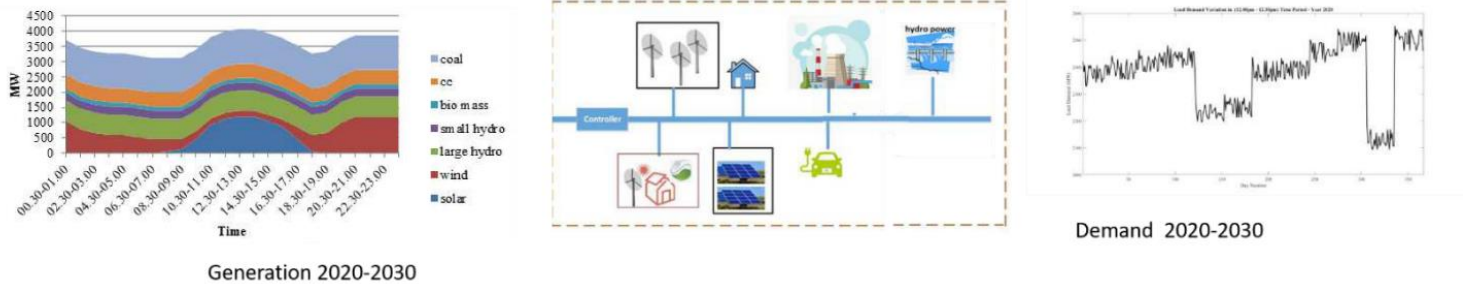


**Figure 2.2-10: Generation and Demand Variations**

However, there must be enough variable generations to cover the variability of demand over the day, see Figure 2.2-10: Generation and Demand Variations

To simulate the time domain load flow for the original IEEE 9 bus system over one month from 1<sup>st</sup> May 2024 to 31<sup>st</sup> May 2024, the loads (Load A, B, and C) are assumed to be changed hourly over the day as per **Figure 2.2-11** and **Figure 2.2-12**, so as the current flow for these loads as per **Figure**

### 2.2-14

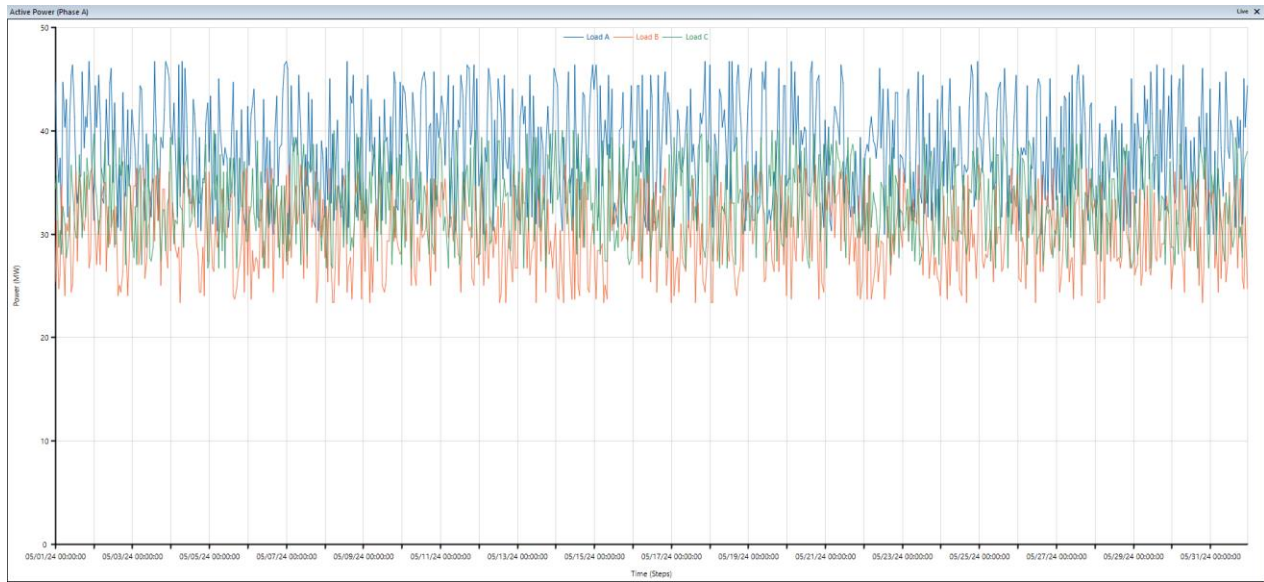


**Figure 2.2-11:** Time Domain Active Power Flow for Phase A for Loads A, B, and C

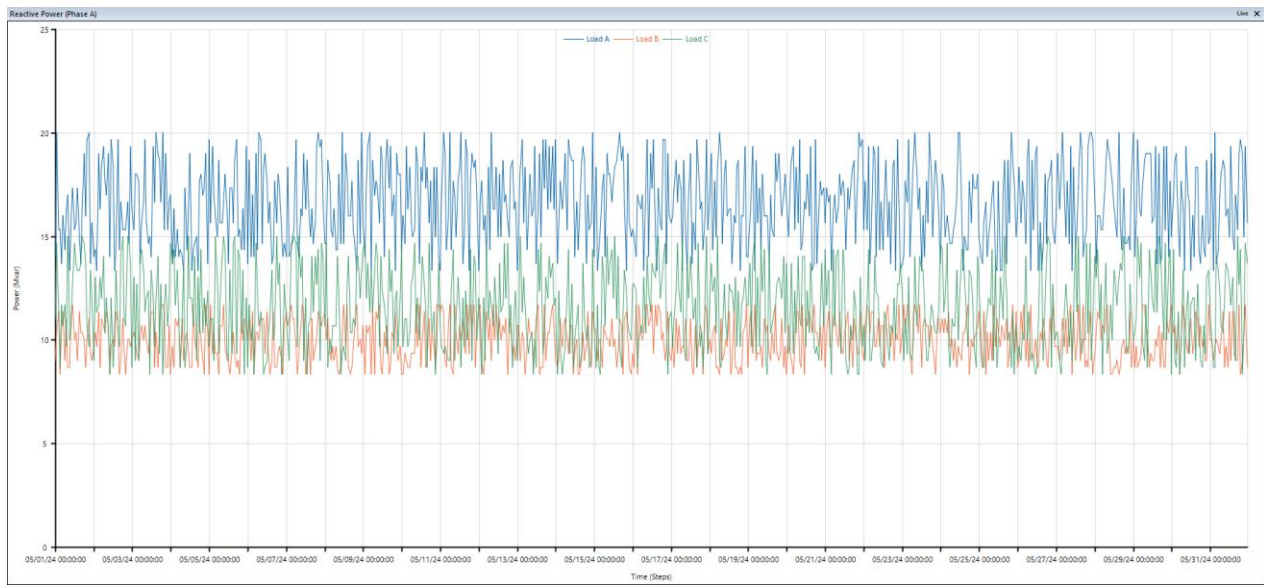


**Figure 2.2-12:** Time Domain Reactive Power Flow for Phase A for Loads A, B, and C

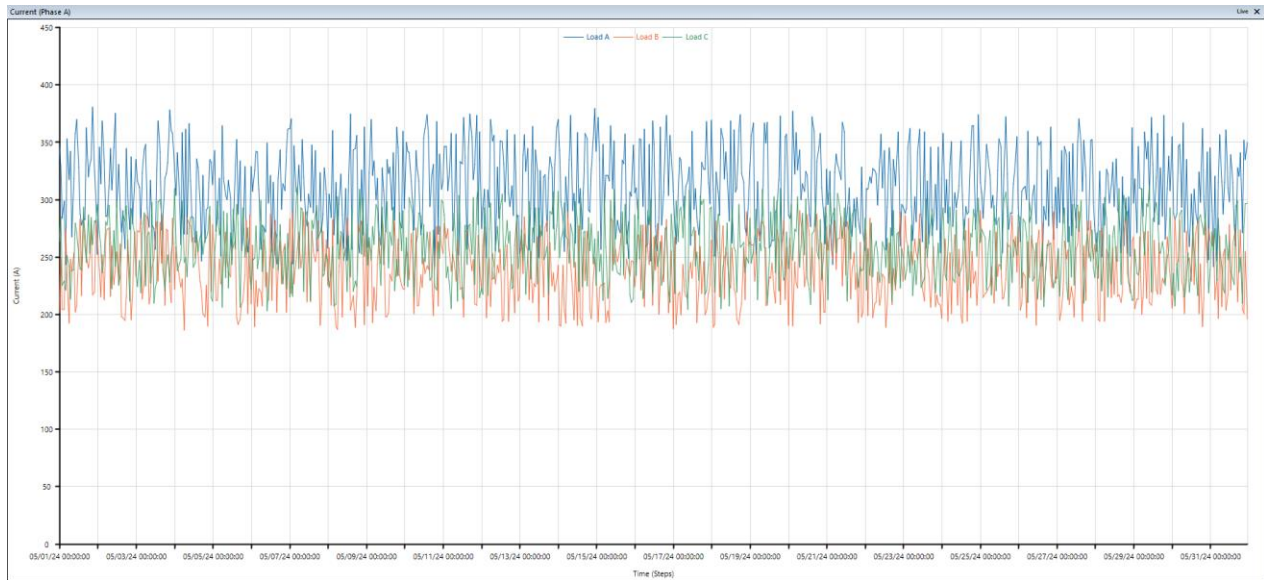


**Figure 2.2-13:**Time Domain Current Flow for Phase A for Loads A, B, and C

The variation of the loads implied a variation of Gen1 active power which is at swing mode of operation, while maintaining the active power for Gen2 and Gen3 which are at reactive power control mode of operation and voltage control mode of operation respectively, see **Figure 2.2-14**

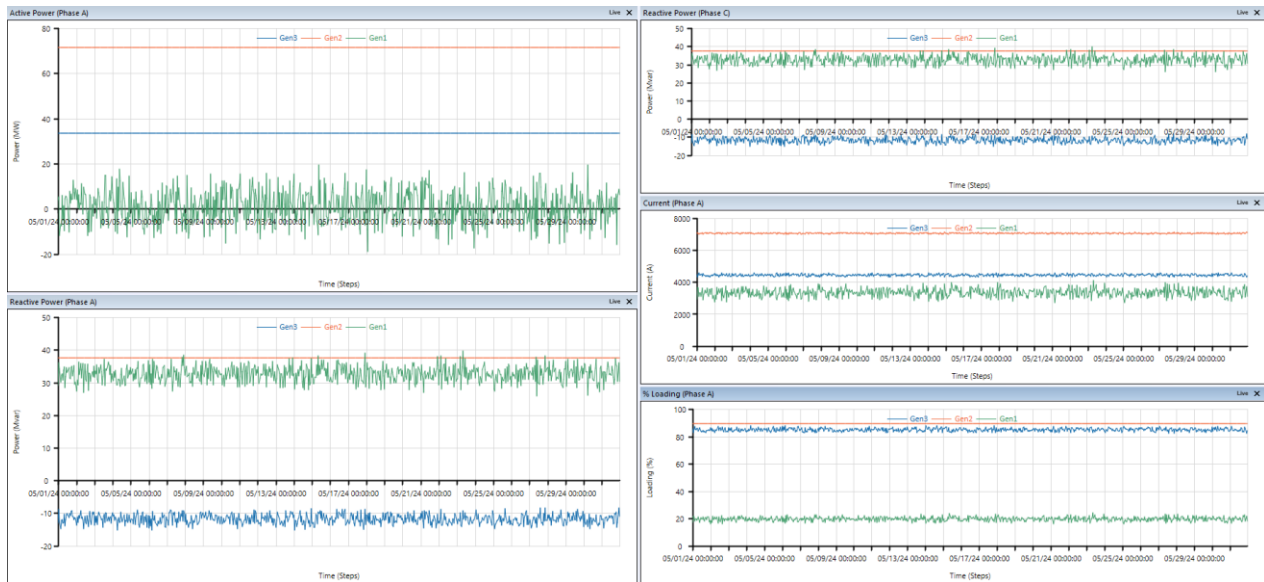


**Figure 2.2-14:**Time Domain Power Flow for Generators 1, 2, and 3

In below **Figure 2.2-15:** Total System Time Domain Load Flow (Source, Load, Losses P and Q)

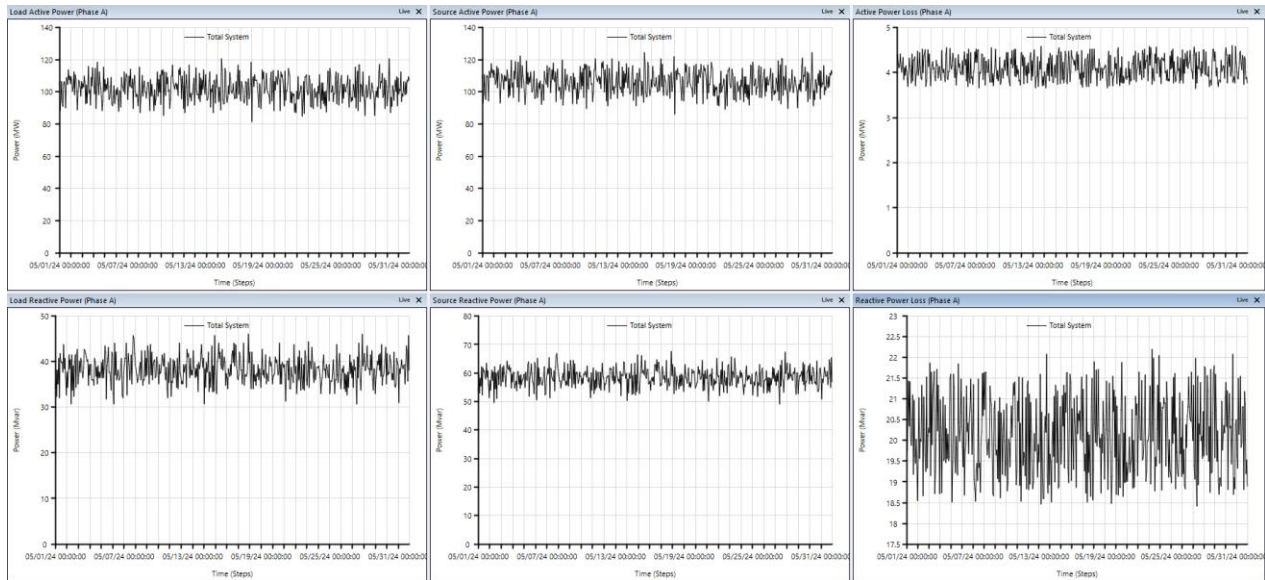


**Figure 2.2-15: Total System Time Domain Load Flow (Source, Load, Losses P and Q)**

## 2.2.6 FAULT CALCULATIONS

Fault calculations (short circuit studies) are essential to design and develop the protective schemes for various parts of the system. The protective scheme consists of current and voltage sensing devices, protective relays and circuit breakers. The system must be protected against the flow heavy short circuit currents by disconnecting / isolating the faulty part of the system by means of CB's operated by protection relays, and for proper choice of the CB and protection relays, the magnitude of the current that would flow during the short circuit condition must be calculated.

Based on above the main purposes conducting the short circuit studies are to find out the short circuit rating of all equipment, to find the breaking and making capacity of the interrupting devices, to find the DC interrupting capability of the circuit breakers, and finally to establish the input for other studies such as Harmonic analysis, transient stability

Present-day electrical power systems are nearly interconnected, which increases the risk of defects and necessitates the interruption of high-speed currents prior to the restoration of normal conditions. There are numerous fault varieties that occur as symmetrical or asymmetrical faults.

Moreover, the classification is illustrated in the most disruptive fault that **Figure 2.2-16** the greatest amount of downtime in network components is a symmetrical or three-phase fault.

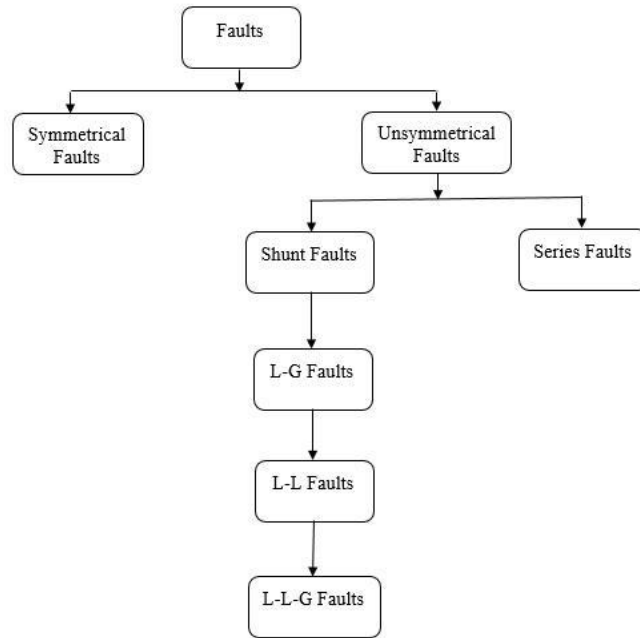


**Figure 2.2-16:**Types of Faults in Electrical Power System

### 2.2.6.1 Symmetrical Three Phase Fault Current

During transient conditions the fault current consists of a symmetrical AC current and a DC component **Figure 2.2-17** shows the simplified equivalent impedance diagram for network.

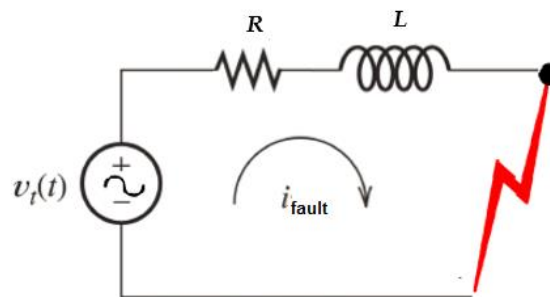


**Figure 2.2-17:** Simplified Equivalent Impedance Diagram

The fault current will be the sum of forced component of the fault current and natural component.

$$i_{fault}(t) = i_F(t) + i_N(t)$$

$i_F(t)$  is the forced component by the voltage source of  $i_{fault}(t)$

$$i_F(t) = \frac{V_m}{Z} \sin(\omega t + \theta - \varphi)$$

$$Z = \sqrt{R^2 + \omega^2 L^2}$$

$$\varphi = \tan^{-1}\left(\frac{\omega L}{R}\right)$$

$i_N(t)$  is the natural component without the voltage source

$$V_L + V_R = 0$$

$$L \frac{di}{dt} + R i = 0$$

$$L \frac{di}{dt} = -R i$$

$$\frac{1}{i} di = -\frac{R}{L} dt$$

Integrating both sides

$$\int \frac{1}{i} di = \int -\frac{R}{L} dt \Rightarrow \ln i = -\frac{R}{L} t$$

Taking exponential for both sides

$$e^{\ln i} = A e^{-\frac{R}{L} t}$$

$$i(t) = A e^{-\frac{R}{L} t}$$

$$i_{fault} = \frac{V_m}{Z} \sin(\omega t + \theta - \varphi) + A e^{-\frac{R}{L}t}$$

To find the constant **A**, then initial condition  $i(0)=0$  should be used

$$0 = \frac{V_m}{Z} \sin(\theta - \varphi) + A e^0$$

$$A = \frac{-V_m}{Z} \sin(\theta - \varphi) \Rightarrow A = \frac{V_m}{Z} \sin(\varphi - \theta)$$

$$i_{fault} = \frac{V_m}{Z} \sin(\omega t + \theta - \varphi) + \frac{V_m}{Z} \sin(\varphi - \theta) e^{-\frac{R}{L}t}$$

$$i_p = \frac{V_m}{Z_p} \sin(\omega t + \theta - \varphi) + \frac{V_{pm}}{Z_p} \sin(\varphi - \theta) e^{-\frac{R}{L}t}$$

$$i_{fault} = I_{pm} \sin(\omega t + \theta - \varphi) + I_{pm} \sin(\varphi - \theta) e^{-\frac{R}{L}t}$$

Drawing above equation will be as shown in **Figure 2.2-18**

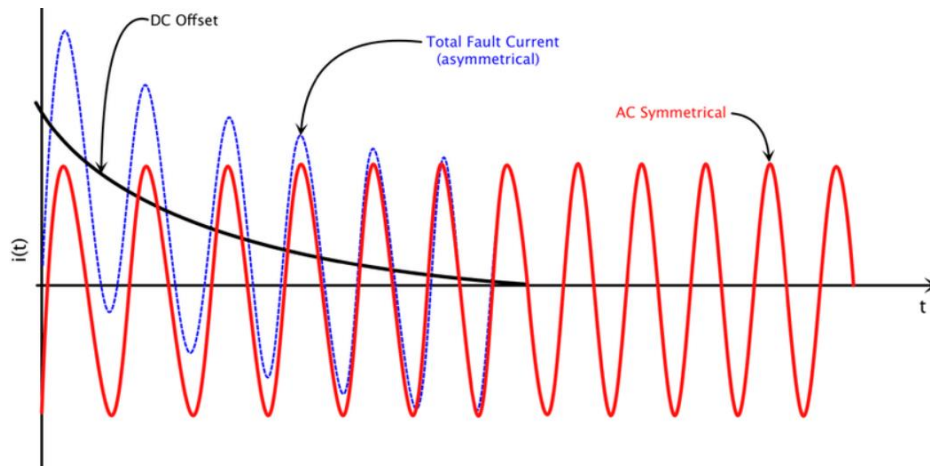


**Figure 2.2-18:** Total (DC and AC components) of a Symmetrical Short Circuit Current

Where

$$i_{p(\text{periodic component})} = I_{pm} \sin(\omega t + \theta - \varphi)$$

$$i_{p(\text{dc component})} = I_{pm} \sin(\varphi - \theta) e^{-\frac{R}{L}t}$$

$Z_p$  is the impedance of the primary circuit.

$$Z_p = \sqrt{R_p^2 + \omega^2 L_p^2}$$

$\alpha$  is the angle of the voltage wave form at the initial moment at  $t=0$

$$\phi = \tan^{-1}\left(\frac{\omega L_p}{R_p}\right)$$

In short circuit,  $\omega L \gg R$  so that  $\phi=90^\circ$

### 2.2.6.2 ETAP Simulation for Symmetrical Three Phase Fault Current at all 9 Buses

Conducting three phase device duty based on IEC 60909 using ETAP, below **Figure 2.2-19**

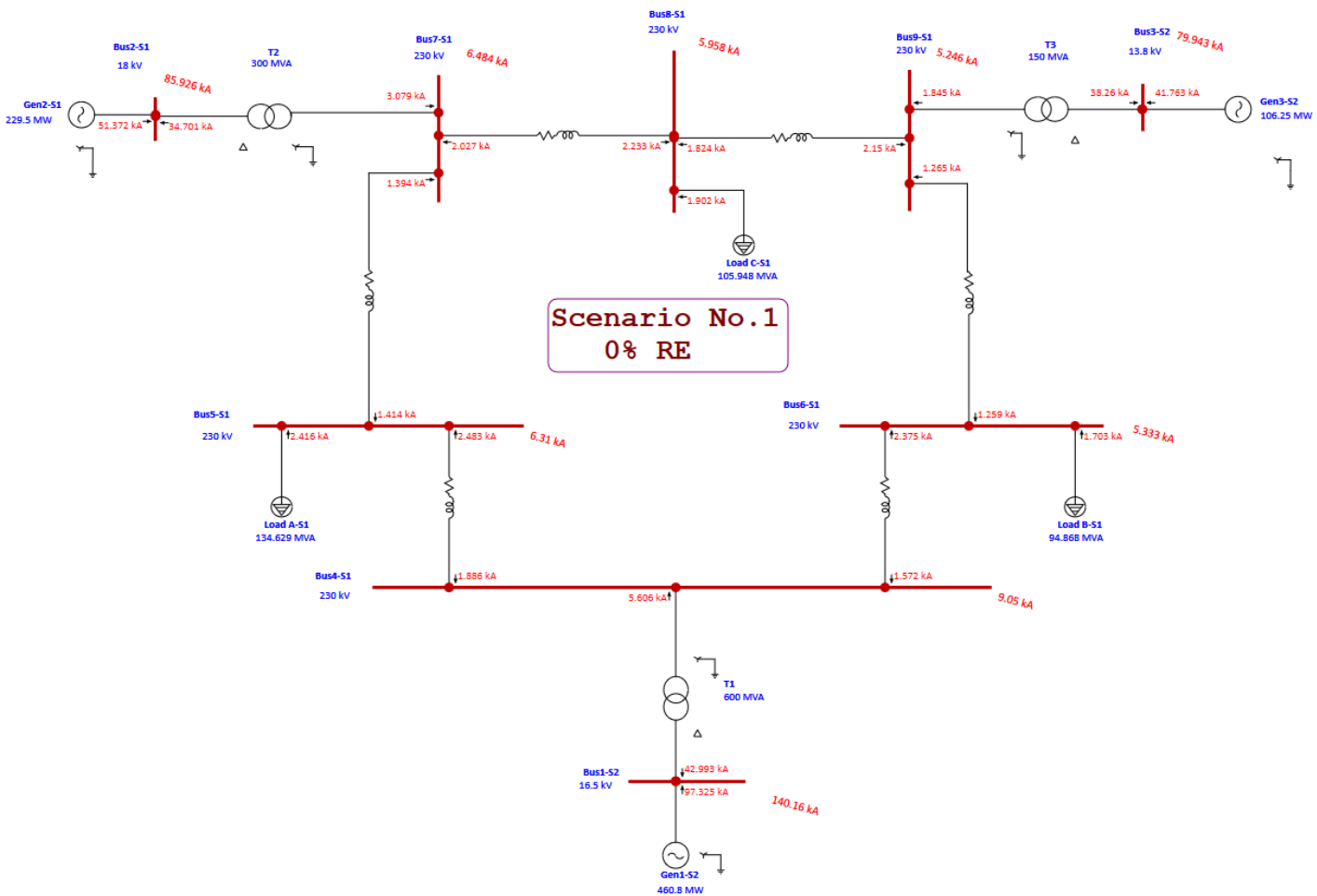


**Figure 2.2-19:** Three Phase Device Duty IEC 60909 – Single Line Diagram

Performing a transient short circuit analysis as per IEC 61363 standard for each of the nine buses, then the graphs for the total fault current, top envelop of fault current, AC component, DC component, and percent DC component of fault current will be as per *Figure 2.2-20* to *Figure 2.2-28*

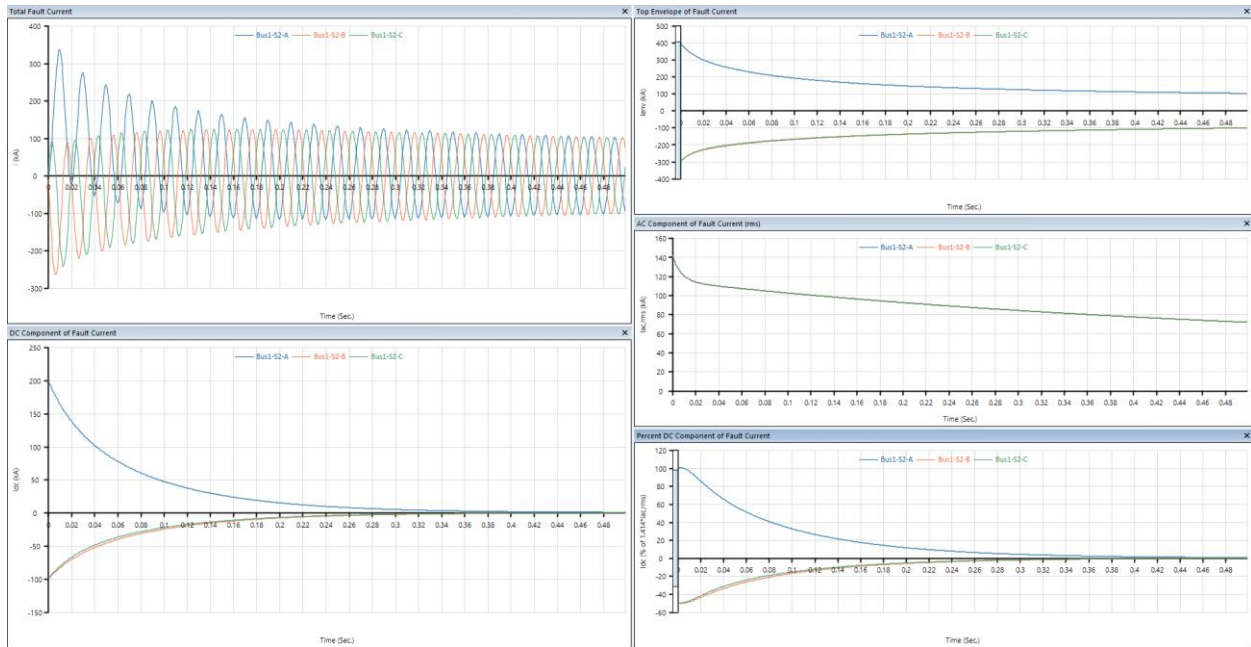


**Figure 2.2-20: Bus No.1 - Transient Short Circuit Current**

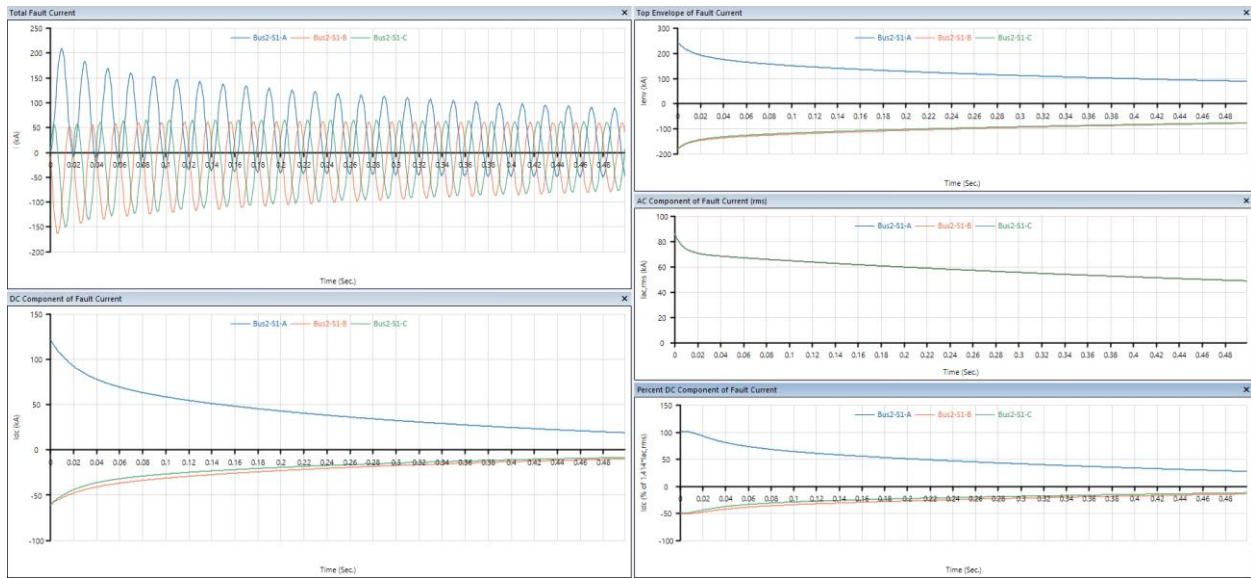


**Figure 2.2-21: Bus No.2-Transient Short Circuit Current**

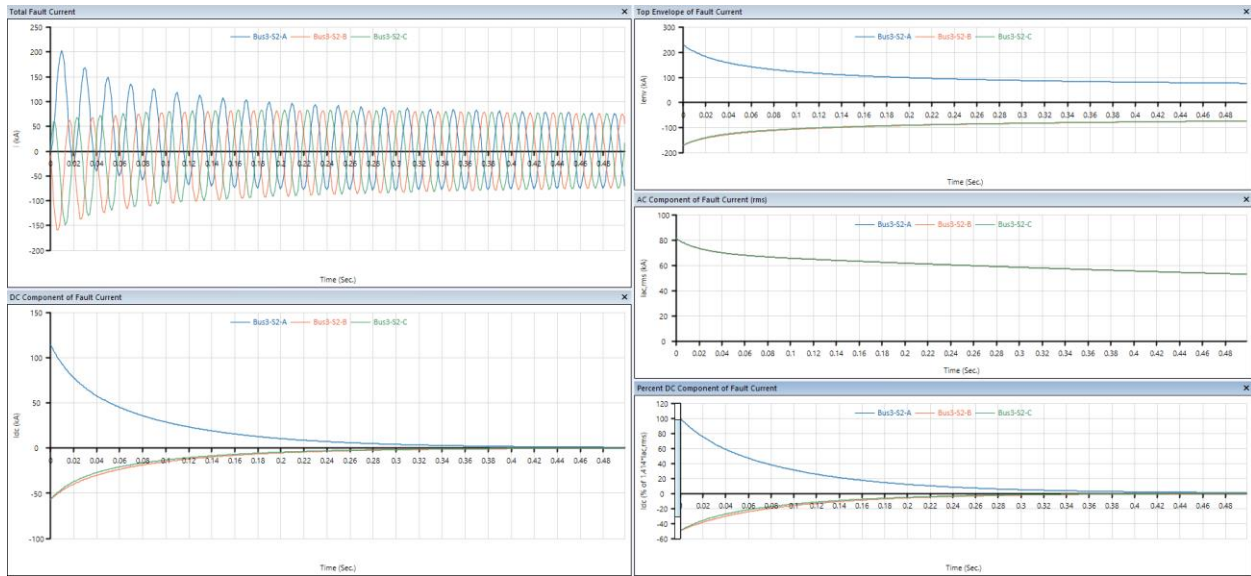


**Figure 2.2-22:Bus No.3-Transient Short Circuit Current**

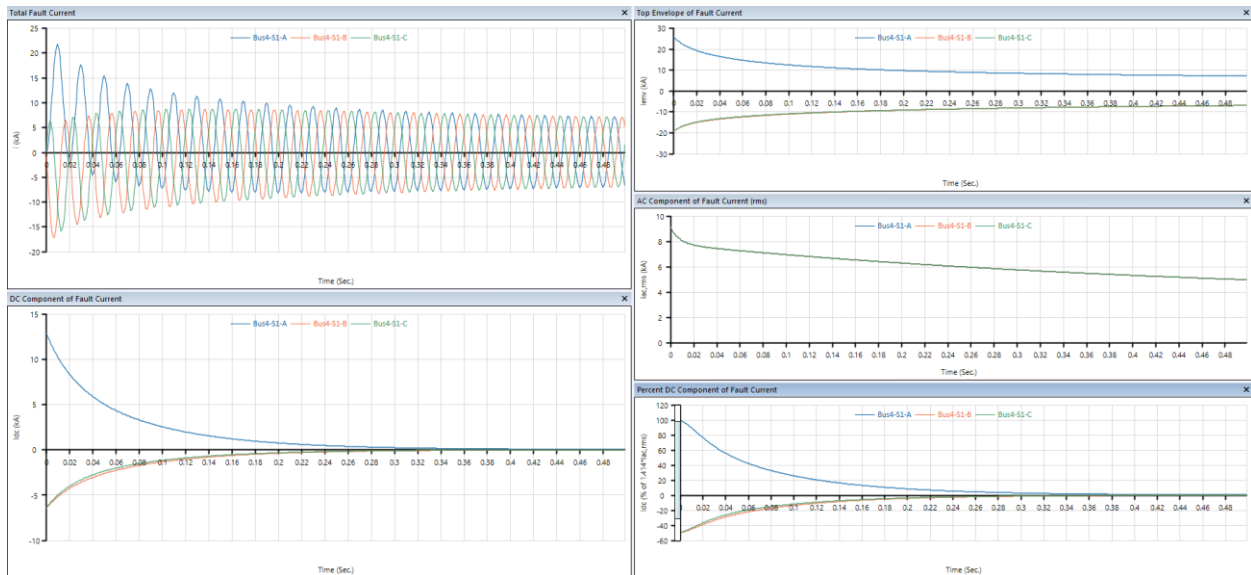


**Figure 2.2-23:Bus No.4-Transient Short Circuit Current**

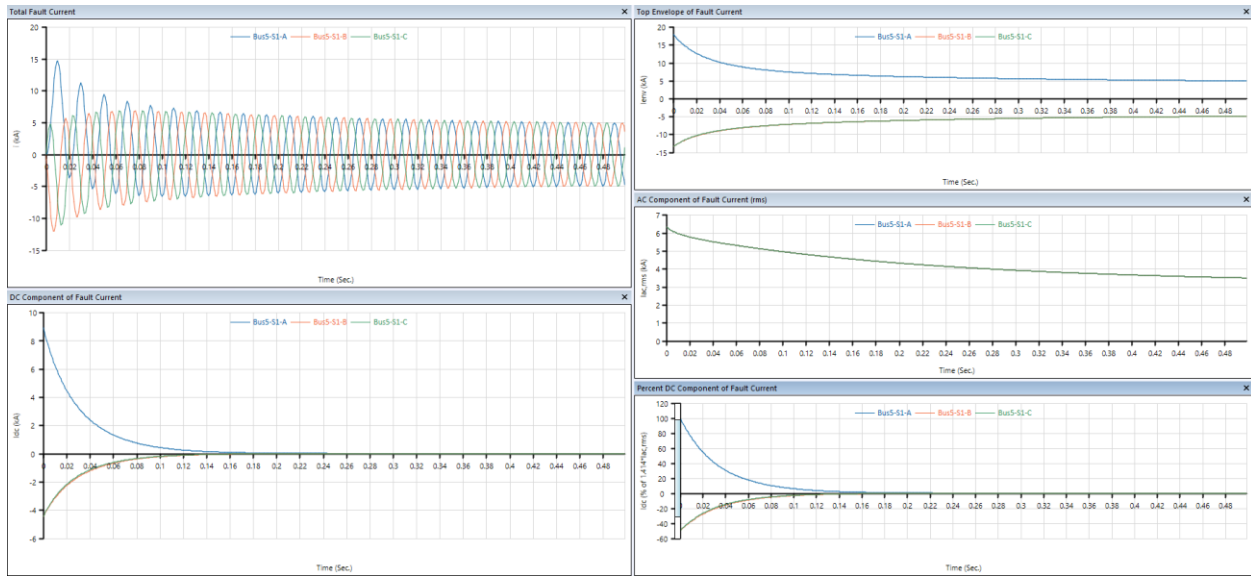


**Figure 2.2-24- Bus No.5-Transient Short Circuit Current**

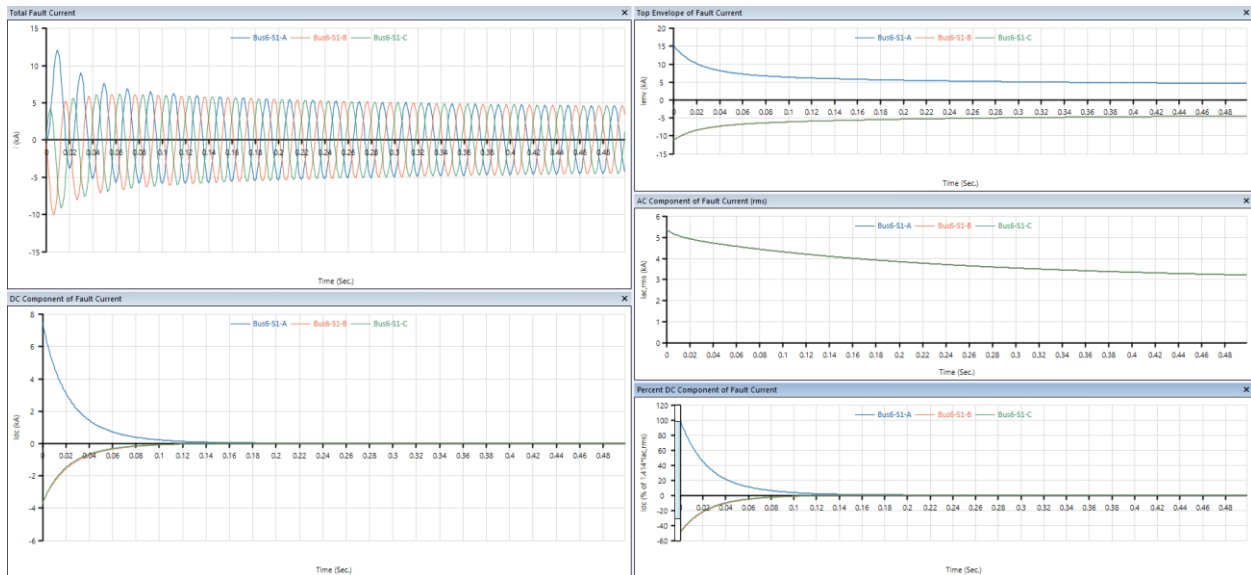


**Figure 2.2-25- Bus No.6-Transient Short Circuit Current**

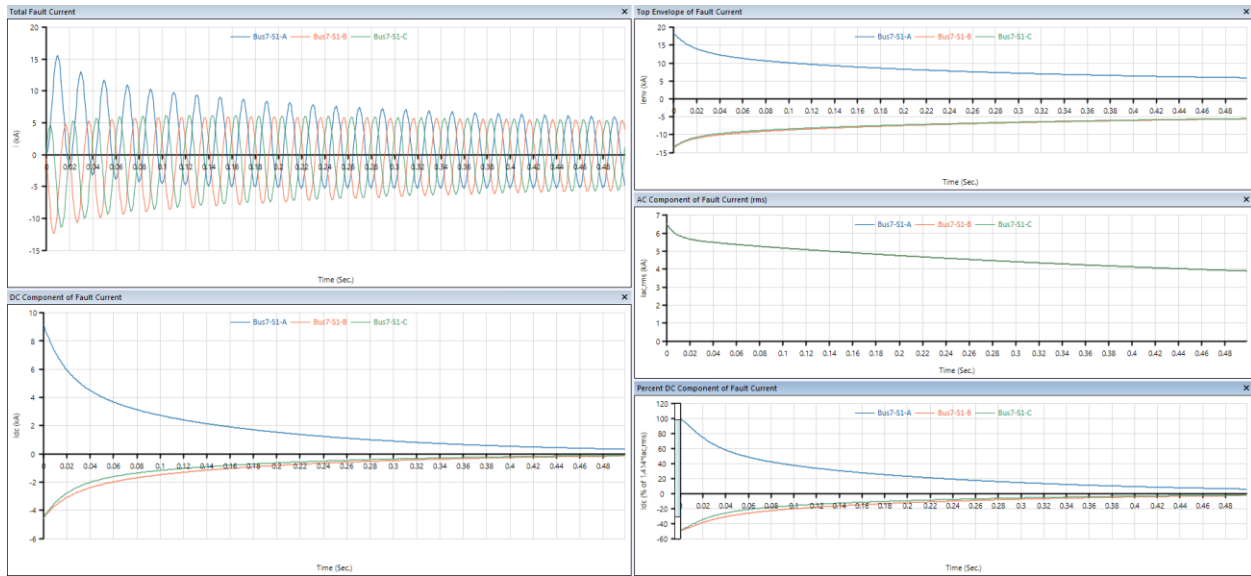


**Figure 2.2-26- Bus No.7-Transient Short Circuit Current**

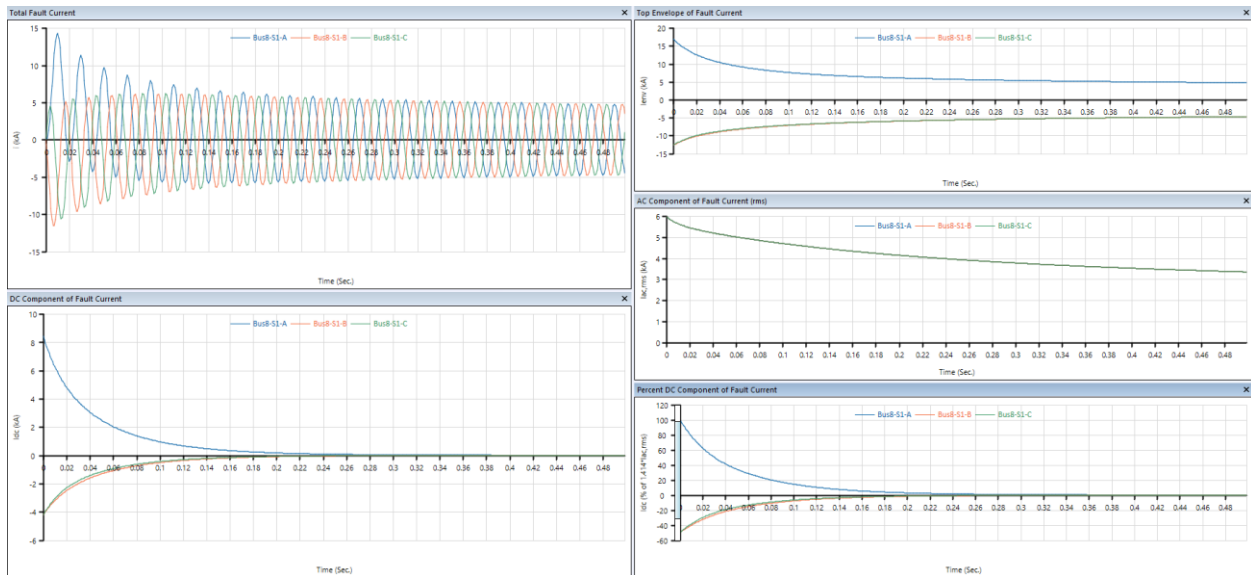


**Figure 2.2-27: Bus No.8-Transient Short Circuit Current**

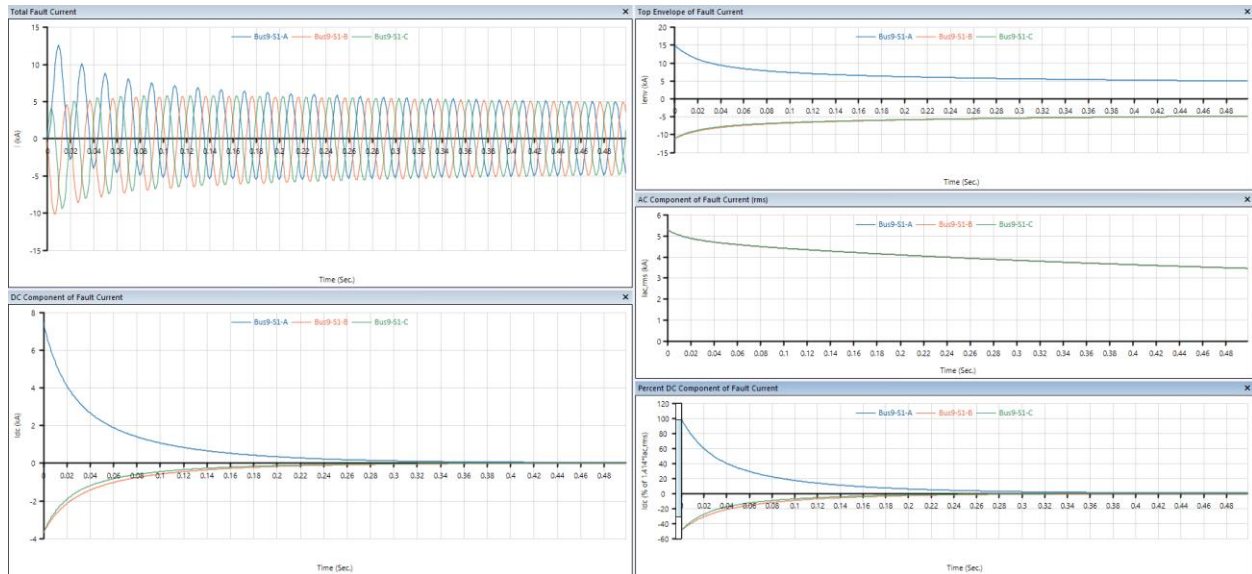


**Figure 2.2-28: Bus No.9-Transient Short Circuit Current**

### 2.2.6.3 Unsymmetrical Types of Faults

Unsymmetrical faults are those in the power system that result in unsymmetrical fault currents, or uneven fault currents in lines with unequal phase displacement. The three lines' currents become uneven when an unsymmetrical fault occurs, which causes a phase displacement between them. In a power system, unsymmetrical failures may happen in three different ways.

Unsymmetrical faults involve only one or two phases or conductors. In unsymmetrical faults the three phase lines become unbalanced. Such types of faults occur between line-to-ground or between lines. An unsymmetrical series fault is between phases or between phase-to-ground, whereas unsymmetrical shunt fault is an unbalanced in the line impedances. Shunt unsymmetrical faults in the three-phase system can be classified as;

1. Single line-to-ground fault (LG).
2. Line-to-line fault (LL).
3. Double Line-to-ground fault (LLG).

### 2.2.6.3.1 Single Line to Ground Fault (L/G)

The most prevalent defect is phase-to-earth, accounting for 80% of all faults. This issue happens when one conductor makes touch with the ground as shown in **Figure 2.2-29** or comes into contact with the neutral wire. It is possible that the cause of the issue is trees collapsing into the power cables. You can see ETAP simulation for L/G fault in **Figure 2.2-30**

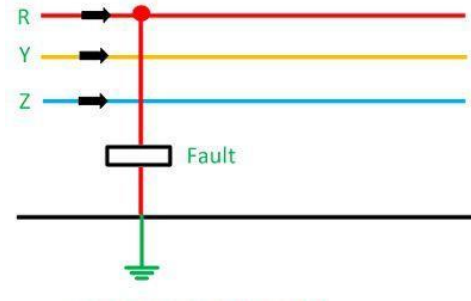


**Figure 2.2-29: Single Line to Ground Fault**

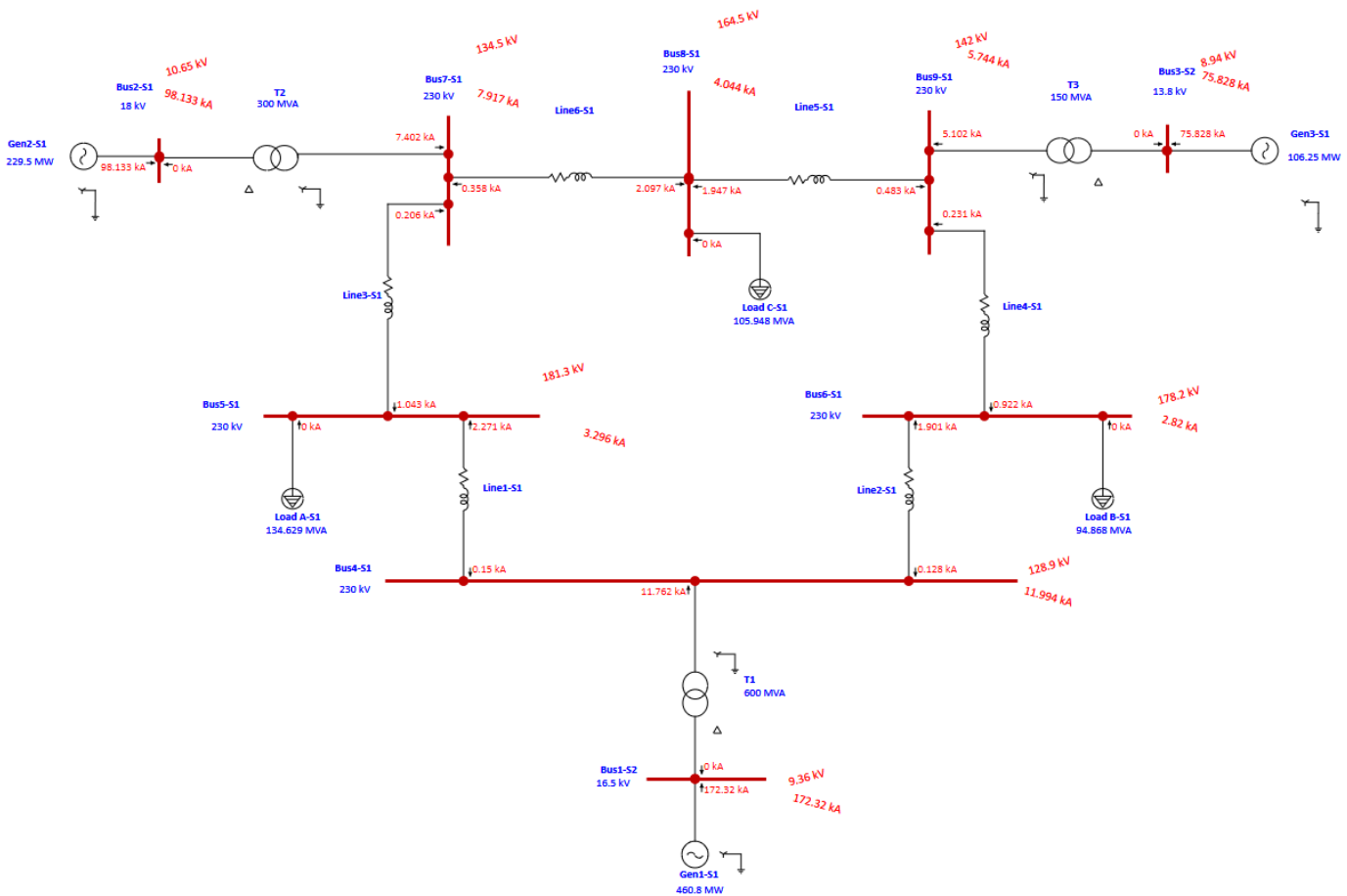


**Figure 2.2-30: Single Line to Ground Fault with ( $V_b$  and  $3I_o$ )**

### 2.2.6.3.2 Double Line Fault (LL)

A double line fault or also known as phase-to-phase fault occurs when two conductors are short-circuited as shown in **Figure 2.2-31**, accounting for 15% of defects. For instance, a bird may perch on a single power wire and inadvertently make contact with another line, or a tree limb might collapse onto two adjacent power lines. You can see ETAP simulation for LL fault in **Figure 2.2-32**

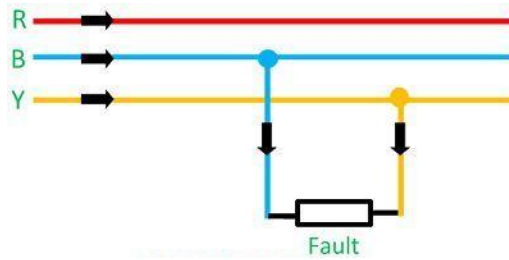


**Figure 2.2-31: Double Line Fault**

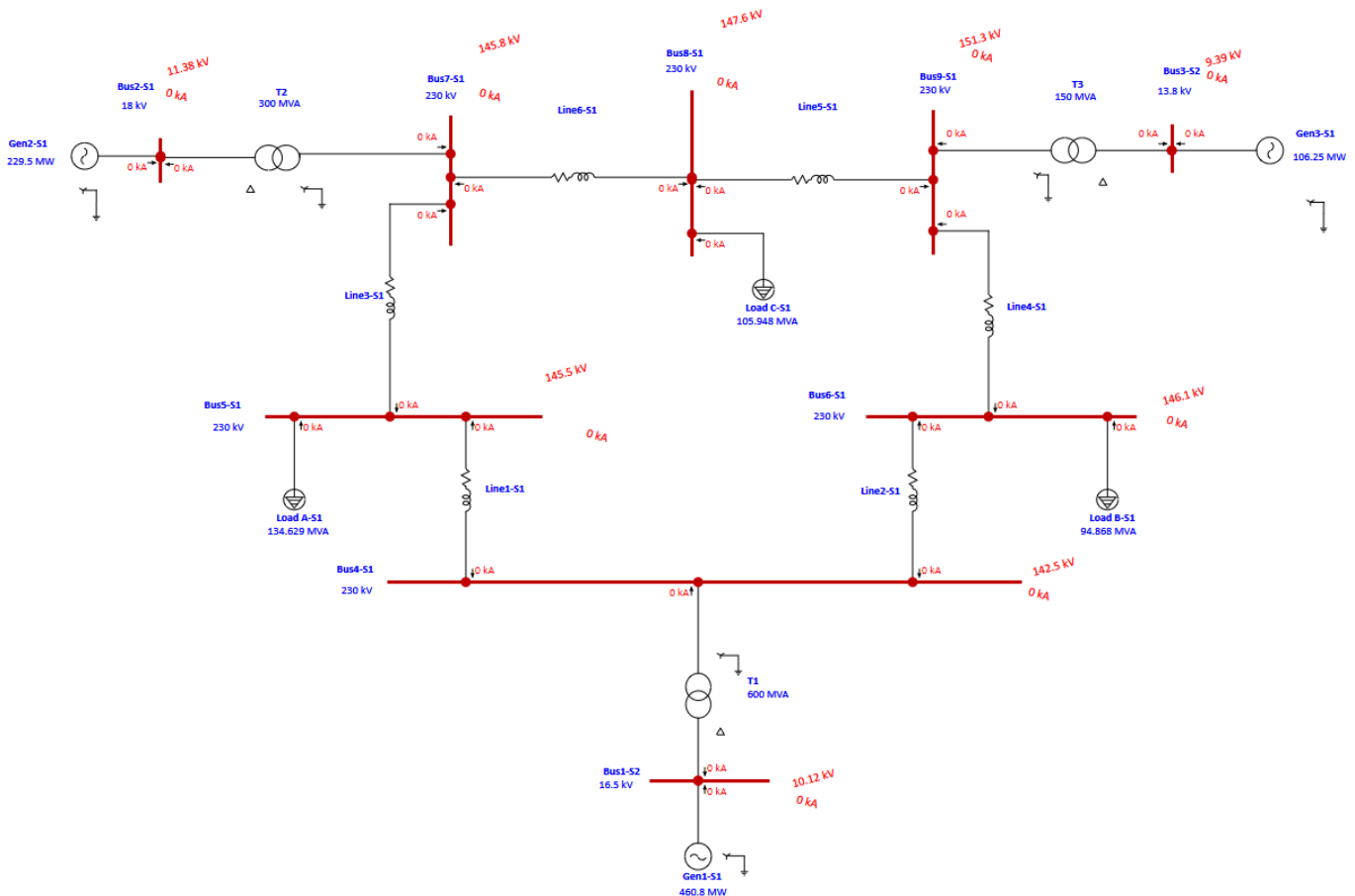


**Figure 2.2-32: Double Line Fault with ( $V_a$  and  $3I_o$ )**

### 2.2.6.3.3 Double Line to Ground Fault (LL/G)

Double line to ground fault or also knows Phase-to-phase-to-earth faults may occur when two conductors are short-circuited with the ground as shown in **Figure 2.2-33** for example when a tree falls on two power lines or due to other factors. You can see ETAP simulation for LL/G fault in **Figure 2.2-34**

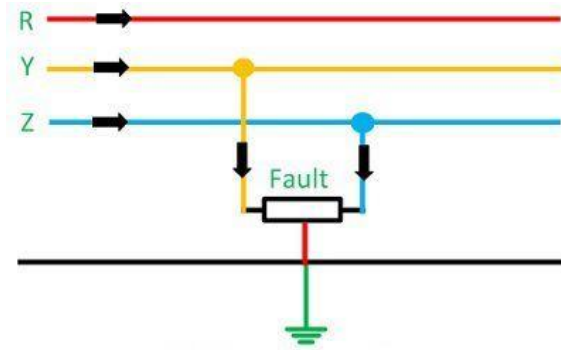


**Figure 2.2-33: Double Line to Ground Fault**

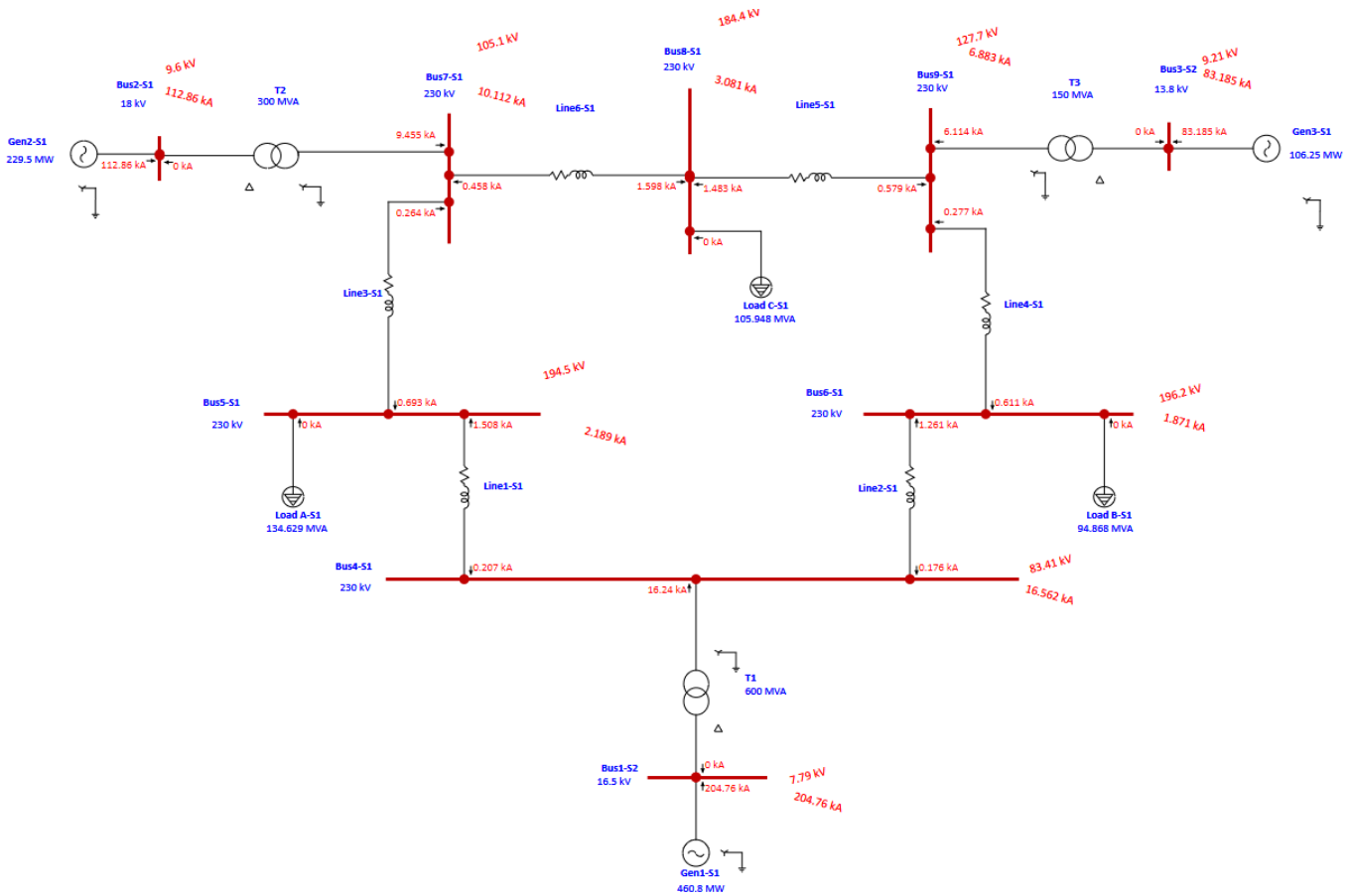


**Figure 2.2-34: Double Line to Ground Fault with ( $V_a$  and  $I_{lo}$ )**

## 2.2.7 STABILITY STUDY

Power system stability can be defined as the ability of an electric power system for a given initial operating condition to regain a state of operating equilibrium condition after being subjected to a physical disturbance with all the system variables bounded so that the system integrity is preserved. The Integrity of the system is preserved when practically the entire power system remains intact with no tripping of generators or loads, except for those disconnected by isolation of the faulted elements or intentionally tripped to preserve the continuity of operation of the rest of the system. It is the ability of electrical machine or power system to regain its original/previous state is called steady state stability. The stability of a system refers to the ability of a system to return to its steady state when subjected to a disturbance. As mentioned before, power is generated by synchronous generators that operate in synchronism with the rest of the system.

A generator is synchronized with a bus when both of them have same frequency, voltage and phase sequence. The power system stability can be defined as the ability of the power system to return to steady state without losing synchronism. Usually, power system stability is categorized into steady state, transient and dynamic stability as shown in **Figure 2.2-35**. If the system is unstable, it will result in a run-away or run-down situation for example, a progressive increase in angular separation of generator rotors or a progressive decrease in bus voltages.

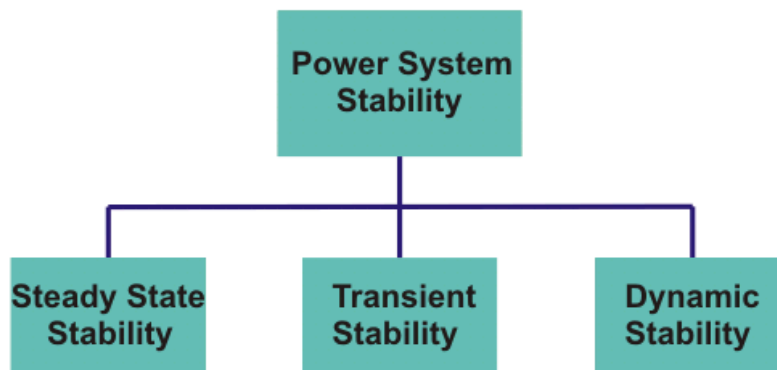


**Figure 2.2-35:** Power System Stability Classifications

A power system is said to be in a steady state operating condition, if all the measured (or calculated) physical quantities describing the operating condition of the system can be considered constant for the purpose of analysis. However, if a sudden change or sequence of changes occurs in one or more of the system parameters or one or more of its operating quantities, the system is said to have undergone a disturbance from its steady state operating condition. The two types of disturbances in a power system are,

- i) *Small disturbance*
- ii) *Large disturbance*

#### **Small disturbance**

If the power system is operating in a steady state condition and it undergoes change, which can be properly analyzed by linearized versions of its dynamic and algebraic equations, a small disturbance is said to have occurred. Example of small disturbance is a change in the gain of the automatic voltage regulator in the excitation system of a large generating unit.

#### **Large disturbance**

A large disturbance is one for which the nonlinear equations describing the dynamics of the power system cannot be validly linearized for the purpose of analysis. Examples of large disturbances are transmission system faults, sudden load changes, loss of generating units and line switching.

#### ***2.2.7.1 Steady State Stability of a Power System***

The steady state stability of a power system is defined as the ability of the system to bring itself back to its stable configuration following a small disturbance in the network (like normal load fluctuation or action of automatic voltage regulator). It can only be considered only during a very gradual and infinitesimally small power change. In case the power flow through the circuit exceeds the maximum power permissible, then there are chances that a particular machine or a group of machines will cease to operate in synchronism and result in yet more disturbances. In such a situation, the steady state limit of the system is said to have reached or in other words the steady state stability limit of a system refers to the

maximum amount of power that is permissible through the system without loss of its steady state stability.

#### 2.2.7.2 *Transient Stability of a Power System*

Transient stability of a power system refers to the ability of the system to reach a stable condition following a large disturbance in the network condition. In all cases related to large changes in the system like sudden application or removal of load, switching operations, line faults or loss due to excitation the transient stability of the system comes into play. It in fact deals with the ability of the system to retain synchronism following a disturbance sustaining for a reasonably long period of time. And the maximum power that is permissible to flow through the network without loss of stability following a sustained period of disturbance is referred to as the transient stability of the system. Going beyond that maximum permissible value for power flow, the system would temporarily be rendered as unstable.

#### 2.2.7.3 *Dynamic Stability of a Power System*

Dynamic stability of a system denotes the artificial stability given to an inherently unstable system by automatic controlled means. It is generally concerned with small disturbances lasting for about 10 to 30 seconds.

#### 2.2.7.4 *Rotor Dynamics and Swing Equation*

The rotor dynamic equation can be given by the equation below.

$$J \frac{d^2\theta_m}{dt^2} = T_a = T_m - T_e$$

Where

J is the total moment of inertia of the rotor mass (kg.m<sup>2</sup>)

$\theta_m$  is the angular displacement of the rotor with respect to a stationary axis ( rad )

t is the time (seconds)

$T_m$  is the machinal torque supplied by the prime mover.

$T_e$  is electrical or electromagnetic torque.

$T_a$  is the accelerating torque.

Since  $\theta_m = \omega t + \delta$

Differentiating both sides of the equations

$$\frac{d\theta_m}{dt} = \omega + \frac{d\delta}{dt}$$

$$\frac{d^2\theta_m}{dt^2} = \frac{d^2\delta}{dt^2}$$

Substituting equation 4-81 in equation 4-79

$$J \frac{d^2\delta}{dt^2} = T_a = T_m - T_e$$

Multiplying both sides of equation 4-82 with  $\omega$

$$\omega \times (T_m - T_e) = \omega \times J \frac{d^2\delta}{dt^2}$$

$$P_m - P_e = M \times \frac{d^2\delta}{dt^2}$$

However, and angular momentum  $M$  is given by below equation

$$M = J\omega \Rightarrow J = \frac{M}{\omega}$$

The rotational kinetic energy is given by below equation

$$W_k = \frac{1}{2}J\omega^2$$

Substituting equation 4-84 in equation 4-85

$$W_k = \frac{1}{2} \left( \frac{M}{\omega} \right) \omega^2 = \frac{1}{2} M \omega_s$$

But the stored kinetic energy for 1MVA is denoted by  $H$

$$H = \frac{W_k}{S}; \text{ so for one unit of Power (1 MVA), } H \text{ (MJ/MVA)} = W_k$$

$$H = \frac{1}{2} M \omega_s \Rightarrow M = \frac{2H}{\omega_s}$$

The swings equation is known by

$$\frac{2H}{\omega_s} \frac{d^2\delta}{dt^2} = P_{mech} - P_{ele}$$

Swing equation can be written by two first order DE's

$$\frac{d\omega}{dt} = \frac{\omega_s}{2H} (P_m - P_e)$$

$$\frac{d\delta}{dt} = \omega - \omega_s$$

The above swing equation is applicable for rotating machines like synchronous generators.

### 2.2.7.5 Stability Study for the Case Study

Assuming the three-phase fault that happened at the beginning of Line L1 connecting BB.4 and BB.5, then the fault will be looked like as if it happened at BB.4 as shown in **Figure 2.2-36**

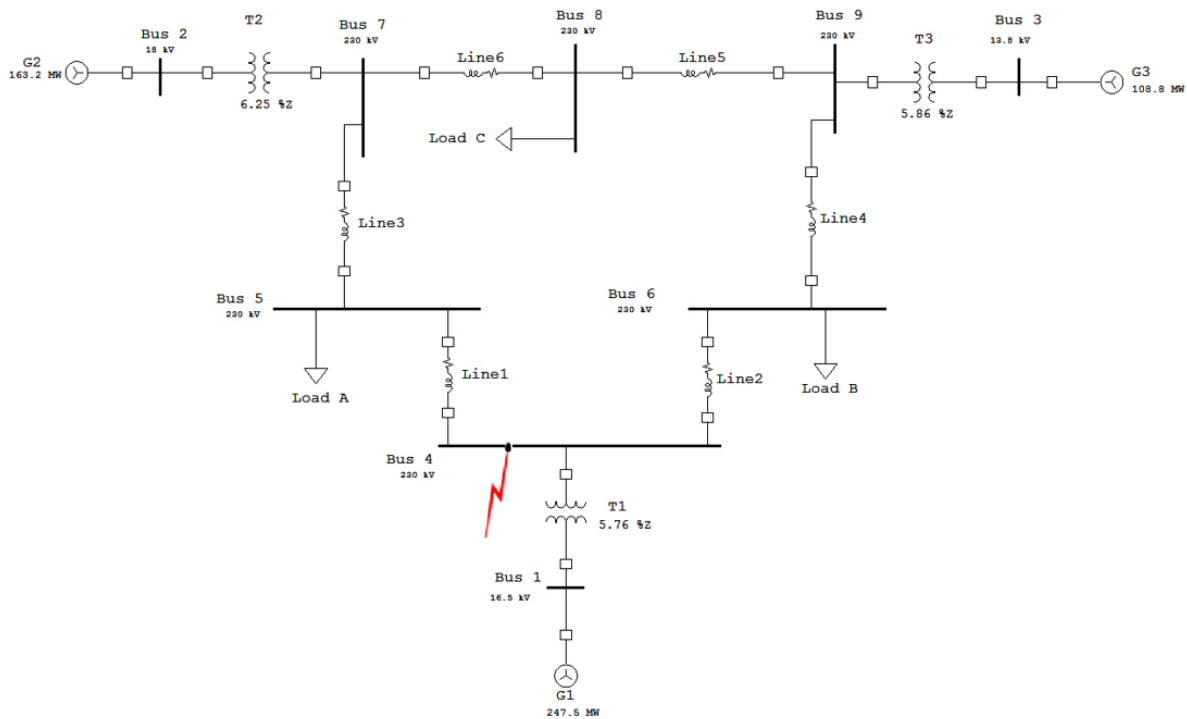


**Figure 2.2-36:** Three-Phase Fault at Beginning of Line 1 (connecting Bus 4 and Bus 5)

The equivalent circuit for **Figure 2.2-36** can be written in PU as shown in **Figure 2.2-37**

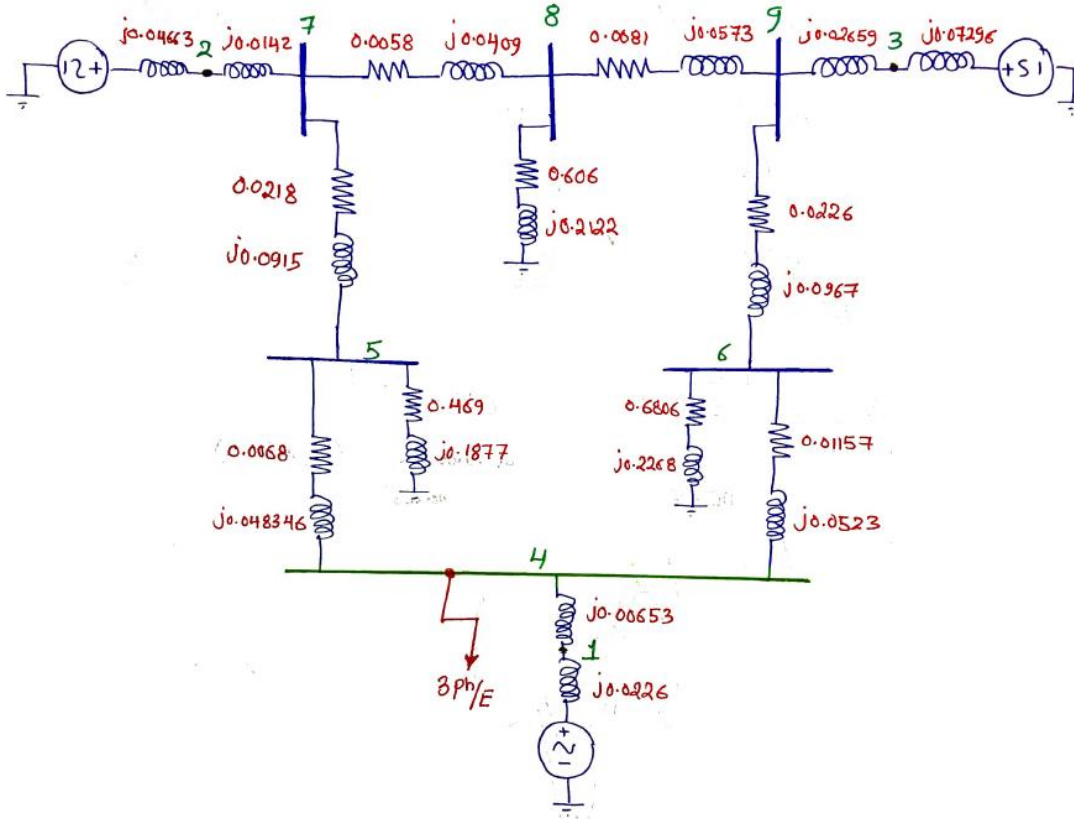


**Figure 2.2-37:** PU Equivalent Circuit in Pre-Fault Condition

### 2.2.7.5.1 Pre-Fault Condition

In pre-fault condition, assuming that generator G1 is delivering to Bus No.4 below PU of power.

$$P_{pu-G1} = \frac{512 \times 0.9}{100} = 4.61 \text{ PU}$$

Then the power angle equation can be written as below based on the equivalent circuit simplified as shown in **Figure 2.2-38:** Simplified Equivalent Circuit No.1 in Pre-Fault Condition.

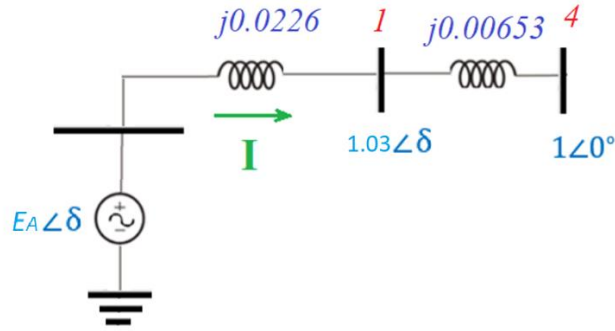


**Figure 2.2-38:** Simplified Equivalent Circuit No.1 in Pre-Fault Condition

The 4.61 PU of power generated from G1 generator to Bus No.4 can be written using the power angle equation below

$$P = \frac{|V_1| \times |V_4|}{|X_{14}|} \sin\delta = \frac{|1.03| \times |1|}{|0.00653|} \sin\delta$$

$$P = 4.61 \text{ PU} = \frac{|1.03| \times |1|}{|0.00653|} \sin\delta \Rightarrow \sin\delta = 0.02922 \Rightarrow \delta = \sin^{-1}(0.02922) = 1.6747^\circ$$

Hence the terminal voltage of the G1 generator is  $1.03\angle 1.6747^\circ$

Based on above, the current  $I$  delivered from the generator G1 terminal to the Bus No.4 through the GSU T1 can be calculated

$$I = \frac{V_1\angle\delta - V_4\angle 0}{jX} = \frac{1.03\angle 1.6747^\circ - 1\angle 0^\circ}{0.00653\angle 90^\circ} = 6.46\angle -44.48^\circ$$

Based on the value of the current, the transient internal generated induced EMF (voltage) for generator G1 can be calculated using the equivalent circuit shown in **Figure 2.2-39:** Internal Generated Voltage for Generator G1 in Pre-Fault Condition

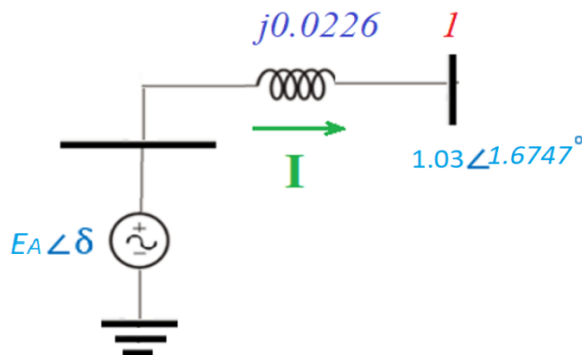


**Figure 2.2-39:** Internal Generated Voltage for Generator G1 in Pre-Fault Condition

$$E' \angle \delta = 1.03 \angle 1.6747^\circ + (6.46 \angle -44.48^\circ) \times (0.0226 \angle 90^\circ) = 1.14 \angle 6.765^\circ$$

The power angle equation relating the internal transient voltage  $E'$  and the infinite bus voltage is determined by the total transfer reactance  $0.10075 \angle 84.4^\circ$  as shown in **Figure 2.2-40**

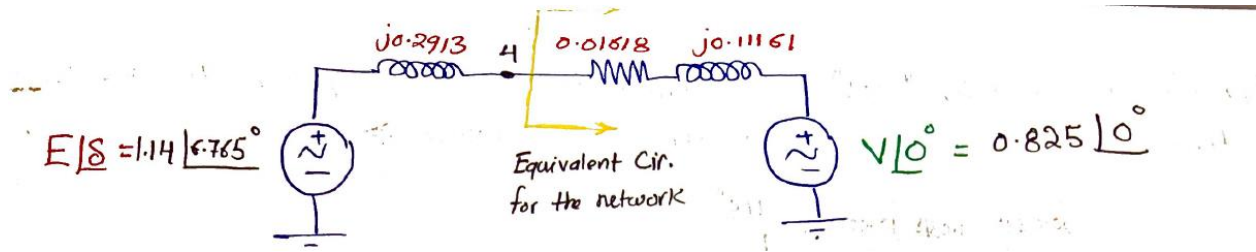


**Figure 2.2-40:** Two Bus System with Transfer Reactance in Pre-Fault Condition

Transfer impedance connecting between sending and receiving end voltage is

$$Z = 0.01618 + j 0.2913 + j 0.11161 = 0.01618 + j 0.40291 = 0.40323 \angle 87.7^\circ$$

$$P_{e-l} = \frac{|E| \times |V|}{|Z|} \sin \delta = \frac{|1.14| \times |0.825|}{|0.40323|} \sin \delta = 2.332 \sin \delta$$

When

$$P_m = P_{e-l}$$

$$1 = 2.332 \sin \delta_o \Rightarrow \sin \delta_o = \frac{1}{2.332} = 0.428816$$

$$\delta_o = \sin^{-1}(0.428816) = 25.4^\circ$$

Where  $\delta$  is angle of the G1 generator with respect to Bus No.4. The power angle curve in pre-fault condition is shown in **Figure 2.2-41: Power Angle Curve in Pre-Fault Condition**

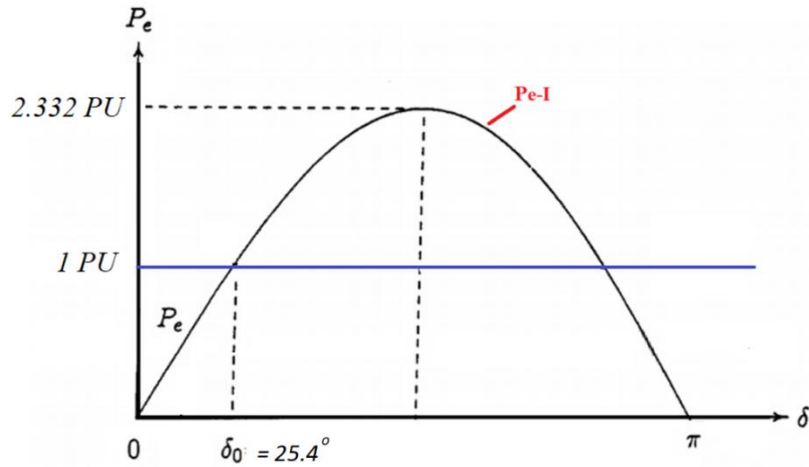


**Figure 2.2-41:** Power Angle Curve in Pre-Fault Condition

### 2.2.7.5.2 During Fault Condition

During the fault at Line 1 that connects between Bus No.4 and Bus No.5, the electrical power system will be subjected to the flow of heavy short circuit current through the system which was already calculated under section 4.7.2 and simulated under section 4.7.3 and it was around 9 kA. This fault happened at the beginning of Line 1 toward BB.4 side, so it looks like as if it happened at the 230 kV BB No.4. Hence the power transferred from generator G1 to the grid will be zero due to this three-phase short circuit, and the power angle curve is as shown in **Figure 2.2-42:**

Power Angle Curve During Fault

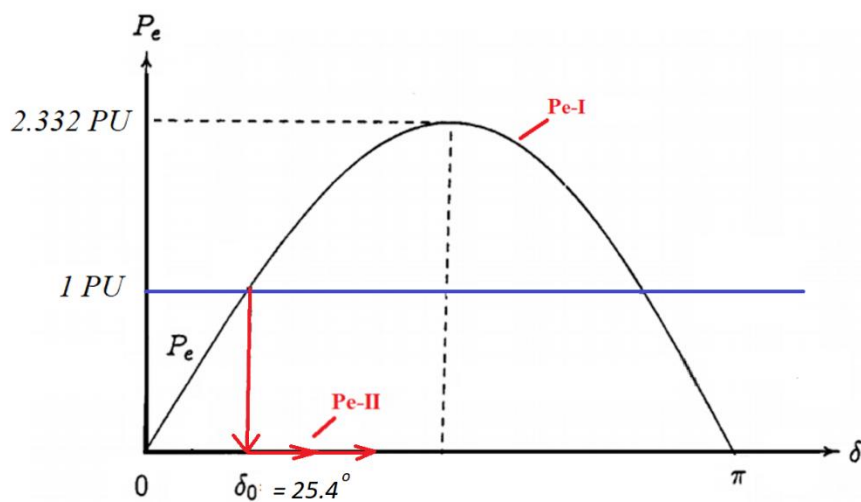


**Figure 2.2-42:** Power Angle Curve During Fault

The protection scheme consists of current and voltage sensing devices which are the CT's and VT's, protection relays and circuit breakers. The selection of these devices mainly depends on various currents that may flow in the fault conditions and the system must be protected against the flow of heavy short circuit current by isolating the faulty part from the healthy part of the system by means of circuit breakers and protection relays.

**2.2.7.5.3 Post Fault Condition**

After fault clearance by tripping the upstream and downstream CB's of the Line No.1, Based on that the system will look like **Figure 2.2-43: Single Line Diagram with Line 1 Outage**

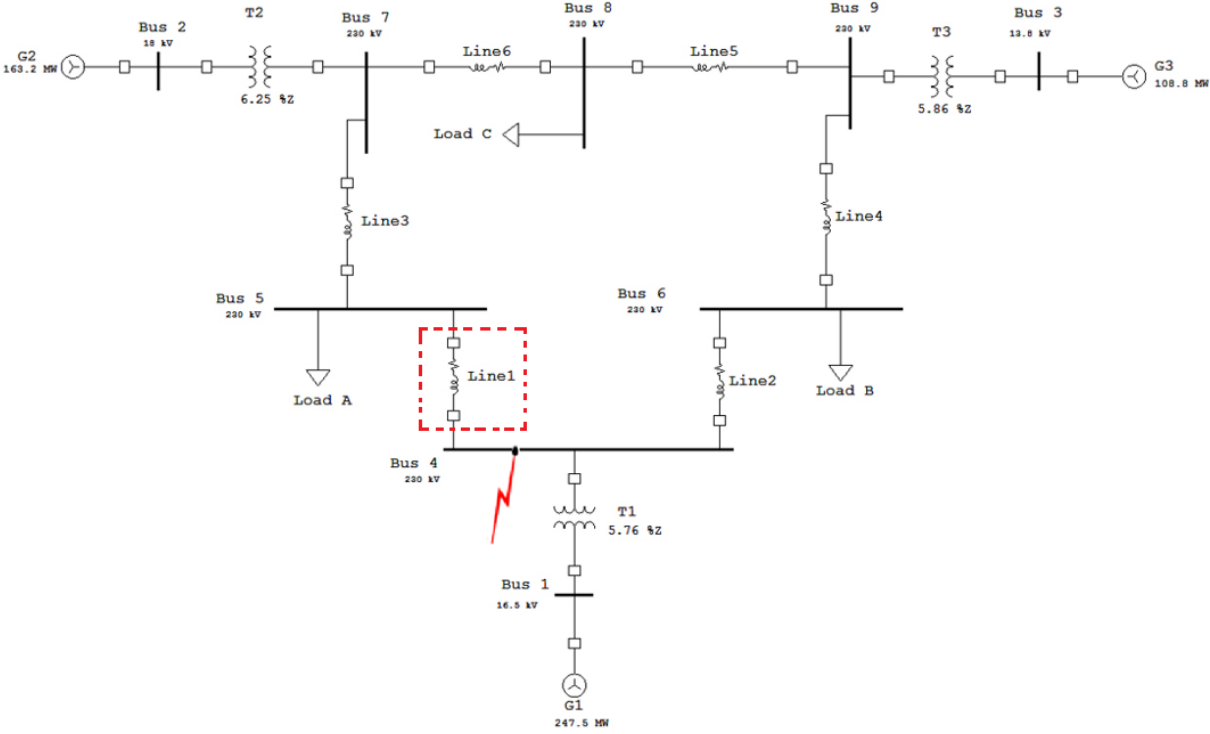


**Figure 2.2-43: Single Line Diagram with Line 1 Outage**

The PU equivalent circuit for the system will be as shown in **Figure 2.2-44: PU Equivalent Circuit after Line 1 is out of**

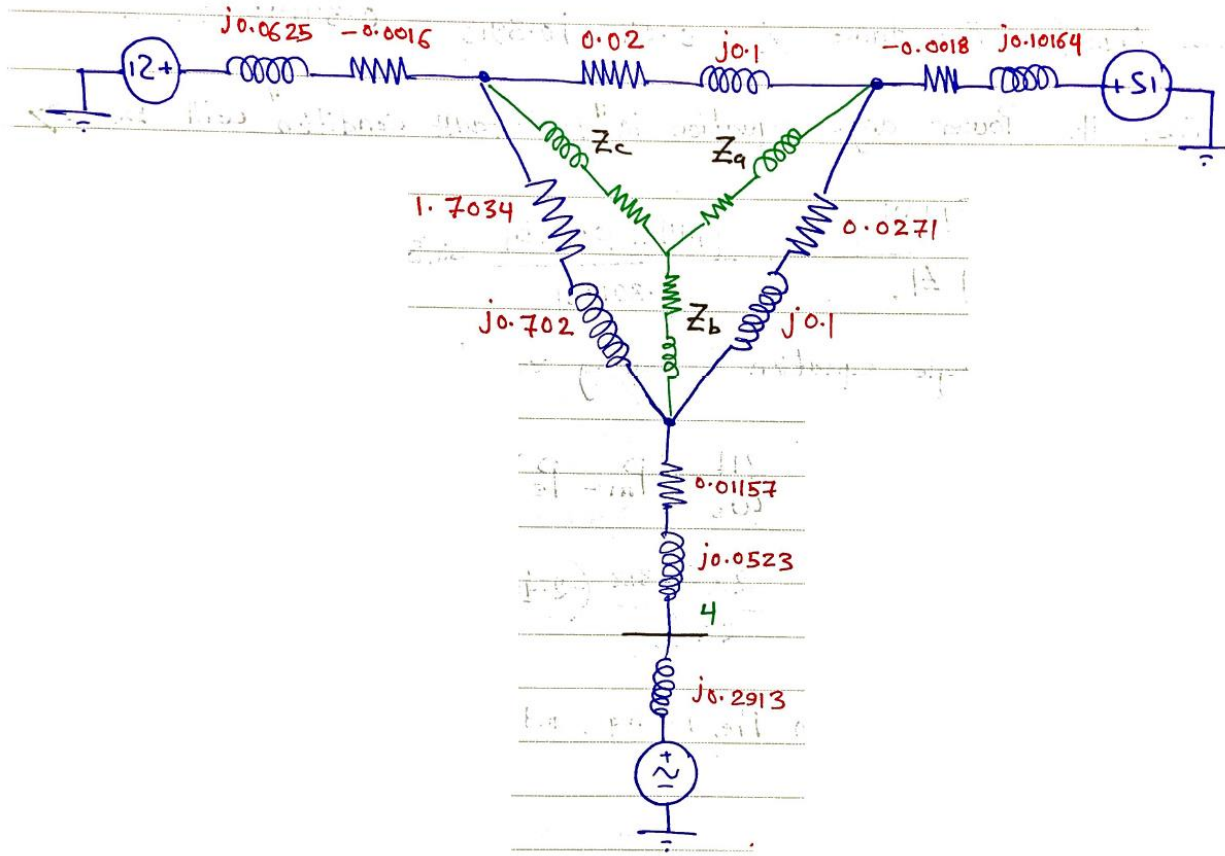


**Figure 2.2-44:** PU Equivalent Circuit after Line 1 is out of Service.

The above circuit can be simplified as shown in **Figure 2.2-45:** Simplified Equivalent Circuit with Line 1 is out of service

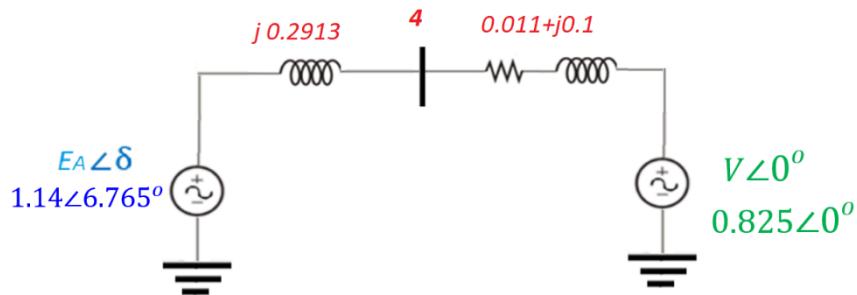


**Figure 2.2-45:** Simplified Equivalent Circuit with Line 1 is out of Service.

Transfer impedance connecting between sending and receiving end voltage is

$$Z = 0.011 + j 0.2913 + j 0.1 = 0.011 + j 0.3913 = 0.39145 \angle 88.39^\circ$$

$$P_{e-III} = \frac{|E| \times |V|}{|Z|} \sin\delta = \frac{|1.14| \times |0.825|}{|0.39145|} \sin\delta = 2.4026 \sin\delta$$

The power angle curves in pre, during, and post fault conditions are shown in **Figure 2.2-46**:

Power Angle Curve in Pre, During, and Post-Fault Condition

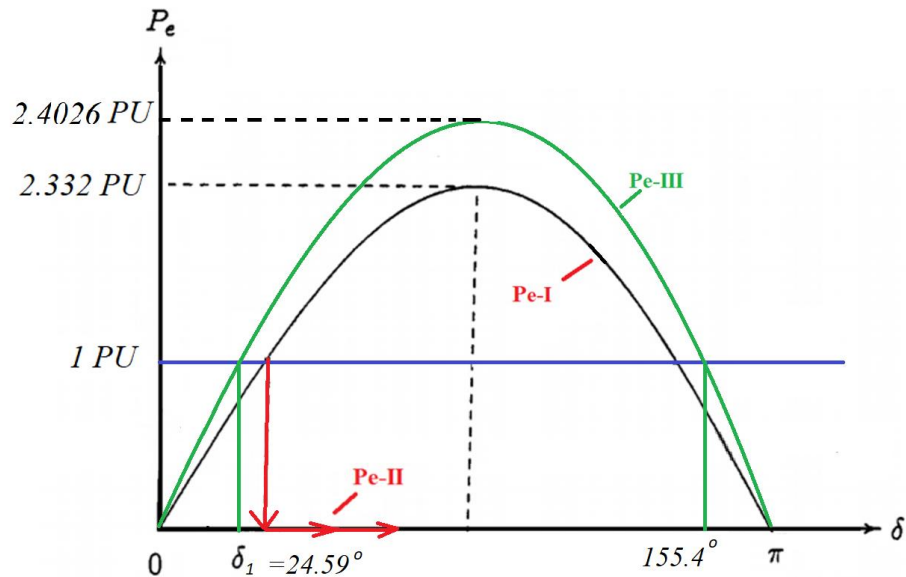


**Figure 2.2-46:** Power Angle Curve in Pre, During, and Post-Fault Condition

Using Equal area criteria, in order for the system to get stabilized, the mechanical energy added to the rotor due to the acceleration (acceleration energy) must be removed in the deceleration, hence accelerating area A1 must be equal to the decelerating area A2.

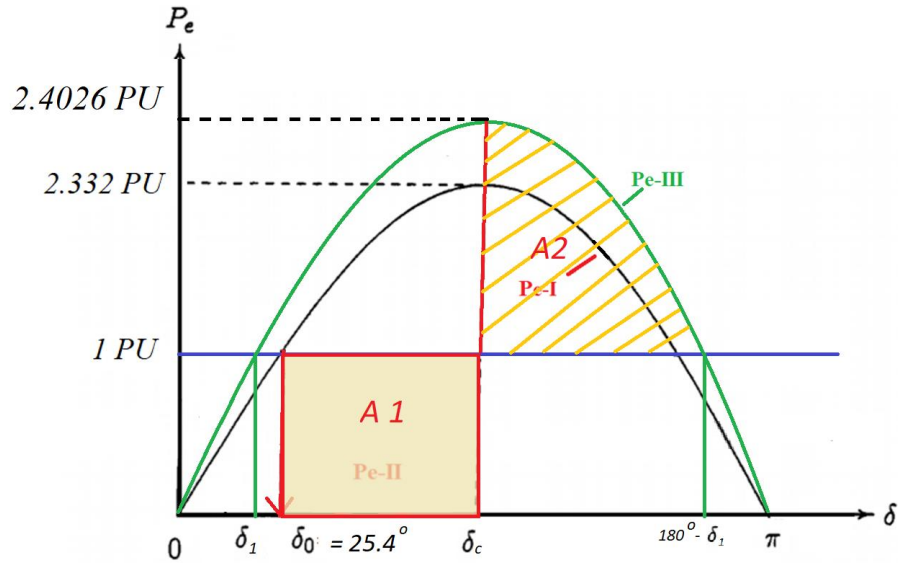


**Figure 2.2-47:** Acceleration and Deceleration Areas

Equating both acceleration and deceleration areas A1 and A2 in **Figure 2.2-47**

$$A_1 = A_2$$

$$\int_{\delta_0}^{\delta_c} (P_m - 0) \cdot d\delta = \int_{\delta_c}^{180^\circ - \delta_1} (P_{e-III} - P_m) \cdot d\delta$$

$$\int_{25.4^\circ}^{\delta_c} (1 - 0) \cdot d\delta = \int_{\delta_c}^{155.4^\circ} (2.4026 \sin\delta - 1) \cdot d\delta$$

$$1 \times (\delta_c - 25.4^\circ) \times \frac{\pi}{180^\circ} = -2.4026 \cos\delta \Big|_{\delta_c}^{155.4^\circ} - 1 \times (155.4^\circ - \delta_c) \times \frac{\pi}{180^\circ}$$

$$\delta_c \cdot \frac{\pi}{180^\circ} - 25.4^\circ \cdot \frac{\pi}{180^\circ}$$

$$= -2.4026 \cos(155.4^\circ) + 2.4026 \cos\delta_c - 155.4^\circ \cdot \frac{\pi}{180^\circ} + \delta_c \cdot \frac{\pi}{180^\circ}$$

$$2.4026 \cos\delta_c = (155.4^\circ - 25.4^\circ) \times \frac{\pi}{180^\circ} + 2.4026 \cos(155.4^\circ)$$

$$\cos\delta_c = 0.0844 \Rightarrow \delta_c = \cos^{-1}(0.0844) = 85.158^\circ$$

To calculate the critical clearing time, then we should be using the swing equation.

$$P_m - P_e = \frac{2H}{\omega_s} \frac{d^2\delta}{dt^2}$$

However, in case of 3 phase fault, the delivered electrical power  $P_e = 0$

$$\frac{d^2\delta}{dt^2} = \frac{d\omega}{dt} = \frac{\omega_s}{2H} (P_m - 0) = \frac{\omega_s}{2H} P_m$$

Integrating both sides of the equation

$$\int \frac{d^2\delta}{dt^2} = \int \frac{d}{dt} \left( \frac{d\delta}{dt} \right) = \int \frac{d\omega}{dt} = \int \frac{\omega_s}{2H} P_m$$

$$\frac{d\delta}{dt} = \int d\omega = \int \frac{\omega_s}{2H} P_m \cdot dt$$

$$\frac{d\delta}{dt} = \omega = \frac{\omega_s}{2H} P_m \cdot t$$

Integrating again both sides of the equation

$$\int d\delta = \int \frac{\omega_s}{2H} P_m t dt$$

$$\delta = \frac{\omega_s}{2H} P_m \frac{t^2}{2} + \delta_o$$

If the critical clearing time is plugged in in above equation

$$\delta_{cr} = \frac{\omega_s}{2H} P_m \frac{t_{cr}^2}{2} + \delta_o$$

With mathematical manipulation, and substituting the critical clearing angle, the critical clearing time can be calculated.

$$\delta_{cr} - \delta_o = \frac{\omega_s}{2H} P_m \frac{t_{cr}^2}{2}$$

$$t_{cr}^2 = \frac{(\delta_{cr} - \delta_o) \times 4H}{\omega_s \times P_m}$$

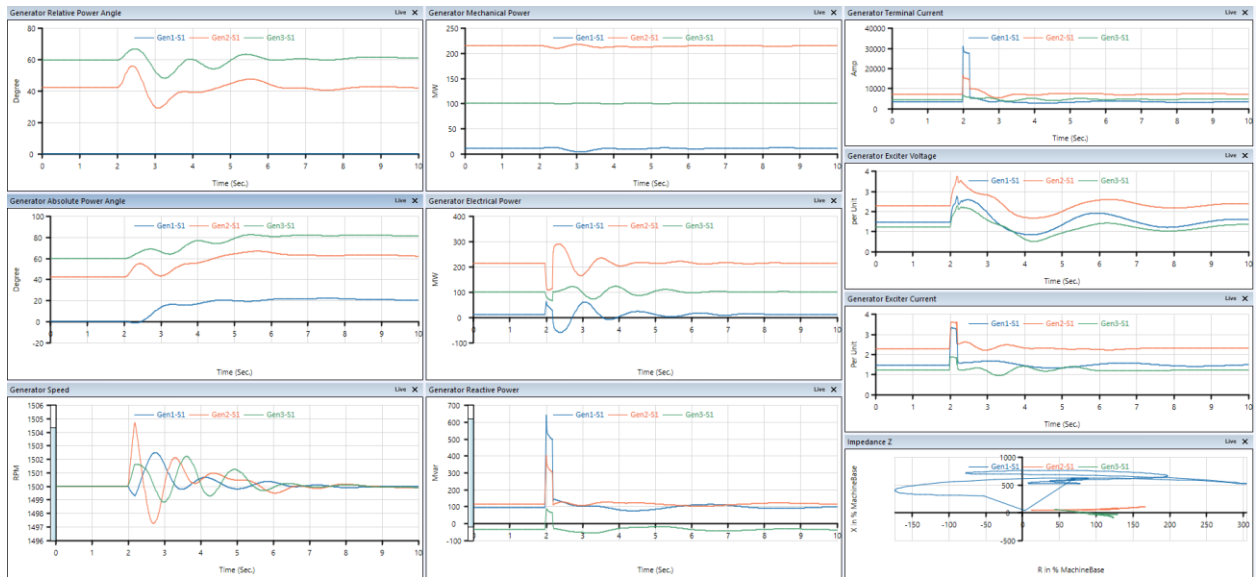
$$t_{cr} = \sqrt{\frac{(\delta_{cr} - \delta_o) \times 4H}{\omega_s \times P_m}}$$

If the above values have been plugged in, then we can calculate the critical clearing time

$$t_{cr} = \sqrt{\frac{(85.158^\circ - 25.4^\circ) \times \frac{\pi}{180^\circ} \times 4 \times 2.6312}{2\pi \times 50 \times 1}}$$

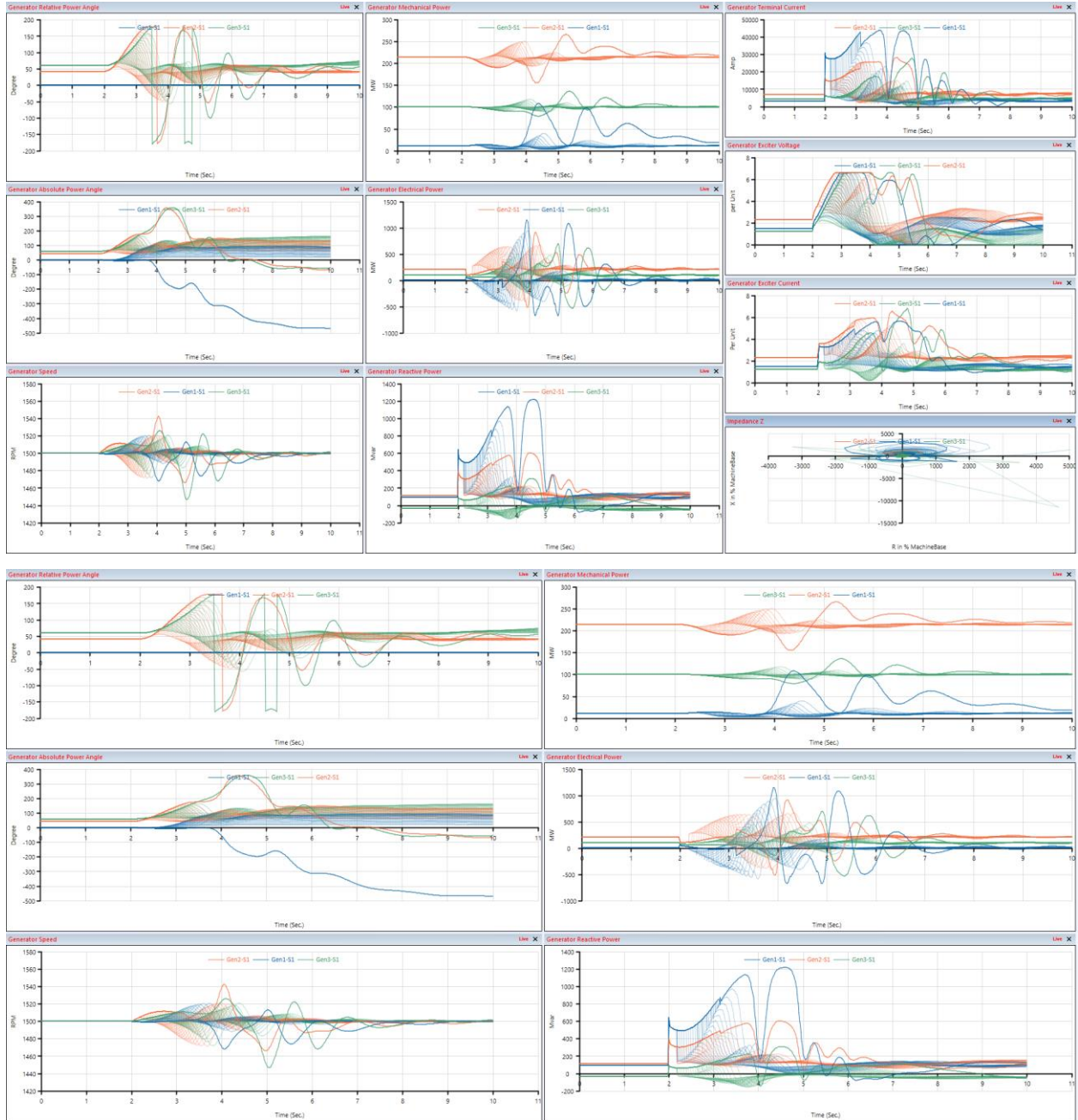
$$t_{cr} = 0.187 \text{ sec} = 187 \text{ m sec}$$

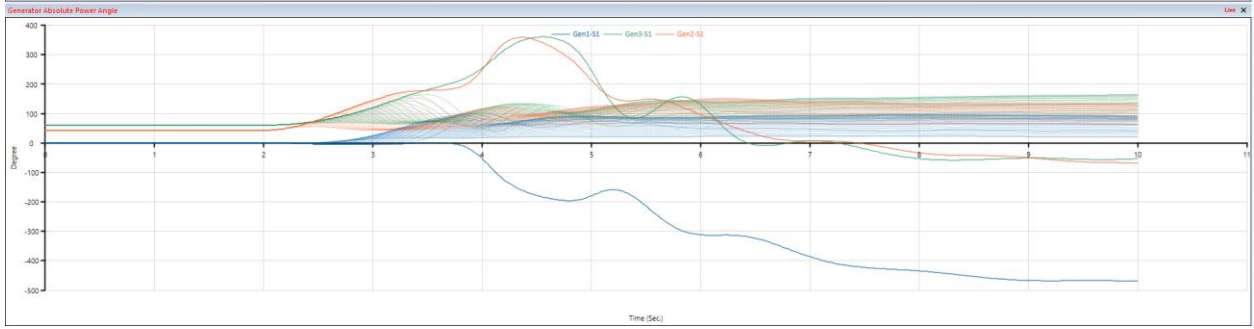
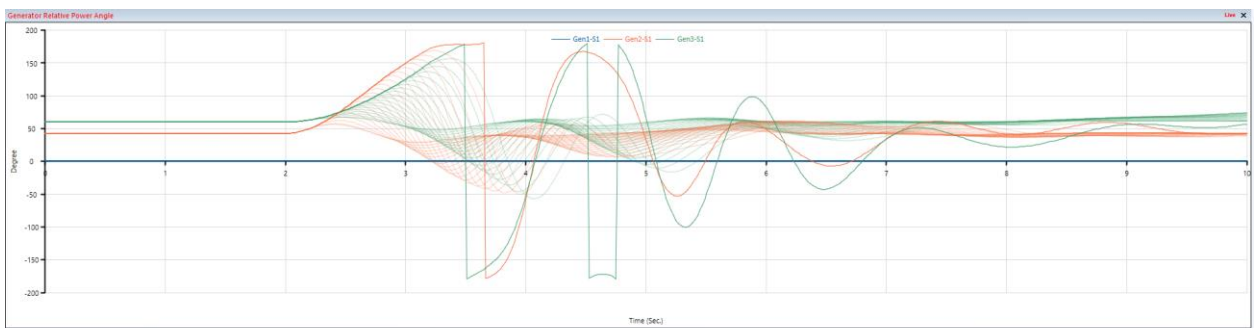
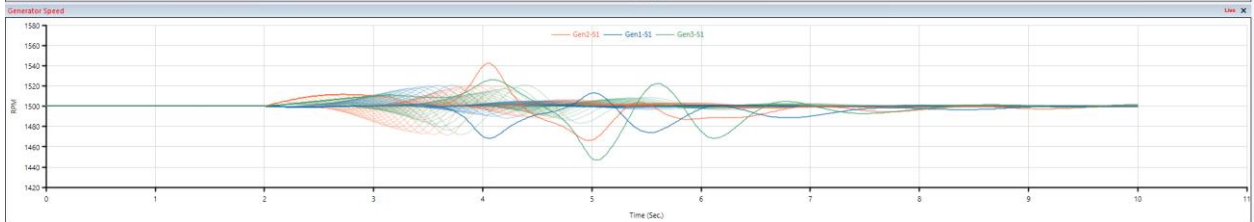
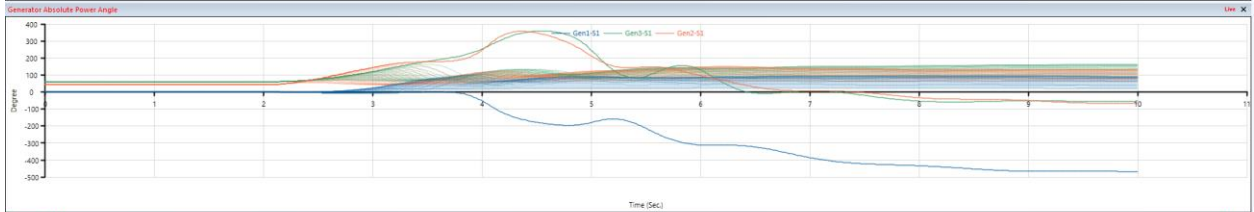
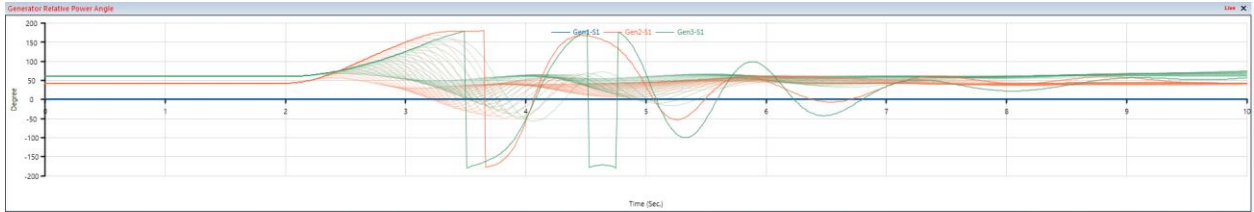
Event 1: ETAP simulation for fault at t=2 sec at the beginning of the Line L1 and fault clearance after 200 m sec is shown in **Figure 2.2-48**



**Figure 2.2-48:** Generators Gen1, 2, and 3 dynamic Response for large disturbance - transient stability study

Event 2: Assuming a three phase faults at BB No.5 occurred at t=2 sec and cleared at t=3.5 sec with reduced fault clearance time by 50 msec each step, see Figure 2.2-49





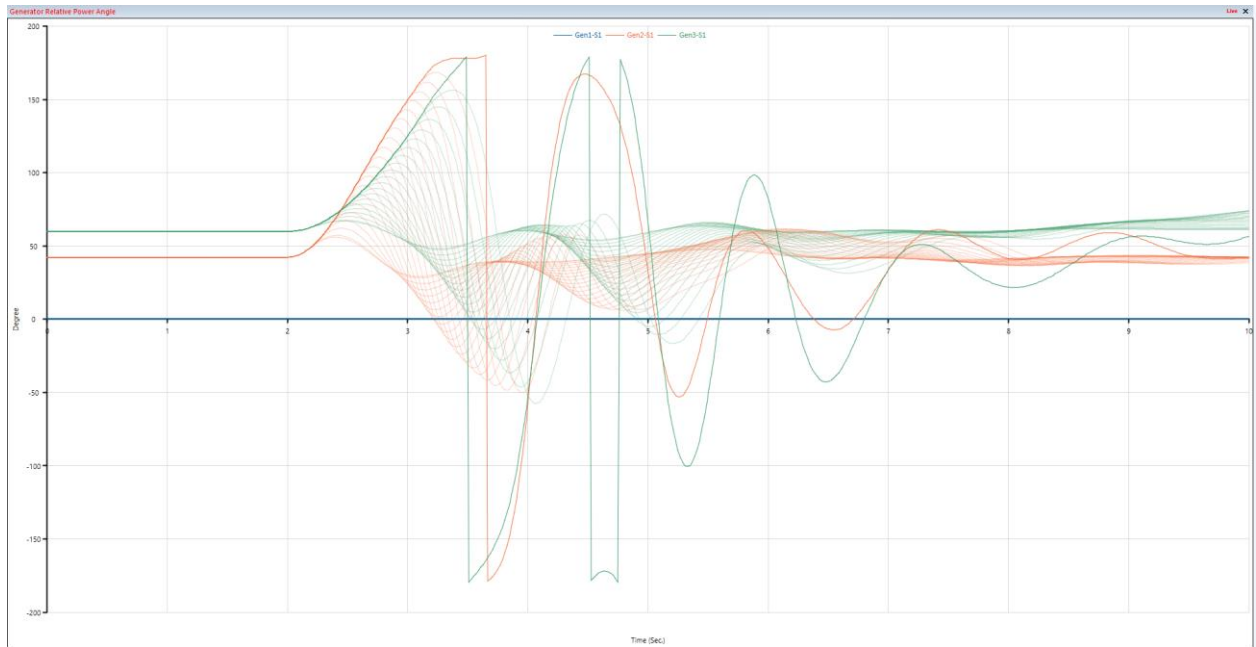


Figure 2.2-49:Generators Gen1, 2, and 3 dynamic Response for large disturbance - transient stability study BB No.5 fault

### 2.2.7.6 Control Systems for Synchronous Machines

Below are the control systems for the synchronous generator

#### 1- Frequency Stability and active power control

- a. Grid Inertial Response – Initial phase: This is the first phase of frequency response. Synchronous generators have a rotational kinetic energy which is stored in the power system as grid inertia or system inertia. This system inertia is an important inherent system property of frequency dynamics and stability.
- b. Control Phase: Three types of controls are considered for frequency control based on the timeline of initiation and functional need.
  - i. Primary Control: It is achieved through the turbine speed governor mechanism which makes the generating units respond quickly to frequency deviation as per speed-droop characteristics of the generator
  - ii. Secondary Control: It is a supplementary corrective action which involves Automatic generation Control (AGC) which delivers reserve power in order to bring back the frequency and the area interchange programs to their target values.

- iii. Tertiary Control: It is done in case of a very large disturbance in the system that cannot be handled by secondary reserves alone

2- Voltage Stability and reactive power control

- a. The synchronous generators are equipped with Automatic Voltage regulation (AVR) control which is a closed loop fashion that adjusts the excitation and control the terminal voltage.
  - i. Steady State Voltage regulation: AVR in the excitation system operating in voltage control mode helps in terminal voltage adjustment
  - ii. VAR compensation and support AVR in the excitation system operating in VAR control mode helps in reactive power support.
- b. Voltage profile improvement is also done by on-load or off-load tap changing transformer

3- Angle Stability

- a. Small Signal Angle Stability: Power system stabilizer (PSS) present in excitation system helps in improving small signal angle stability of the system.
- b. Transient Stability Improvement: High speed excitation along with PSS and several other controls are present for large signal stability enhancement

To mimic the control functionalities of the conventional synchronous machines, grid forming control system is used in which the system generates and sustains its own voltage, ensuring synchronization. It provides immediate assistance for voltage and frequency and enhances stability and resilience, which is particularly important for grids with little power capacity.

Grid Forming Performance:

- 1- Contribute to grid strength.
- 2- Contribute to short circuit current injection.
- 3- Reduces system unbalance.
- 4- Provide inertial response.
- 5- Contribute to frequency control.
- 6- Island operation.

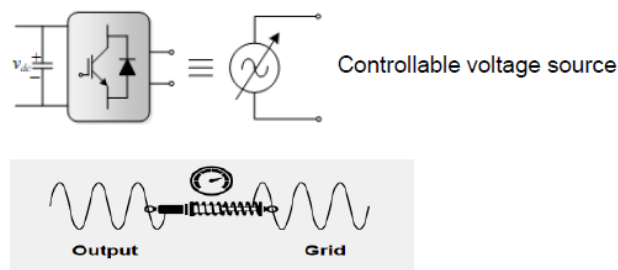


Figure 2.2-50: Grid Forming Principle

## 2.2.8 Power System Differential Equations

The electrical power systems can be modeled using differential equations that are derived from the simple ohm's law and Kirchhoff's voltage law. For example, if we take Figure 2.2-51: Line connecting between two buses i and j:

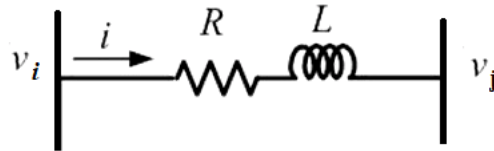


Figure 2.2-51: Line connecting between two buses i and j

Applying Kirchhoff's voltage law, then

$$v_i = v_j + Ri + L \frac{di}{dt}$$

$$L \frac{di}{dt} = v_i - v_j - Ri$$

$$\frac{di}{dt} = \frac{v_i - v_j}{L} - \frac{R}{L} i$$

We will develop a dynamic mathematical model for the IEEE 9 bus system which can be used for steady state and dynamic conditions. This mathematical model of a three-phase IEEE 9 bus power system with a single-circuit short-length transmission lines, **Figure 2.2-52**: IEEE 9 bus system with equivalent circuit. has been developed through a system of differential equations for current, bus voltage calculations and algebraic equations for load-bus and fault location voltage calculations. The idea of this procedure has been based on nodal voltages technique and on differentiation of Kirchhoff's current law (KCL) applied to each non-reference node of the system, the result of which a system of algebraic equations for nodal voltages has been obtained [21]. Currents flowing through the electric power system components have been determined by solving their respective differential equations.

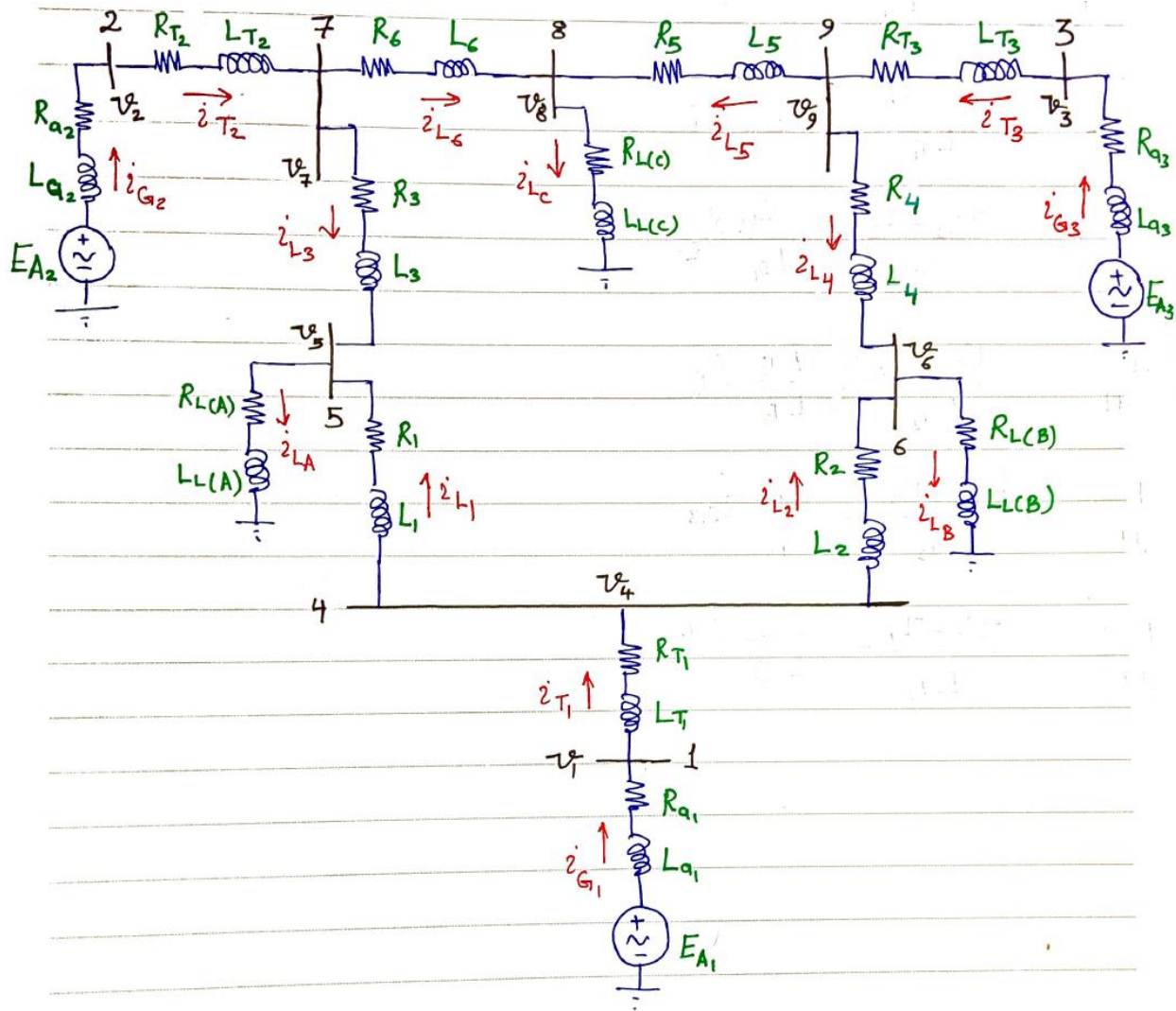


Figure 2.2-52: IEEE 9 bus system with equivalent circuit.

Modeling the system should be performed in a step-by-step manner as per below.

Step No.1: Write the differential equations for all branches.

For generators and its generator step up transformers

$$\frac{di_{G1}}{dt} = \frac{E_{A1} - v_1}{L_{a1}} - \frac{R_{a1}}{L_{a1}} \times i_{G1}$$

$$\frac{di_{T1}}{dt} = \frac{v_1 - v_4}{L_{T1}} - \frac{R_{T1}}{L_{T1}} \times i_{T1}$$

$$\frac{di_{G2}}{dt} = \frac{E_{A2} - v_2}{L_{a2}} - \frac{R_{a2}}{L_{a2}} \times i_{G2}$$

$$\frac{di_{T2}}{dt} = \frac{v_2 - v_7}{L_{T2}} - \frac{R_{T2}}{L_{T2}} \times i_{T2}$$

$$\frac{di_{G3}}{dt} = \frac{E_{A3} - v_3}{L_{a3}} - \frac{R_{a3}}{L_{a3}} \times i_{G3}$$

$$\frac{di_{T3}}{dt} = \frac{v_3 - v_9}{L_{T3}} - \frac{R_{T3}}{L_{T3}} \times i_{T3}$$

For the transmission lines

$$\frac{di_{l1}}{dt} = \frac{v_4 - v_5}{L_{l1}} - \frac{R_{l1}}{L_{l1}} \times i_{l1}$$

$$\frac{di_{l2}}{dt} = \frac{v_4 - v_6}{L_{l2}} - \frac{R_{l2}}{L_{l2}} \times i_{l2}$$

$$\frac{di_{l3}}{dt} = \frac{v_7 - v_5}{L_{l3}} - \frac{R_{l3}}{L_{l3}} \times i_{l3}$$

$$\frac{di_{l4}}{dt} = \frac{v_9 - v_6}{L_{l4}} - \frac{R_{l4}}{L_{l4}} \times i_{l4}$$

$$\frac{di_{l5}}{dt} = \frac{v_9 - v_8}{L_{l5}} - \frac{R_{l5}}{L_{l5}} \times i_{l5}$$

$$\frac{di_{l6}}{dt} = \frac{v_7 - v_8}{L_{l6}} - \frac{R_{l6}}{L_{l6}} \times i_{l6}$$

For the loads

$$\frac{di_{L(A)}}{dt} = \frac{v_5}{L_A} - \frac{R_A}{L_A} \times i_A$$

$$\frac{di_{L(B)}}{dt} = \frac{v_6}{L_B} - \frac{R_B}{L_B} \times i_B$$

$$\frac{di_{L(C)}}{dt} = \frac{v_8}{L_C} - \frac{R_C}{L_C} \times i_C$$

Step No.2: Apply KCL for all buses.

$$\text{Bus No. 1} \Rightarrow i_{G1} = i_{T1}$$

$$\text{Bus No. 2} \Rightarrow i_{G2} = i_{T2}$$

$$\text{Bus No. 3} \Rightarrow i_{G3} = i_{T3}$$

$$\text{Bus No. 4} \Rightarrow i_{T1} = i_{l1} + i_{l2}$$

$$\text{Bus No. 5} \Rightarrow i_{l1} + i_{l3} = i_{L(A)}$$

$$\text{Bus No. 6} \Rightarrow i_{l2} + i_{l4} = i_{L(B)}$$

$$\text{Bus No. 7} \Rightarrow i_{T2} = i_{l3} + i_{l6}$$

$$\text{Bus No. 8} \Rightarrow i_{l5} + i_{l6} = i_{L(C)}$$

$$\text{Bus No. 9} \Rightarrow i_{T3} = i_{l4} + i_{l5}$$

*Step No.3: Differentiate the KCL equations for all buses.*

$$\text{Bus No. 1} \Rightarrow i_{G1} = i_{T1} \Rightarrow \frac{di_{G1}}{dt} = \frac{di_{T1}}{dt}$$

$$\text{Bus No. 2} \Rightarrow i_{G2} = i_{T2} \Rightarrow \frac{di_{G2}}{dt} = \frac{di_{T2}}{dt}$$

$$\text{Bus No. 3} \Rightarrow i_{G3} = i_{T3} \Rightarrow \frac{di_{G3}}{dt} = \frac{di_{T3}}{dt}$$

$$\text{Bus No. 4} \Rightarrow i_{T1} = i_{l1} + i_{l2} \Rightarrow \frac{di_{T1}}{dt} = \frac{di_{l1}}{dt} + \frac{di_{l2}}{dt}$$

$$\text{Bus No. 5} \Rightarrow i_{l1} + i_{l3} = i_{L(A)} \Rightarrow \frac{di_{l1}}{dt} + \frac{di_{l3}}{dt} = \frac{di_{L(A)}}{dt}$$

$$\text{Bus No. 6} \Rightarrow i_{l2} + i_{l4} = i_{L(B)} \Rightarrow \frac{di_{l2}}{dt} + \frac{di_{l4}}{dt} = \frac{di_{L(B)}}{dt}$$

$$\text{Bus No. 7} \Rightarrow i_{T2} = i_{l3} + i_{l6} \Rightarrow \frac{di_{T2}}{dt} = \frac{di_{l3}}{dt} + \frac{di_{l6}}{dt}$$

$$\text{Bus No. 8} \Rightarrow i_{l5} + i_{l6} = i_{L(C)} \Rightarrow \frac{di_{l5}}{dt} + \frac{di_{l6}}{dt} = \frac{di_{L(C)}}{dt}$$

$$\text{Bus No. 9} \Rightarrow i_{T3} = i_{l4} + i_{l5} \Rightarrow \frac{di_{T3}}{dt} = \frac{di_{l4}}{dt} + \frac{di_{l5}}{dt}$$

*Step No.4: Substitute the Differential equations of step No.1 in step 4.*

$$\text{Bus No. 1} \Rightarrow \frac{di_{G1}}{dt} = \frac{di_{T1}}{dt} \Rightarrow \frac{E_{A1} - v_1}{L_{a1}} - \frac{R_{a1}}{L_{a1}} \times i_{G1} = \frac{v_1 - v_4}{L_{T1}} - \frac{R_{T1}}{L_{T1}} \times i_{T1} \Rightarrow$$

$$v_1 \left( \frac{1}{L_{a1}} + \frac{1}{L_{T1}} \right) - v_4 \left( \frac{1}{L_{T1}} \right) = \frac{E_{A1}}{L_{a1}} - \frac{R_{a1}}{L_{a1}} \times i_{G1} + \frac{R_{T1}}{L_{T1}} \times i_{T1}$$

$$\text{Bus No. 2} \Rightarrow \frac{di_{G2}}{dt} = \frac{di_{T2}}{dt} \Rightarrow \frac{E_{A2} - v_2}{L_{a2}} - \frac{R_{a2}}{L_{a2}} \times i_{G2} = \frac{v_2 - v_7}{L_{T2}} - \frac{R_{T2}}{L_{T2}} \times i_{T2} \Rightarrow$$

$$v_2 \left( \frac{1}{L_{a2}} + \frac{1}{L_{T2}} \right) - v_7 \left( \frac{1}{L_{T2}} \right) = \frac{E_{A2}}{L_{a2}} - \frac{R_{a2}}{L_{a2}} \times i_{G2} + \frac{R_{T2}}{L_{T2}} \times i_{T2}$$

$$\text{Bus No. 3} \Rightarrow \frac{di_{G3}}{dt} = \frac{di_{T3}}{dt} \Rightarrow \frac{E_{A3} - v_3}{L_{a3}} - \frac{R_{a3}}{L_{a3}} \times i_{G3} = \frac{v_3 - v_9}{L_{T3}} - \frac{R_{T3}}{L_{T3}} \times i_{T3}$$

$$v_3 \left( \frac{1}{L_{a3}} + \frac{1}{L_{T3}} \right) - v_9 \left( \frac{1}{L_{T3}} \right) = \frac{E_{A3}}{L_{a3}} - \frac{R_{a3}}{L_{a3}} \times i_{G3} + \frac{R_{T3}}{L_{T3}} \times i_{T3}$$

$$\begin{aligned} \text{Bus No. 4} \Rightarrow \frac{di_{T1}}{dt} &= \frac{di_{l1}}{dt} + \frac{di_{l2}}{dt} \Rightarrow \frac{v_1 - v_4}{L_{T1}} - \frac{R_{T1}}{L_{T1}} \times i_{T1} \\ &= \frac{v_4 - v_5}{L_{l1}} - \frac{R_{l1}}{L_{l1}} \times i_{l1} + \frac{v_4 - v_6}{L_{l2}} - \frac{R_{l2}}{L_{l2}} \times i_{l2} \end{aligned}$$

$$v_4 \left( \frac{1}{L_{l1}} + \frac{1}{L_{l2}} + \frac{1}{L_{T1}} \right) - v_1 \left( \frac{1}{L_{T1}} \right) - v_5 \frac{1}{L_{l1}} - v_6 \left( \frac{1}{L_{l2}} \right) = -\frac{R_{T1}}{L_{T1}} \times i_{T1} + \frac{R_{l2}}{L_{l2}} \times i_{l2} + \frac{R_{l1}}{L_{l1}} \times i_{l1}$$

$$\text{Bus No. 5} \Rightarrow \frac{di_{l1}}{dt} + \frac{di_{l3}}{dt} = \frac{di_{L(A)}}{dt} \Rightarrow \frac{v_4 - v_5}{L_{l1}} - \frac{R_{l1}}{L_{l1}} \times i_{l1} + \frac{v_7 - v_5}{L_{l3}} - \frac{R_{l3}}{L_{l3}} \times i_{l3} = \frac{v_5}{L_A} - \frac{R_A}{L_A} \times i_A$$

$$v_5 \left( \frac{1}{L_A} + \frac{1}{L_{l1}} + \frac{1}{L_{l3}} \right) - v_4 \left( \frac{1}{L_{l1}} \right) - v_7 \left( \frac{1}{L_{l3}} \right) = -\frac{R_{l1}}{L_{l1}} \times i_{l1} + -\frac{R_{l3}}{L_{l3}} \times i_{l3} + \frac{R_A}{L_A} \times i_A$$

$$\text{Bus No. 6} \Rightarrow \frac{di_{l2}}{dt} + \frac{di_{l4}}{dt} = \frac{di_{L(B)}}{dt} \Rightarrow \frac{v_4 - v_6}{L_{l2}} - \frac{R_{l2}}{L_{l2}} \times i_{l2} + \frac{v_9 - v_6}{L_{l4}} - \frac{R_{l4}}{L_{l4}} \times i_{l4} = \frac{v_6}{L_B} - \frac{R_B}{L_B} \times i_B$$

$$v_6 \left( \frac{1}{L_A} + \frac{1}{L_{l2}} + \frac{1}{L_{l4}} \right) - v_4 \left( \frac{1}{L_{l2}} \right) - v_9 \left( \frac{1}{L_{l4}} \right) = -\frac{R_{l2}}{L_{l2}} \times i_{l2} - \frac{R_{l4}}{L_{l4}} \times i_{l4} + \frac{R_B}{L_B} \times i_B$$

$$\begin{aligned}
\text{Bus No. 7} &\Rightarrow \frac{di_{T2}}{dt} = \frac{di_{l3}}{dt} + \frac{di_{l6}}{dt} \Rightarrow \frac{v_2 - v_7}{L_{T2}} - \frac{R_{T2}}{L_{T2}} \times i_{T2} \\
&= \frac{v_7 - v_5}{L_{l3}} - \frac{R_{l3}}{L_{l3}} \times i_{l3} + \frac{v_7 - v_8}{L_{l6}} - \frac{R_{l6}}{L_{l6}} \times i_{l6} \\
v_7 \left( \frac{1}{L_{T2}} + \frac{1}{L_{l3}} + \frac{1}{L_{l6}} \right) - v_2 \left( \frac{1}{L_{T2}} \right) - v_5 \left( \frac{1}{L_{l3}} \right) - v_8 \left( \frac{1}{L_{l6}} \right) &= -\frac{R_{T2}}{L_{T2}} \times i_{T2} + \frac{R_{l3}}{L_{l3}} \times i_{l3} + \frac{R_{l6}}{L_{l6}} \times i_{l6}
\end{aligned}$$

$$\begin{aligned}
\text{Bus No. 8} &\Rightarrow \frac{di_{l5}}{dt} + \frac{di_{l6}}{dt} = \frac{di_{L(C)}}{dt} \Rightarrow \frac{v_9 - v_8}{L_{l5}} - \frac{R_{l5}}{L_{l5}} \times i_{l5} + \frac{v_7 - v_8}{L_{l6}} - \frac{R_{l6}}{L_{l6}} \times i_{l6} = \frac{v_8}{L_C} - \frac{R_C}{L_C} \times i_C \\
v_8 \left( \frac{1}{L_C} + \frac{1}{L_{l5}} + \frac{1}{L_{l6}} \right) - v_9 \left( \frac{1}{L_{l5}} \right) - v_7 \left( \frac{1}{L_{l6}} \right) &= -\frac{R_{l6}}{L_{l6}} \times i_{l6} - \frac{R_{l5}}{L_{l5}} \times i_{l5} + \frac{R_C}{L_C} \times i_C
\end{aligned}$$

$$\begin{aligned}
\text{Bus No. 9} &\Rightarrow \frac{di_{T3}}{dt} = \frac{di_{l4}}{dt} + \frac{di_{l5}}{dt} \Rightarrow \frac{v_3 - v_9}{L_{T3}} - \frac{R_{T3}}{L_{T3}} \times i_{T3} \\
&= \frac{v_9 - v_6}{L_{l4}} - \frac{R_{l4}}{L_{l4}} \times i_{l4} + \frac{v_9 - v_8}{L_{l5}} - \frac{R_{l5}}{L_{l5}} \times i_{l5}
\end{aligned}$$

$$v_9 \left( \frac{1}{L_{T3}} + \frac{1}{L_{l4}} + \frac{1}{L_{l5}} \right) - v_3 \left( \frac{1}{L_{T3}} \right) - v_6 \left( \frac{1}{L_{l4}} \right) - v_8 \left( \frac{1}{L_{l5}} \right) = -\frac{R_{T3}}{L_{T3}} \times i_{T3} + \frac{R_{l4}}{L_{l4}} \times i_{l4} + \frac{R_{l5}}{L_{l5}} \times i_{l5}$$

Step No.5: Re-writing the equations in step No.4 into matrix form

$$[L] \times [V] = [I]$$

$$[V] = [L]^{-1} \times [I]$$

Matrix L can be written per below

$\frac{1}{L_{a1}} + \frac{1}{L_{T1}}$	0	0	$\frac{-1}{L_{T1}}$	0	0	0	0	0
0	$\frac{1}{L_{a2}} + \frac{1}{L_{T2}}$	0	0	0	0	$\frac{-1}{L_{T2}}$	0	0
0	0	$\frac{1}{L_{a3}} + \frac{1}{L_{T3}}$	0	0	0	0	0	$\frac{-1}{L_{T3}}$
$\frac{-1}{L_{T1}}$	0	0	$\frac{1}{L_{l1}} + \frac{1}{L_{l2}} + \frac{1}{L_{T1}}$	$\frac{-1}{L_{l1}}$	$\frac{-1}{L_{l2}}$	0	0	0
0	0	0	$\frac{-1}{L_{l1}}$	$\frac{1}{L_A} + \frac{1}{L_{l1}} + \frac{1}{L_{l3}}$	0	$\frac{-1}{L_{l3}}$	0	0
0	0	0	$\frac{1}{L_{l2}}$	0	$\frac{1}{L_A} + \frac{1}{L_{l2}} + \frac{1}{L_{l4}}$	0	0	$\frac{1}{L_{l4}}$
						$\frac{1}{L_{T2}} + \frac{1}{L_{l3}} + \frac{1}{L_{l6}}$		
							$\frac{1}{L_C} + \frac{1}{L_{l5}} + \frac{1}{L_{l6}}$	
								$\frac{1}{L_{T3}} + \frac{1}{L_{l4}} + \frac{1}{L_{l5}}$

Below is the MATLAB m.file code

```

% IEEE 9 bus system - Power System Modeling and Simulation at Normal Operating
Condition
clc
clear

```

```

clear var
h=0.314;
T=500;
t=[0:h:T];
EA1=1;EA2=1;EA3=1;
V1=zeros(1,length(t)); V2=zeros(1,length(t));
V3=zeros(1,length(t));V4=zeros(1,length(t));
V5=zeros(1,length(t)); V6=zeros(1,length(t));
V7=zeros(1,length(t));V8=zeros(1,length(t));V9=zeros(1,length(t));

f=50;
W=2*pi*f;

RT1=0.00256;RT2=0.00256;RT3=0.00256;
LT1=0.1;LT2=0.1;LT3=0.1;

Ra1=0.0114;Ra2=0.0114;Ra3=0.0114;
La1=0.0769;La2=0.0769;La3=0.0769;

R1=0.00256;R2=0.00256;R3=0.00256;R4=0.00256;R5=0.00256;R6=0.00256;
L1=0.1;L2=0.1;L3=0.1;L4=0.1;L5=0.1;L6=0.1;

RA=0.0114;RB=0.0114;RC=0.0114;
LA=0.0769;LB=0.0769;LC=0.0769;

L=[ (1/La1+1/LT1), 0, 0, -(1/LT1), 0, 0, 0, 0, 0 ;
    0, (1/La2+1/LT2), 0, 0, 0, 0, -(1/LT2), 0, 0 ;
    -(1/LT1), 0, 0, (1/LT1+1/L1+1/L2), -(1/L1), -(1/L2), 0, 0, 0 ;
    0, 0, (1/La3+1/LT3), 0, 0, 0, 0, 0, -(1/LT3) ;
    0, 0, 0, -(1/L1), (1/L1+1/L3+ 1/LA), 0, -(1/L3), 0, 0 ;
    0, 0, 0, -(1/L2), 0, 1/L2+1/L4+1/LB, 0, 0, -(1/L4) ;
    0, -(1/LT2), 0, 0, -(1/L3), 0, (1/LT2+1/L3+1/L6), -(1/L6), 0;
    0, 0, 0, 0, 0, 0, -(1/L6), (1/L5+1/L6+1/LC), -(1/L5) ;
    0, 0, -(1/LT3), 0, 0, -(1/L4), 0, -1/L5, (1/L4+1/L5+1/LT3)];

X=inv(L);

iT1=0;iG1=0;iT2=0;iG2=0;iT3=0;iG3=0;

iL1=0;iL2=0;iL3=0;iL4=0;iL5=0;iL6=0;

iA=0;iB=0;iC=0;

i(1,:)=[iG1, iT1, iG2, iT2, iG3, iT3, iL1, iL2, iL3, iL4, iL5, iL6, iA, iB, iC];
V=[0 ; 0 ; 0 ; 0 ; 0 ; 0 ; 0 ; 0 ; 0 ; 0 ]; % V1 , V2 , V3 , V4 , V5 , V6 , V7 , V8 ,V9

for j=1:length(t)-1
y = i(j,:);

f=@(t,i) [(EA1*sin(t)-V(1,j))/La1-(Ra1/La1)*i(1); %d_iG1/d_t
          (V(1,j)-V(4,j))/LT1-(RT1/LT1)*i(2); %d_iT1/d_t
          (EA2*sin(t)-V(2,j))/La2-(Ra2/La2)*i(3); %d_iG2/d_t
          (V(2,j)-V(4,j))/LT2-(RT2/LT2)*i(4); %d_iT2/d_t

```

```

(EA3*sin(t)-V(3,j))/La3-(Ra3/La3)*i(5); %d_iG3/d_t
(V(3,j)-V(4,j))/LT3-(RT3/LT3)*i(6); %d_iT3/d_t
(V(4,j)-V(5,j))/L1-(R1/L1)*i(7); %d_iL1/d_t
(V(4,j)-V(6,j))/L2-(R2/L2)*i(8); %d_iL2/d_t
(V(7,j)-V(5,j))/L3-(R3/L3)*i(9); %d_iL3/d_t
(V(9,j)-V(6,j))/L4-(R4/L4)*i(10); %d_iL4/d_t
(V(9,j)-V(8,j))/L5-(R5/L5)*i(11); %d_iL5/d_t
(V(7,j)-V(8,j))/L6-(R6/L6)*i(12); %d_iL6/d_t
(V(5,j)/LA)-(RA/LA)*i(13); %d_iLA/d_t
(V(6,j)/LB)-(RB/LB)*i(14); %d_iLB/d_t
(V(8,j)/LC)-(RC/LC)*i(15)]; %d_iLC/d_t

k1=h*f(t(j),y);
k2=h*f((t(j)+0.5*h),(y+0.5*k1*h));
k3=h*f((t(j)+0.5*h),(y+0.5*k2*h));
k4=h*f((t(j)+0.5*h),(y+k3*h));

i(j+1,:)=i(j,:)+((k1+2*k2+2*k3+k4)/6.0)';

L=[(1/La1+1/LT1) , 0 , 0 , -(1/LT1) , 0 , 0 , 0 , 0 , 0 ;
    0 , (1/La2+1/LT2) , 0 , 0 , 0 , -(1/LT2) , 0 , 0 , 0 ;
    -(1/LT1) , 0 , 0 , (1/LT1+1/L1+1/L2) , -(1/L1) , -(1/L2) , 0 , 0 , 0 ;
    0 , 0 , (1/La3+1/LT3) , 0 , 0 , 0 , 0 , 0 , -(1/LT3) ;
    0 , 0 , 0 , -(1/L1) , (1/L1+1/L3+ 1/LA) , 0 , -(1/L3) , 0 , 0 ;
    0 , 0 , 0 , -(1/L2) , 0 , 1/L2+1/L4+1/LB , 0 , 0 , -(1/L4) ;
    0 , -(1/LT2) , 0 , 0 , -(1/L3) , 0 ,(1/LT2+1/L3+1/L6) , -(1/L6) , 0 ;
    0 , 0 , 0 , 0 , 0 , -(1/L6) , (1/L5+1/L6+1/LC) , -(1/L5) ;
    0 , 0 , -(1/LT3) , 0 , 0 , -(1/L4) , 0 , -1/L5 , (1/L4+1/L5+1/LT3)];

%[iG1, iT1, iG2, iT2, iG3, iT3, iL1, iL2, iL3, iL4, iL5, iL6, iA,
iB, iC]
%i(1), i(2), i(3), i(4), i(5), i(6), i(7) , i(8), i(9), i(10), i(11), i(12), i(13)
, i(14), i(15)
X=inv(L);
A=[ (EA1*sin(t(j+1))/La1)-(Ra1/La1)*i(j+1,1)+(RT1/LT1)*i(j+1,2);
    (EA2*sin(t(j+1))/La2)-(Ra2/La2)*i(j+1,3)+(RT2/LT2)*i(j+1,4);
    (EA3*sin(t(j+1))/La3)-(Ra3/La3)*i(j+1,5)+(RT3/LT3)*i(j+1,6);
    -(RT1/LT1)*i(j+1,2)+(R1/L1)*i(j+1,4)+(R2/L2)*i(j+1,6);
    -(R1/L1)*i(j+1,7)-(R3/L3)*i(j+1,9)+(RA/LA)*i(j+1,13);
    -(R2/L2)*i(j+1,8)-(R4/L4)*i(j+1,10)+(RB/LB)*i(j+1,14);
    -(RT2/LT2)*i(j+1,4)-(R3/L3)*i(j+1,9)+(R6/L6)*i(j+1,12);
    -(R6/L6)*i(j+1,12)-(R5/L5)*i(j+1,11)+(RC/LC)*i(j+1,15);
    -(RT3/LT3)*i(j+1,6)-(R4/L4)*i(j+1,10)+(R5/L5)*i(j+1,11)];

V(:,j+1)=X*A;

end
%[iG1, iT1, iG2, iT2, iG3, iT3, iL1, iL2, iL3, iL4, iL5, iL6, iA,
iB, iC]

```

```

%i(1), i(2), i(3), i(4), i(5), i(6), i(7) , i(8), i(9), i(10), i(11), i(12), i(13)
, i(14), i(15)
iG1=i(:,1); iT1=i(:,2); iG2=i(:,3); iT2=i(:,4); iG3=i(:,5); iT3=i(:,6);

iL1=i(:,7); iL2=i(:,8); iL3=i(:,9); iL4=i(:,10); iL5=i(:,11); iL6=i(:,12);

iA=i(:,13); iB=i(:,14); iC=i(:,15);

V1=V(1,:); V2=V(2,:); V3=V(3,:); V4=V(4,:); V5=V(5,:); V6=V(6,:); V7=V(7,:);
V8=V(8,:); V9=V(9,:);

figure
plot(t/314,i);
hold
grid on;
xlabel('time');
ylabel('Currents in all branches in P.U');
axis auto
legend('iG1','iT1','iG2','iT2','iG3','iT3','iG','iL1','iL2','iL3','iL4','iL5','iL6',
'iA','iB','iC');

figure
plot(t/314,V);
hold
grid on;
xlabel('time');
ylabel('Voltages at all 9 buses in P.U')
axis auto
legend('V1','V2','V3','V4','V5','V6','V7','V8','V9') ;

% Grid Current
figure
plot(t/314,i(:,1),t/314,i(:,3),t/314,i(:,5))
hold
grid on
xlabel('time')
ylabel('Generators Current in P.U');
legend('i generators current ')
figure
plot(t/314,V(4,:));
hold;
grid on;
xlabel('time');
ylabel('V at IEEE 9 Bus system');

subplot(2,2,1);
plot(t/314,i);
grid on;
title('Subplot 1: Currents in all branches PU')
legend('iG1','iT1','iG2','iT2','iG3','iT3','iG','iL1','iL2','iL3','iL4','iL5','iL6',
'iA','iB','iC');

```

```

subplot(2,2,2);
plot(t/314,V);
grid on;
title('Subplot 2: 9-Bus Voltages in PU')
legend('V1','V2','V3','V4','V5','V6','V7','V8','V9') ;

subplot(2,2,3);
plot(t/314,i(:,13),t/314,i(:,14),t/314,i(:,15));
grid on;
title('Subplot 3: Load Currents in P.U')
legend('iLA','iLB','iLC') ;

subplot(2,2,4);
plot(t/314,i(:,1),t/314,i(:,3),t/314,i(:,5));
grid on;
title('Subplot 4: Total Currents from Generators in PU')
legend('iG1','iG2','iG3') ;

```

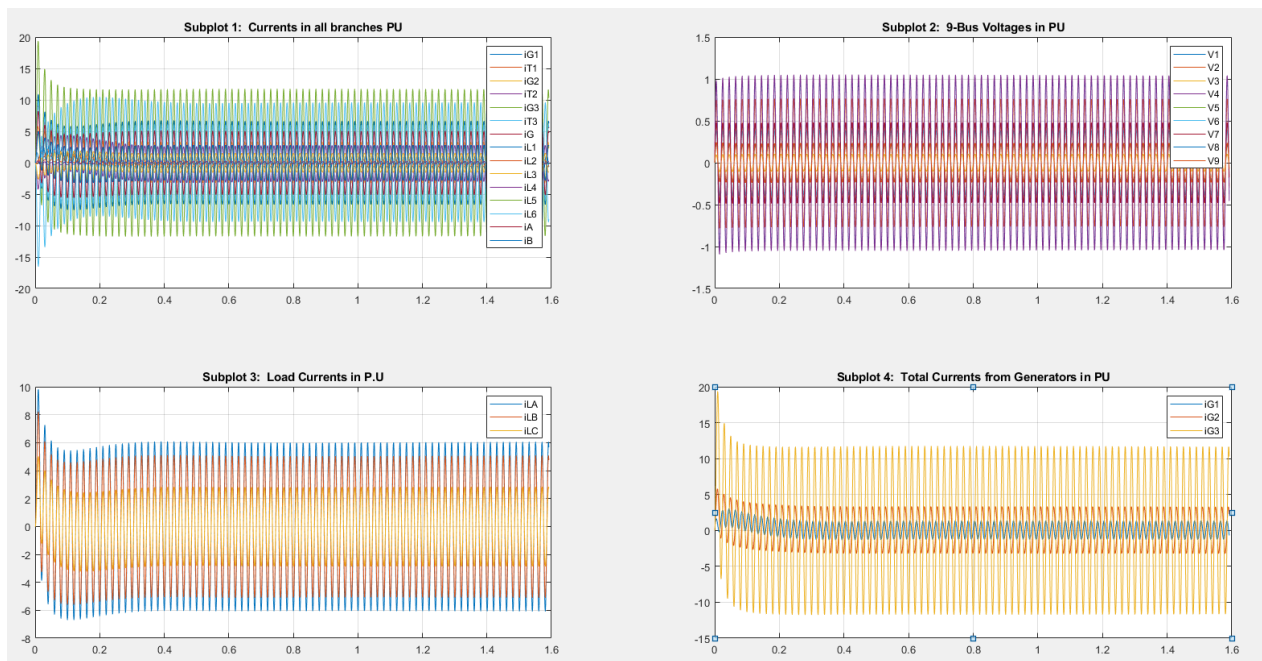


Figure 2.2-53: MATLAB m.file Output

Above model was under normal operating conditions, however, to simulate the fault there are different approaches like adding a shunt element at fault location and decrease the shunt resistance and inductance parameters to almost zero, also there is another approach in which we reduce the load parameters at the fault location and reduce them to zero

```

% Power System Modeling and Simulation-Dynamic Short Circuit at BB No.9 ( load C
terminals )
clc
clear
clear var
h=0.314;
T=500;
t=[0:h:T];

```

```

EA1=1;EA2=1;EA3=1;
V1=zeros(1,length(t)); V2=zeros(1,length(t));
V3=zeros(1,length(t));V4=zeros(1,length(t));
V5=zeros(1,length(t)); V6=zeros(1,length(t));
V7=zeros(1,length(t));V8=zeros(1,length(t));V9=zeros(1,length(t));

f=50;
W=2*pi*f;

RT1=0.00256;RT2=0.00256;RT3=0.00256;
LT1=0.1;LT2=0.1;LT3=0.1;

Ra1=0.0114;Ra2=0.0114;Ra3=0.0114;
La1=0.0769;La2=0.0769;La3=0.0769;

R1=0.00256;R2=0.00256;R3=0.00256;R4=0.00256;R5=0.00256;R6=0.00256;
L1=0.1;L2=0.1;L3=0.1;L4=0.1;L5=0.1;L6=0.1;
RA=0.0114;RB=0.0114;RC=0.0114;
LA=0.0769;LB=0.0769;LC=0.0769;

L=[ (1/La1+1/LT1), 0, 0, -(1/LT1), 0, 0, 0, 0, 0 ;
    0, (1/La2+1/LT2), 0, 0, 0, -(1/LT2), 0, 0, 0 ;
    -(1/LT1), 0, 0, (1/LT1+1/L1+1/L2), -(1/L1), -(1/L2), 0, 0, 0 ;
    0, 0, (1/La3+1/LT3), 0, 0, 0, 0, 0, -(1/LT3) ;
    0, 0, 0, -(1/L1), (1/L1+1/L3+ 1/LA), 0, -(1/L3), 0, 0 ;
    0, 0, 0, -(1/L2), 0, 1/L2+1/L4+1/LB, 0, 0, -(1/L4) ;
    0, -(1/LT2), 0, 0, -(1/L3), 0, (1/LT2+1/L3+1/L6), -(1/L6), 0;
    0, 0, 0, 0, 0, -(1/L6), (1/L5+1/L6+1/LC), -(1/L5) ;
    0, 0, -(1/LT3), 0, 0, -(1/L4), 0, -1/L5, (1/L4+1/L5+1/LT3)];

X=inv(L);

iT1=0; iG1=0; iT2=0; iG2=0; iT3=0; iG3=0;

iL1=0; iL2=0; iL3=0; iL4=0; iL5=0; iL6=0;

iA=0; iB=0; iC=0;

i(1,:)=[iG1, iT1, iG2, iT2, iG3, iT3, iL1, iL2, iL3, iL4, iL5, iL6, iA, iB, iC];
V=[0 ; 0 ; 0 ; 0 ; 0 ; 0 ; 0 ; 0 ; 0 ; 0 ]; % V1 , V2 , V3 , V4 , V5 , V6 , V7 , V8 ,V9

for j=1:length(t)-1
y = i(j,:)';

f=@(t,i) [(EA1*sin(t)-V(1,j))/La1-(Ra1/La1)*i(1); %d_iG1/d_t
(V(1,j)-V(4,j))/LT1-(RT1/LT1)*i(2); %d_iT1/d_t
(EA2*sin(t)-V(2,j))/La2-(Ra2/La2)*i(3); %d_iG2/d_t
(V(2,j)-V(4,j))/LT2-(RT2/LT2)*i(4); %d_iT2/d_t
(EA3*sin(t)-V(3,j))/La3-(Ra3/La3)*i(5); %d_iG3/d_t
(V(3,j)-V(4,j))/LT3-(RT3/LT3)*i(6); %d_iT3/d_t
(V(4,j)-V(5,j))/L1-(R1/L1)*i(7); %d_iL1/d_t
(V(4,j)-V(6,j))/L2-(R2/L2)*i(8); %d_iL2/d_t
(V(7,j)-V(5,j))/L3-(R3/L3)*i(9); %d_iL3/d_t

```

```

(V(9,j)-V(6,j))/L4-(R4/L4)*i(10); %d_iL4/d_t
(V(9,j)-V(8,j))/L5-(R5/L5)*i(11); %d_iL5/d_t
(V(7,j)-V(8,j))/L6-(R6/L6)*i(12); %d_iL6/d_t
(V(5,j)/LA)-(RA/LA)*i(13); %d_iLA/d_t
(V(6,j)/LB)-(RB/LB)*i(14); %d_iLB/d_t
(V(8,j)/LC)-(RC/LC)*i(15)]; %d_iLC/d_t

k1=h*f(t(j),y);
k2=h*f((t(j)+0.5*h),(y+0.5*k1*h));
k3=h*f((t(j)+0.5*h),(y+0.5*k2*h));
k4=h*f((t(j)+0.5*h),(y+k3*h));

i(j+1,:)=i(j,:)+((k1+2*k2+2*k3+k4)/6.0)';

if j<0.35*length(t)
RC=0.0114; LC=0.0769;
L=[(1/La1+1/LT1), 0, 0, -(1/LT1), 0, 0, 0, 0, 0;
0, (1/La2+1/LT2), 0, 0, 0, 0, -(1/LT2), 0, 0;
-(1/LT1), 0, 0, (1/LT1+1/L1+1/L2), -(1/L1), -(1/L2), 0, 0, 0;
0, 0, (1/La3+1/LT3), 0, 0, 0, 0, 0, -(1/LT3);
0, 0, 0, -(1/L1), (1/L1+1/L3+ 1/LA), 0, -(1/L3), 0, 0;
0, 0, 0, -(1/L2), 0, 1/L2+1/L4+1/LB, 0, 0, -(1/L4);
0, -(1/LT2), 0, 0, -(1/L3), 0, (1/LT2+1/L3+1/L6), -(1/L6), 0;
0, 0, 0, 0, 0, 0, -(1/L6), (1/L5+1/L6+1/LC), -(1/L5);
0, 0, -(1/LT3), 0, 0, -(1/L4), 0, -1/L5, (1/L4+1/L5+1/LT3)];
X=inv(L);
A=[ (EA1*sin(t(j+1))/La1)-(Ra1/La1)*i(j+1,1)+(RT1/LT1)*i(j+1,2);
(EA2*sin(t(j+1))/La2)-(Ra2/La2)*i(j+1,3)+(RT2/LT2)*i(j+1,4);
(EA3*sin(t(j+1))/La3)-(Ra3/La3)*i(j+1,5)+(RT3/LT3)*i(j+1,6);
-(RT1/LT1)*i(j+1,2)+(R1/L1)*i(j+1,4)+(R2/L2)*i(j+1,6);
-(R1/L1)*i(j+1,7)-(R3/L3)*i(j+1,9)+(RA/LA)*i(j+1,13);
-(R2/L2)*i(j+1,8)-(R4/L4)*i(j+1,10)+(RB/LB)*i(j+1,14);
-(RT2/LT2)*i(j+1,4)-(R3/L3)*i(j+1,9)+(R6/L6)*i(j+1,12);
-(R6/L6)*i(j+1,12)-(R5/L5)*i(j+1,11)+(RC/LC)*i(j+1,15);
-(RT3/LT3)*i(j+1,6)-(R4/L4)*i(j+1,10)+(R5/L5)*i(j+1,11)];

V(:,j+1)=X*A;

elseif j>=0.35*length(t) && j<=0.7*length(t)
RC=0.000000002; LC=0.000000001;
L=[(1/La1+1/LT1), 0, 0, -(1/LT1), 0, 0, 0, 0, 0;
0, (1/La2+1/LT2), 0, 0, 0, 0, -(1/LT2), 0, 0;
-(1/LT1), 0, 0, (1/LT1+1/L1+1/L2), -(1/L1), -(1/L2), 0, 0, 0;
0, 0, (1/La3+1/LT3), 0, 0, 0, 0, 0, -(1/LT3);
0, 0, 0, -(1/L1), (1/L1+1/L3+ 1/LA), 0, -(1/L3), 0, 0;
0, 0, 0, -(1/L2), 0, 1/L2+1/L4+1/LB, 0, 0, -(1/L4);
0, -(1/LT2), 0, 0, -(1/L3), 0, (1/LT2+1/L3+1/L6), -(1/L6), 0;
0, 0, 0, 0, 0, 0, -(1/L6), (1/L5+1/L6+1/LC), -(1/L5);
0, 0, -(1/LT3), 0, 0, -(1/L4), 0, -1/L5, (1/L4+1/L5+1/LT3)];
X=inv(L);
A=[ (EA1*sin(t(j+1))/La1)-(Ra1/La1)*i(j+1,1)+(RT1/LT1)*i(j+1,2);
(EA2*sin(t(j+1))/La2)-(Ra2/La2)*i(j+1,3)+(RT2/LT2)*i(j+1,4);
(EA3*sin(t(j+1))/La3)-(Ra3/La3)*i(j+1,5)+(RT3/LT3)*i(j+1,6);
-(RT1/LT1)*i(j+1,2)+(R1/L1)*i(j+1,4)+(R2/L2)*i(j+1,6);

```

```

-(R1/L1)*i(j+1,7)-(R3/L3)*i(j+1,9)+(RA/LA)*i(j+1,13);
-(R2/L2)*i(j+1,8)-(R4/L4)*i(j+1,10)+(RB/LB)*i(j+1,14);
-(RT2/LT2)*i(j+1,4)-(R3/L3)*i(j+1,9)+(R6/L6)*i(j+1,12);
-(R6/L6)*i(j+1,12)-(R5/L5)*i(j+1,11)+(RC/LC)*i(j+1,15);
-(RT3/LT3)*i(j+1,6)-(R4/L4)*i(j+1,10)+(R5/L5)*i(j+1,11)];

V(:,j+1)=X*A;

else j> 0.7*length(t);
RC=0.0114; LC=0.0769;
L=[(1/La1+1/LT1) , 0 , 0 , -(1/LT1) , 0 , 0 , 0 , 0 , 0 ;
0 , (1/La2+1/LT2) , 0 , 0 , 0 , 0 , -(1/LT2) , 0 , 0 ;
-(1/LT1) , 0 , 0 , (1/LT1+1/L1+1/L2) , -(1/L1) , -(1/L2) , 0 , 0 , 0 ;
0 , 0 , (1/La3+1/LT3) , 0 , 0 , 0 , 0 , 0 , -(1/LT3) ;
0 , 0 , 0 , -(1/L1) , (1/L1+1/L3+ 1/LA) , 0 , -(1/L3) , 0 , 0 ;
0 , 0 , 0 , -(1/L2) , 0 , 1/L2+1/L4+1/LB , 0 , 0 , -(1/L4) ;
0 , -(1/LT2) , 0 , 0 , -(1/L3) , 0 , (1/LT2+1/L3+1/L6) , -(1/L6) , 0 ;
0 , 0 , 0 , 0 , 0 , 0 , -(1/L6) , (1/L5+1/L6+1/LC) , -(1/L5) ;
0 , 0 , -(1/LT3) , 0 , 0 , -(1/L4) , 0 , -1/L5 , (1/L4+1/L5+1/LT3)];
X=inv(L);
A=[ (EA1*sin(t(j+1))/La1)-(Ra1/La1)*i(j+1,1)+(RT1/LT1)*i(j+1,2);
(EA2*sin(t(j+1))/La2)-(Ra2/La2)*i(j+1,3)+(RT2/LT2)*i(j+1,4);
(EA3*sin(t(j+1))/La3)-(Ra3/La3)*i(j+1,5)+(RT3/LT3)*i(j+1,6);
-(RT1/LT1)*i(j+1,2)+(R1/L1)*i(j+1,4)+(R2/L2)*i(j+1,6);
-(R1/L1)*i(j+1,7)-(R3/L3)*i(j+1,9)+(RA/LA)*i(j+1,13);
-(R2/L2)*i(j+1,8)-(R4/L4)*i(j+1,10)+(RB/LB)*i(j+1,14);
-(RT2/LT2)*i(j+1,4)-(R3/L3)*i(j+1,9)+(R6/L6)*i(j+1,12);
-(R6/L6)*i(j+1,12)-(R5/L5)*i(j+1,11)+(RC/LC)*i(j+1,15);
-(RT3/LT3)*i(j+1,6)-(R4/L4)*i(j+1,10)+(R5/L5)*i(j+1,11)];

V(:,j+1)=X*A;

end

end

%iG1, iT1, iG2, iT2, iG3, iT3, iL1, iL2, iL3, iL4, iL5, iL6, iA,
iB, iC]
%i(1), i(2), i(3), i(4), i(5), i(6), i(7) , i(8), i(9), i(10), i(11), i(12), i(13)
, i(14), i(15)
iG1=i(:,1); iT1=i(:,2); iG2=i(:,3); iT2=i(:,4); iG3=i(:,5); iT3=i(:,6);
iL1=i(:,7); iL2=i(:,8); iL3=i(:,9); iL4=i(:,10); iL5=i(:,11); iL6=i(:,12);
iA=i(:,13); iB=i(:,14); iC=i(:,15);

V1=V(1,:); V2=V(2,:); V3=V(3,:); V4=V(4,:); V5=V(5,:); V6=V(6,:);V7=V(7,:);
V8=V(8,:); V9=V(9,:);

figure
plot(t/314,i);
hold
grid on;
xlabel('time');
ylabel('Currents in all branches in P.U');

```

```

axis auto
legend('iG1','iT1','iG2','iT2','iG3','iT3','iG','iL1','iL2','iL3','iL4','iL5','iL6',
'iA','iB','iC');

figure
plot(t/314,V);
hold
grid on;
xlabel('time');
ylabel('Voltages at all 9 buses in P.U')
axis auto
legend('V1','V2','V3','V4','V5','V6','V7','V8','V9') ;

% Grid Current
figure
plot(t/314,i(:,1),t/314,i(:,3),t/314,i(:,5))
hold
grid on
xlabel('time')
ylabel('Generators Current in P.U');
legend('i generators current ')
figure
plot(t/314,V(4,:));
hold;
grid on;
xlabel('time');
ylabel('V at IEEE 9 Bus system');

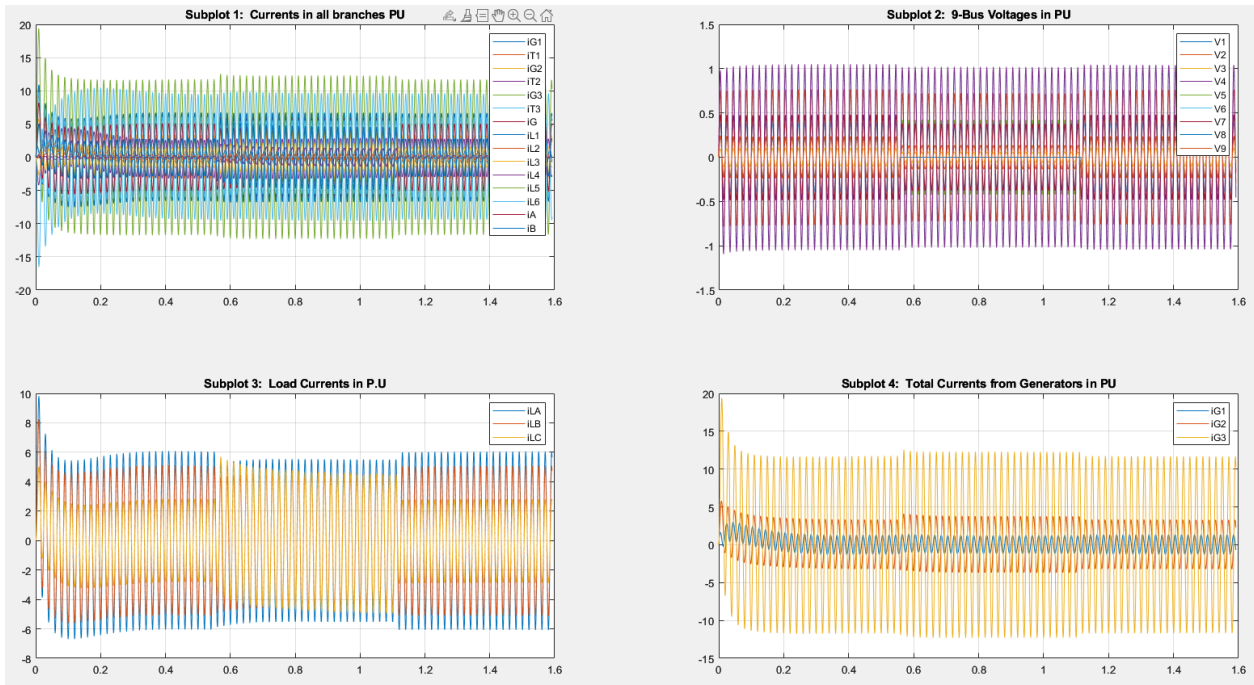
subplot(2,2,1);
plot(t/314,i);
grid on;
title('Subplot 1: Currents in all branches PU')
legend('iG1','iT1','iG2','iT2','iG3','iT3','iG','iL1','iL2','iL3','iL4','iL5','iL6',
'iA','iB','iC');

subplot(2,2,2);
plot(t/314,V);
grid on;
title('Subplot 2: 9-Bus Voltages in PU')
legend('V1','V2','V3','V4','V5','V6','V7','V8','V9') ;

subplot(2,2,3);
plot(t/314,i(:,13),t/314,i(:,14),t/314,i(:,15));
grid on;
title('Subplot 3: Load Currents in P.U')
legend('iLA','iLB','iLC') ;

subplot(2,2,4);
plot(t/314,i(:,1),t/314,i(:,3),t/314,i(:,5));
grid on;
title('Subplot 4: Total Currents from Generators in PU')
legend('iG1','iG2','iG3') ;

```



### 2.2.9 Voltage Stability Study

Voltage collapse remains the primary and most significant risk to a power system. This is because power systems are consistently operated close to their stability limit as a result of economic and environmental limitations. Ensuring the stability and security of a power system is of paramount importance and presents a complex challenge.

Voltage stability phenomena occur when:

- 1- The voltage at the receiving end decreases significantly below its usual value and does not recover even after activating restorative devices such as var compensators.
- 2- The voltage oscillates continuously because it lacks sufficient dampening to counteract external perturbations.

As a result of the fact that conducting an efficient voltage stability analysis is essential for system planning and long-term interoperability, voltage stability analysis provides an assessment of these weak, unstable, and uncontrollable areas of the electrical network that may put future load growth at risk due to some unexpected voltage collapse.

According to the following definition provided by the IEEE task force, voltage stability is defined as follows: The ability of a power system to maintain a constant and steady state operating voltage at all of its buses after they have been subjected to a disturbance from a certain beginning operating point/condition is what is meant by the term "voltage stability." The status of the system enters the voltage instability area when an uncontrolled and continuous reduction in system voltage is the consequence of a disturbance, an increase in load demand, or any other change in the state of the system.

Another crucial concept to clarify is voltage collapse, which arises from voltage instability. Voltage collapse occurs when the post-disturbance equilibrium voltage near the loads falls below permissible limits. It is a process that leads to voltage instability and results in a very low voltage profile in the critical area of the system. A voltage breakdown might result in either a complete or partial blackout.

A vast variety of phenomena are covered by voltage stability; for engineers working with induction motors, HVAC loads, or HVDC lines, this is a fast-moving phenomenon.

For some engineers, however, it's a slow phenomenon that involves things like load tap changes.

Reasons/Causes for Voltage Instability:

- 1- Centralized generation and longer distance this typically occurs in mature power systems so therefore an extensive use of existing generation and transmission, few centralized generations source, large power plants, few voltage control busses, longer electrical distance between generation and load
- 2- Extensive use of shunt capacitor banks for reactive power compensation, though this is not a problem, but it creates a fragile network prone to voltage collapse.
- 3- Voltage instability caused by line and generator outages cause the system to operate closer to the limits, so that any such large disturbance such as a loss of generating unit or heavily loaded line can cause a cascading event in the system.
- 4- Natural or small gradual increase in system load, whereby the load growth if not pay

attention may result of voltage instability.

The system is said to be in a voltage stable state, if at a given operating condition for every bus in the system, the bus voltage magnitude increase as the reactive power injection at the same bus is increased.

A system is voltage unstable if for at least one bus in the system the bus voltage magnitude decrease as the reactive power injects at the same bus is increased.

Voltage Stability criteria states that:

- 1- For a system to be said as “**Stable**”, if the reactive power injection increased the bus voltage will be increased, which is said to be positive voltage sensitivity **+V-Q**.
- 2- For a system to be said as “**Un-Stable**”, if the reactive power injection increased the bus voltage will be decreased, which is said to be negative voltage sensitivity **-V-Q**.

#### 2.2.9.1 Network Feasibility

The system model used must represent the problem being studied so that when analyzing distribution networks, the transmission or sub transmission networks are treated as sources operating at a given voltage. On the other hand, when analyzing the transmission or sub transmission networks, the distribution networks are treated as sinks of real and reactive power and referred to as composite loads or simply loads.

A distribution network is connected to the transmission network at the grid supply point where a change in voltage may cause complicated dynamic interactions inside the distribution network itself due to:

- 1- Voltage control action arising from transformer tap changing.
- 2- Control action associated with reactive power compensation and/or small embedded generators.
- 3- A low supply voltage causes changes in the power demand as a result of induction motors stalling and/or the extinguishing of discharge lighting.
- 4- operation of protective equipment by overcurrent or under-voltage relays, electromechanically held contactors and so on;

5- re-ignition of discharge lighting and self-start induction motors when the supply voltage recovers.

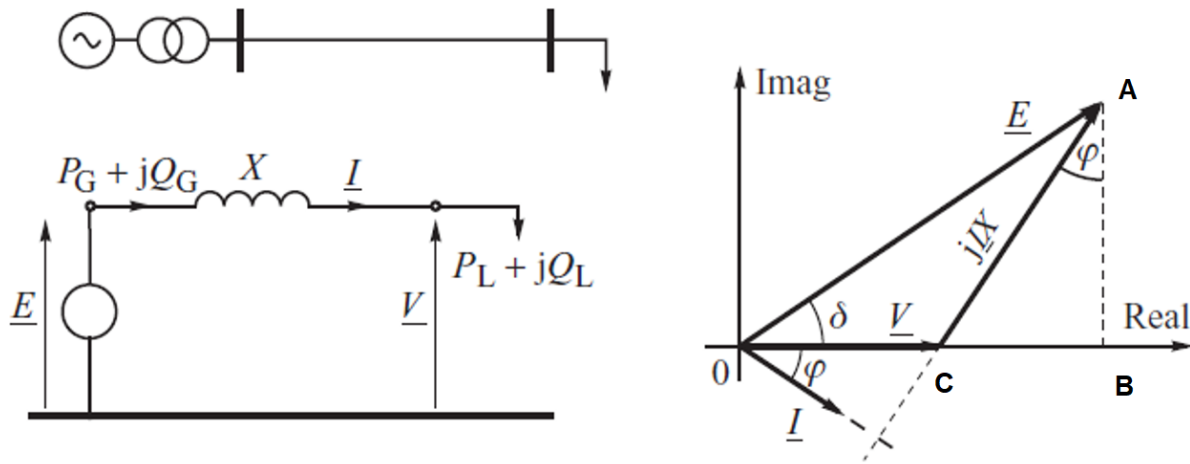


**Figure 2.2-54:**Equivalent circuit of the transmission link and its phasor diagram.

The composite network is presented by its static voltage characteristics to determine the *network feasibility or the network loadability*.

$$V \angle 0^\circ = E \angle \delta - jIX$$

$$E \angle \delta = V \angle 0^\circ + jIX$$

Based upon the phasor diagram:

$$\overline{AB} = I \cdot X \cos(\varphi) = E \sin(\delta)$$

So that we can find  $I \cdot \cos(\varphi)$

$$I \cdot \cos(\varphi) = \frac{E \sin(\delta)}{X}$$

Also, Based upon the simplified phasor diagram:

$$\overline{BC} = I \cdot X \sin(\varphi) = E \cos(\delta) - V$$

So that we can find  $I \cdot \sin(\varphi)$

$$I \cdot \sin(\varphi) = \frac{E \cos(\delta) - V}{X}$$

However, we know that output active /reactive power are given by

$$P_L = P_L(V) = V I \cos(\varphi) = V \left\{ \frac{E \cdot \sin(\delta)}{X} \right\} = \frac{E V}{X} \sin(\delta)$$

$$Q_L = Q_L(V) = V I \sin(\varphi) = V \left\{ \frac{E \cdot \cos(\delta) - V}{X} \right\} = \frac{E V}{X} \cos(\delta) - \frac{V^2}{X}$$

Taking the square of each equation

$$P_L^2 = \left\{ \frac{E V}{X} \sin(\delta) \right\}^2 = \left\{ \frac{E V}{X} \right\}^2 \sin^2(\delta)$$

$$Q_L^2 = \left\{ \frac{E V}{X} \cos(\delta) - \frac{V^2}{X} \right\}^2 = \left\{ \frac{E V}{X} \right\}^2 \cos^2(\delta) - 2 \frac{E V^3}{X^2} \cos(\delta) + \left\{ \frac{V^2}{X} \right\}^2$$

Adding  $P_L^2$  to  $Q_L^2$

$$P_L^2 + Q_L^2 = \left\{ \frac{E V}{X} \right\}^2 \sin^2(\delta) + \left\{ \frac{E V}{X} \right\}^2 \cos^2(\delta) - 2 \frac{E V^3}{X^2} \cos(\delta) + \left\{ \frac{V^2}{X} \right\}^2$$

$$P_L^2 + Q_L^2 = \left\{ \frac{E V}{X} \right\}^2 [\sin^2(\delta) + \cos^2(\delta)] - 2 \frac{E V^3}{X^2} \cos(\delta) + \left\{ \frac{V^2}{X} \right\}^2$$

But as per trigonometric identity  $\sin^2(\delta) + \cos^2(\delta) = 1$

$$P_L^2 + Q_L^2 = \left\{ \frac{E V}{X} \right\}^2 - 2 \frac{E V^3}{X^2} \cos(\delta) + \left\{ \frac{V^2}{X} \right\}^2$$

$$\left\{ \frac{E V}{X} \right\}^2 = P_L^2 + Q_L^2 + 2 \frac{E V^3}{X^2} \cos(\delta) - \left\{ \frac{V^2}{X} \right\}^2$$

Substituting  $Q_L^2$

$$\left\{ \frac{E V}{X} \right\}^2 = P_L^2 + \left\{ \left\{ \frac{E V}{X} \right\}^2 \cos^2(\delta) - 2 \frac{E V^3}{X^2} \cos(\delta) + \left\{ \frac{V^2}{X} \right\}^2 \right\} + 2 \frac{E V^3}{X^2} \cos(\delta) - \left\{ \frac{V^2}{X} \right\}^2$$

$$\left\{\frac{E V}{X}\right\}^2 = P_L^2 + \left\{\left\{\frac{E V}{X}\right\}^2 \cos^2(\delta) - 2 \frac{E V^3}{X^2} \cos(\delta) + \left\{\frac{V^2}{X}\right\}^2\right\} + 2 \frac{E V^3}{X^2} \cos(\delta) - \left\{\frac{V^2}{X}\right\}^2$$

$$\left\{\frac{E V}{X}\right\}^2 = P_L^2 + \left\{\frac{E V}{X}\right\}^2 \cos^2(\delta) = P_L^2 + \left\{\left\{\frac{E V}{X}\right\} \cos(\delta)\right\}^2$$

But

$$Q_L = \frac{E V}{X} \cos(\delta) - \frac{V^2}{X} \Rightarrow \frac{E V}{X} \cos(\delta) = Q_L + \frac{V^2}{X}$$

$$\left\{\frac{E V}{X}\right\}^2 = P_L^2 + \left\{\left\{\frac{E V}{X}\right\} \cos(\delta)\right\}^2 = P_L^2 + \left\{Q_L + \frac{V^2}{X}\right\}^2$$

Let  $P_L(V) = P_n$  and  $Q_L(V) = Q_n = P_n \tan(\varphi)$

$$\left\{\frac{E V}{X}\right\}^2 = P_n^2 + \left\{Q_n + \frac{V^2}{X}\right\}^2 = P_n^2 + \left\{P_n \tan(\varphi) + \frac{V^2}{X}\right\}^2$$

$$\left\{\frac{E V}{X}\right\}^2 = P_n^2 + \left\{P_n \tan(\varphi) + \frac{V^2}{X}\right\}^2 = P_n^2 + \left\{P_n^2 \tan^2(\varphi) + 2P_n \tan(\varphi) \frac{V^2}{X} + \left\{\frac{V^2}{X}\right\}^2\right\}$$

$$\left\{\frac{E V}{X}\right\}^2 - \left\{\frac{V^2}{X}\right\}^2 = P_n^2 + \left\{P_n \tan(\varphi) + \frac{V^2}{X}\right\}^2 = P_n^2 + P_n^2 \tan^2(\varphi) + 2P_n \tan(\varphi) \frac{V^2}{X}$$

But

$$\tan(\varphi) = \frac{\sin(\varphi)}{\cos(\varphi)}$$

$$P_n^2 + P_n^2 \left(\frac{\sin(\varphi)}{\cos(\varphi)}\right)^2 + 2P_n \frac{\sin(\varphi)}{\cos(\varphi)} \frac{V^2}{X} = \left\{\frac{E V}{X}\right\}^2 - \left\{\frac{V^2}{X}\right\}^2$$

$$P_n^2 + P_n^2 \left( \frac{\sin(\varphi)}{\cos(\varphi)} \right)^2 + 2P_n \frac{\sin(\varphi)}{\cos(\varphi)} \frac{V^2}{X} = \frac{V^2}{X^2} \{E^2 - V^2\}$$

$$P_n^2 + P_n^2 \left( \frac{\sin^2(\varphi)}{\cos^2(\varphi)} \right) + 2P_n \frac{\sin(\varphi)}{\cos(\varphi)} \frac{V^2}{X} = \frac{V^2}{X^2} \{E^2 - V^2\}$$

Multiplying both side with  $\cos^2(\varphi)$

$$P_n^2 \cos^2(\varphi)^2 + P_n^2 \sin^2(\varphi) + 2P_n \sin(\varphi) \cos(\varphi) \frac{V^2}{X} = \frac{V^2}{X^2} \{E^2 - V^2\} \cos^2(\varphi)$$

$$P_n^2 (\sin^2(\varphi) + \cos^2(\varphi)) + 2P_n \sin(\varphi) \cos(\varphi) \frac{V^2}{X} = \frac{V^2}{X^2} \{E^2 - V^2\} \cos^2(\varphi)$$

But as per trigonometric identity  $\sin^2(\varphi) + \cos^2(\varphi) = 1$

$$P_n^2 + 2P_n \frac{V^2}{X} \sin(\varphi) \cos(\varphi) = \frac{V^2}{X^2} \{E^2 - V^2\} \cos^2(\varphi)$$

The left-hand side of this equation is an incomplete square of sum

$$\left\{ P_n + \frac{V^2}{X} \sin(\varphi) \cos(\varphi) \right\}^2 = P_n^2 + 2P_n \frac{V^2}{X} \sin(\varphi) \cos(\varphi) + \left( \frac{V^2}{X} \right)^2 \sin^2(\varphi) \cos^2(\varphi)$$

$$P_n^2 + 2P_n \frac{V^2}{X} \sin(\varphi) \cos(\varphi) = \left\{ P_n + \frac{V^2}{X} \sin(\varphi) \cos(\varphi) \right\}^2 - \left( \frac{V^2}{X} \right)^2 \sin^2(\varphi) \cos^2(\varphi)$$

$$\left\{ P_n + \frac{V^2}{X} \sin(\varphi) \cos(\varphi) \right\}^2 - \left( \frac{V^2}{X} \right)^2 \sin^2(\varphi) \cos^2(\varphi) = \frac{V^2}{X^2} \{E^2 - V^2\} \cos^2(\varphi)$$

$$\left\{P_n + \frac{V^2}{X} \sin(\varphi) \cos(\varphi)\right\}^2 = \left(\frac{V^2}{X}\right)^2 \sin^2(\varphi) \cos^2(\varphi) + \frac{V^2}{X^2} \{E^2 - V^2\} \cos^2(\varphi)$$

$$\left\{P_n + \frac{V^2}{X} \sin(\varphi) \cos(\varphi)\right\}^2 = \frac{V^2}{X^2} \cos^2(\varphi) \{E^2 - V^2 + V^2 \sin^2(\varphi)\}$$

$$\left\{P_n + \frac{V^2}{X} \sin(\varphi) \cos(\varphi)\right\}^2 = \frac{V^2}{X^2} \cos^2(\varphi) \{E^2 + V^2(-1 + \sin^2(\varphi))\}$$

$$\left\{P_n + \frac{V^2}{X} \sin(\varphi) \cos(\varphi)\right\}^2 = \frac{V^2}{X^2} \cos^2(\varphi) \{E^2 - V^2 \cos^2(\varphi)\}$$

Taking square root for both sides

$$P_n + \frac{V^2}{X} \sin(\varphi) \cos(\varphi) = \frac{V}{X} \cos(\varphi) \sqrt{E^2 - V^2 \cos^2(\varphi)}$$

$$P_n = -\frac{V^2}{X} \sin(\varphi) \cos(\varphi) + \frac{V}{X} \cos(\varphi) \sqrt{E^2 - V^2 \cos^2(\varphi)}$$

Multiplying with  $\frac{E^2}{E^2}$

$$P_n = -\frac{V^2}{X} \frac{E^2}{E^2} \sin(\varphi) \cos(\varphi) + \frac{V}{X} \frac{E^2}{E^2} \cos(\varphi) \sqrt{1 - \frac{V^2}{E^2} \cos^2(\varphi)} \times E$$

$$P_n = -\frac{E^2}{X} \frac{V^2}{E^2} \sin(\varphi) \cos(\varphi) + \frac{E^2}{X} \frac{V}{E} \cos(\varphi) \sqrt{1 - \frac{V^2}{E^2} \cos^2(\varphi)}$$

Let

$$v = \frac{V}{E} \Rightarrow v^2 = \frac{V^2}{E^2}$$

$$P_n = -\frac{E^2}{X} v^2 \sin(\varphi) \cos(\varphi) + \frac{E^2}{X} v \cos(\varphi) \sqrt{1 - v^2 \cos^2(\varphi)}$$

Dividing both sides on  $\frac{E^2}{X}$

$$p_n = \frac{P_n}{\left(\frac{E^2}{X}\right)} = -v^2 \sin(\varphi) \cos(\varphi) + v \cos(\varphi) \sqrt{1 - v^2 \cos^2(\varphi)}$$

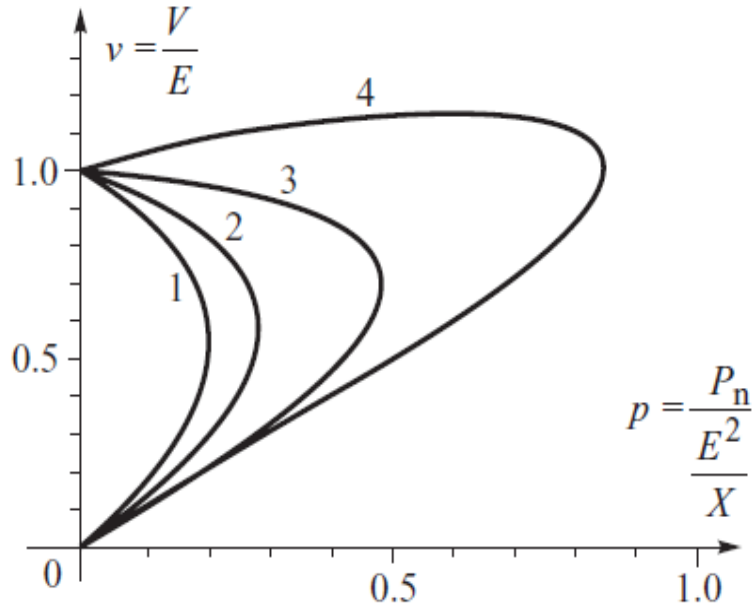


Figure 2.2-55: Nose Curve at different power factor angle (1)  $\varphi=45^\circ$  lag , (2)  $\varphi=30^\circ$  lag, (3)  $\varphi=0^\circ$  lag, (4)  $\varphi=30^\circ$  lead

If we continue in this trajectory with larger load values, we will see that we will approach about 57% of the bus voltage and then at some point the load flow does not converge (which is the point of voltage collapse) because of that the traditional load flow will not converge because of the singularity of the power flow Jacobian matrix at the PoVC therefore the traditional power flow method cannot be used to determine the voltage stability point and a different methodology must be used, ETAP uses **continuation power flow** method to essentially get to the point of instability and to draw the voltage points and determine the effect of the load increase in the network and the impact on the voltage all the way at the PoVC

Voltage stability or voltage collapse is often viewed as a steady state viability problem suitable for static power flow analysis the ability to transfer reactive power from production sources to consumption sinks during steady state operating conditions is a major aspect of voltage stability, therefore there some recommended analysis methods based on static models, one of the most popular ones being is P-V and Q-V curve analysis. This analysis is used for reactive power reserve calculation, active power margin and combined with contingency analysis to determine the loadability of a power system network.

P is the load Power, V is the voltage of the bus

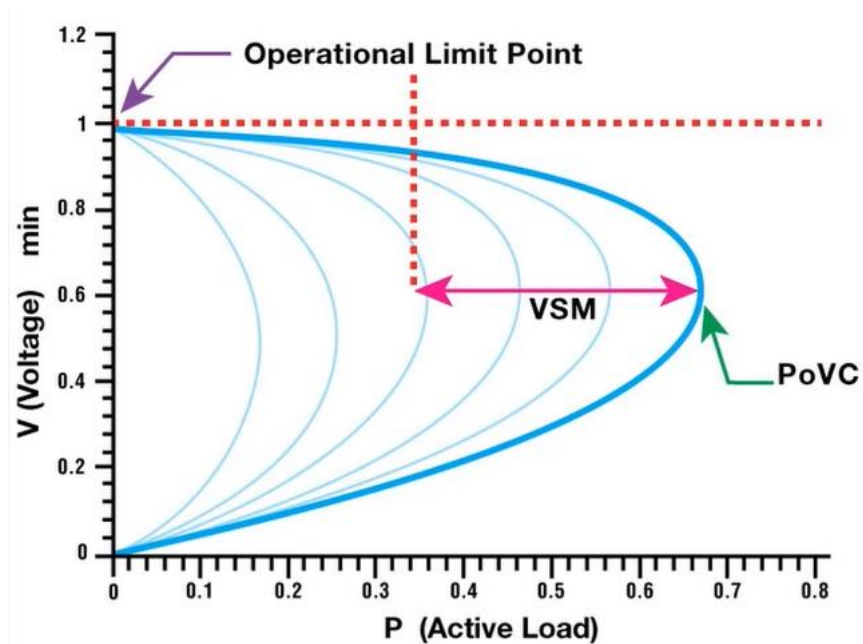
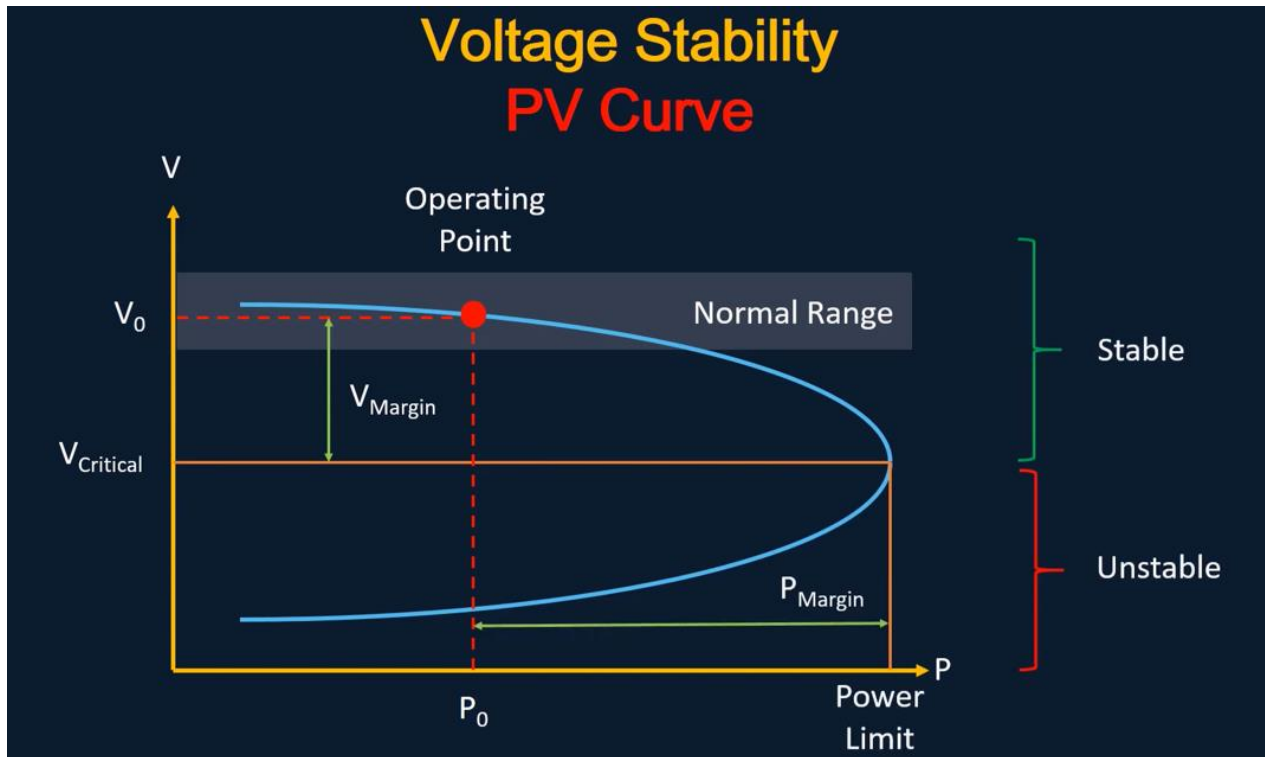


Figure 2.2-56: P-V curve at different power factors

The curve shows how the voltage falls as the demand increases, as we increase the active power drawn, we expect the voltage to drop. The nose of the POV curve shown here is the point of voltage collapse or PoVC defines the maximum demand that can be served and the associated critical voltage.



**Figure 2.2-57:** Voltage Stability Range for P-V curve

The red point is at the initial operating conditions, as the load increases there will be a real power value where the voltage will collapse but does this value of voltage happened to be within the normal operating range or the critical range of the system is the key point to be analyzed

The distance between the operating point and the nose point is typically given as real power margin and the distance between the operating point and the critical point as far as the voltage considered is the voltage margin. Above the nose curve the system is said to be stable and below the nose point you are essentially voltage unstable

### 2.2.9.2 Sensitivity Analysis

This analysis analyzes every single bus in the system and provides a ranking. The ranking is provided to know what is the sensitivity of that bus with respect to the voltage as the reactive power is adjusted in the system

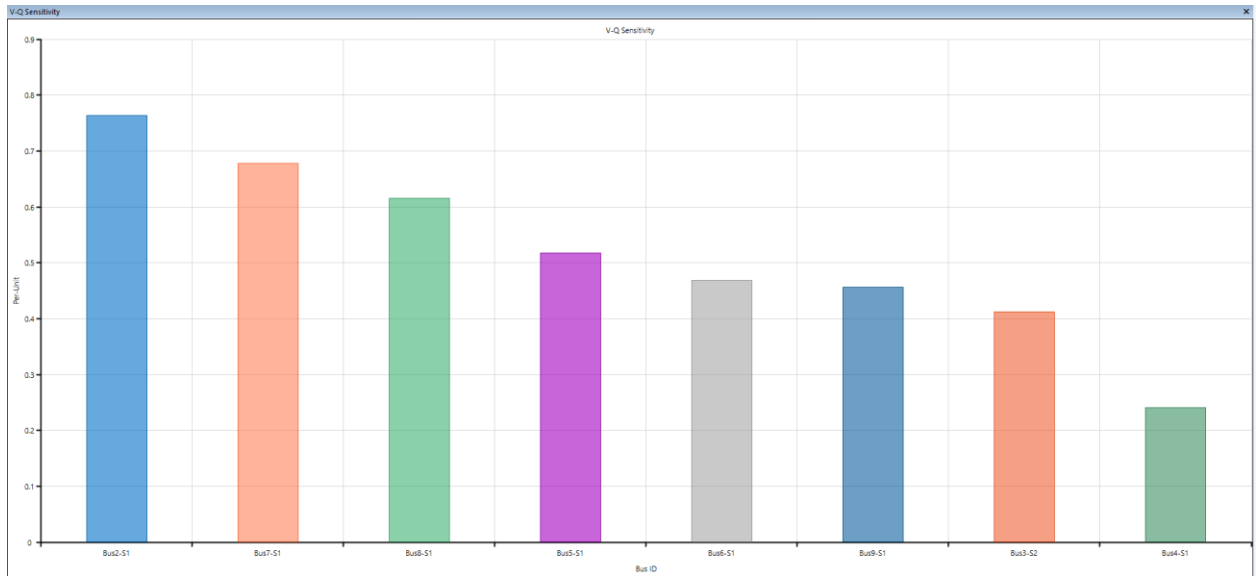


**Figure 2.2-58:** V-Q sensitivity for original IEEE 9 bus system ( with 0% renewable penetration )

For every reactive power change there is a corresponding active (real) power change, then the bus which has the maximum sensitivity to this reactive power change is given rank no.1 followed by the remaining ranks. If we run the P-V and Q-V analysis for the entire system, in this case we can analyze the effect of real and reactive power changes on every single bus in the network.

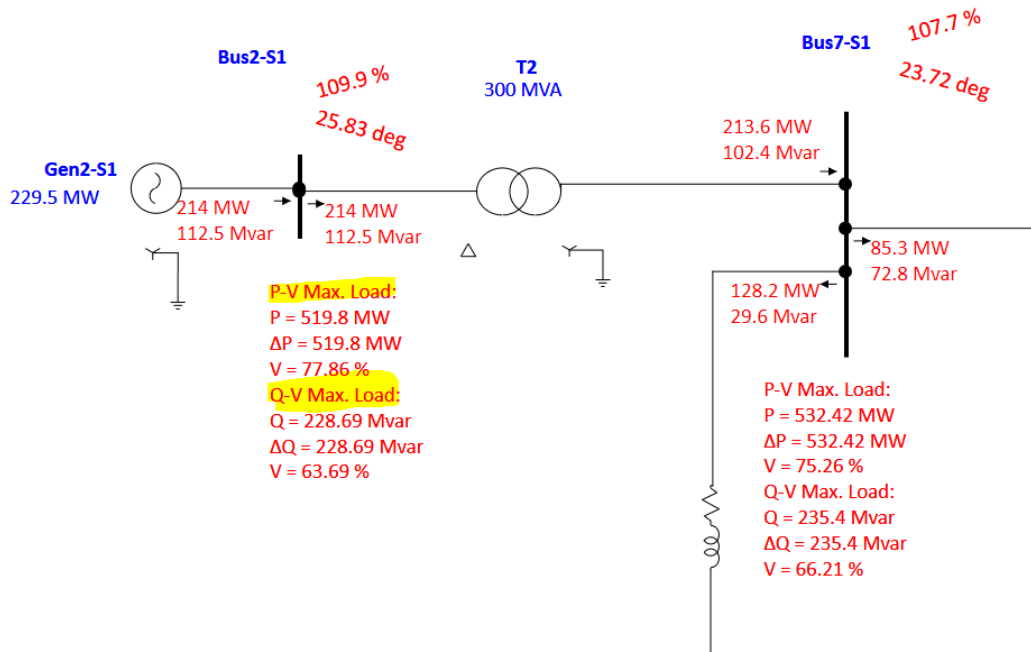


**Figure 2.2-59:** Bus No.2 P-V and Q-V results

In the above case for Bus No.2, we can increase load beyond the current loadability which is (214 MW) of real power, we can further increase the real power **P** by about 519 MW before we see a voltage collapse which will be at 77.86%. Similarly, beyond the point 112.5 MVAR of reactive

power consumption, if we add additional reactive power load of about 228.69MVar the voltage will collapse at about 63.69%. Therefore, we can see what our real and reactive power loadability is before the point of collapse. This in other words gives us the **voltage margin** and the **reactive power margin** that we need for our system.

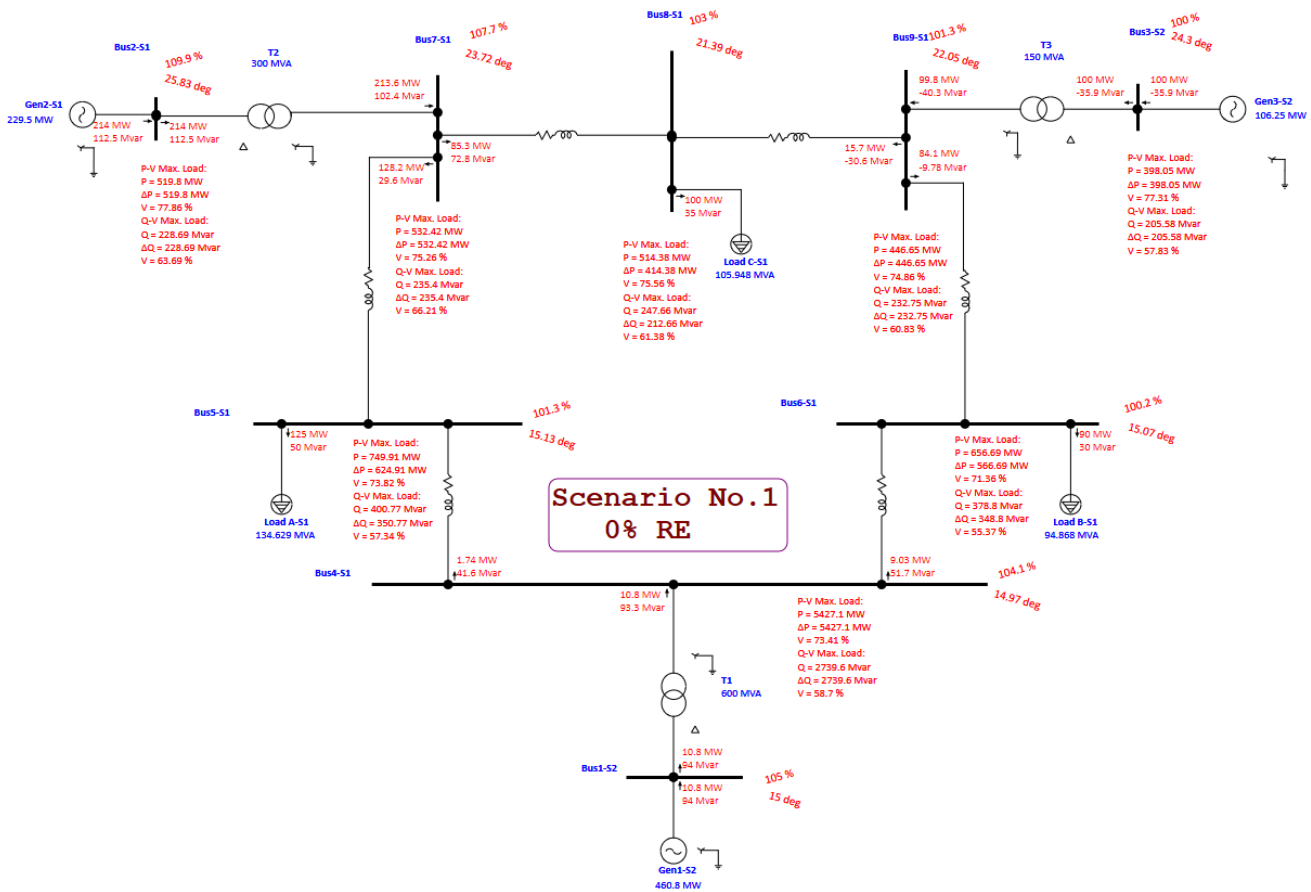


Figure 2.2-60: P-V and Q-V Analysis ETAP simulation output

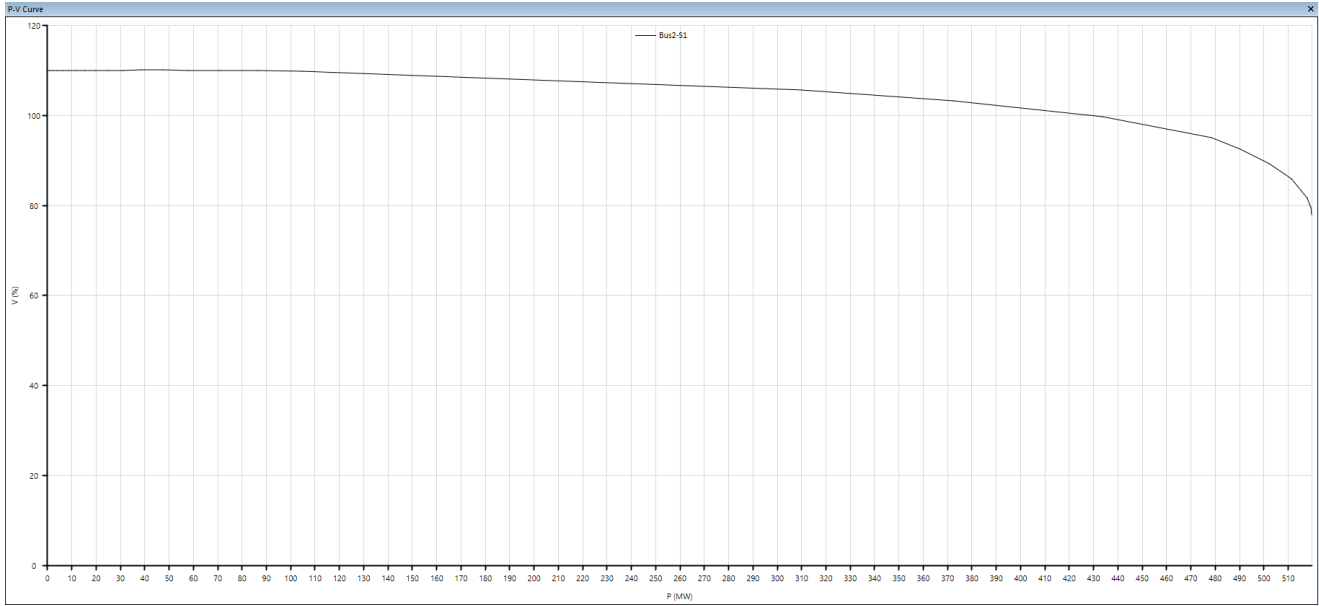


Figure 2.2-61: Bus No.2 P-V Curve

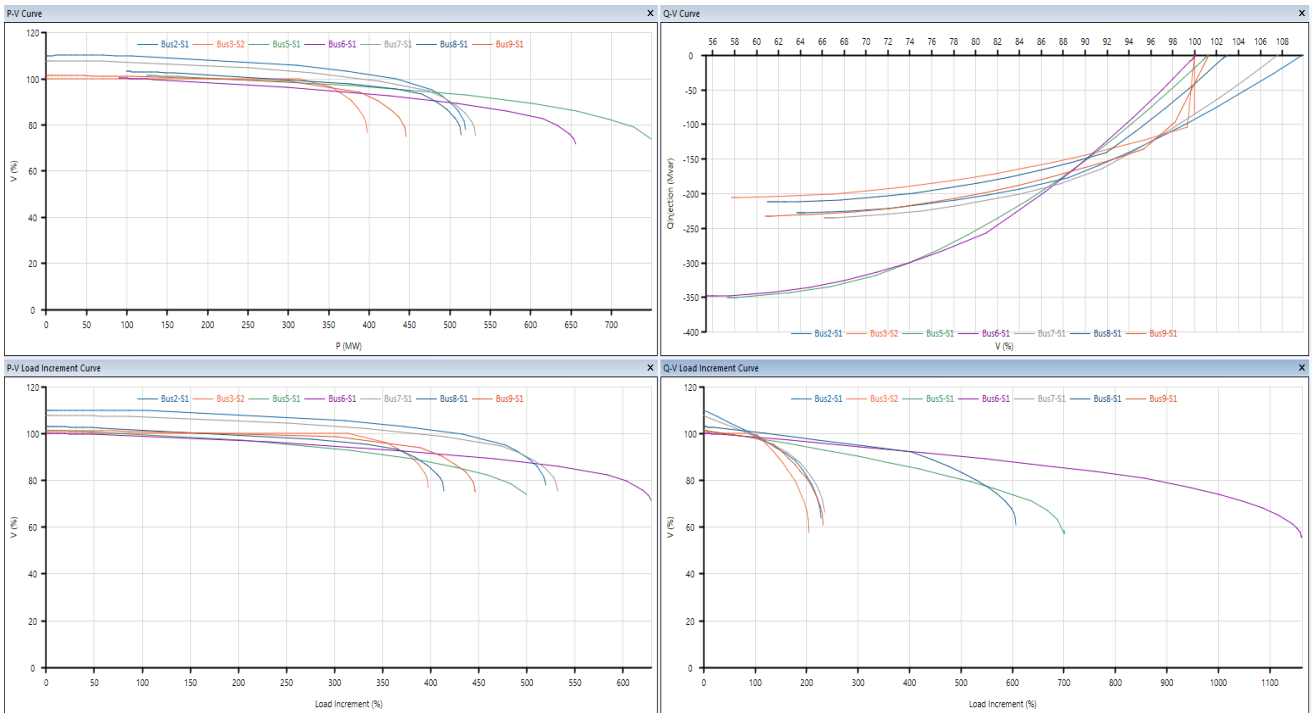


Figure 2.2-62: Voltage P-V and Q-V curves for all 9 buses of IEEE 9-Bus system

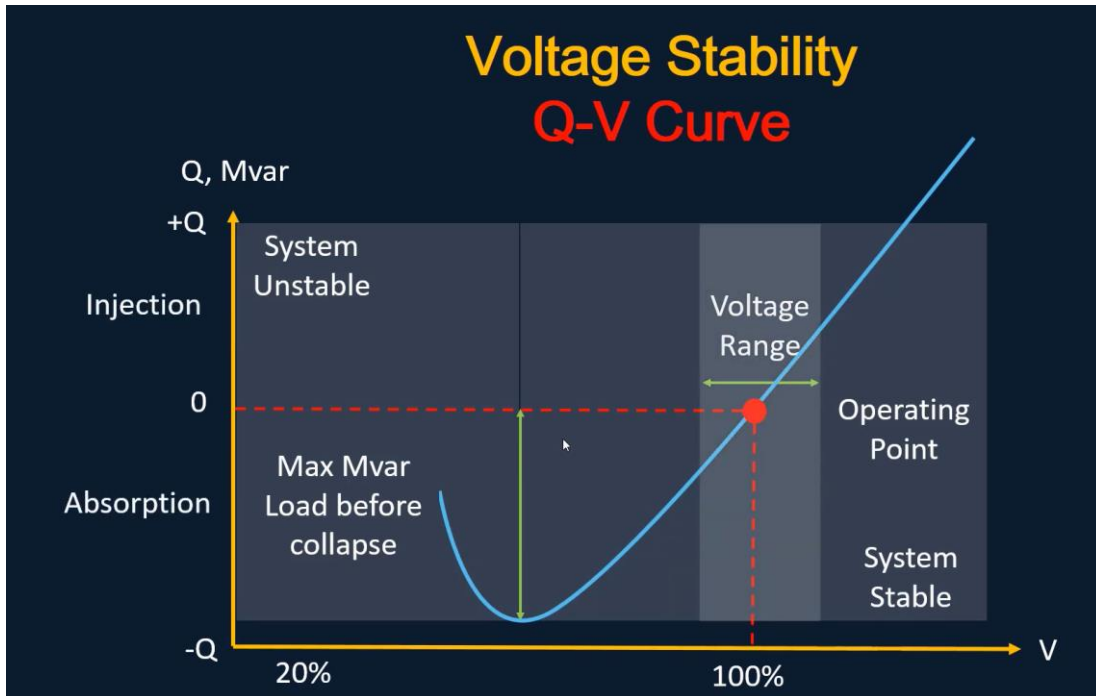


Figure 2.2-63: Voltage Stability Range for Q-V curve

The load changes affect the value of reactive power and in the Q-V plot we see the same effect as well. There is a **knee point** that is calculated that identifies the stability limit value also known as the **voltage stability margin** and the distance is also known as the reactive power margin. As it is the maximum reactive, power load that can be connected or increased before a collapse is reached [47]

High or low voltage stability margin indicator values becomes a measure of the security level of the bus where the high voltage stability margin value indicates that the bus is safe and visa-versa. The nose point is where the rate of change or the  $dQ/dv$  is equal to zero, this is also known as the voltage stability limit or voltage instability point

### 2.2.10 Harmonic Analysis

Harmonics are a power quality problem that is caused by the distortion ( deviation from pure sinusoidal waveform ) in the power system due to either nonlinear types of loads such as (Variable Frequency Drives (VFD's), large computer systems, SCADA systems, etc.) that draw a non-sinusoidal pattern current although the voltage applied is a perfect sine wave, or due to power

energy converters ( i.e. inverters and rectifiers ) which main principle is based on the electronic switching circuits.

This power quality problem has a significant impact on power regulation and consumption, premature failure of equipment, low power factor, resonating and harmonic heating of power factor correction capacitor. This distortion can be either in current or voltage, for example, high current distortion causes increase in eddy currents losses in transformers and generators, increase in power losses in conductors, transformers, and generators, Neutral overload, increase in line current within power system, overheating of electrical machines (motors, transformers, generators) also overheating in capacitors and cables. On the other hand, voltage distortion causes failures in switch mode power supplies, generators AVR malfunction, incorrect meters reading, and malfunction of electronic equipment that relies on zero voltage crossing.

#### *2.2.10.1 IEEE 519 Standard*

Harmonics are inherently present in the electrical power system, and it is impossible to eliminate them. Hence, managing harmonics in power system is a joint responsibility involving both plant owners and grid off-taker (utility), then the IEEE 519 standard was basically created to establish a limit for the harmonic distortion, defines limit for harmonic currents and voltages at PoCC, and provide directions on how to mitigate these harmonics.

There are several terms that should be reviewed upon performing Harmonic Analysis:

- 1- Short Circuit Ratio or *SCR* is defined as the ratio of the short circuit current  $I_{s,c}$  available at point of common coupling PoCC to the maximum fundamental load current  $I_L$ . A low SCR typically expresses a weak power source (grid) while a higher SCR expresses a stiff power source (grid)
  
- 2- Maximum Load Current  $I_L$  is the average current of the maximum demand for the preceding 12 months.

- 3- Total Harmonic Distortion or THD refers to the accumulative effect of several sine waves with varying amplitudes and frequencies on the basic sinusoidal waveform that should be produced by an alternating current source.

#### 2.2.10.2 Sources of Harmonics

Which equipment can create a high frequency component? Some power electronic devices or high switching devices, or some magnetization equipment (3<sup>rd</sup> order harmonic), grid will create harmonics because it is not a single network, but it is connection of multiple sources and loads. Harmonic study is an approximation study only because we are not going to provide, however we are going to provide the exact harmonic condition, some standard harmonic conditions and we are going to check whenever that type of harmonic in the network, how the network is going to be reacting for that.

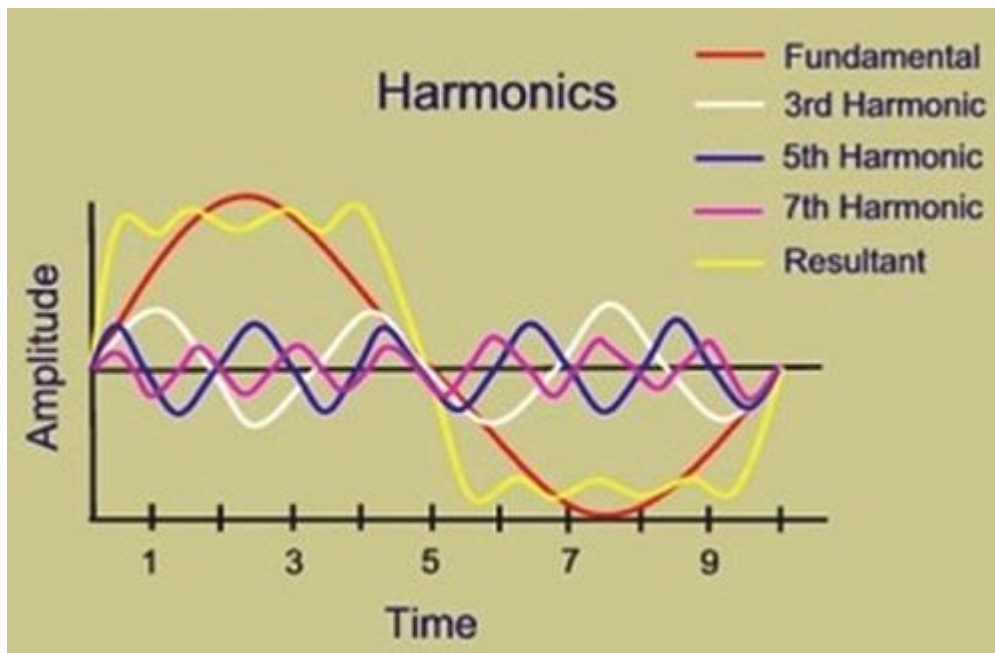


**Figure 2.2-64:** Harmonic Waveform for fundamental, 3<sup>rd</sup>, 5<sup>th</sup>, 7<sup>th</sup> order, and Resultant

Basically Linear & Non-linear types of loads are being extensively used in any electrical load scenario. Linear load is defined as whose impedance is constant throughout its applied voltage cycle. Resistive, inductive & capacitive loads are coming under linear category.

Whereas Non-linear load is defined as whose impedance is continuously varying to its applied voltage cycle. SMPS, electronic equipment, SCR/IGBT devices, UPS systems etc are coming under

non-linear category. However, harmonics are distortion of the normal electrical current waveform, generally transmitted by nonlinear loads that draw a non-sinusoidal current from a sinusoidal voltage source. A harmonic current increases power system heat loss reduces system efficiency. Harmonic currents can have a significant impact on electrical distribution systems and the facilities they feed.

Switch-mode power supplies (SMPS), variable speed motors and drives, photocopiers, personal computers, laser printers, fax machines, battery chargers and UPSs are examples of nonlinear loads. Single-phase non-linear loads are prevalent in modern office buildings, while three-phase, non-linear loads are widespread in factories and industrial plants. Harmonics should not be confused with spikes, dips, impulses, oscillations or other forms of transients. Power system harmonics is an area that is receiving a great deal of attention recently. The increase in proportion of non-linear load has prompted more stringent recommendations (IEEE Std. 519 & IEC61000-4-7) and stricter limits imposed by utilities.

The above waveform was created due to 150Hz frequency (3<sup>rd</sup> harmonic), but there are N number of frequencies multipliers. Total harmonic distortion (THD or THD) is a measurement of the harmonic distortion present in a signal and is defined as the ratio of the sum of the powers of all harmonic components to the power of the fundamental frequency. Distortion factor, a closely related term, is sometimes used as a synonym.

$$THD_F = \frac{\sqrt{V_2^2 + V_3^2 + V_4^2 + V_5^2 + \dots + V_n^2}}{V_1}$$

THD is the total harmonic distortion and  $V_n$  is the RMS voltage of the nth harmonic

So, the THD is a measure for the effect of all higher frequency components which are present in the network. And we will be using individual order of Harmonic by studying the distortion that is happening from the individual order of harmonic, for example, below is the effect due to 3<sup>rd</sup> order of Harmonic on the fundamental frequency.

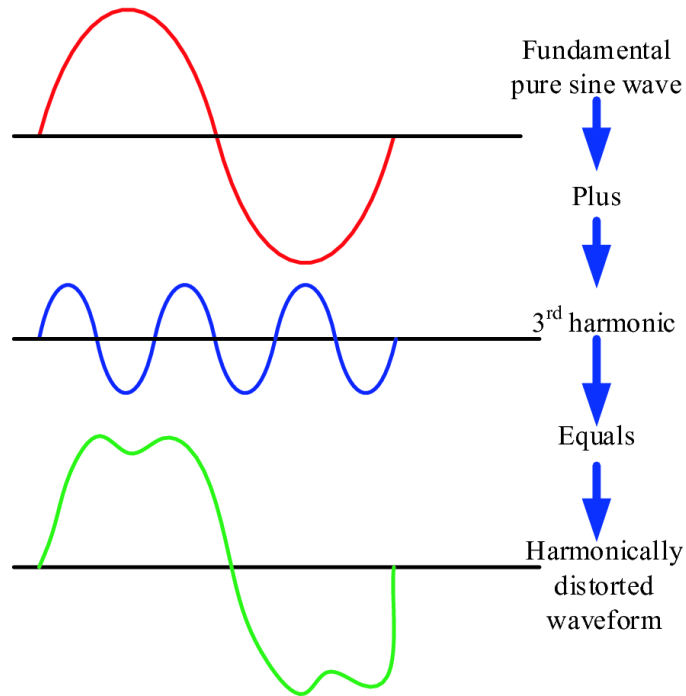


**Figure 2.2-65:** Effect of 3<sup>rd</sup> order harmonic (starting with positive cycle) on resultant distorted waveform

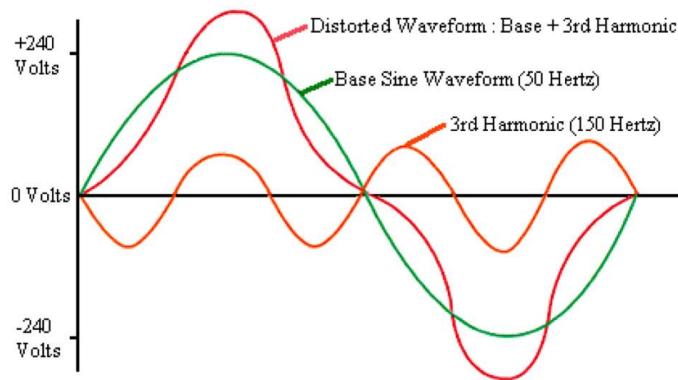


**Figure 2.2-66:**Effect of 3<sup>rd</sup> Order harmonic (starting with negative cycle) on resultant distorted waveform

Sine waves are symmetric about origin. Figure 1 shows various harmonic contents like 3rd, 5th & 7th & the resultant yellow color appears to be square wave. A square wave is actually combination of infinite series of sine wave harmonics, added together.

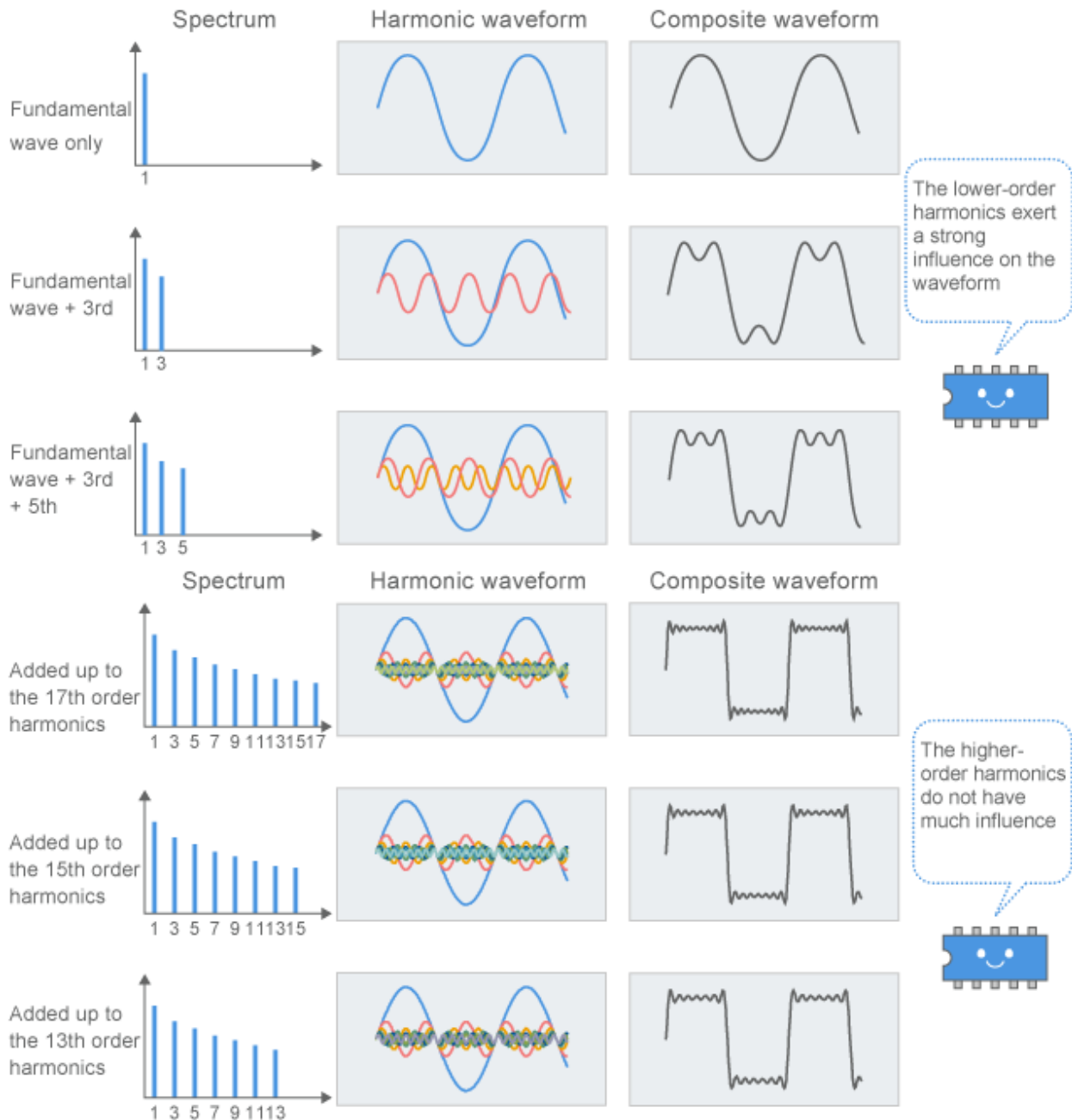


Figure 2.2-67: Several Harmonics waveforms and the composite waveform

In power system, there are limitation of harmonic value, and we need to maintain the harmonic level within some percentage, so if the harmonic value exceeded greater than some level it will cause:

- 1- Some miss-operation of electronic device.
- 2- Increase the power losses in the network.
- 3- Increase the reactive power consumption.
- 1- Reduce the lifetime of the equipment in the network.

To avoid these problems, we will be using some allowable limits for the total harmonic distortions to maintain the harmonic level of the network within that limit so for that we will be using some harmonic filters and to design the harmonic filter values, we will perform the harmonic study for that. Power electronic (inverters, UPS, VFD's) and high switching devices cause harmonics, also some magnetization equipment cause 3<sup>rd</sup> harmonic, also the grid can cause harmonic

**Case 1- Assuming Power grid harmonic model for the Synchronous Machines (ONLY) without XMFR for the power transformers**

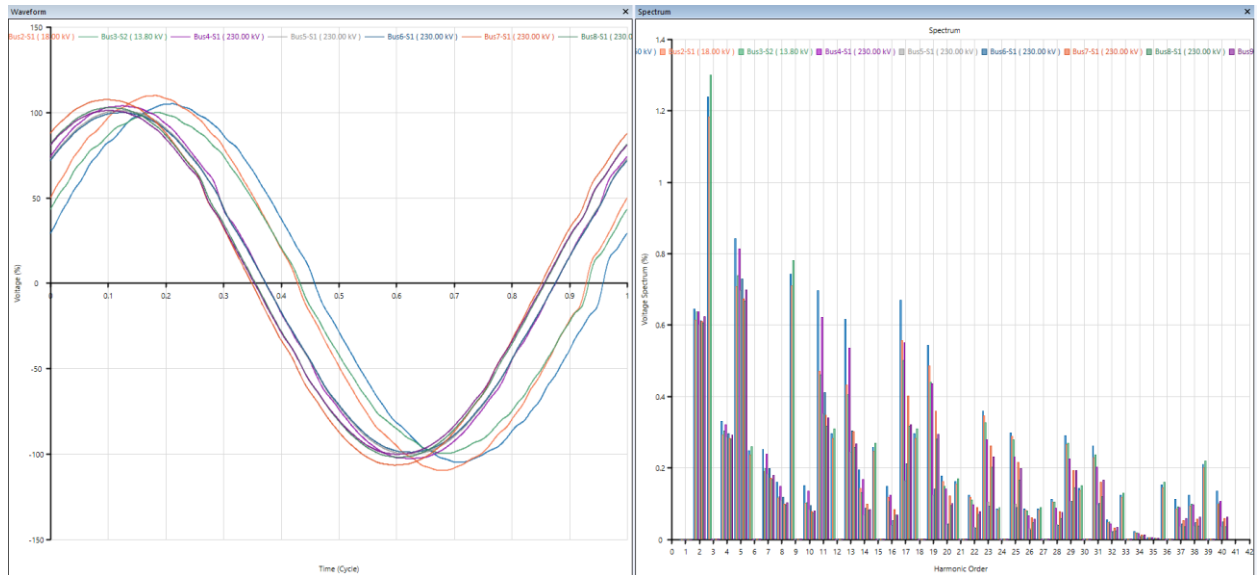


Figure 2.2-68: ETAP Voltage THD (%) Harmonic Analysis for all IEEE 9 bus system without transformer harmonic model

**Case 2- Assuming XMFR harmonic model for power transformers + Power grid harmonic model for the Synchronous Machines**

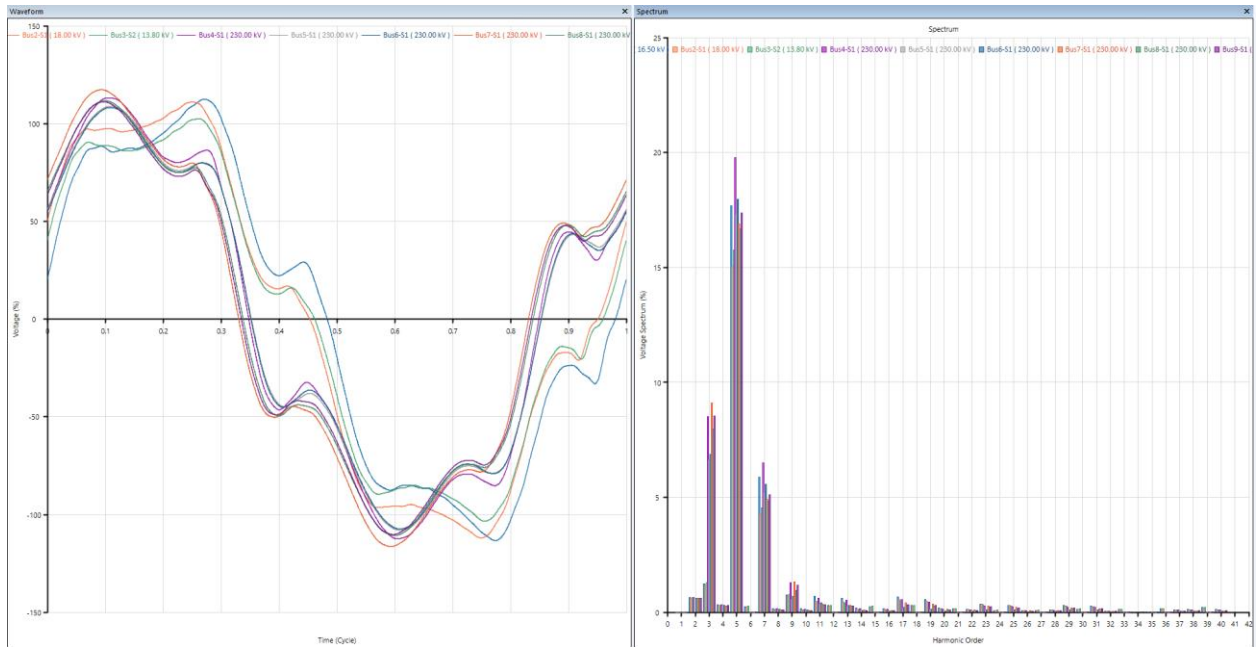


Figure 2.2-69:ETAP Voltage THD (%) Harmonic Analysis for all IEEE 9 bus system with transformer harmonic model

Harmonic impedance scan is shown in Figure 2.2-70

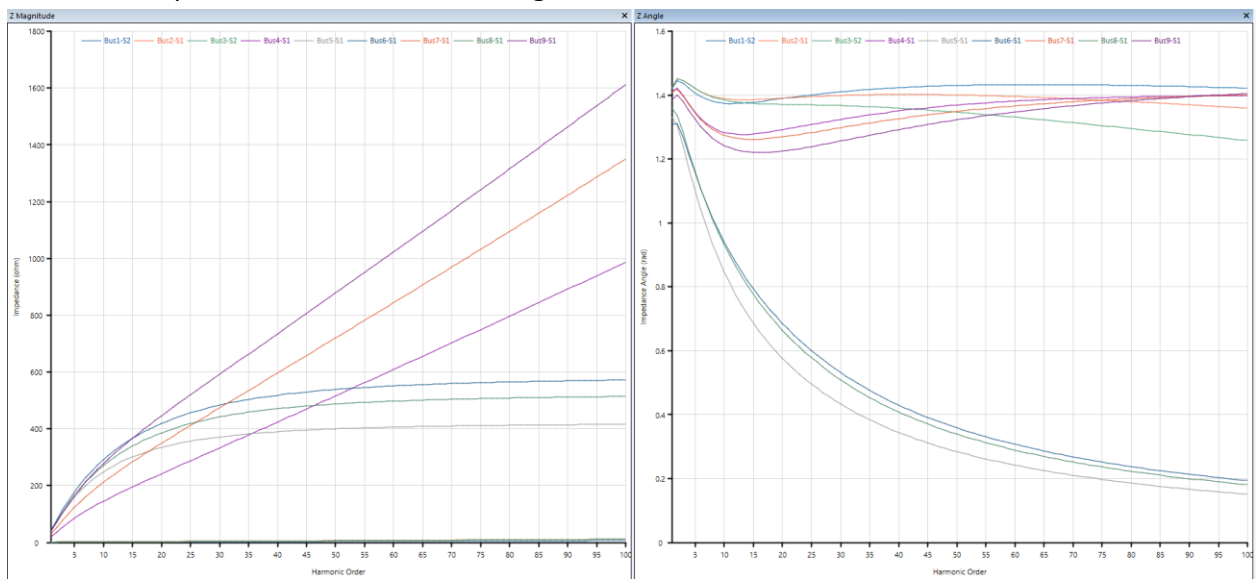


Figure 2.2-70: ETAP Harmonic Impedance Scan Z magnitude and Z angle

### 2.2.11 Contingency Analysis

Contingency analysis is the most significant aspect of a power system assessment because it assesses the power system's ability to handle the load without exceeding voltage and equipment loading restrictions in case of contingency.

It is unrealistic to build a power system with no breakdowns, failures, and faults. Faults in the power system must be isolated immediately so that the remainder of the system can work without interruption and the system returns to its normal stable operating condition. The post-fault circumstances are entirely different from the pre-fault situations in terms of the flow of power in the branches and the voltage at all the buses. Therefore, it is important to investigate the behavior of the system in its steady state following incidents including malfunctions and equipment failures or outages. Various equipment outages lead to distinct variations in power flow and voltage hence identifying the crucial outage before doing a simulation is challenging.

Therefore, it is advisable to conduct simulations in order to analyze the steady state behavior of the system subsequent to the individual apparatus failures. The term for this is "contingency analysis."

Contingency analysis is used to examine the response of a power system in the event of equipment failure. Contingency situations include several operational methods that may be examined, including the potential loss of a generator, transmission line, transformer, or load.

Preventing every unexpected interruption in the electrical system is difficult, thus evaluating potential outages to forecast their repercussions is critical. Contingency analysis is a valuable method for assessing power system security. It simulates any single or multiple outages to forecast power system condition variables after the disruption.

The N-1 contingency is a widely accepted criterion for evaluating the security of power infrastructure. According to this criterion, the intended power system should be able to resist any single component failure without violating any other component limitations, while still sustaining all system loads.

The N-1 contingency may be inadequate in situations when several component failures occur concurrently. N-K contingency analysis is designed to address the occurrence of numerous component failures. The N-K contingency refers to the ability of a power system to endure K number (2, 3) of component failures concurrently.

### Switching modes of Operation

The power system must possess the necessary attributes of system dependability and continuous operation. In the event of equipment outage, the remaining equipment guarantees a consistent and dependable power supply, while adhering to equipment loading and voltage requirements. The load flow analysis should include scenarios that demonstrate the system's ability to operate well under exceptional situations, such as transformer and motor loss or repair, grid supply failure, and so on.

### Load Flow Scenarios

In the context of load-flow evaluations for industrial applications, it is customary to encounter a restricted range of feasible scenarios for investigation. The comprehensive assessment and analysis of all occurrences of equipment maintenance or failure has significant importance.

Running ETAP contingency analysis with N-1 and N-2 in the following scenarios

#### 1- Generators Outages

Equipment Rating	DeviceID1	DeviceType1	Outage2	DeviceID2	DeviceType2	VVsp	DeltaP	DeltaQ	SSsp	Combined
Outage1										
2	Gen3-S1	Syn Gen	0			1.823565	84.25004	0.6670477	0.0761514	0
2	Gen3-S1	Syn Gen	3	Gen2-S1	Syn Gen	2.707521	1261.55	1.242212	0.04417973	0

## 2- Buses Outages

Equipment Rating	DeviceID1	DeviceType1	Outage2	DeviceID2	DeviceType2	VVsp	DeltaP	DeltaQ	SSsp	Combined
Outage1										
1	Bus1-S1	Bus	0			400	1	1	0	0
2	Bus2-S1	Bus	0			44.77453	792.9346	1.202065	0.07372336	0
3	Bus3-S1	Bus	0			46.15139	84.25003	0.6670477	0.07615139	0
4	Bus4-S1	Bus	0			355.6667	1	1	7.50E-21	0
5	Bus5-S1	Bus	0			46.00863	44.71667	1.055794	0.1345115	0
6	Bus6-S1	Bus	0			45.13018	276.3037	0.4467896	0.1292828	0
7	Bus7-S1	Bus	0			89.19996	709.1525	1.316782	0.07636761	0
8	Bus8-S1	Bus	0			48.83294	293.7845	1.260359	0.1260195	0
9	Bus9-S1	Bus	0			91.78465	29.66653	0.7064821	0.07631073	0
2	Bus2-S1	Bus	10	Bus1-S1	Bus	400	1	1	0	0
3	Bus3-S1	Bus	10	Bus1-S1	Bus	400	1	1	0	0
4	Bus4-S1	Bus	10	Bus1-S1	Bus	400	1	1	0	0
5	Bus5-S1	Bus	10	Bus1-S1	Bus	400	1	1	0	0
6	Bus6-S1	Bus	10	Bus1-S1	Bus	400	1	1	0	0
7	Bus7-S1	Bus	10	Bus1-S1	Bus	400	1	1	0	0
8	Bus8-S1	Bus	10	Bus1-S1	Bus	400	1	1	0	0
9	Bus9-S1	Bus	10	Bus1-S1	Bus	400	1	1	0	0
3	Bus3-S1	Bus	11	Bus2-S1	Bus	90.71967	1261.55	1.242213	0.04417974	0
4	Bus4-S1	Bus	11	Bus2-S1	Bus	355.6667	1	1	7.50E-21	0
5	Bus5-S1	Bus	11	Bus2-S1	Bus	89.3134	22.37382	1.375907	0.05986899	0
6	Bus6-S1	Bus	11	Bus2-S1	Bus	89.2275	680.6476	1.395309	0.06248932	0
7	Bus7-S1	Bus	11	Bus2-S1	Bus	89.19996	709.1525	1.316782	0.07636761	0
8	Bus8-S1	Bus	11	Bus2-S1	Bus	89.08395	661.2988	0.559266	0.05963528	0
9	Bus9-S1	Bus	11	Bus2-S1	Bus	142.4495	2279.287	3.222193	0.05493006	0
4	Bus4-S1	Bus	12	Bus3-S1	Bus	355.6667	1	1	7.50E-21	0
5	Bus5-S1	Bus	12	Bus3-S1	Bus	95.96231	10.28689	1.296035	0.0722431	0
6	Bus6-S1	Bus	12	Bus3-S1	Bus	92.56716	9.270747	0.8995863	0.07225055	0
7	Bus7-S1	Bus	12	Bus3-S1	Bus	146.3171	746.3343	3.803333	0.05888569	0
8	Bus8-S1	Bus	12	Bus3-S1	Bus	93.3764	258.7477	1.465676	0.07270121	0
9	Bus9-S1	Bus	12	Bus3-S1	Bus	91.78465	29.66653	0.7064821	0.07631073	0
5	Bus5-S1	Bus	13	Bus4-S1	Bus	355.6667	1	1	7.50E-21	0
6	Bus6-S1	Bus	13	Bus4-S1	Bus	355.6667	1	1	7.50E-21	0
7	Bus7-S1	Bus	13	Bus4-S1	Bus	355.6667	1	1	7.50E-21	0
8	Bus8-S1	Bus	13	Bus4-S1	Bus	355.6667	1	1	7.50E-21	0
9	Bus9-S1	Bus	13	Bus4-S1	Bus	355.6667	1	1	7.50E-21	0
6	Bus6-S1	Bus	14	Bus5-S1	Bus	311.3333	0.9999998	1	3.32E-16	0
7	Bus7-S1	Bus	14	Bus5-S1	Bus	133.6524	22.37382	1.375908	0.059869	0
8	Bus8-S1	Bus	14	Bus5-S1	Bus	177.9764	1.215568	0.6462097	0.05174081	0
9	Bus9-S1	Bus	14	Bus5-S1	Bus	266.8742	16.2505	0.8268268	0.003025411	0
7	Bus7-S1	Bus	15	Bus6-S1	Bus	266.8652	588.7943	0.8180814	0.006270716	0
8	Bus8-S1	Bus	15	Bus6-S1	Bus	182.4424	256.9431	1.660604	0.07393464	0
9	Bus9-S1	Bus	15	Bus6-S1	Bus	136.4033	9.270814	0.8995851	0.07225065	0
8	Bus8-S1	Bus	16	Bus7-S1	Bus	133.5194	661.2988	0.5592661	0.05963528	0
9	Bus9-S1	Bus	16	Bus7-S1	Bus	222.41	626.3689	0.7071866	0.01817336	0
9	Bus9-S1	Bus	17	Bus8-S1	Bus	137.8191	258.7477	1.465676	0.07270121	0

### 3- Line Outages

Equipment Rating		DeviceID1	DeviceType1	Outage2	DeviceID2	DeviceType2	VVsp	DeltaP	DeltaQ	SSsp	Combined
Outage1		Line1-S1	Line	0			1.15889	0.1992653	1.155133	0.123052	0
1		Line2-S1	Line	0			1.231053	4.724794	1.160374	0.1231993	0
2		Line3-S1	Line	0			1.542616	770.3619	0.9691133	0.1362534	0
3		Line4-S1	Line	0			0.6509441	279.317	0.2804366	0.1297445	0
4		Line5-S1	Line	0			2.808305	10.55921	0.5051532	0.1240826	0
5		Line6-S1	Line	0			4.556898	299.9735	2.081135	0.1294565	0
6		Line2-S1	Line	7	Line1-S1	Line	311.3333	0.9999998	1	4.13E-17	0
2		Line3-S1	Line	7	Line1-S1	Line	46.00862	44.71667	1.055794	0.1345114	0
3		Line4-S1	Line	7	Line1-S1	Line	266.8742	16.2505	0.8268262	0.003025412	0
4		Line5-S1	Line	7	Line1-S1	Line	177.9764	1.215568	0.6462097	0.05174081	0
5		Line6-S1	Line	7	Line1-S1	Line	133.6524	22.37382	1.375908	0.05986901	0
6		Line3-S1	Line	8	Line2-S1	Line	266.8652	588.7943	0.8180814	0.006270718	0
4		Line4-S1	Line	8	Line2-S1	Line	45.13018	276.3037	0.4467896	0.1292828	0
5		Line5-S1	Line	8	Line2-S1	Line	136.4033	9.270814	0.8995846	0.07225065	0
6		Line6-S1	Line	8	Line2-S1	Line	182.4424	256.9431	1.660604	0.07393464	0
4		Line4-S1	Line	9	Line3-S1	Line	222.41	626.3689	0.7071863	0.01817337	0
5		Line5-S1	Line	9	Line3-S1	Line	133.5194	661.2988	0.5592663	0.05963528	0
6		Line6-S1	Line	9	Line3-S1	Line	89.19996	709.1525	1.316782	0.07636762	0
5		Line5-S1	Line	10	Line4-S1	Line	91.78465	29.66653	0.7064812	0.07631073	0
6		Line6-S1	Line	10	Line4-S1	Line	137.8191	258.7477	1.465675	0.07270121	0
6		Line6-S1	Line	11	Line5-S1	Line	48.83294	293.7845	1.260358	0.1260195	0

### 4- Transformer Outages

Equipment Rating		DeviceID1	DeviceType1	Outage2	DeviceID2	DeviceType2	VVsp	DeltaP	DeltaQ	SSsp	Combined
Outage1		T1	Transformer	0			355.6667	1	1	7.50E-21	0
1		T2	Transformer	0			44.77453	792.9346	1.202065	0.07372336	0
2		T3	Transformer	0			46.15139	84.25003	0.6670477	0.07615139	0
3		T2	Transformer	4	T1	Transformer	355.6667	1	1	7.50E-21	0
2		T3	Transformer	4	T1	Transformer	355.6667	1	1	7.50E-21	0
3		T3	Transformer	5	T2	Transformer	90.71967	1261.55	1.242213	0.04417974	0

## 2.3 Chapter Six: Grid Connected Solar PV Plant and Wind Farm- Grid Impact Study and ETAP Simulation for Modified IEEE 9 Bus System



### 2.3.1 Overview and Grid Code Compliance

All generators connected to the transmission system must be complied with Transmission System Operator (TSO) grid code. In this case study, the TSO is the entity who controls the 230kV High voltage system of the IEEE 9 bus system. The compliance with grid code requires that both active  $P$  and reactive power  $Q$  are supplied to the PoCC within the acceptable voltage and frequency ranges defined in the Transmission Interconnection Code (TIC) of the grid provider. PV plants / wind farms connected to MV or HV networks should be designed and constructed in order to be viewed as a single generator connected to the Point of Common Coupling PoCC. Therefore, a control and automation system should be considered in order to fully fulfill the grid code requirements.

#### 2.3.1.1 INTERMIT RENEWABLE RESOURCE (IRR) OPERATION

It must be possible to operate IRR plant in reactive power control mode and follow any operating point within the range  $\cos\phi = 0.95$  leading under-excited to  $\cos\phi = 0.85$  lagging over-excited at

PoCC as shown in **Figure 2.3-1** below. For active power supply below the nominal power, **Figure 2.3-1** indicates the minimum reactive power and power factor requirements.

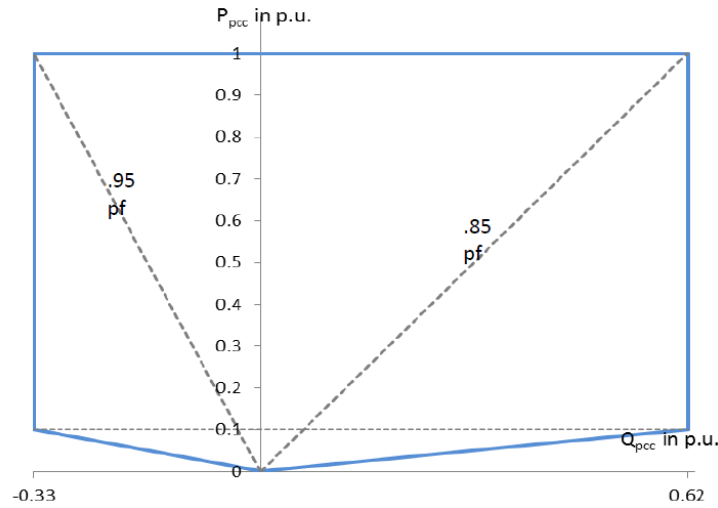


**Figure 2.3-1:** Minimum P-Q Diagram to be fulfilled by IRR Plant [32]

The reactive support must be dynamic in nature for the equivalent of the nominal plant (sum of IRR) capacity, and the rest of the reactive support may be provided by automatically switched capacitors at the point of interconnection. The IRR shall be capable of providing reactive power support in any of three modes: voltage set point control, power factor set point, or reactive power set point control. An implementation example for the steady-state VAR settings and controller design are shown in **Figure 2.3-2**

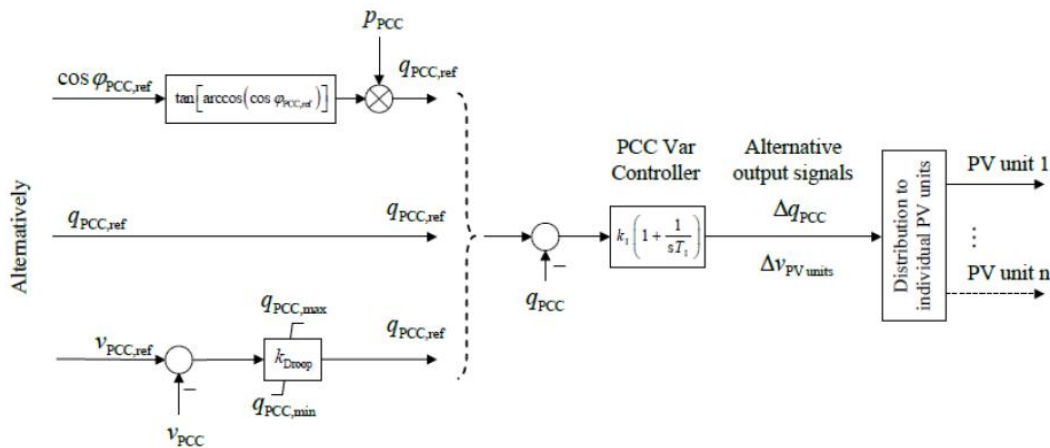


**Figure 2.3-2:** Definition and Control of PoCC Reactive Power

The rate of change for the reactive support in VARs ( $Q$ ) shall satisfy the following requirements:

1. Rate of change from zero to the maximum or minimum VAR support (0 to  $Q_{max}$  or 0 to  $Q_{min}$ ) shall be achievable within 2 s to 5 s.
2. Rate of change to swing the support between the maximum and minimum VAR support ( $Q_{max}$  to  $Q_{min}$  or  $Q_{min}$  to  $Q_{max}$ ) shall be achievable within 10 s.

According to the above considerations, the P-Q characteristic at PoCC should be as shown in **Figure 2.3-3**

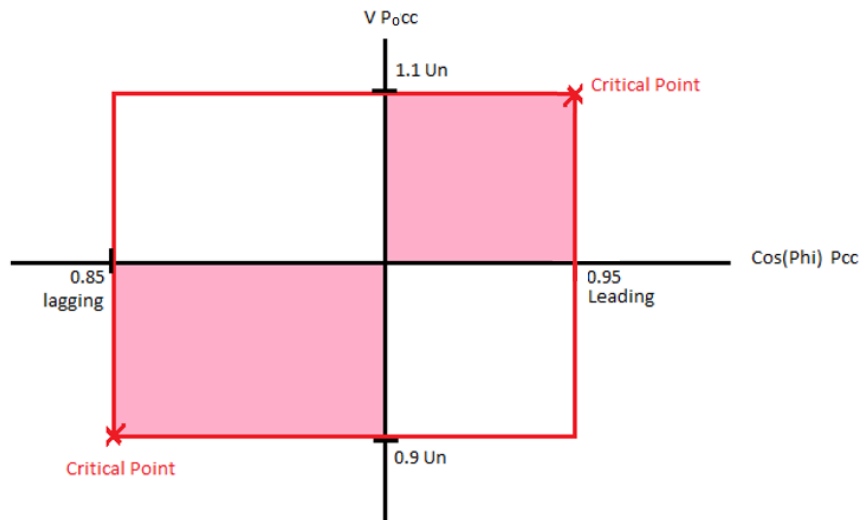


**Figure 2.3-3:** V-PF Characteristics at PoCC

Additionally, the full lagging reactive capability of 0.85 PF of the IRR nominal capacity shall be made available at 100% to 90% of the nominal voltage. The full leading reactive capability of 0.95 PF of the IRR nominal capacity shall be made available at 100% to 110% of the nominal voltage.

### 2.3.1.2 Fault Ride Through (Zero and LVRT)

The Low Voltage Ride-Through (LVRT) specifies the capability range for IRRs to remain connected to the system during and following grid faults, including the requirement to participate in dynamic voltage control. The dynamic voltage control, to be superimposed on the steady state voltage control, is to be implemented as a fast-local control to change the reactive current output of the IRR as necessary to counter the sudden voltage change resulting from grid faults and disturbances. A voltage falls below the red line triggers the permitted disconnection of the unit. IRR must be

capable of remaining connected at or above this limit during and immediately after any short circuit, balanced or unbalanced, which is correctly isolated by protection schemes even in the case of action by the second level protection. IRR must survive a zero-voltage dip of at least the depth shown in the solid red line at the PCC in Figure 2.3-4 [32].

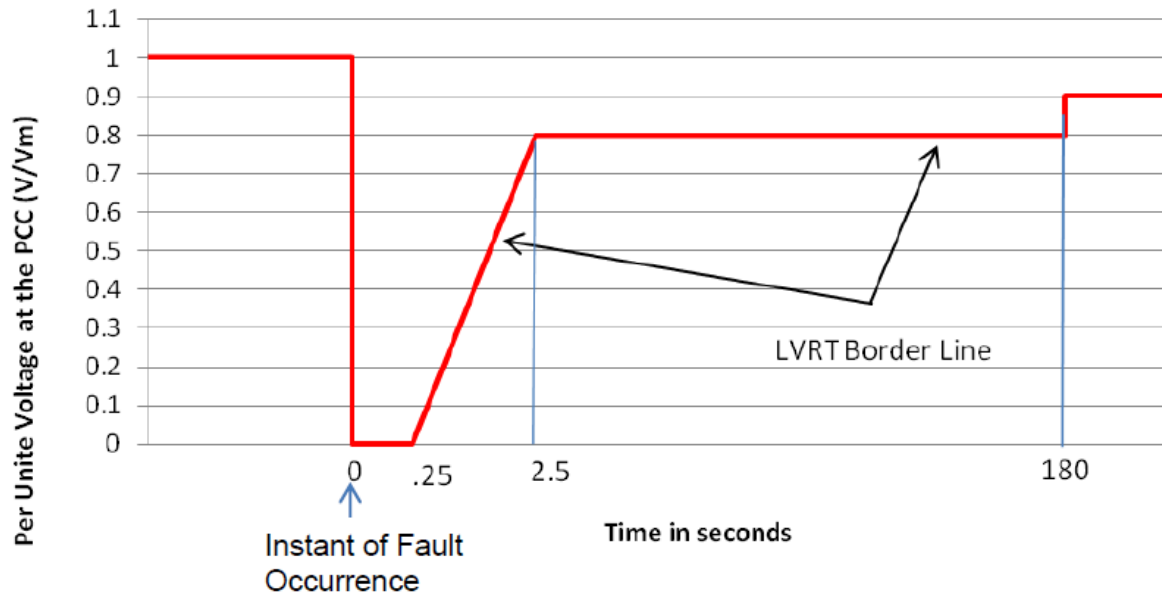


**Figure 2.3-4:** Definition of Voltage Characteristic at the PCC for LVRT

### 2.3.1.3 Frequency Requirements of IRR

Under extreme system fault conditions and large disturbances, all IRR units must be disconnected from the grid at a frequency greater than 51.5 Hz. At a frequency less than 47.5 Hz the generator may be disconnected if such frequency stays longer than 20 s (in accordance with Table 2.3-1). Where under and over frequency relays are installed, these relays shall be set such that the automatic removal of the IRR from TSO’s Transmission Network meets the requirements shown in Table 2.3-1. TSO, however, may specify slightly different tripping points for various generators in order to avoid having all generators on the Transmission Network trip at the same time in a frequency constraint.

**Table 2.3-1:** Frequency Relaying Requirements

Frequency Range	Delay to Trip
51.5 Hz < Freq	0.5 s
47.5 Hz ≤ Freq ≤ 51.5 Hz	Continuous Operation
47.0 Hz < Freq < 47.5 Hz	20 s
Freq ≤ 47.0 Hz	0.5 s

#### 2.3.1.4 Voltage Requirements of IRR

TSO Transmission Grid Code defines that the transmission network under Normal Operation shall operate within the ranges shown in Table 2.3-2.

**Table 2.3-2:** Voltage Range for Normal Operation.

Voltage Level	IRR Continuous Operation Range
230 kV system	207kV (-10%) to 253kV (+10%)
33 kV system	29.7 kV (-10%) to 36.3 kV (+10%)

IRRs shall remain continuously connected to the transmission network at maximum available active power or controlled Active Power output for normal and disturbed system conditions for step changes in Transmission System voltage of up to 10 % per Table 2.3-3.

**Table 2.3-3:** Voltage Relaying Requirements

Voltage Range (% V <sub>nominal</sub> )	Delay to Trip
120 ≤ V	No Time Delay
115 ≤ V < 120	0.2s
110 < V < 115	60 s*
90 ≤ V ≤ 110	Continuous Operation
80 ≤ V < 90	180 s*
0 < V < 80	0.25s to 2.5s per LVRT graph
V = 0	0.25 s

\*IRRs with equipment capable of staying on-line for longer duration must activate that capability in coordination with TSO

#### 2.3.2 Grid Connected Photo Voltic Plant

The proposal is to replace the SM-2 which nominal total capacity of 270MVA, PF=85%, P=230MW, however it was set to deliver 213 MW at PoCC, by a 270MVA Grid connected PV

plant which PoCC at IEEE 9 bus system is Bus No.7 as per Scenario No.3 shown below **Figure 2.3-5:Grid Connected PV plant with IEEE 9 Bus System (Bus No.7: POCC)**

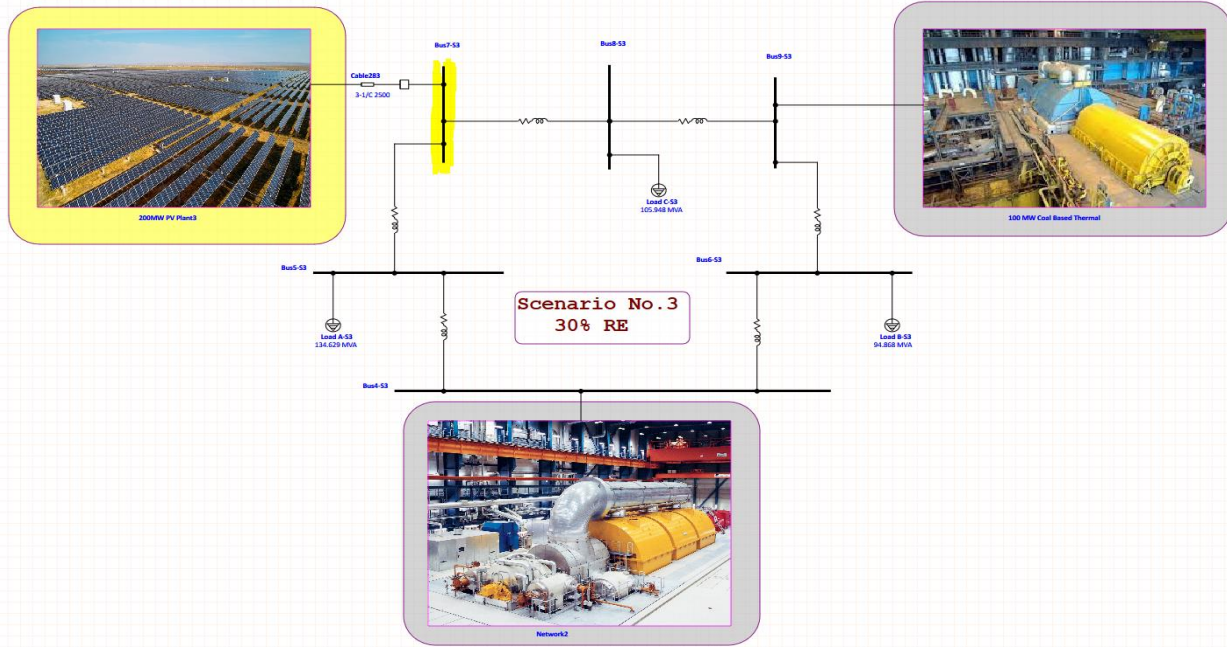


**Figure 2.3-5:Grid Connected PV plant with IEEE 9 Bus System (Bus No.7: POCC)**

The proposed PV plant with below parameters

**Table 2.3-4: Proposed Grid Connected PV plant Parameters.**

Item	Parameter
Active Power (MW ac)	200
Voltage at PoCC (kV)	230
DC Capacity (MWp)	240
Design Temperature (Ambient Temperature) (°C)	-5°C ~ + 40
Active Power Losses from inverters terminals up to the PoCC	7.5 %
Grid Reactive Power Capability	0.85 over excited 0.95 under excited
Voltage Range	(0.9 -1.1) Un

**2.3.2.1 PV PLANT ARCHITECTURE DRAWING**

The PV plant will be designed based on central inverter stations or power collection stations, whereby each inverter station will receive the DC electrical power from the PV generator (array) and convert it into AC electrical power. Generally, the number of inverters will depend on the plant capacity and the size of each inverter. Each inverter station contains 2 X central inverters, a solar step-up transformer that steps up the LV power from the output of the inverter terminals into MV power, and MV Ring main Unit (RMU). A group of inverter stations will be connected in series through MV RMU's connected through MV power cables, and these groups are connected to MV main switchgear in parallel, as indicated in the single line diagram **Figure 2.3-6: PV Plant Architecture**. This main MV switchgear contains the PV incoming feeders, outgoing transformer feeders, and bus sections. Hence, the power flow of the PV plant can be controlled by switching the circuit breakers on and off. From the main MV switchgear comes the step-up (MV/HV) power transformers that will step up the MV voltage into HV level ready for connection with the grid primary switching SS, which will be considered as PoCC of that PV plant.

It is assumed that the substation is designed in a manner where it divides the PV plant generation into three sections. Each section is sized to be adequate to evacuate 67 MW of generation towards the grid. In normal operation condition of each section, there are three 33/230 kV, 125 MVA power transformers operating at the same time to evacuate all the energy towards grid, while all bus couplers are open. Bus couplers are closed only in case of failure of any of the three transformers, in order to divert the power path into the grid through the remaining two transformers, which are sized to be adequate enough. It is important to highlight that it is not allowed to close both bus couplers of the same section at the same time, to minimize the possible short circuit current that is coming from the utility.

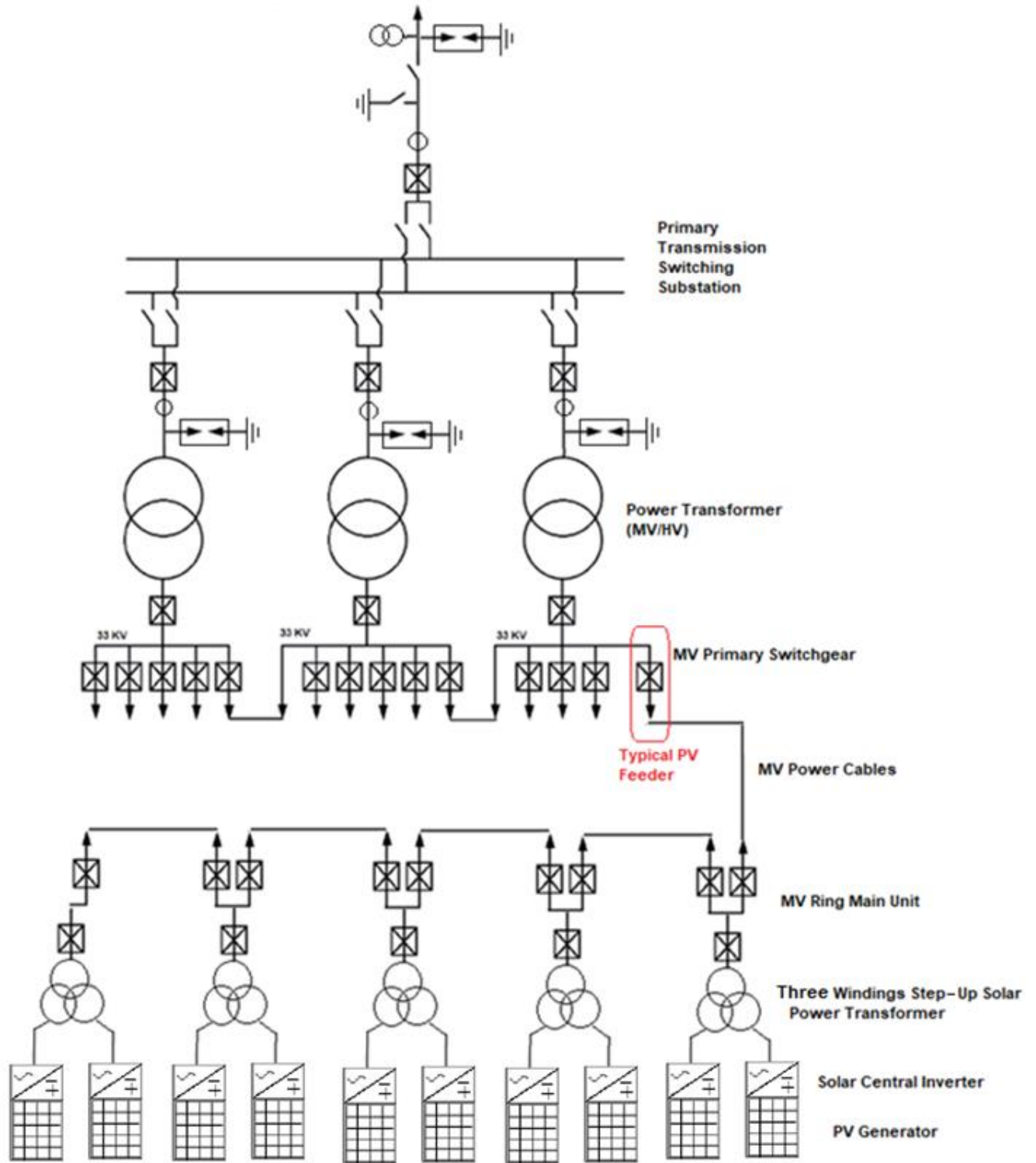


**Figure 2.3-6:** PV Plant Architecture drawing.

### 2.3.2.2 ACTIVE AND REACTIVE POWER REQUIRED BY THE SOLAR INVERTERS

#### 2.3.2.2.1 Active Power

The required active power  $P$  that should be available at the inverters output terminals is affected by the power losses from the inverter terminals all the way till the PoCC. Hence, to achieve the required nominal active power  $P$  at the PoCC, the power losses should be considered. The power required at inverter terminals can be calculated as below:

$$P_{\text{required at inverters terminal}} = P_{@PoCC} \times (1 + \Delta P_{\text{losses}} \%) = 200 \text{ MW} \times (1 + 0.075) = 215 \text{ MW}$$

#### 2.3.2.2.2 Reactive Power

The required reactive power  $Q$  that should be available at the PoCC should comply with the grid code requirement of the grid reactive power capability which is 0.85 over excited to 0.95 under excited.

##### 2.3.2.2.2.1 0.85 Over-Excited (O/E)

$$\text{In 0.85 over-excited: } PF = \cos(\varphi) = 0.85 \Rightarrow \varphi = \cos^{-1}(0.85) = 31.78^\circ$$

The reactive power can be calculated from the available parameters in **Table 2.3-4**

$$\begin{aligned} Q_{O/E} &= S \times \sin(\varphi) = \left( \frac{P}{\cos(\varphi)} \right) \times \sin(\varphi) = P \times \tan(\varphi) = 200 \times \tan(31.78^\circ) \\ &= 124 \text{ MVar Capacitive} \end{aligned}$$

$$Q_{O/E(PU)} = \left( \frac{124}{200} \right) = 0.62 \text{ pu}$$

##### 2.3.2.2.2.2 0.95 Under-Excited (U/E)

$$\text{In 0.95 under-excited: } PF = \cos(\varphi) = 0.95 \Rightarrow \varphi = \cos^{-1}(0.95) = 18.19^\circ$$

The reactive power can be calculated from the available parameters in **Table 2.3-4**:

$$\begin{aligned} Q_{U/E} &= S \times \sin(\varphi) = \left( \frac{P}{\cos(\varphi)} \right) \times \sin(\varphi) = P \times \tan(\varphi) = 200 \times \tan(18.19^\circ) \\ &= 66 \text{ MVar Inductive} \end{aligned}$$

$$Q_{U/E(PU)} = \left( \frac{66}{200} \right) = 0.33 \text{ pu}$$

### 2.3.2.3 VOLTAGE RISE DURING MAXIMUM REACTIVE POWER FEED

The calculation uses the same formula for the voltage drop on the lines/cables as well as on the transformer, using basic parameters like inductive/resistive components of their respective impedance, the module of the current, and the displacement angle (i.e.  $\phi$ ).

For transformers:

$$Z_T = Z_{cc}\% \times \frac{V^2}{S}$$
$$R = \frac{Z}{\sqrt{1 + (X/R)^2}}$$

$$X = R \times (X/R)$$

For a given current  $I$  and displacement angle  $\phi$  you can calculate the voltage drop/rise as follows:

$$\Delta V_T = \sqrt{3} \times I \times (R_T \times \cos\phi + X_T \times \sin\phi)$$

For lines/cables:

$$\Delta V_L = \sqrt{3} \times I \times (R_L \times \cos\phi + X_L \times \sin\phi)$$

Where  $R_L$  and  $X_L$  are the active and reactive component of the line/cable impedance.

#### 2.3.2.3.1 Power Factor 0.85

The voltage rises on the inverter terminals due reactive power injection (in maximum over excited = PF = **0.85**)

**A- LV/MV Transformer – 4 MVA, 0.66/33 KV (Zsc% = 6.00), X/R=8**

$$Z = Z_{cc}\% \times \frac{V^2}{S} = 0.06 \times \frac{33,000^2}{4,000,000} = 16.33 \Omega$$

$$R = \frac{Z}{\sqrt{1 + (X/R)^2}} = \frac{16.33}{\sqrt{1 + (8)^2}} = 2.025 \Omega$$

$$X = R \times (X/R) = 2.025 \times 8 = 16.203 \Omega$$

$$I_{max-TR} = \frac{S}{\sqrt{3} \times V} = \frac{4,000,000}{\sqrt{3} \times 33,000} = 70 \text{ A}$$

$$\Delta V_T = \sqrt{3} \times I \times (R_T \times \cos\phi + X_T \times \sin\phi)$$

$$\Delta V_T = \sqrt{3} \times 70 \times (2.025 \times 0.85 + 16.203 \times 0.53) = \mathbf{1,249.88 \text{ V}}$$

$$\Delta V_T \% = \frac{\Delta V}{V} \times 100\% = \frac{1,249.88}{33,000} \times 100\% = \mathbf{3.78\%}$$

### B- 33kV Power Cable

The selected 33kV power cable is 18/30 (36) kV single core Aluminum Conductor XLPE Insulated AWA, with below list of cross-sectional area in **Table 2.3-5: Power Cables Voltage Drop at 0.85 PF**

**Table 2.3-5: Power Cables Voltage Drop at 0.85 PF**

From	To	Cable Size (mm <sup>2</sup> )	Number of Runs	Length per Run (meter)	R (Ω/m)	X (Ω/m)	R (Ω)	X (Ω)	Voltage Drop ΔV
1 <sup>st</sup> Block	2 <sup>nd</sup> Block	185	1	295	0.000164	0.000128	0.58	0.45	
2 <sup>nd</sup> Block	3 <sup>rd</sup> Block	185	1	268	0.000164	0.000128	0.53	0.41	
3 <sup>rd</sup> Block	4 <sup>th</sup> Block	240	1	296	0.000125	0.000121	0.44	0.43	
4 <sup>th</sup> Block	5 <sup>th</sup> Block	240	2	1,047	0.0000625	0.0000605	0.79	0.76	
5 <sup>th</sup> Block	Connection Point	400	2	712	0.0000389	0.0000665	0.33	0.57	
Total voltage drops at 33kV side at 0.85 PF as per the results from ETAP simulation, Annex K									<b>957 V</b>

$$R = R_{\Omega/Km} \times L_{km}$$

$$X = X_{\Omega/Km} \times L_{km}$$

$$I_{max-TR} = \frac{S}{\sqrt{3} \times V} = \frac{4,000,000}{\sqrt{3} \times 33,000} = 70 \text{ A}$$

injected in each block

$$\Delta V_L = \sqrt{3} \times I \times (R_L \times \cos\varphi + X_L \times \sin\varphi)$$

$$\Delta V_L \% = \frac{\Delta V}{V} \times 100\% = \frac{957}{33,000} \times 100\% = \mathbf{2.9\%}$$

**C- MV/HV Transformer – 125MVA, 33/230 KV (Zs.c% = 12.5%), X/R=39**

$$Z = Z_{cc}\% \times \frac{V^2}{S} = 0.125 \times \frac{230,000^2}{125,000,000} = 52.9 \Omega$$

$$R = \frac{Z}{\sqrt{1 + (X/R)^2}} = \frac{52.9}{\sqrt{1 + (39)^2}} = 1.356 \Omega$$

$$X = R \times (X/R) = 1.356 \times 39 = 52.882 \Omega$$

$$I_{max-TR} = \frac{S}{\sqrt{3} \times V} = \frac{\sqrt{P^2 + Q^2}}{\sqrt{3} \times V} = \frac{\sqrt{200,000,000^2 + 124,000,000^2}}{\sqrt{3} \times 230,000} = 590.707 A$$

Assuming that the current is evenly divided between the transformers (3 x 125 MVA; which are running in parallel) = 590.707 / 3 = **197** Amps (for each transformer).

$$\Delta V_T = \sqrt{3} \times I \times (R_T \times \cos\varphi + X_T \times \sin\varphi)$$

$$\Delta V_T = \sqrt{3} \times 197 \times (1.356 \times 0.85 + 52.882 \times 0.53) = 9,956.64$$

$$\Delta V_T \% = \frac{\Delta V}{V} \times 100\% = \frac{9,956.64}{230,000} \times 100\% = \mathbf{4.3\%}$$

In conclusion, the total voltage rises equals to:

$$\Delta V_{total}^{0.85 O/E} = 3.78\% + 2.9\% + 4.33\% = 11.01\% \approx \mathbf{11\%}$$

**2.3.2.3.2 Power factor 0.95**

The voltage drops on the inverter terminals due reactive power absorption (in maximum under excited = PF =**0.95**)

**A- LV/MV Transformer – 4MVA, 0.66/33 KV (Zsc% = 6%)**

$$Z = Z_{cc}\% \times \frac{V^2}{S} = 0.06 \times \frac{33,000^2}{4,000,000} = 16.33 \Omega$$

$$R = \frac{Z}{\sqrt{1 + (X/R)^2}} = \frac{16.33}{\sqrt{1 + (8)^2}} = 2.025 \Omega$$

$$X = R \times (X/R) = 1.625 \times 8 = 16.203 \Omega$$

$$I_{max-TR} = \frac{S}{\sqrt{3} \times V} = \frac{4,000,000}{\sqrt{3} \times 33,000} = 70 A$$

$$\Delta V_T = \sqrt{3} \times I \times (R_T \times \cos\phi + X_T \times \sin\phi)$$

$$\Delta V_T = \sqrt{3} \times 70 \times (2.025 \times 0.95 + 16.203 \times 0.31) = \mathbf{842.24 V}$$

$$\Delta V_T\% = \frac{\Delta V}{V} \times 100\% = \frac{842.24}{33,000} \times 100\% = \mathbf{2.55\%}$$

### B- 33kV Power Cable

The selected 33kV power cable is 18/30 (36) kV single core Aluminum Conductor XLPE Insulated AWA, with below list of cross-sectional area in **Table 2.3-6**

**Table 2.3-6:**Power Cables Voltage Drop at 0.95 PF

From	To	Cable Size (mm <sup>2</sup> )	Number of Runs	Length per Run	R (Ω/m)	X (Ω/m)	R (Ω)	X (Ω)	Voltage Drop ΔV
1 <sup>st</sup> Block	2 <sup>nd</sup> Block	185	1	294.83	0.000164	0.000128	0.58	0.45	
2 <sup>nd</sup> Block	3 <sup>rd</sup> Block	185	1	268.83	0.000164	0.000128	0.53	0.41	
3 <sup>rd</sup> Block	4 <sup>th</sup> Block	240	1	296.33	0.000125	0.000121	0.44	0.43	
4 <sup>th</sup> Block	5 <sup>th</sup> Block	240	2	1,047.58	0.0000625	0.0000605	0.79	0.76	
5 <sup>th</sup> Block	Connection Point	400	2	712.33	0.0000389	0.0000665	0.33	0.57	
Total voltage drops at 33kV side at 0.95 PF as per the results from ETAP simulation, Annex L									<b>277.2</b>

$$R = R_{\Omega/Km} \times L_{km}$$

$$X = X_{\Omega/Km} \times L_{km}$$

$$I_{max-TR} = \frac{S}{\sqrt{3} \times V} = \frac{4,000,000}{\sqrt{3} \times 33,000} = 70 \text{ A}$$

injected in each block

$$\Delta V_L = \sqrt{3} \times I \times (R_L \times \cos\varphi + X_L \times \sin\varphi)$$

$$\Delta V_L \% = \frac{\Delta V}{V} \times 100\% = \frac{277.2}{33,000} \times 100\% = \mathbf{0.84\%}$$

### C- MV/HV Transformer – 125MVA, 33/230 KV (Zs.c% = 12.5%), X/R=39

$$ZZ = Z_{cc}\% \times \frac{V^2}{S} = 0.125 \times \frac{230,000^2}{125,000,000} = 52.9 \Omega$$

$$R = \frac{Z}{\sqrt{1 + (X/R)^2}} = \frac{52.9}{\sqrt{1 + (39)^2}} = 1.356 \Omega$$

$$X = R \times (X/R) = 1.356 \times 39 = 52.882 \Omega$$

$$I_{max-TR} = \frac{S}{\sqrt{3} \times V} = \frac{\sqrt{P^2 + Q^2}}{\sqrt{3} \times V} = \frac{\sqrt{200,000,000^2 + 124,000,000^2}}{\sqrt{3} \times 230,000} = 590.707 \text{ A}$$

Assuming that the current is evenly divided between the transformers (3 x 125 MVA; which are running in parallel) = 590.707 / 3 = **197 A** (for each transformer).

$$\Delta V_T = \sqrt{3} \times I \times (R_T \times \cos\varphi + X_T \times \sin\varphi)$$

$$\Delta V_T = \sqrt{3} \times 197 \times (1.356 \times 0.95 + 52.882 \times 0.31) = \mathbf{6,033.216 \text{ V}}$$

$$\Delta V_T \% = \frac{\Delta V}{V} \times 100\% = \frac{6,033.216}{230,000} \times 100\% = \mathbf{2.623\%}$$

A detailed grid impact study is required to define the exact percentage using advanced simulation tools.

In conclusion, the total voltage rise equals to:

$$\Delta V_{total} = 2.55\% + 0.84\% + 2.623\% = 5.73\%$$

0.95 U/E

### 2.3.2.4 SOLAR INVERTER P-Q CHARACTERISTICS

The capability curve for the typical solar inverter is shown in **Figure 2.3-7** below. while **Figure 2.3-8** shows the load capacity curve under different temperature conditions.

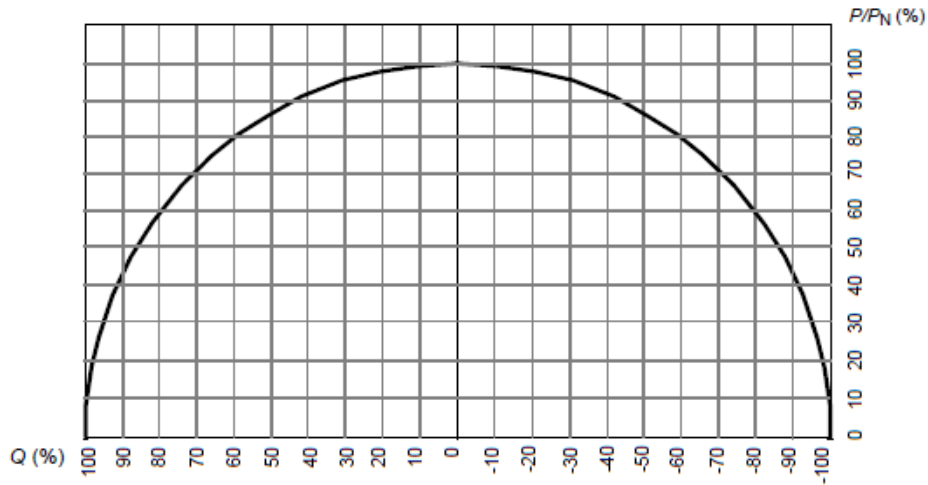


**Figure 2.3-7:** P-Q Capability Curve for PVS 980-2000 kVA

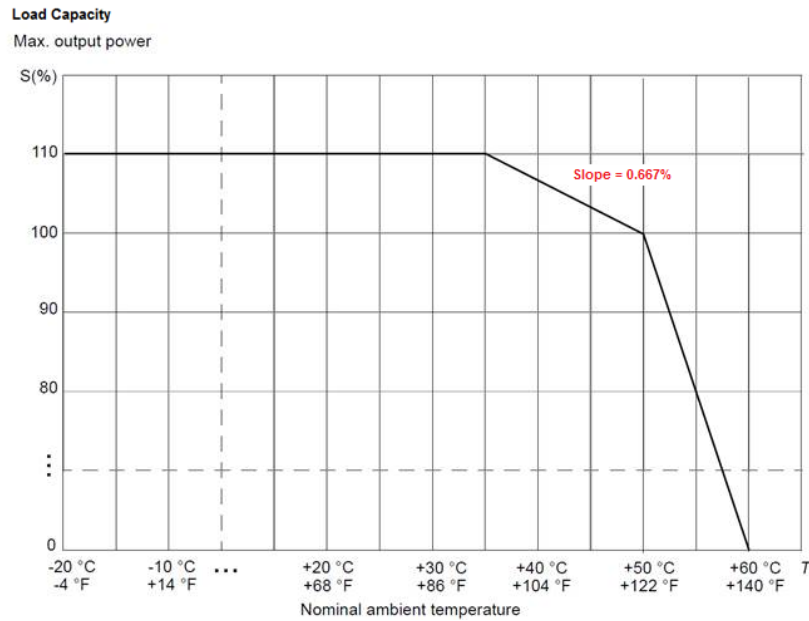


**Figure 2.3-8:** Load Capacity curve under different temperature conditions; 2066 kVA @ 45°C

From **Figure 2.3-3** , the nominal inverter terminal voltage at 0.85 PF can be calculated as below:

$$V_{inv} = 0.9 \times \left(1 + \frac{\Delta V}{100}\right) \times V_n$$

$$V_{inv} = 0.9 \times \left(1 + \frac{11}{100}\right) \times V_n = 0.99 \times V_n \approx 1 \times V_n$$

The required apparent power S per inverter and at 45°C

$$S_{inverter} = 1 \times S_n = 1 \times 2066 = \mathbf{2,066 \text{ kVA}}$$

Since the total required active power at the inverter terminals was calculated to be

$$\begin{aligned} P_{required @ inverters terminal} &= P_{@ PoCC} \times (1 + \Delta P_{losses} \%) = 200 \text{ MW} \times (1 + 0.075) \\ &= 215 \text{ MW} \end{aligned}$$

Assuming 120 central solar inverters, then the power required from each inverter will be

$$P_{inverter} = \frac{215 \text{ MW}}{120} = \mathbf{1,792 \text{ kW}}$$

Based on above the power factor to be set for each inverter will be

$$PF = \frac{P}{S} = \frac{1,792 \text{ kW}}{2,066 \text{ kVA}} = \mathbf{0.867}$$

The P-Q Capability Assessment considering the resistance of the power transformers, resistance and reactance of the MV power cables, is listed in **Errore. L'origine riferimento non è stata trovata..**

**Table 2.3-7: P-Q Capability Assessment**

Conditions at PoCC	Conditions at inverter terminals	Inverter capability
$V_{PoCC} = 0.9 \times V_n$	$V_{inv} = 1 \times V_n$	$S_{max} = 2,066 \text{ kVA}$
$\text{Cos}(\varphi)_{PoCC} = 0.85 \text{ Over Excited}$	$\text{Cos}(\varphi)_{inv} = \mathbf{0.867} \text{ Over Excited}$	$P_{max} = 1,792 \text{ kW}$

Using 120 x PVS980-2000 kVA, and 60 MV Step up Stations (4,000 kVA): 215MW / 120 Inverters = **1,792 kW** (Active Power is required from each inverter). By setting a continuous P.F on the inverter to **0.867**, the required active power will be achieved, and the inverter characteristics will be as follows (taking into consideration the voltage conditions and the design temperature). **Table 2.3-8** shows the inverter characteristics based on above settings.

**Table 2.3-8:** Inverter Characteristics at P.F = 0.867,  $V_{inv} = 1 \times V_n$ , Design Temp =45°C, and  $V_{PoCC} = 0.9 V_n$

<b>Inverter Characteristics at P.F = 0.867, <math>V_{inv} = V_n</math> Design Temperature = 45°C, <math>V_{PoCC} = 0.9V_n</math></b>	
Inverter Apparent Power (S) at <b>50°C</b>	2,000 kVA
Inverter Apparent Power (S) at <b>45°C</b>	2,066 kVA
Inverter Apparent Power (S) at <b>45°C and <math>1 \times V_n</math></b>	2,066 kVA
Inverter Real Power (P); Power Limit	1,792 kW
Inverter Reactive Power (Q)	1,028 kVAR

Therefore:

- P total available at inverter terminals =  $1,792 \times 120 = \mathbf{215.004 \text{ MW}}$
- Q total available at inverter terminals =  $1,028 \times 120 = \mathbf{123.360 \text{ MVAR}}$

As concluded above, the active power at PoCC has been achieved considering the 120 x PVS 980-2000 kVA, however, still the reactive power at PoCC not yet achieved. However, in order to use reactive power capabilities of the 120 x PVS 980-2000 kVA solar inverters, there are three main options:

- 1- Limiting the amount of active power delivered (**Figure 2.3-9, a**),
- 2- Oversizing the inverter (**Figure 2.3-9, b**).

The first of these options implies a reduction in the PV production and therefore, it would lead to reduced earnings for the PV system owner [39]. And the second option implies either a greater number of solar inverters than the originally required number of solar inverters or oversizing the solar inverters capacity.

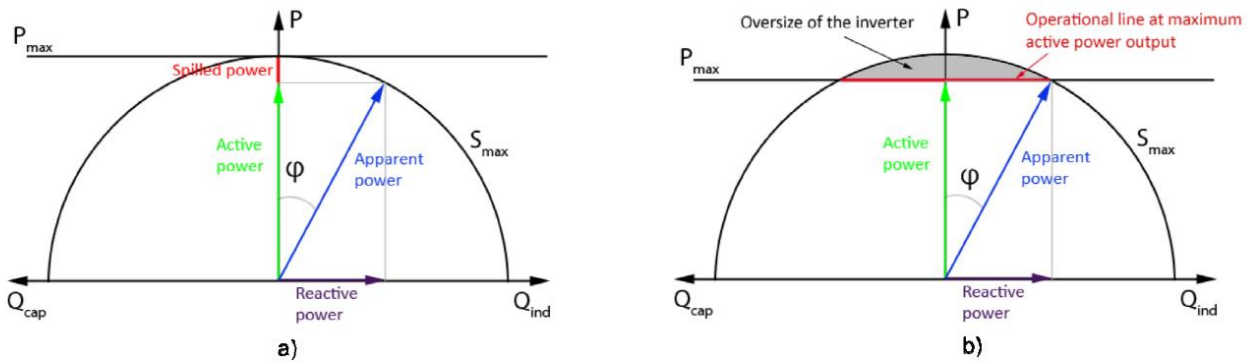


**Figure 2.3-9:** Methods of Exporting Q from Solar Inverters [14]

3- Static or dynamic shunt compensator: by these the reactive power capabilities of solar inverters in which the originally designed numbers/capacity of solar inverters are kept the same (without increasing their numbers/capacity), and at the same time the required amount of reactive power Q will be supplied and achieved at PoCC. This solution includes, in addition to the solar inverters, the operation of PV plant with predetermined reactive power (MVar) open rack MV capacitor banks that are connected in parallel to PV plant in order to meet the base reactive power load and to fulfill the required reactive power as per grid code requirements and to compensate the reactive power absorbed by the solar power transformers. **Figure 2.3-10** shows the above described.

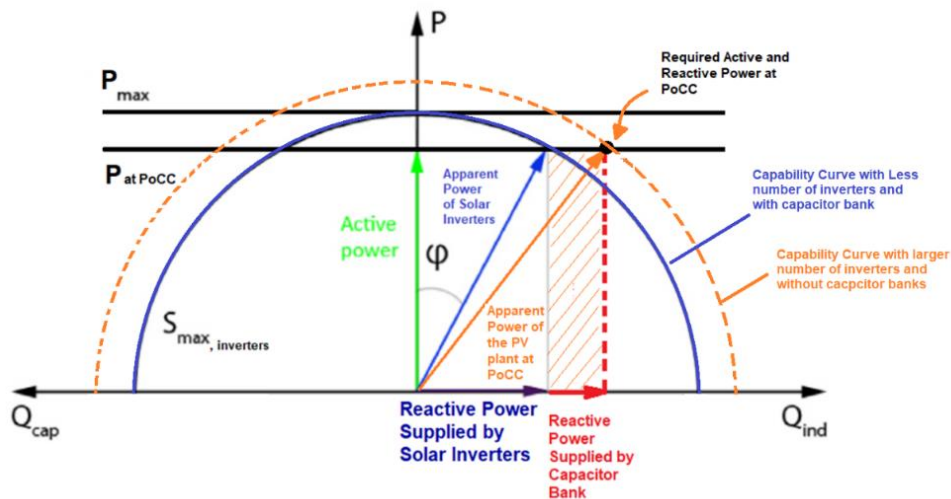


**Figure 2.3-10:** Capacitor Bank Implementation for Exporting Q to the Grid

This solution includes, in addition to the 120 x PVS 980-2000 KVA solar inverters, the operation of PV plant with predetermined reactive power (MVAR) open rack MV capacitor banks that are connected in parallel to PV plant in order to meet the required reactive power as per grid code requirements and to compensate the reactive power absorbed by the solar power transformers. **Figure 2.3-11** shows the above described.

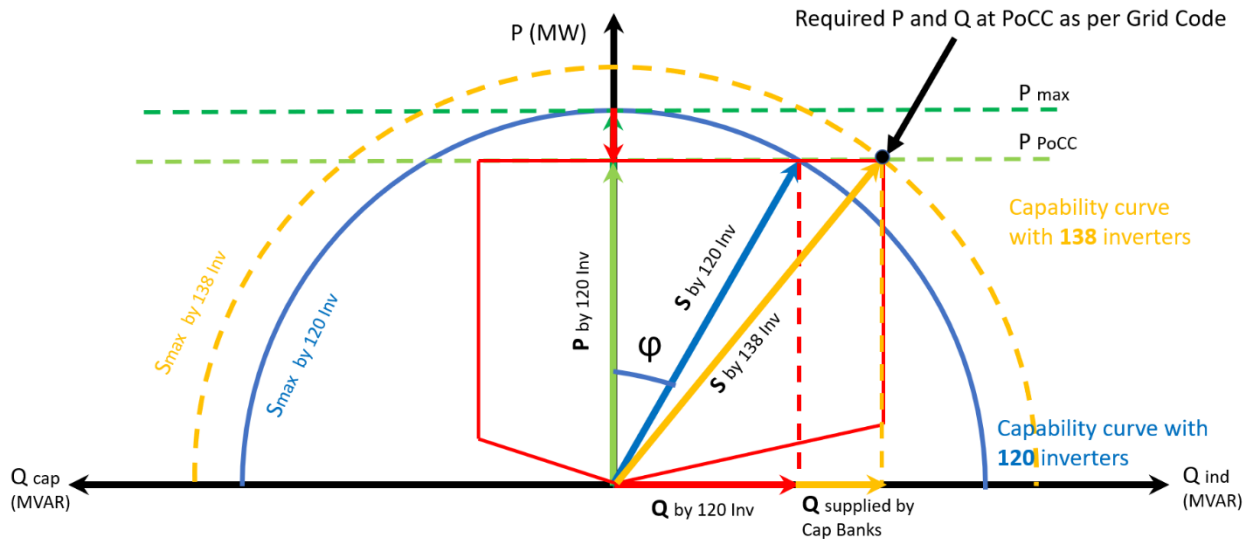


**Figure 2.3-11:** Capacitor Bank Implementation for Exporting Q to the Grid

However, the reactive power needed by the power transformers (within the PV plant) needs to be calculated in order to achieve the reactive power at PoCC, section 4.15 below discusses the calculation of the needed reactive power by power transformers

### 2.3.2.5 CALCULATION OF NEEDED REACTIVE POWER BY POWER TRANSFORMERS

The power transformers distributed all over the PV plant absorbs part of the generated reactive power from the solar inverters, and this absorbed reactive power is necessary for their operations, hence the reactive power at PoCC will be reduced by this absorbed amount.

#### 2.3.2.5.1 LV/MV Transformers Needed Reactive Power

For 4 MVAR Power Transformers (MV step-up stations 1 - 60)

$$Q_{\text{Needed by TR}} = 3 \times I^2 \times X = 3 \times (\beta I_{FL})^2 \times X = 3 \times \left( \beta \times \frac{S}{\sqrt{3} V} \right)^2 \times X\% \times \frac{V^2}{S}$$

$$Q_{\text{Needed by TR}} = \beta^2 \times S \times X\%$$

$$Q_{\text{Needed by 4MVA TR}} = (81\%)^2 \times 4,000,000 \times 6.5\% = 0.17 \text{ MVAR}$$

Total transformer LV/MV needed reactive power is: 0.17 MVAR/TR x 60 TR's = 10.2 MVAR

### 2.3.2.5.2 MV/HV Transformers Needed Reactive Power

Knowing that the  $Z_{cc}\%$  is 12.5% for MV/HV transformers, and if the three transformers are running at the same time and the total plant capacity is distributed equally between the three transformers, then the loading factor for each transformer will be  $\beta = 80.9/125 = 64.47\%$  Loading, then each transformer will consume the following reactive power:

$$Q_{\text{Needed by 125MVA TR}} = (66.47\%)^2 \times 125,000,000 \times 12.5\% = 6.545 \text{ MVAR/ Transformer}$$

Since the three transformers operating at the same time, then total MV/HV transformers reactive power consumption will be:

$$6.545 \text{ MVAR/TR} \times 3 \text{ TR's} = 19.635 \text{ MVAR}$$

The total transformer losses (MV + HV) = 10.2 MVAR + 19.635 MVAR = 29.835 MVAR

The reactive power requirements at the inverter terminals are:

$$\text{Over Excited} \Rightarrow Q = 124 \text{ MVAR} + 29.835 = 153.835 \text{ MVAR (out of inverters capability)}$$

$$\text{Under Excited} \Rightarrow Q = 66 \text{ MVAR} - 29.835 = 36.165 \text{ MVAR (within the inverters capability)}$$

### 2.3.2.6 DESIGN OF THE PREDETERMINED REACTIVE POWER (MVAR) OPEN RACK MV CAPACITOR BANKS

The rated power of the banks should be close to the maximum reactive power absorbed by the PV inverters under the following limitations [8]:

$$0.5 \times |P \tan \varphi| \leq Q_c \leq 0.02 \times S_{sc}$$

Where

$P \tan \varphi$  is a maximum reactive power absorbed by PV inverters

$S_{sc}$  is a short-circuit power at PoCC.

The absorbed reactive power happens when PF is 0.95 under-excited:

$$P.F = \cos(\varphi) = 0.95 \Rightarrow \varphi = \cos^{-1}(0.95) = 18.19^\circ$$

The reactive power can be calculated from the available parameters:

$$Q_{U/E} = P \times \tan(\varphi) = 200 \times \tan(18.19^\circ) = 66 \text{ MVAR}$$

The  $S_{sc}$  at PoCC is already given 2,634.06 MVA

$$0.5 \times |66| \leq Q_c \leq 0.02 \times 2634.06$$

$$33 \leq Q_c \leq 52.68$$

Since the total transformer losses (MV + HV) = 10.2 MVAR + 19.635 MVAR = 29.835 MVAR

Based on above the proposed size of the total capacitor bank is 30 MVAR which will be distributed at the three sections 3 x 10 MVAR

However, in contingency, the total capacitor bank is 36 MVAR which will be distributed at the three sections 3 x 12 MVAR

#### 2.3.2.6.1 Open Rack Capacitor Bank

The proposed open rack capacitor bank has parameters as per

**Table 2.3-9** Technical Parameters of Open Rack Capacitor Bank

Item	Parameter
Rated voltage kV	36
Rated frequency Hz	50

Rated output MVAR	10
Connection	Y-Y
Fuses	Internal
Lightning impulse withstand voltage kV	250
Power frequency withstand voltage kV	95

The proposed open rack mechanically switched open rack capacitor bank

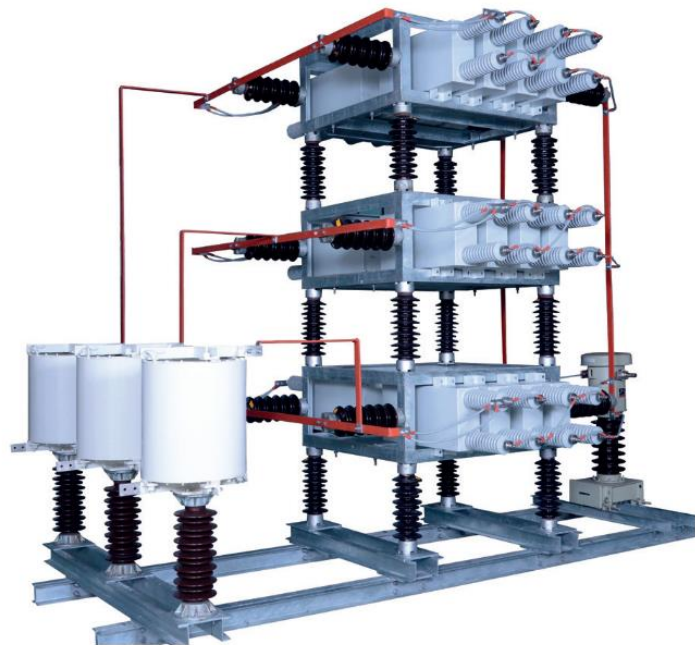


**Figure 2.3-12:** Proposed Open Rack Capacitor Bank

2.3.2.7 PV Plant Single Line Diagram Drawing with MV Capacitor Banks

The new single line diagram for the PV plant after utilizing the capacitor banks (in red) will be as shown in **Errore. L'origine riferimento non è stata trovata.**

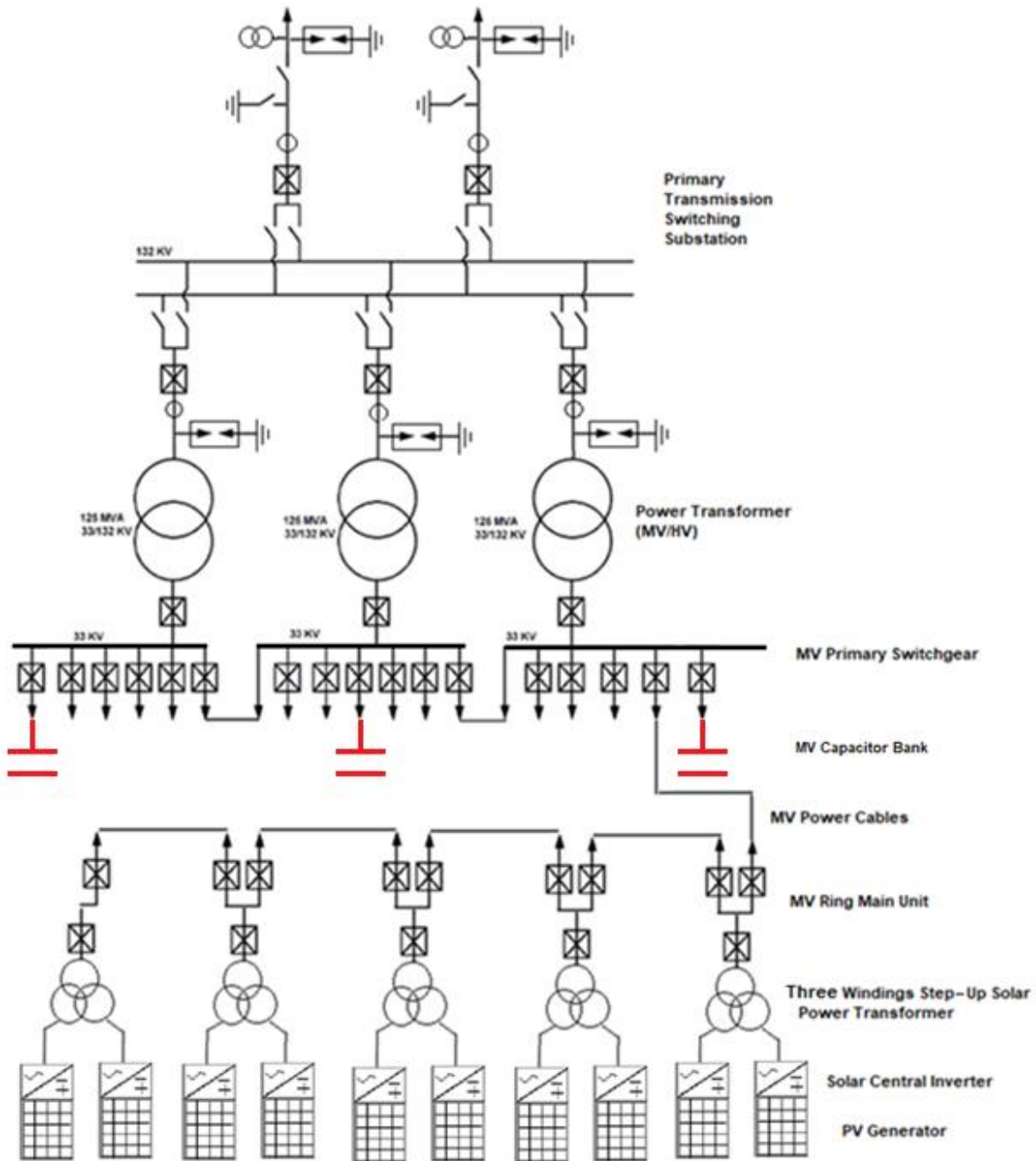
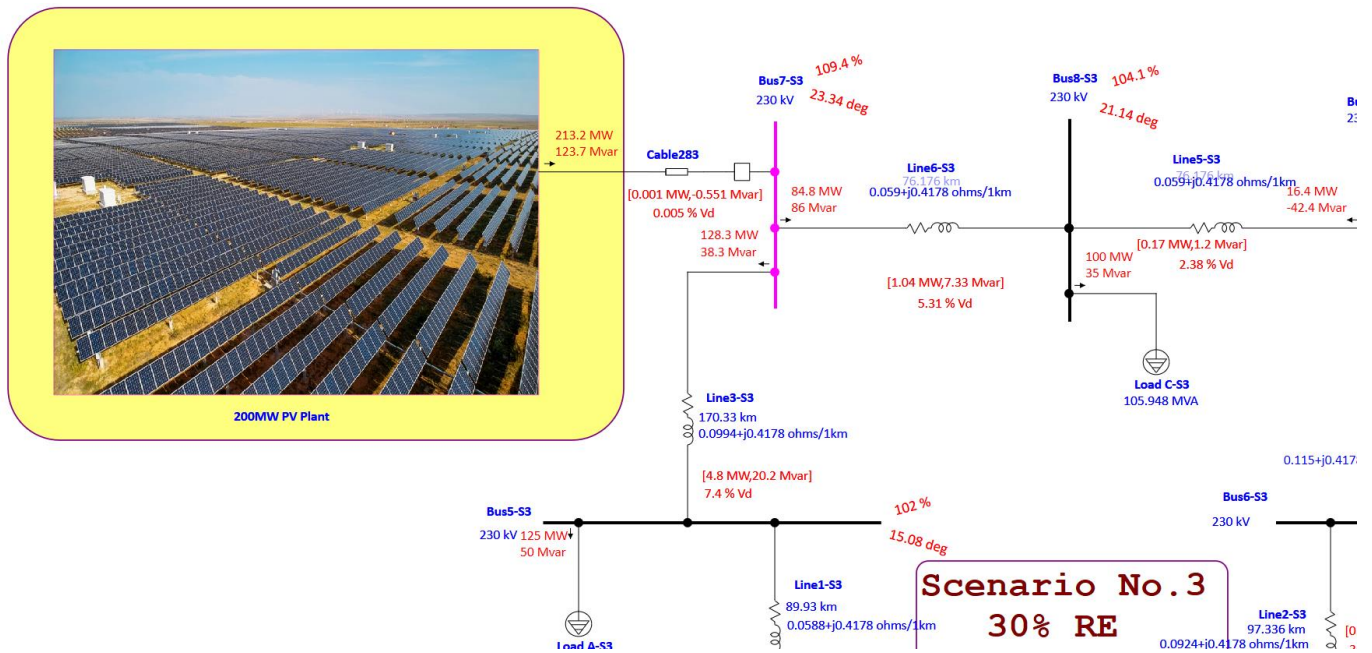


Figure 2.3-13: PV Plant Single Line Diagram Drawing with MV Capacitor Banks

### 2.3.2.8 Power Flow on ETAP Software

The same has been verified with ETAP software. **Figure 2.3-14:** Active and Reactive (P and Q) delivered by 200MW Grid Connected PV Plant shows a screen shot from ETAP one line view window for the active and reactive power injected from the PV plant at IEEE 9 bus system Bus No. 7 which is the PoCC.



**Figure 2.3-14:** Active and Reactive (P and Q) delivered by 200MW Grid Connected PV Plant

In this case study, the 200MW was built accurately started from the IRR unit till the PoCC as per the architecture **Figure 2.3-6:** PV Plant Architecture drawing., and **Figure 2.3-15:** P and Q delivered by the 200MW PV plant at the MV/HV Station

As shown above both the active and reactive power is supplied at the PoCC and this means that the grid connected PV plant comply with the grid code

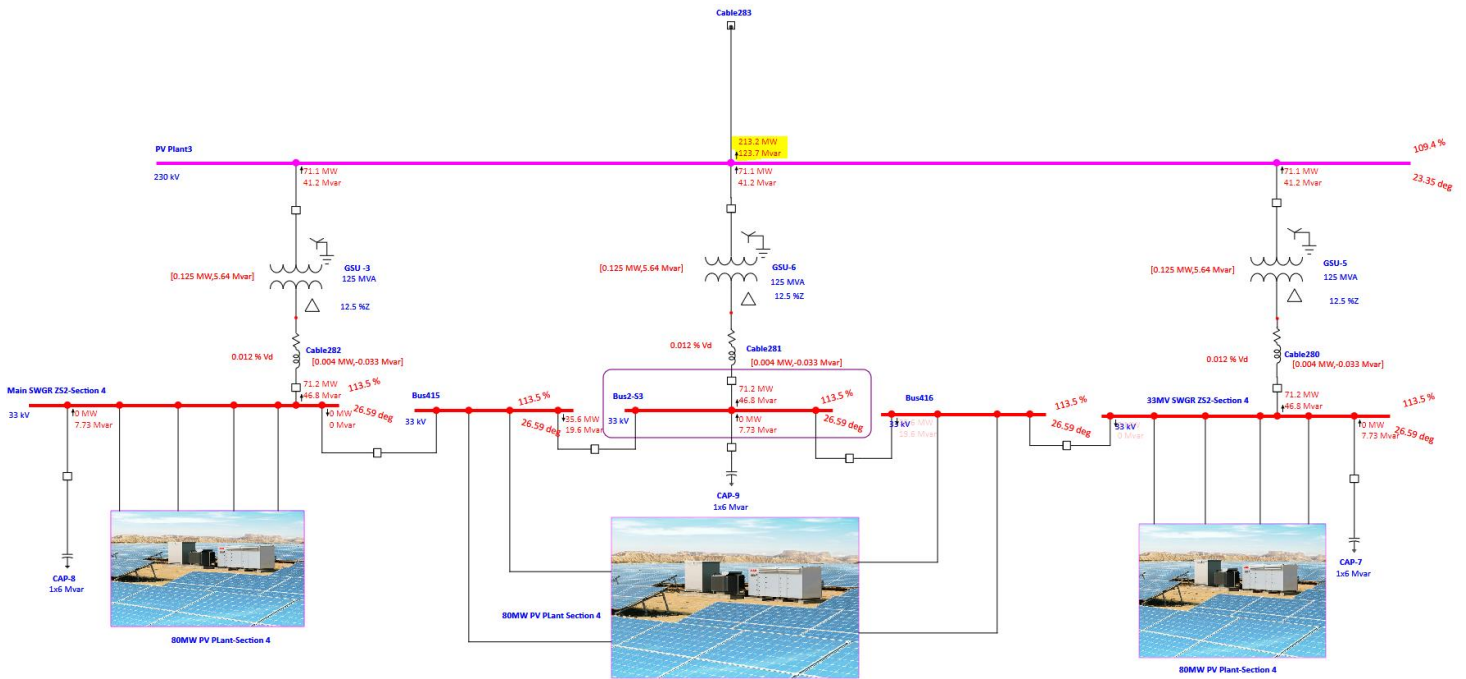


**Figure 2.3-15:** P and Q delivered by the 200MW PV plant at the MV/HV Station

### 2.3.2.9 Fault Simulation with ETAP software

Fault simulation of 3 phase fault at PoCC has been conducted. ETAP short circuit calculation is performed based on IEC 60909 as shown in **Figure 2.3-16**, This short circuit current of **3.877 kA** is the sum of the short circuit currents from the grid side (2.027 + 1.394) kA and PV side 0.461 kA

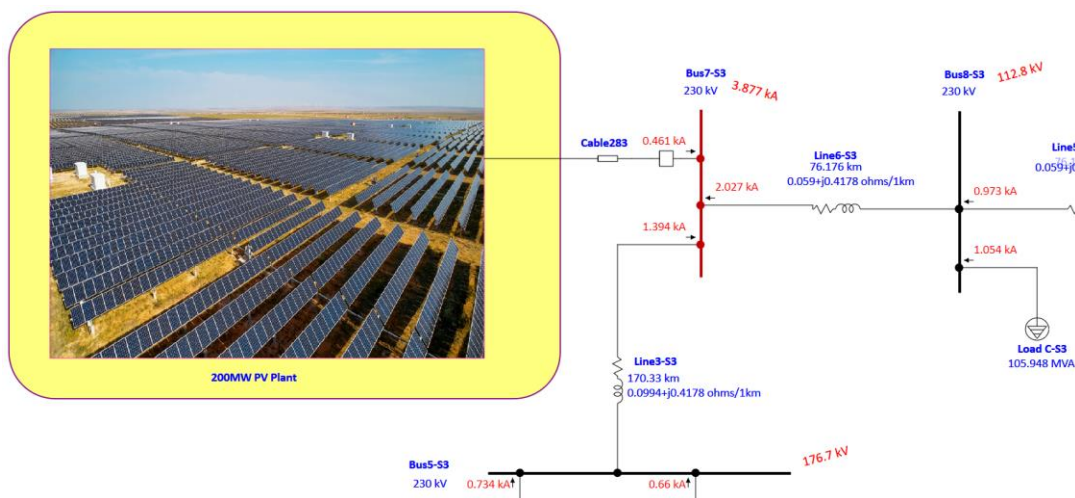


**Figure 2.3-16:** ETAP - Run 3-Phase Device Duty using IEC 60909 at PoCC Bus No.7 IEEE 90 Bus

However, if a three-phase fault current at 230kV HV Bus of the PV plant step up substation, then the fault current was 3.875 kA as shown in Figure 2.3-17

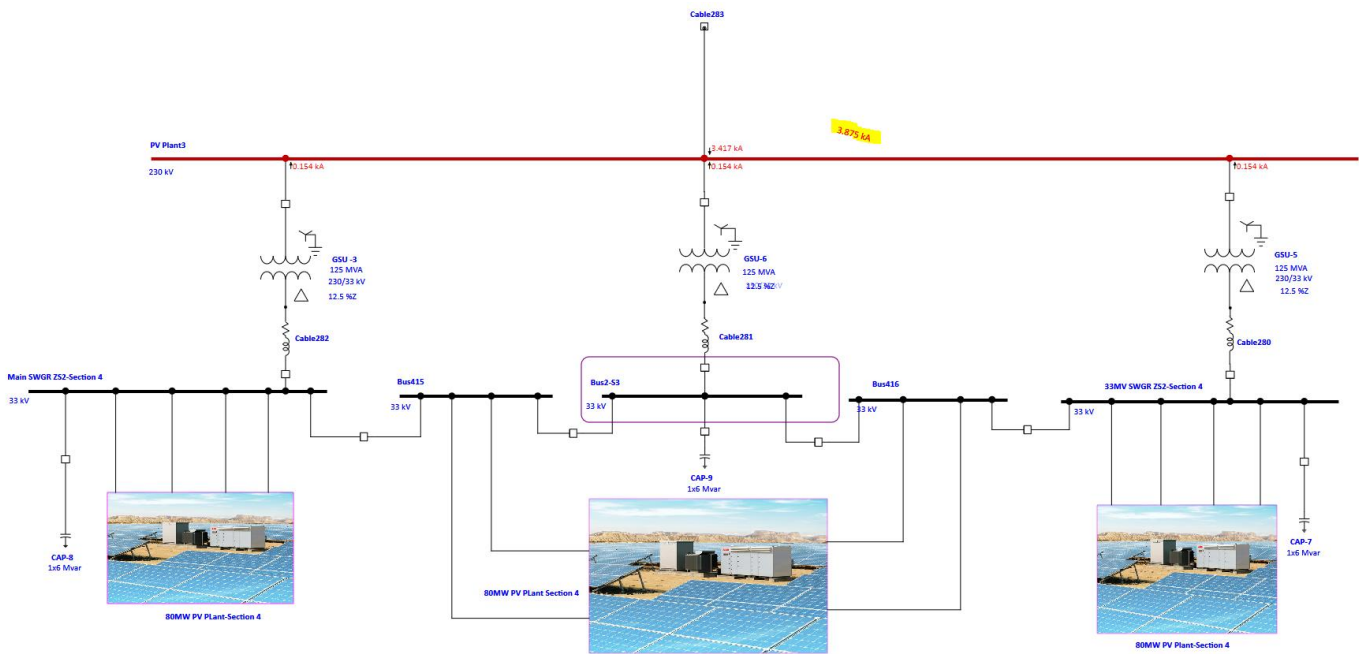


Figure 2.3-17:ETAP - Run 3-Phase Device Duty using IEC 60909 at HV Bus of Solar Step-Up station.

A transient short circuit analysis was conducted using ETAP as per IEC 61363 as shown in **Figure 2.3-18**

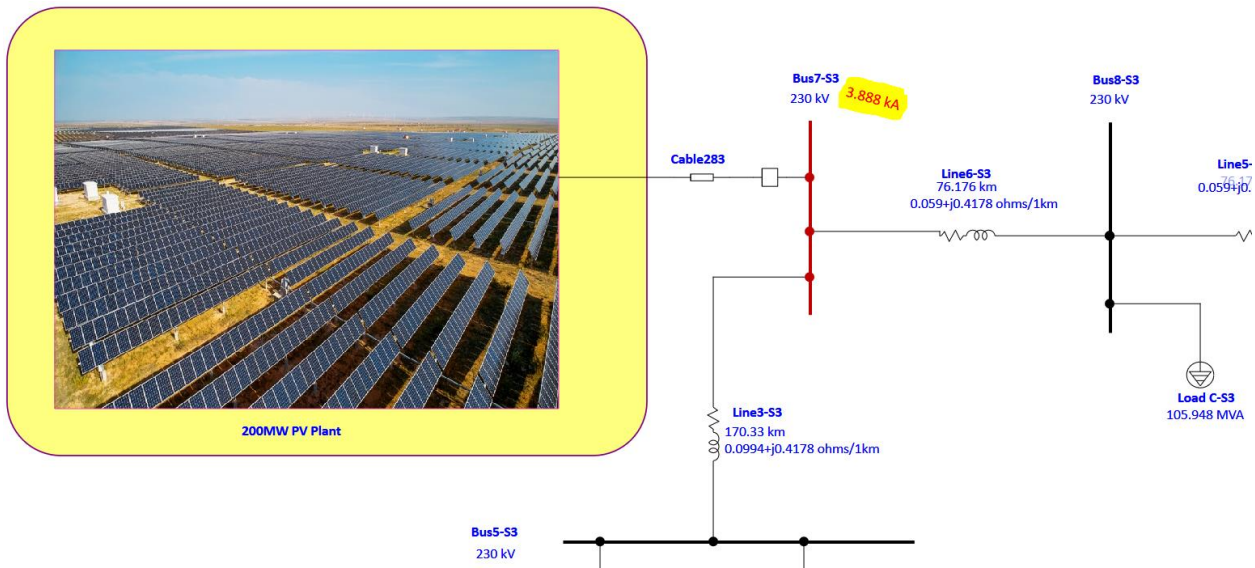
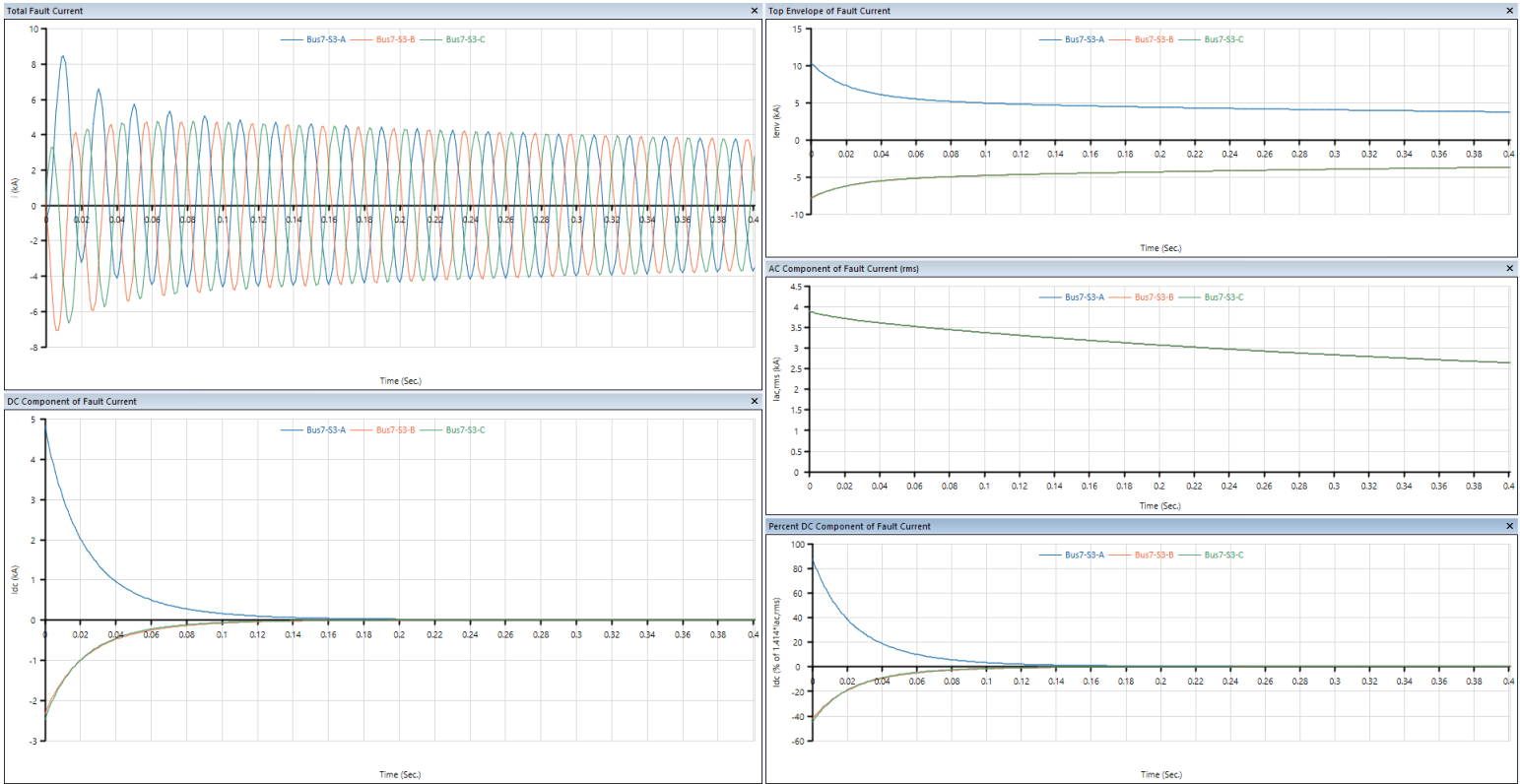


Figure 2.3-18: ETAP - Run Transient Short Circuit using IEC 61363

**Figure 2.3-19** shows the graphs generated from ETAP software upon simulating the transient short circuit current at PoCC



**Figure 2.3-19:** Three Phase Fault Current as Per IEC 61363 at PoCC (Bus 7 of IEEE 9 Bus system )

### 2.3.2.10 Harmonic Analysis at PoCC Using ETAP

In our case study, the 200MW grid connected PV plant, one harmonic model has been introduced for each solar inverter which is typical IEEE-12 pulse. accordingly harmonic analysis has been performed for each of the following cases: 120 solar inverters + 3 X 7 MVAR capacitor banks. Both time domain graph that shows the overall resultant distorted waveform, as well as the frequency domain graph for the voltage at PoCC have been drawn, and both current THD and voltage THD at PoCC have been simulated.

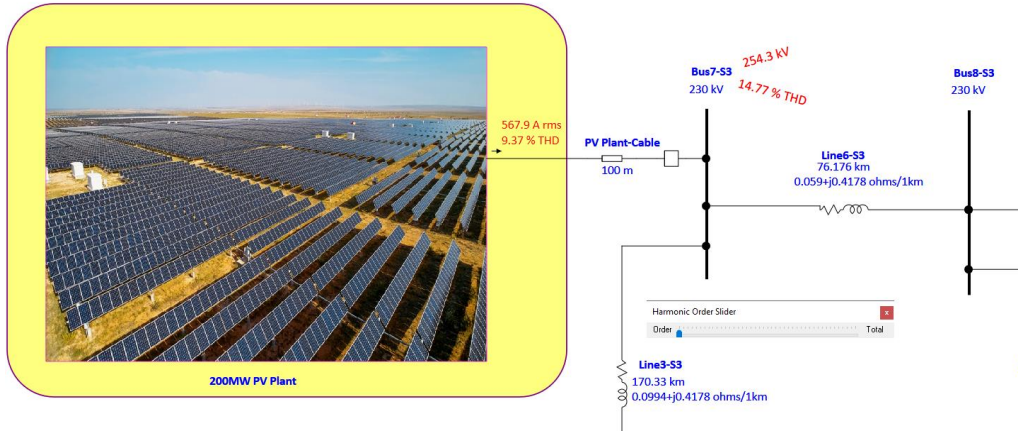


Figure 2.3-20: Voltage and Current Total Harmonic Distortion (THD) at PoCC of PV Plant

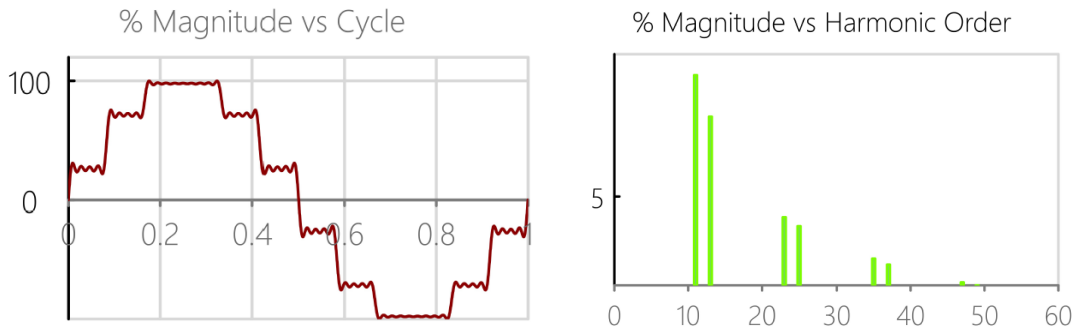


Figure 2.3-21: IEEE 12-Pulse Pre-defined Harmonic Model (Waveform and Spectrum)

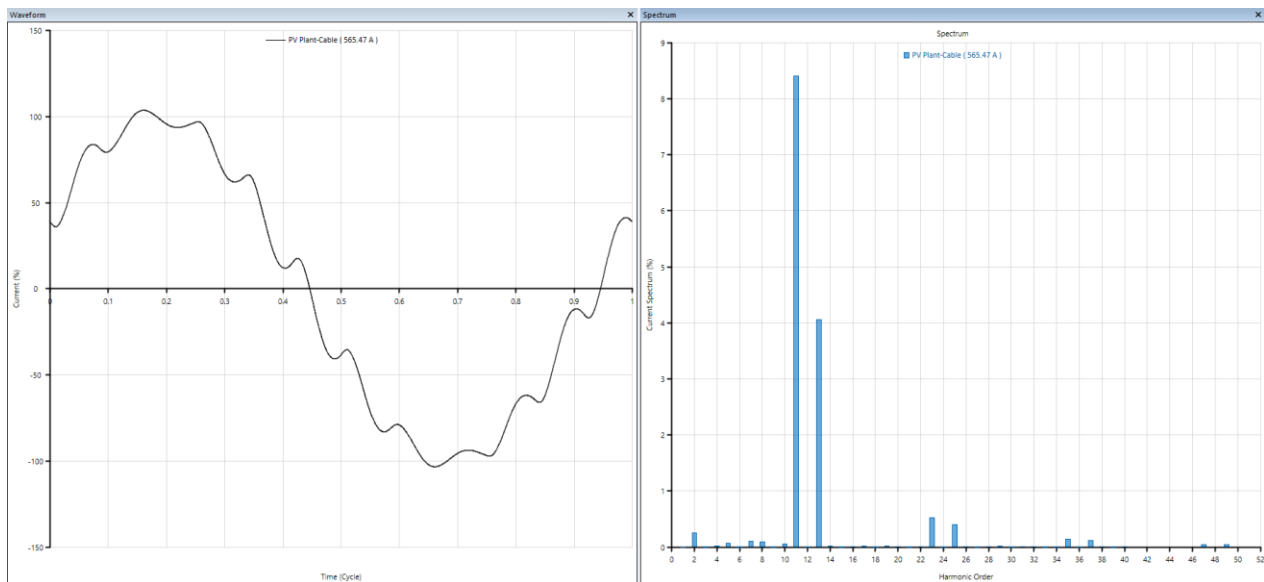


Figure 2.3-22: Current THD (%) Cable Intertie for PV plant

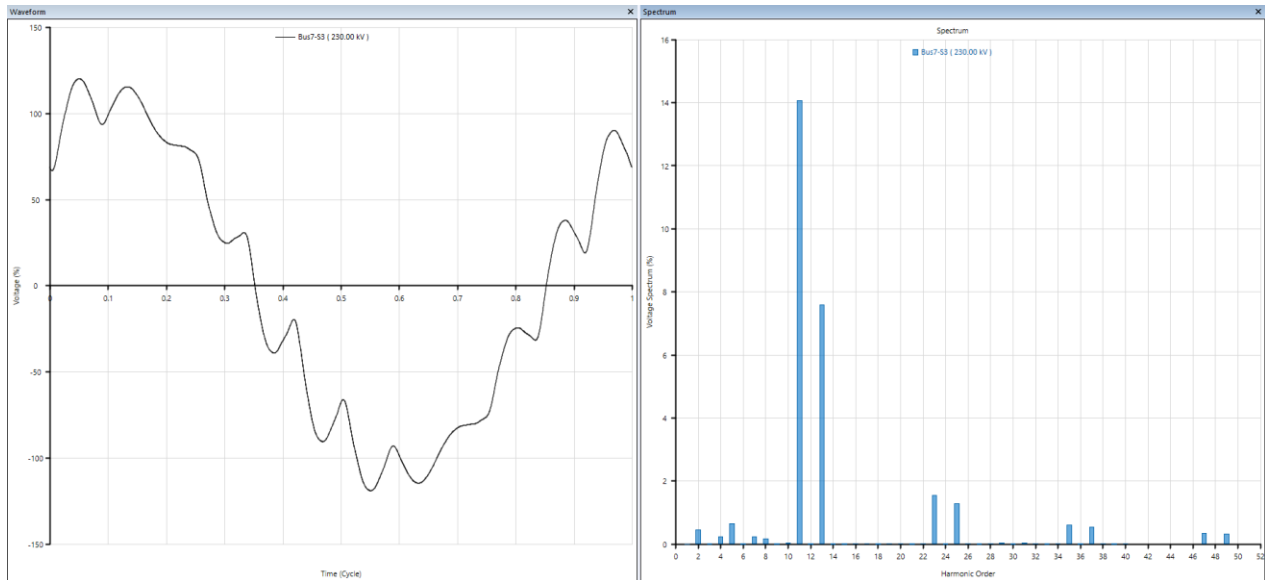


Figure 2.3-23: Voltage THD (%) Bus 7 - PoCC for PV plant

If harmonic frequency scan has been conducted, then we will notice that at 8<sup>th</sup> harmonic order, the driving point impedance.

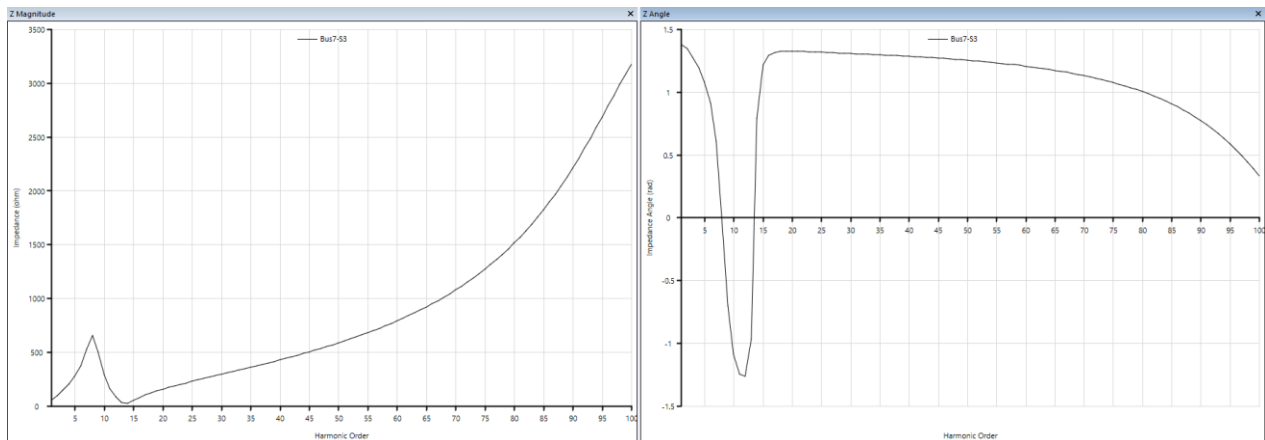
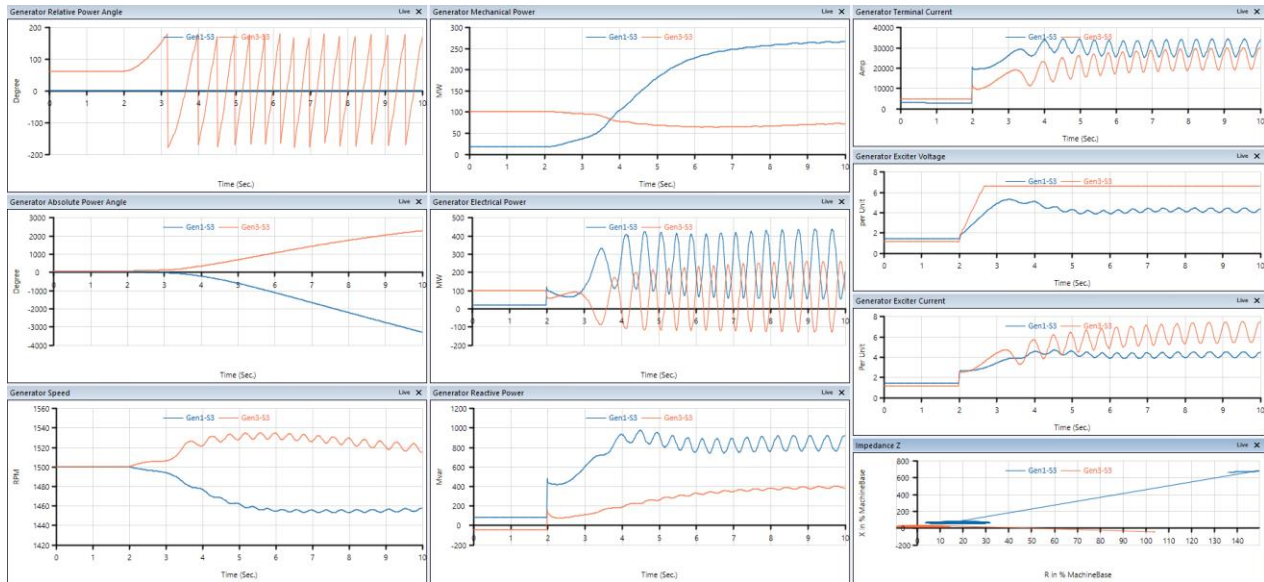


Figure 2.3-24: Harmonic Frequency Scan Z magnitude and Z angle

### 2.3.2.11 Transient Stability Using ETAP

Under this section, several types of disturbances will be introduced into the system and simulated using ETAP, and after that ability of the “modified IEEE 9 bus system with 200MW solar plant integration” is going to be examined.

#### 2.3.2.11.1 First Disturbance: Three Phase Balanced Fault at Bus No.7 without Fault Clearance



**Figure 2.3-25:** Generator Gen 1 and Gen 3 dynamic response due to 3 Phase fault at BB No.7 without fault clearance

The system lost its stability and the generators G1 and G3 lost their synchronism.

**2.3.2.11.2 First Disturbance: Three Phase Balanced Fault at Bus No.7 with Fault Clearance after 1 sec**

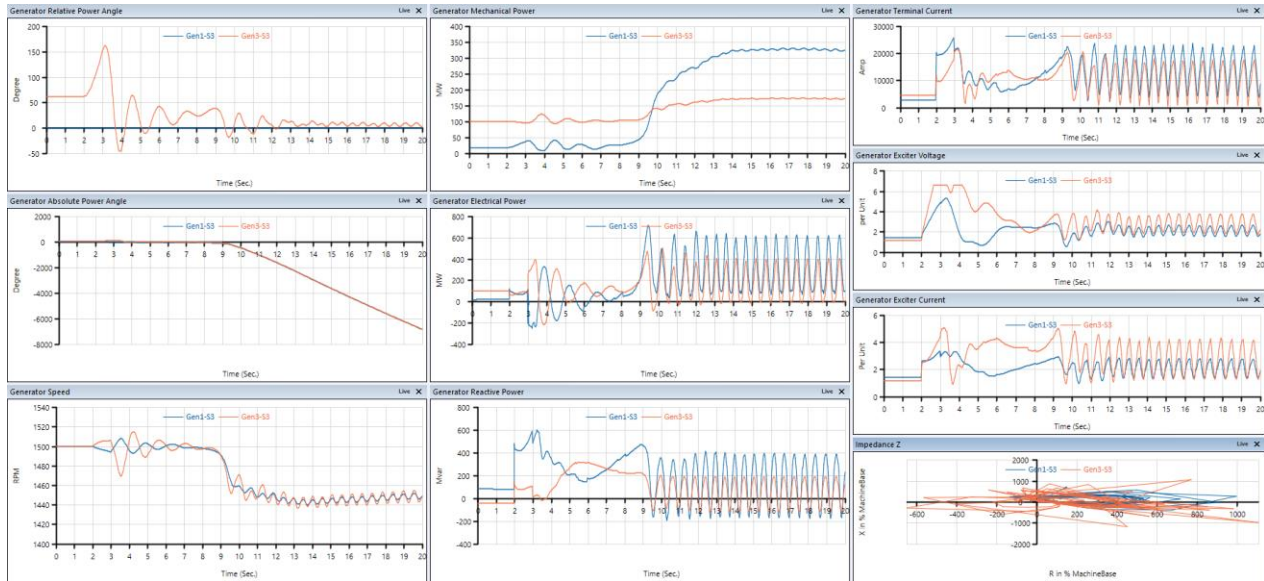


**Figure 2.3-26:**Generator Gen 1 and Gen 3 dynamic response due to 3 Phase fault at BB No.7 with fault clearance after 1 sec

Fault Clearing Time of 1 sec is not sufficient to return the system stability and forced the system back to its equilibrium.

**2.3.2.11.3 First Disturbance: Three Phase Balanced Fault at Bus No.7 with Fault Clearance after 0.5 sec**

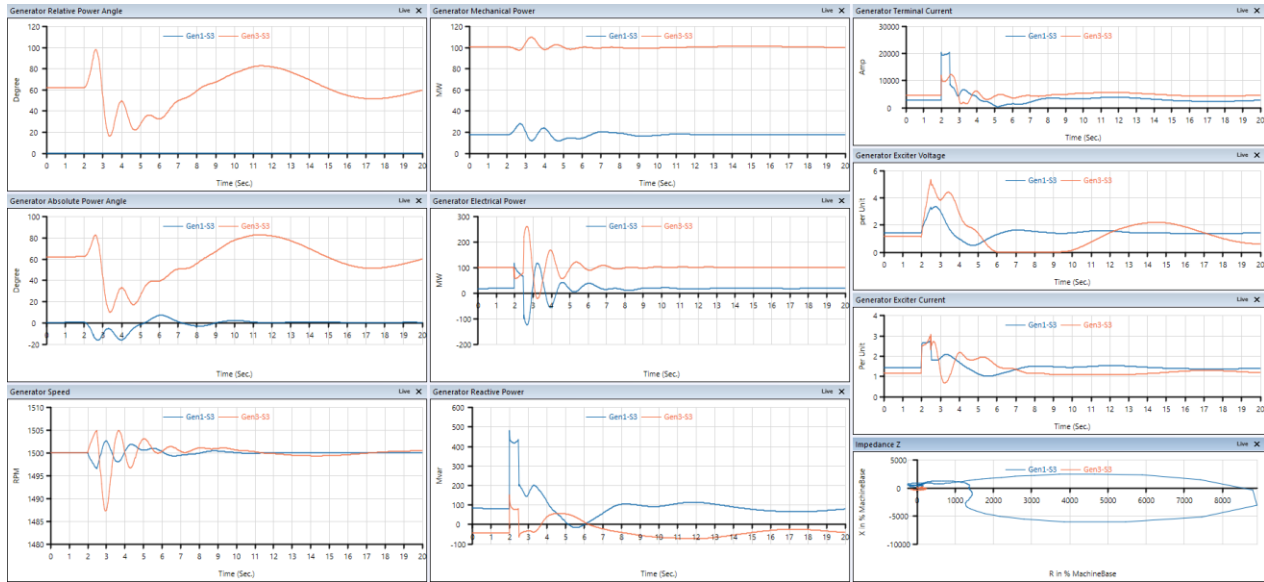


Figure 2.3-27: Generator Gen 1 and Gen 3 dynamic response due to 3 Phase fault at BB No.7 with fault clearance after 0.5 sec

**2.3.2.11.4 Second Disturbance: Three Phase Balanced Fault at Line 1 without Fault Clearance**

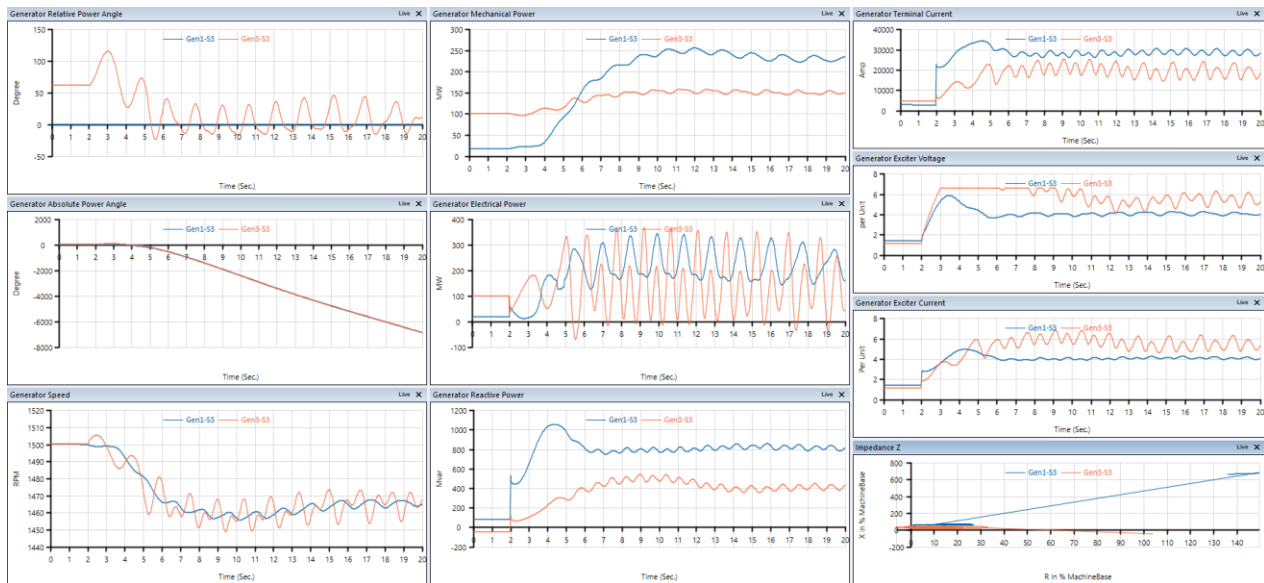


Figure 2.3-28: Generator Gen 1 and Gen 3 dynamic response due to 3 Phase fault at Line No.1 without fault clearance

### 2.3.2.11.5 Second Disturbance: Three Phase Balanced Fault at Line 1 with Fault Clearance

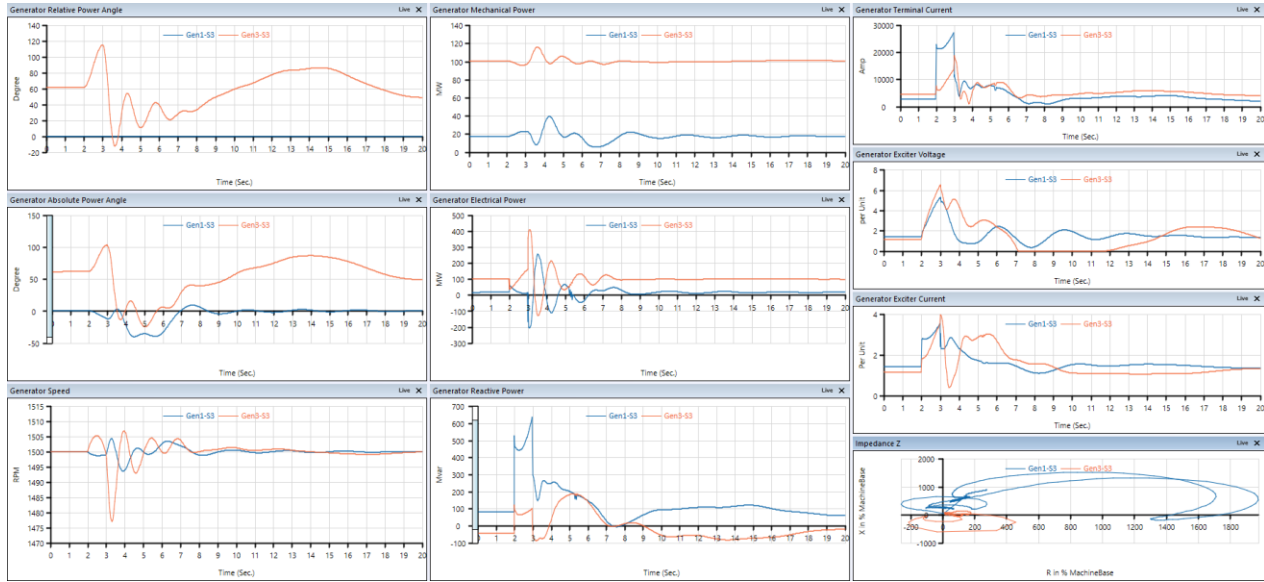


Figure 2.3-29:Generator Gen 1 and Gen 3 dynamic response due to 3 Phase fault at Line No.1 with fault clearance

### 2.3.2.11.6 Third Disturbance: Loss of 200MW PV Plant at t=5 sec

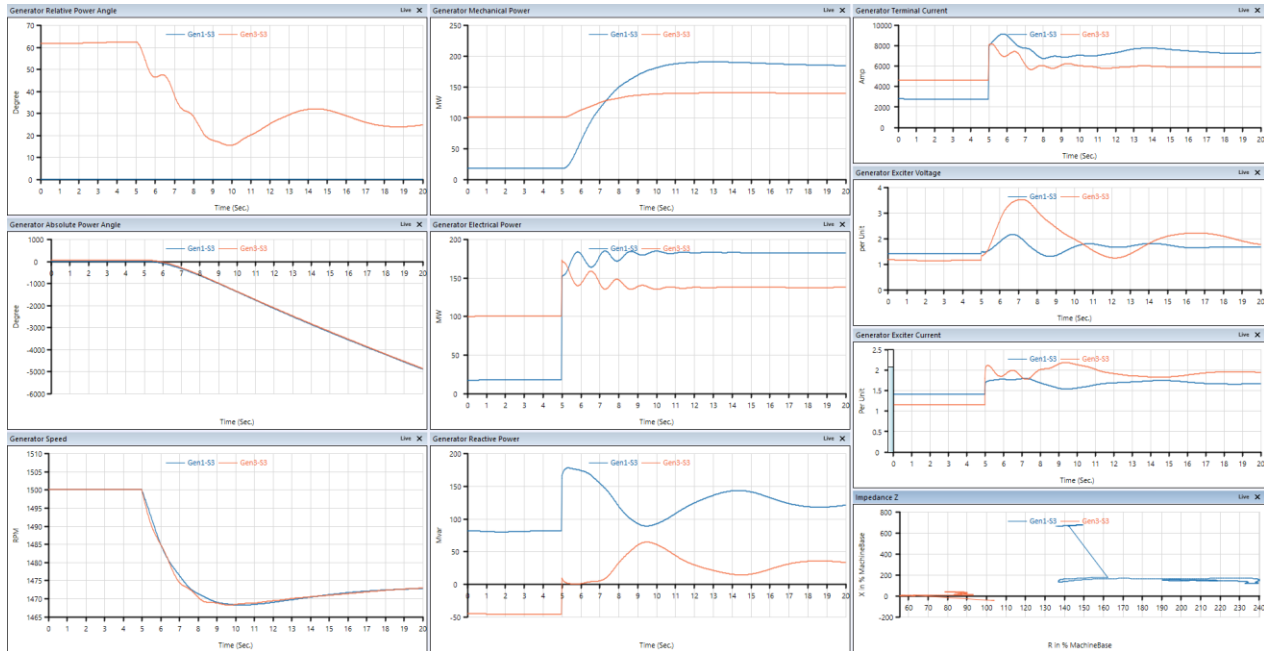


Figure 2.3-30:Generator Gen 1 and Gen 3 dynamic response due to loss of 200MW PV plant at t=5 sec

### 2.3.2.11.7 Forth Disturbance: Sudden Load Change

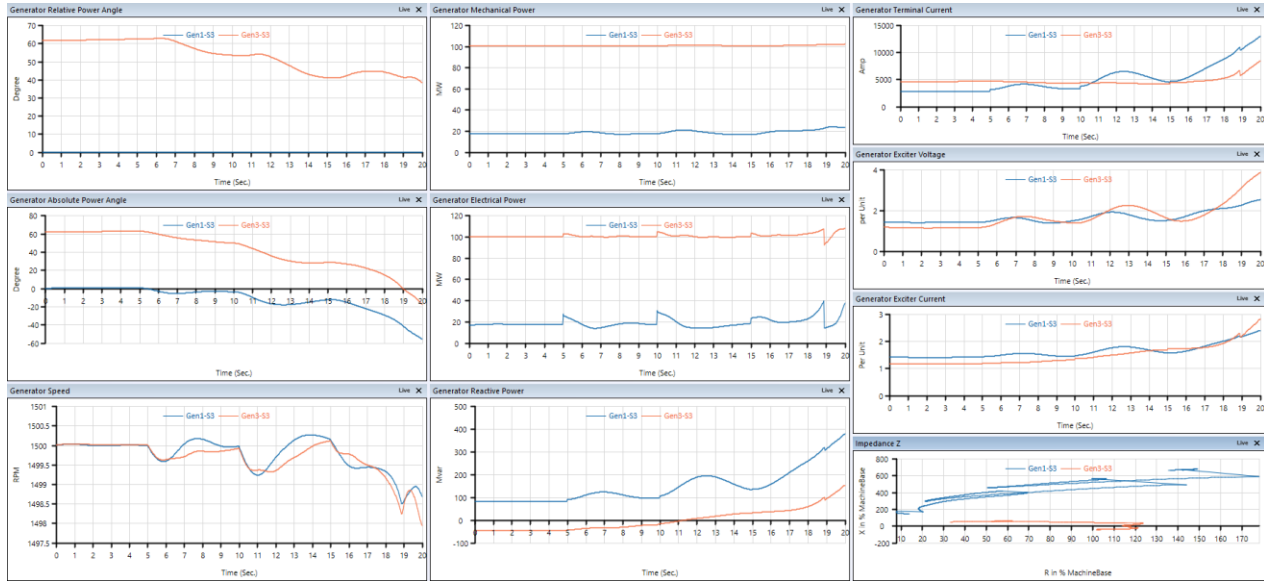


Figure 2.3-31: Generator Gen 1 and Gen 3 dynamic response due to Sudden Load Change

### 2.3.2.11.8 Fifth Disturbance: Tripping/ Disconnection of Line 4

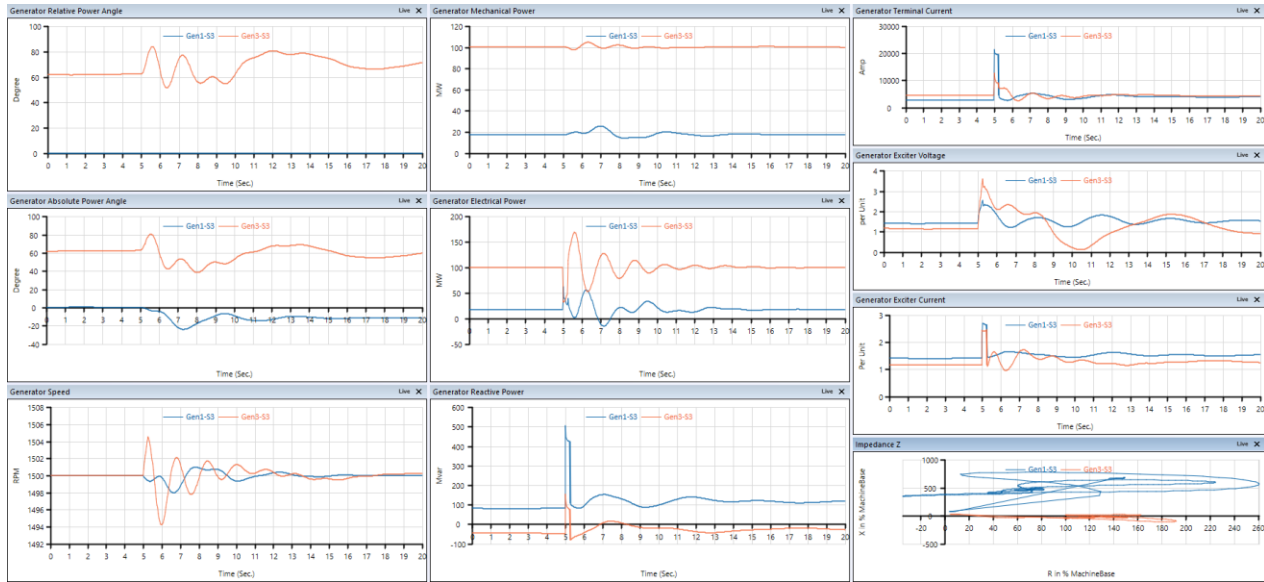


Figure 2.3-32: Generator Gen 1 and Gen 3 dynamic response due to Tripping of Line No.4

### 2.3.2.12 Voltage Stability Study Using ETAP

ETAP voltage sensitivity analysis for IEEE transmission buses and MV collection switchgear as shown in Figure 2.3-33 and Figure 2.3-34

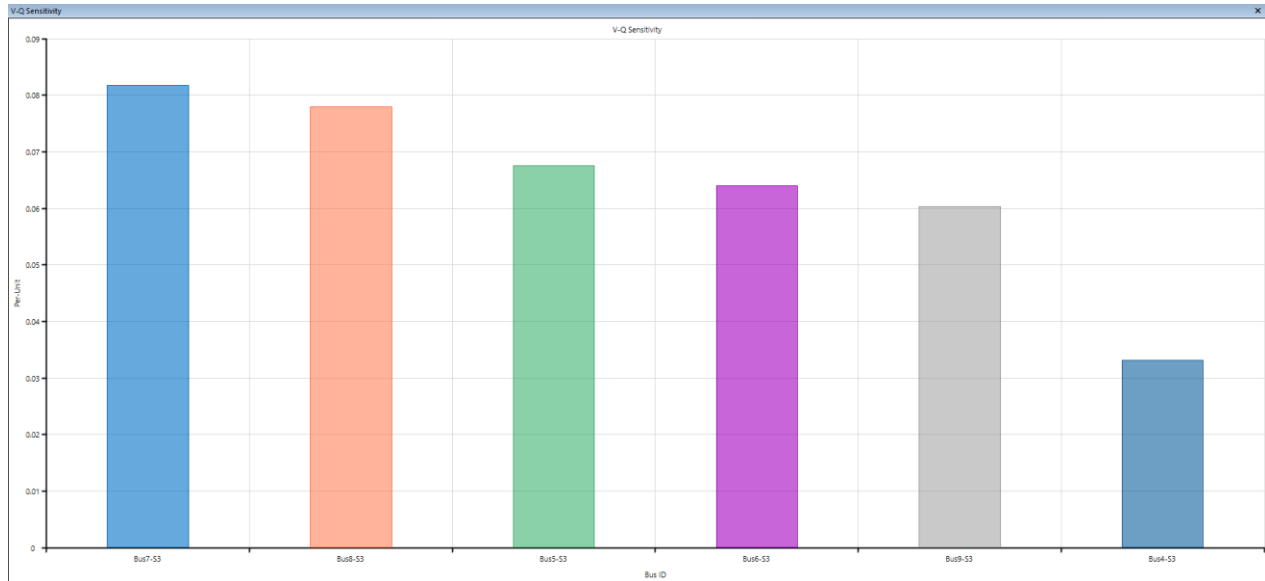


Figure 2.3-33: V-Q Sensitivity for 9 Buses of IEEE 9 Bus system

Voltage sensitivity analysis for the 33kV MV collection switchgear which is the 33kV side of PV plant

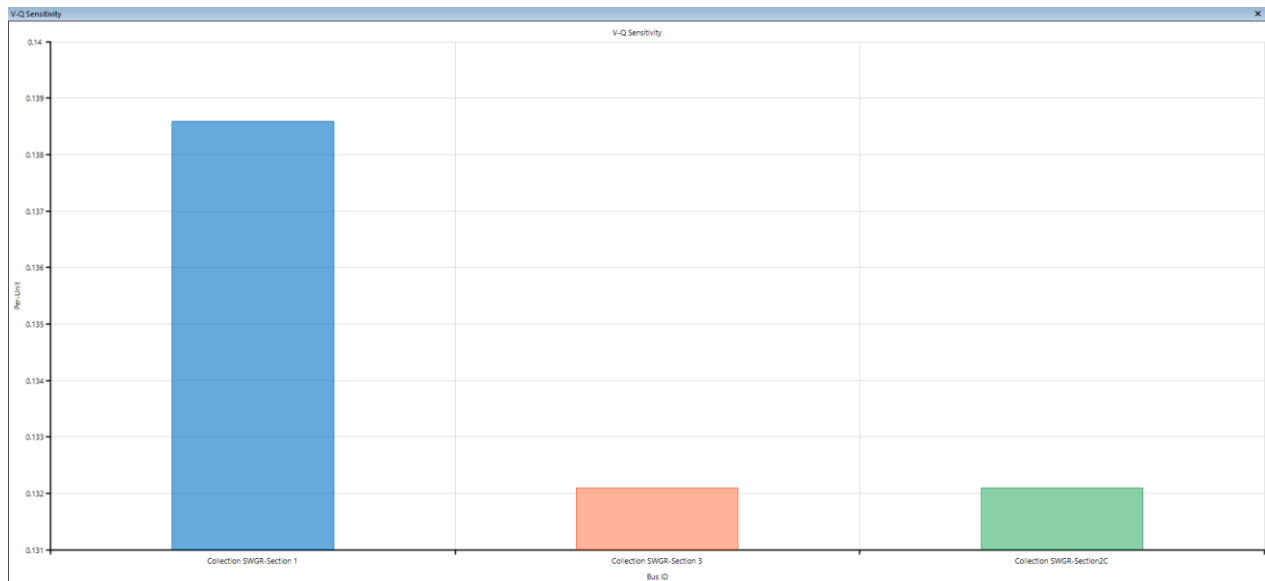


Figure 2.3-34: V-Q Sensitivity Analysis for MV PV plant collection switchgear

In below Figure 2.3-35 and Figure 2.3-36 the PV and QV for the IEEE 9 buses and PV plant MV collection switchgear

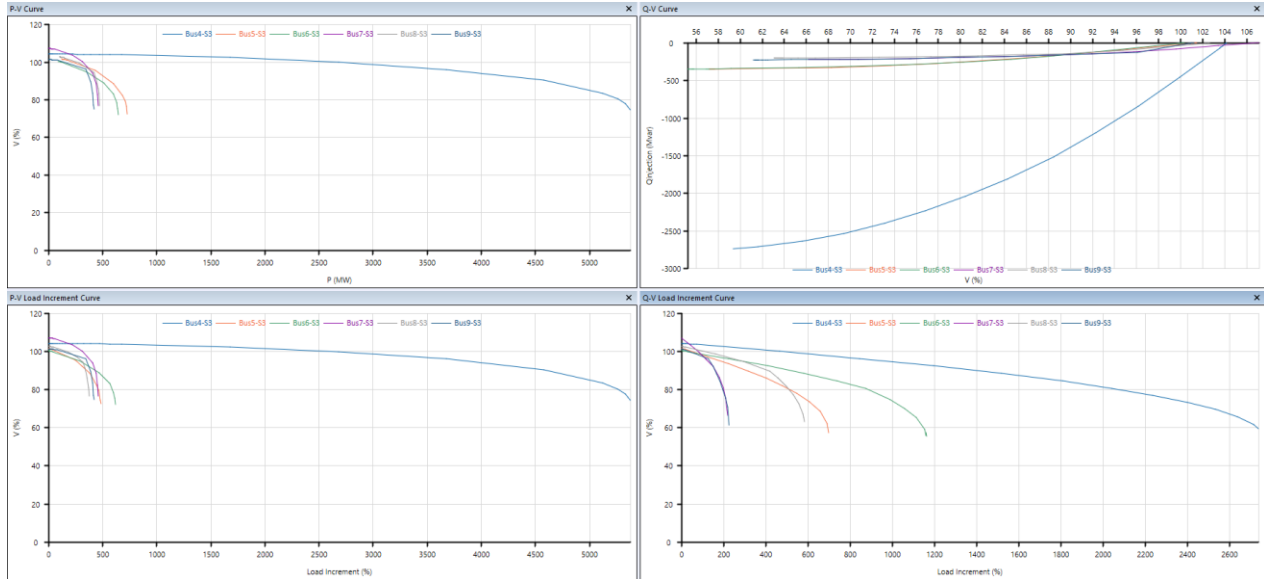


Figure 2.3-35: P-V and Q-V for 9 Buses of IEEE 9 bus system

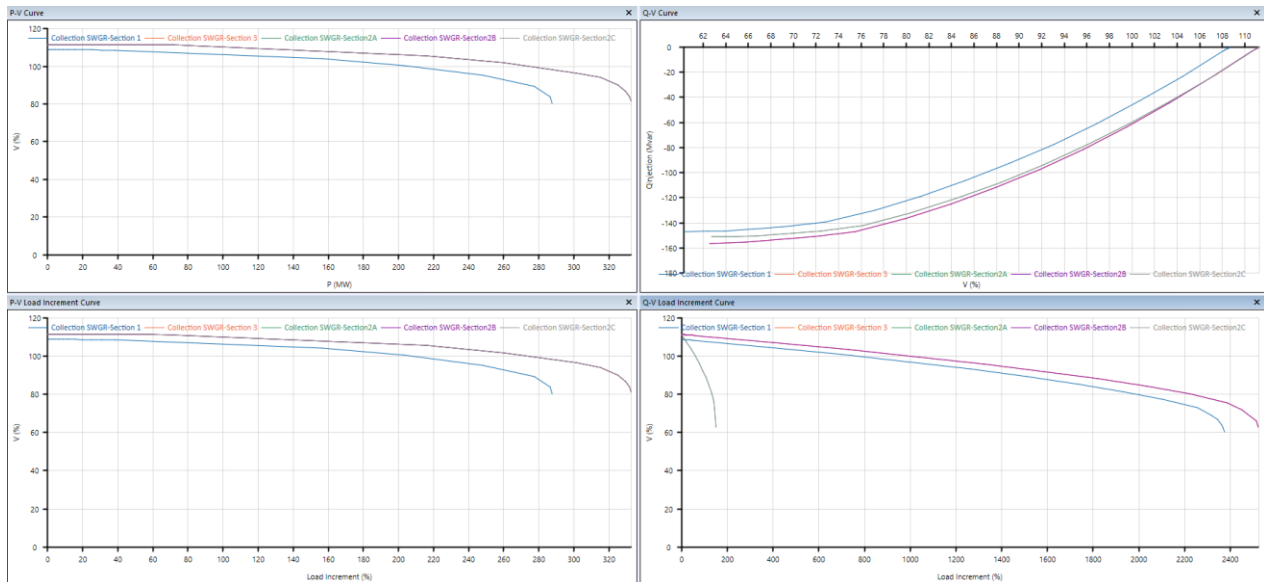
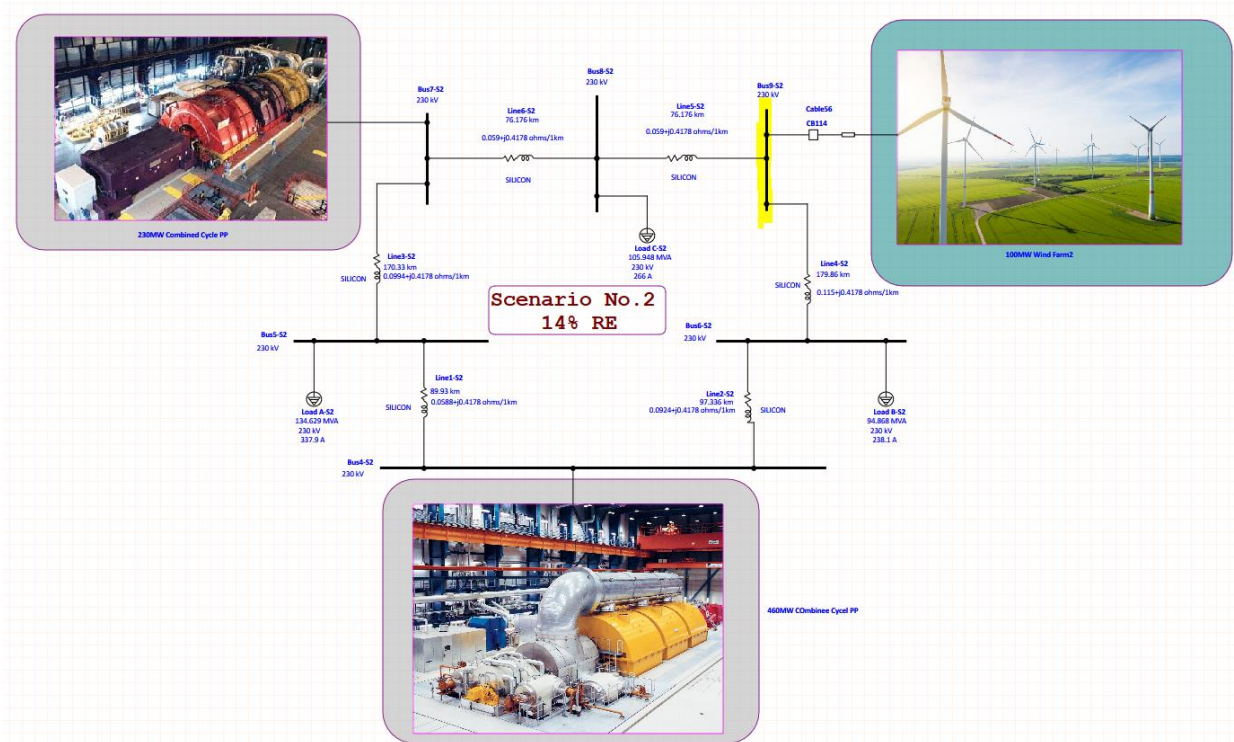


Figure 2.3-36: P-Q and Q-V curves for MV side main collection SWGR of PV plant

### 2.3.3 Grid Connected Wind Farm

The proposal is to replace SM-3 of the IEEE 9 bus system, which nominal total capacity is 125MVA, PF=85%, P=106.25MW, however it was set to deliver 100 MW at PoCC, by a 125MVA Grid connected Wind farm which PoCC at IEEE 9 bus system is Bus No.9 (highlighted in yellow) as per Scenario No.2 shown below



The proposed wind farm is with below parameters as per **Table 2.3-10**

**Table 2.3-10: Proposed Grid Connected Wind Farm Parameters**

Item	Parameter
Active Power (MW ac)	100
Voltage at PoCC (kV)	230
Design Temperature (Ambient Temperature) (°C)	-5 °C ~ + 40
Active Power Losses from inverters terminals up to the PoCC	7.5 %
Grid Reactive Power Capability- Over excited	0.85
Grid Reactive Power Capability- Under excited	0.95
Voltage Range	(0.9 -1.1) Un

WTG's (type 3 and 4) converters are traditionally designed to operate with unity power factor ( $\cos \phi = 1$ ) i.e. operational points along the vertical axis, where the maximum real power P output corresponds to the intersection with the semi-circumference. However, in order to utilize the reactive power Q capabilities of smart converters and generate reactive power Q along with active power P, there are two main options: limiting the amount of active power delivered (**Figure 2.3-9, a**), or oversizing the converters (**Figure 2.3-9, b**). Obviously, the first of these options implies a reduction in the PV production and therefore, it would lead to reduced earnings for the PV system owner [39]. And the second option implies either a greater number of WTG's than the originally required number or oversizing the WTG's.

However, there will be a third option to use static or dynamic shunt compensator and by these the reactive power capabilities of converter in which the originally designed numbers/capacity of WTG's are kept the same (without increasing their numbers/capacity), and at the same time the required amount of reactive power Q will be supplied and achieved at PoCC. This solution includes, in addition to the WTG's, the operation of wind farm with predetermined reactive power (MVar) open rack MV capacitor banks that are connected in parallel to wind farm in order to meet the base reactive power load and to fulfill the required reactive power as per grid code requirements and to compensate the reactive power absorbed by the step-up transformers. **Figure 2.3-10** shows the above described.

#### 2.3.3.1 *Wind Farm ARCHITECTURE DRAWING*

The wind farm will be designed based on a collection of WTG's, each WTG contains the electrical generator and its associated converters inside the nacelle; in Type 3 (DFIG) system a back-to-back converter is used in which the stator windings of the DFIG are directly connected to the power grid, while the rotor windings are connected to the grid through RSC, capacitor "DC Link", GSC and filter, while in Type 4 (PMSG) the generator stator terminal is connected to the generator-side converter (GSC) and the line-side converter (LSC) is connected to the grid. Generally, the number of WTG's will depend on the plant capacity and the size of turbine. Each wind turbine contains a step-up transformer that steps up the LV into MV power, and MV Ring main Unit (RMU). A group

of WTG's will be connected in series through MV RMU's connected through MV power cables, and these groups are connected to MV main switchgear in parallel, as indicated in the single line diagram **Figure 2.3-37: Wind Farm Architecture drawing**. This main MV switchgear contains the WTG incoming feeders, outgoing transformer feeder, and bus section. Hence, the power flow of the wind farm can be controlled by switching the circuit breakers on and off. From the main MV switchgear comes the step-up (MV/HV) power transformers that will step up the MV voltage into HV level ready for connection with the grid primary switching SS, which will be considered as PoCC of that wind farm.

It is assumed that the substation is designed in a manner where it divides the wind farm generation into two sections. Each section is sized to be adequate to evacuate 100 MW of generation towards the grid. In normal operation condition of each section, there are two 33/230 kV, 125 MVA power transformers operating at the same time to evacuate all the energy towards grid, while all bus couplers are open. Bus couplers are closed only in case of failure of any of the two transformers, in order to divert the power path into the grid through the remaining one transformer, which are sized to be adequate enough.

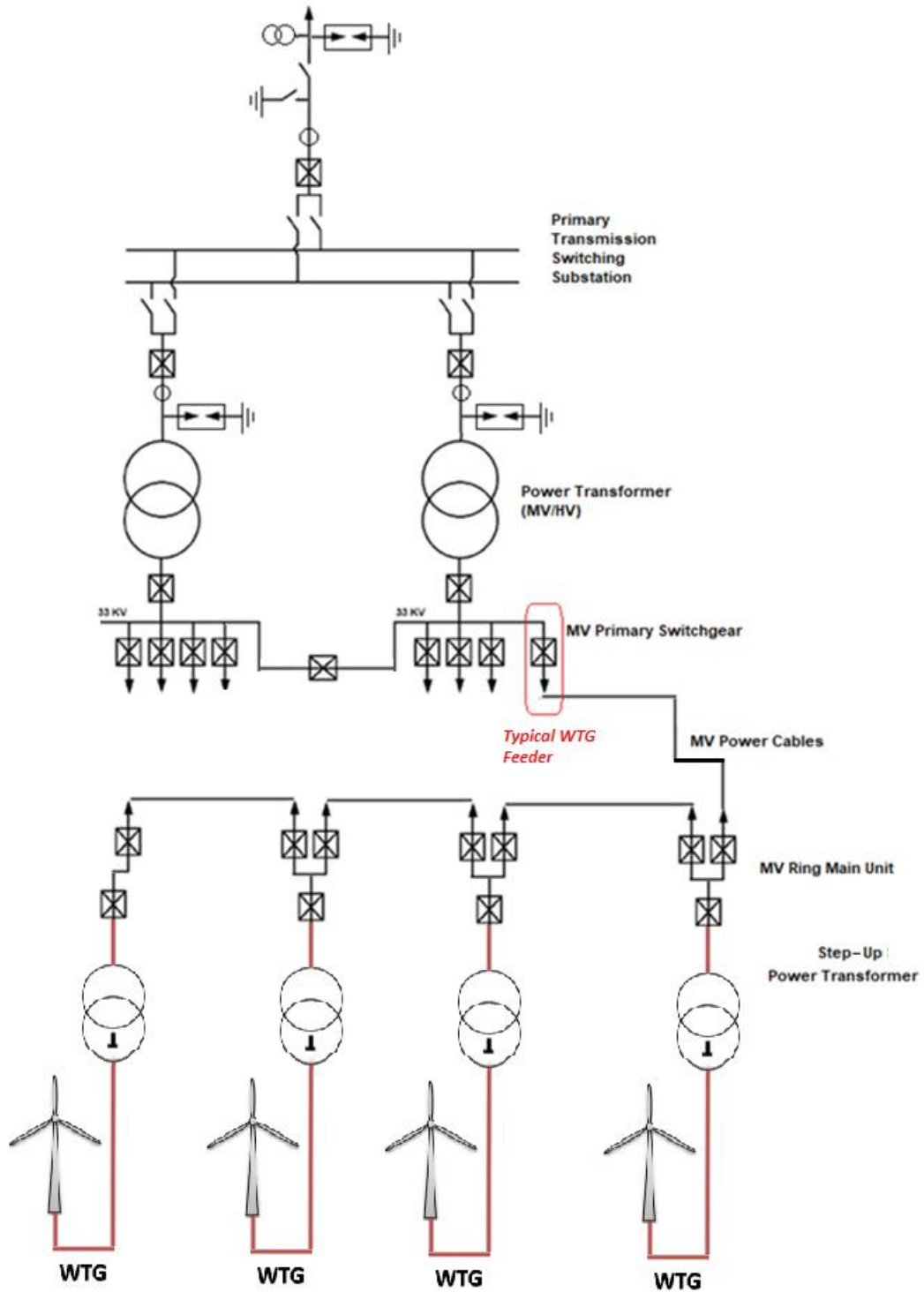


Figure 2.3-37: Wind Farm Architecture drawing.

### 2.3.3.2 ACTIVE AND REACTIVE POWER REQUIRED BY THE WTG'S

#### 2.3.3.2.1 Active Power

The required active power  $P$  that should be available at the WTG output terminals is affected by the power losses from the WTG terminals to the PoCC. Hence, in order to achieve the required active power  $P$  at the PoCC, the power losses should be considered. The power required at WTG can be calculated as below:

$$P_{\text{required at WTG terminal}} = P_{@ \text{PoCC}} \times (1 + \Delta P_{\text{losses}} \%) = 100 \text{ MW} \times (1 + 0.075) = 107.5 \text{ MW}$$

#### 2.3.3.2.2 Reactive Power

The required reactive power  $Q$  that should be available at the PoCC should comply with the grid code requirement of the grid reactive power capability which is 0.85 over excited to 0.95 under excited.

##### 2.3.3.2.2.1 0.85 Over-Excited (O/E)

$$\text{In 0.85 over-excited: } PF = \cos(\varphi) = 0.85 \Rightarrow \varphi = \cos^{-1}(0.85) = 31.78^\circ$$

The reactive power can be calculated from the available parameters in **Table 2.3-10**:

$$\begin{aligned} Q_{O/E} &= S \times \sin(\varphi) = \left( \frac{P}{\cos(\varphi)} \right) \times \sin(\varphi) = P \times \tan(\varphi) = 100 \times \tan(31.78^\circ) \\ &= 62 \text{ MVar Capacitive} \end{aligned}$$

$$Q_{O/E(PU)} = \left( \frac{62}{100} \right) = 0.62 \text{ pu}$$

##### 2.3.3.2.2.2 0.95 Under-Excited (U/E)

$$\text{In 0.95 under-excited: } PF = \cos(\varphi) = 0.95 \Rightarrow \varphi = \cos^{-1}(0.95) = 18.19^\circ$$

The reactive power can be calculated from the available parameters in **Table 2.3-10**:

$$\begin{aligned} Q_{U/E} &= S \times \sin(\varphi) = \left( \frac{P}{\cos(\varphi)} \right) \times \sin(\varphi) = P \times \tan(\varphi) = 100 \times \tan(18.19^\circ) \\ &= 33 \text{ MVar Inductive} \end{aligned}$$

$$Q_{U/E(PU)} = \left( \frac{33}{100} \right) = 0.33 \text{ pu}$$

### 2.3.3.3 VOLTAGE RISE DURING MAXIMUM REACTIVE POWER FEED

The calculation uses the same formula for the voltage drop on the lines/cable as well as on the transformer, using basic parameters like inductive/resistive components of their respective impedance, the module of the current, and the displacement angle (i.e.  $\phi$ ).

For transformers:

$$Z_T = Z_{cc}\% \times \frac{V^2}{S}$$
$$R = \frac{Z}{\sqrt{1 + (X/R)^2}}$$
$$X = R \times (X/R)$$

For a given current  $I$  and displacement angle  $\phi$  you can calculate the voltage drop/rise as follows:

$$\Delta V_T = \sqrt{3} \times I \times (R_T \times \cos\phi + X_T \times \sin\phi)$$

For lines/cables:

$$\Delta V_L = \sqrt{3} \times I \times (R_L \times \cos\phi + X_L \times \sin\phi)$$

Where  $R_L$  and  $X_L$  are the active and reactive component of the line/cable impedance.

#### 2.3.3.3.1 Power Factor 0.85

The voltage rises on the WTG terminals due reactive power injection (in maximum over excited = PF = 0.85)

**A- LV/MV Transformer – 4.5MVA, 0.690/33 KV ( $Z_{sc}\% = 7.15$ ),  $X/R=8.5$**

$$Z = Z_{cc}\% \times \frac{V^2}{S} = 0.0715 \times \frac{33,000^2}{4,500,000} = 4.235 \Omega$$

$$R = \frac{Z}{\sqrt{1 + (X/R)^2}} = \frac{4.235}{\sqrt{1 + (8.5)^2}} = 0.4948 \Omega$$

$$X = R \times (X/R) = 0.4948 \times 8.5 = 4.2 \Omega$$

$$I_{max-TR} = \frac{S}{\sqrt{3} \times V} = \frac{4,500,000}{\sqrt{3} \times 33,000} = 78.73 \text{ A}$$

$$\Delta V_T = \sqrt{3} \times I \times (R_T \times \cos\phi + X_T \times \sin\phi)$$

$$\Delta V_T = \sqrt{3} \times 78.73 \times (0.4948 \times 0.85 + 4.2 \times 0.53) = \mathbf{360.89 \text{ V}}$$

$$\Delta V_T \% = \frac{\Delta V}{V} \times 100\% = \frac{360.89}{33,000} \times 100\% = \mathbf{1.1\%}$$

### B- 33kV Power Cable

The selected 33kV power cable is 18/30 (36) kV single core Aluminum Conductor XLPE Insulated AWA, with below list of cross-sectional area in **Table 2.3-10**

**Table 2.3-11: Power Cables Voltage Drop at 0.85 PF**

From	To	Cable Size (mm <sup>2</sup> )	Number of Runs	Length per Run (meter)	R (Ω/m)	X (Ω/m)	R (Ω)	X (Ω)	Voltage Drop ΔV
1 <sup>st</sup> Block	2 <sup>nd</sup> Block	95	1	615	0.000164	0.000128	0.58	0.45	19
2 <sup>nd</sup> Block	3 <sup>rd</sup> Block	155	1	1042	0.000164	0.000128	0.53	0.41	26.9
3 <sup>rd</sup> Block	4 <sup>th</sup> Block	300	1	676	0.000125	0.000121	0.44	0.43	24.9
4 <sup>th</sup> Block	Connection Point	300	2	1906	0.0000625	0.0000605	0.79	0.76	33.6
Total voltage drops at 33kV side at 0.85 PF as per the results from ETAP simulation, Annex K									<b>180V LL</b>

$$R = R_{\Omega/Km} \times L_{km}$$

$$X = X_{\Omega/Km} \times L_{km}$$

$$I_{max-TR} = \frac{S}{\sqrt{3} \times V} = \frac{4,500,000}{\sqrt{3} \times 33,000} = 78.73 \text{ A}$$

injected in each block

$$\Delta V_L = \sqrt{3} \times I \times (R_L \times \cos\phi + X_L \times \sin\phi)$$

$$\Delta V_L \% = \frac{\Delta V}{V} \times 100\% = \frac{180.826}{33,000} \times 100\% = \mathbf{0.548\%}$$

**C- MV/HV Transformer – 100MVA, 33/230 KV (Zs.c% = 12%), X/R=43.211**

$$Z = Z_{cc}\% \times \frac{V^2}{S} = 0.12 \times \frac{230,000^2}{100,000,000} = 63.48 \Omega$$

$$R = \frac{Z}{\sqrt{1 + (X/R)^2}} = \frac{63.48}{\sqrt{1 + (43.211)^2}} = 1.4686 \Omega$$

$$X = R \times (X/R) = 1.468 \times 43.211 = 63.43 \Omega$$

$$I_{max-TR} = \frac{S}{\sqrt{3} \times V} = \frac{\sqrt{P^2 + Q^2}}{\sqrt{3} \times V} = \frac{\sqrt{100,000,000^2 + 62,000,000^2}}{\sqrt{3} \times 230,000} = 295.35 A$$

Assuming that the current is evenly divided between the transformers (3 x 125 MVA; which are running in parallel) = 295.35 / 2 = **147.675** Amps (for each transformer).

$$\Delta V_T = \sqrt{3} \times I \times (R_T \times \cos\varphi + X_T \times \sin\varphi)$$

$$\Delta V_T = \sqrt{3} \times 147.675 \times (1.4686 \times 0.85 + 63.43 \times 0.53) = 8,918.1$$

$$\Delta V_T \% = \frac{\Delta V}{V} \times 100\% = \frac{5,707.35}{230,000} \times 100\% = \mathbf{3.87\%}$$

In conclusion, the total voltage rises equals to:

$$\Delta V_{total} = 1.1\% + 0.548\% + 3.87\% = 5.518\% \approx \mathbf{5.5\%}$$

**2.3.3.3.2 Power factor 0.95**

The voltage drops on the inverter terminals due reactive power absorption (in maximum under excited = PF =**0.95**)

**A- LV/MV Transformer – 4.5MVA, 0.690/33 KV (Zsc% = 7.15), X/R=8.5**

$$Z = Z_{cc}\% \times \frac{V^2}{S} = 0.0715 \times \frac{33,000^2}{4,500,000} = 4.235 \Omega$$

$$R = \frac{Z}{\sqrt{1 + (X/R)^2}} = \frac{4.235}{\sqrt{1 + (8.5)^2}} = 0.4948 \Omega$$

$$X = R \times (X/R) = 0.4948 \times 8.5 = 4.2 \Omega$$

$$I_{max-TR} = \frac{S}{\sqrt{3} \times V} = \frac{4,500,000}{\sqrt{3} \times 33,000} = 78.73 A$$

$$\Delta V_T = \sqrt{3} \times I \times (R_T \times \cos\phi + X_T \times \sin\phi)$$

$$\Delta V_T = \sqrt{3} \times 78.73 \times (0.4948 \times 0.95 + 4.8 \times 0.31) = \mathbf{267.01 V}$$

$$\Delta V_T \% = \frac{\Delta V}{V} \times 100\% = \frac{267.01}{33,000} \times 100\% = \mathbf{0.81\%}$$

### A- 33kV Power Cable

The selected 33kV power cable is 18/30 (36) kV single core Aluminum Conductor XLPE Insulated AWA, with below list of cross-sectional area in **Table 2.3-12**

**Table 2.3-12: Power Cables Voltage Drop at 0.95 PF**

From	To	Cable Size (mm <sup>2</sup> )	Number of Runs	Length per Run (meter)	R (Ω/m)	X (Ω/m)	R (Ω)	X (Ω)	Voltage Drop ΔV
1 <sup>st</sup> Block	2 <sup>nd</sup> Block	95	1	615	0.000164	0.000128	0.58	0.45	
2 <sup>nd</sup> Block	3 <sup>rd</sup> Block	155	1	1042	0.000164	0.000128	0.53	0.41	
3 <sup>rd</sup> Block	4 <sup>th</sup> Block	300	1	676	0.000125	0.000121	0.44	0.43	
4 <sup>th</sup> Block	Connection Point	300	2	1906	0.0000625	0.0000605	0.79	0.76	
Total voltage drops at 33kV side at 0.85 PF as per the results from ETAP simulation, Annex K									<b>957 V</b>

$$R = R_{\Omega/Km} \times L_{km}$$

$$X = X_{\Omega/Km} \times L_{km}$$

$$I_{max-TR} = \frac{S}{\sqrt{3} \times V} = \frac{4,500,000}{\sqrt{3} \times 33,000} = 78.73 A$$

injected in each block

$$\Delta V_L = \sqrt{3} \times I \times (R_L \times \cos\varphi + X_L \times \sin\varphi)$$

$$\Delta V_L \% = \frac{\Delta V}{V} \times 100\% = \frac{277.2}{33,000} \times 100\% = \mathbf{0.84\%}$$

**B- MV/HV Transformer – 100MVA, 33/230 KV (Zs.c% = 12%), X/R=43.211**

$$Z = Z_{cc}\% \times \frac{V^2}{S} = 0.12 \times \frac{230,000^2}{100,000,000} = 63.48 \Omega$$

$$R = \frac{Z}{\sqrt{1 + (X/R)^2}} = \frac{63.48}{\sqrt{1 + (43.211)^2}} = 1.4686 \Omega$$

$$X = R \times (X/R) = 1.468 \times 43.211 = 63.43 \Omega$$

$$I_{max-TR} = \frac{S}{\sqrt{3} \times V} = \frac{\sqrt{P^2 + Q^2}}{\sqrt{3} \times V} = \frac{\sqrt{100,000,000^2 + 33,000,000^2}}{\sqrt{3} \times 230,000} = 264.33 \text{ A}$$

Assuming that the current is evenly divided between the transformers (2 x 100 MVA; which are running in parallel) = 264.33 / 2 = **132.168** Amps (for each transformer).

$$\Delta V_T = \sqrt{3} \times I \times (R_T \times \cos\varphi + X_T \times \sin\varphi)$$

$$\Delta V_T = \sqrt{3} \times 132.168 \times (1.4686 \times 0.95 + 63.43 \times 0.31) = 4,820.7$$

$$\Delta V_T \% = \frac{\Delta V}{V} \times 100\% = \frac{4,820.7}{230,000} \times 100\% = \mathbf{2.1\%}$$

In conclusion, the total voltage rises equals to:

$$\Delta V_{total} = 0.81\% + 2.9\% + 2.1\% = 7.55\% \approx \mathbf{5.81\%}$$

A detailed grid impact study is required to define the exact percentage using advanced simulation tools.

#### 2.3.3.4 WTG Converter P-Q CHARACTERISTICS

The capability curve for the WTG- converter is shown in **Figure 2.3-13** below. The blue curve shows the PQ capability at 35°C while the red one shows the same at 50°C (load capacity curve under different temperature conditions).

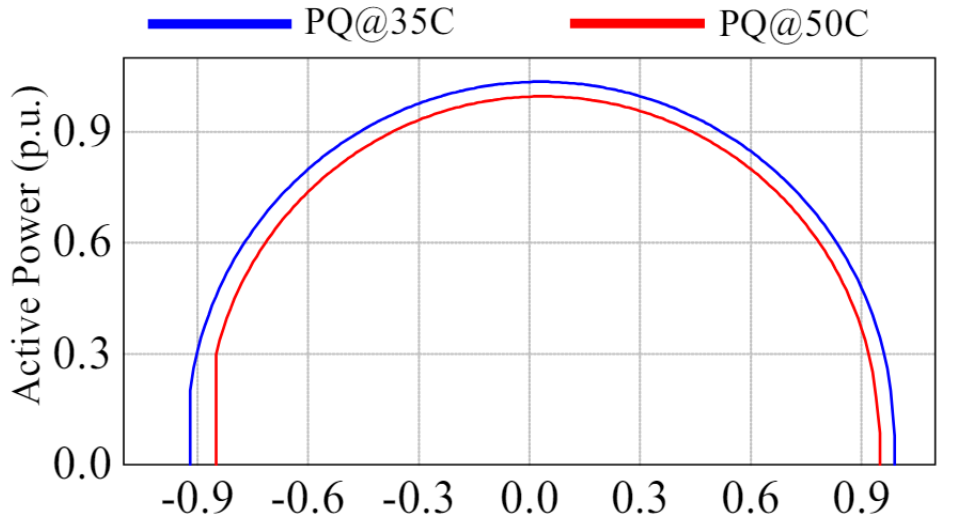


**Figure 2.3-38:** P-Q Capability Curve for WTG Converter

Nominal converter terminal voltage of the WTG at 0.85 PF is calculated as below:

$$V_{WTG} = 0.9 \times \left(1 + \frac{\Delta V}{100}\right) \times V_n$$

$$V_{WTG} = 0.9 \times \left(1 + \frac{5.5}{100}\right) \times V_n = 0.9495 \times V_n \approx \mathbf{0.95} \times V_n$$

The required apparent power S per WTG converter and at 45°C

$$S_{inverter} = \mathbf{0.95} \times S_n = 1 \times 4,941 = \mathbf{4,693.95 \text{ kVA}}$$

Since the total required active power at the WTG terminals was calculated to be

$$P_{required @ WTG} = P_{@ PoCC} \times (1 + \Delta P_{losses} \%) = 100 \text{ MW} \times (1 + 0.075) = 107.5 \text{ MW}$$

Assuming 28 Wind Turbine Generator (WTG), then the power required from each WTG will be:

$$P_{WTG} = \frac{107.5 \text{ MW}}{28} = \mathbf{3,839 \text{ kW}}$$

However, if we set each WTG at 90% generation, then the real power delivered by each WTG will be 3,780 kW, Based on above the power factor at WTG converter terminal will be

$$PF = \frac{P}{S} = \frac{3,780 \text{ kW}}{4,693.95 \text{ kVA}} = \mathbf{0.8053}$$

The P-Q Capability Assessment for the WTG is listed in **Table 2.3-13**

**Table 2.3-13:** P-Q Capability Assessment for WTG

Conditions at PoCC	Conditions at converter terminals	Converter capability
$V_{PoCC} = 0.9 \times V_n$	$V_{WTG} = 0.95 \times V_n$	$S_{max} = 4,693.95 \text{ kVA}$
$\text{Cos}(\varphi)_{PoCC} = 0.85$ Over Excited	$\text{Cos}(\varphi)_{WTG} = \mathbf{0.8053}$ Over Excited	$P_{max} = 3,780 \text{ kW}$

Using 28 x WTG-4,941.2 kVA, 0.8053 PF, 4,200kW (however it is set to deliver 90% of its generation = 90% X 4200 kW= 3,780kW), and 28 WTG's transformers (4,500 kVA), then 107.5MW / 28 WTG = **3,839 kW** (maximum active power is required from each WTG). By setting a continuous P.F on the inverter to **0.8053**, the required active power will be achieved, and the WTG characteristics will be as follows **Table 2.3-14** shows the WTG characteristics based on above settings.

**Table 2.3-14:** WTG Characteristics at P.F = 0.805,  $V_{WTG} = 0.95 \times V_n$

WTG Characteristics at P.F = 0.8053, $V_{WTG} = 0.95 \times V_n$	
WTG Apparent Power (S) at 50°C	4,941 kVA
WTG Apparent Power (S) at 50°C <u>and</u> 0.95 X $V_n$	4,639.95 kVA
WTG Real Power (P); Power Limit	3,780 kW
WTG Reactive Power (Q)	2,690 kVAR

Therefore:

- P total available at WTG terminals = 3,780 x 28 = **105.8 MW**
- Q total available at WTG terminals = 2,690 x 28 = **75.320 MVAR**

As concluded above, the active power at PoCC has been achieved considering the 28 x WTG 4200KW-4941 kVA, however, still the reactive power at PoCC not yet achieved.

As discussed earlier, in order to use reactive power capabilities of the 28 x WTG 4200KW-4941 kVA, there are three main options:

WTG's are traditionally designed to operate with unity power factor ( $\cos \phi = 1$ ) i.e. operational points along the vertical axis, where the maximum real power  $P$  output corresponds to the intersection with the semi-circumference. However, in order to utilize the reactive power  $Q$  capabilities of smart converters and generate reactive power  $Q$  along with active power  $P$ , there are three main options: limiting the amount of active power delivered (**Figure 2.3-9, a**), or oversizing the WTG and converter (**Figure 2.3-9, b**), use static or dynamic shunt compensators and by these the reactive power capabilities of converters in which the originally designed numbers/capacity of WTG's are kept the same, and at the same time the required amount of reactive power  $Q$  will be supplied and achieved at PoCC. This solution includes, in addition to the 28 x WTG's, the operation of wind farm with predetermined reactive power (MVAR) open rack MV capacitor banks that are connected in parallel to wind farm in order to meet the required reactive power as per grid code requirements and to compensate the reactive power absorbed by the step-up power transformers. **Figure 2.3-39** shows the above described.

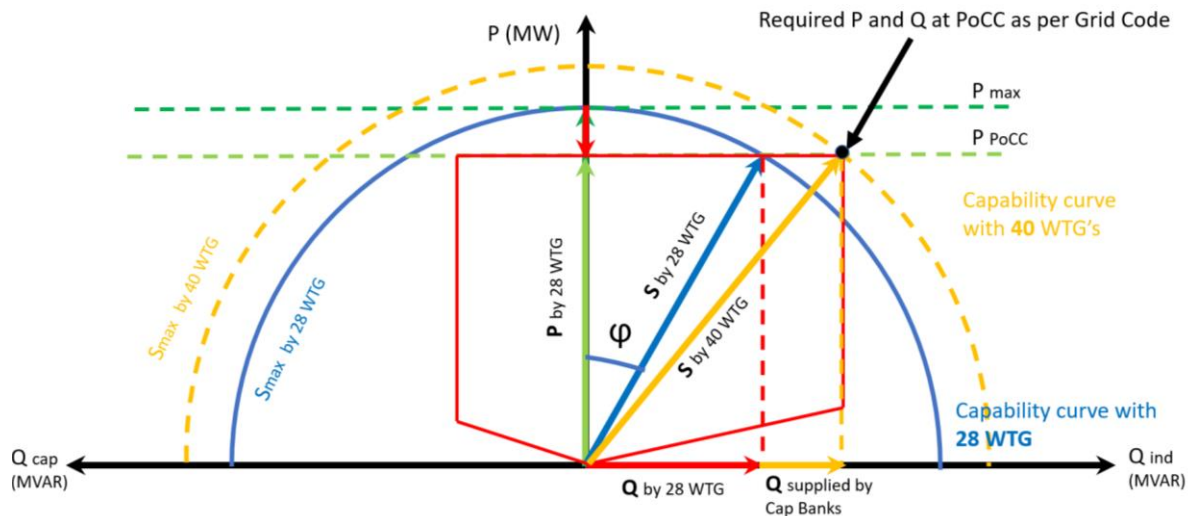


**Figure 2.3-39:** Capacitor Bank Implementation for Exporting  $Q$  to the Grid

However, the reactive power needed by the power transformers (within the wind farm) needs to be calculated in order to achieve the reactive power at PoCC.

### 2.3.3.5 CALCULATION OF NEEDED REACTIVE POWER BY POWER TRANSFORMERS

The power transformers distributed all over the wind farm absorbs part of the generated reactive power from the WTG's, and this absorbed reactive power is necessary for their operations, hence the reactive power at PoCC will be reduced by this absorbed amount.

#### 2.3.3.5.1 LV/MV Transformers Needed Reactive Power

For 4.5 MVA Power Transformers (WTG's 1 - 28)

$$Q_{\text{Needed by TR}} = 3 \times I^2 \times X = 3 \times (\beta I_{FL})^2 \times X = 3 \times \left( \beta \times \frac{S}{\sqrt{3} V} \right)^2 \times X\% \times \frac{V^2}{S}$$

$$Q_{\text{Needed by TR}} = \beta^2 \times S \times X\%$$

$$Q_{\text{Needed by 4.5MVA TR}} = (88.13\%)^2 \times 4,500,000 \times 7.15\% = 0.250 \text{ MVA}r$$

Total transformer LV/MV needed reactive power is: 0.250 MVAr/TR x 28 TR's = 7 MVAr

#### 2.3.3.5.2 MV/HV Transformers Needed Reactive Power

Knowing that the  $Z_{cc}\%$  is 12% for MV/HV transformers, and if the two transformers are running at the same time and the total plant capacity is distributed equally between the two transformers, then the loading factor for each transformer will be  $\beta = 63.1/100 = 63.1\%$  Loading, then each transformer will consume the following reactive power:

$$Q_{\text{Needed by 100MVA TR}} = (63.1\%)^2 \times 100,000,000 \times 12\% = 4.777 \text{ MVA}r / \text{Transformer}$$

Since the two transformers operating at the same time, then total MV/HV transformers reactive power consumption will be:

$$4.777 \text{ MVA}r/\text{TR} \times 2 \text{ TR's} = 9.5 \text{ MVA}r$$

The total transformer losses (MV + HV) = 7 MVAr + 9.5 MVAr = **16.5 MVAr**

The reactive power requirements at the WTG terminals are:

Over Excited =>  $Q = 62 \text{ MVAR} + 16.5 = 78.5 \text{ MVAR}$  (out the WTG capability)

Under Excited =>  $Q = 33 \text{ MVAR} - 16.5 = 16.5 \text{ MVAR}$  (within the WTG capability)

However, in contingency and when one of the 2 GSU's are out of service, then one transformer is evacuating the full capacity of the wind farm, then the loading factor for the transformer will be  $120.2 / 100 = 120.2\%$ , then each transformer will consume the following reactive power:

$$Q_{\text{by } 100\text{MVA TR}}^{\text{Needed}} = (120.2\%)^2 \times 100,000,000 \times 12\% = 17.28 \text{ MVar/ Transformer}$$

The total transformer losses (MV + HV) =  $7 \text{ MVAR} + 17.28 \text{ MVAR} = \mathbf{24.25 \text{ MVAR}}$

The reactive power requirements at the WTG terminals are:

Over Excited =>  $Q = 62 \text{ MVAR} + 24.25 = 86.28 \text{ MVAR}$  (out the WTG capability)

Under Excited =>  $Q = 33 \text{ MVAR} - 24.25 = 8.75 \text{ MVAR}$  (within the WTG capability)

### 2.3.3.6 DESIGN OF THE PREDETERMINED REACTIVE POWER (MVar) OPEN RACK MV CAPACITOR BANKS

The rated power of the banks should be close to the maximum reactive power absorbed by the PV inverters under the following limitations [8]:

$$0.5 \times |P \tan \varphi| \leq Q_c \leq 0.02 \times S_{sc}$$

Where;

$P \tan \varphi$  is a maximum reactive power absorbed by WTG's

$S_{sc}$  is a short-circuit power at PoCC.

The absorbed reactive power happens when PF is 0.95 under-excited:

$$P.F = \cos(\varphi) = 0.95 \Rightarrow \varphi = \cos^{-1}(0.95) = 18.19^\circ$$

The reactive power can be calculated from the available parameters:

$$Q_{U/E} = P \times \tan(\varphi) = 100 \times \tan(18.19^\circ) = 33 \text{ MVAR}$$

The  $S_{SC}$  at PoCC is already given 1,552.05 MVA

$$0.5 \times |33| \leq Q_c \leq 0.02 \times 1552.05$$

$$16.5 \leq Q_c \leq 31$$

Since the total transformer losses (MV + HV) = 6.123 MVAR + 11.484 MVAR = **17.607 MVAR**

Based on above the proposed size of the total capacitor bank is 20 MVAR which will be distributed at the three sections 2 x 10 MVAR. However, in contingency, the total capacitor bank is 36 MVAR which will be distributed at the three sections 2 x 18 MVAR. The proposed open rack capacitor bank has parameters as per **Table 2.3-15**

**Table 2.3-15** Technical Parameters of Open Rack Capacitor Bank

Item	Parameter
Rated voltage kV	36
Rated frequency Hz	50
Rated output MVAR	18
Connection	Y-Y
Fuses	Internal
Lightning impulse withstand voltage kV	250
Power frequency withstand voltage kV	95

The proposed capacitor bank is shown in **Figure 2.3-12: Proposed Open Rack Capacitor Bank**

### 2.3.3.7 Wind Farm Single Line Diagram with MV Capacitor Banks

The new single line diagram for the wind farm after utilizing the capacitor banks (in red) will be as shown in **Figure 2.3-40: Wind Farm Single Line Diagram Drawing with MV Capacitor Banks**

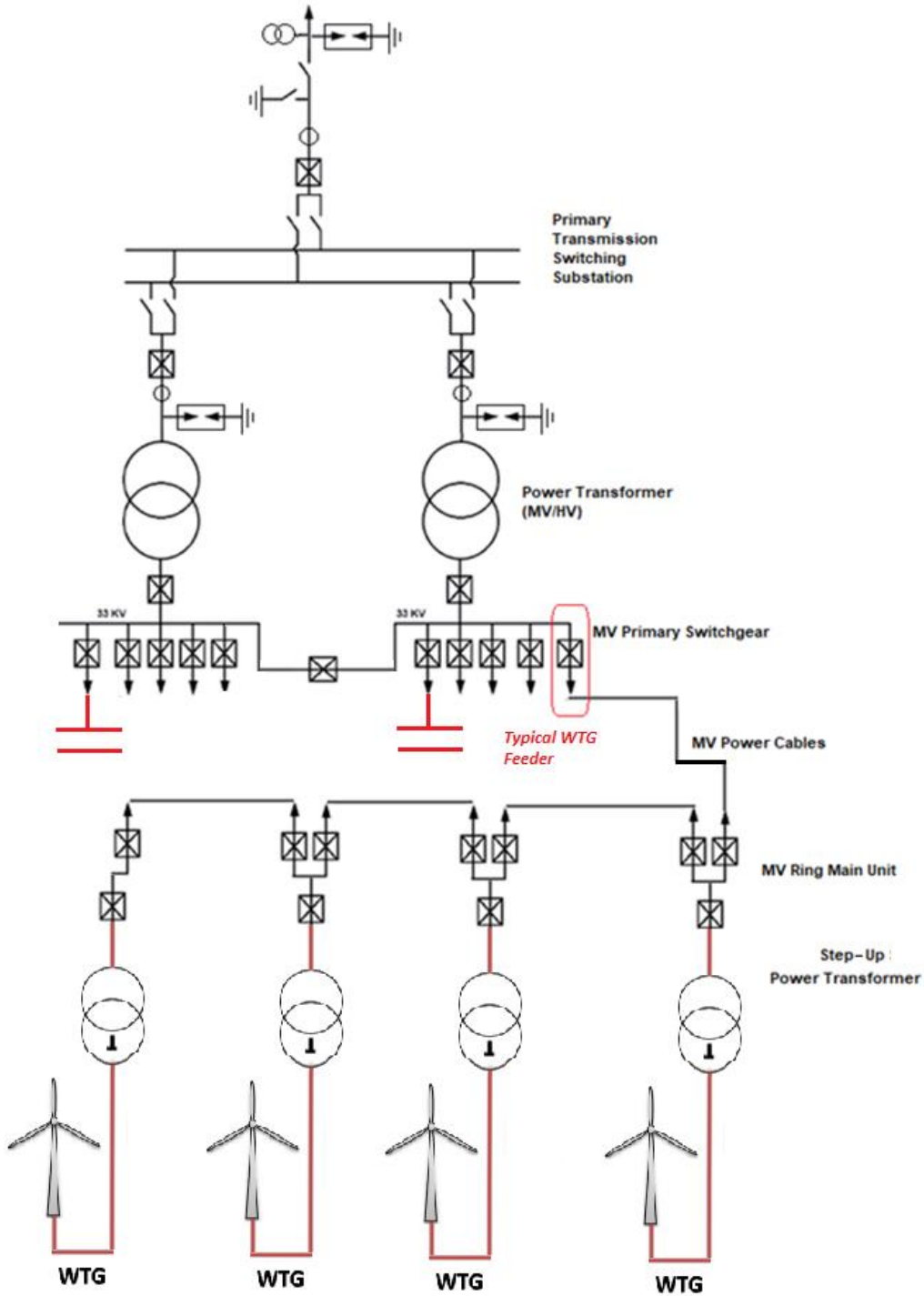


**Figure 2.3-40: Wind Farm Single Line Diagram Drawing with MV Capacitor Banks**

### 2.3.3.8 Power Flow on ETAP Software

The same has been verified with ETAP software **Figure 2.3-41**: Active and Reactive (P and Q) delivered by 100MW Grid Connected Wind Farm shows a screen shot from ETAP one line view window for the active and reactive power injected from the PV plant at IEEE 9 bus system Bus No. 9 which is the PoCC.

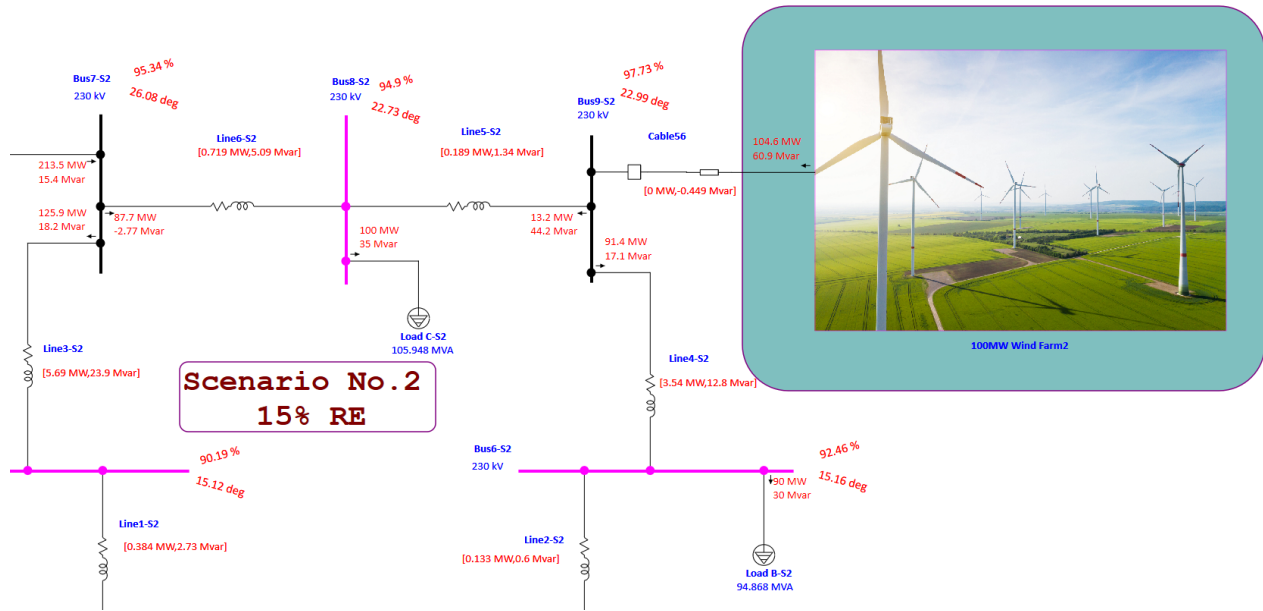


**Figure 2.3-41:** Active and Reactive (P and Q) delivered by 100MW Grid Connected Wind Farm

In this case study, the 100MW was built accurately started from the IRR unit till the PoCC as per the architecture **Figure 2.3-6: PV Plant Architecture drawing.**, and **Figure 2.3-41:** Active and Reactive (P and Q) delivered by 100MW *Grid Connected Wind Farm*

As shown above both the active and reactive power is supplied at the PoCC and this means that the grid connected wind farm comply with the grid code

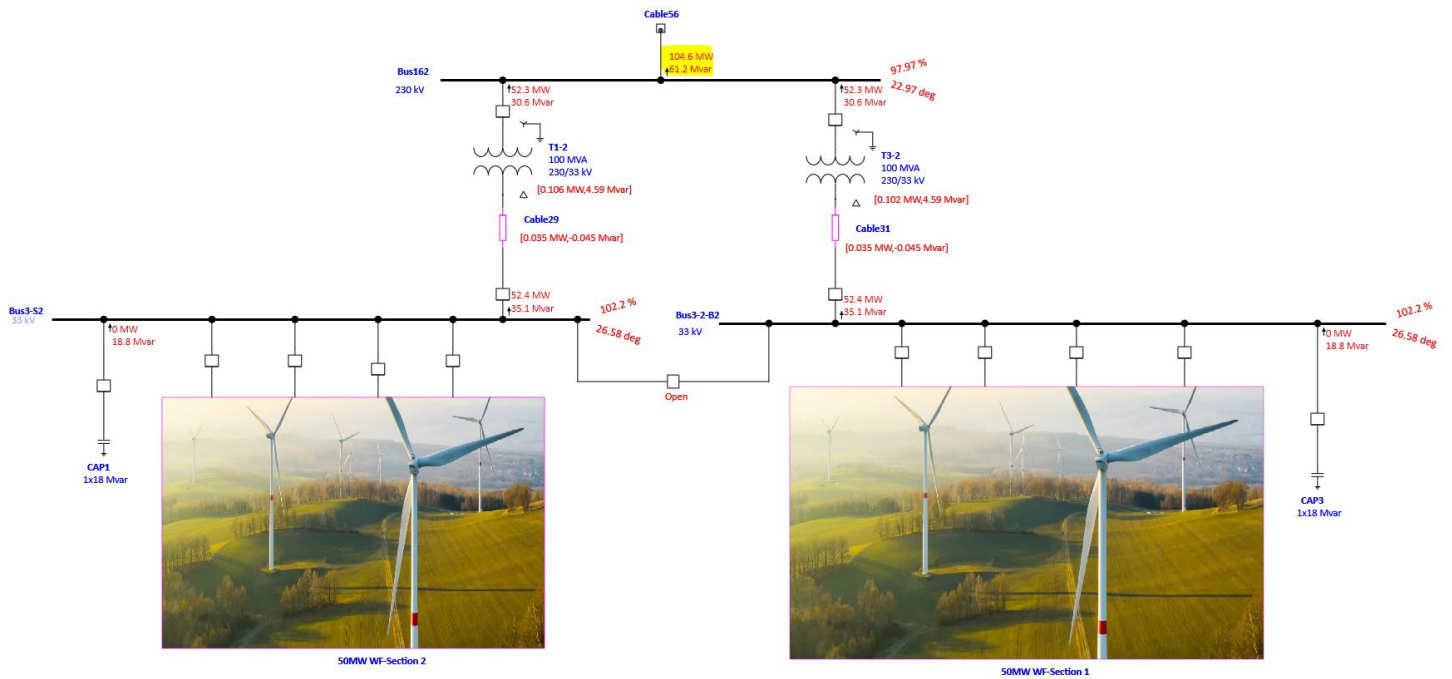


**Figure 2.3-42:** P and Q delivered by the 100MW Wind Farm at the MV/HV Station

### 2.3.3.9 Fault Simulation with ETAP software

Fault simulation of 3 phase fault at PoCC has been conducted. ETAP short circuit calculation is performed based on IEC 60909 as shown in **Figure 2.3-43**, This three-phase short circuit current of **3.896 kA** is the sum of the short circuit currents from the grid side (2.15 + 1.265) kA and wind farm side 0.491 kA



A transient short circuit analysis was conducted using ETAP as per IEC 61363 as shown **Figure 2.3-45**

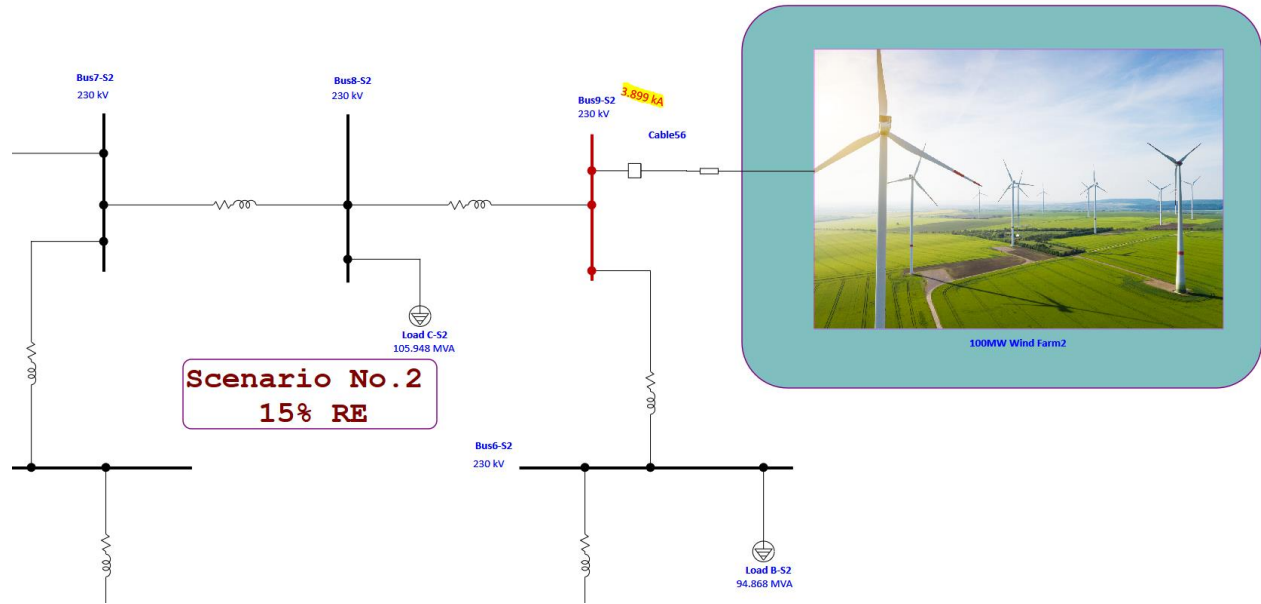


**Figure 2.3-45:** ETAP - Run Transient SC using IEC 61363

**Figure 2.3-46** shows the graphs generated from ETAP software upon simulating the transient short circuit current at PoCC (Bus 9).

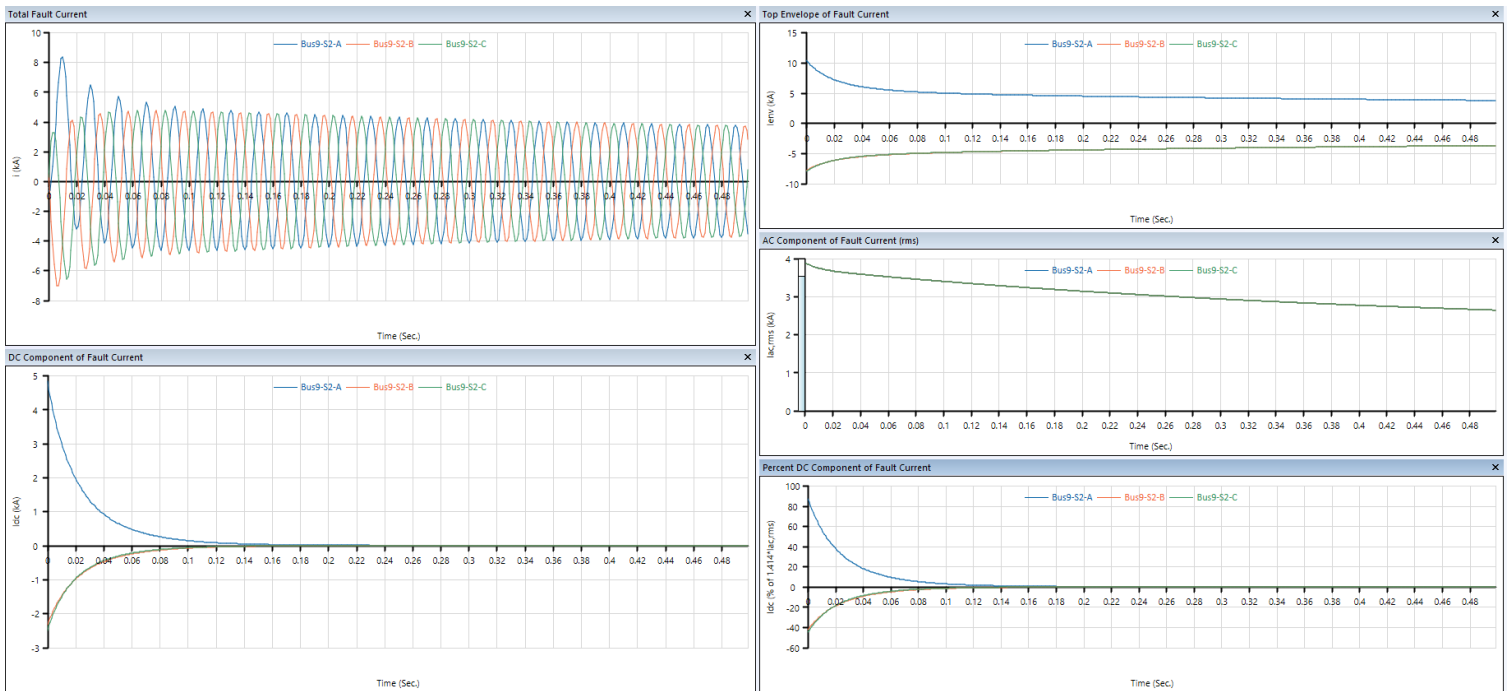


**Figure 2.3-46:** Three Phase Fault Current as Per IEC 61363 at PoCC ( Bus 9 of IEEE 9 Bus system )

### 2.3.3.10 Harmonic Analysis at PoCC Using ETAP

In our case study, the 100MW grid connected PV plant, one harmonic model has been introduced for each converter of the Type 4 WTG which is typical IEEE-12 pulse. accordingly harmonic analysis has been performed for each of the following cases: 44 WTG's + 2 X 18 MVAR capacitor banks. Both time domain graph that shows the overall resultant distorted waveform, as well as the frequency domain graph for the voltage at PoCC have been drawn, and both current THD and voltage THD at PoCC have been simulated.

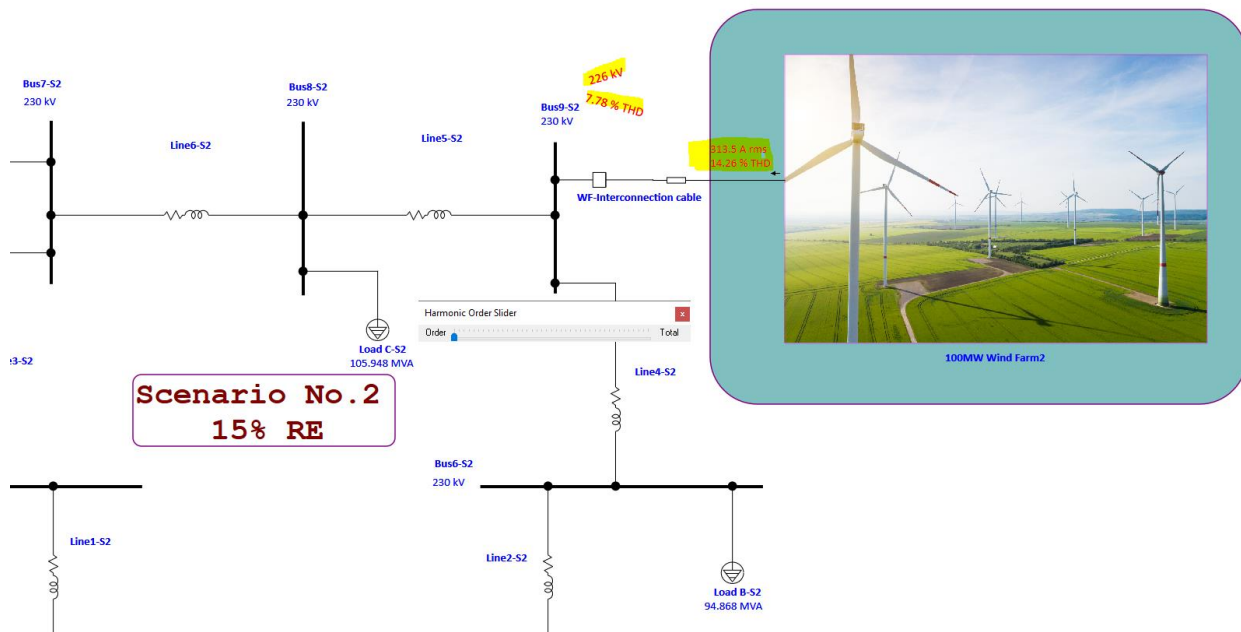


Figure 2.3-47: Voltage and Current Total Harmonic Distortion (THD) at PoCC of Wind farm.

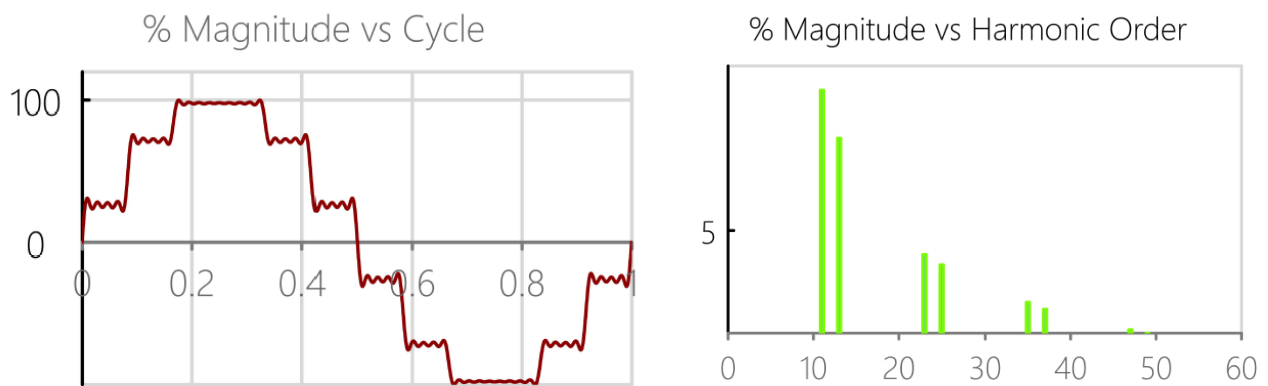


Figure 2.3-48: IEEE 12 Pulse Pre-defined Harmonic Model (Waveform and Spectrum)

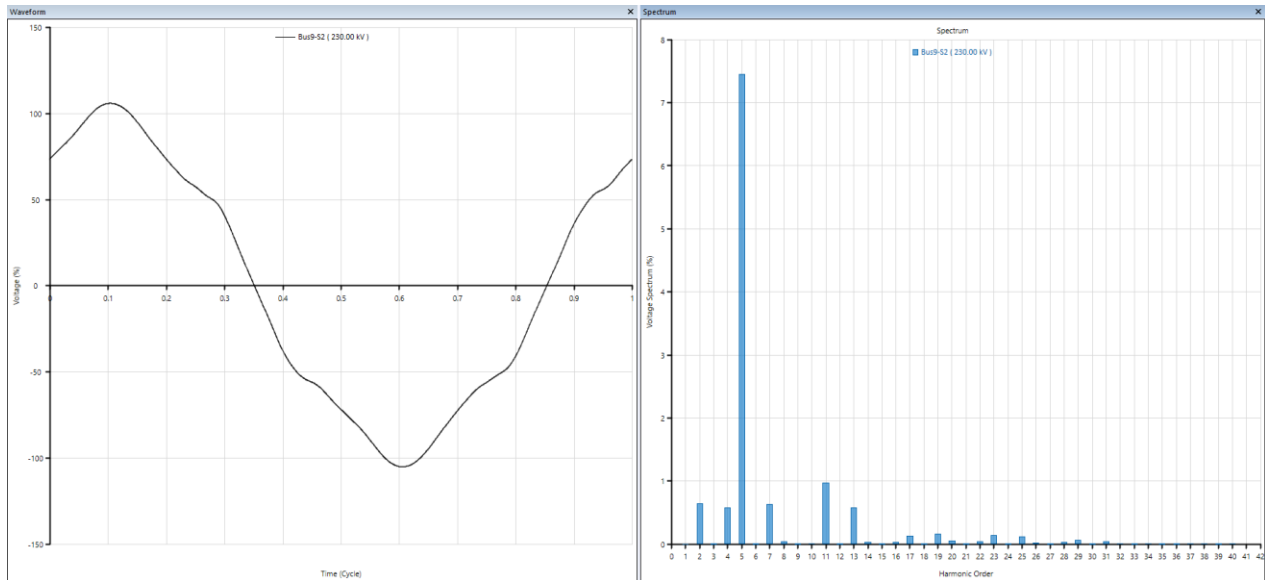


Figure 2.3-49: Voltage (THD)% Harmonic Waveform and Spectrum at Wind Farm PoCC (Bus 9)

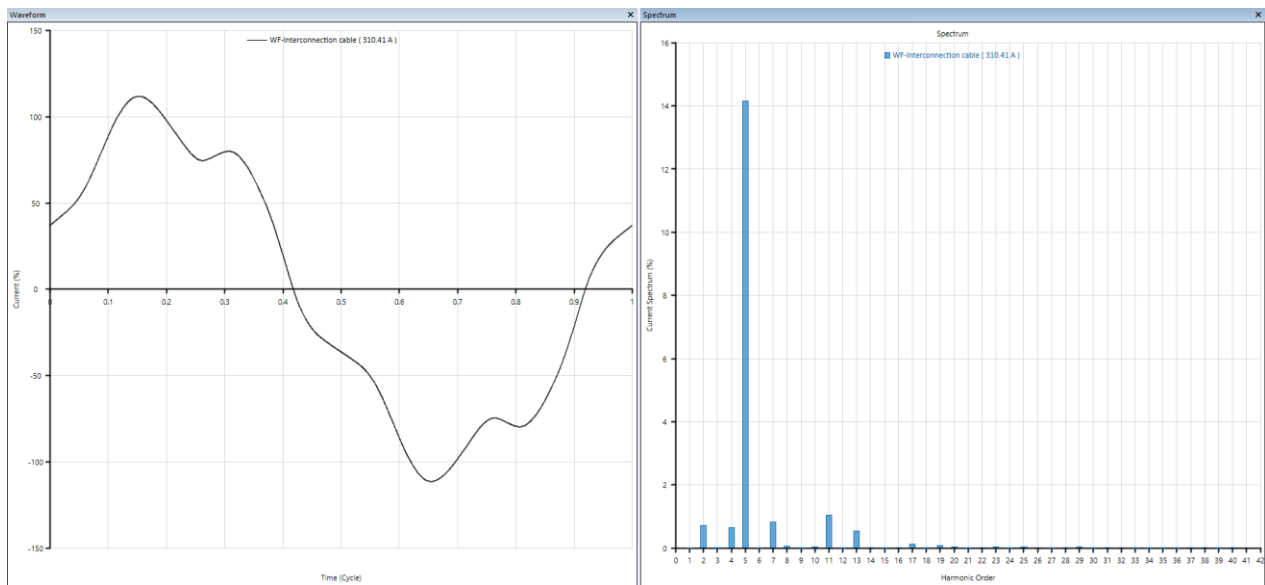


Figure 2.3-50: Current (THD)% Harmonic Waveform and Spectrum at Wind Farm PoCC (cable inertia)

If harmonic frequency scan has been conducted, then we will notice that at 5<sup>th</sup> harmonic order, the driving point impedance.

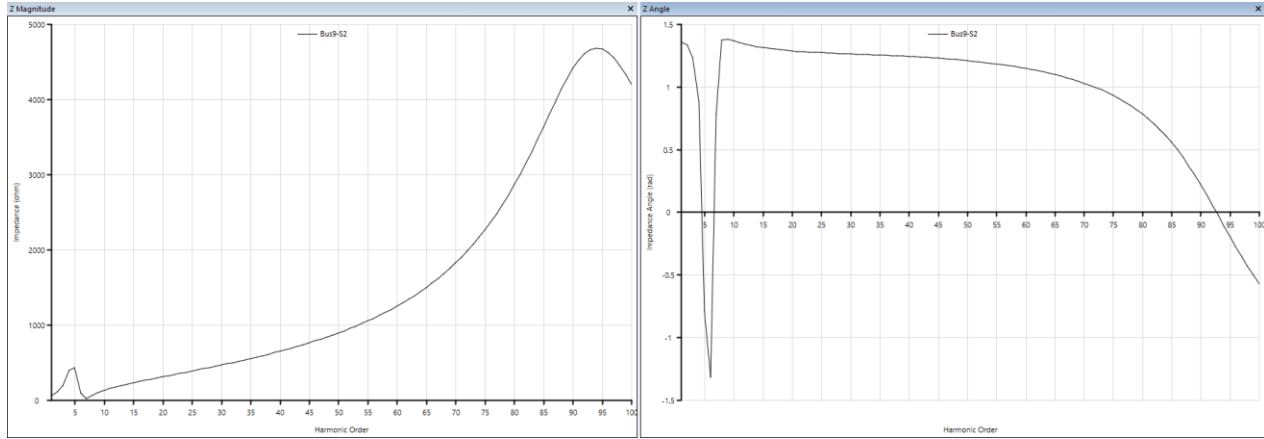


Figure 2.3-51: Harmonic Frequency Scan (Z magnitude and Z angle)

### 2.3.3.11 Transient Stability Using ETAP

Under this section, several types of disturbances will be introduced into the system and simulated using ETAP, and after that, the ability of the “modified IEEE 9 bus system with 100MW wind farm integration” is going to be examined to return to its normal stable operating condition.

#### 2.3.3.11.1 First Disturbance: Three Phase Balanced Fault at Bus No.9 without Fault Clearance

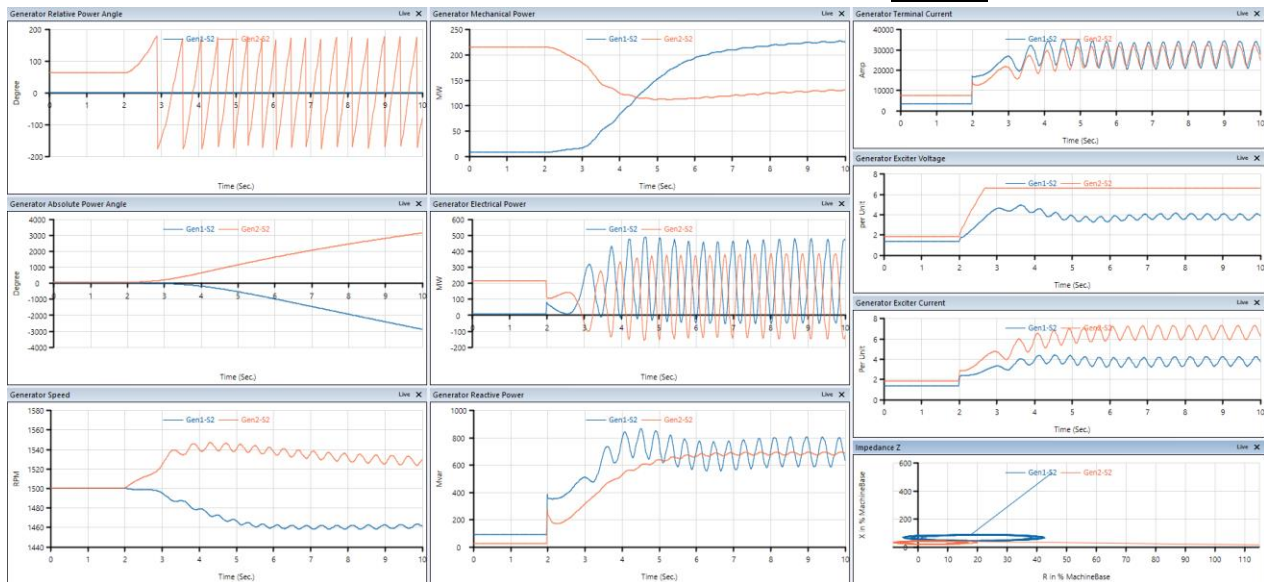
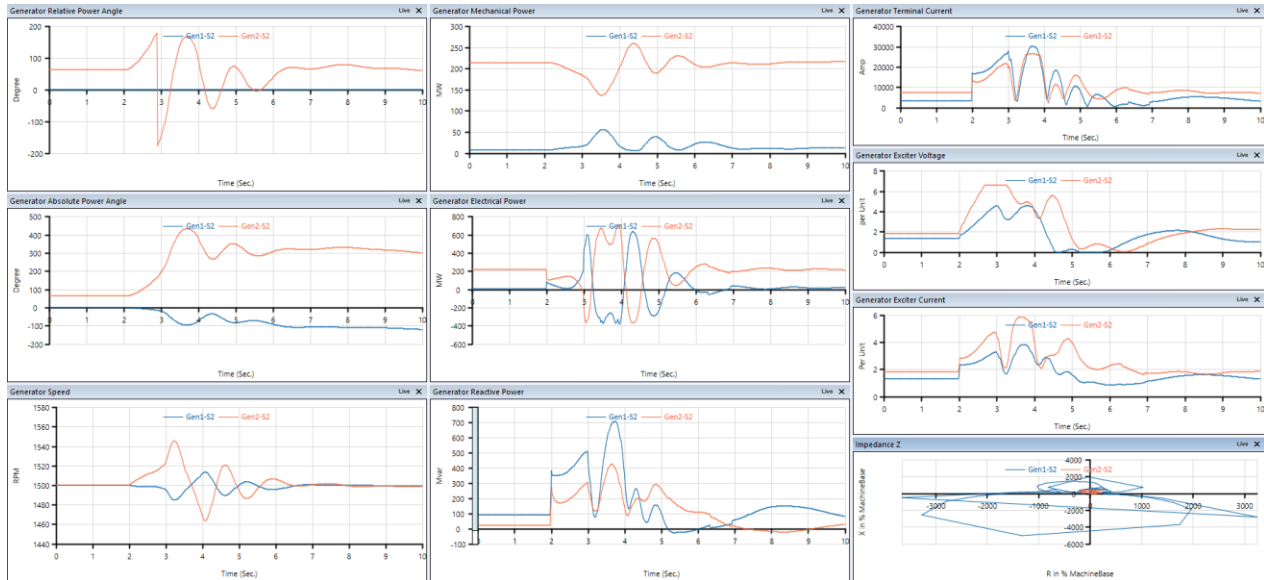


Figure 2.3-52: Generator Gen 1 and Gen 2 dynamic response due to 3 Phase fault at BB No.9 without fault clearance

The system lost its stability and the generators G1 and G2 lost their synchronism.

**2.3.3.11.2 First Disturbance: Three Phase Balanced Fault at Bus No.9 with Fault Clearance after 1 sec**



**Figure 2.3-53:**Generator Gen 1 and Gen 2 dynamic response due to 3 Phase fault at BB No.9 with fault clearance after 1 sec

FCT of 1 sec is not sufficient to return the system stability and forced the system back to its equilibrium.

**2.3.3.11.3 First Disturbance: Three Phase Balanced Fault at Bus No.9 with Fault Clearance after 0.5 sec**

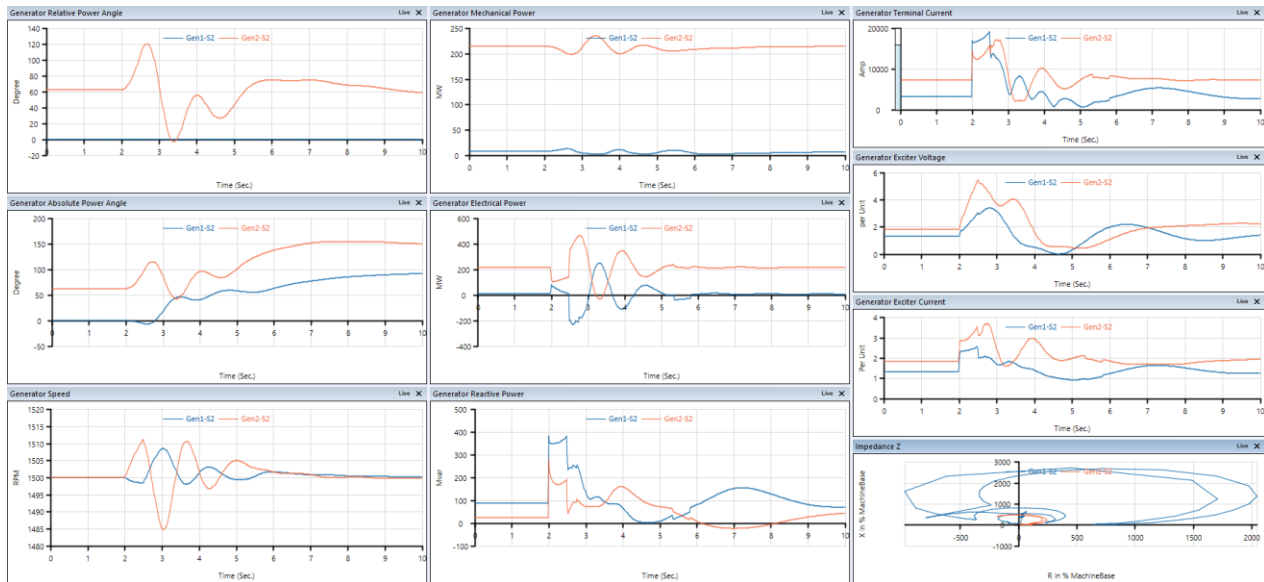


**Figure 2.3-54:**Generator Gen 1 and Gen 2 dynamic response due to 3 Phase fault at BB No.9 with fault

### 2.3.3.11.4 Second Disturbance: Three Phase Balanced Fault at Line-1 without Fault Clearance

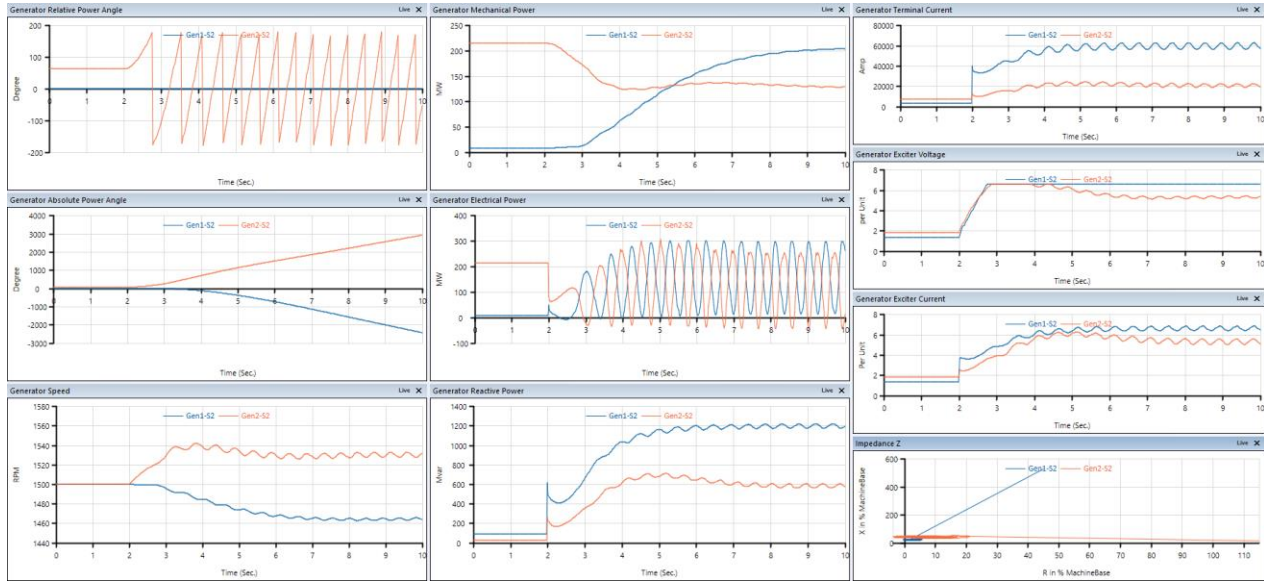


Figure 2.3-55: Generator Gen 1 and Gen 2 dynamic response due to 3 Phase fault at Line No.1 without fault clearance

### 2.3.3.11.5 Second Disturbance: Three Phase Balanced Fault at Line-1 with Fault Clearance

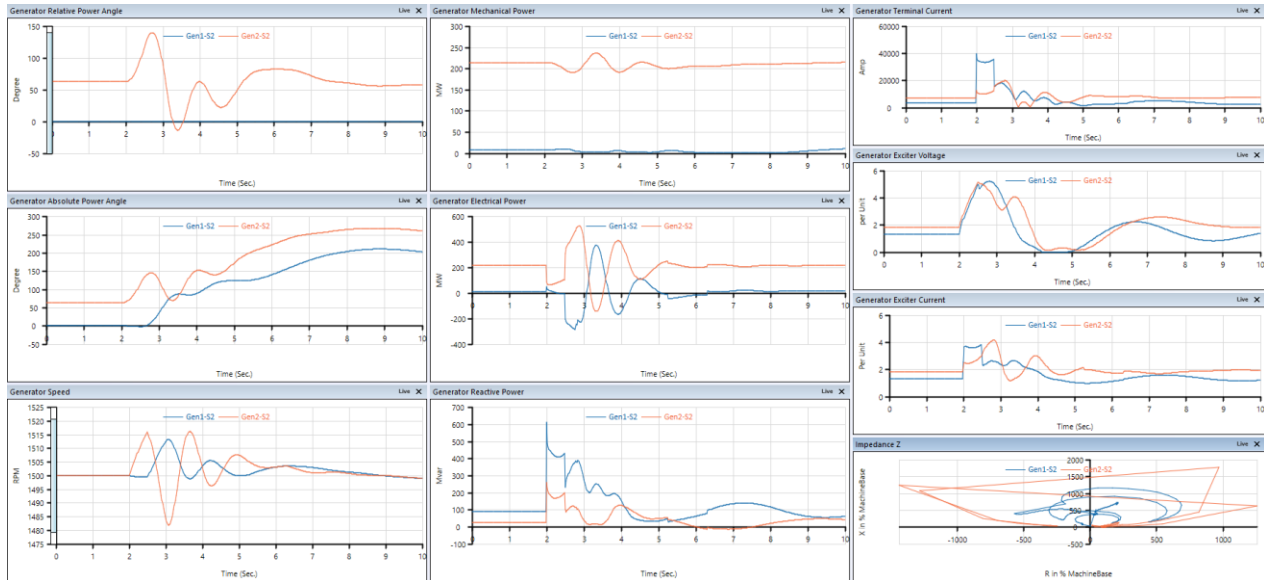


Figure 2.3-56: Generator Gen-1 and Gen-2 dynamic response due to 3-Phase fault at Line No.1 with fault clearance

### 2.3.3.11.6 Third Disturbance: Loss of 100MW WF at t=5 sec

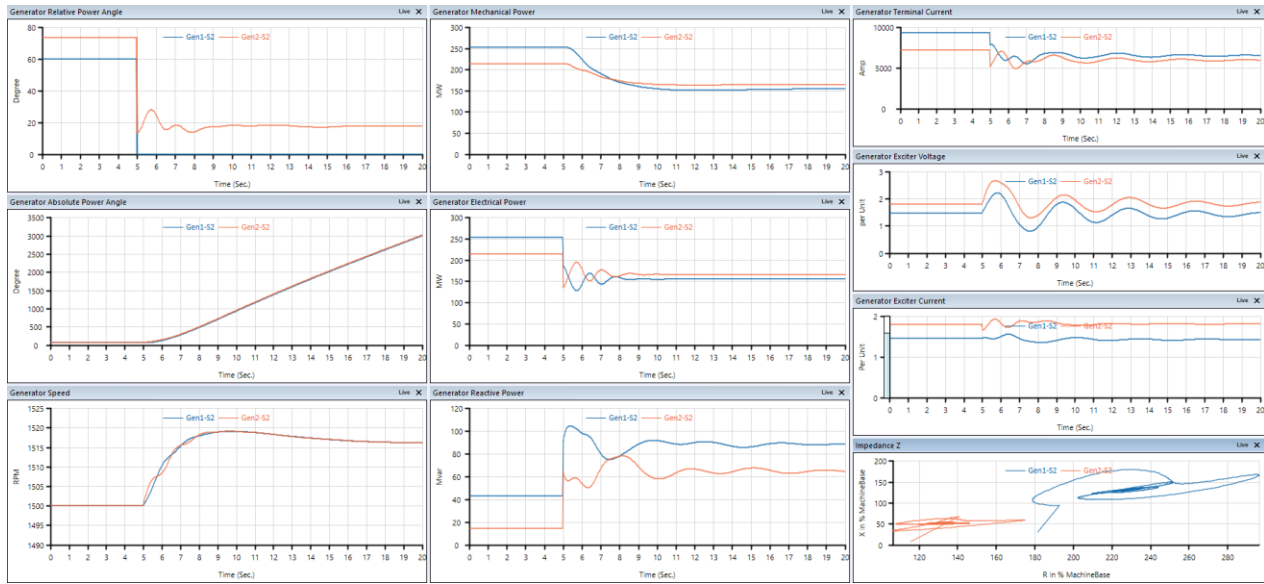


Figure 2.3-57: Generator Gen 1 and Gen 2 dynamic response due to loss of Wind farm at t=5 sec

### 2.3.3.11.7 Forth Disturbance: Gradual Incremental Penetration of WF Plant

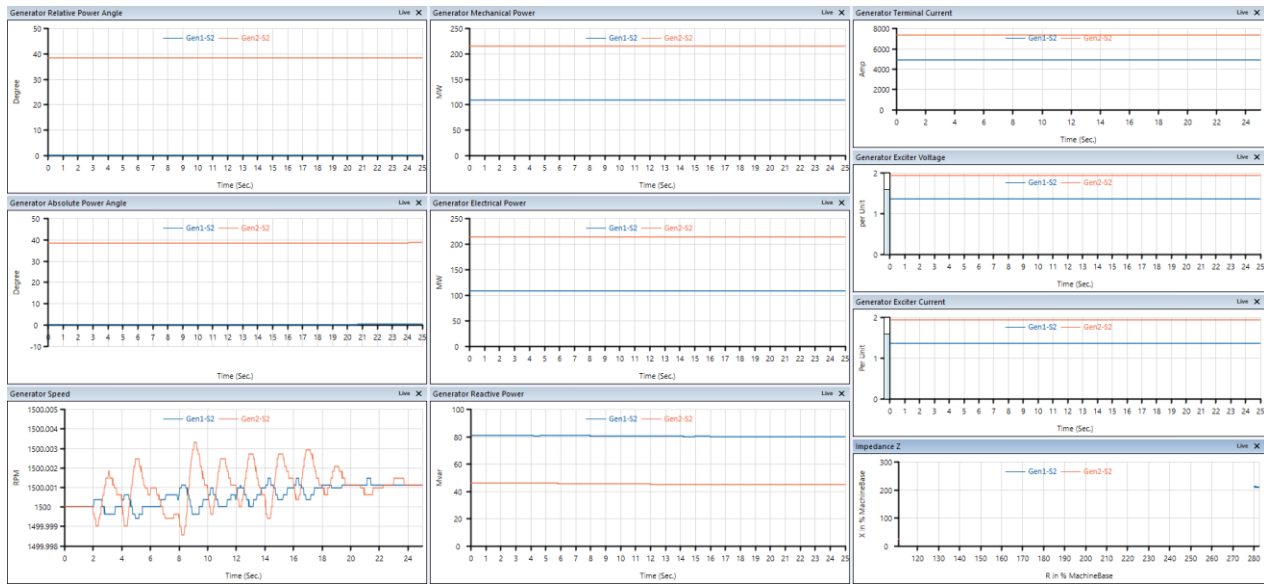
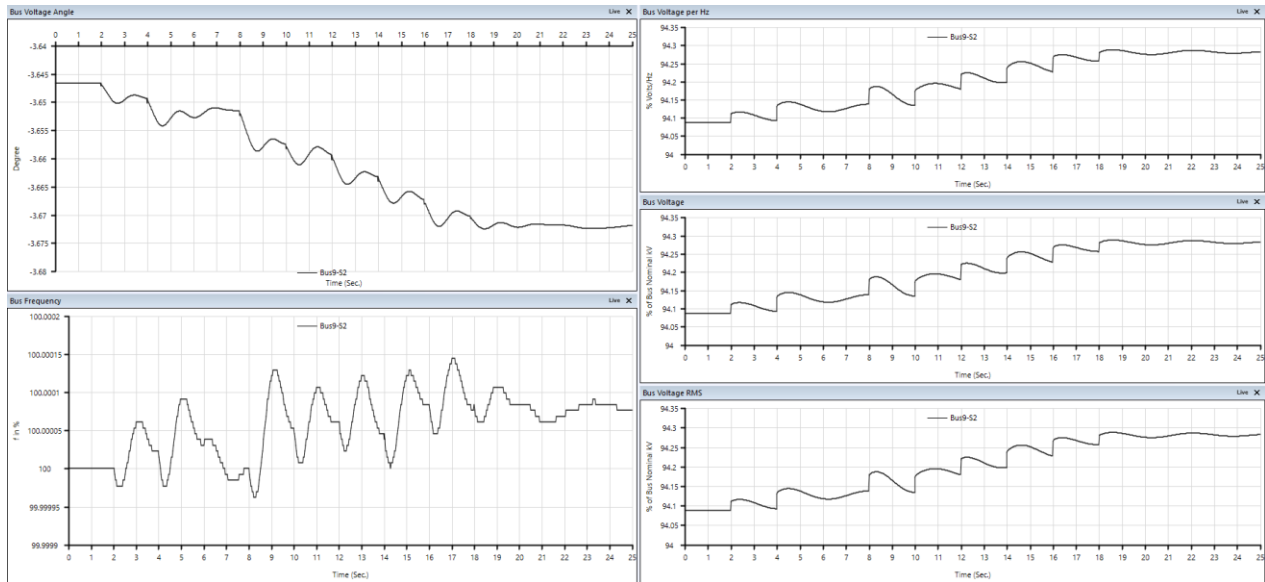


Figure 2.3-58: Generator Gen 1 and Gen 2 dynamic response with the gradual penetration of Wind Farm



**Figure 2.3-59:** PoCC for Wind Farm (Bus No.9) dynamic response with the gradual penetration of Wind Farm

**2.3.3.11.8 Fifth Disturbance: Sudden Load Change**

Load A assumed to be changes by 10% at t= 2 sec, then load B changed by 20% at t=5 sec, and load C changed by 25% t t=10 sec

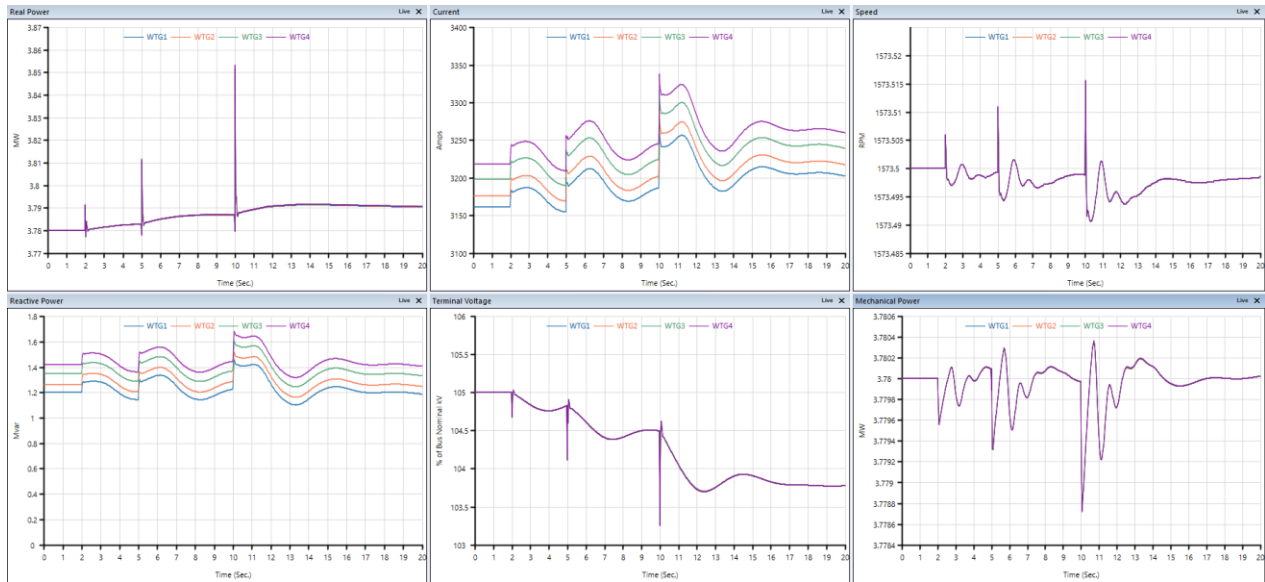


**Figure 2.3-60:** WTG's 1,2,3 and 4 dynamic responses for load change

**2.3.3.11.9 Sixth Disturbance: Tripping/ Disconnection of Line 4**

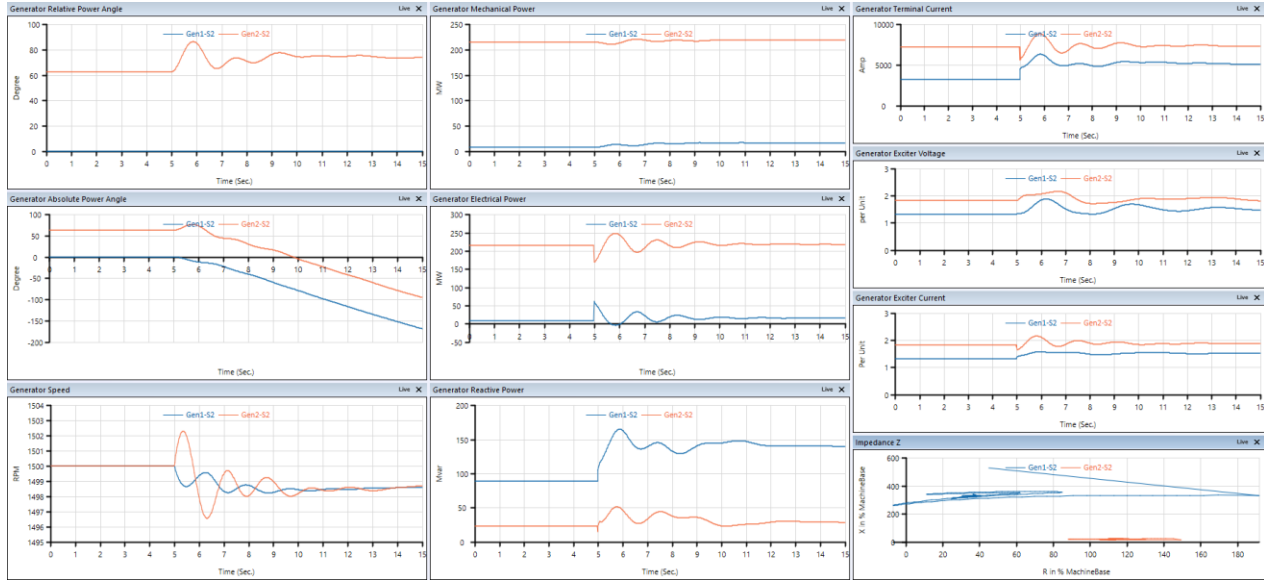


Figure 2.3-61:Generator Gen 1 and Gen 2 dynamic response due to Disconnection of Line 4

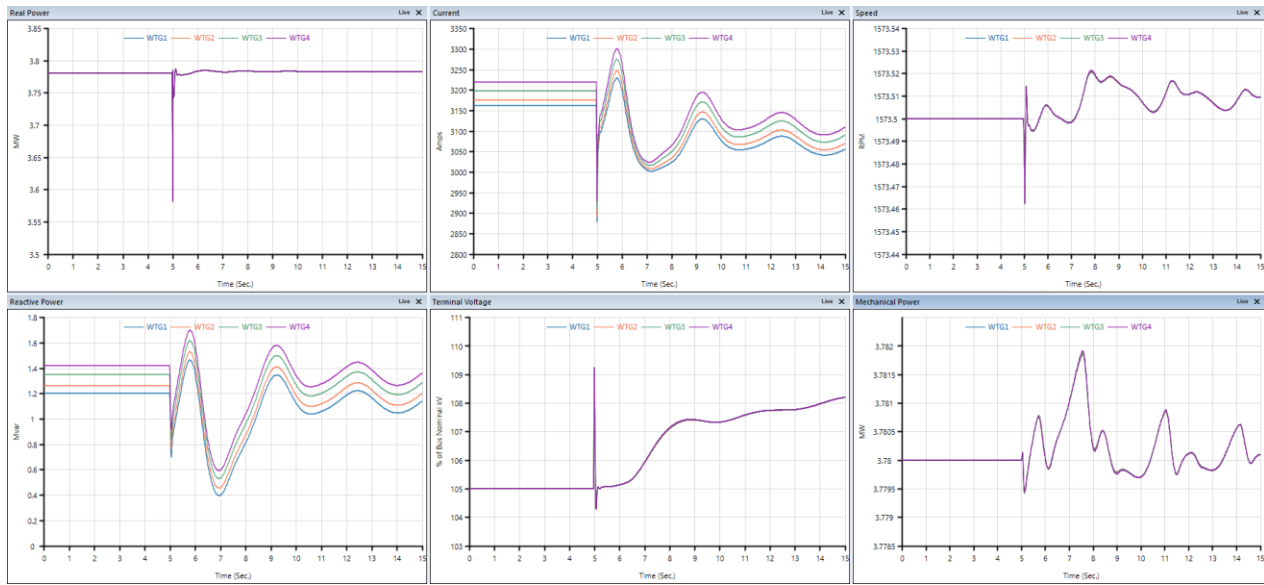


Figure 2.3-62:WTG's 1,2,3 and 4 dynamic responses for disconnection of Line 4

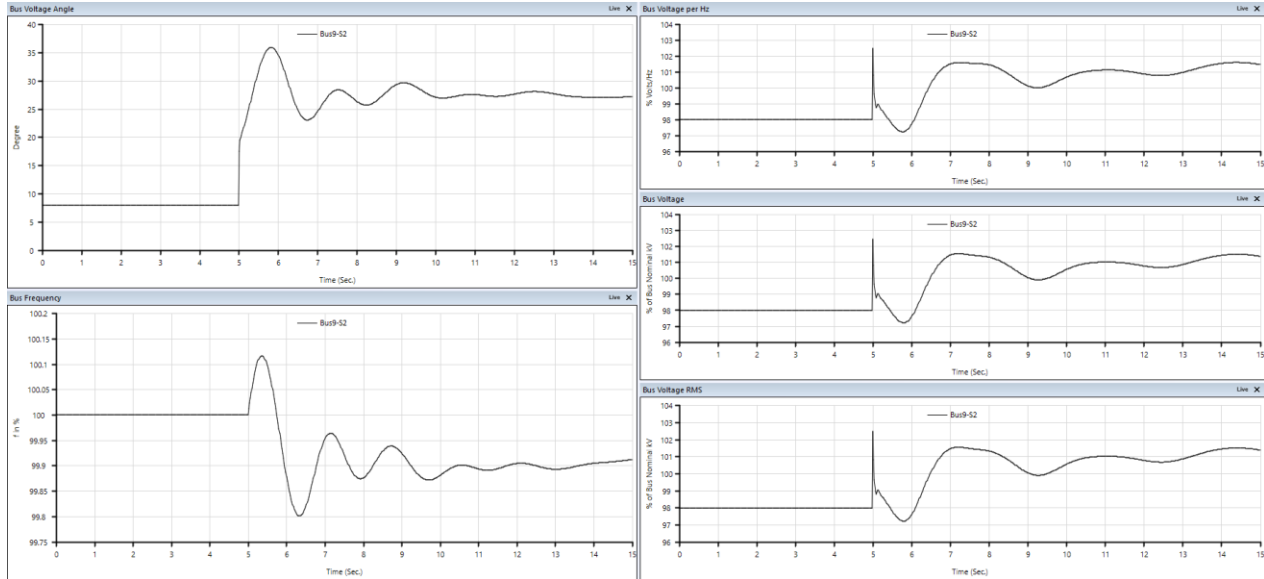


Figure 2.3-63: Bus No.9 (WF PoCC) dynamic responses for disconnection of Line 4

### 2.3.3.12 Voltage Stability Study Using ETAP

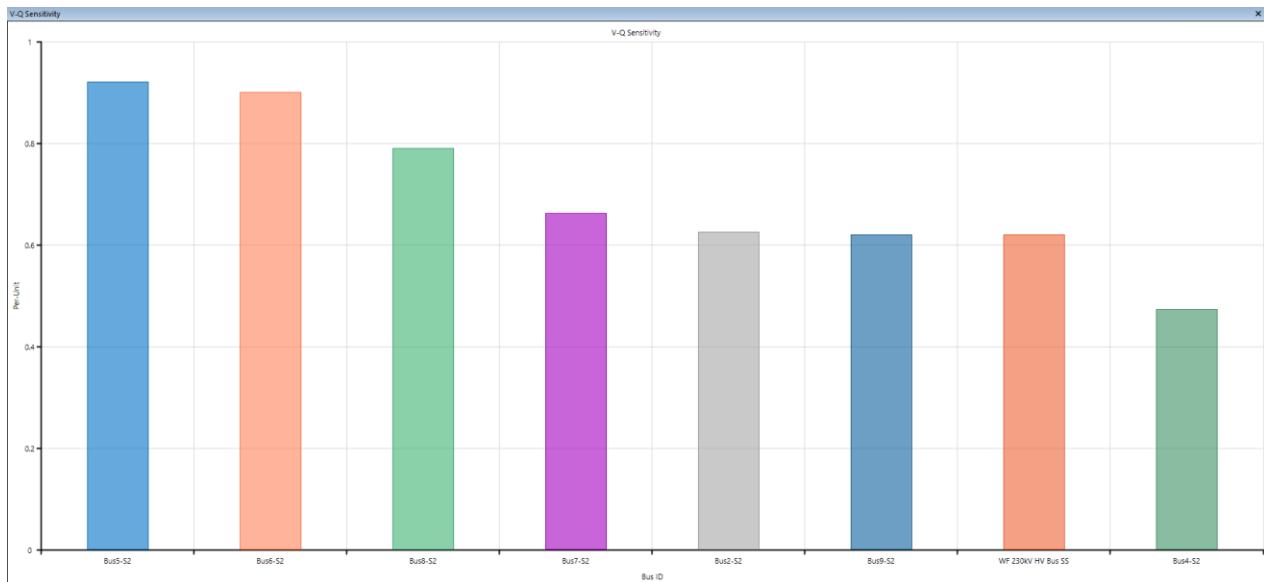


Figure 2.3-64: V-Q Sensitivity - transmission buses

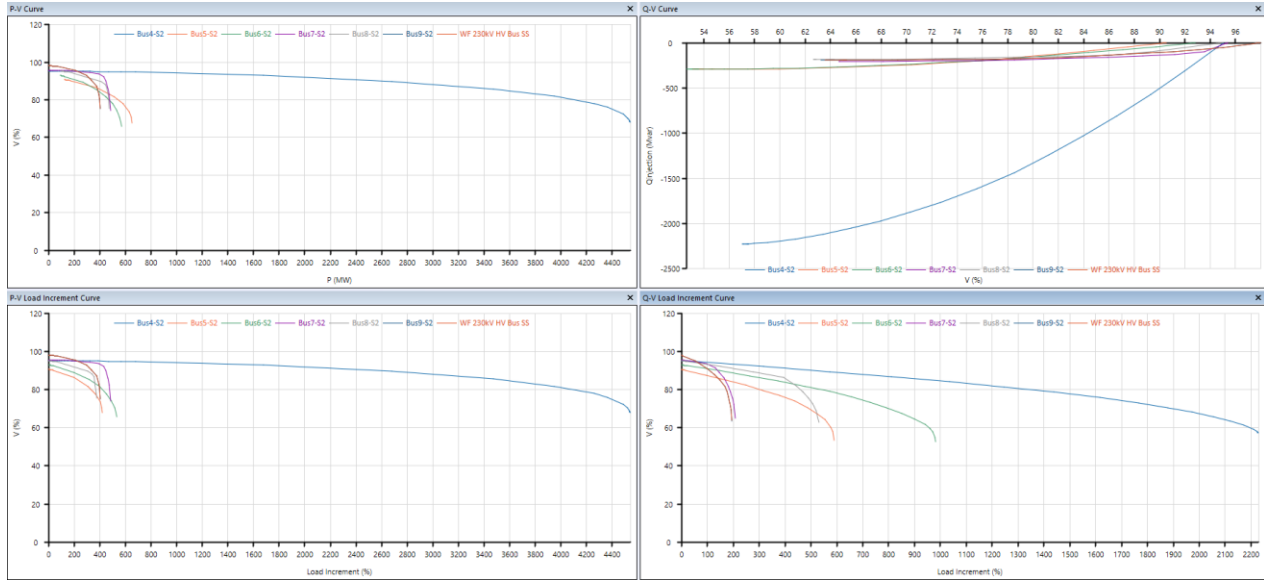


Figure 2.3-65: P-V and Q-V for Transmission Buses

## 2.4 Chapter Seven: 100% Renewables Grid Integrated to IEEE 9 Bus System



The feasibility and credibility of a complete transition from fossil-fuel based electric power and energy system (EPES) to fossil-free EPES, has been a subject of increasing interest within the energy sector. supporters of a 100% renewable energy scenario argue that there is a growing amount of evidence supporting the idea that replacing fossil fuels and nuclear energy with a completely renewable energy system so that this newly sustainable and green energy system will be completely 100% renewable energy system, is a technologically feasible, stable, secure, interoperable, and economically efficient way to decrease carbon emissions in the global energy system.

This thesis aims to surpass the feasibility and credibility discussion around the 100% renewable energy system scenario by conducting a in depth analysis of this 100% renewable energy scenario for IEEE 9 bus system. This thesis aims to identify the prevalent challenges and opportunities in terms of stability, security, and interoperability associated with a swift and comprehensive transition towards more ambitious renewable energy objectives. Additionally, it offers policy suggestions that are relevant to this transition.

Planning, optimization, and traceability are required in order to operate a power system that has a high penetration of renewable energy sources such as solar, wind, hydro, and biomass. This transition in the electrical power and energy system will be gradual until we reach the goal of accomplishing 100% renewable energy. To accomplish this goal, we will need to achieve 100% renewable energy. This helps to facilitate the transition to an energy system that is net zero, and it necessitates the development of new tools and digital technologies.

In order to verify the aforementioned, the IEEE 9 bus system, which is considered to be a small-scale electrical power system, was selected as the case study. Following that, the results will be implemented into our large-scale power systems.

Large generators and turbines with massive rotating parts make up conventional generation power plants. These power plants are electromechanically connected to the electrical power system, which allows them to naturally contribute an inertial response. In reality, traditional generators lower their rotational speed in the event of a sudden breakdown in the generation or connection of an extra load, releasing part of the kinetic energy stored in the huge spinning components as electrical energy to maintain the normal system frequency. Renewable generators, including wind and photovoltaic generators, don't add to the system's inertia as conventional generators do, and therefore can't provide more power to the system in the event of a disruption [46].

Under this chapter, the proposal is that the conventional IEEE 9 Bus System fossil fuel conventional power generation stations are replaced with Fossil Free Primary Energy Sources (Solar / Wind / Hydro) 125MVA Wind Farm replaces SM3, 270MVA PV Plant Replacing SM2, and 512MVA Hydro Electric Power Plant replaces SM1, and by this the full power generation of the IEEE bus system will be fully from 100% Renewable energy sources.

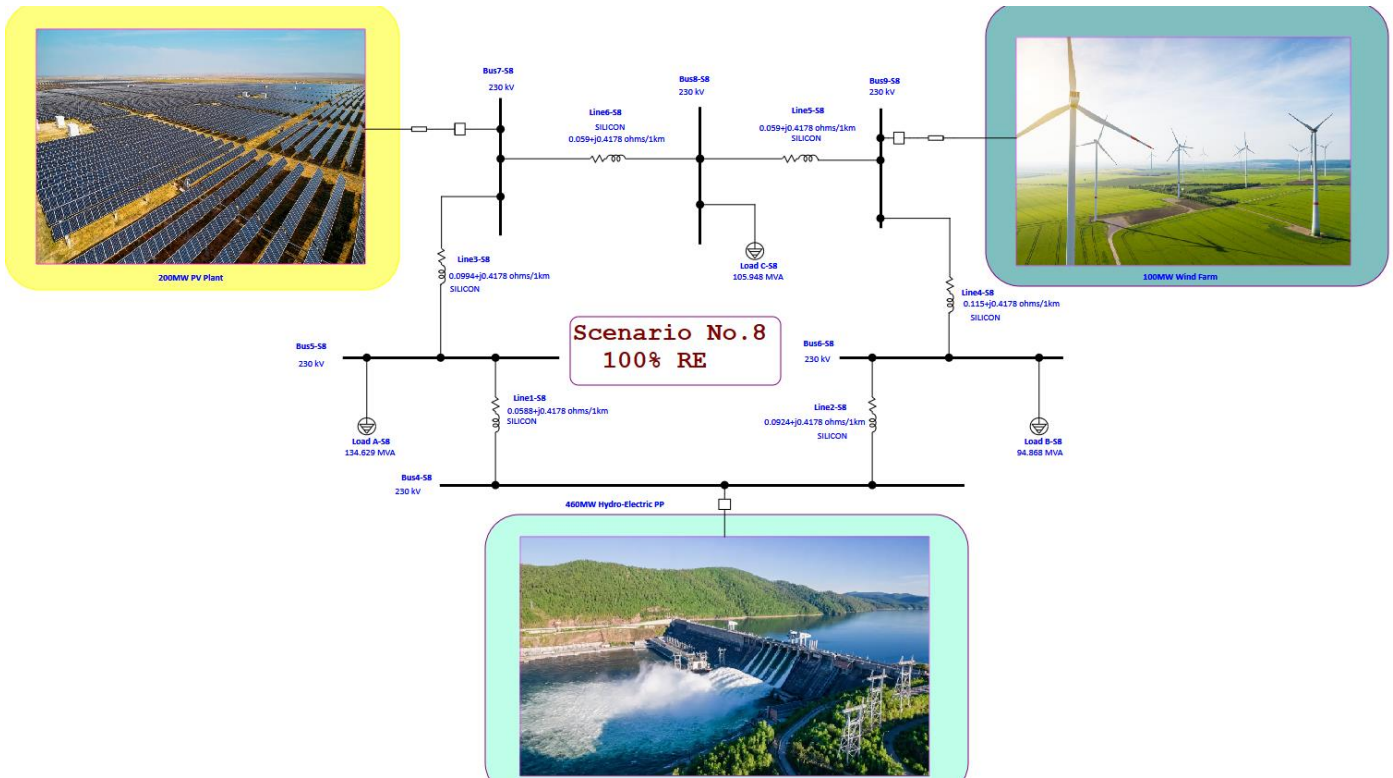


Figure 2.4-1:ETAP model for IEEE 9 bus system with 100% Renewable Energy Sources

However, Solar and Wind farms are unlike synchronous generator in thermal power plants are asynchronously integrated into the grid through inverters, hence they do not contribute to grid inertia.

While Hydroelectric power plants are based on conventional synchronous machines which are driven by hydro turbines which is a renewable energy source and, in the meantime, the synchronous generator contributes to the total system inertia. Hydroelectric facilities excel in meeting short-term peak power needs more effectively than fossil-fuel and nuclear power plants. One method used is "pumped storage," which involves reusing the same water several times.

Pumped storage is a technique used to store water for times of high electricity demand. It involves pumping water that has previously passed through turbines back up to a storage pool located above the power plant. This is often done during periods of low energy demand, such as during the nighttime. During periods of high demand and increased system load, the water is subsequently directed to flow back through the turbine-generators.

### 2.4.1.1 Power Flow on ETAP Software

The same has been verified with ETAP software. **Figure 2.3-14: Active and Reactive (P and Q) delivered by 200MW Grid Connected PV Plant** shows a screen shot from ETAP one line view window for the active and reactive power injected from the renewable power plants into the IEEE 9 bus transmission system and

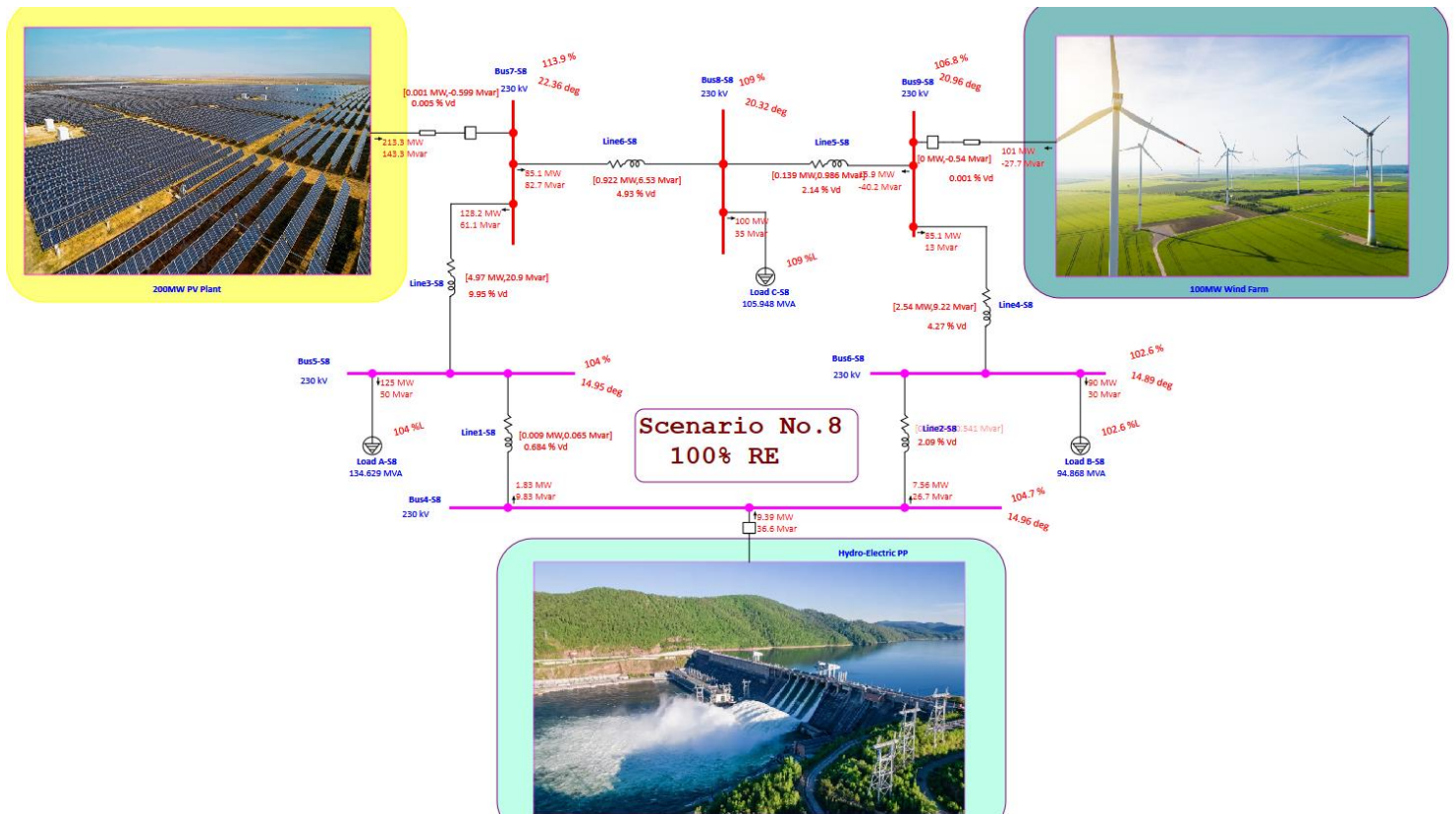


**Figure 2.4-2: Power Flow for IEEE 9 bus system with 100% Renewable generations.**

As shown both active and reactive power is delivered by the renewable primary energy sources (solar/wind/hydro) to the IEEE transmission network, and the load required power is delivered by these renewable energy sources

### 2.4.1.2 Time Domain Load Flow on ETAP Software

Simulation a Time Domain Load Flow (TDLF) analysis for one complete month started from 1/5/2024 till 31/5/2024 for the 100% Renewable IEEE 9-Bus electric power and energy system with Fossil Free Primary Energy Sources (Solar / Wind / Hydro) with 512MVA Hydroelectric Power Plant replaces SM1, 270MVA PV Plant Replacing SM2, and 125MVA Wind Farm replaces SM3. , the loads (Load A, B, and C) are assumed to be changed hourly over the day and so as the renewable primary energy sources (solar/wind) generated power is recorded too.

See below **Figure 2.4-3** load curve for load A over one day.

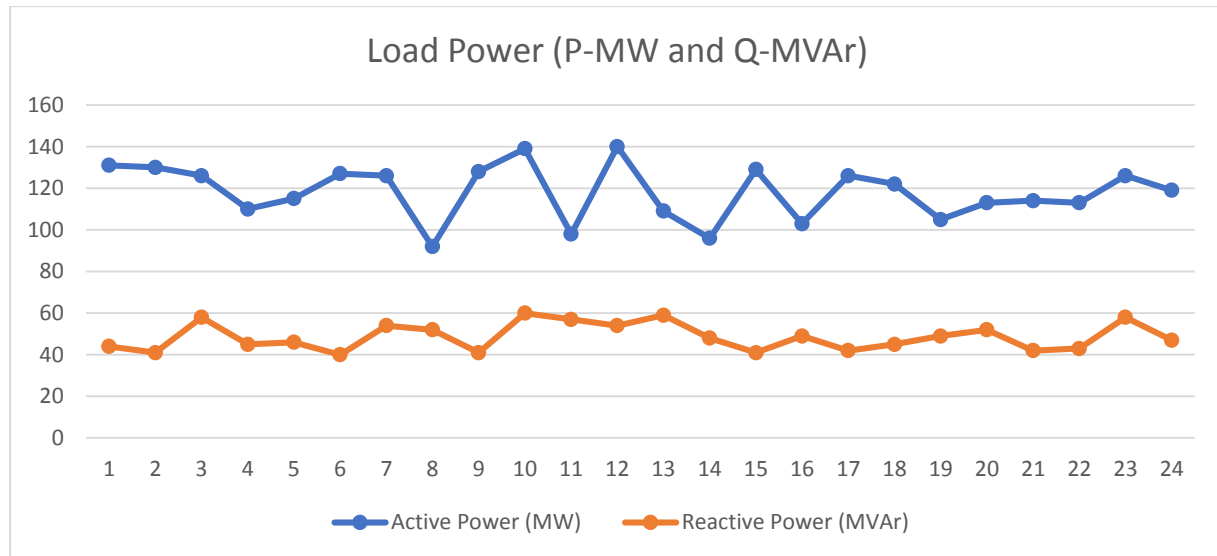


**Figure 2.4-3:** Load curve for Load A for one day (24 hour)

Also, see below the solar and wind variable power generated.

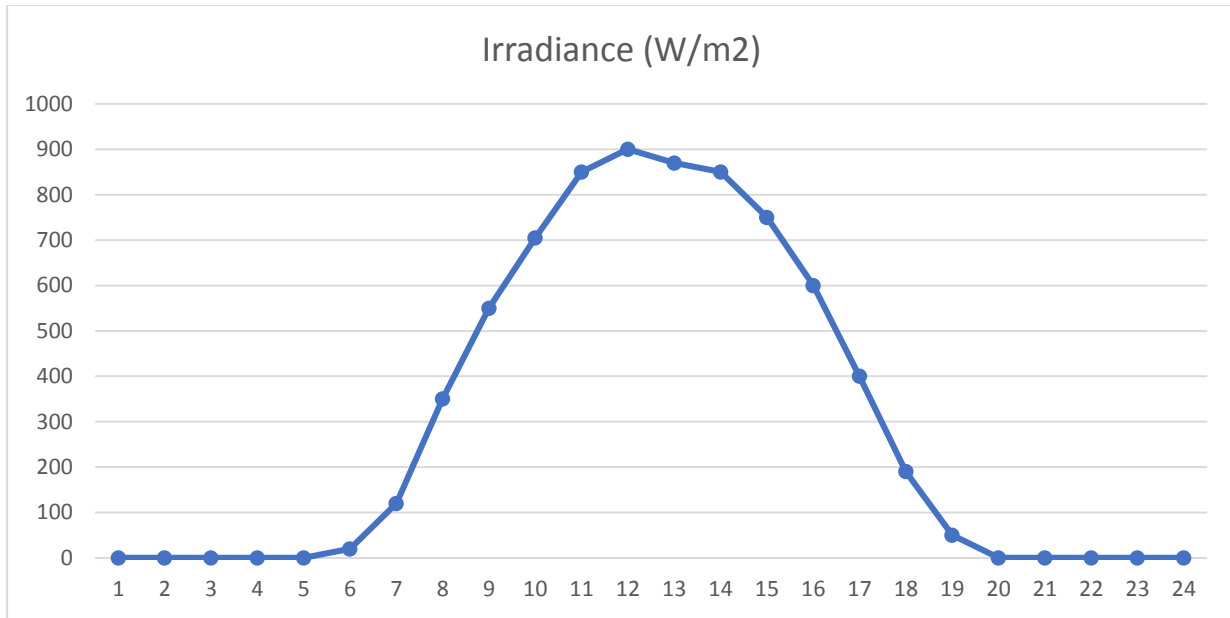


Figure 2.4-4: Irradiance in W/m2 for Solar PV plant for one day

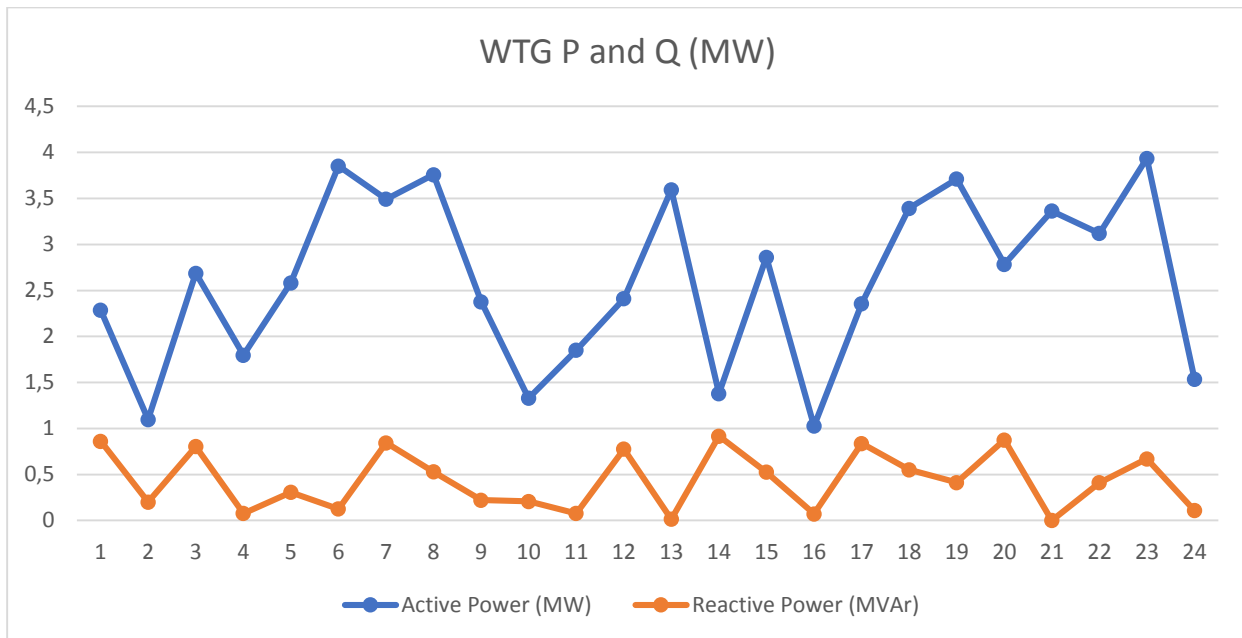


Figure 2.4-5: Wind Turbine Generator P and Q variation for one day

After this, and upon running the time domain load flow (TDLF) for one complete month started from 01/05/2024 till 31/05/2024, below is the total system performance.

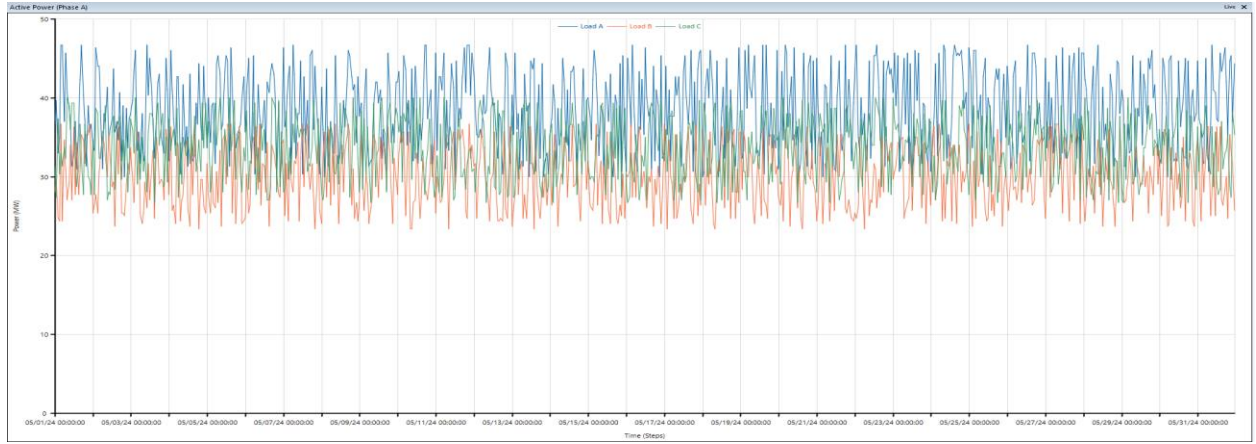


Figure 2.4-6: Loads A, B, and C variations over one month.

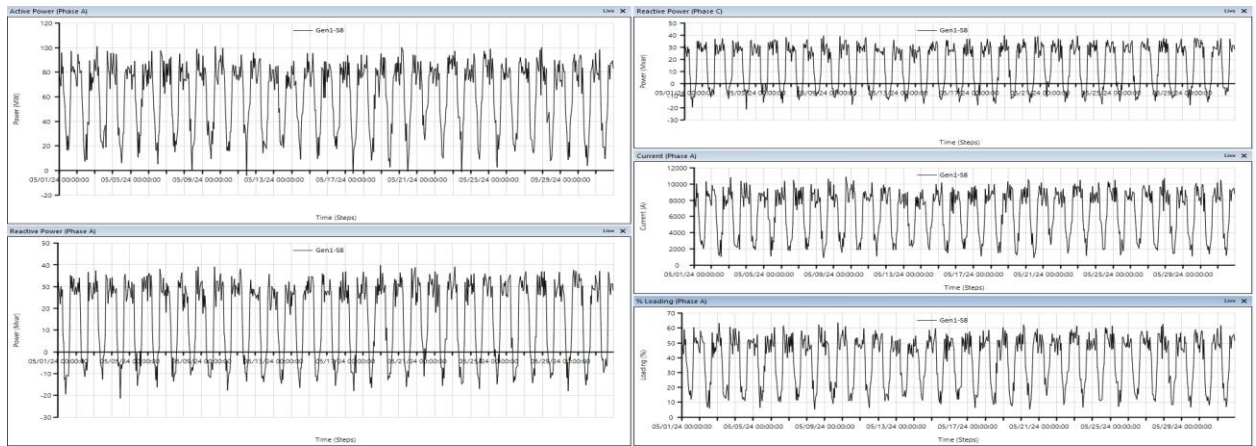


Figure 2.4-7: Hydroelectric Generator No.1 time domain power flow main parameters.

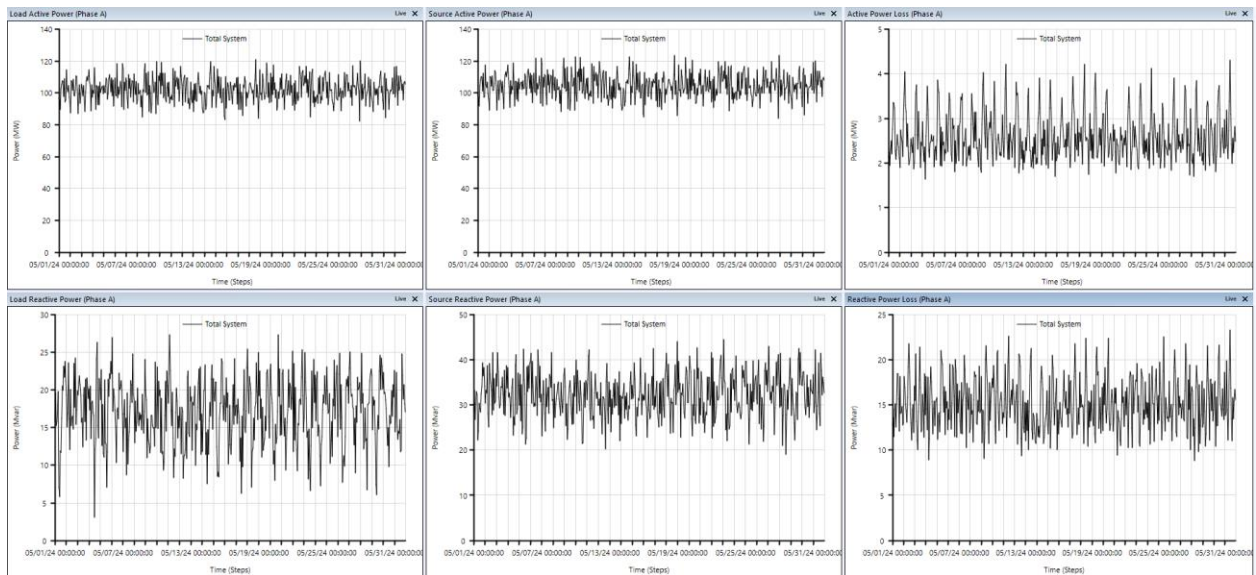


Figure 2.4-8: Total system performance over one complete month

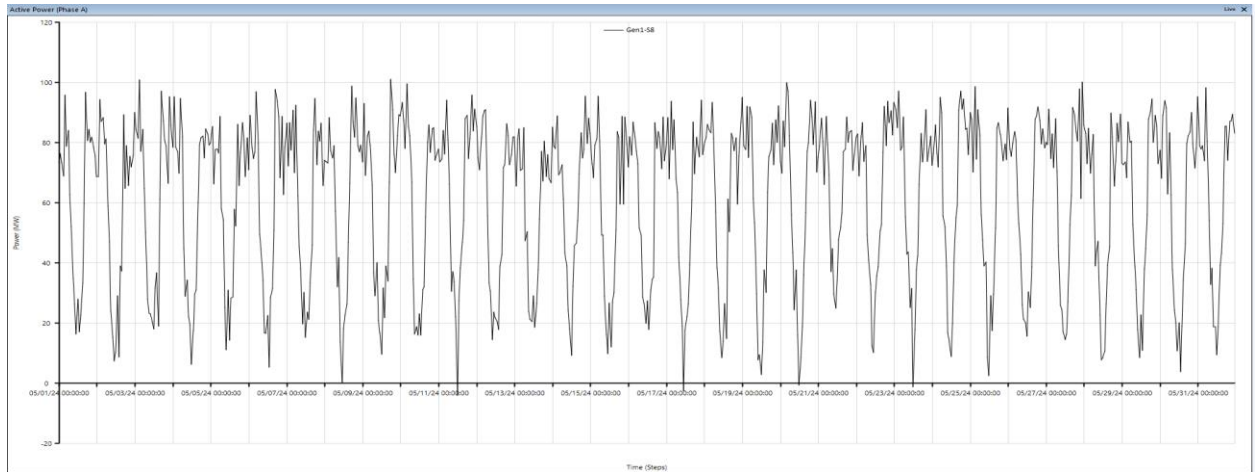


Figure 2.4-9: Hydro Electric Generator Active Power Flow over one complete month.

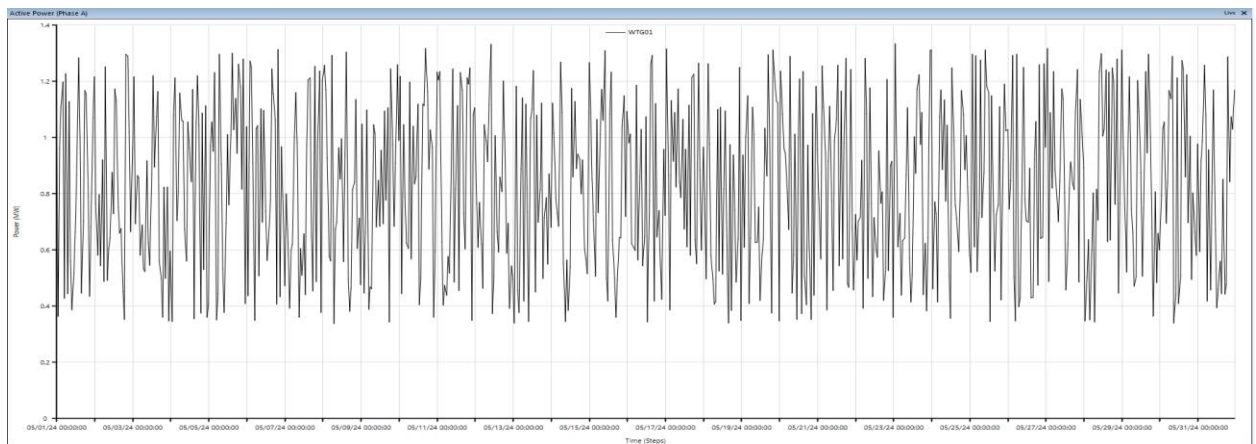


Figure 2.4-10: Wind Turbine Generator Active Power Flow over one complete month.

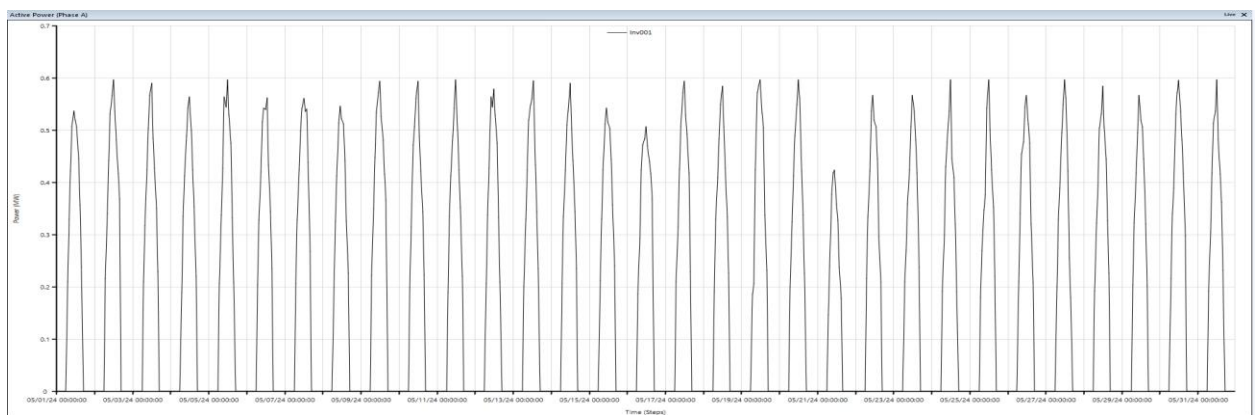
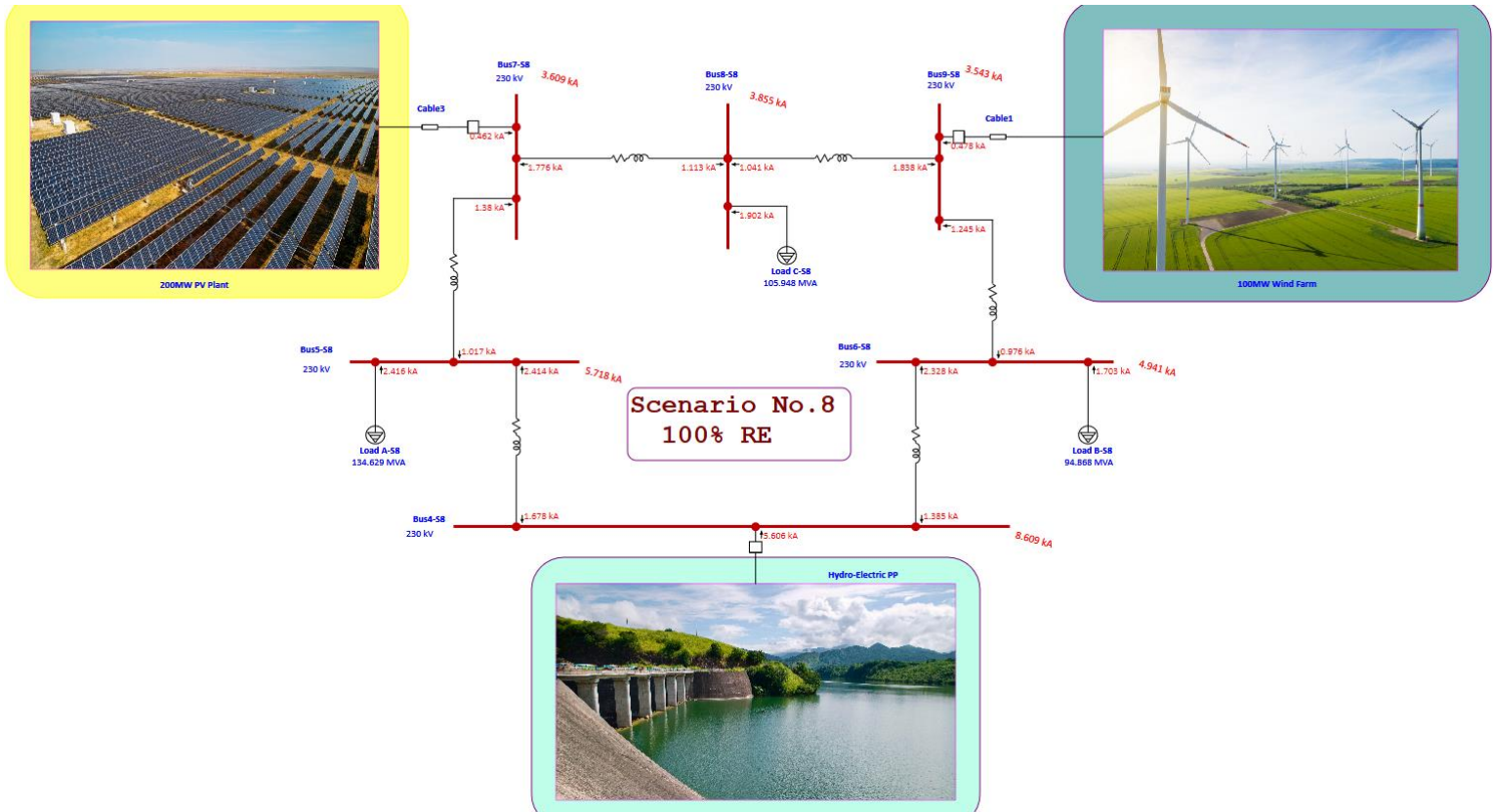


Figure 2.4-11: PV Generator Active Power Flow over one complete month.

### 2.4.1.3 Fault Simulation with ETAP software

Fault simulation of three phase fault at all transmission buses has been conducted using ETAP short circuit calculation is performed based on IEC 60909 as shown **Figure 2.4-12**



**Figure 2.4-12:** ETAP - Run 3-Phase Device Duty using IEC 60909 at Transmission Buses of IEEE 9 Bus system

The source of the short circuit at all buses contributed from all types of sources like hydroelectric generator, wind turbine generator, and solar PV generator, however the contribution from all inverters-based resources like solar and wind are minimal compared to the large synchronous machines in the hydroelectric power plants

Besides, a transient short circuit analysis was conducted using ETAP as per IEC 61363 as shown in **Figure 2.4-13**

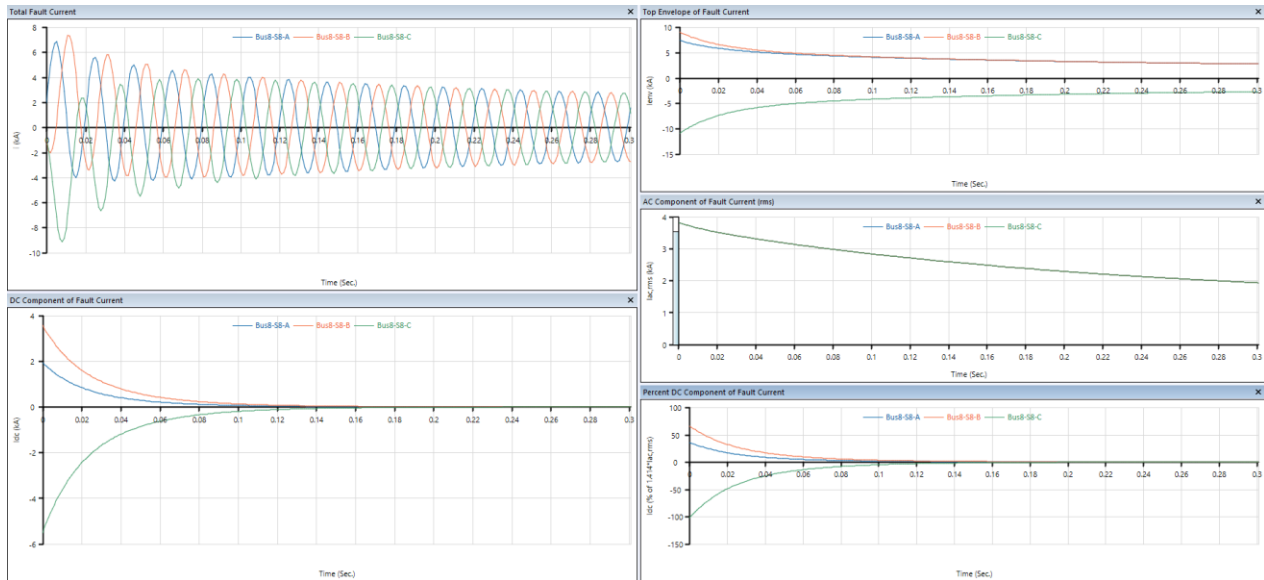


**Figure 2.4-13:** ETAP - Run Transient SC using IEC 61363

**Figure 2.3-19** shows the graphs generated from ETAP software upon simulating the transient short circuit current at Bus No.8

#### 2.4.1.4 Harmonic Analysis at PoCC Using ETAP

In our case study, the 200MW grid connected PV plant and 100MW wind farm, one harmonic model has been introduced for each solar inverter /WTG converter which is typical IEEE-12 pulse as shown in **Figure 2.4-14**. Both time domain graph that shows the overall resultant distorted waveform, as well as the frequency domain graph for the voltage at PoCC have been drawn, and both current THD and voltage THD at PoCC have been simulated. See below **Figure 2.4-15**

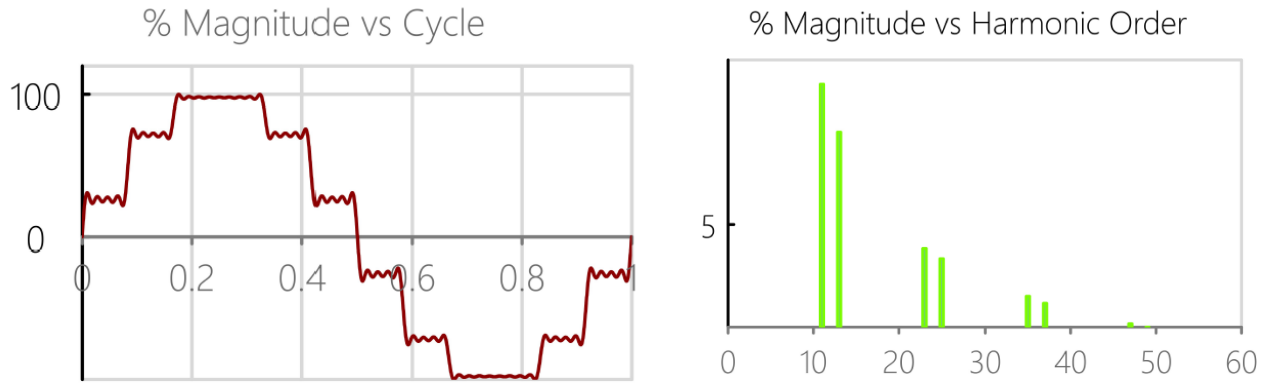


Figure 2.4-14: IEEE 12 Pulse Pre-defined Harmonic Model (Waveform and Spectrum)

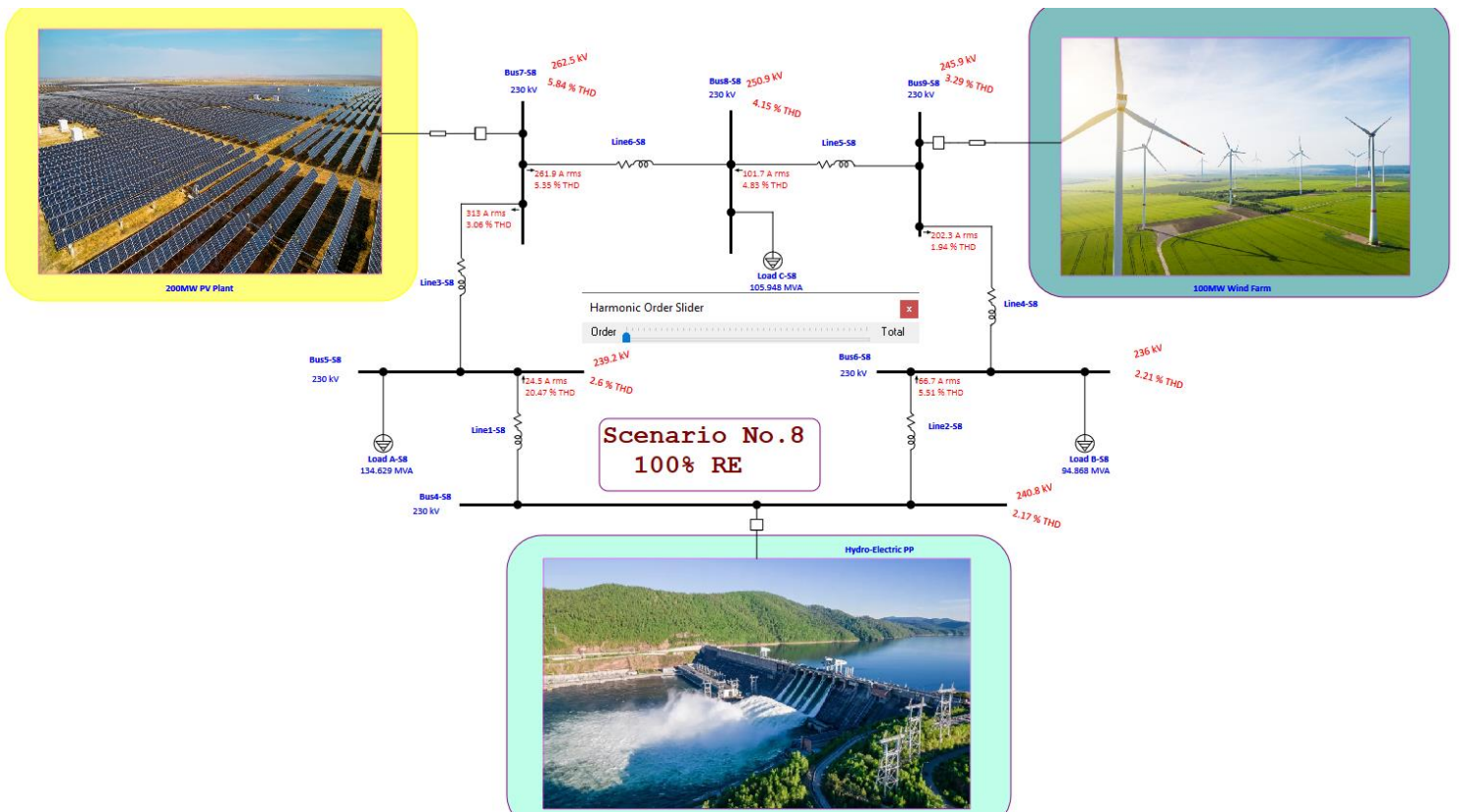


Figure 2.4-15: ETAP Harmonic Analysis output voltage and current THD (%) on Single Line Diagram

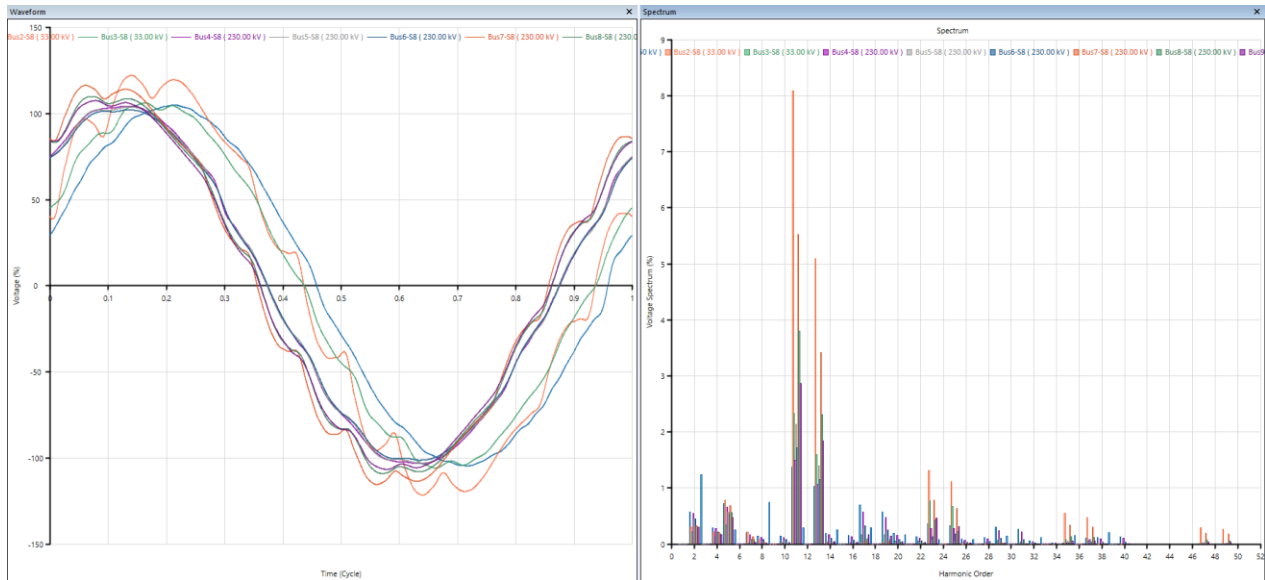


Figure 2.4-16: Distorted waveform and spectrum for main buses

If harmonic frequency scan has been conducted, then we will notice that at 8<sup>th</sup> harmonic order, the driving point impedance is maximum for bus No.2, and at the 23<sup>rd</sup> and 93<sup>rd</sup> harmonic for Bus No.9 the driving point impedance is maximum too.

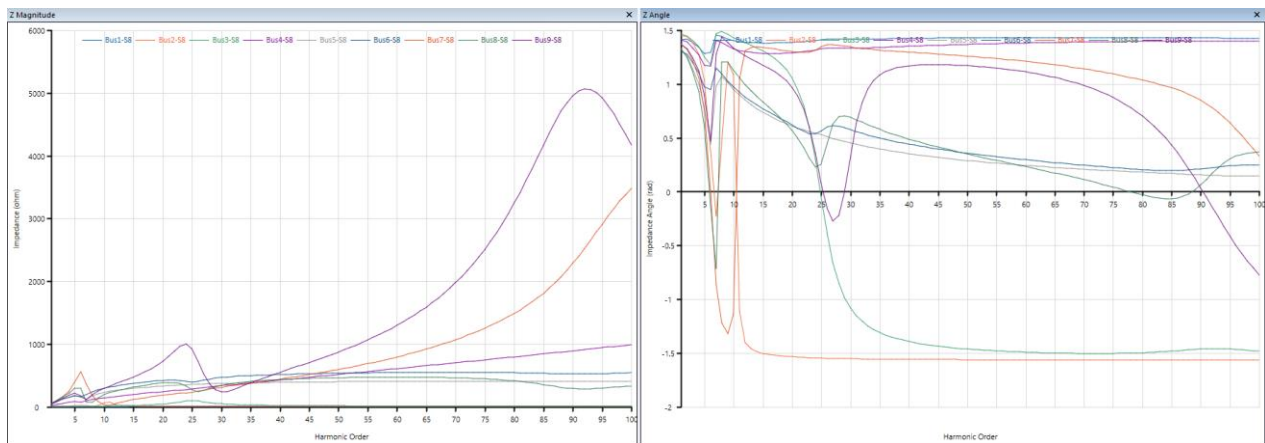


Figure 2.4-17: Harmonic Impedance Scan (Z magnitude and Z angle)

#### 2.4.1.5 Transient Stability Using ETAP

Under this section, several types of disturbances will be introduced into the system and simulated using ETAP, and after that ability of the “modified IEEE 9 bus system with 100% Renewable Energy system” is going to be examined to return to its normal stable operating condition.

### 2.4.1.5.1 First Disturbance: Three Phase Balanced Fault at PV plant POCC with/without Fault Clearance

The full response and behavior for the hydroelectric power plant generator G1 in response to this large disturbance (three phase fault at PV plant PoCC) is shown below in **Figure 2.4-18**

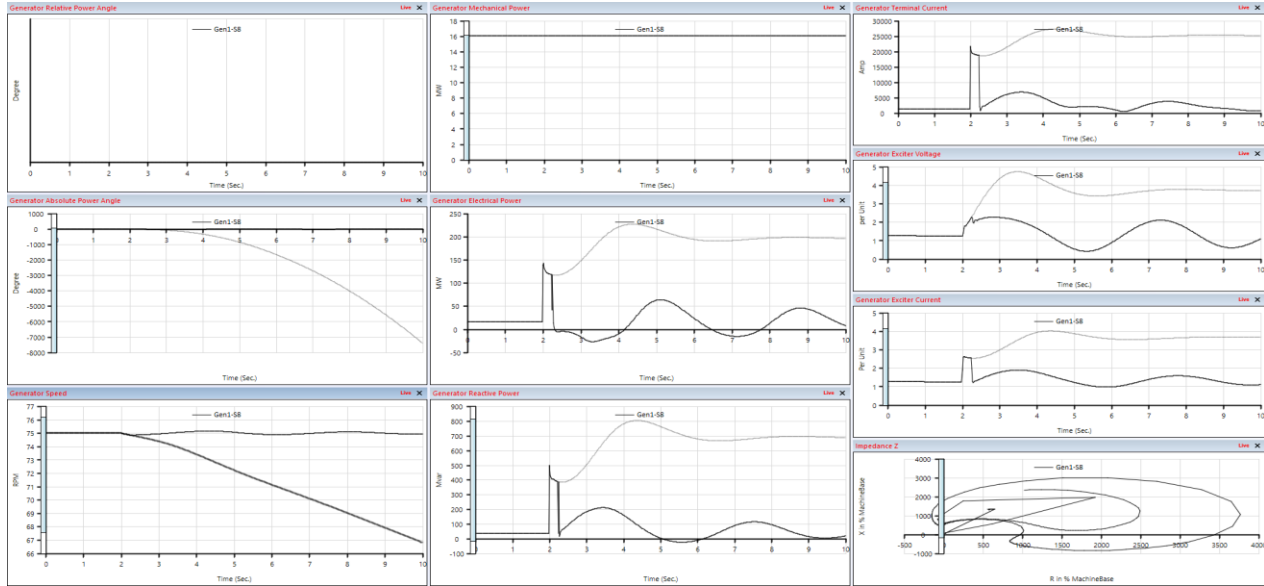


**Figure 2.4-18:** Hydroelectric generator Gen1 dynamic response for a fault at PV plant PoCC with and without fault clearance.

Also, in below the PV plant PoCC bus main parameters behavior

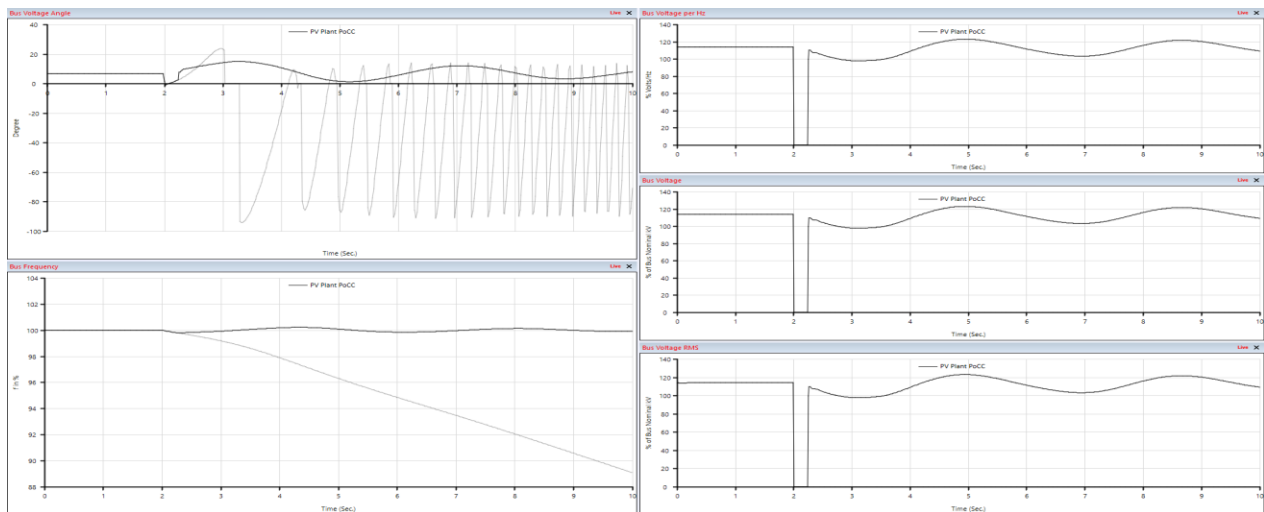


**Figure 2.4-19:** PV plant PoCC dynamic response for a fault at PV plant PoCC with and without fault clearance.

Below **Figure 2.4-20** is the PoCC bus voltage angle with and without fault clearance.

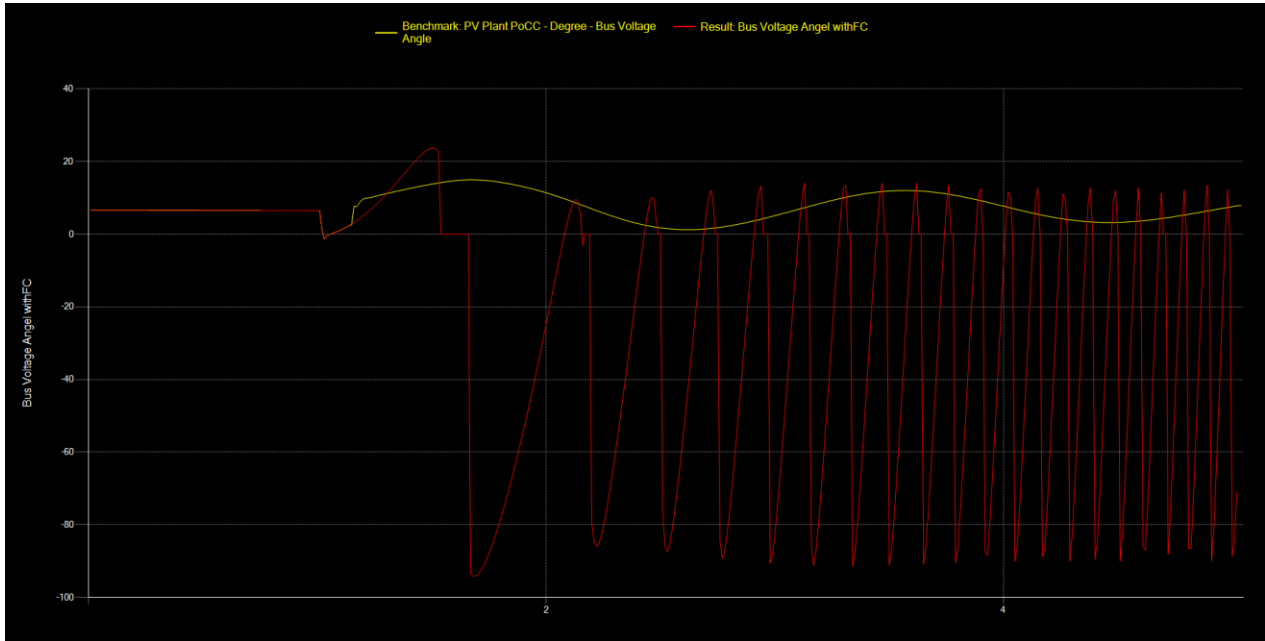


**Figure 2.4-20:** PoCC bus voltage angle with and without fault clearance.

**2.4.1.5.2 Second Disturbance: Three Phase Balanced Fault at WF PoCC with/without Fault Clearance**

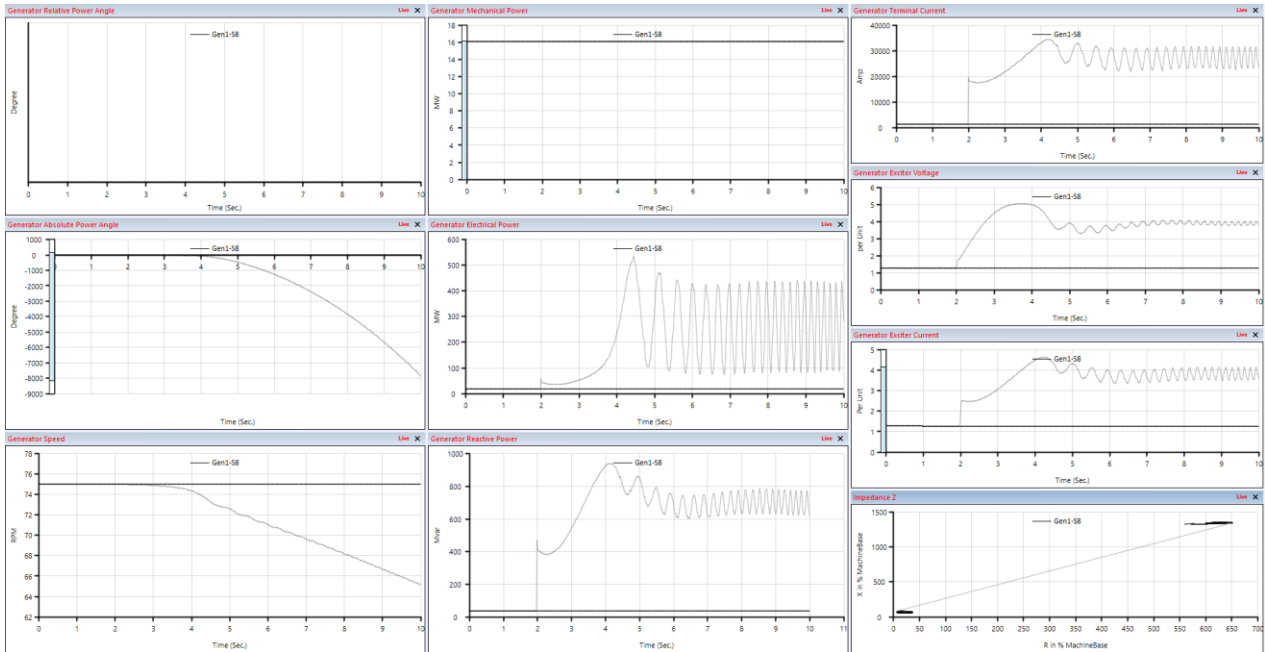


**Figure 2.4-21:** Dynamic Response for HE Gen-1 Three Phase Balanced Fault at WF PoCC with 1 sec FCT

Fault clearing time of 1 sec is not sufficient to return the system stability and forced the system back to its equilibrium.

**2.4.1.5.3 Third Disturbance: Three Phase Balanced Fault at Bus No.8 with Fault Clearance after 0.5 sec**

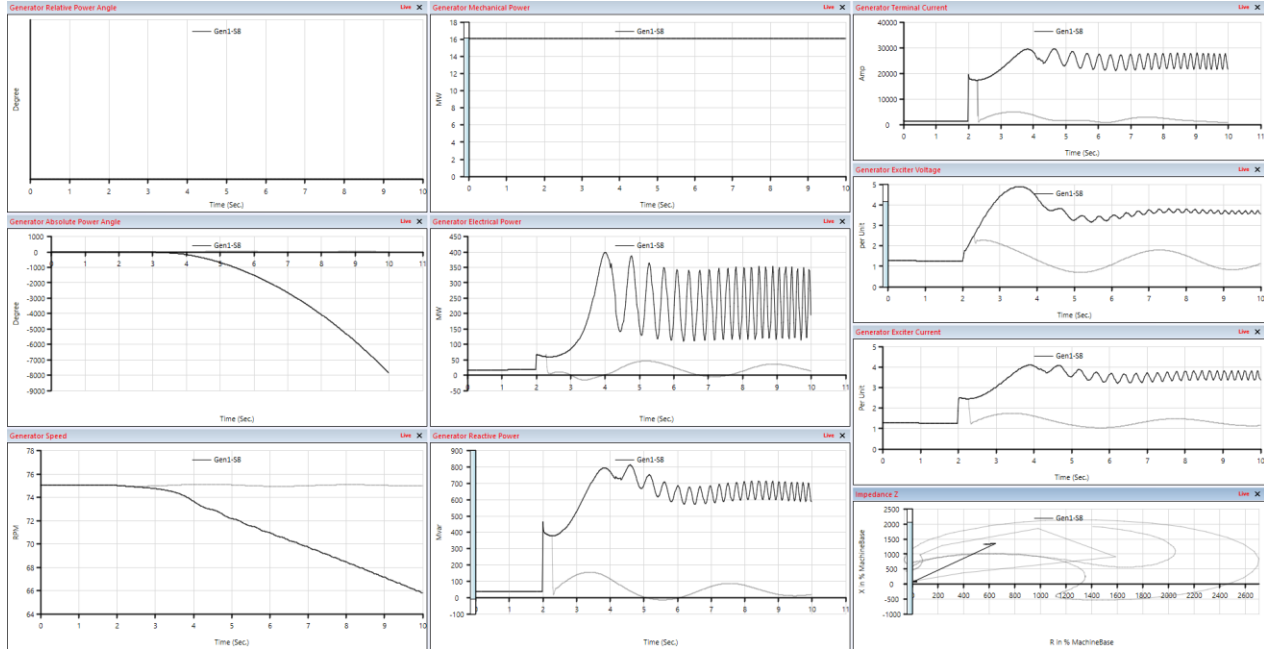


Figure 2.4-22: Dynamic Response for HE Gen-1 Three Phase Balanced Fault at WF PoCC with 0.5 sec FCT

**2.4.1.5.4 Forth Disturbance: Three Phase Balanced Fault at Line 6 with/without Fault Clearance**

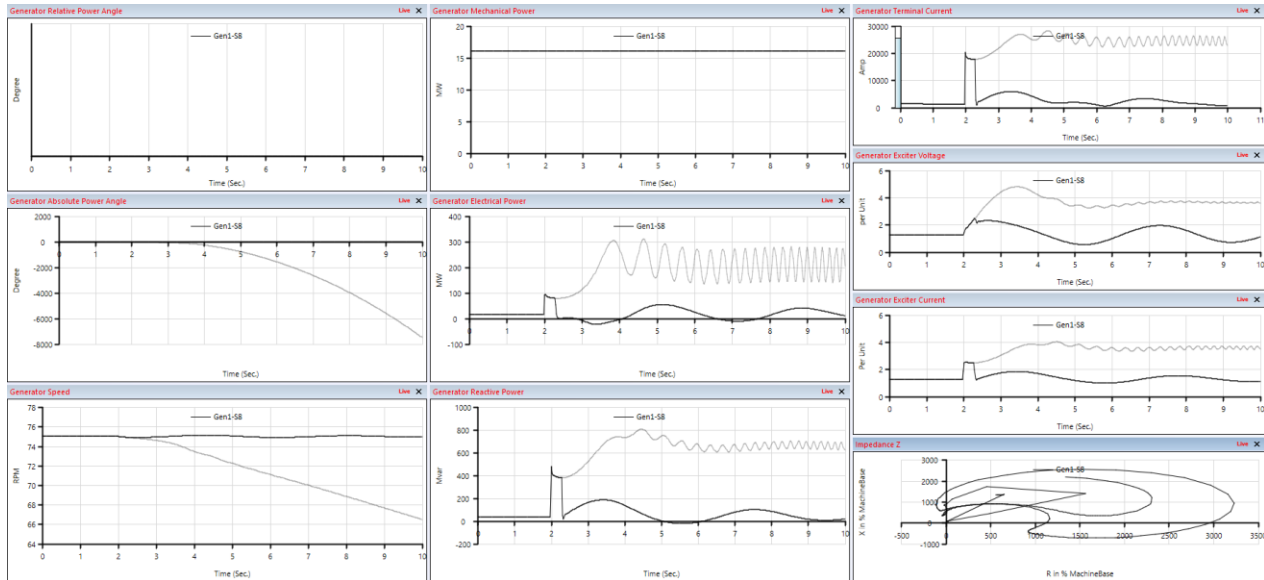


Figure 2.4-23: generator Gen1 response due to Three Phase Balanced Fault at Line 6 with/without Fault Clearance

### 2.4.1.5.5 Fifth Disturbance: Loss of 200MW PV Plant at t=5 sec

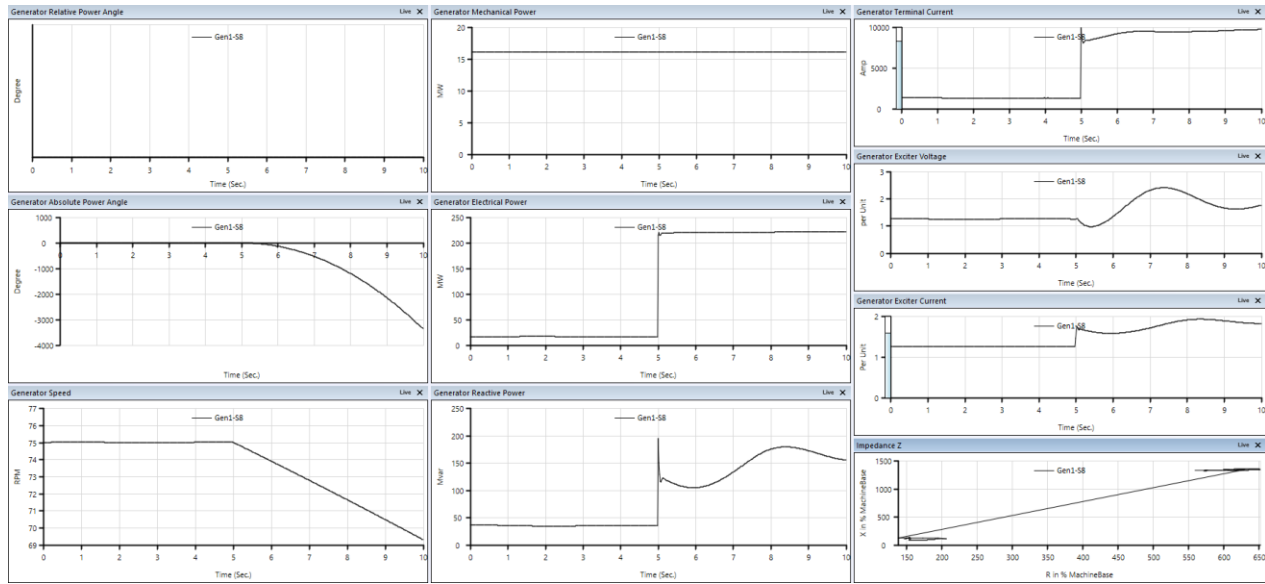


Figure 2.4-24: Generator Gen1 response due to Loss of 200MW PV Plant at t=5 sec

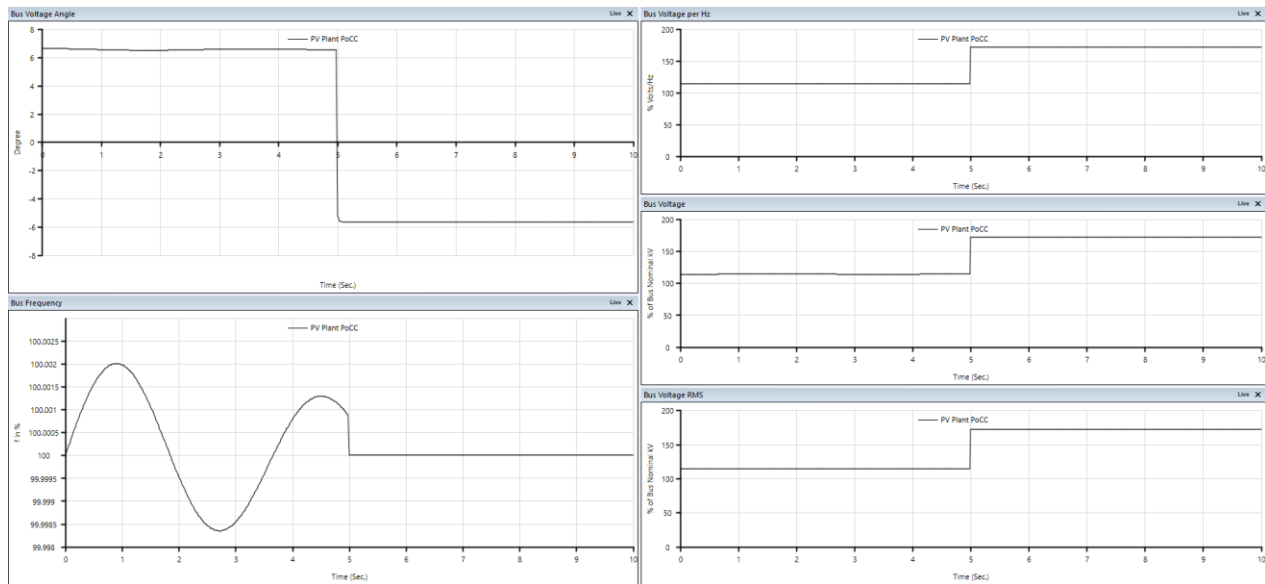


Figure 2.4-25: PV plant PoCC dynamic response due to Loss of 200MW PV Plant

### 2.4.1.5.6 Sixth Disturbance: Loss of 100MW WF at t=5 sec

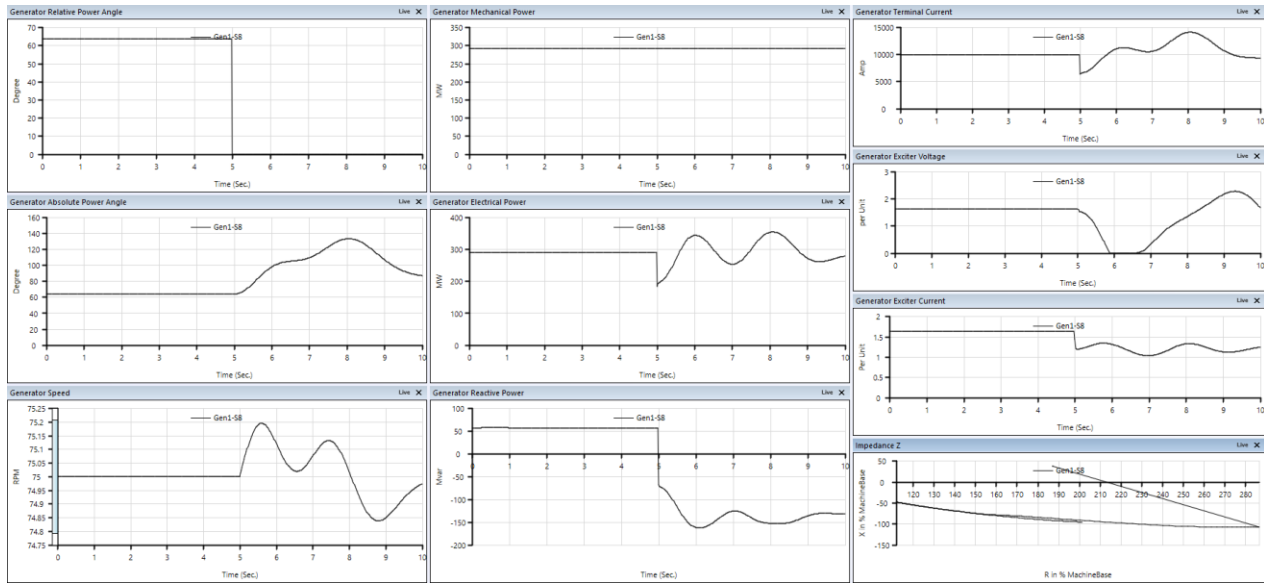


Figure 2.4-26:Generator Gen1 response due to Loss of 100MW Wind Farm at t=5 sec

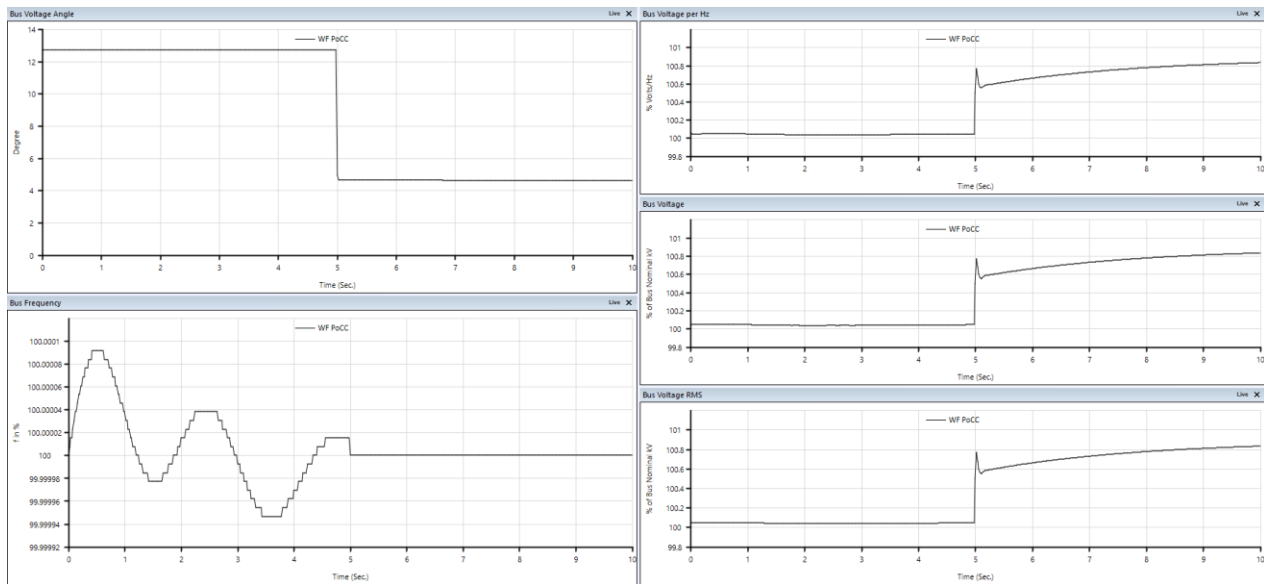


Figure 2.4-27:Wind farm PoCC dynamic response due to Loss of 100MW Wind farm

### 2.4.1.5.7 Seventh Disturbance: Sudden Load Change

Loads A, B and C are assumed to be increased by 20% each 5 sec one at a time

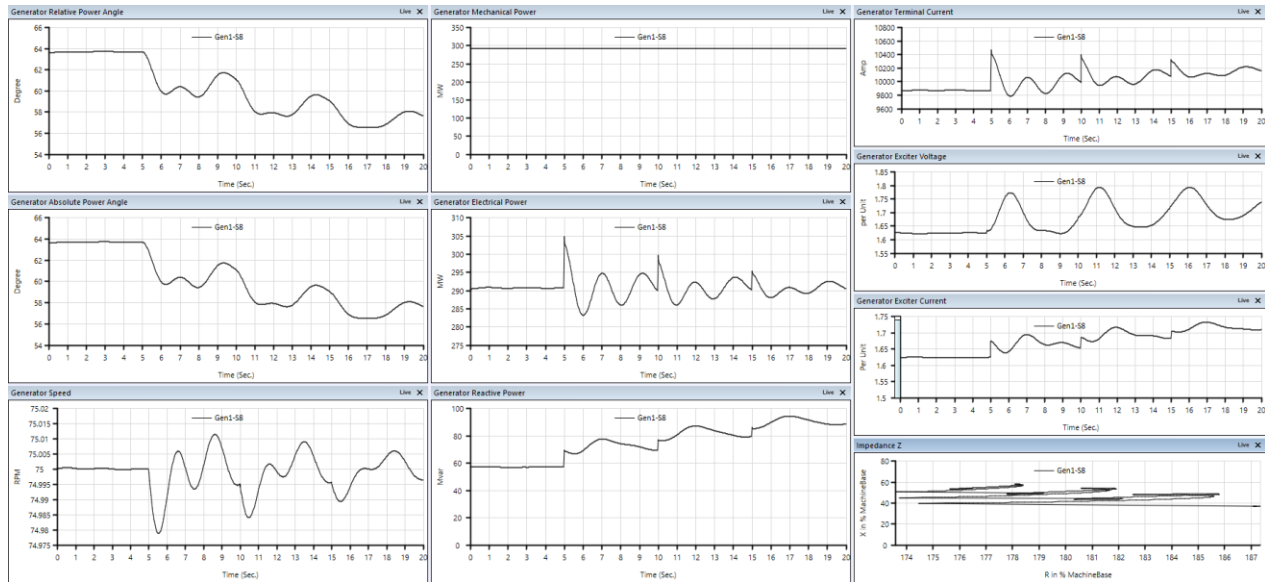


Figure 2.4-28: Generaroe G1 dynamic response due to Loads A, B, and C change

### 2.4.1.5.8 Eighth Disturbance: Tripping/ Disconnection of Line 4

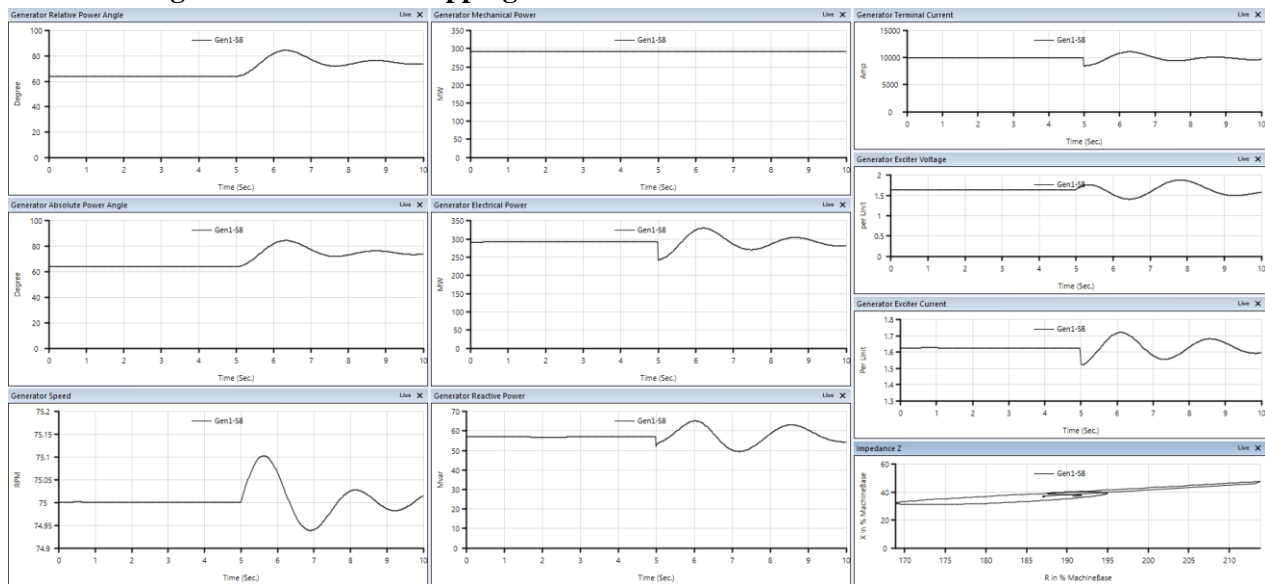


Figure 2.4-29:Generaroe G1 dynamic response due to Line 4 disconnection

### 2.4.1.6 Voltage Stability Study Using ETAP

#### Voltage sensitivity Analysis for IEEE transmission buses

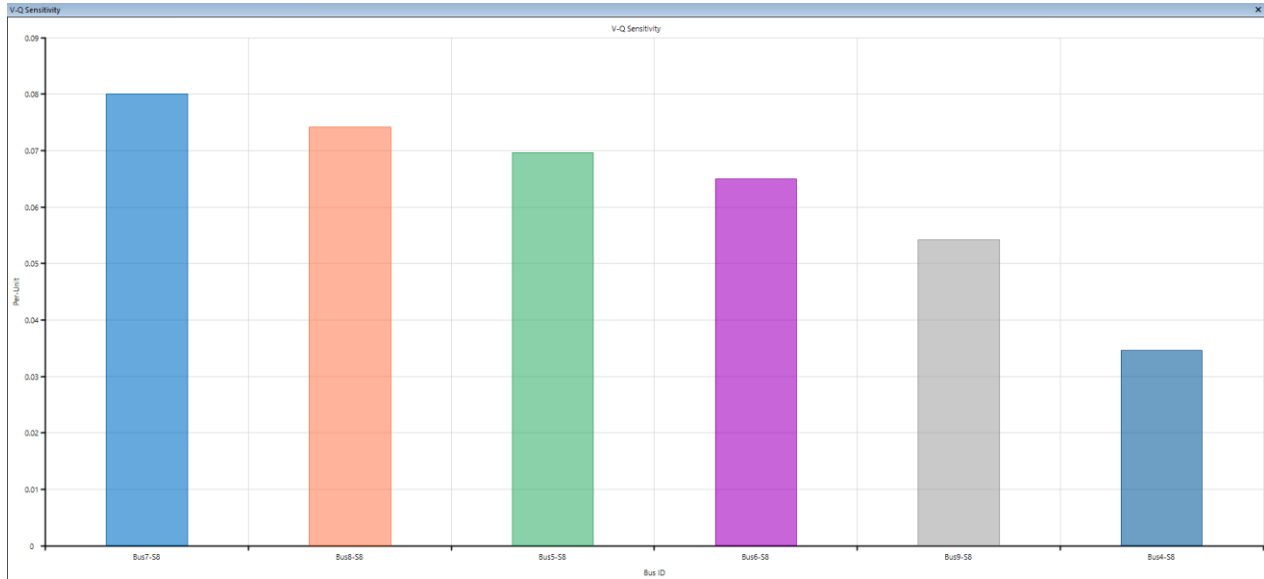


Figure 2.4-30: V-Q Sensitivity Analysis

Q-V and P-V analysis for all IEEE 9-bus – transmission buses are shown in Figure 2.4-31 and Figure 2.4-32

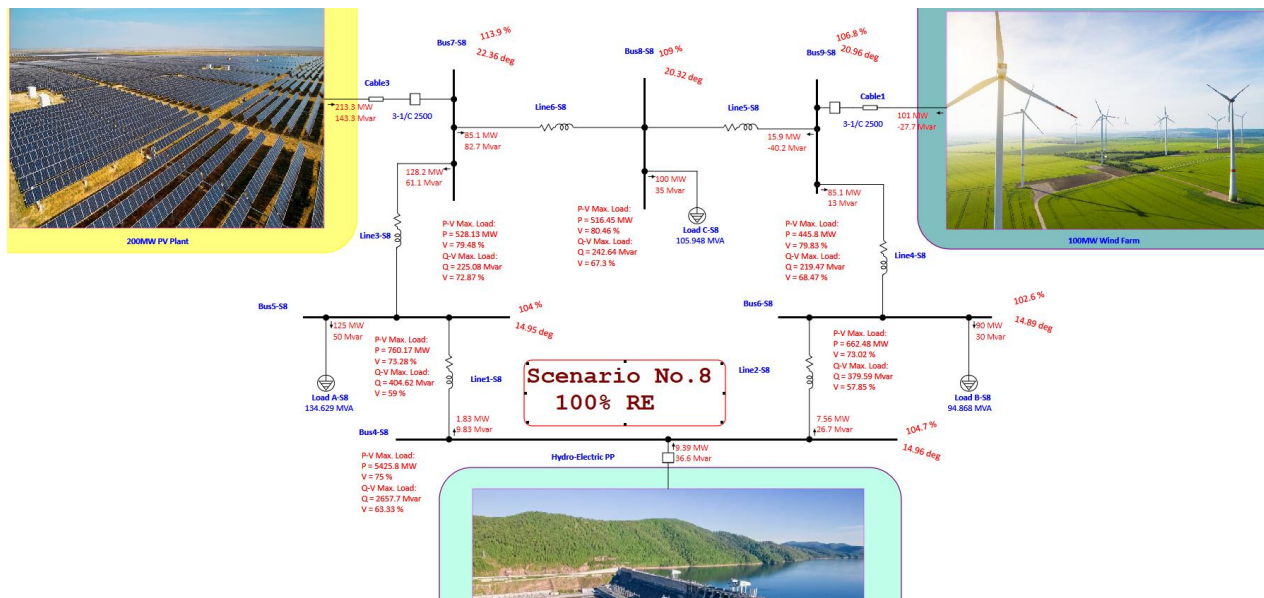


Figure 2.4-31: ETAP P-V and Q-V simulation output of Voltage Stability Study

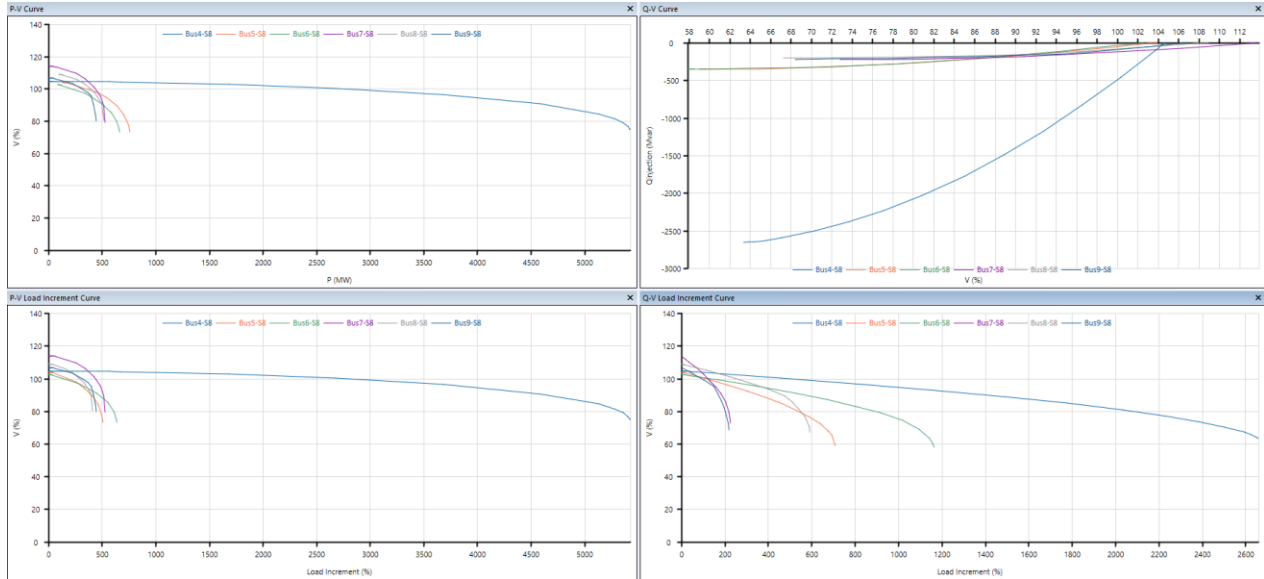


Figure 2.4-32: P-V and Q-V curves for all transmission buses

#### 2.4.1.7 Security

Energy security is sometimes used to promote renewable energy solutions and it is primary objective of energy policy since it enables the requirements of energy users to be satisfied [51]. A state of energy security is one in which the energy system is able to operate in a sustainable manner within the dimensions that are being addressed without being subject to any dangers. For the purpose of this inquiry, six different factors are usually chosen: availability, variety, cost, environment, health, and employment.

To enhance energy security, a more robust approach is needed. Enhanced financial system and governments with more stability. Energy security policies are seen as being interrelated. with policies pertaining to economic development, stability, poverty reduction, and the improvement of living standards, ensuring political stability and delivering public services

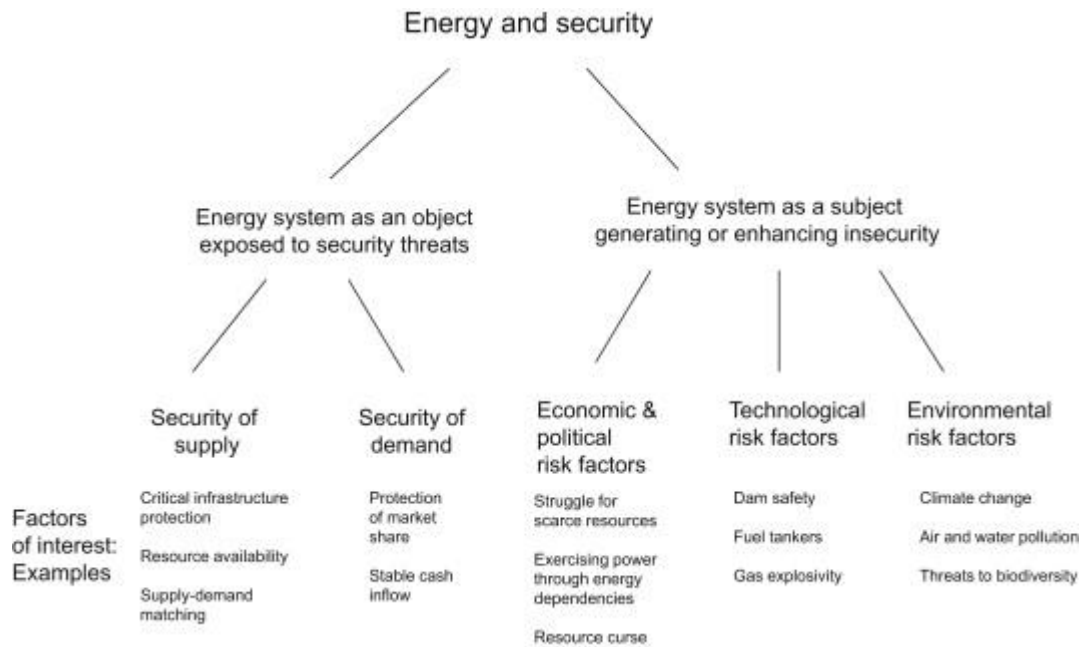


Figure 2.4-33: Energy and Security Classification

#### 2.4.1.8 Interoperability

There will be an increase in the complexity of energy systems as the world moves toward achieving net zero emissions. When there is a larger dependence on intermittent power and energy sources like solar and wind, it is necessary to have a system that is able to use, store, or sell extra electricity ( the surplus of energy ) when available energy is high or demand is low, and then draw upon reserves when the reverse is true [50].

In this chapter, scenario No.8, the full power generated for the IEEE 9 bus system will be from renewable energy sources, and to maximize the power generated from solar and wind, the electrical power system must be interoperable with high ability of several networks, systems, devices, applications, or components to share and utilize information safely and efficiently.

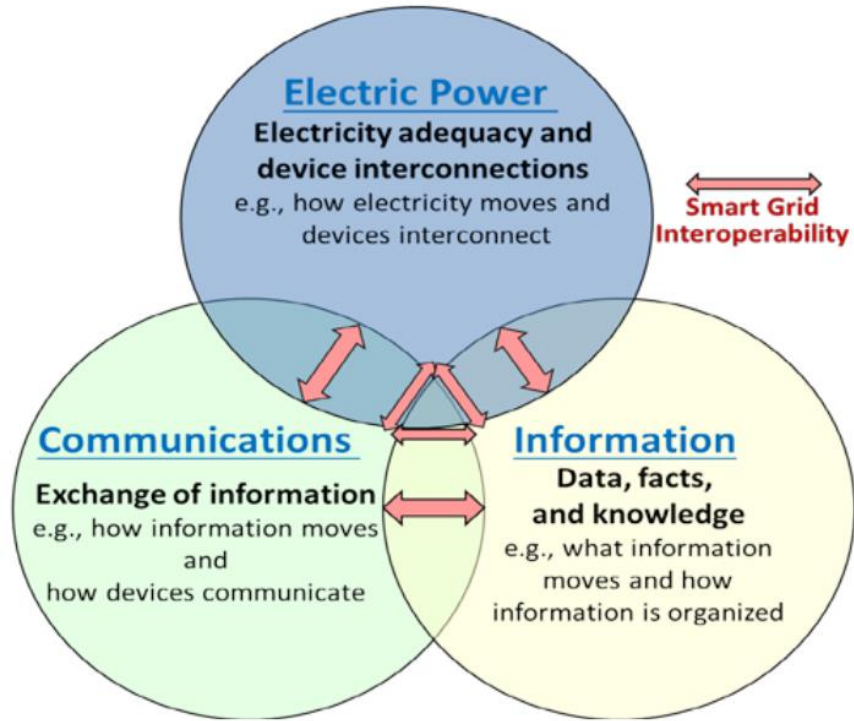


Figure 2.4-34: Smart Grid Interoperability pillars

The 2030 standard is a guide published by the Institute of Electrical and Electronics Engineers (IEEE) that provides a knowledge base on terminology, characteristics, and functional performance of the Smart Grid. It establishes the 2030 Smart Grid Interoperability Reference Model (SGIRM), which allows for extensibility, scalability, and upgradeability. The SGIRM defines the integrated architectural perspectives for power systems, communications technology, and information technology. The emphasis of the SGIRM is on functional interfaces, logical connections, and data flows. IEEE Standard 2030 also includes design tables and classification of data flow characteristics, as well as templates for identifying power perspective needs and integrating information-communication technology protocols and standards. These protocols and standards address reliability, security, cyber issues, quality of service, and communication mediums [48].

## PART THREE



### 3.1 CHAPTER EIGHT: DATA COLLECTION AND ANALYSIS

In this chapter, data collection and data analysis have been conducted through collecting, inspecting, cleaning, transforming, and modeling the data from the ETAP software simulation outputs using eight (8) sustainable energy transformation scenarios, and the main purpose is to extract information and insights from raw data to support power system planning and decision-making about the applicability for the results on a larger scale electrical power system.

The data analysis process involves a structured sequence of steps listed below that lead from raw data to insightful information with actionable steps, and the steps are as

### 3.1.1 Data Collection:

First step in data analysis is the data collection where the relevant data have been gathered from the simulation results of eight (8) sustainable energy scenarios for the IEEE-9 bus system using the Electric Transient Analyzer Program (ETAP) software as per below eight (8) scenarios:

1. Original IEEE 9 bus system with 0% Renewable penetration of IEEE 9-Bus System with Fossil Fuel Primary Energy Sources driven Synchronous Machines SM1, SM2, and SM3.
2. 14% Renewable Contribution with IEEE 9-Bus System with Fossil Fuel Primary Energy Sources driven Synchronous Machines SM1 and SM2 + 125MVA Wind Farm replaces SM3.
3. 30% Renewable Contribution with IEEE 9-Bus System with Fossil Fuel Primary Energy Sources driven Synchronous Machines SM1 and SM3 + 270MVA PV plant replaces SM2.
4. 44% Renewable Contribution for IEEE 9-Bus System with Fossil Fuel Primary Energy Sources driven Synchronous Machine SM1 with 270MVA PV Plant Replacing SM2+ 125MVA Wind Farm replaces SM3.
5. 56% Renewable Contribution for IEEE 9-Bus System with Fossil Fuel Primary Energy Sources driven Synchronous Machines SM2 and SM3 with 512MVA Hydro Electric Power Plant replacing SM1.
6. 70% Renewable Contribution for IEEE 9-Bus System with Fossil Fuel Primary Energy Sources driven Synchronous Machine SM2 with 512MVA Hydro Electric Power Plant replacing SM1 + 125MVA Wind farm replaces SM3.
7. 85% Renewable Contribution for IEEE 9-Bus System with Fossil Fuel Primary Energy Sources driven Synchronous Machine SM3 with 512MVA Hydro Electric Power Plant replacing SM1 + 270MVA PV plant replaces SM2.
8. 100% Renewable for IEEE 9-Bus System with Fossil Free Primary Energy Sources (Solar / Wind / Hydro) with 512MVA Hydroelectric Power Plant replaces SM1+270MVA PV Plant Replacing SM2+ 125MVA Wind Farm replaces SM3.

The scenarios listed above are as per tabulation and graph below:

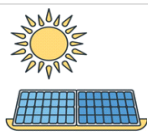
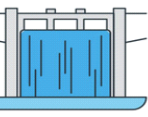
Technology	S1 - 0% Renewable	S2- 14% Renewable - Wind	S3 - 30% Renewable - Solar	S4 - 44% Renewable - Wind & Solar	S5 - 56% Renewable - Hydro	S6- 70% Renewable - Hydro & Wind	S7- 86% Renewable - Hydro & Solar	S8 - 100% Renewable - Hydro, Wind , & solar
	100%	86%	70%	56%	44%	30%	14%	0%
	0%	14%	0%	14%	0%	14%	0%	14%
	0%	0%	30%	30%	0%	0%	30%	30%
	0%	0%	0%	0%	56%	56%	56%	56%

Figure 3.1-1: Eight (8) sustainable energy scenarios and contribution in (%) of MW per technology.

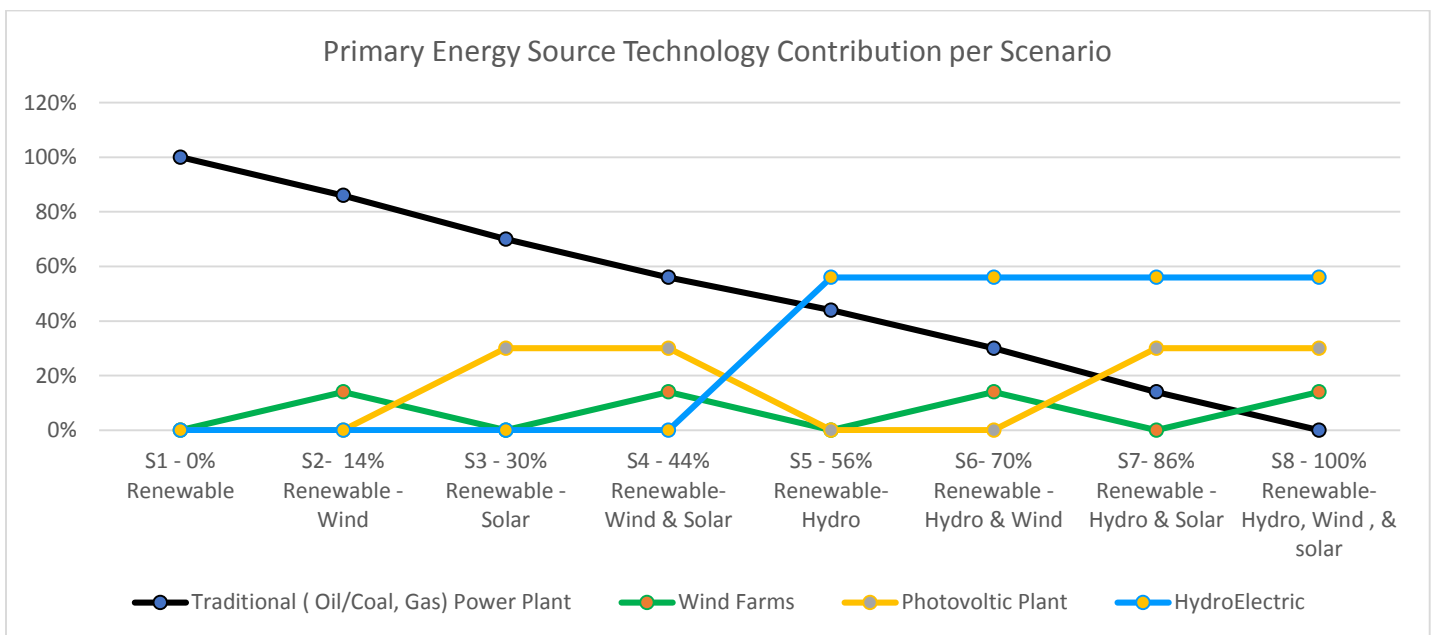


Figure 3.1-2: Primary Energy Source Technology Contribution per Scenario

The data collected will be from three (3) main sources:

*3.1.1.1 Data Source No.1:*

Data from simulation of a Time Domain Load Flow (TDLF) analysis for one complete month started from 1/5/2024 till 31/5/2024 for each scenario of the 8 scenarios, under which the Levelized Cost of Energy (LOCE), and estimated CO2 emissions have been calculated based on the total system, power / energy output reports from ETAP for each scenario for the whole month. See below sample for the data output from TDLF for one day for the 8th Scenario (100% Renewable energy). However, the actual outputs from the ETAP are for the full month of May with 31 days, and below you can see the summary for the energy generated (MWh) for the 100% renewable scenario showing the contribution of each energy technology over the whole month.

Date	Time	S8-RE 100% $\sigma$ Source kW	S8-RE 100% $\sigma$ Source kvar	S8-RE 100% $\sigma$ Wind kW	S8-RE 100% $\sigma$ Solar kW	S8-RE 100% $\sigma$ AC Load kW	S8-RE 100% $\sigma$ AC Load kvar	S8-RE 100% $\sigma$ Losses kW
2024-05-01	00:00:00	351431.4	98448.5	69695.1	0.0	343000	46485.3	8431.4
2024-05-01	01:00:00	337404.7	123547.7	70848.1	0.0	329000	70558.8	8404.7
2024-05-01	02:00:00	298471.5	87106.0	73555.3	0.0	292000	48625.2	6471.5
2024-05-01	03:00:00	335217.1	114439.2	77786.2	0.0	327000	61906.7	8217.1
2024-05-01	04:00:00	293215.7	81355.8	67162.4	0.0	287000	44943.2	6215.7
2024-05-01	05:00:00	324350.3	112603.3	74598.4	0.2	317000	67049.4	7350.3
2024-05-01	06:00:00	299636.7	113813.4	68408.2	5.1	293000	72556.9	6636.7
2024-05-01	07:00:00	331444.9	75443.7	66842.4	75410.5	325000	39386.3	6444.9
2024-05-01	08:00:00	317305.5	83671.9	65364.1	118264.6	311000	47923.2	6305.5
2024-05-01	09:00:00	315320.0	92056.1	76697.5	151593.7	307000	46831.4	8320.0
2024-05-01	10:00:00	305536.3	76177.9	68187.5	182405.0	296000	23862.6	9536.3
2024-05-01	11:00:00	325583.1	85580.7	72993.3	193134.7	315000	27359.7	10583.1
2024-05-01	12:00:00	373658.8	101107.7	64235.2	186696.9	364000	45142.0	9658.8
2024-05-01	13:00:00	275056.1	96526.0	69633.5	182037.2	265000	42974.4	10056.1
2024-05-01	14:00:00	332362.1	91490.6	69928.3	160296.3	324000	44910.4	8362.1
2024-05-01	15:00:00	261093.1	72404.5	75824.0	127977.1	254000	35519.1	7093.1
2024-05-01	16:00:00	309355.0	65745.5	72273.4	85491.4	303000	31946.0	6355.0
2024-05-01	17:00:00	329368.7	92207.9	72003.3	17.9	322000	45963.1	7368.7
2024-05-01	18:00:00	297705.0	108358.6	67794.6	0.8	291000	66487.2	6705.0
2024-05-01	19:00:00	305634.4	90768.4	75721.0	0.0	299000	50545.2	6634.4
2024-05-01	20:00:00	322607.4	101581.1	70201.9	0.0	315000	55920.9	7607.4
2024-05-01	21:00:00	322597.0	112102.1	70549.7	0.0	315000	64213.2	7597.0
2024-05-01	22:00:00	345314.7	115846.4	71426.8	0.0	337000	64071.5	8314.7
2024-05-01	23:00:00	284047.3	96019.3	65591.3	0.0	278000	58795.3	6047.3

### 3.1.1.2 Data Source No.2

Second source of data was collected from simulation output from a transient stability study for the 8 scenarios based one major disturbance of 3 phase balanced fault (major disturbance) at busbar No.8 at which Load C is connected, and the simulation was performed for total simulation time of 10 sec. See below sample for the data output up to 0.5 sec.

Time (Sec.)	S1 Gen1 - Degree - Absolute Power Angle	S2 Gen1 - Degree - Absolute Power Angle	S3 Gen1 - Degree - Absolute Power Angle	S4Gen1 - Degree - Absolute Power Angle	S5 Gen1 - Degree - Absolute Power Angle	S6 Gen1 - Degree - Absolute Power Angle	S7 Gen1 - Degree - Absolute Power Angle	S8 Gen1 - Degree - Absolute Power Angle
0	0	0	0	0	0	0	0	0
0.001	-0.0001	-0.0001	0	0	-0.0001	-0.0001	0	0
0.021	-0.0214	-0.0304	-0.0098	-0.0175	-0.0195	-0.0284	-0.0096	-0.0173
0.041	-0.0767	-0.1127	-0.0336	-0.0649	-0.0703	-0.1058	-0.0329	-0.0641
0.061	-0.1635	-0.2454	-0.0701	-0.1416	-0.1505	-0.2308	-0.0687	-0.1401
0.081	-0.2795	-0.4265	-0.1185	-0.2476	-0.2581	-0.4021	-0.1163	-0.2449
0.101	-0.4223	-0.654	-0.178	-0.3824	-0.3913	-0.618	-0.175	-0.3783
0.121	-0.5896	-0.9259	-0.2479	-0.5457	-0.548	-0.8768	-0.2439	-0.5401
0.141	-0.7789	-1.2403	-0.3272	-0.7371	-0.7262	-1.1769	-0.3225	-0.7297
0.161	-0.9882	-1.5951	-0.4154	-0.9562	-0.9241	-1.5167	-0.4098	-0.947
0.181	-1.2153	-1.9886	-0.5116	-1.2027	-1.1397	-1.8945	-0.5054	-1.1915
0.201	-1.4579	-2.4187	-0.6151	-1.4761	-1.3712	-2.3088	-0.6085	-1.4629
0.221	-1.7139	-2.8835	-0.7255	-1.7761	-1.6166	-2.7579	-0.7186	-1.7611
0.241	-1.9814	-3.3813	-0.8419	-2.1025	-1.8742	-3.2402	-0.8351	-2.0858
0.261	-2.2581	-3.91	-0.9638	-2.4548	-2.142	-3.7542	-0.9574	-2.4367
0.281	-2.5421	-4.468	-1.0908	-2.8329	-2.4181	-4.2984	-1.085	-2.8137
0.301	-2.8314	-5.0532	-1.2222	-3.2364	-2.7009	-4.871	-1.2175	-3.2167
0.321	-3.1238	-5.664	-1.3575	-3.6652	-2.9884	-5.4707	-1.3544	-3.6455
0.341	-3.4175	-6.2985	-1.4963	-4.1189	-3.2787	-6.0958	-1.4953	-4.1
0.361	-3.7104	-6.9549	-1.6381	-4.5973	-3.5701	-6.745	-1.6397	-4.5802
0.381	-4.0007	-7.6315	-1.7825	-5.1003	-3.8608	-7.4167	-1.7873	-5.086
0.401	-4.2863	-8.3267	-1.929	-5.6277	-4.149	-8.1094	-1.9378	-5.6174
0.421	-4.5656	-9.0388	-2.0773	-6.1794	-4.4329	-8.822	-2.0907	-6.1745
0.441	-4.8366	-9.7664	-2.227	-6.7551	-4.7108	-9.5529	-2.2457	-6.7572
0.461	-5.0978	-10.508	-2.3778	-7.3548	-4.9811	-10.3012	-2.4027	-7.3657
0.481	-5.3474	-11.2623	-2.5294	-7.9784	-5.2422	-11.0655	-2.5613	-8.0001
0.5	-5.5724	-11.9895	-2.6738	-8.5929	-5.4803	-11.8056	-2.7132	-8.6268

### 3.1.1.3 Data Source No.3:

In this part, the third source of data was collected from the following power system analysis studies for each scenario:

- 1- Power Flow Study
- 2- Short circuit calculation
- 3- Harmonic analysis
- 4- Voltage stability study

And the data will be collected in tabulated form.

Parameter	Bus ID	S1-0% RE-LFA	S2-15% RE-Wind-LFA	S3-30% RE-S	S4-44% Renewable-Wind & Solar	S5-56% RE-Hydro	S6-70% Renewable-Hydro & Wind	S7-86% Renewable-Hydro & Solar	S8-100% Renewable-Hydro Wind & solar
Voltage (%)	Bus4	104.14	104.5	104.23	104.73	103.81	104.5	104.23	104.73
Voltage (%)	Bus5	101.28	102.75	102	104.04	97.86	102.75	102	104.04
Voltage (%)	Bus6	100.17	102.28	100.4	103.24	99.38	102.28	100.4	103.24
Voltage (%)	Bus7	107.66	110.96	109.4	113.99	96.53	110.96	109.4	113.99
Voltage (%)	Bus8	103	107.27	104.09	109.91	95.99	107.27	104.09	109.91
Voltage (%)	Bus9	101.31	106.46	101.71	106.59	98.68	106.46	101.71	106.59
IK (kA)	Bus4	23.00549	22.76598	22.59304	22.11614	23.00549	22.76598	22.59304	22.11614
IK (kA)	Bus5	15.18746	15.1079	14.23707	13.86426	15.18746	15.1079	14.23707	13.86426
IK (kA)	Bus6	12.37801	11.8274	12.26805	11.51928	12.37801	11.8274	12.26805	11.51928
IK (kA)	Bus7	16.37965	15.62532	8.615823	7.885878	16.37965	15.62532	8.615823	7.885878
IK (kA)	Bus8	14.6354	12.39531	11.231	9.068916	14.6354	12.39531	11.231	9.068916
IK (kA)	Bus9	12.82856	8.589867	11.8635	7.648338	12.82856	8.589867	11.8635	7.648338
V THD(%)	Bus4	1.599465	2.143059	3.342208	3.314471	1.599465	2.143059	3.342208	3.314471
V THD(%)	Bus5	1.111309	1.947327	5.712369	5.790743	1.111309	1.947327	5.712369	5.790743
V THD(%)	Bus6	1.199279	2.965355	4.004113	3.50748	1.199279	2.965355	4.004113	3.50748
V THD(%)	Bus7	1.207567	2.346195	14.7744	14.46055	1.207567	2.346195	14.7744	14.46055
V THD(%)	Bus8	1.1157655	3.704657	10.18458	8.795355	1.157655	3.704657	10.18458	8.795355
V THD(%)	Bus9	1.245399	5.35119	6.964278	5.081095	1.245399	5.35119	6.964278	5.081095
TIF(%)	Bus4	46.17002	47.87619	66.50759	64.95781	46.17002	47.87619	66.50759	64.95781
TIF(%)	Bus5	18.32175	19.52453	94.97775	91.7423	18.32175	19.52453	94.97775	91.7423
TIF(%)	Bus6	20.32936	28.25331	65.57305	51.72615	20.32936	28.25331	65.57305	51.72615
TIF(%)	Bus7	35.32992	31.34585	264.5687	250.7905	35.32992	31.34585	264.5687	250.7905
TIF(%)	Bus8	28.62062	19.02004	174.6032	143.8202	28.62062	19.02004	174.6032	143.8202
TIF(%)	Bus9	33.84841	21.43471	120.3863	67.74123	33.84841	21.43471	120.3863	67.74123

Parameters	Line	S1-0% RE-LFA	S2-15% RE-Wind-LFA	S3-30% RE-Solar	S4-44% Renewable-Wind & Solar	S5-56% RE-Hydro	S6-70% Renewable-Hydro & Wind	S7-86% Renewable-Hydro & Solar	S8-100% Renewable-Hydro Wind & solar
Max Flow	Line 1	40.475	25.119	31.6	8.971	73.362	25.118	31.6	18.988
Max Flow	Line 2	49.707	28.549	48.091	18.988	36.72	28.549	48.091	18.988
Max Flow	Line 3	9.525	24.882	38.259	40.029	7.639	24.882	38.259	40.029
Max Flow	Line 4	-9.777	-11.458	-8.438	-11.012	-8.591	-11.458	-8.438	-11.012
Max Flow	Line 5	-30.572	-42.437	-25.971	-25.971	33.49	-42.437	-25.971	-25.971
Max Flow	Line 6	68.284	52.551	78.64	61.454	7.662	52.551	78.64	61.454
Current THD (%)	Line 1	2.592237	5.348912	12.84762	46.48418	2.592237	5.348912	12.84762	46.48418
Current THD (%)	Line 2	1.551484	11.99233	2.959993	13.05807	3.592237	11.99233	2.959993	13.05807
Current THD (%)	Line 3	0.8924079	1.500784	7.441057	7.474623	6.952237	1.500784	7.441057	7.474623
Current THD (%)	Line 4	1.001428	5.585556	3.810825	4.288519	6.592237	5.585556	3.810825	4.288519
Current THD (%)	Line 5	0.8938988	30.87888	13.1554	35.07969	12.592237	30.87888	13.1554	35.07969
Current THD (%)	Line 6	0.8812547	5.07812	11.75543	15.10139	10.592237	5.07812	11.75543	15.10139

### 3.1.2 Data Cleaning:

After this, and upon running the time domain load flow (TDLF) for one complete month started from 01/05/2024 till 31/05/2024, ETAP will generate a full and detailed report with complete data (source No.1 of data) from each scenario, then we should identify and rectify errors, missing values, and inconsistencies in the dataset because data cleaning and augmentation are crucial for accurate analysis. Also, ETAP will generate the maximum output power in MW and the time at which it occurred. In addition to the above, the maximum and minimum voltage along with bus no. and the time at which it occurred.

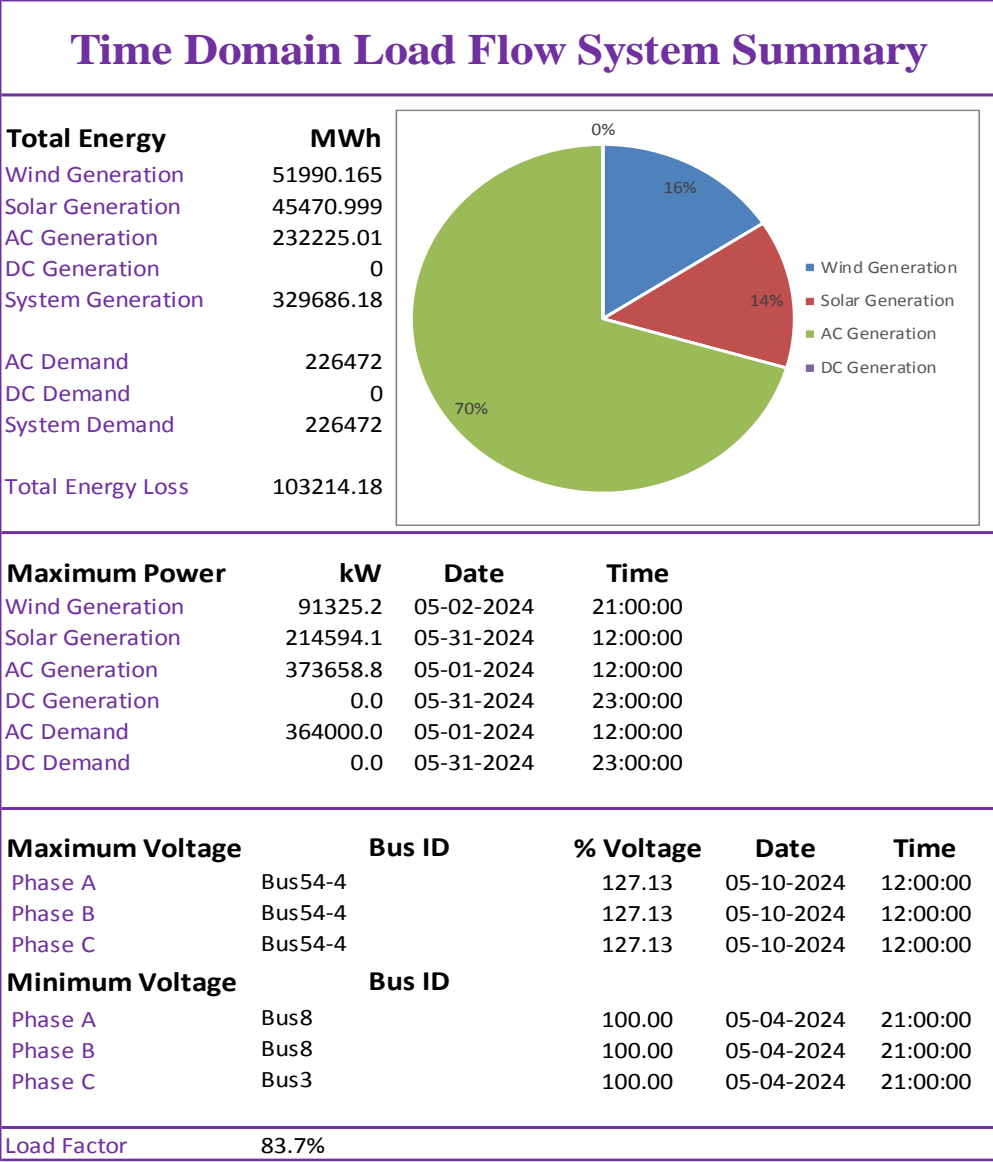


Figure 3.1-3:ETAP time domain load flow summary for 100% Renewable Energy Sources

As part of the data cleaning and data preparation, the LCOE and CO2 emissions have been calculated for each scenario as per attached excel sheet. In below subsections more elaboration about the LCOE and CO2 emissions are discussed

A financial evaluation and sustainability analysis have been conducted for a time domain load flow over one month for the last scenario (S8-100% renewable energy). Following this, for the third set of data source, it will be collected after conducting several power system studies like (power flow,

short circuit calculation, harmonic analysis, and voltage stability studies) using ETAP, then a comparative analysis has been carried out for various power system studies. Then, a transient stability study has been conducted for one major disturbance (three 3- phase balanced fault at t=0 sec and fault were cleared at t=500 m sec) for a full simulation time of 10 secs. Subsequently, a data analysis has been performed, which will involve inspecting, cleaning, transforming, and modeling the data to extract valuable information. Additionally, hidden patterns will be discovered, and numerical data will be converted into practical insights. These insights will assist decision makers in strategizing and planning for a sustainable energy future in a larger-scale electrical power system.

### 3.1.3 Exploratory Data Analysis (EDA):

Under this part, preliminary analysis is conducted to understand the data's characteristics, distributions, and relationships. Visualization techniques are often used here.

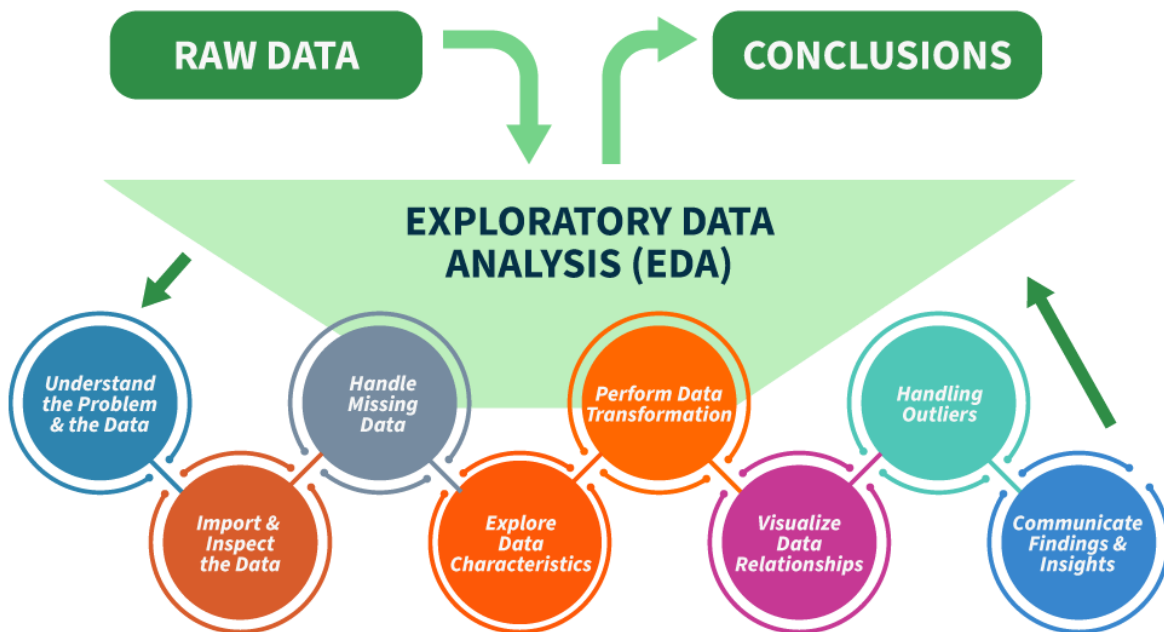


Figure 3.1-4: Exploratory Data Analysis Chart

The LCOE is listed up to year 2022, however based on the above available data and its pattern we will be predicting how much would the LCOE be in 2024 using the linear regression, and in order to perform the linear regression we will be using the excel sheet data analysis functionality.

Power generation costs (USD/kWh)			
Year	PhotoVolic	On-shore Wind	Hydroelectric
2010	0.445	0.107	0.04
2011	0.332	0.102	0.04
2012	0.248	0.099	0.04
2013	0.191	0.094	0.05
2014	0.172	0.083	0.05
2015	0.129	0.072	0.04
2016	0.113	0.067	0.05
2017	0.089	0.063	0.05
2018	0.075	0.054	0.04
2019	0.066	0.047	0.04
2020	0.059	0.039	0.05
2021	0.051	0.035	0.05
2022	0.049	0.033	0.06

PV LCOE regression data analysis summary output generated from Excel.

SUMMARY OUTPUT PV									
<i>Regression Statistics</i>									
Multiple R	0.924402357								
R Square	0.854519719								
Adjusted R Square	0.83997169								
Standard Error	0.035603286								
Observations	12								
<i>ANOVA</i>									
	df	SS	MS	F	Significance F				
Regression	1	0.074456	0.074455727	58.73783785	1.71108E-05				
Residual	10	0.012676	0.001267594						
Total	11	0.087132							
		Coefficients	Standard Error	t Stat	P-value	Lower 95%	Upper 95%	Lower 95.0%	Upper 95.0%
Intercept		46.1440303	6.003727	7.685897757	1.66941E-05	32.76689338	59.52116723	32.76689338	59.52116723
	2010	-0.022818182	0.002977	-7.664061446	1.71108E-05	-0.029452011	-0.016184352	-0.02945201	-0.016184352

Figure 3.1-5: Linear regression for LCOE for PV

However, PV LCOE data from 2010 till 2022 showing an exponential trajectory, hence using the “Data Analysis” option in excel sheet, we will be using the “Exponential Smoothing”, we will get the following.

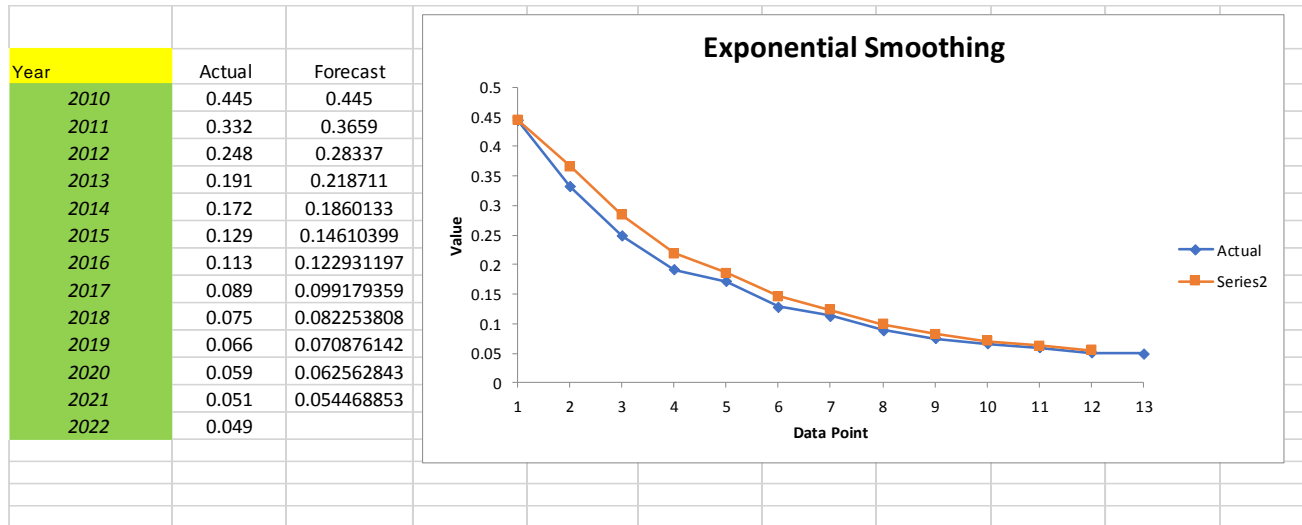


Figure 3.1-6: Exponential Smoothing for LCOE for PV

SUMMARY OUTPUT Wind								
<i>Regression Statistics</i>								
Multiple R								
R Square								
Adjusted R Square								
Standard Error								
Observations								
ANOVA								
	<i>df</i>	<i>SS</i>	<i>MS</i>	<i>F</i>	<i>Significance F</i>			
Regression	1	0.006702	0.006702385	795.232735	7.30723E-11			
Residual	10	8.43E-05	8.42821E-06					
Total	11	0.006787						
	<i>Coefficients</i>	<i>Standard Error</i>	<i>t Stat</i>	<i>P-value</i>	<i>Lower 95%</i>	<i>Upper 95%</i>	<i>Lower 95.0%</i>	<i>Upper 95.0%</i>
Intercept	13.8709359	0.489552	28.33396625	6.97243E-11	12.78014716	14.96172463	12.78014716	14.96172463
2010	-0.006846154	0.000243	-28.19987119	7.30723E-11	-0.007387085	-0.006305223	-0.00738708	-0.006305223

Figure 3.1-7: Linear regression for LCOE for Wind Energy

SUMMARY OUTPUT - HydroElectric								
<i>Regression Statistics</i>								
Multiple R								
R Square								
Adjusted R Square								
Standard Error								
Observations								
ANOVA								
	<i>df</i>	<i>SS</i>	<i>MS</i>	<i>F</i>	<i>Significance F</i>			
Regression	1	0.000118	0.000118182	3.391304348	0.095356366			
Residual	10	0.000348	3.48485E-05					
Total	11	0.000467						
	<i>Coefficients</i>	<i>Standard Error</i>	<i>t Stat</i>	<i>P-value</i>	<i>Lower 95%</i>	<i>Upper 95%</i>	<i>Lower 95.0%</i>	<i>Upper 95.0%</i>
Intercept	-1.786515152	0.995458	-1.794667134	0.102942283	-4.004533046	0.431502743	-4.00453305	0.431502743
2010	0.000909091	0.000494	1.841549442	0.095356366	-0.000190842	0.002009024	-0.00019084	0.002009024

Figure 3.1-8: Linear regression for LCOE for Hydro Electric

## POWER GENERATION COSTS (2010-2022 USD/KWH)

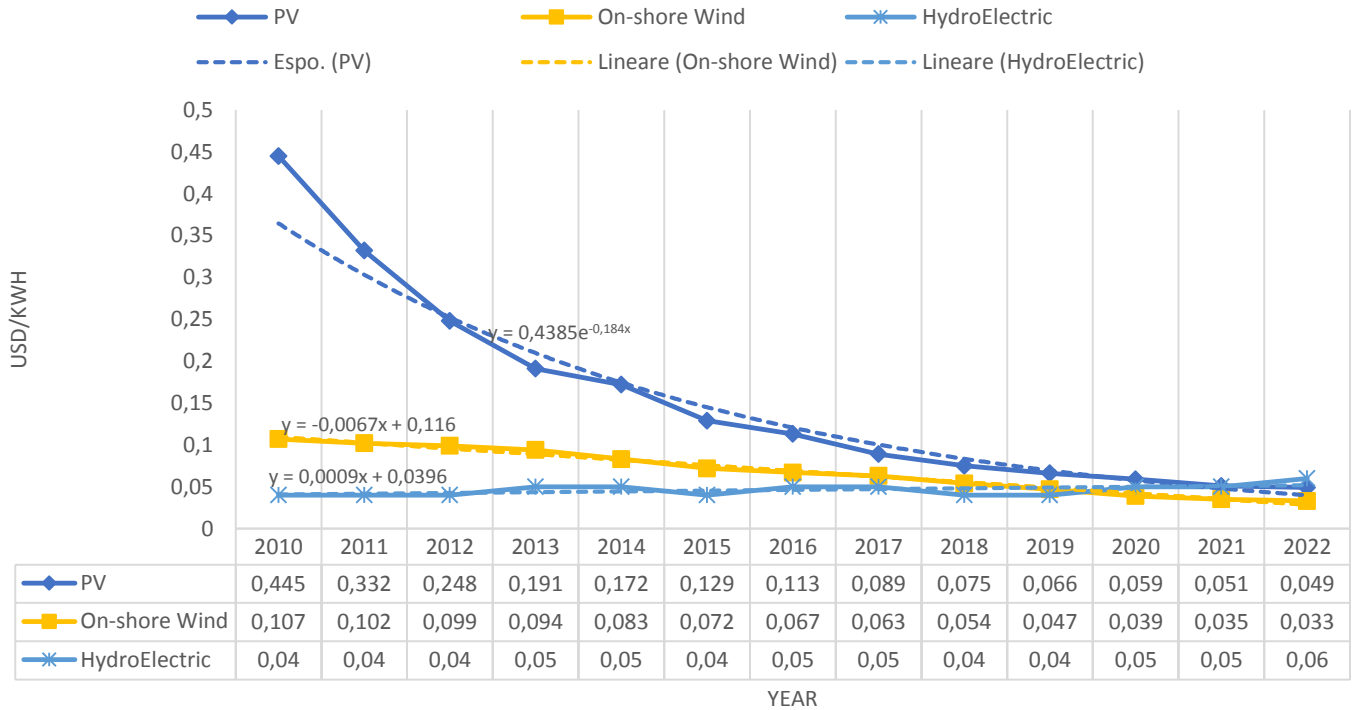
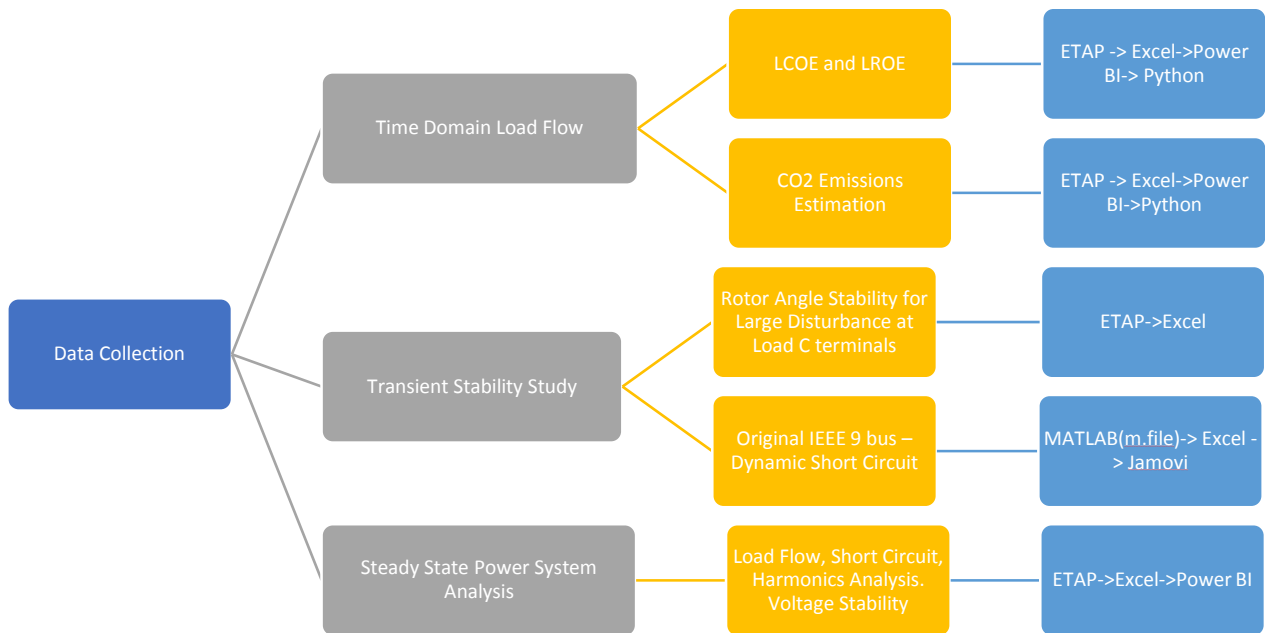


Figure 3.1-9: Power Generation Cost per Technology ( 2010-2022) in USD/KWh

Based on the performed time domain load flow (TDLF) for one complete month started from 01/05/2024 till 31/05/2024, ETAP will generate a full and detailed report and from each scenario.

Exploratory data analysis and data visualization will be conducted using the following data analysis tool/coding programs.

1. MS Excel
2. Power BI
3. Python
4. MATLAB
5. Jamovi



### 3.1.4 Data Transformation:

Under this section, the data will be prepared for analysis by extracting the data, transforming them and finally loading them encoding categorical variables, scaling features, and handling outliers, using **Power BI** following below steps:

- 1- Prepare the data in which we start cleaning and scrubbing the data.
- 2- Model the data: augmenting the data: providing additional information (closing the gaps and adding more data to the exiting data) like creating relationships between the data.

#### 3.1.4.1 LCOE and LROE

The LCOE will be calculated **hourly** for the month of May 2024 based on the actual energy generated from each technology.

$$LCOE \text{ (USD)} = LCOE \text{ (USD/KWh)} \times \text{Energy (KWh)}$$

LROE (USD) will be calculated based on the tariff (USD/KWh) and the actual load absorbed by the transmission system operator.

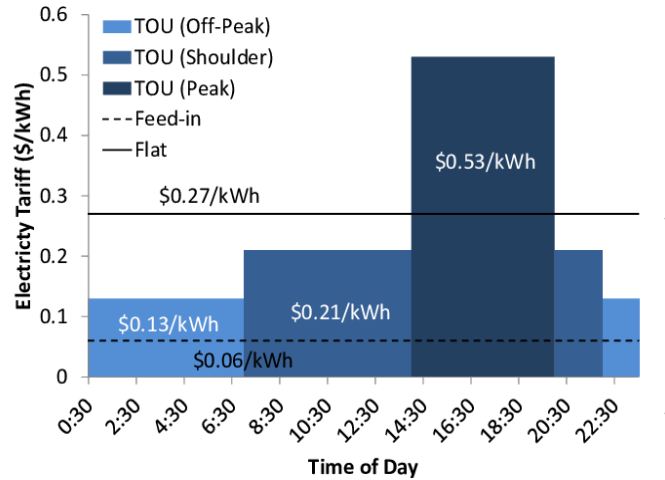


Figure 3.1-10: Electricity tariff USD/kWh

### 3.1.4.2 CO<sub>2</sub> emissions

The CO<sub>2</sub> will be calculated **hourly** for the month of May 2024 based on the actual energy generated from each technology.

$$CO_2 \text{ (g)} = CO_2 \text{ (g/KWh)} \times \text{Energy (KWh)}$$

### 3.1.5 Model Building:

For the TDLF data obtained after running the ETAP simulation for one month, we will now conduct a python model to import the data, read them, perform a load forecasting for the 100% renewable energy option (scenario No.8) using **linear regression** via Python and MATLABtools.

#### 3.1.5.1 Python:

For the TDLF data obtained after running the ETAP simulation for one month, we will now conduct a python model to import the data, read them, perform a load forecasting for the 100% renewable energy option (scenario No.8) using linear regression via Python and Jamovi tools.

Below is the python code the load forecasting linear regression and solar generation forecasting

```
df.info()

import pandas as pd
import numpy as np

# Upload and read the dataset
from google.colab import files

uploaded = files.upload()
df = pd.read_csv('Python 100% RE.csv')

# Print the information about the dataframe
df.info()

# Print the descriptive statistics of the dataframe
df.describe()
# This code uses Linear Regression Algorithm for Load Forecasting based
on the one Month

# Initialize A and B as empty lists
A = []
B = []

# Calculate the values of A and D
n = len(df)
for i in range(n):
    A.append(df.iloc[i, 0] * df.iloc[i, 7])
    B.append(df.iloc[i, 0] * df.iloc[i, 0])
print(A)
# Calculate the values of a and b
a1 = ((n * sum(A)) - (sum(df.iloc[:, 0]) * sum(df.iloc[:, 7]))) / (n *
sum(B) - (sum(df.iloc[:, 0])) ** 2)
b1 = ((sum(df.iloc[:, 7]) * sum(B)) - ((sum(df.iloc[:, 0])) * (sum(A)))) /
(n * sum(B) - (sum(df.iloc[:, 0])) ** 2)

# Print the values of a1, b1
print(a1)
print(b1)

print('The linear regression for Load Forecast Y=aX+b is : Load Forecast
(KW)=', a , 'X Number of Days + ' , b )
# This code uses Linear Regression Algorithm for CO2 emmissions
estimation based on the one Month
```

```

# Initialize U and V as empty lists
U = []
V = []

# Calculate the values of U and V
n = len(df)
for i in range(n):
    U.append(df.iloc[i, 0] * df.iloc[i, 11])
    V.append(df.iloc[i, 0] * df.iloc[i, 0])

# Calculate the values of a and b
a2 = ((n * sum(U)) - (sum(df.iloc[:, 0]) * sum(df.iloc[:, 11]))) / (n *
sum(V) - (sum(df.iloc[:, 0])) ** 2)
b2 = ((sum(df.iloc[:, 11]) * sum(V)) - ((sum(df.iloc[:, 0])) * (sum(U))))
/ (n * sum(V) - (sum(df.iloc[:, 0])) ** 2)

# Print the values of a2, b2
print(a2)
print(b2)

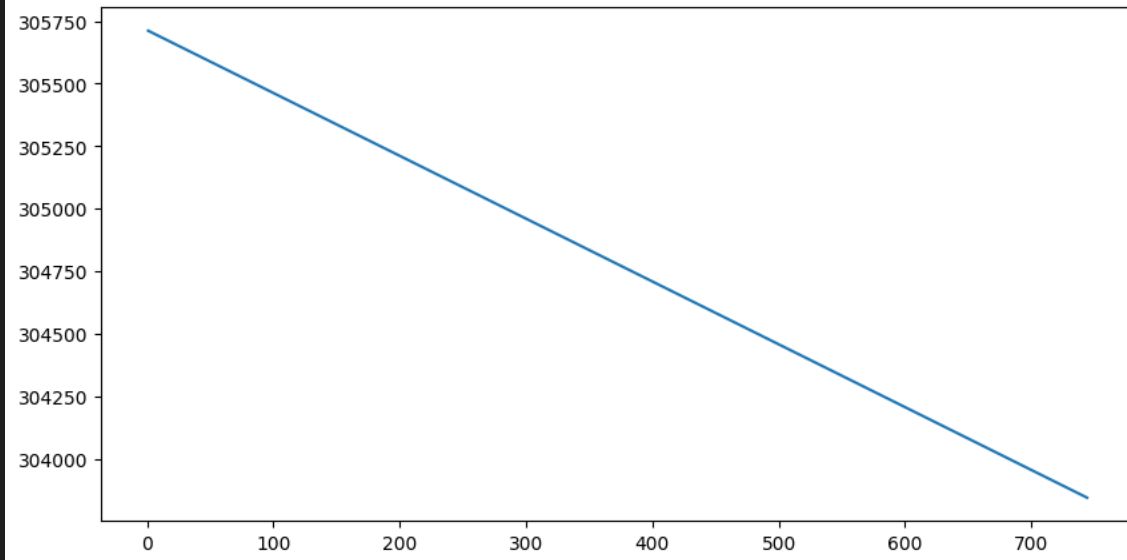
print('The linear regression for CO2 emmission Y=aX+b is : CO2 emmission
in (g)=' , a2 , 'X Number of Days + ' , b2 )
# Import libraries
import matplotlib.pyplot as plt
import numpy as np

# Creating vectors X and Y
X = df.iloc[:, 0]
Y = a1*X+b1

fig = plt.figure(figsize = (10, 5))
# Create the plot
plt.plot(X, Y)

# Show the plot
plt.show()

```



```

# This code calculate the profit and GM (%)

# Initialize U and V as empty lists
Profit = []
GM = []

# Calculate the values of U and V
n = len(df)
for i in range(n):
    Profit.append(df.iloc[i, 12] - df.iloc[i, 10])

GM=(sum(Profit) / sum(df.iloc[:, 12]))*100

print(Profit)
print(GM)
# Import libraries
from matplotlib import pyplot as plt
import numpy as np

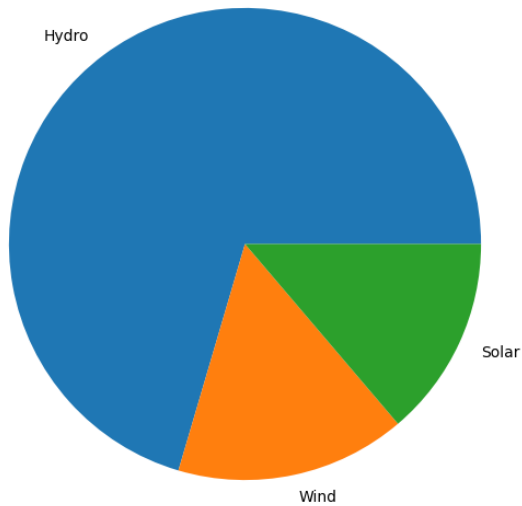
# Creating dataset
Energy_Technology = ['Hydro', 'Wind', 'Solar']

Energy = [sum(df.iloc[:, 3]), sum(df.iloc[:, 5]), sum(df.iloc[:, 6])]

# Creating plot
fig = plt.figure(figsize=(10, 7))
plt.pie(Energy, labels=Energy Technology)

```

```
# show plot
plt.show()
```



```
# The frequency response in the post fault conditions for the 8 scenarios
in ETAP shows a second order system response
# The main purpose of this code is to plot the second order system
response
```

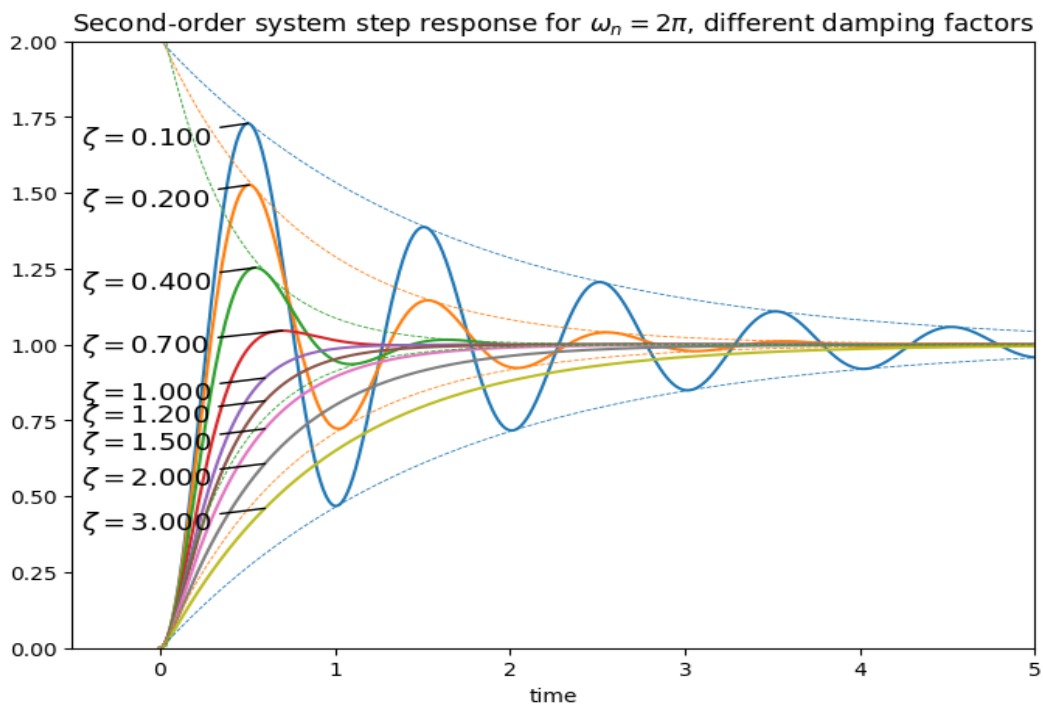
```
import numpy as np
import matplotlib.pyplot as plt
from scipy.signal import lti, lsim, step

zeta_range = [0.1, 0.2, 0.4, 0.7, 1.0, 1.2, 1.5, 2.0, 3.0]
wn = 2*np.pi
t = np.arange(0,5,0.005)
n = len(t)
plt.figure(figsize=(8,6))
hlines = []
for k, zeta in enumerate(zeta_range):
    H = lti([wn*wn], [1,2*zeta*wn,wn**2])
    _,y = H.step(T=t)
    hlines.append(plt.plot(t,y))
    if zeta >= 1:
        klbl = int(n * 0.12)
        t1 = t[klbl]
        y1 = y[klbl]
```

```

else:
    zcomp = np.sqrt(1-zeta**2)
    wd = zcomp*wn
    tl = np.pi/wd
    yl = 1+np.exp(-np.pi*zeta/zcomp)
    plt.annotate('$\\zeta=%.3f$' % zeta, xy=(tl,yl), xytext=(-0.45,yl),
                xycoords='data', textcoords='data',
                arrowprops=dict(arrowstyle="--", shrinkB=0),
                verticalalignment='top',
                fontsize=13
    )
for k, zeta in enumerate ([z for z in zeta_range if z < 0.5]):
    A = 1/np.sqrt(1-zeta**2)
    hl2 = plt.plot(t,1+A*np.exp(-zeta*wn*t), '--',
                  t,1-A*np.exp(-zeta*wn*t), '--')
    for hl in hl2:
        hl.set_color(hlines[k][0].get_color())
        hl.set_linewidth(hlines[k][0].get_linewidth()*0.4)
plt.xlim([-0.5,5])
plt.ylim([0,2])
plt.xlabel('time')
plt.title('Second-order system step response for '
          +'$\\omega_n = 2\\pi$, '
          +'different damping factors'
          )

```



### 3.1.5.2 *Jamovi:*

### 3.1.6 **Model Evaluation:**

Based on the above model, we will assess the models' performance using Root Mean Squared Error. The Root Mean Square Error (RMSE) is the measure of the standard deviation of the residuals, which are the errors in the predictions. Residuals quantify the distance between data points and the regression line, whereas RMSE quantifies the dispersion of these residuals. Put simply, it quantifies the degree of data clustering around the line of best fit.

$$RMSE = \sqrt{\sum_{i=1}^n \frac{(\hat{y}_i - y_i)^2}{n}}$$

```
# root mean square calculated by sklearn package

from sklearn.metrics import mean_squared_error

# Initialize y as a list of all values in the 7th column of df
y_Actual = df.iloc[:, 7]

y_pred=[]
y_error=[]
y_error_square=[]

# Calculate the values of y predicted
n = len(df)
for i in range(n):
    y_pred.append(a1*df.iloc[i,0] + b1)
    y_error.append(y_Actual[i]-y_pred[i])
    y_error_square=np.array(y_error)**2

print(y_pred)
mse = math.sqrt(sum(y_error_square/n))

print('Root mean square error', mse)
```

### 3.1.7 Interpretation and Visualization:

Under this section, we will translate the model's results into actionable insights. Visualizations, tables, and summary statistics will help in conveying findings effectively. Based on the conducted three main categories for data, the data visualization will be as per below

#### 3.1.7.1 Time Domain Load Flow

Parameter	S1 - 0% Renewable	S2- 15% Renewable - Wind	S3 - 30% Renewable - Solar	S4 - 45% Renewable - Wind & Solar	S5 - 56% Renewable - Hydro	S6- 75% Renewable - Hydro & Wind	S7- 85% Renewable - Hydro & Solar	S8 - 100% Renewable - Hydro, Wind, & solar
Source kW	236,547,793.40	234,897,524.44	231,918,551.77	233,519,385.23	235,120,700.80	234,469,906.35	232,541,703.05	232,514,339.05
Source kvar	130,183,968.96	85,628,682.41	104,250,290.87	71,181,398.26	130,633,860.64	85,261,185.12	103,612,173.39	70,421,000.82
Wind kWh	-	51,999,323.05	-	52,072,768.21	-	52,051,798.10	-	52,066,601.73
Solar kWh	-	-	45,470,998.80	45,470,998.86	-	-	45,470,998.78	45,470,998.86
AC Load kWh	227,431,000.09	227,236,998.90	226,233,000.14	227,734,998.68	225,981,000.28	226,793,998.92	226,868,999.79	226,754,998.93
AC Load kvar	85,311,999.98	49,109,894.30	71,267,411.68	37,486,506.71	85,657,000.07	48,699,994.89	70,691,009.79	36,889,542.66
Losses kWh	9,116,793.31	7,660,525.54	5,685,551.62	5,784,386.55	9,139,700.52	7,675,907.42	5,672,703.25	5,759,340.12
LCOE ( USD)	25,231,764.63	26,771,713.60	26,966,057.80	28,855,214.72	18,935,053.77	17,098,935.19	17,482,814.66	17,897,137.14
CO2 (Kg)	210,093,865.17	209,200,143.85	207,846,638.01	209,841,245.39	92,410,272.77	40,664,969.85	31,300,214.86	3,367,100.93
LROE (USD)	62,206,590.04	62,195,209.70	61,654,610.06	62,075,069.66	61,874,090.05	61,918,179.75	62,235,689.95	61,992,469.75
Profit	36,974,825.41	35,423,496.10	34,688,552.27	33,219,854.94	42,939,036.28	44,819,244.56	44,752,875.28	44,095,332.60
Profit (%)	59%	57%	56%	54%	69%	72%	72%	71%

Figure 3.1-11: Summary of Time Domain load flow for 8 scenarios.

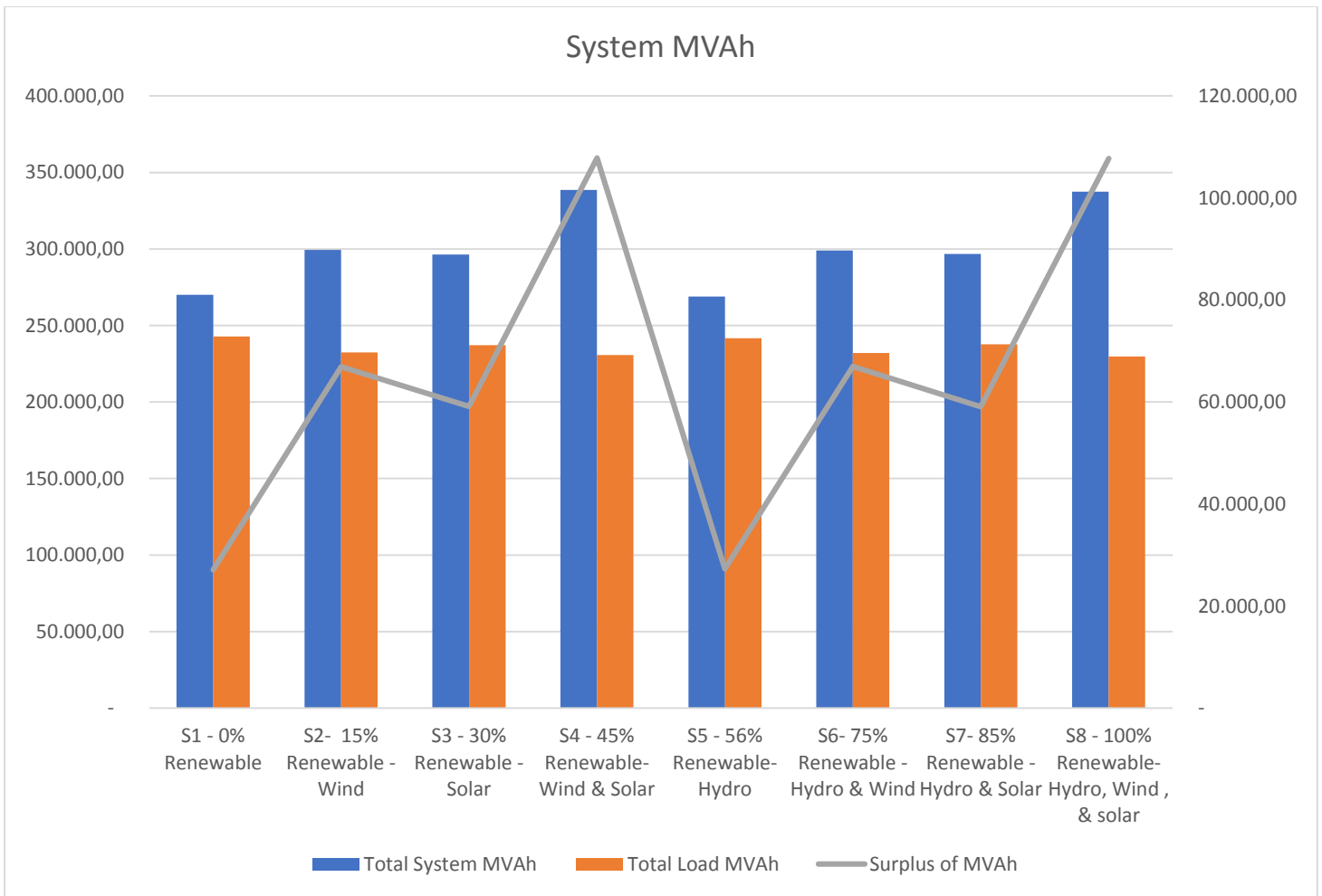


Figure 3.1-12: Total system MVAh for each scenario and surplus of Energy

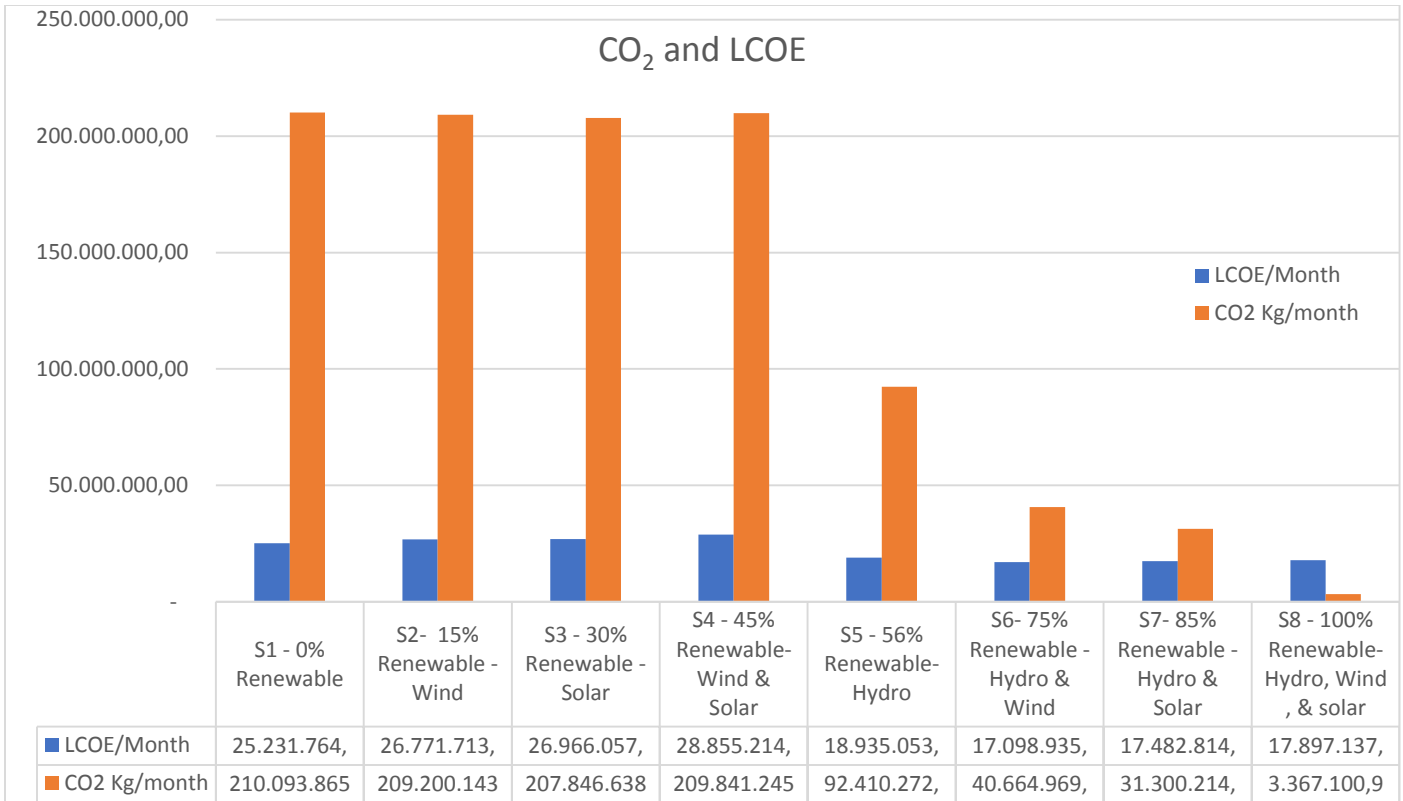


Figure 3.1-13: CO<sub>2</sub> and LCOE for each Scenario for one complete month

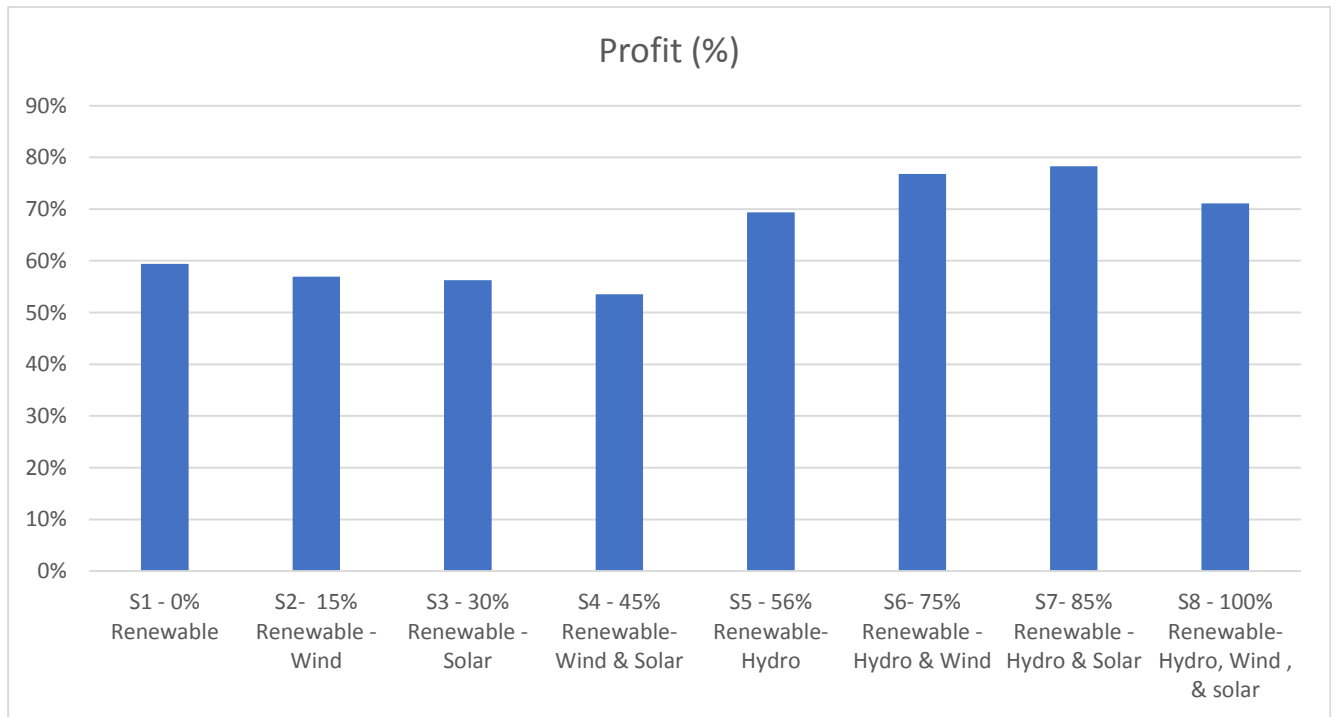


Figure 3.1-14: Profit (%) for one complete month for each scenario

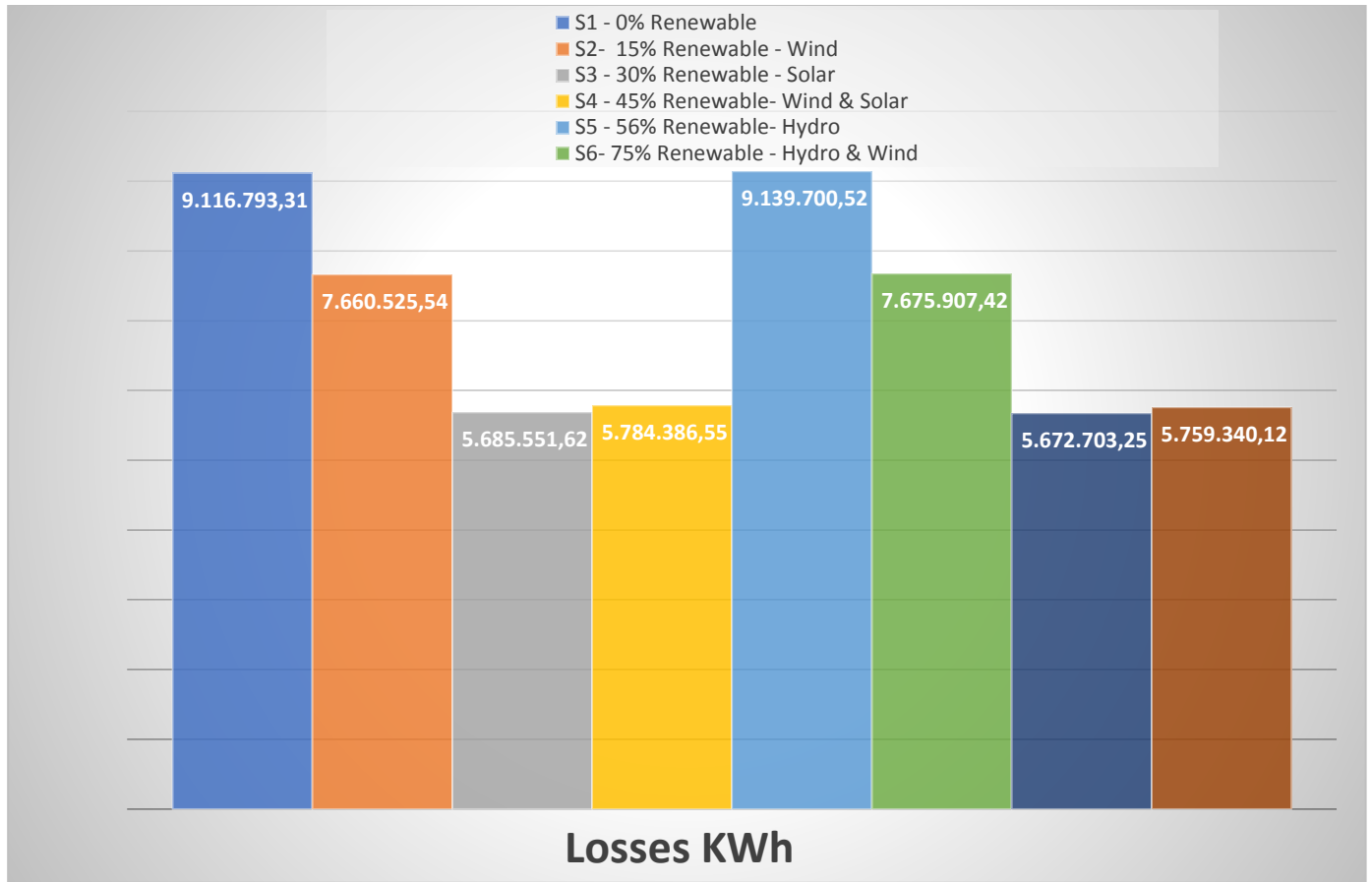


Figure 3.1-15: Losses in KWh for each scenario.

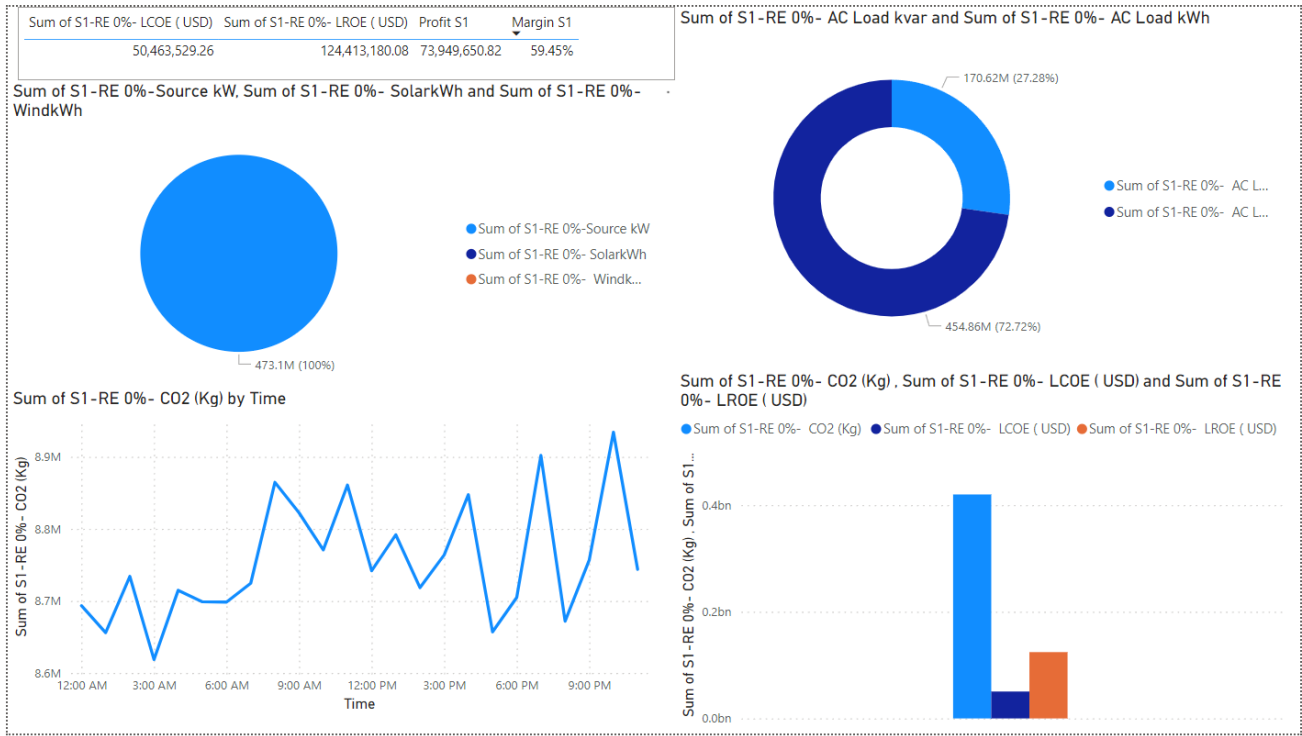


Figure 3.1-16:PowerBI Dashboard for S1-0% Renewable Energy

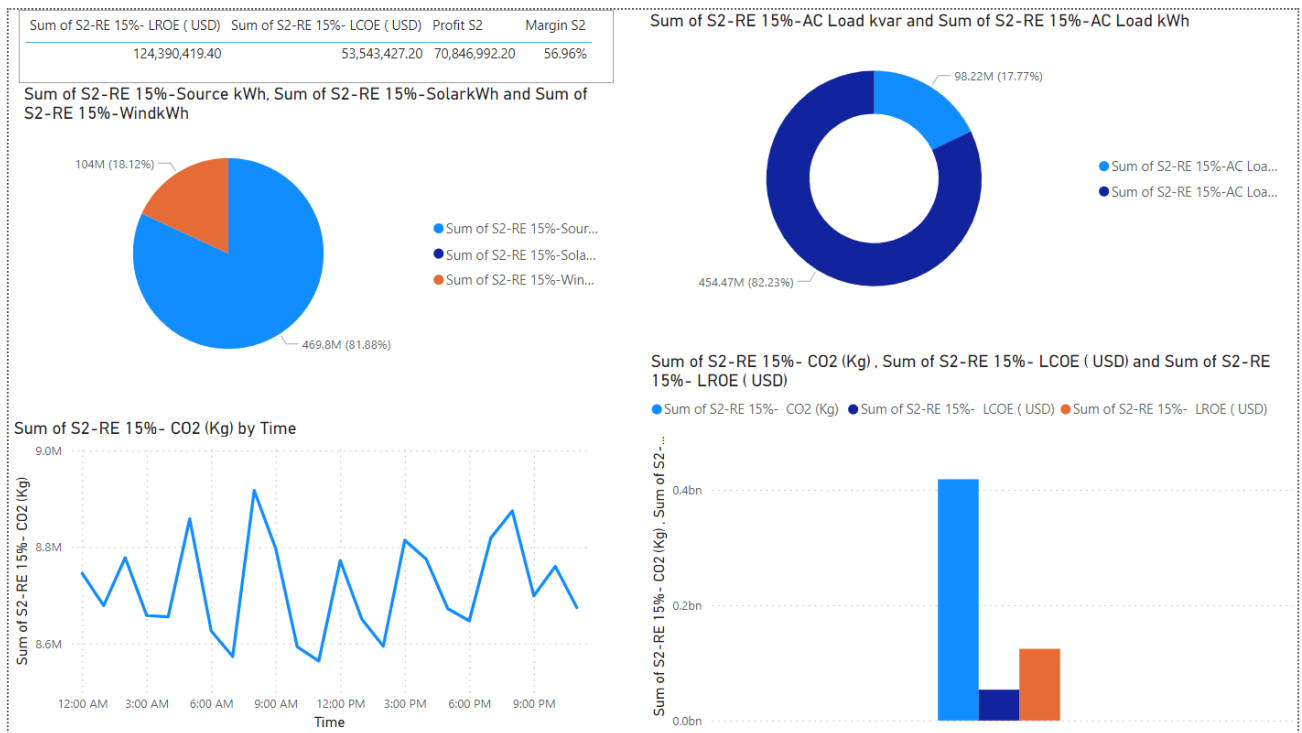


Figure 3.1-17:PowerBI Dashboard for S2-15% Renewable Energy (Wind)

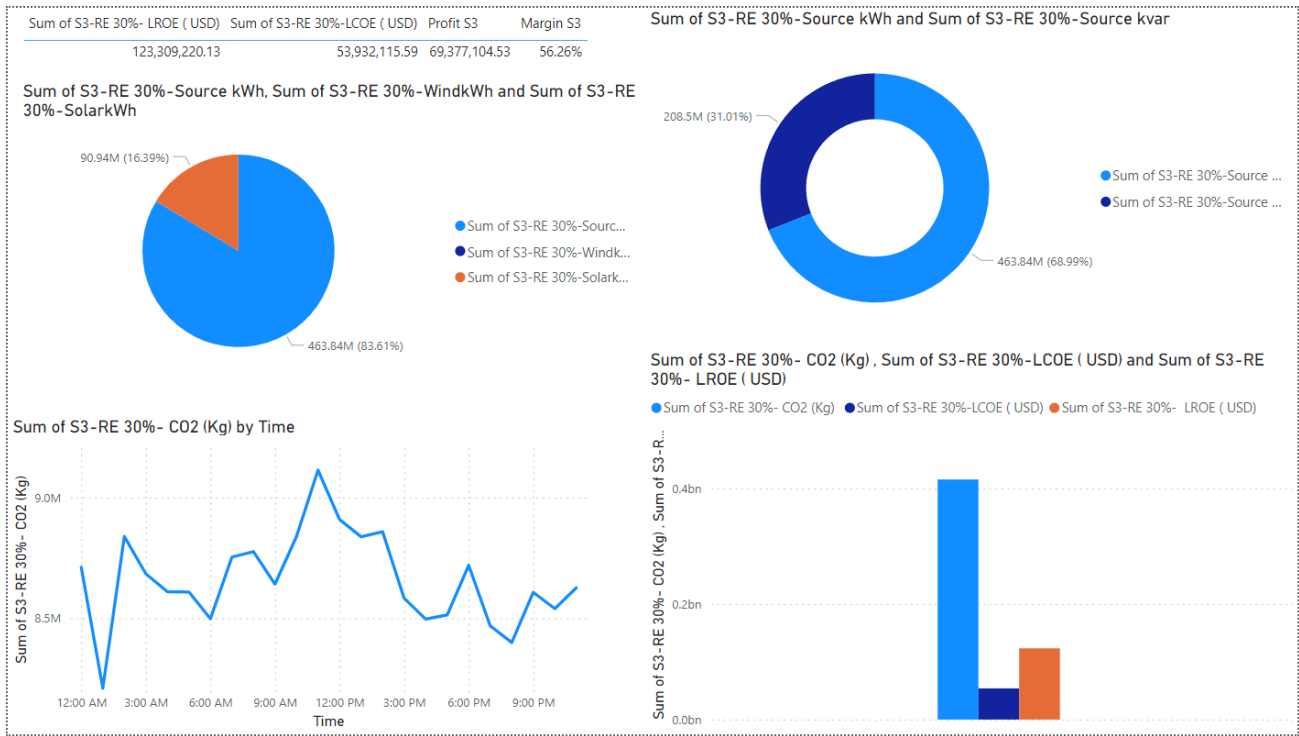


Figure 3.1-18:PowerBI Dashboard for S3-30% Renewable Energy (Solar)

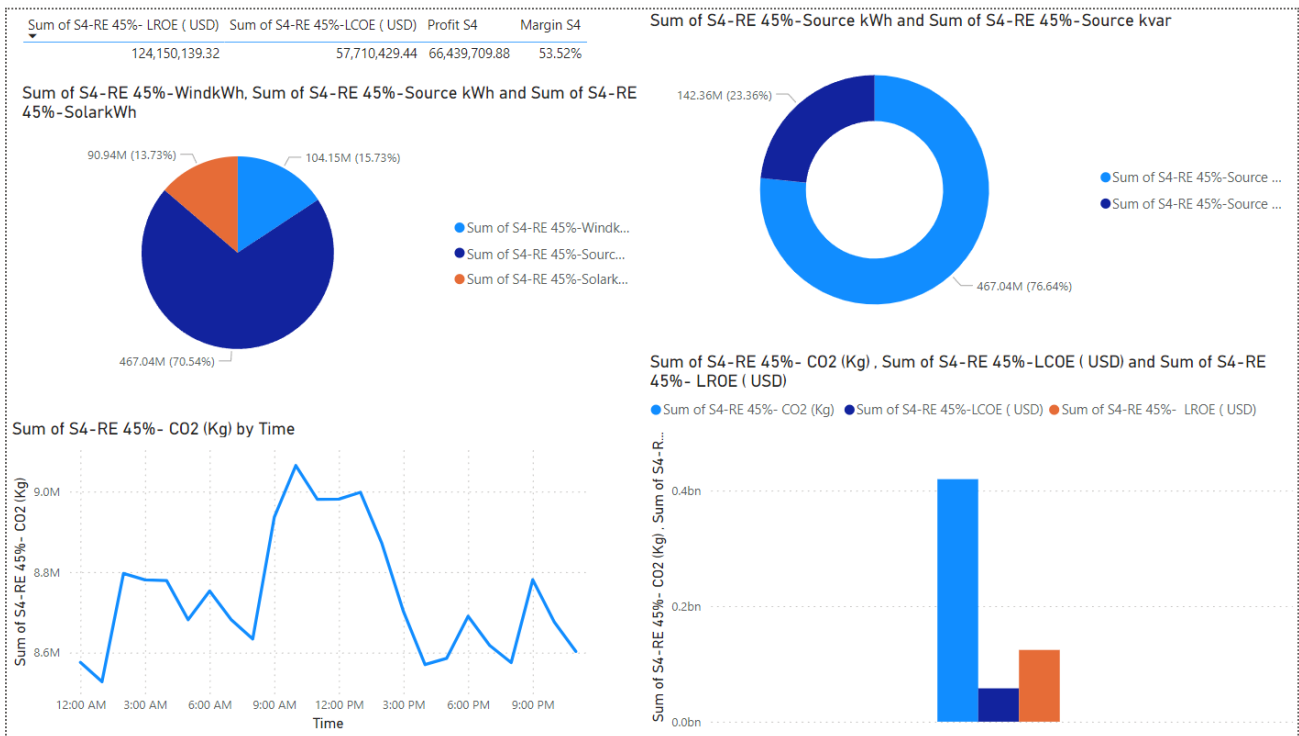


Figure 3.1-19:PowerBI Dashboard for S4-45% Renewable Energy (Wind + Solar)

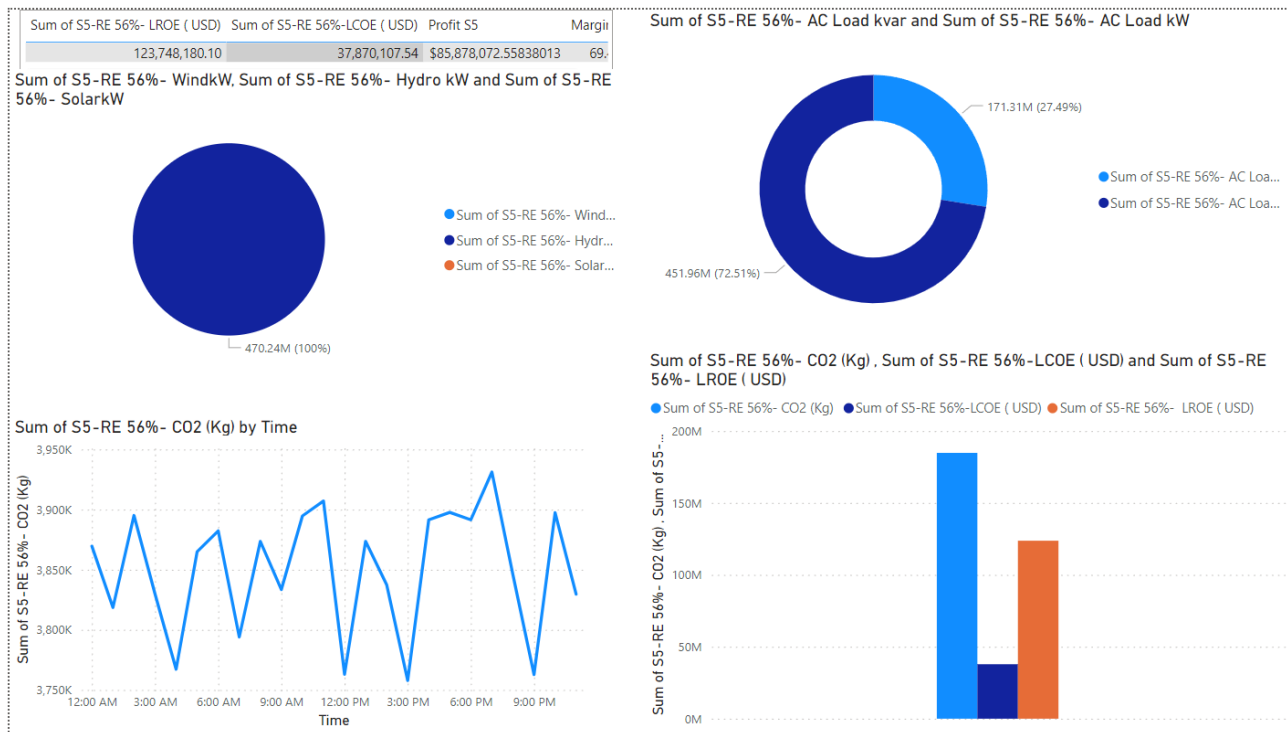


Figure 3.1-20:PowerBI Dashboard for S5-56% Renewable Energy (Hydro)

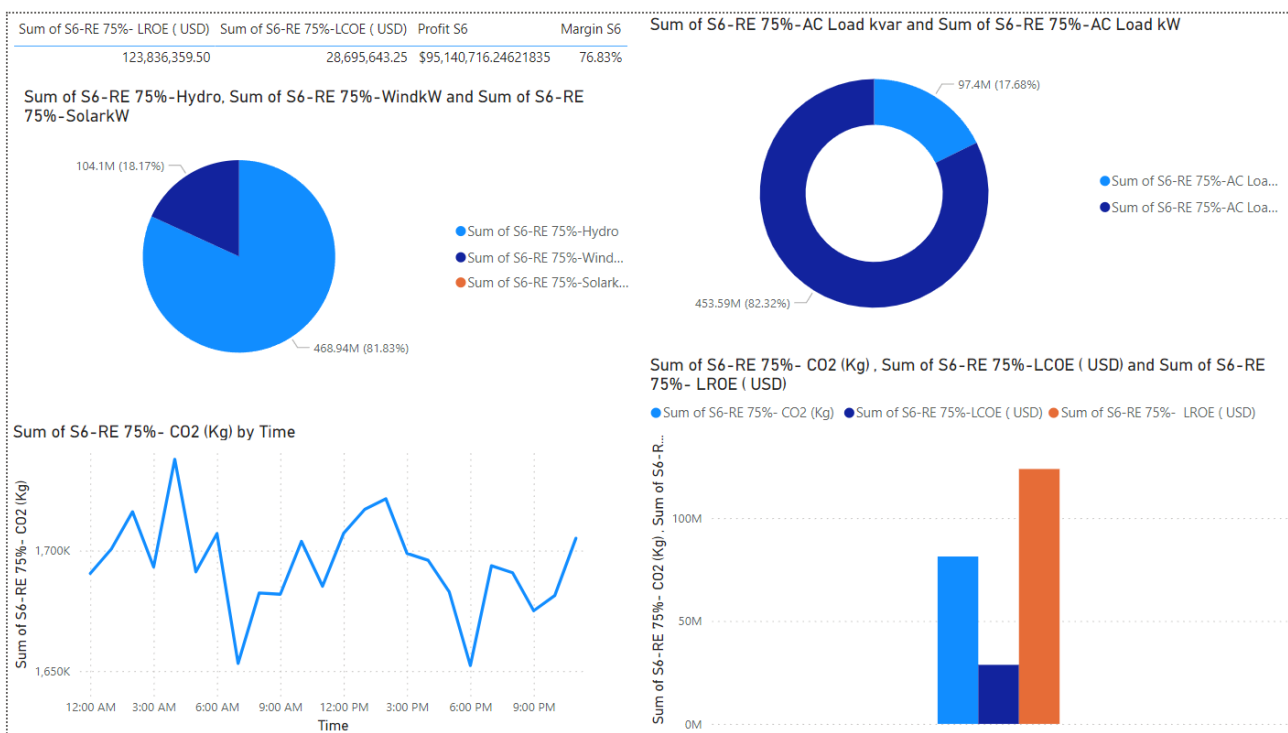


Figure 3.1-21:PowerBI Dashboard for S6-75% Renewable Energy (Hydro+Wind)

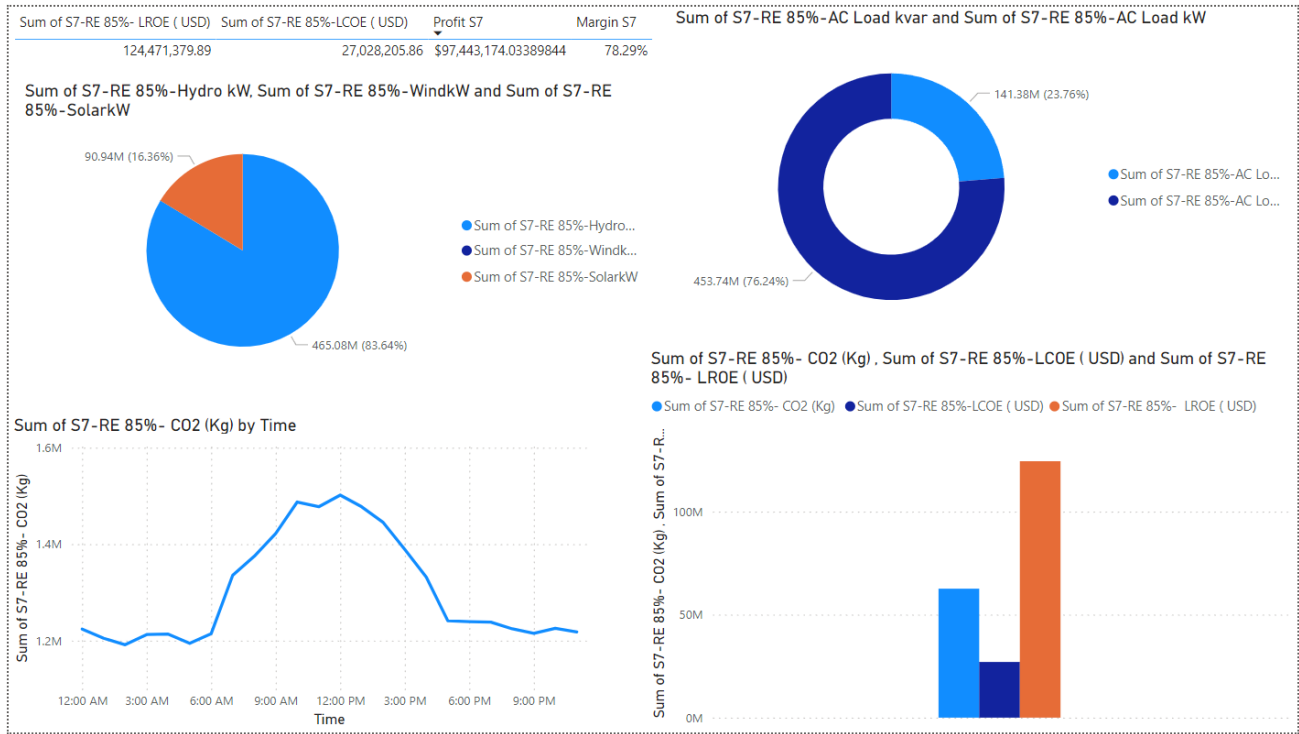


Figure 3.1-22:PowerBI Dashboard for S7-85% Renewable Energy (Hydro+Solar)

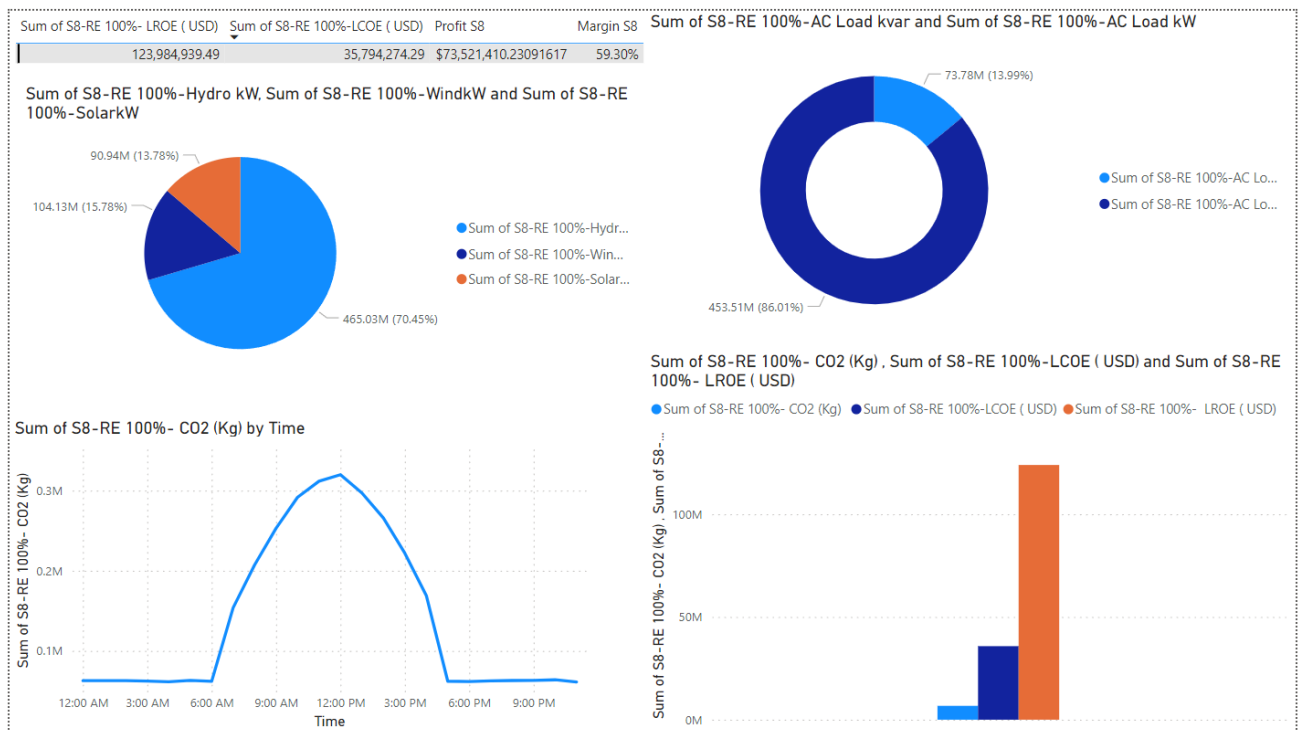


Figure 3.1-23:PowerBI Dashboard for S6-100% Renewable Energy (Hydro+Wind+Solar)

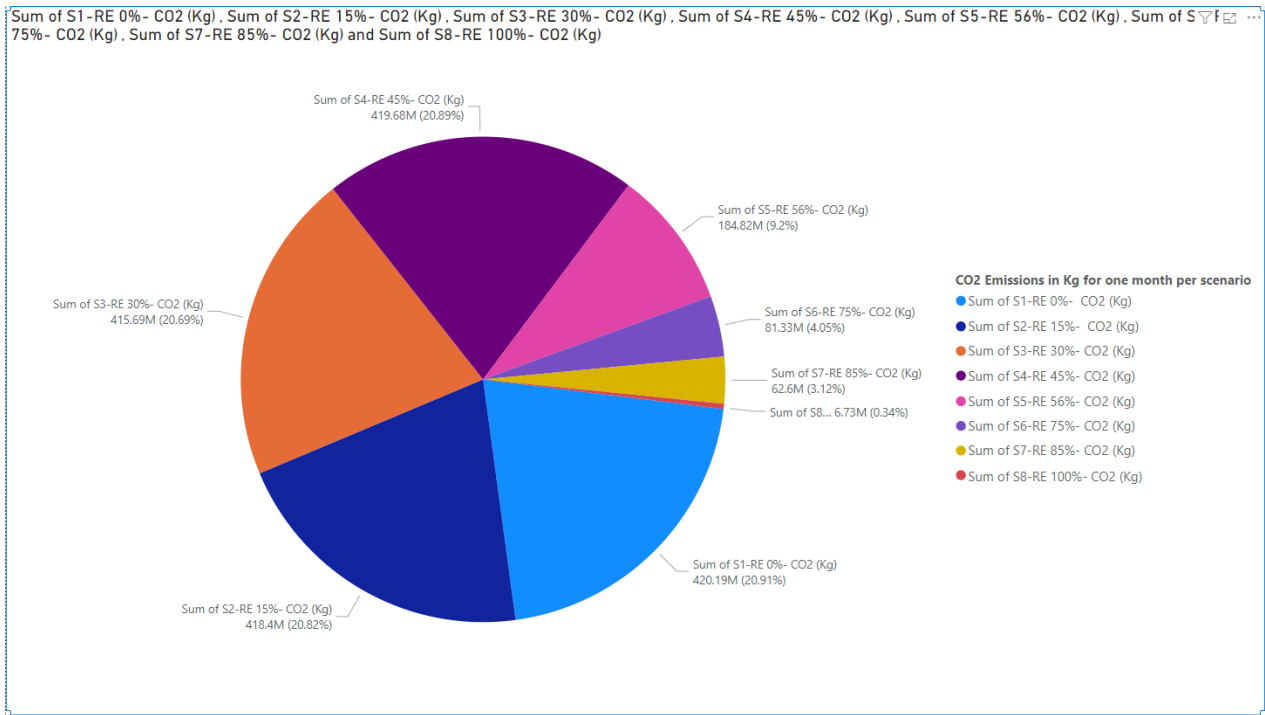


Figure 3.1-24: CO2 emissions per Scenario

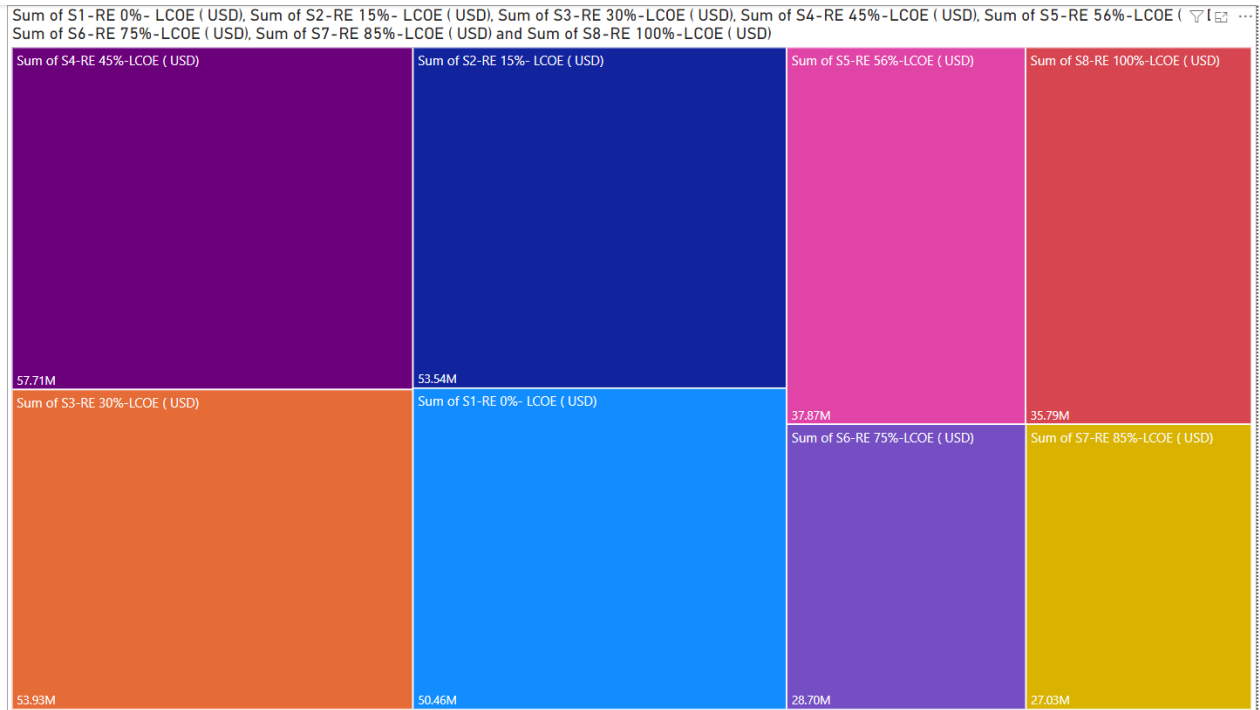


Figure 3.1-25: LCOE per Scenario

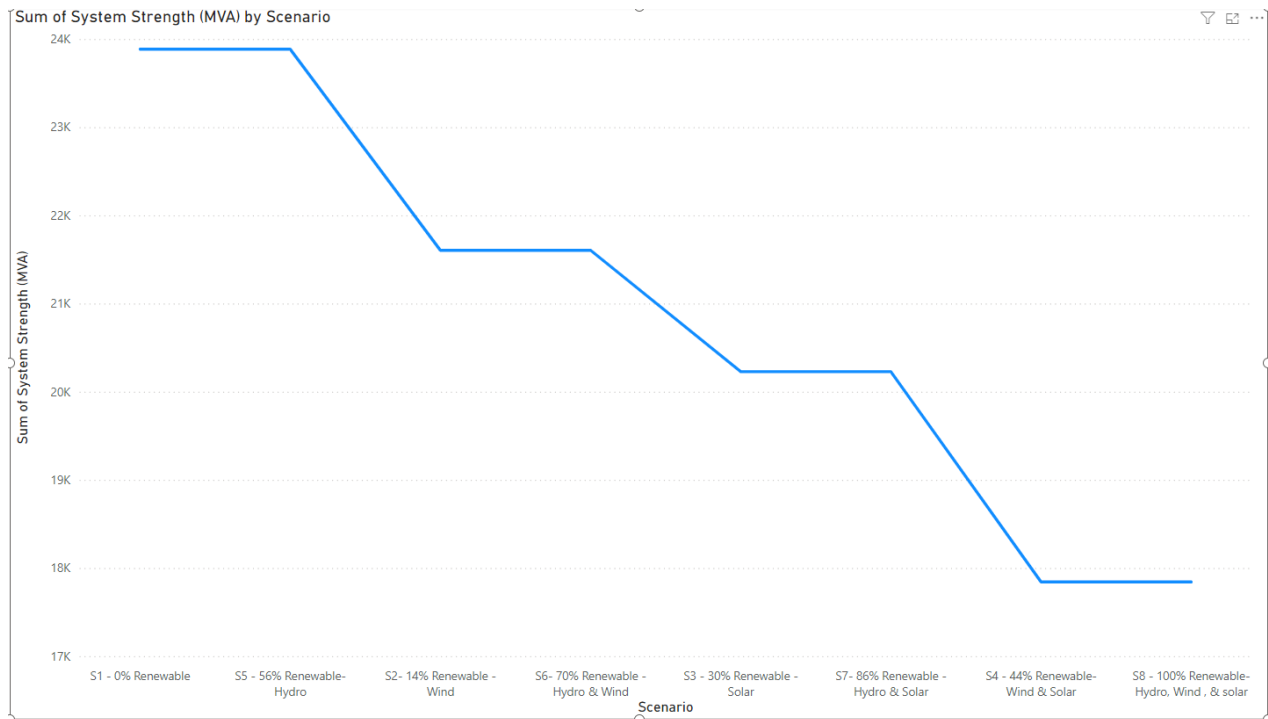


Figure 3.1-26: Short Circuit Power (MVA<sub>sc</sub>) for each scenario

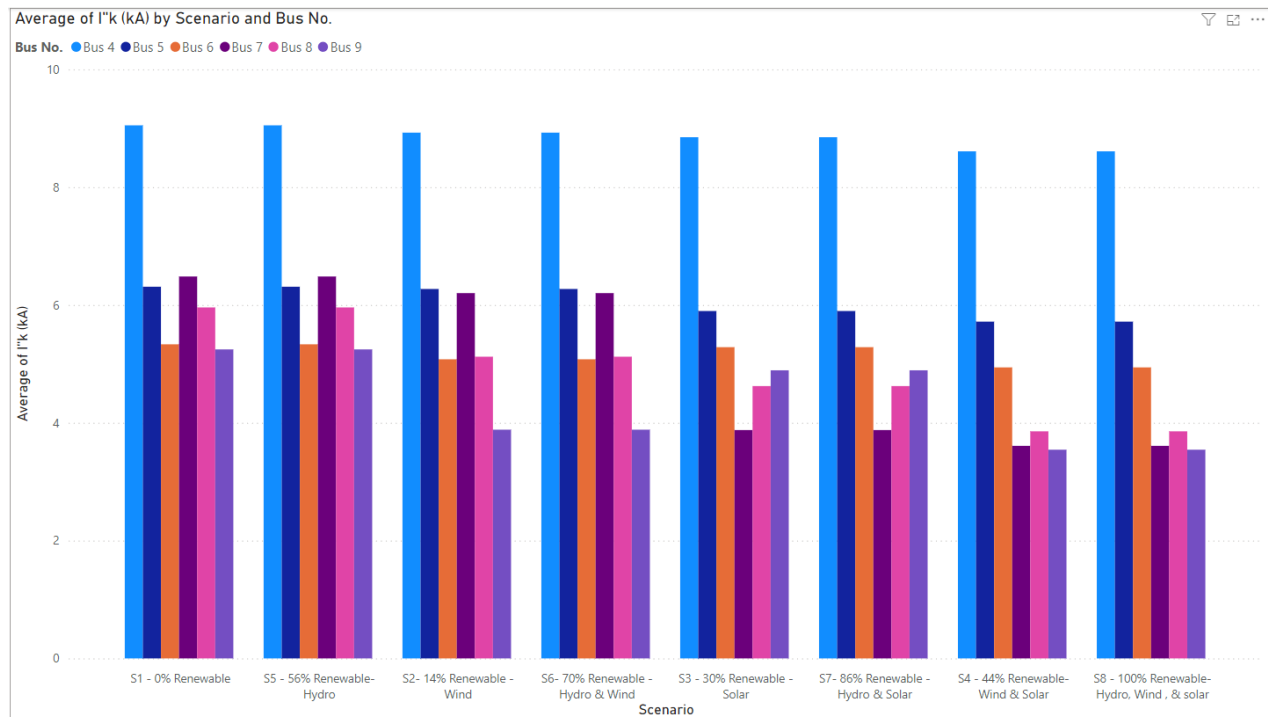


Figure 3.1-27: Three phase short circuit current I''k(kA) for each 230kV bus per scenario

### 3.1.7.2 Transient Stability Study

For the 8 scenarios, the generator G1 response for the exact same large disturbance of 3-phase fault at 230kV Bus Bar No.8 (at load C terminals) for each scenario was simulated and thoroughly examined in pre-, during-, and post-fault condition. After this, a diagnostic data analysis technique was performed to understand the cause-and-effect relationships within the data.

The generator G1 response for a 3-phase fault at BB No.8 (Load C terminals) for each scenario is illustrated in below Figure 3.1-28 .

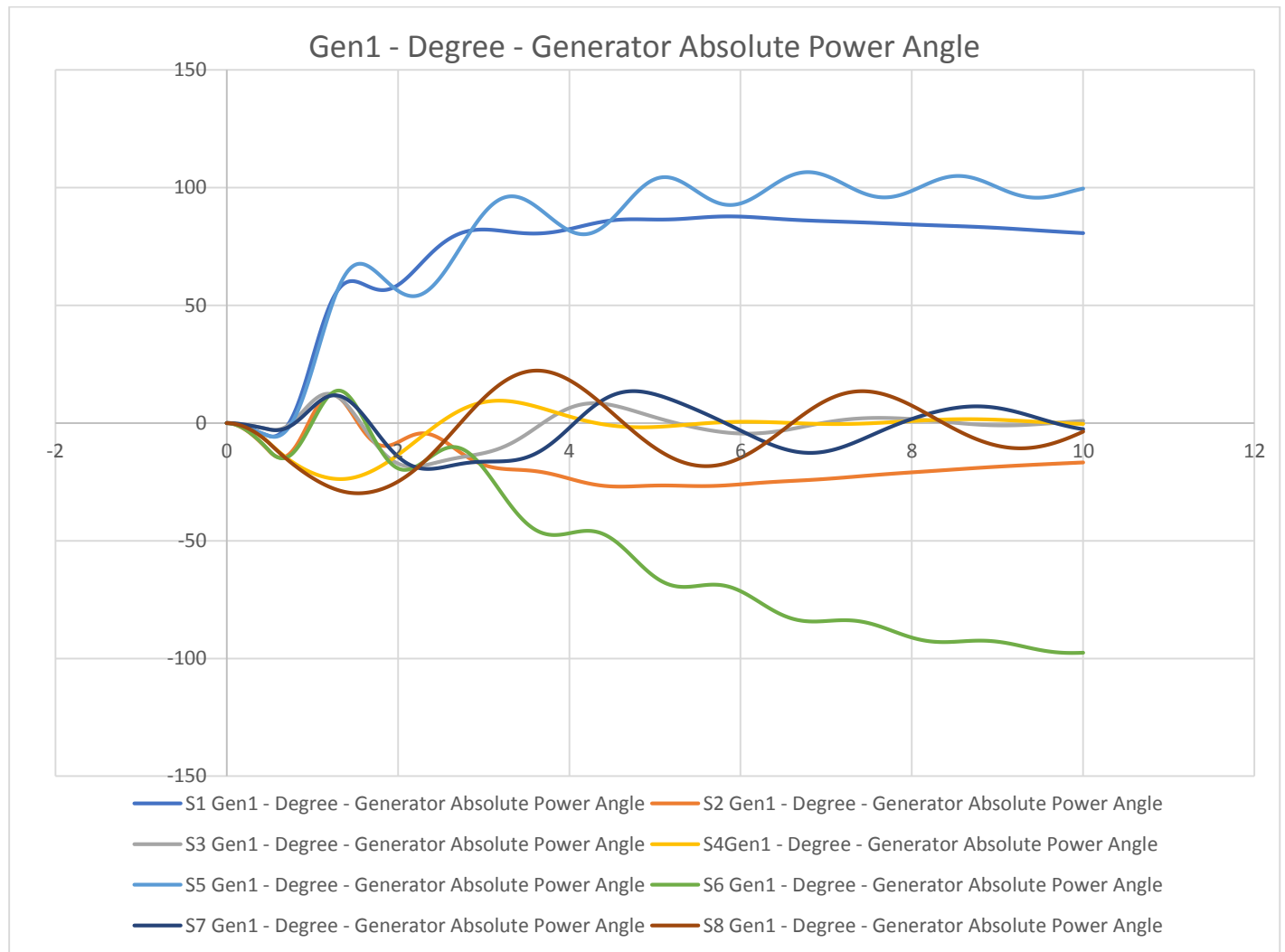


Figure 3.1-28: Gen1 - Degree - Generator Absolute Power Angle

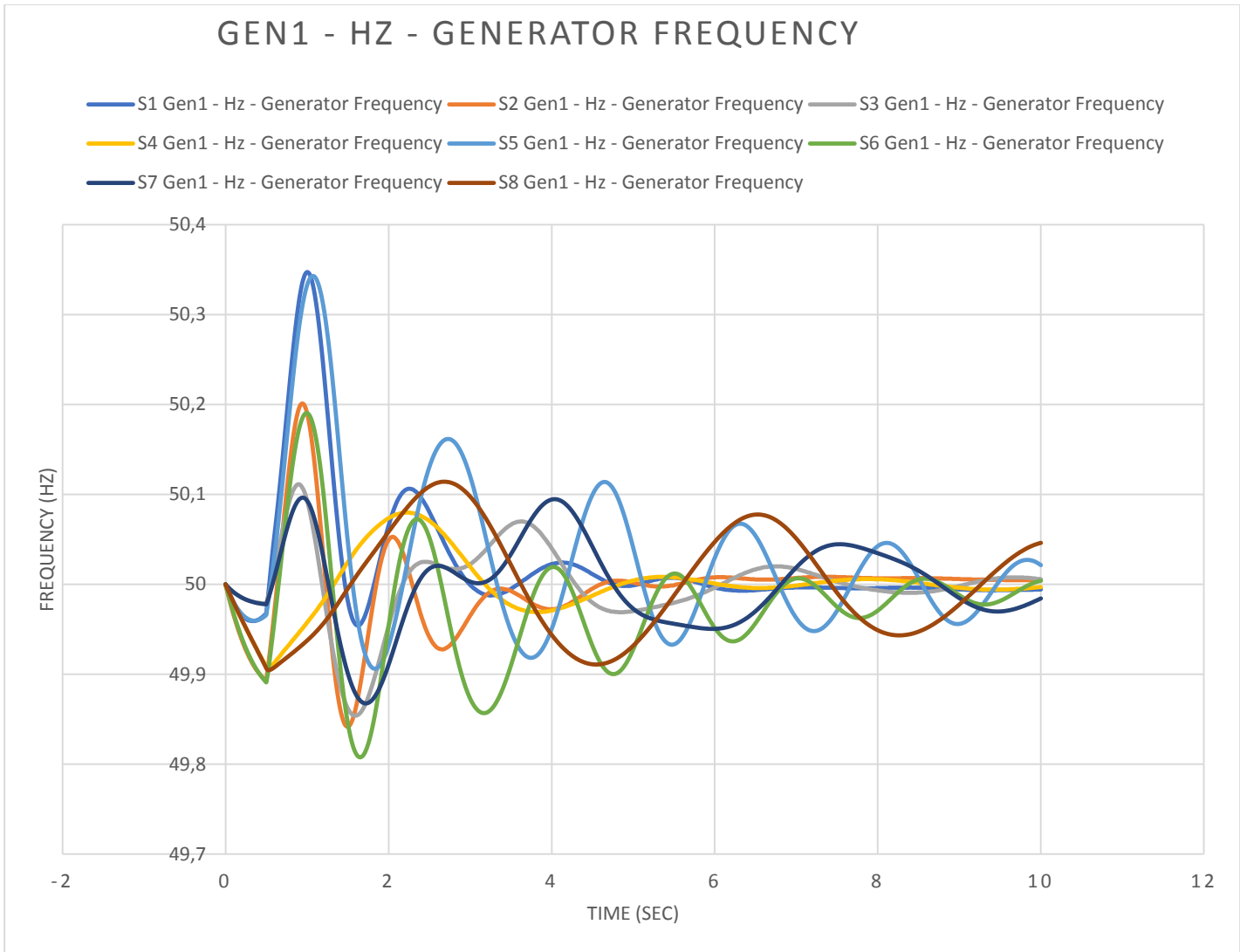


Figure 3.1-29: Generator 1 frequency dynamic response for each scenario

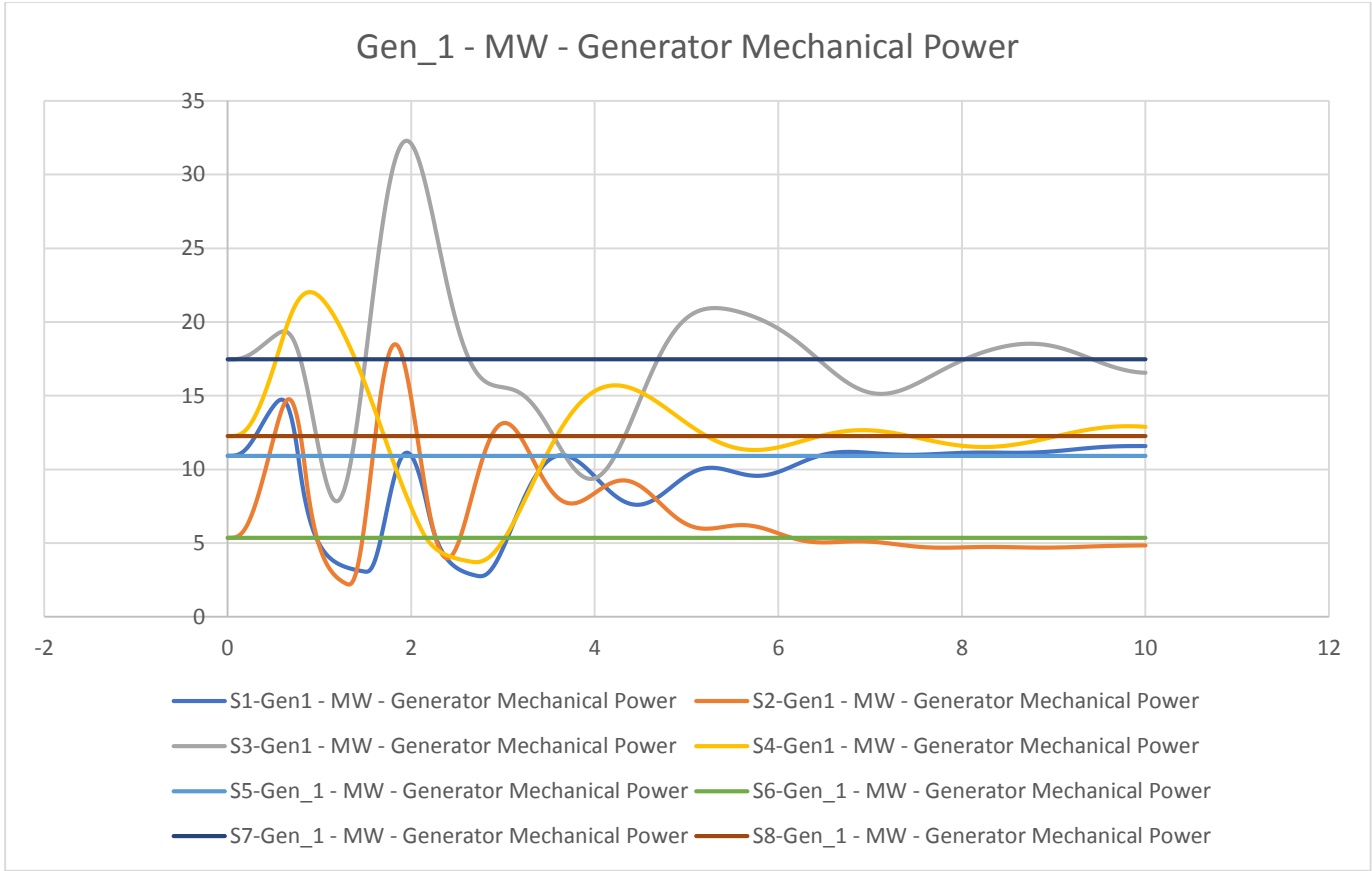


Figure 3.1-30:Gen1 - Generator Mechanical Power ( in MW)

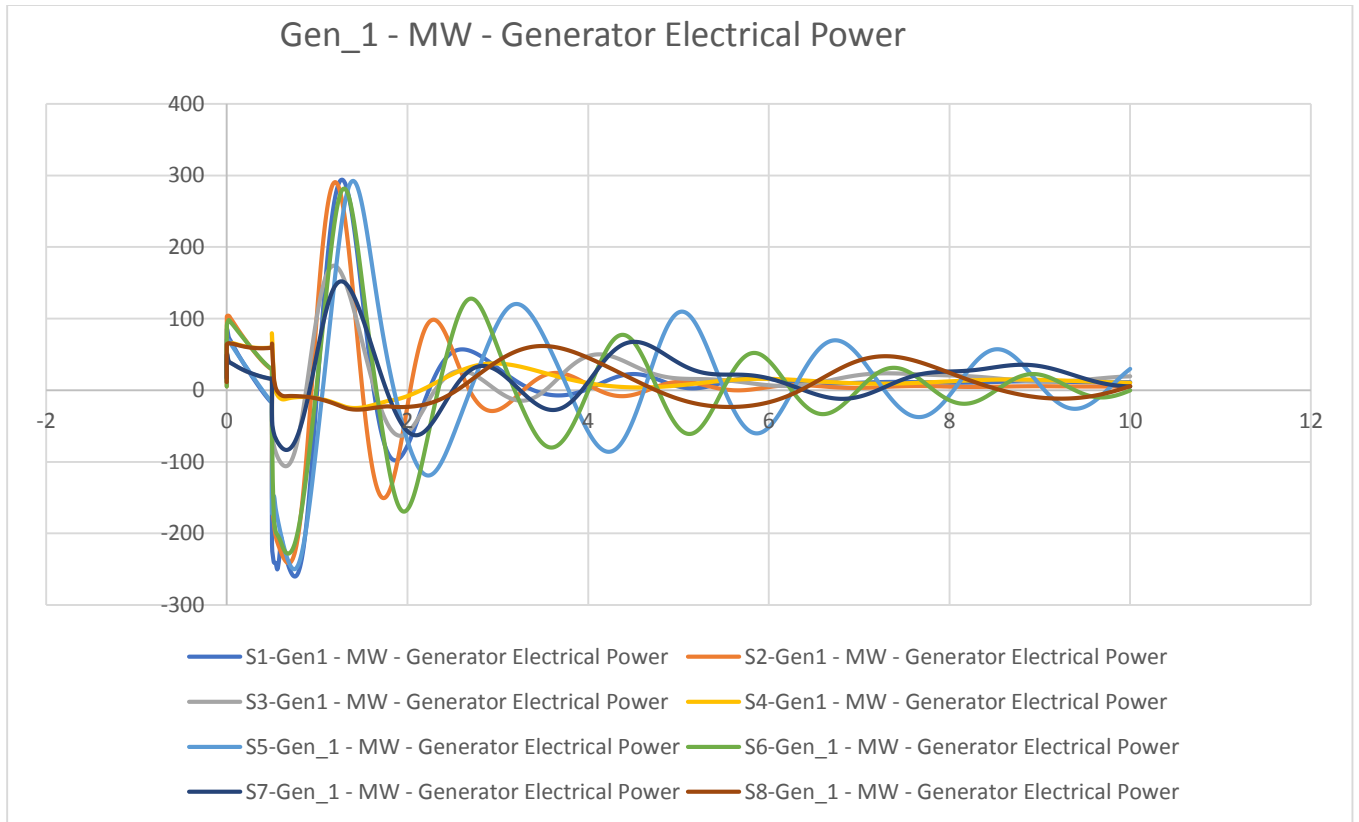


Figure 3.1-31:Gen\_1 - MW - Generator Electrical Power

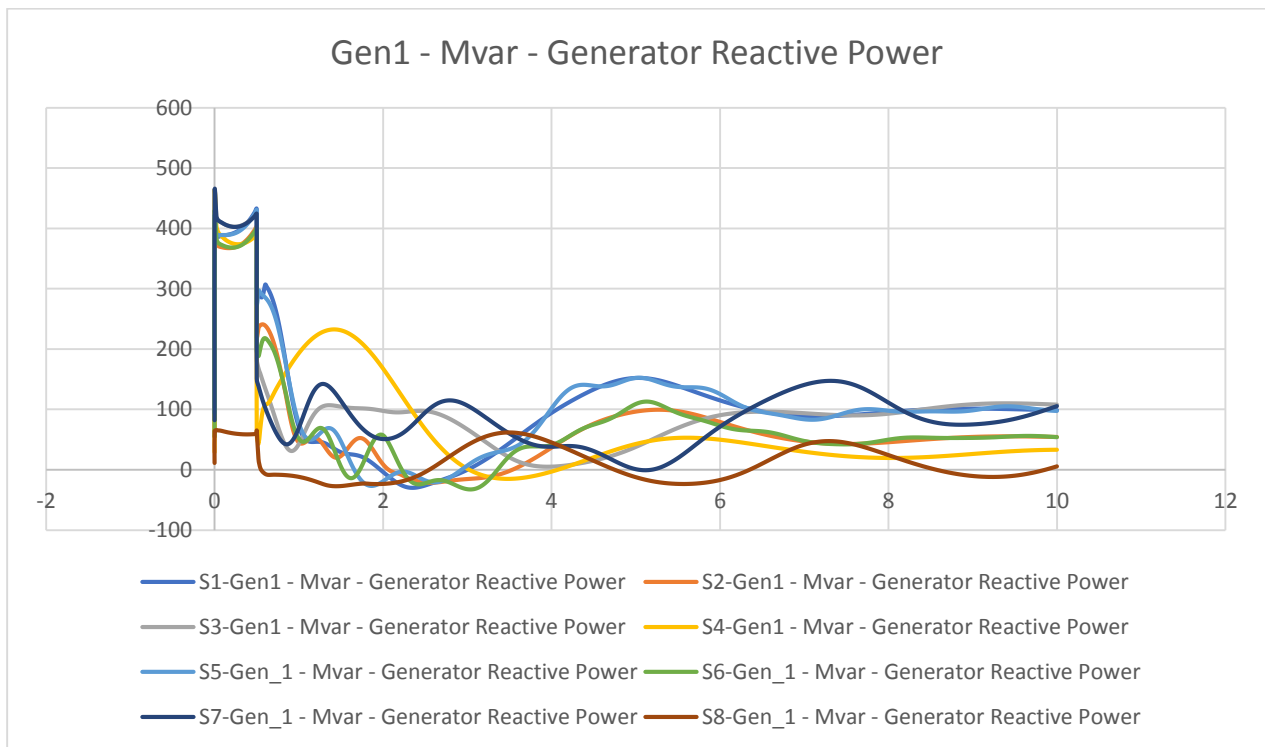


Figure 3.1-32:Gen1 - Mvar - Generator Reactive Power

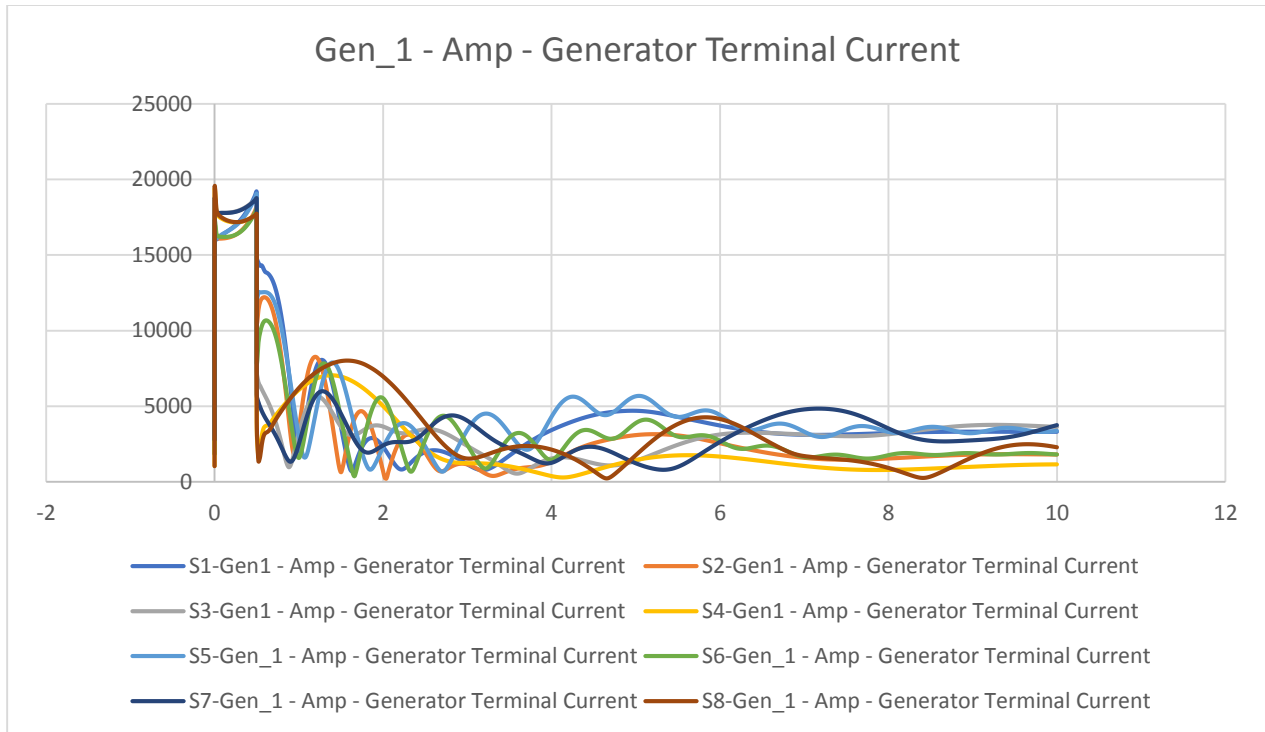


Figure 3.1-33:Gen1 - Generator Terminal Current (Amp)

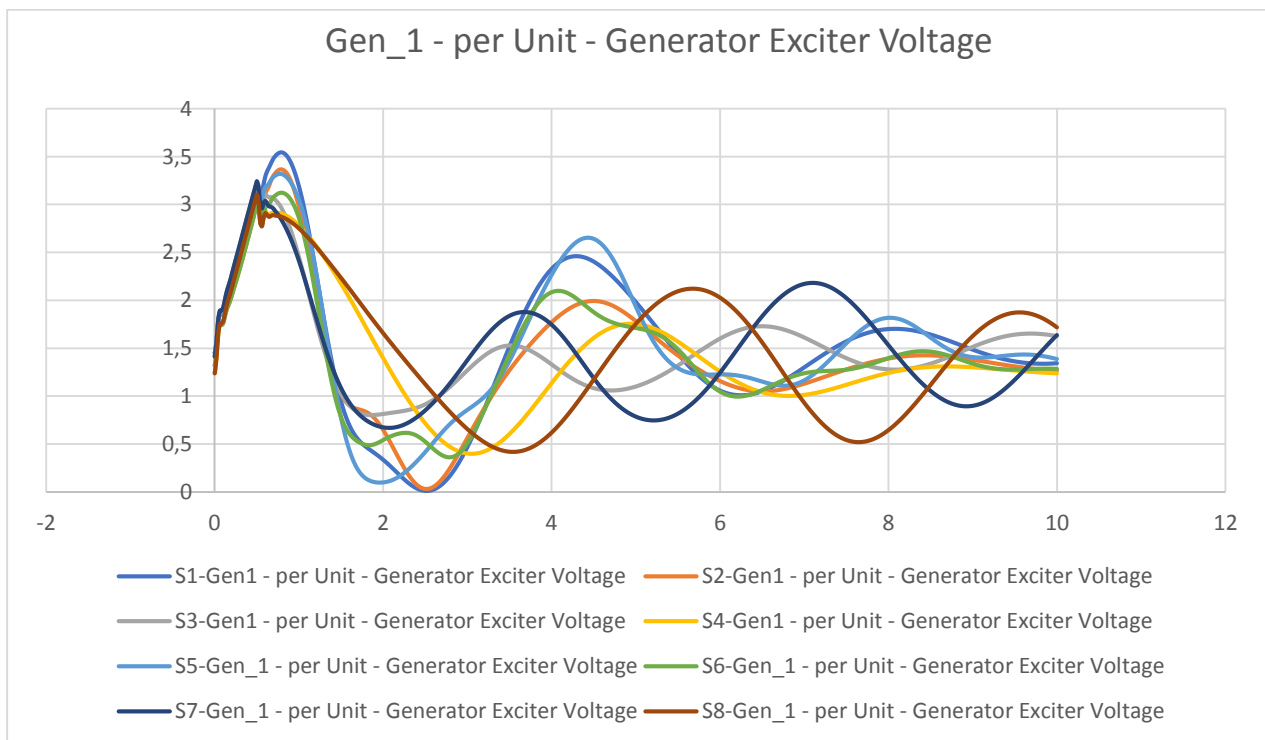


Figure 3.1-34:Gen\_1- Generator Exciter Voltage (PU)

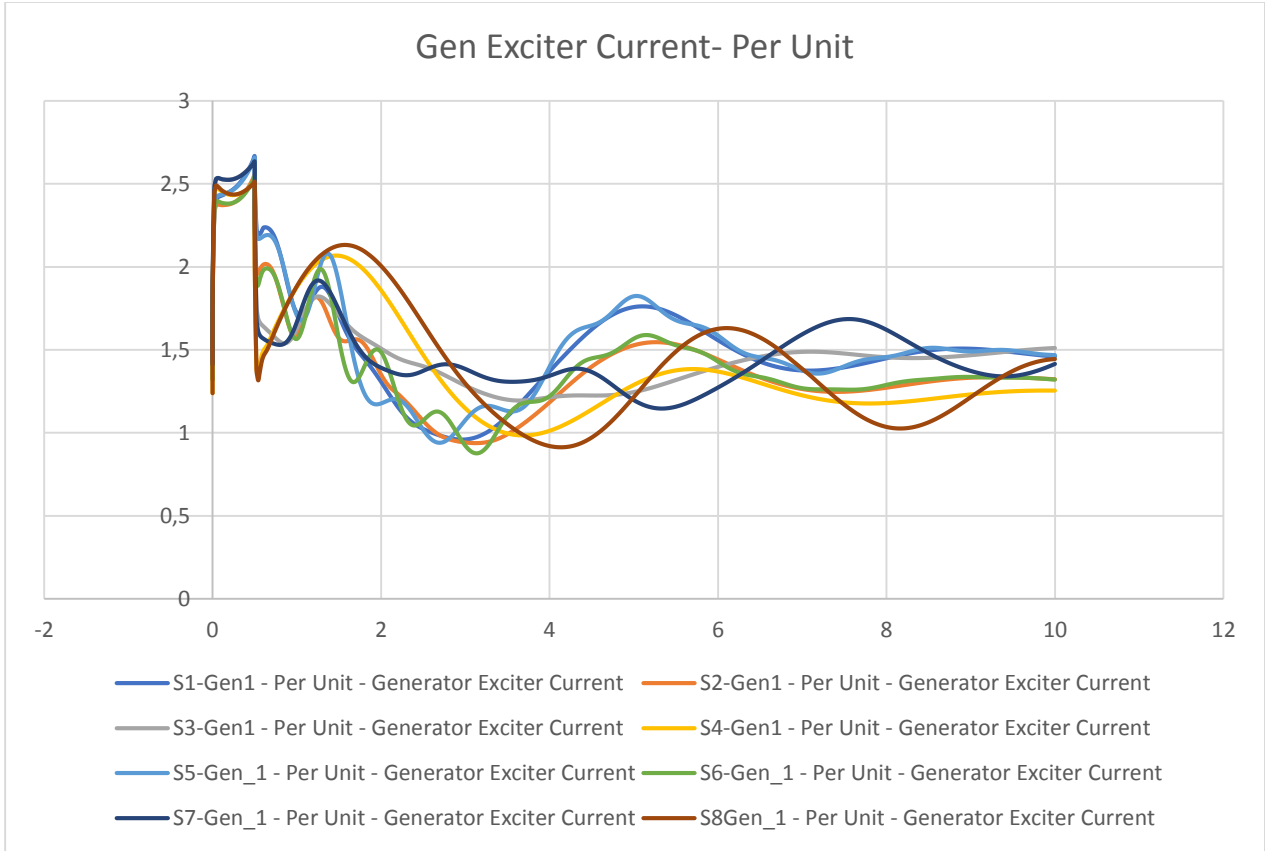


Figure 3.1-35:Gen Exciter Current- Per Unit

### 3.1.7.3 Steady State Power System Studies

Upon analysing the load flow data for the 8 scenarios, below is the summary.

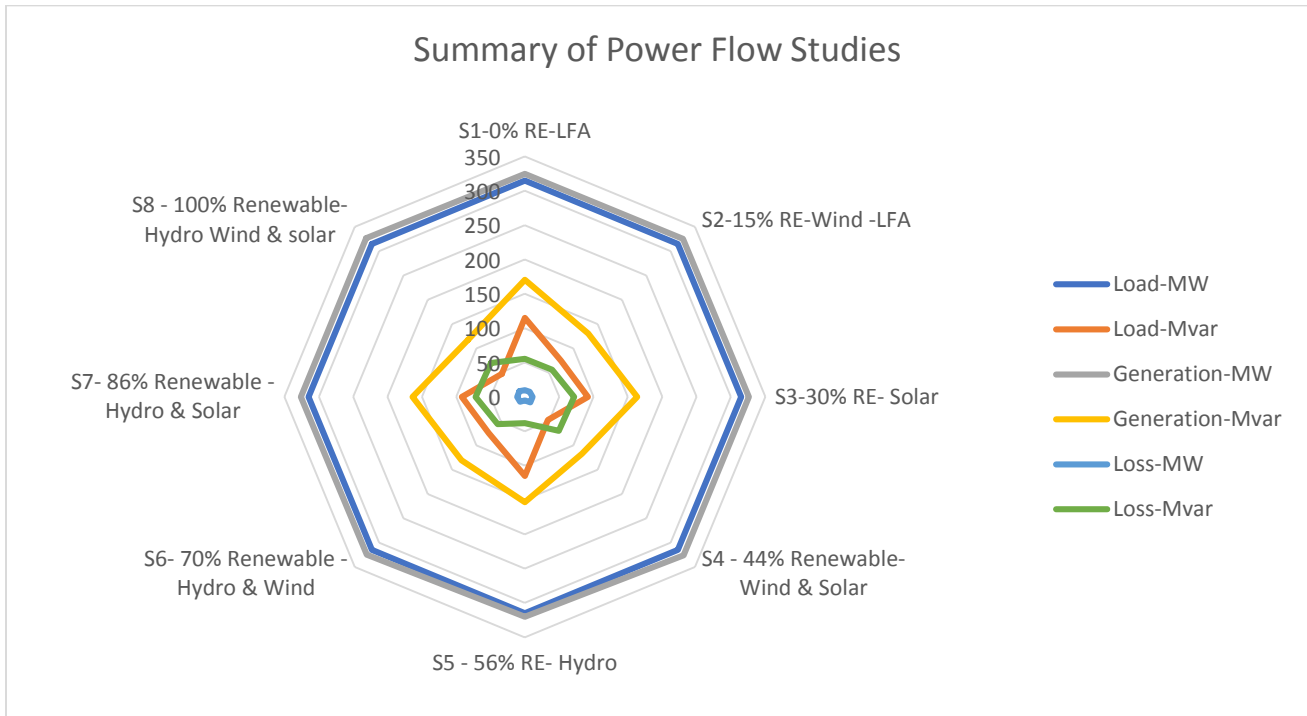


Figure 3.1-36: Summary of Load Flow Study for 8 scenarios.

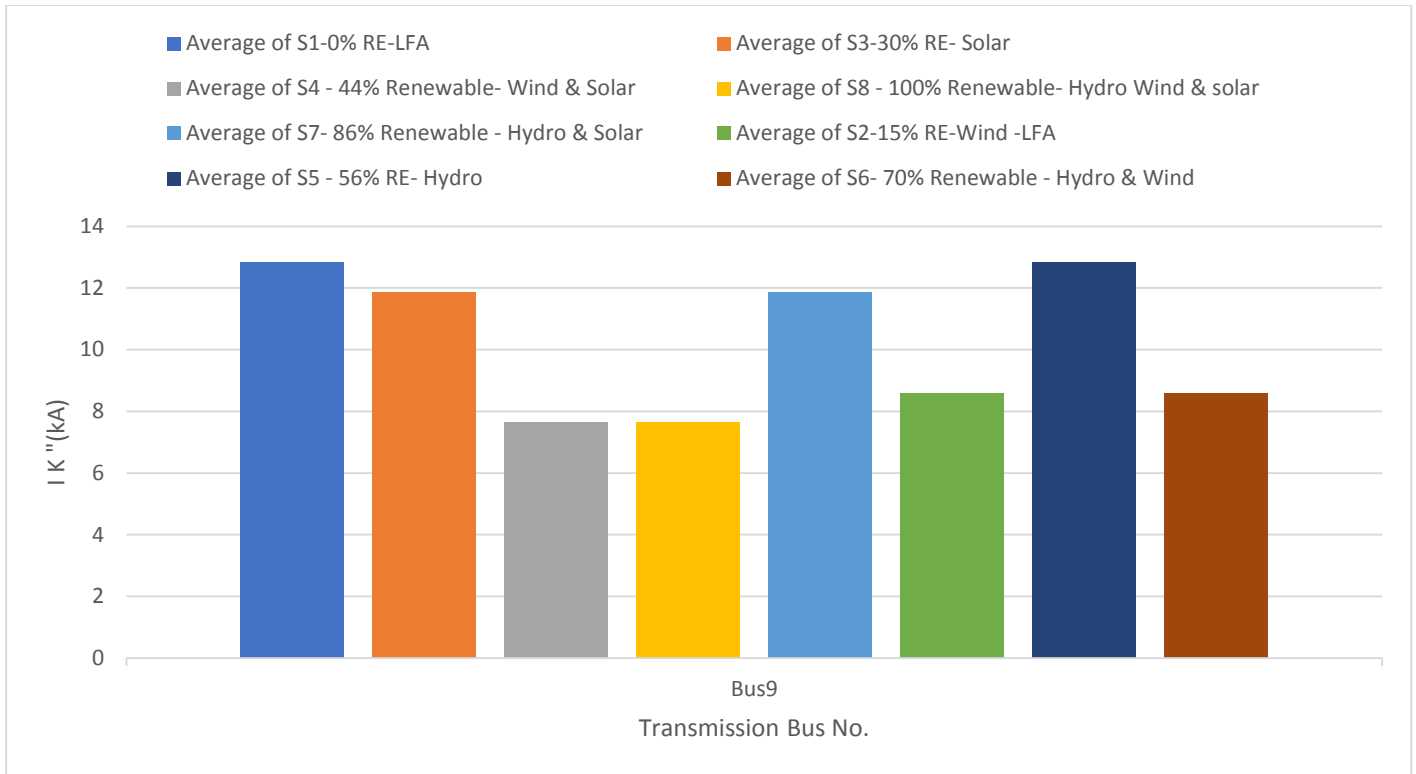


Figure 3.1-37: 3 Phase Short Circuit Current IK'' (kA) for Bus No.9 for each scenario.

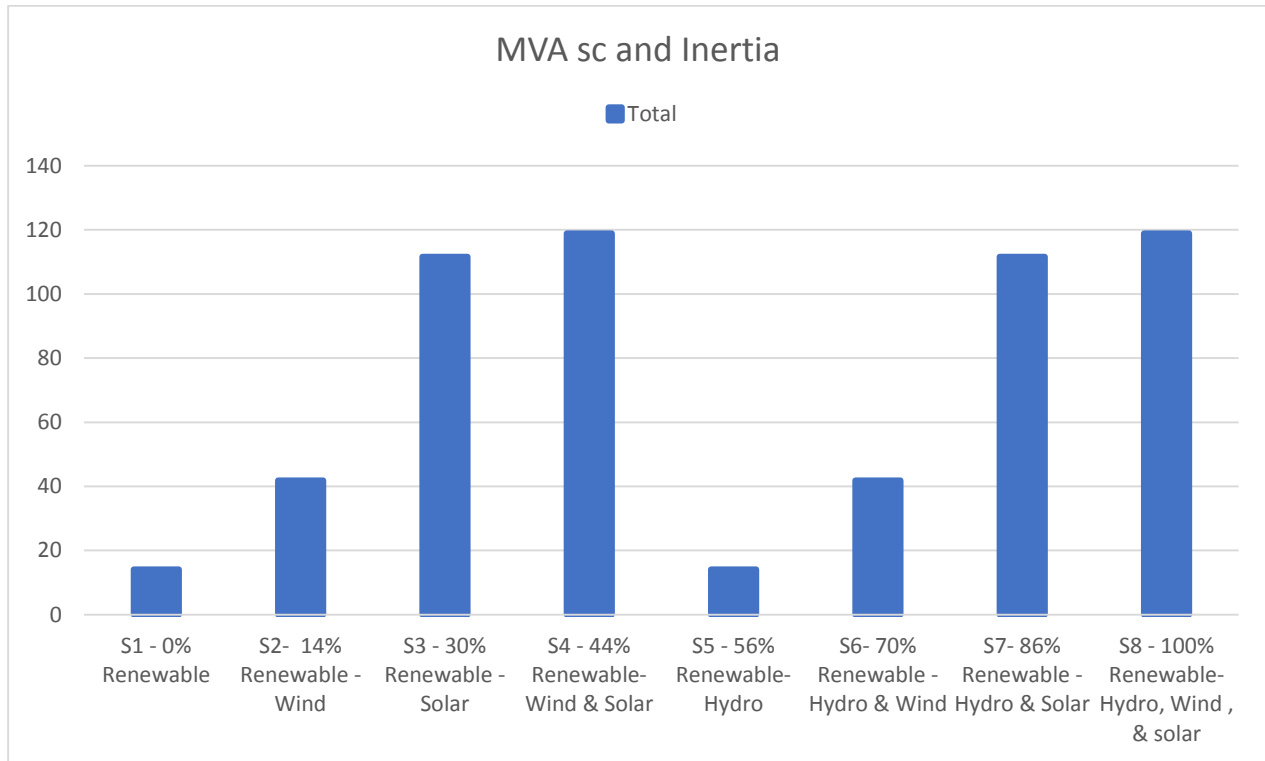


Figure 3.1-38: MVA sc and Inertia

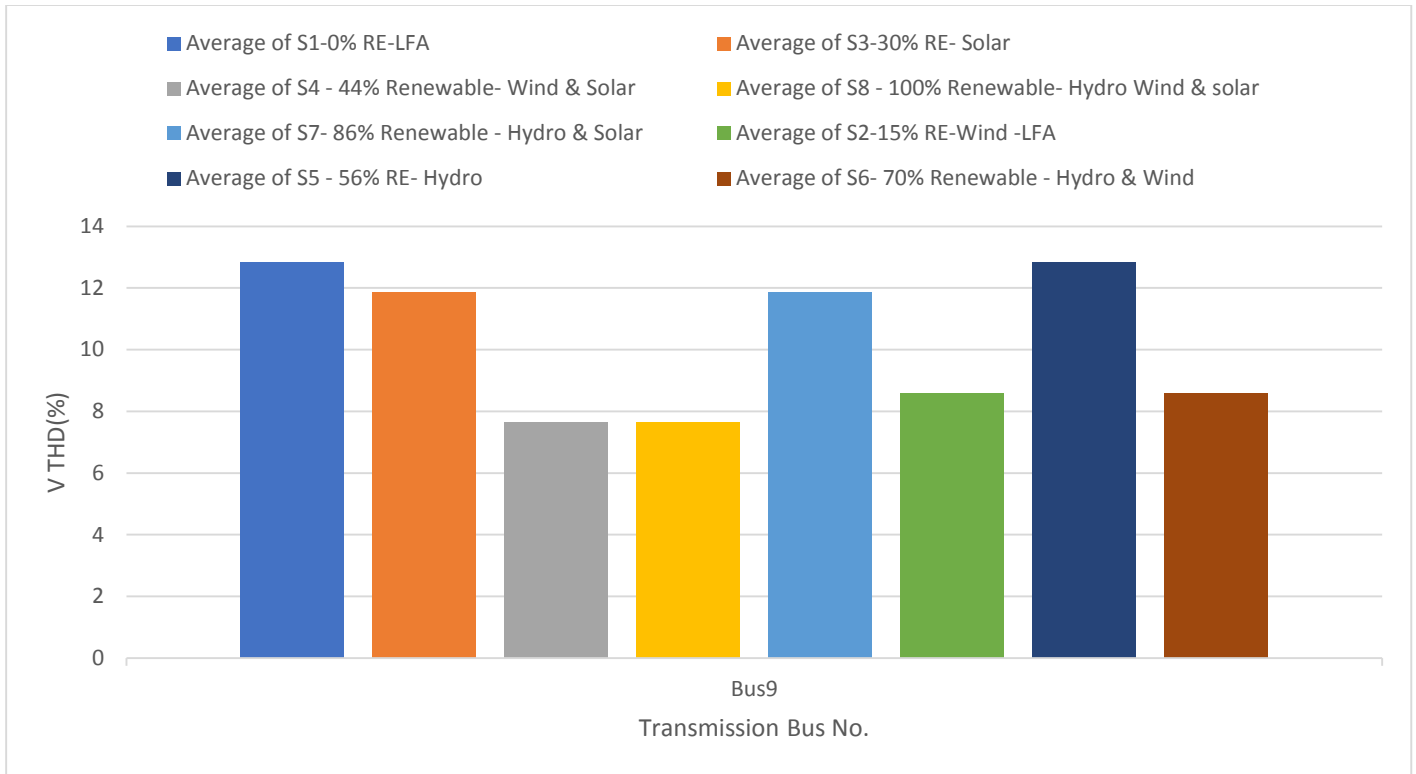


Figure 3.1-39: Voltage THD(%) for Bus No.9 for each scenario.

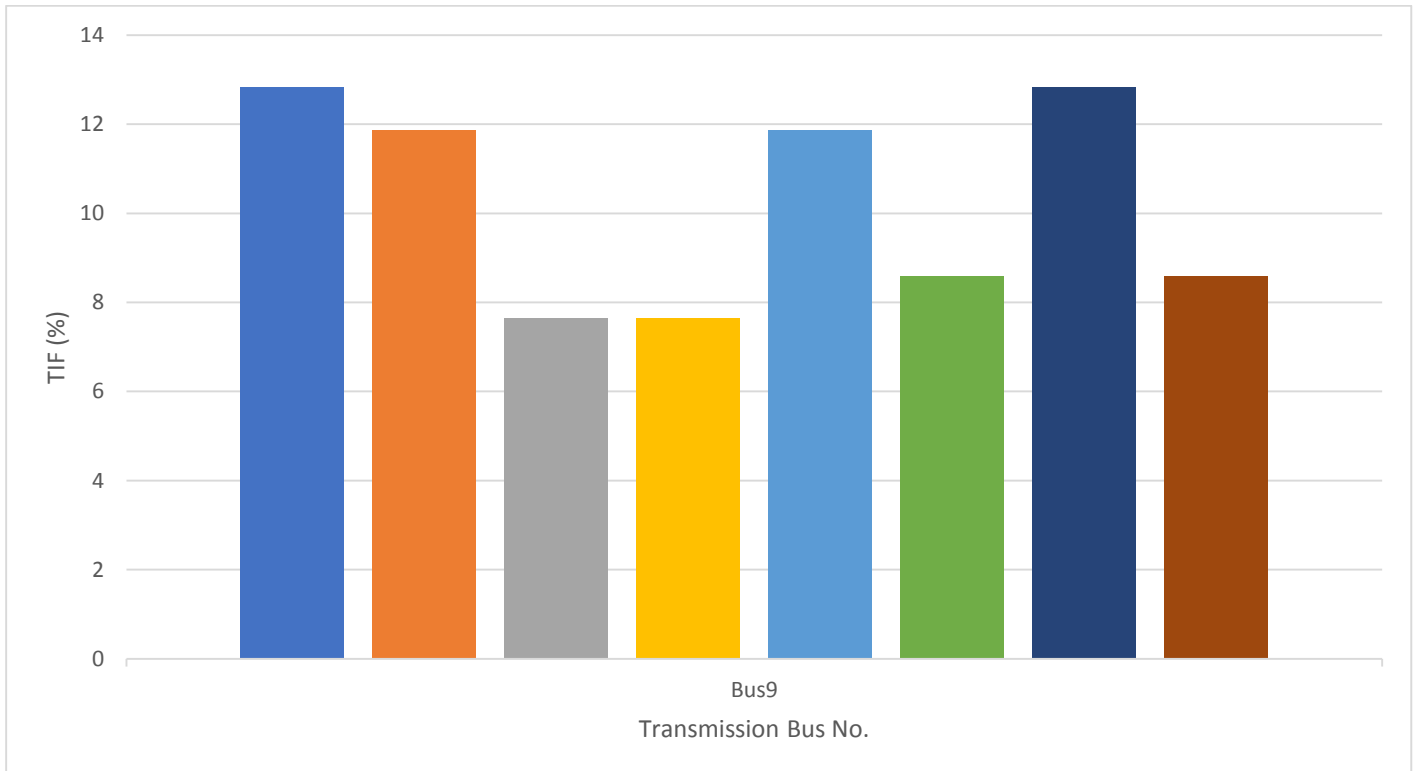


Figure 3.1-40: TIF(%) for Bus No.9 for each scenario.

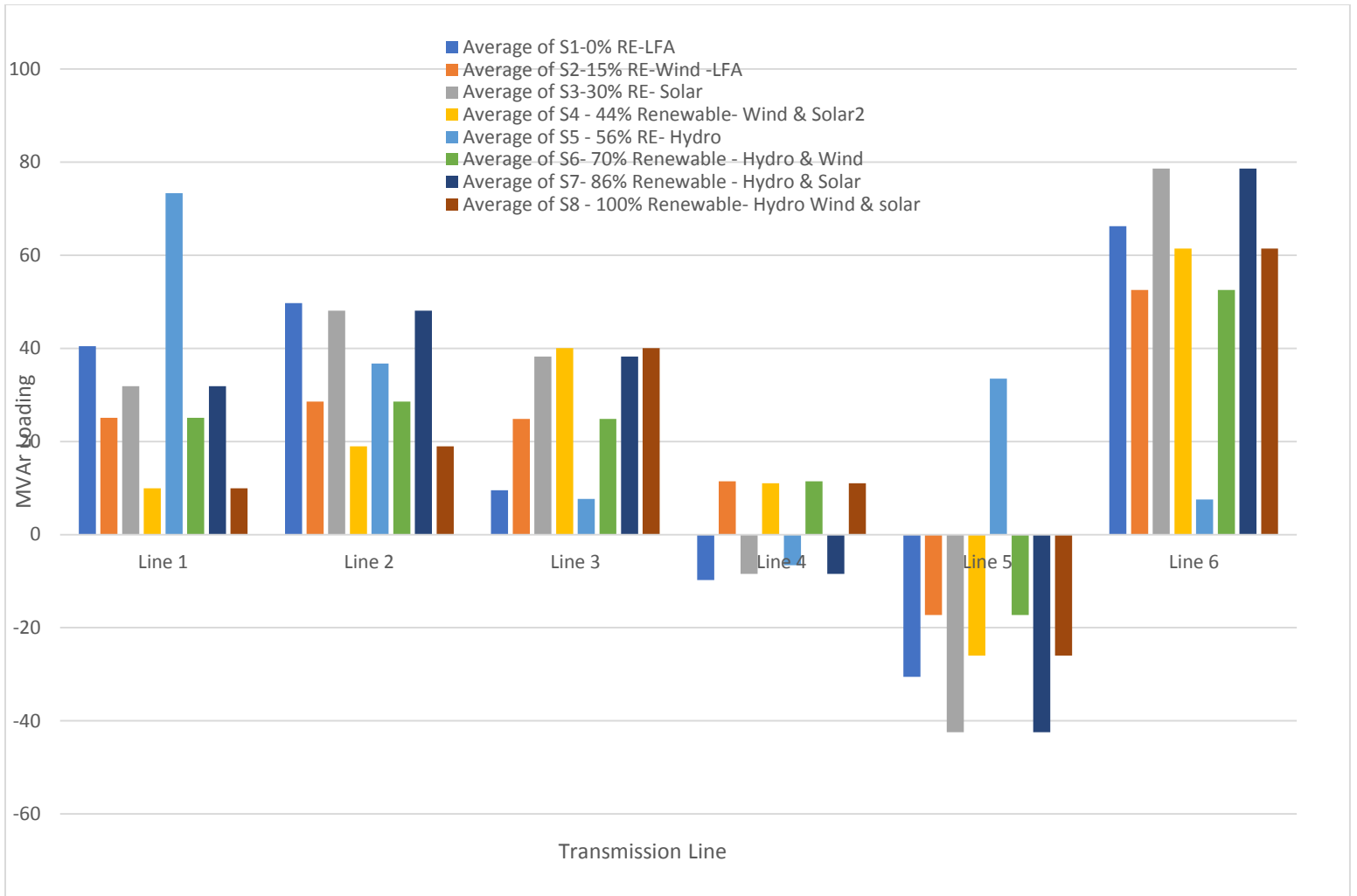


Figure 3.1-41: Reactive Power Loading for all transmission lines per Scenario.

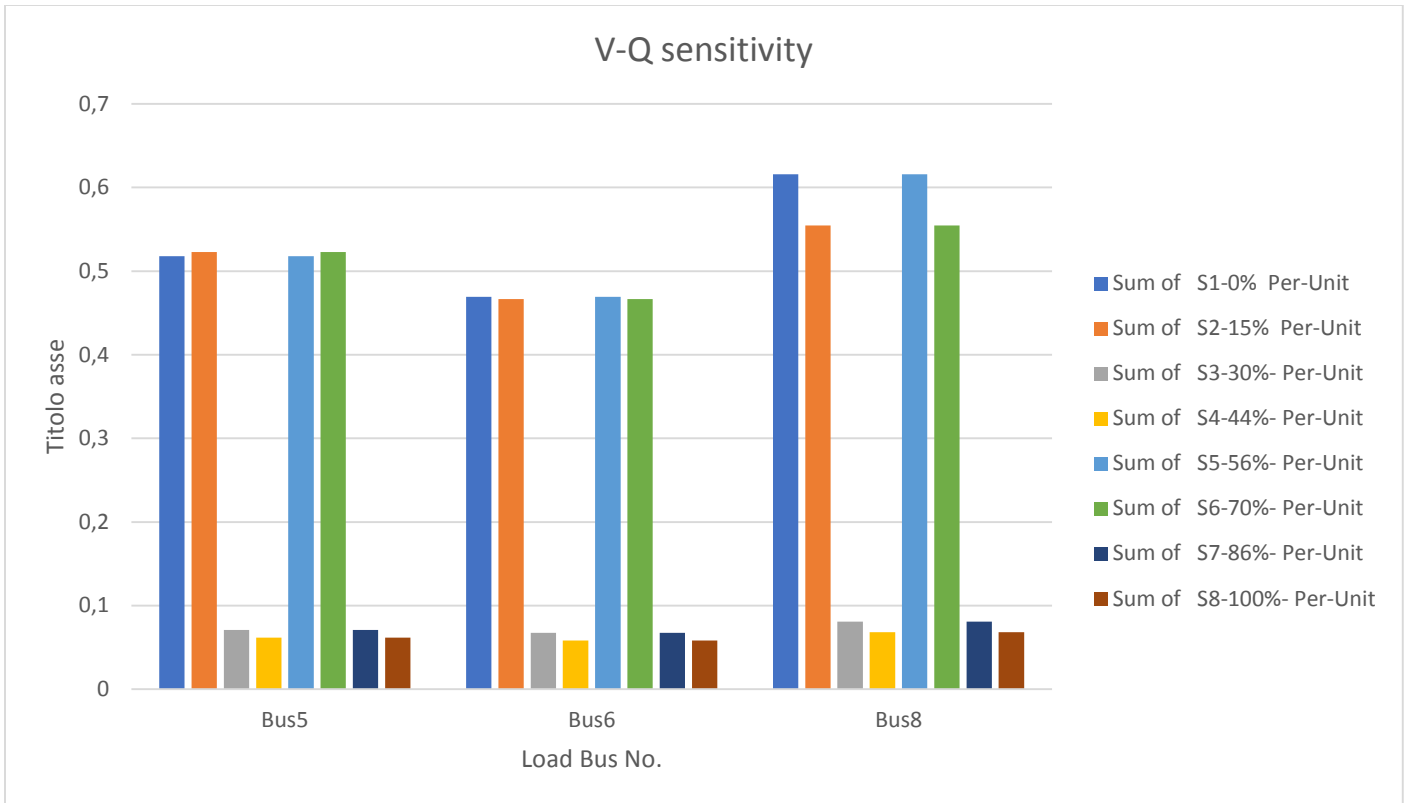


Figure 3.1-42: V-Q sensitivity for load buses for each scenario.

### 3.2 Chapter Nine: CONCLUSIONS

This chapter consolidates the key insights derived from the investigation of the analysis for the challenges of transition towards sustainable 100% renewable electrical power and energy system along with power quality solutions on stability, security, and interoperability of the IEEE 9 bus system. It summarizes the main findings, their implications, and any recommendations that may have been made, also it offers a succinct summary of the research, establishing the relationship between the issues and the study's initial objectives.

In this thesis, the transition from fossil fuel-based synchronous machines to grid integrated and interconnected sustainable 100% renewable electric power energy systems (EPES) were analyzed in depth manner by taking a small-scale sample electrical power IEEE 9 bus system, simulating

different sustainable scenarios with variety of gradual renewable integration contributions. The findings will subsequently be applied to our large-scale power systems.

The original IEEE 9-bus system with 0% renewable ( first scenario ) was deeply analyzed and verified through performing per-unit analysis, power flow study, time domain load flow, P-Q capability checks, steady state and dynamic short circuit calculations, transient stability study, voltage stability study, harmonic analysis, contingency analysis, and a system of differential equations for currents, sending and receiving-end bus voltages, and fault voltage at PoCC, and the same have been verified using ETAP software. This work all has been done in part 2 chapter 4.

After this, in chapter 5 and 6, the grid impact study of equivalent PV plant replacing SM2 and wind farm replacing SM3 has been analyzed respectively. Then in chapter 7, the 100% IEEE 9 bus system was deeply analyzed.

Increased renewables penetration and switching in and out of Inverter Based Resources (IBRs) will negatively impact the stability and reliability of the power system, it is no longer possible to do so without causing a significant impact on grid stability, whereby there are several challenges that expected to come with more renewables such as lower short circuit power and system strength, lower system inertia which causes increased rate of change of frequency (RoCoF), power imbalance results in reduced frequency, injection of more harmonics into the grid, voltage dips and post-fault voltage recovery profiles.

Based on the data analysis for the collected data, the following conclusions can be made:

### **3.2.1 Time Domain Load Flow Analysis**

According to the TDLF performed for all the scenarios, we can conclude the following:

- 1- In all the scenarios, the source MVAh covers the load MVAh, however the highest surplus of energy was in scenario No.4 (45% renewable contribution from solar and wind) and No.8 (100% renewable contribution from hydro, solar and wind )

- 2- The first and second highest energy losses (in KWh) were from scenario No.1 with 0% renewable contribution and No.5 with 56% renewable contribution only from Hydro without IBR solar and wind.
- 3- The lowest energy losses (in KWh) were in scenarios with highest renewable integration ( S7 with 86% RE contribution and S8 with 100% RE contribution)
- 4- The highest levelized cost of energy among the 8 scenarios was scenario No.4 with 45% renewable penetration (solar and wind) with total 28.86 M USD / month, while the lowest LCOE scenario was scenario No.6 with 70% renewable integration (hydro and wind) with 17.09 M USD/month.
- 5- The highest 3 profitable scenarios were S7 with 78% GM, S6 with 77% GM and S8 71% GM
- 6- The lowest CO<sub>2</sub> emissions were released from the last scenario No.8 (100% renewable integration) with only a 3,367 Tons of CO<sub>2</sub>.
- 7- The highest CO<sub>2</sub> emission scenarios came from scenario No.1,2,3, and 4 and at which the renewable contribution is less than 50%

### 3.2.2 Transient Stability Study

According to the TSS performed for all the scenarios, and assuming same type of large disturbance occurs in all the scenarios, we can conclude the following:

- 1- The generator Gen-1 post fault absolute angle for S1 and S4 (in which the total system inertia is the highest and there is no IBR renewable integration) showed the highest post fault absolute angle in a range between 80-100 degree.

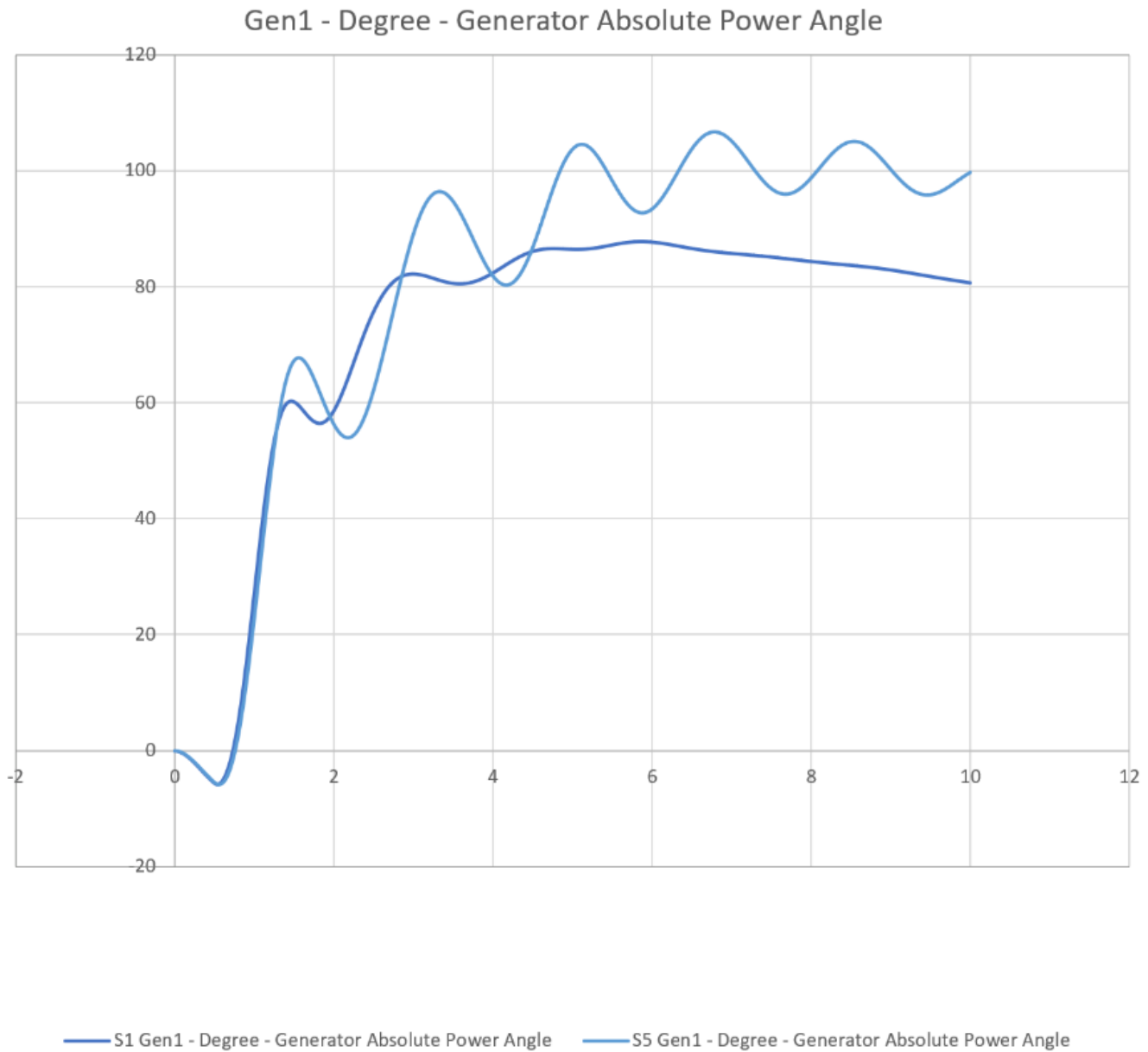


Figure 3.2-1: Generator 1 absolute angle with 0% IBR

2- While the scenarios with **Wind farm integration** shows a negative post fault absolute angle, where the higher the renewable integration shows a more deteriorated post fault absolute angle as show in S6 with 75% Renewable energy.

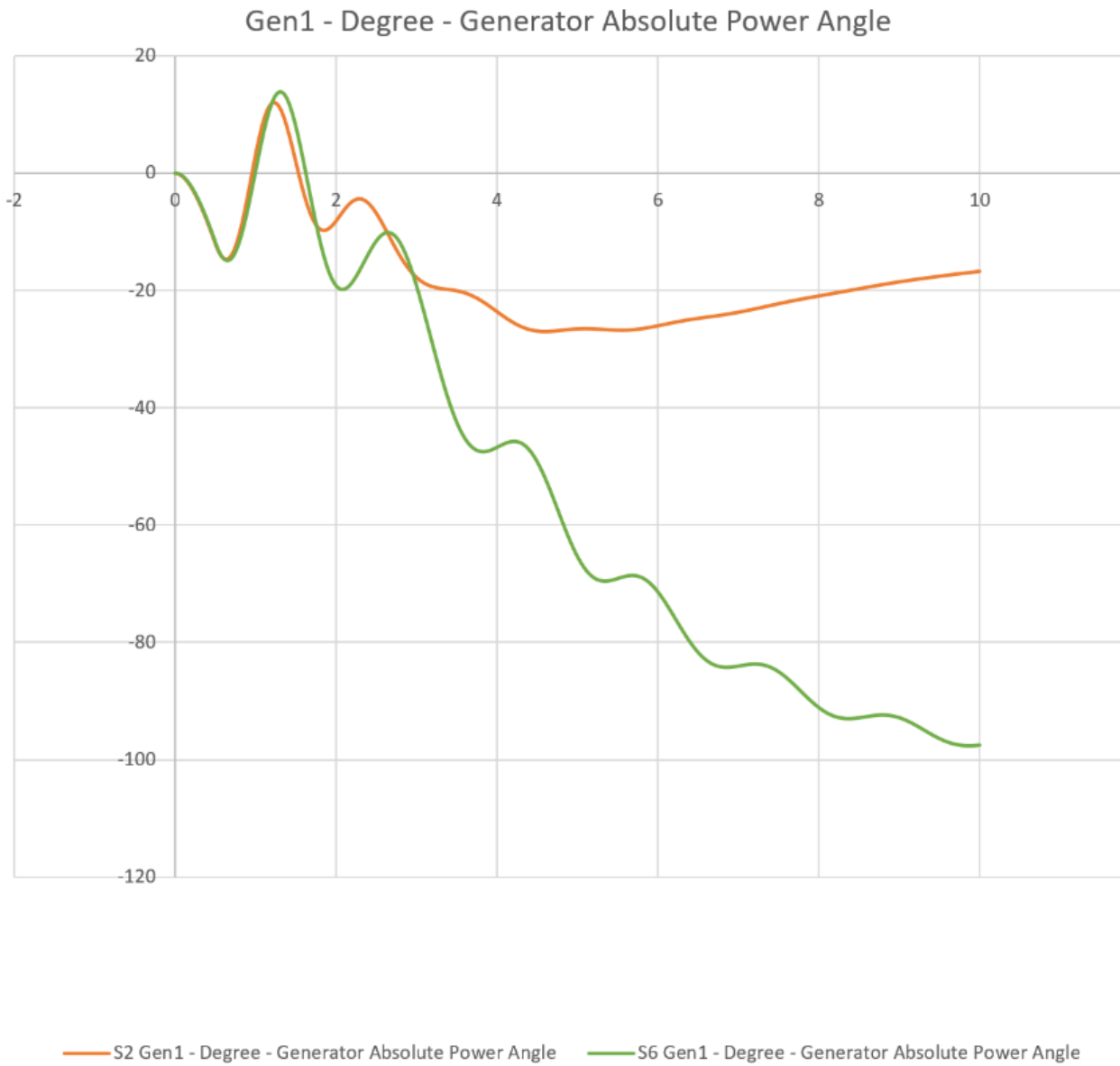


Figure 3.2-2: Generator Absolute Angle for scenarios with wind integration.

- 3- The scenario with **solar integration** (S3: 30% RE & S7: 86% RE) shows oscillatory post fault absolute angle behavior with decreasing magnitude.

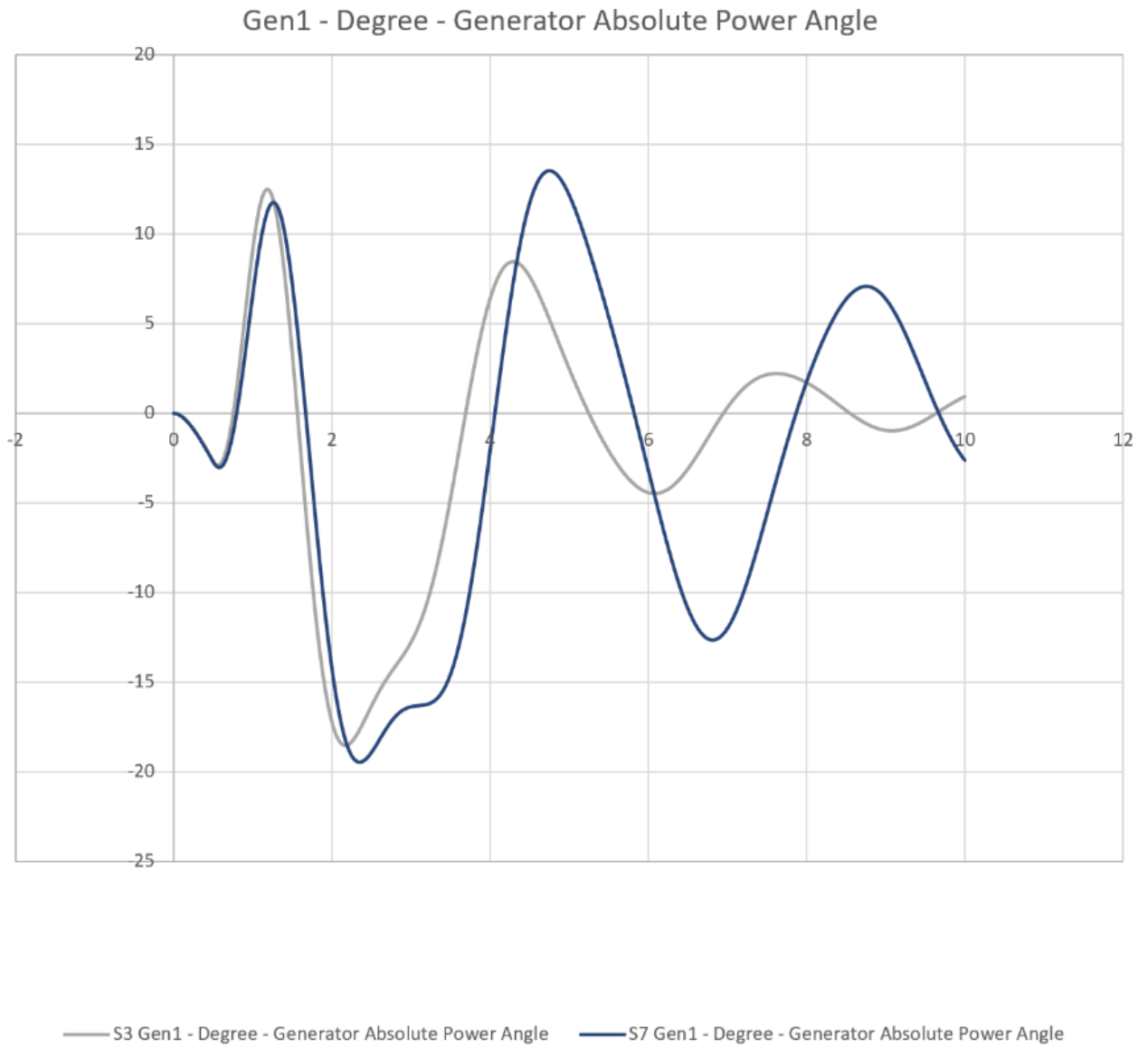


Figure 3.2-3: Generator Absolute Angle for scenarios with Solar integration.

4- However, the scenario with full IBR integration (solar and wind ) shows a more oscillation in 100% RE scenario than the 45% RE integration.

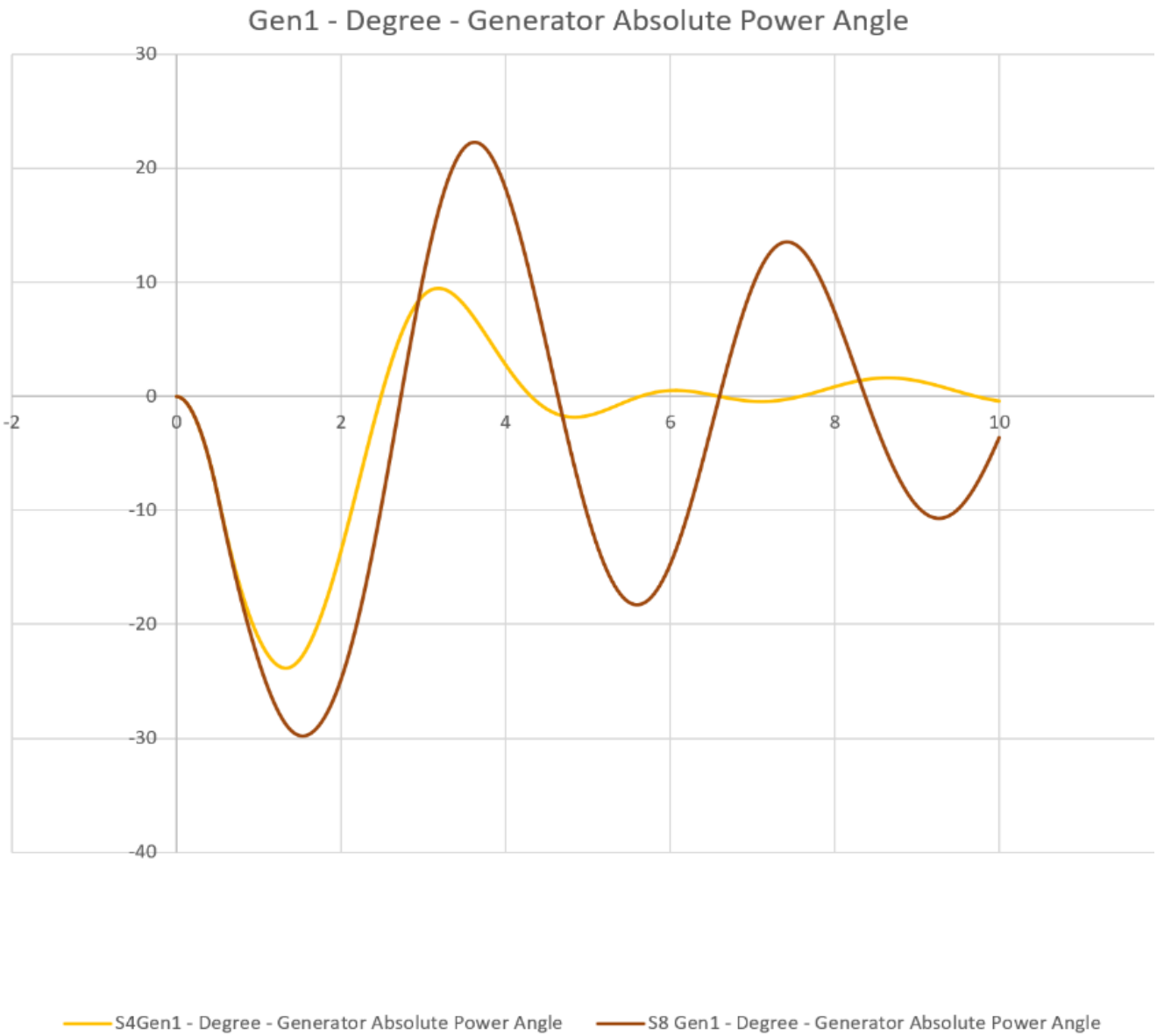


Figure 3.2-4:Generator Absolute Angle for scenarios with solar and wind integration.

- 5- With more IBR integration (solar and wind), the total inertia of the system decreases which affect the Rate of Change of Frequency (RoCoF) as shown in the red rectangle and makes it steeper as more IBR integration contributed in the overall energy system

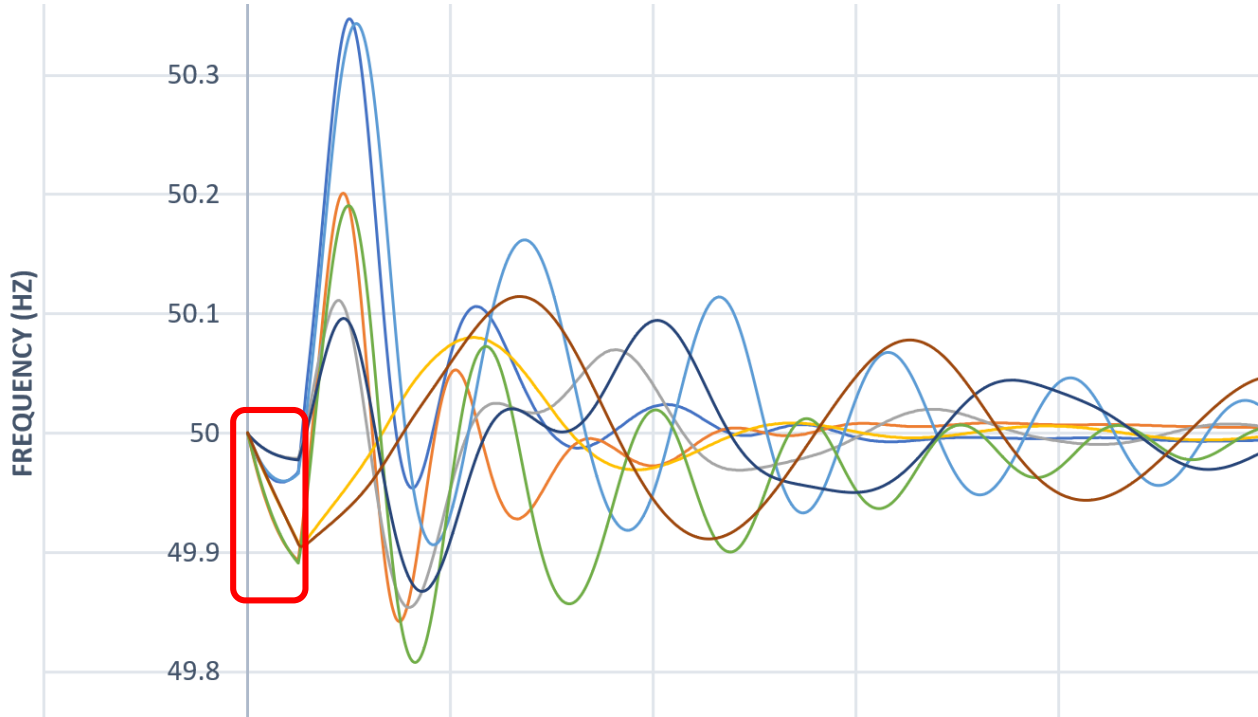


Figure 3.2-5: RoCoF effect.

- 6- The frequency response in post fault condition shows a second order system response with different damping coefficient  $\zeta$  and peak values, whereby the lower damping coefficient and higher peaks were seen in the scenarios with no IBR (solar and wind ) contributions like in S1 and S5.
- 7- In the case of only wind contribution like in S2 and S6, a steeper RoCoF trajectory was seen, and the frequency took  $t= 6$  sec in S2 to reach to steady state, while it took much longer  $t=12$  sec in higher renewable contribution like in the case of S6

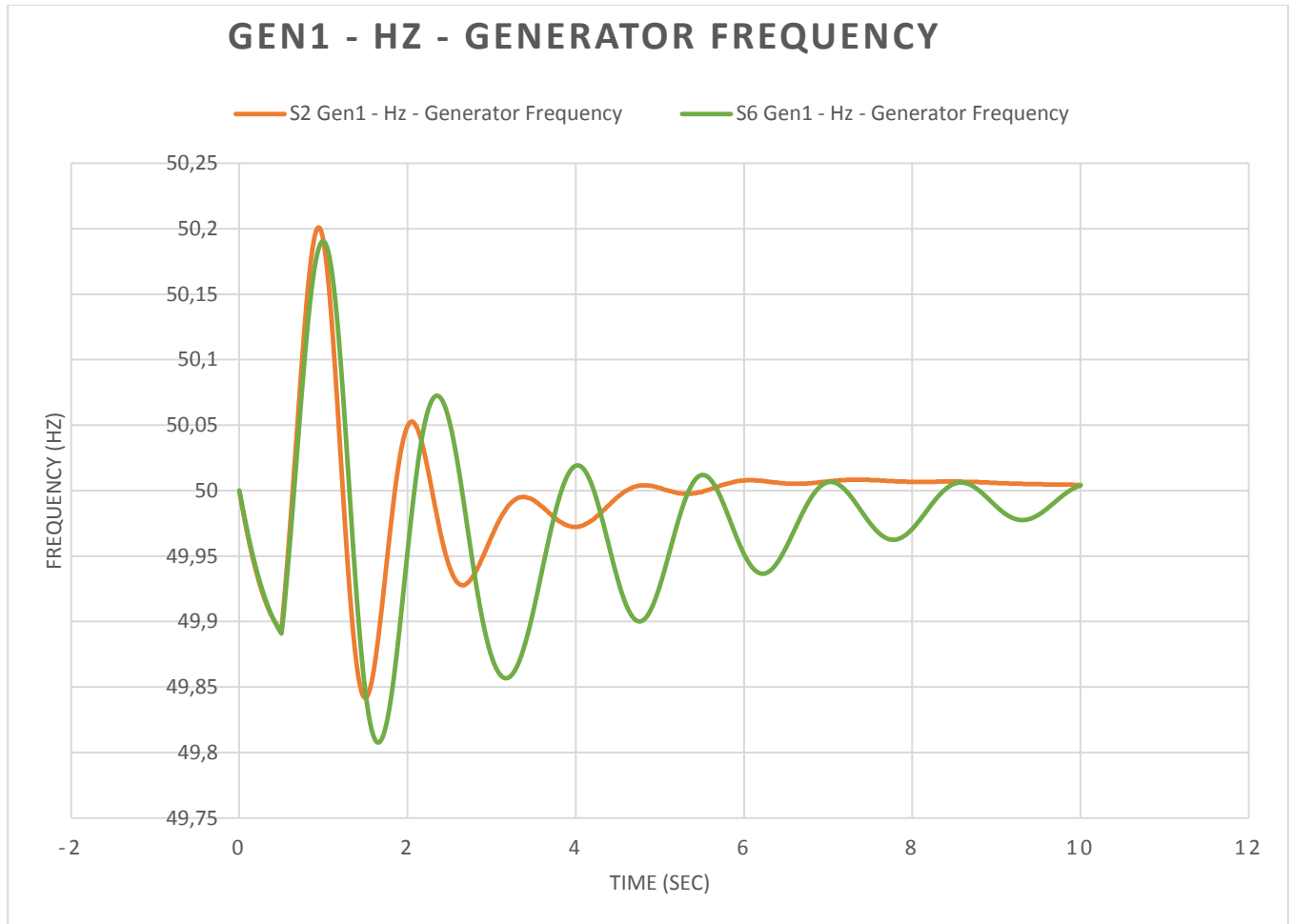


Figure 3.2-6:RoCoF with Wind Integration

- 8- In case of solar integration, the frequency response shows less overshoot but more oscillatory behavior.

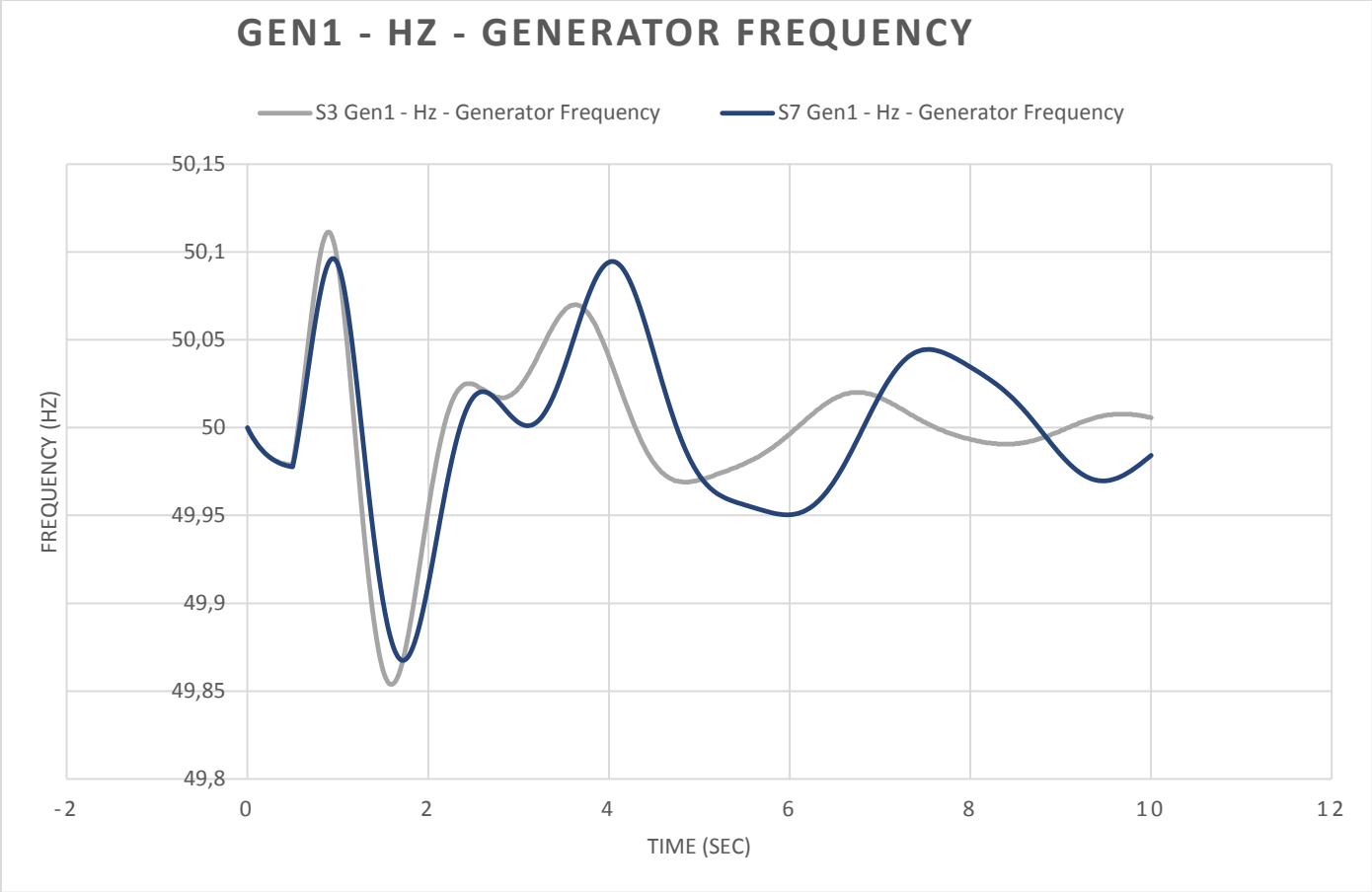


Figure 3.2-7:RoCoF with Solar Integration

9- The difference between the S1 0% renewable energy to S8 100% renewable integration is clearly shown in Figure 3.2-8 below, the RoCoF is more in S8 than S1, the overshoot in S1 higher than that in S8 by 0.478%, and the system in S1 reaches to the steady state frequency much faster than that in S8

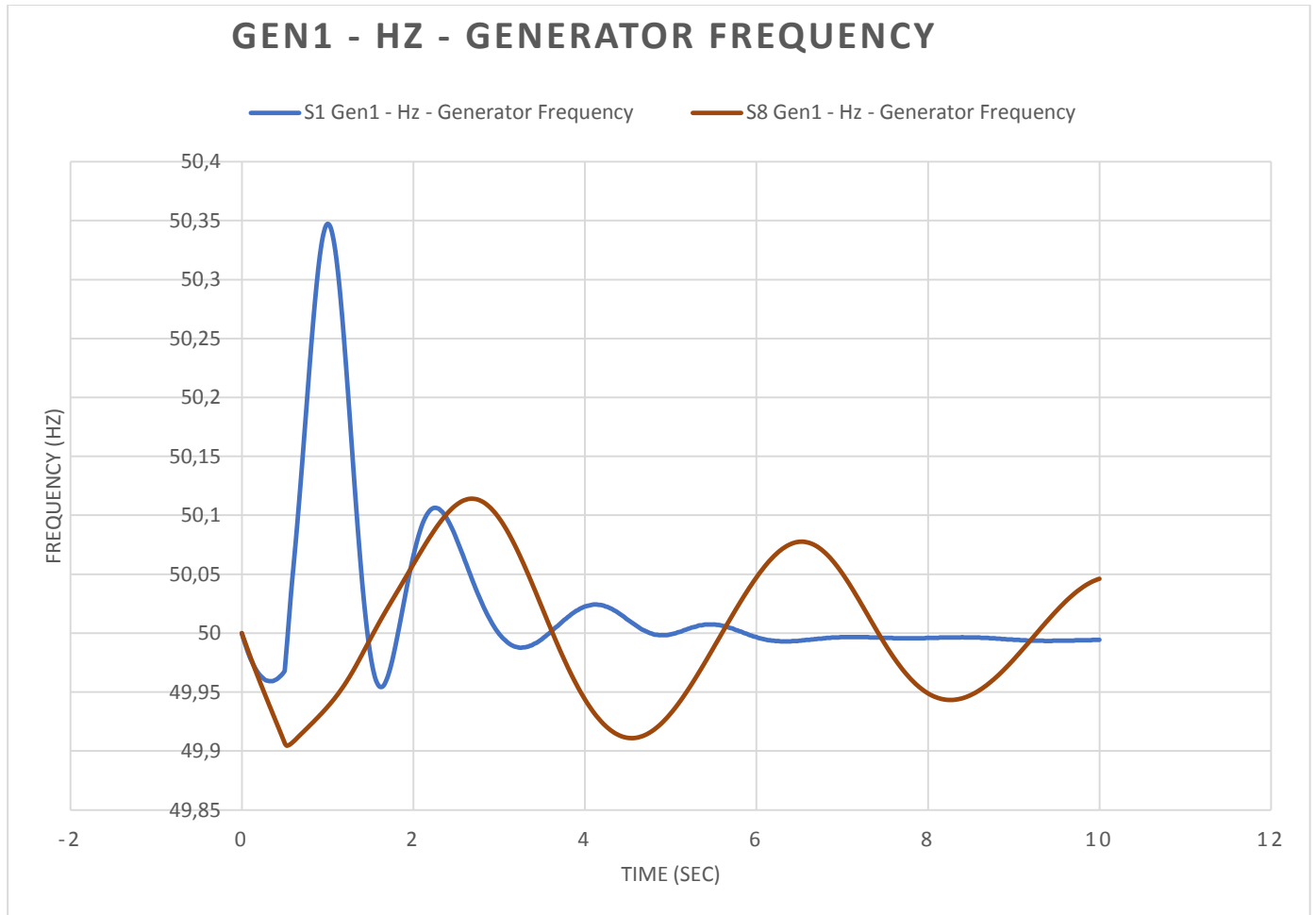


Figure 3.2-8: RoCoF effect between 0% RE to 100% RE

10- The mechanical power for Gen 1 for scenarios 1,2,3, and 4 in which the synchronous machine was driven by steam turbines show an oscillatory response, while Gen 1 for scenarios 5,6,7, and 8 in which synchronous machines was driven by hydro turbine show a constant response

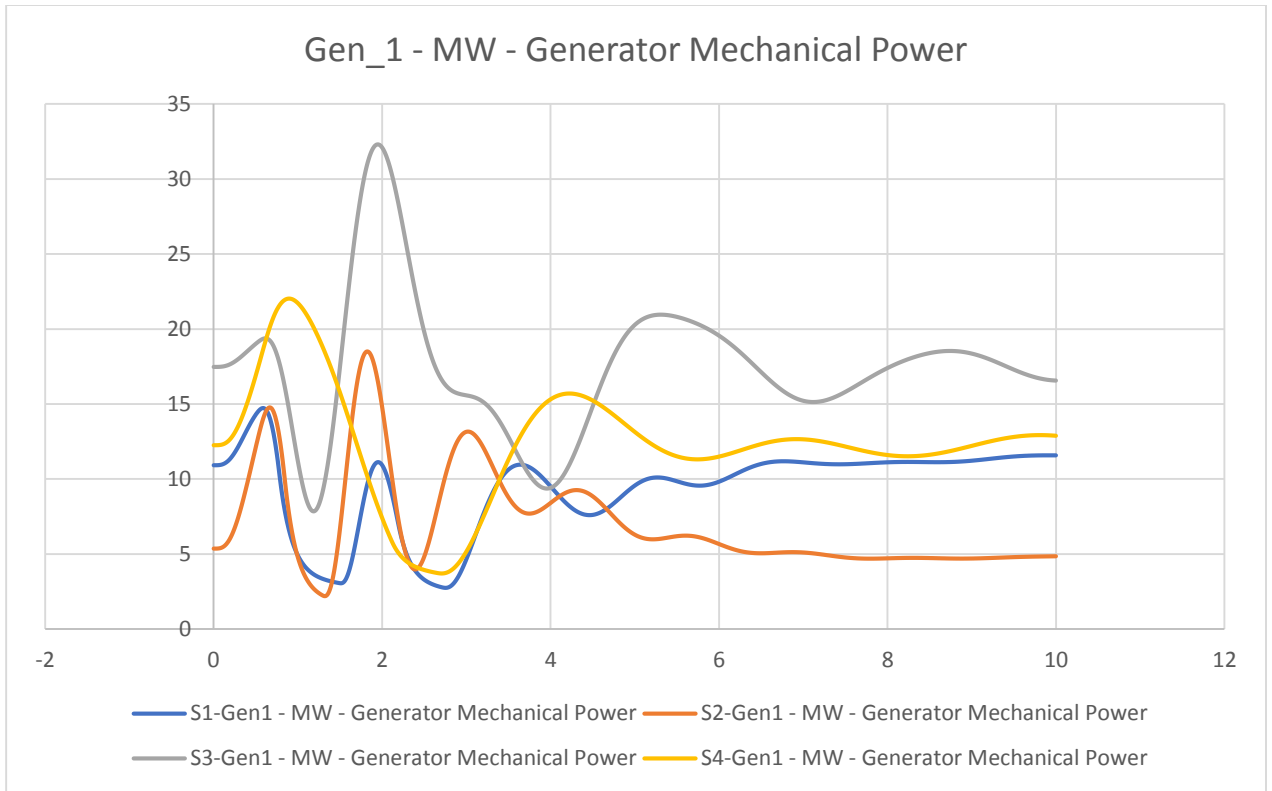


Figure 3.2-9: Mechanical Power Oscillation for steam turbine driven generators.

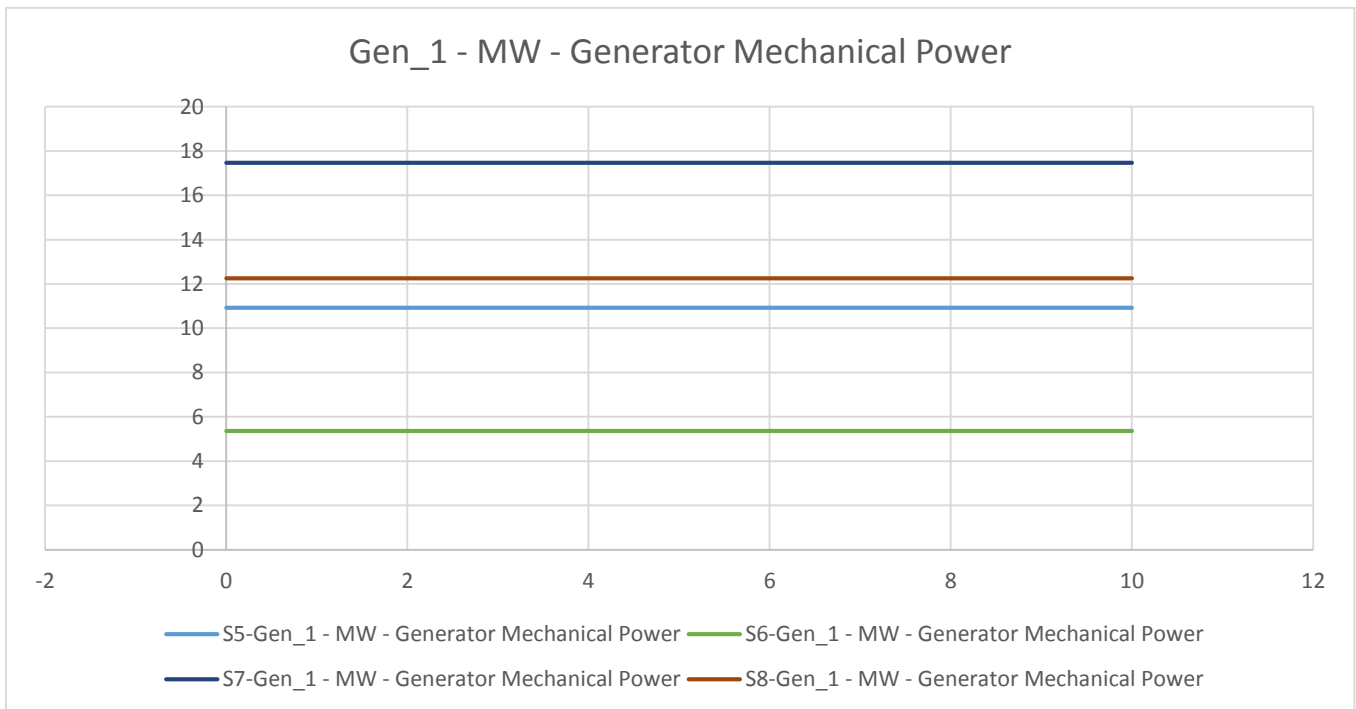


Figure 3.2-10: Mechanical Power Oscillation for hydro turbine driven generators.

11- The output electrical power in post fault condition for all the scenarios without solar & wind together contribution shows an oscillatory second order response, however, when solar and wind becomes together, then the electrical power response shows less oscillation.

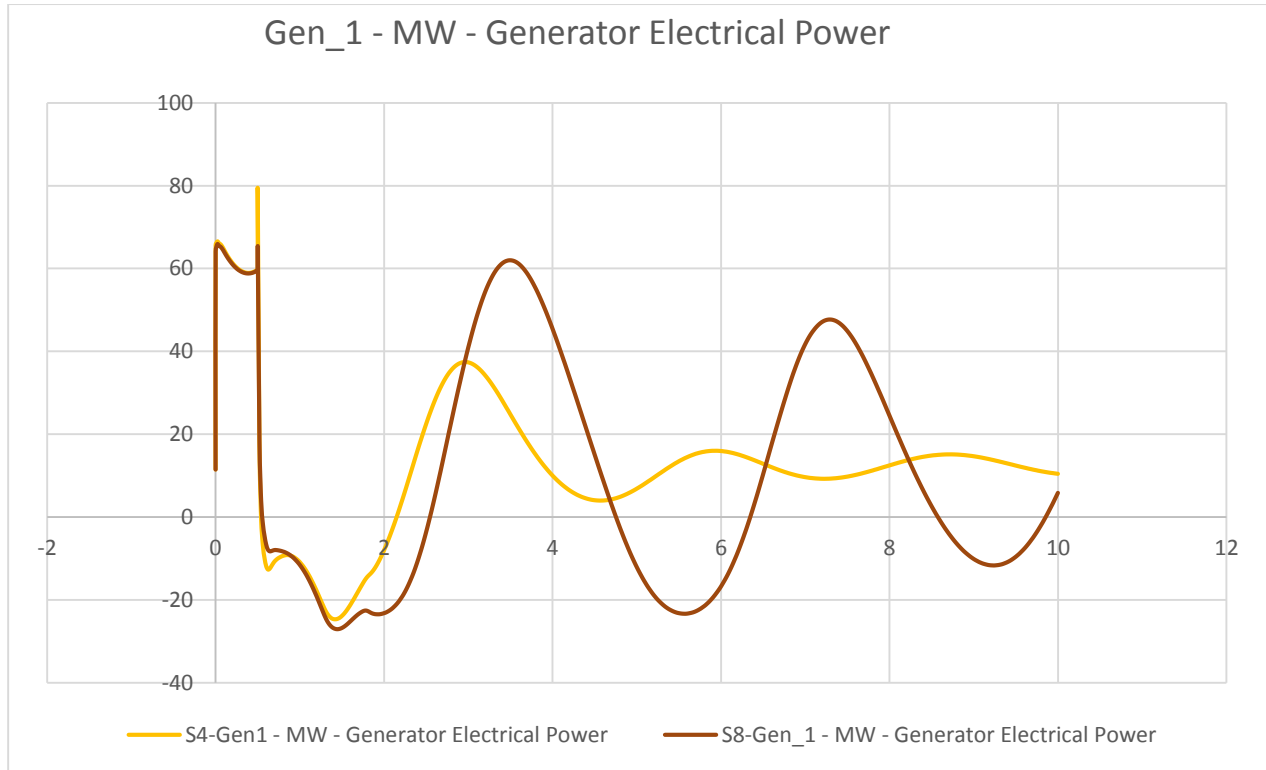


Figure 3.2-11: Electric Power dynamic response for solar and wind contributing together

12- During fault condition the generator Gen1 in all scenarios (except the last scenario 100% RE) contributes with high reactive power 4 times its nominal reactive power, while in last scenario S8:100% RE it contributes only with the nominal reactive power Q

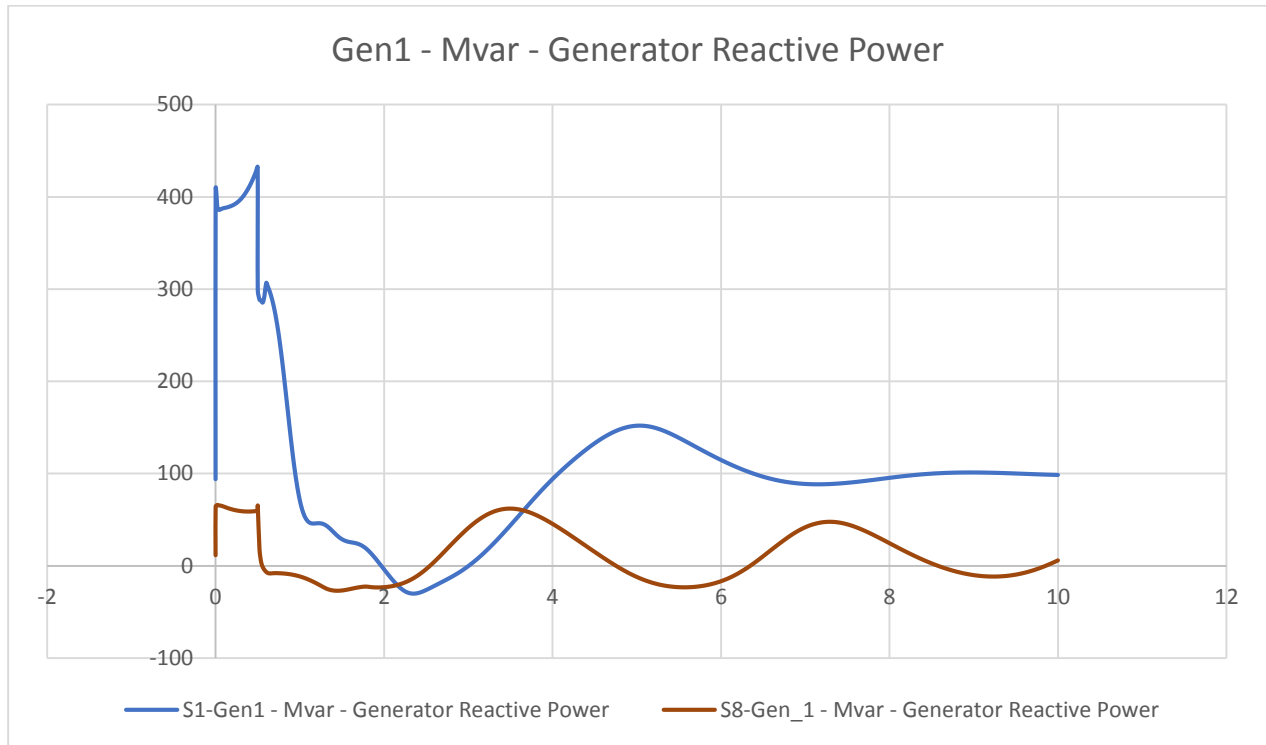


Figure 3.2-12: Reactive power Contribution in postfault condition between 0% and 100% RE

13- The electrical current injected by the Gen-1 on all scenarios is almost same with slight differences in oscillatory behavior.

### 3.2.3 Power System Analysis

According to the *Power Flow Analysis* performed for all the scenarios, we can conclude the following:

- 1- The available generation in MW covers the total demand in MW and the same applies for the MVAR.
- 2- The highest generation in MW was seen for scenarios 4 with and 8 with total generation of 326.492 MW.
- 3- It was observed that the MW losses increased as the IBR (solar and wind) integration increased.

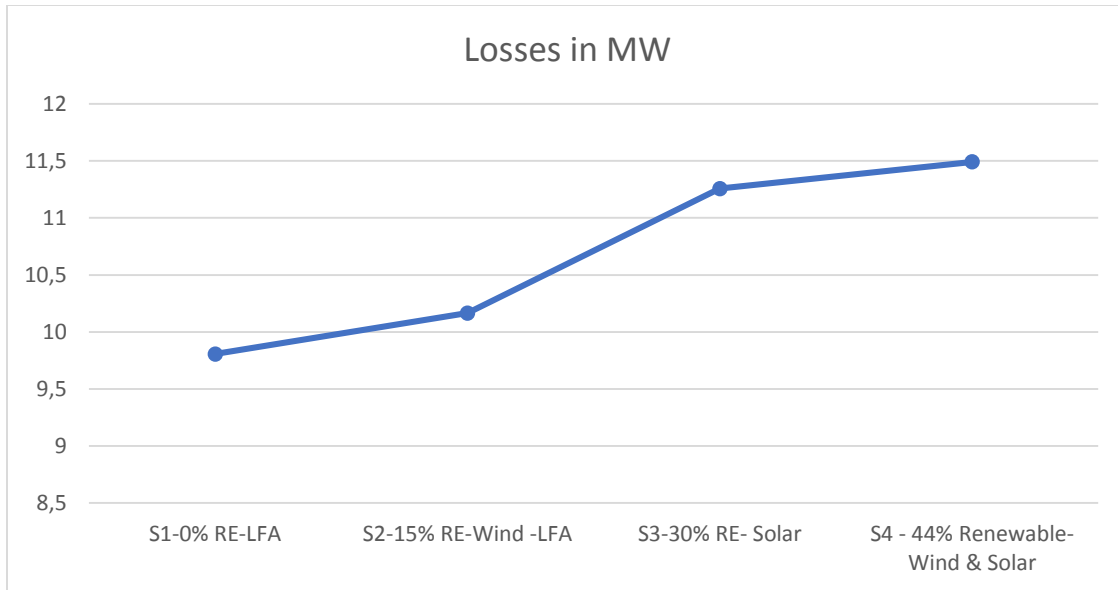


Figure 3.2-13: MW Losses for scenarios 1,2,3, and 4

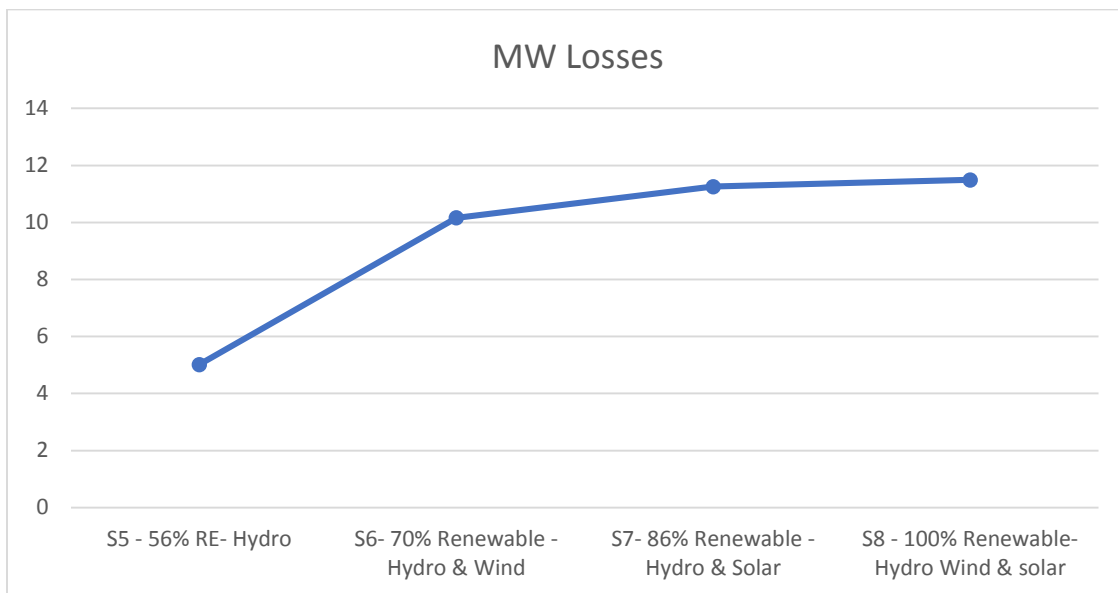


Figure 3.2-14:MW Losses for scenarios 5,6,7, and 8

4- The lowest MW losses was observed for scenario No.5 with 56% Hydro integration

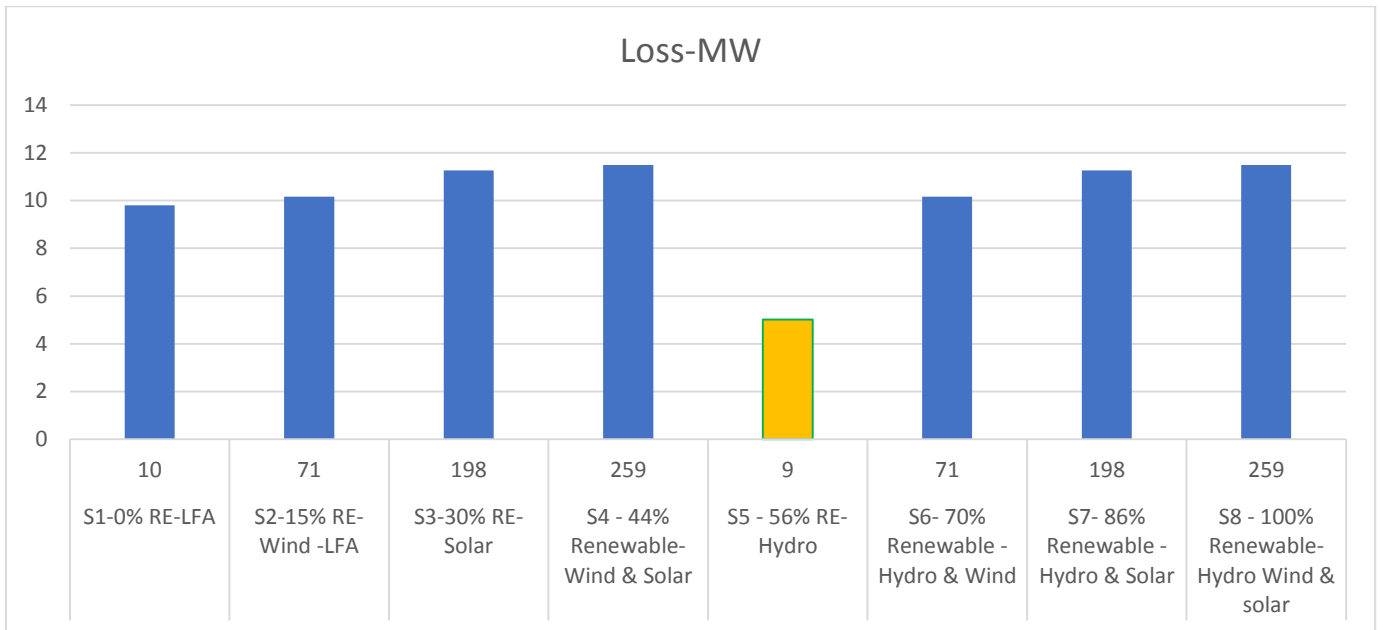


Figure 3.2-15: MW Losses for each Scenario.

According to the short circuit analysis performed for all the scenarios, we can conclude the following:

- 1- It was noticed that as the IBR (solar and wind) contribution increased, the short circuit level for the transmission buses decreased.

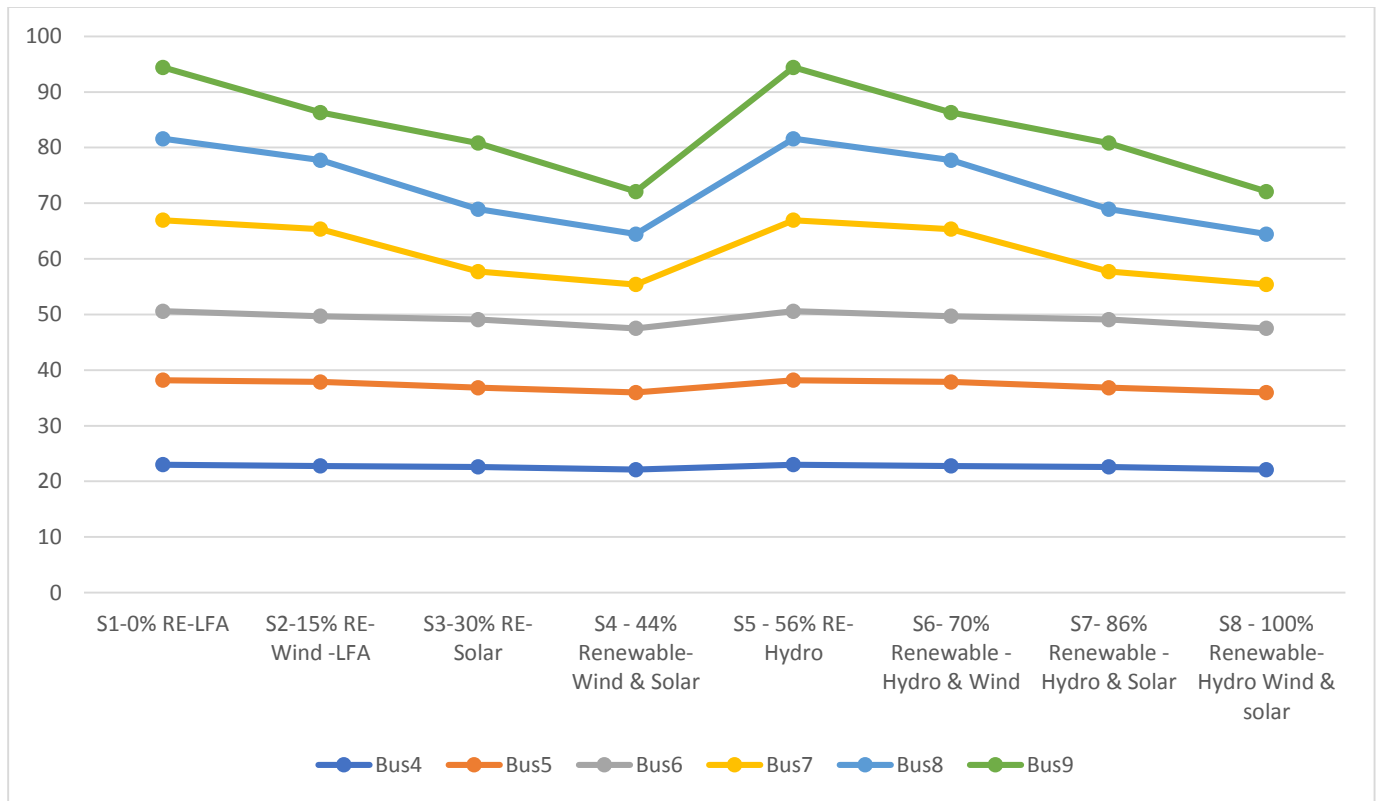


Figure 3.2-16: Short Circuit Current  $I_{K''}$  (kA) for transmission buses for the 8 scenarios

2- As the inertia decreased in the system the short circuit power and short circuit current decreased

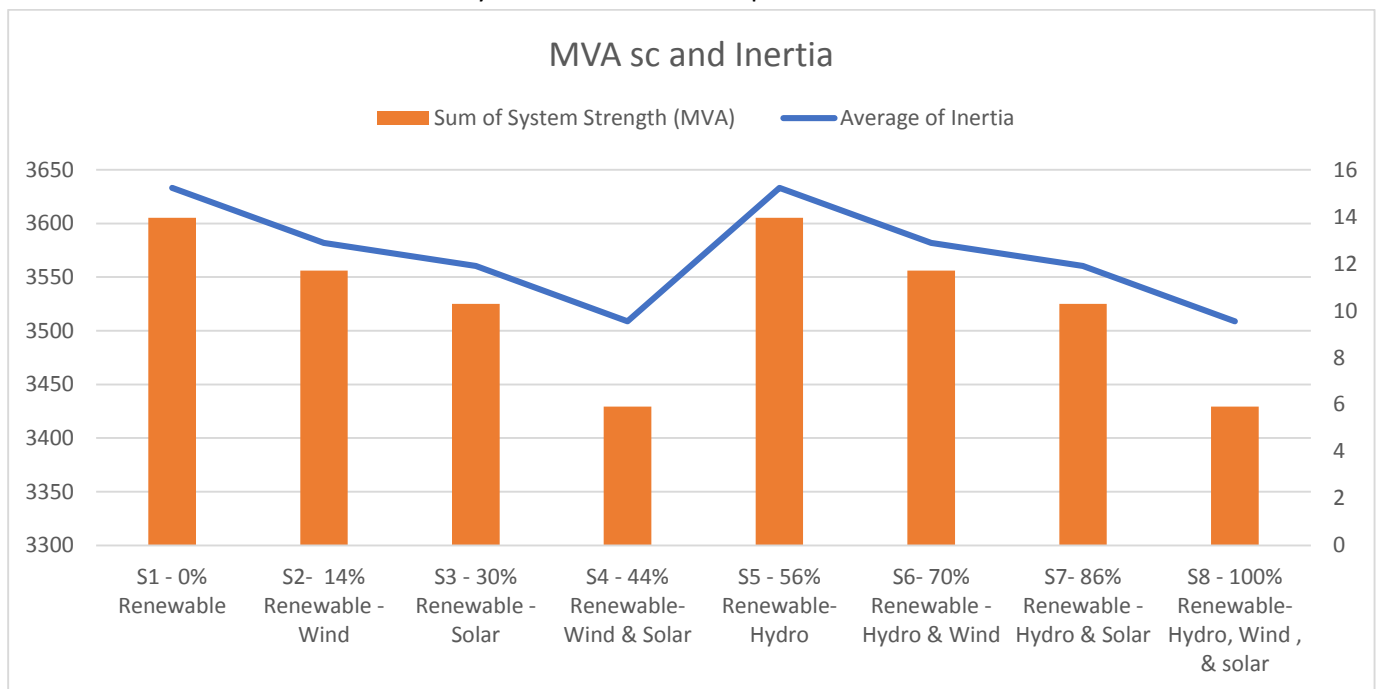


Figure 3.2-17: MVA sc and Inertia per scenario

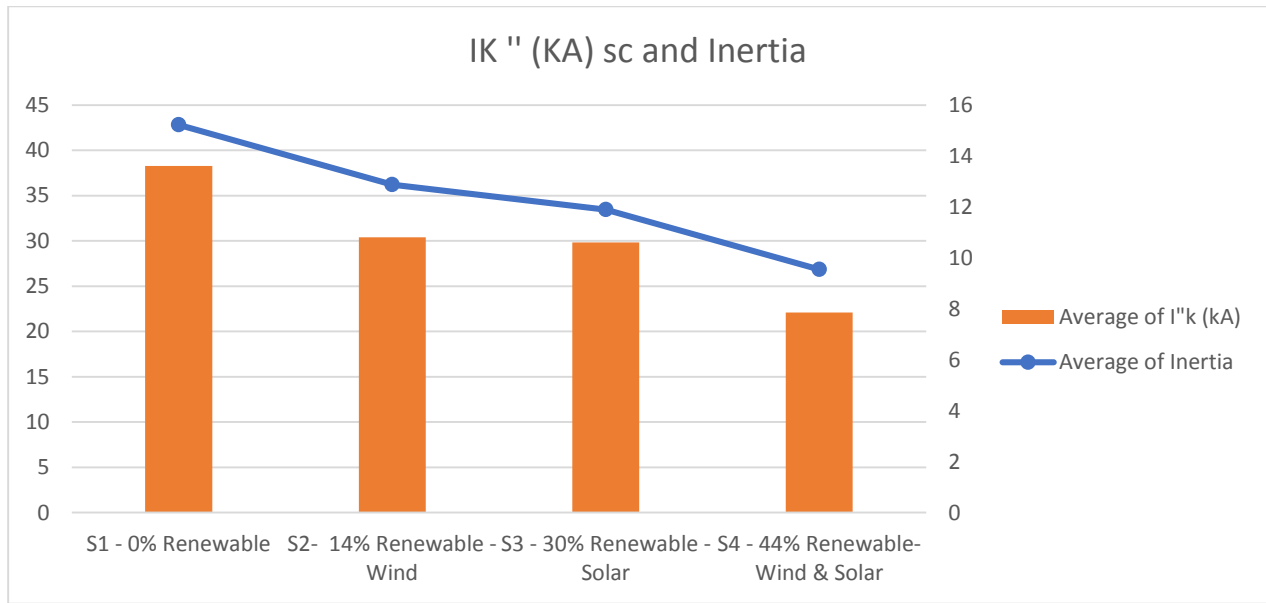


Figure 3.2-18: IK''(kA) short circuit current and inertia for the scenarios 1, 2, 3 , and 4

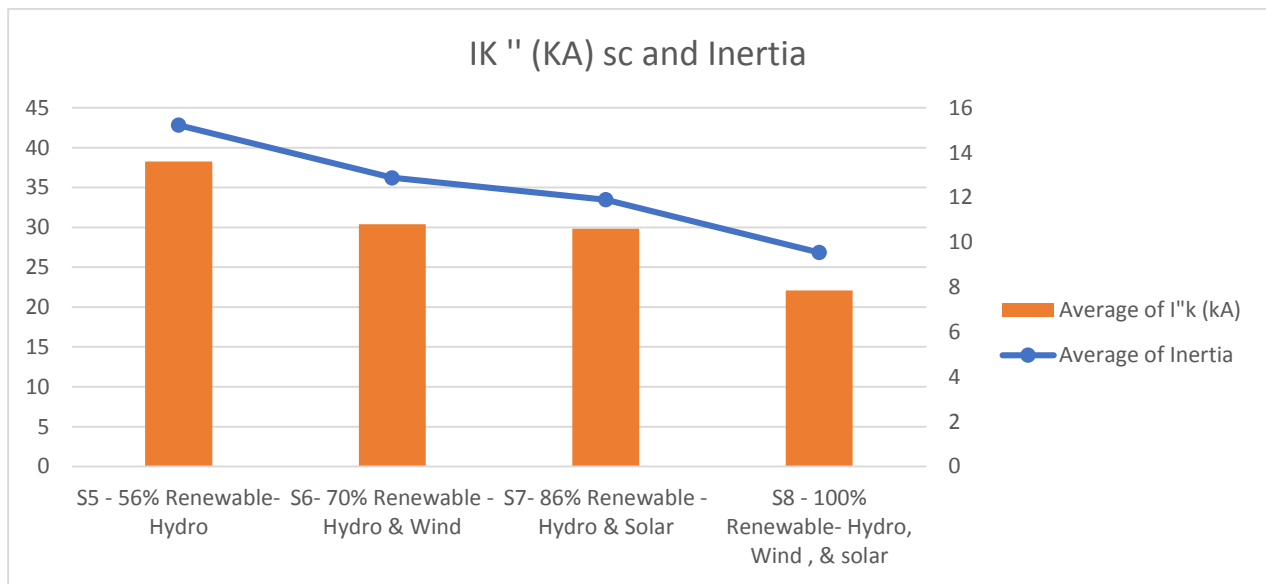


Figure 3.2-19: IK''(kA) short circuit current and inertia for the scenarios 5, 6, 7 , and 8

- 1- The peak and rms symmetrical short circuit current as the IBR (solar and wind) integration increases

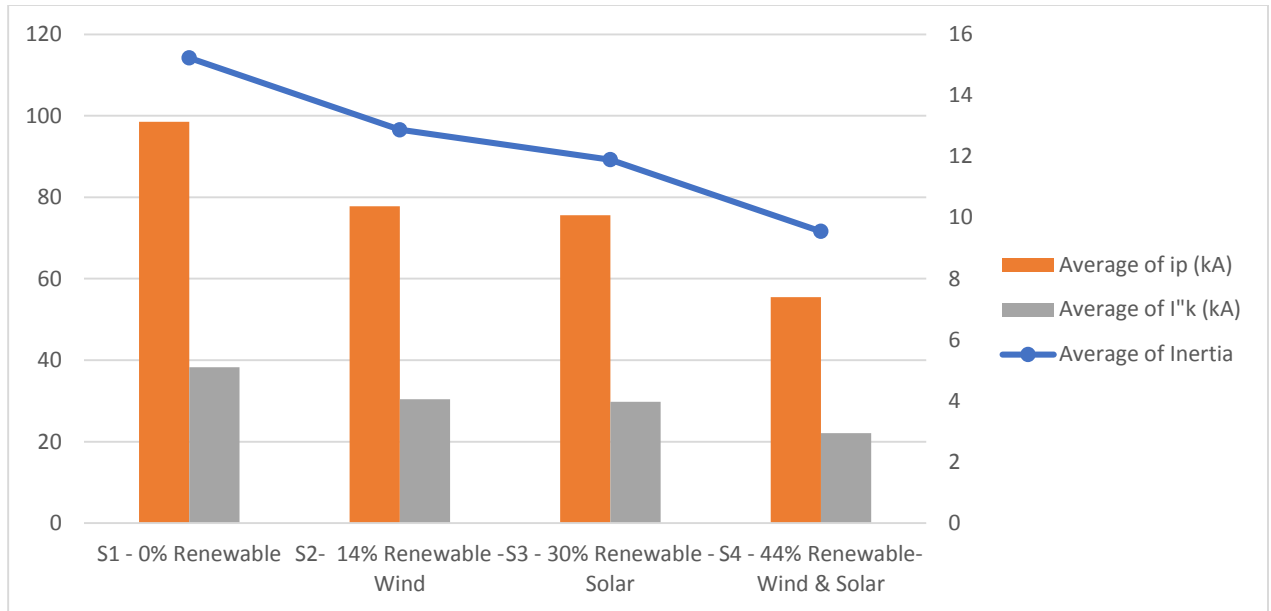


Figure 3.2-20:  $i_p(kA)$ ,  $I''_k(kA)$  and Inertia for scenarios 1,2,3, and 4

According to the Harmonic Analysis performed for all the scenarios, we can conclude the following:

- 1- As the IBR renewable integration increased (specifically the solar), this will lead to increase the voltage total harmonic distortion for both voltage and current

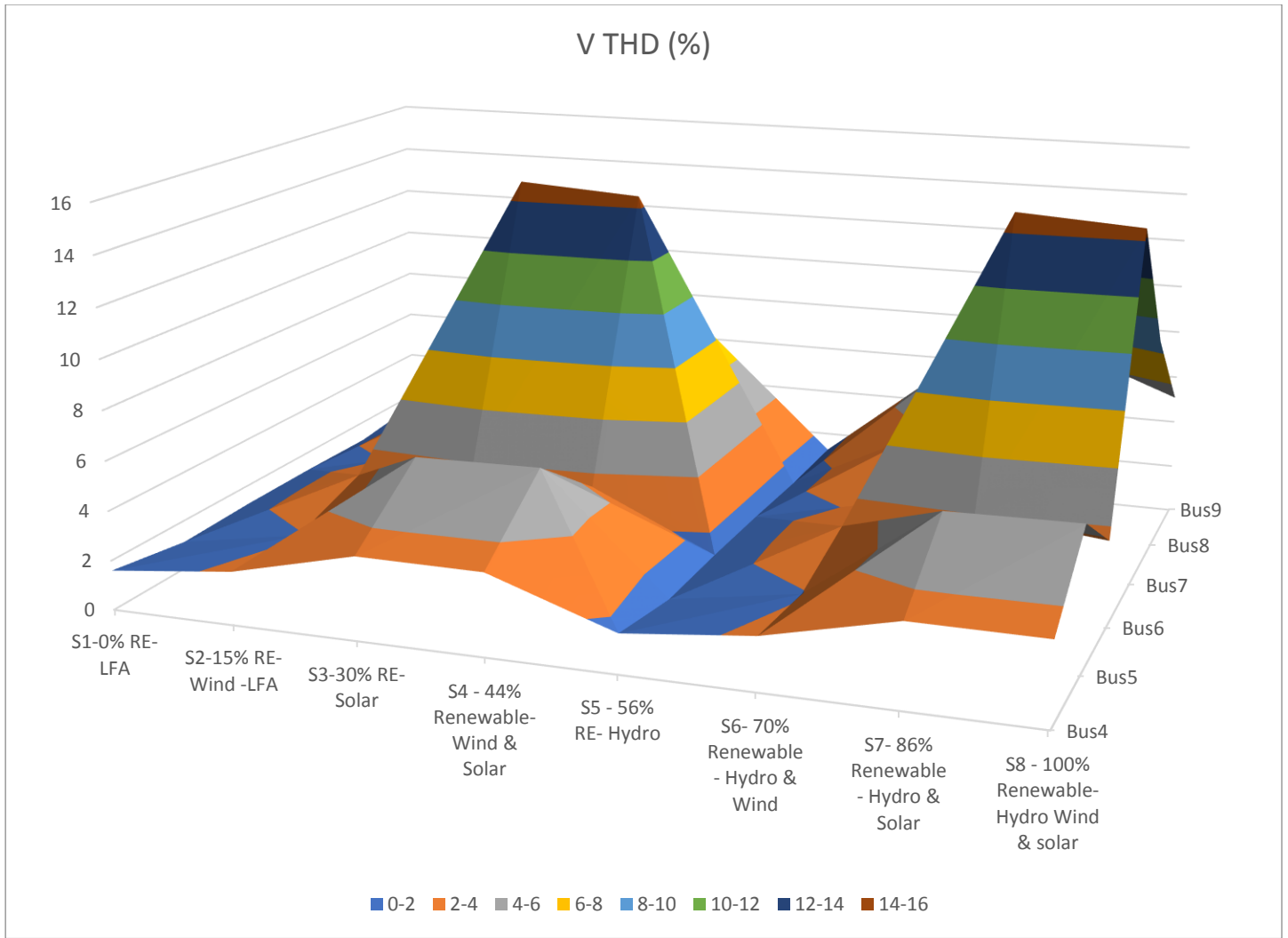


Figure 3.2-21: Voltage THD (%) for transmission buses for the 8 scenarios.

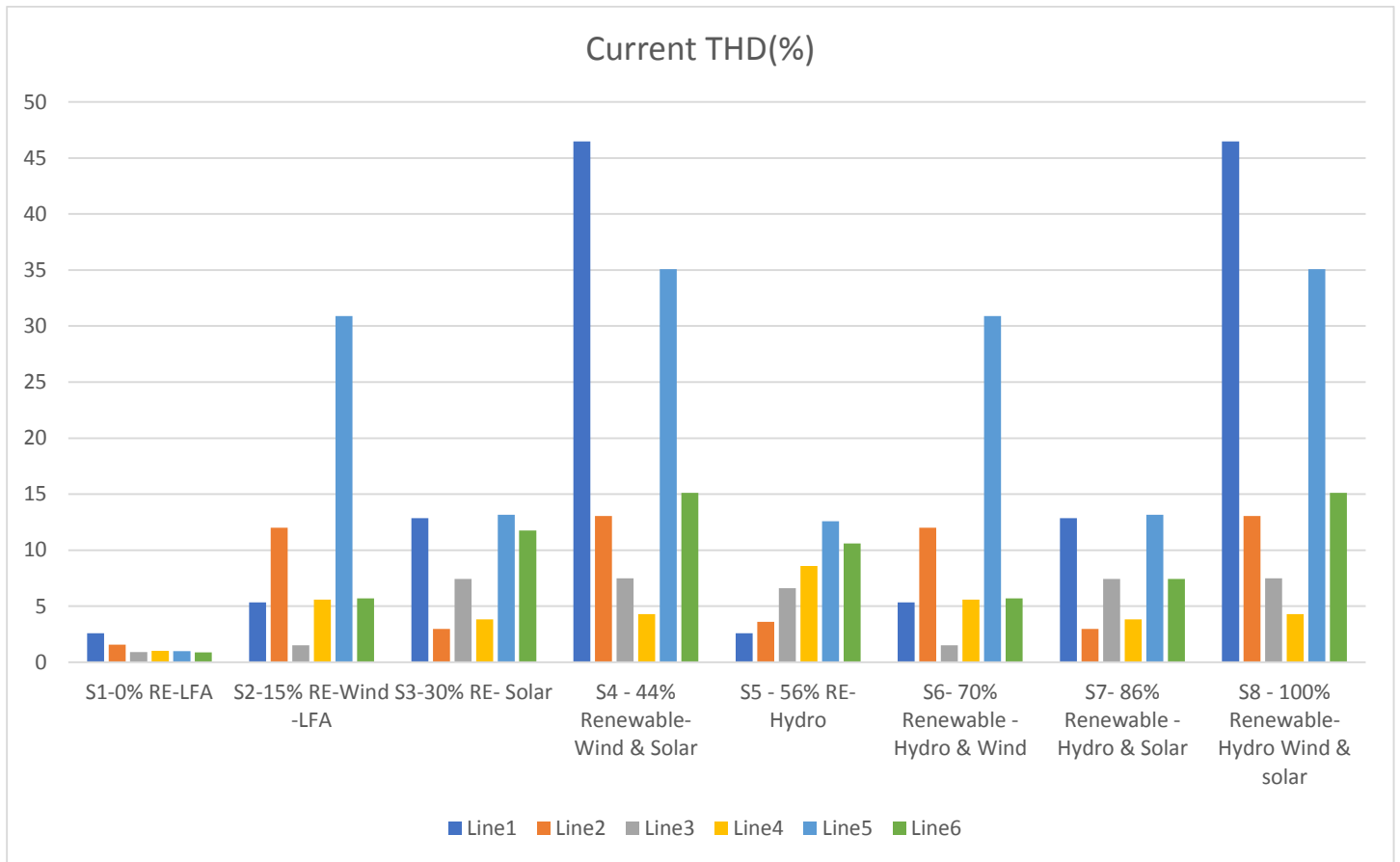


Figure 3.2-22:Current THD (%) for transmission buses for the 8 scenarios.

According to the *Voltage Stability and Voltage Sensitivity Analysis* performed for all the scenarios, we can conclude the following:

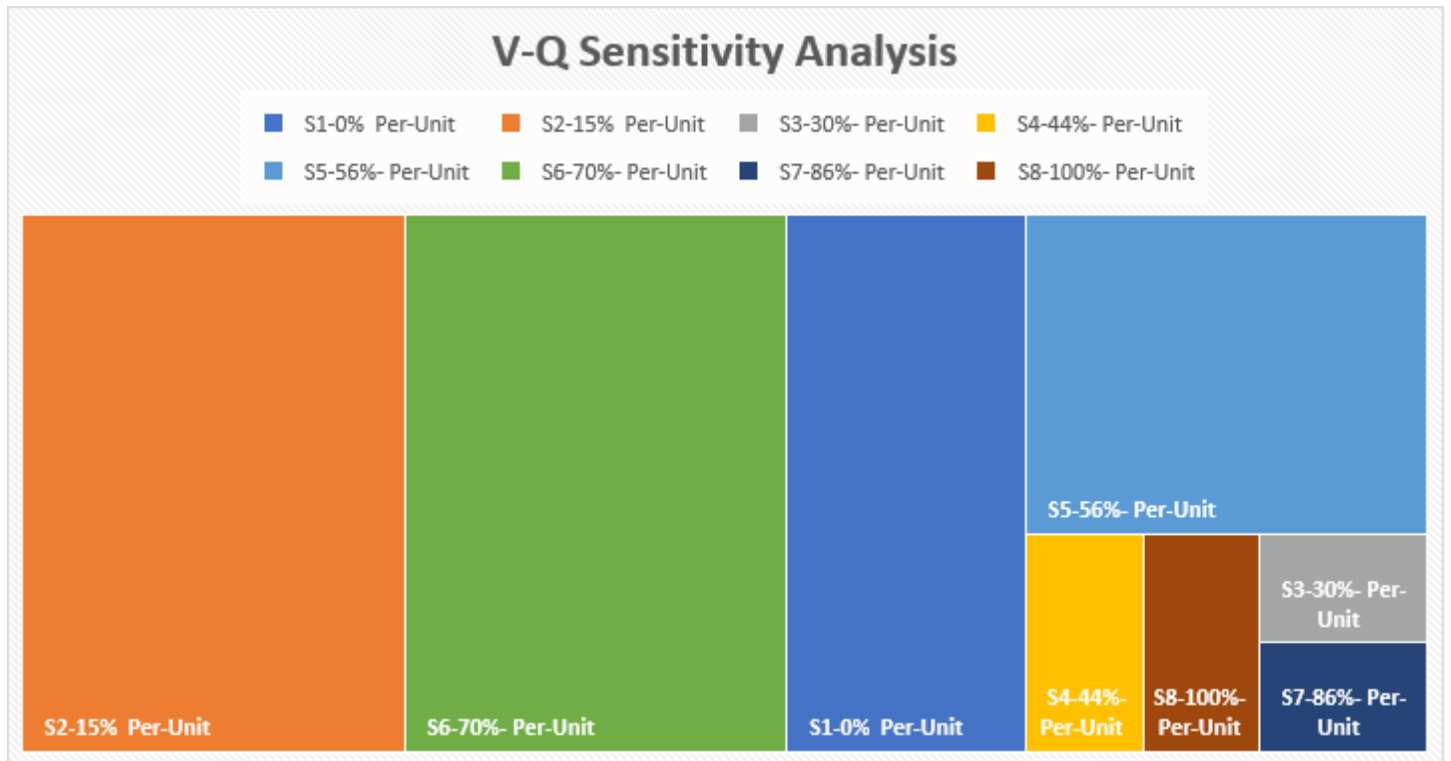


Figure 3.2-23: V-Q sensitivity analysis

### 3.3 Chapter Ten: RECOMMENDATIONS AND FUTURE WORKS

The recommendations for the study are as follows:

#### 3.3.1 Time Domain Load Flow

1. The conducted time domain load flow study was for one month (May 2024 for 31 days), and it is recommended for the future to run it for one year.
2. It is recommended to propose a several 100% renewable energy scenario without any rotating mass like the case of hydroelectric power plant.
3. To explore the financial analysis, LCOE and LROE among a new 100% scenarios.
4. Perform a complete financial analysis (CAPEX/OPEX assessment) for IEEE 9 bus system with 100% RE system with IoT implementation.

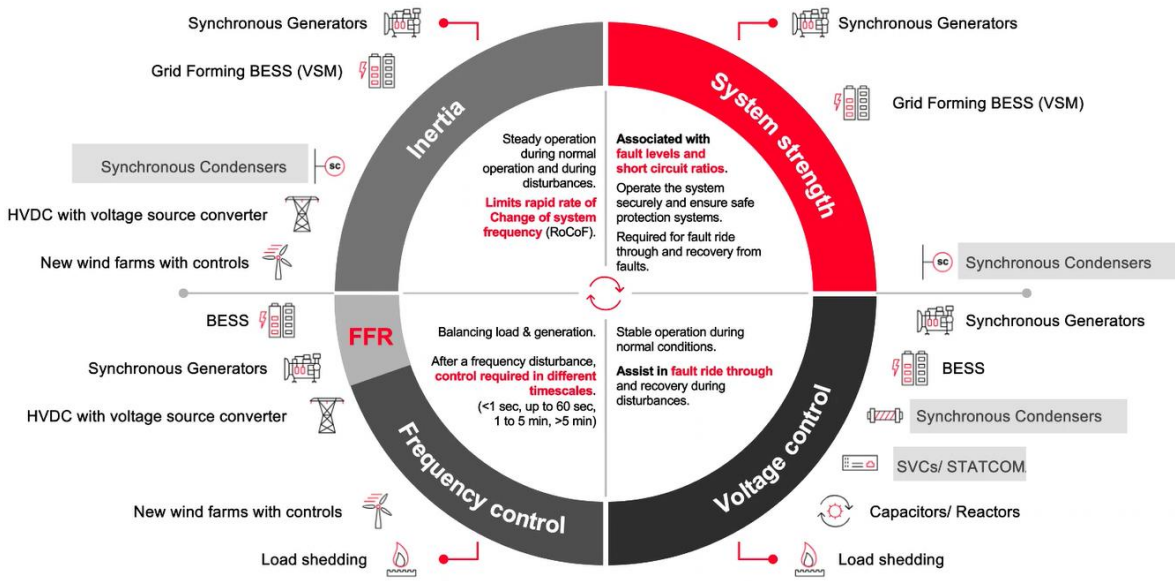
5. Examining how much we should increase the renewable integration to achieve carbon neutrality.

### **3.3.2 Transient Stability Study**

1. Only one large disturbance was examined, which was a three-phase fault at BB No.8, however several other small and large disturbances could be examined.
2. The dynamic behavior for the synchronous machine was examined, however other equipment like busbars, wind turbines, inverters could be examined too.
3. Fault clearing time could be recorded for several scenarios at several renewable penetration.

### **3.3.3 Power System Analysis**

1. It is recommended on the future to examine the effect of dynamic shunt compensators on stabilizing the voltage level.
2. To increase the inertial response, it is recommended to add synchronous condensers to increase the short circuit level.
3. It is recommended in the future to use harmonic filters to reduce the THD (%) to the acceptable limit set by the TSO's.



## Bibliography

Kalogirou, S. A., 2013. *Solar energy engineering: processes and systems..* s.l.: Academic Press.

1. Kalogirou, Soteris A. Solar energy engineering: processes and systems. Academic Press, 2013.
2. Duffie, John A., and William A. Beckman. Solar engineering of thermal processes. John Wiley & Sons, 2013.
3. Patel, Mukund R. Wind and solar power systems: design, analysis, and operation. CRC press, 2005.
4. Nag, P. K. Power plant engineering. Tata McGraw-Hill Education, 2002.
5. Yolcan, O.O., 2023. World energy outlook and state of renewable energy: 10-Year evaluation. *Innovation and Green Development*, 2 (4), 100070.
6. Panwar, N.L., Kaushik, S.C. and Kothari, S., 2011. Role of renewable energy sources in environmental protection: A review. *Renewable and sustainable energy reviews*, 15(3), pp.1513-1524.
7. Hussein, N., 2016. Greenhouse Gas Emissions Reduction Potential of Jordan's Utility Scale Wind and Solar Projects. *Jordan Journal of Mechanical & Industrial Engineering*, 10(3).
8. Wu, Q.H., Bose, A., Singh, C., Chow, J.H., Mu, G., Sun, Y., Liu, Z., Li, Z. and Liu, Y., 2023. Control and stability of large-scale power system with highly distributed renewable energy generation: Viewpoints from six aspects. *CSEE Journal of Power and Energy Systems*, 9(1), pp.8-14.

9. Kimbark, E.W., 1995. Power system stability (Vol. 1). John Wiley & Sons.
10. Wu, Q.H., Bose, A., Singh, C., Chow, J.H., Mu, G., Sun, Y., Liu, Z., Li, Z. and Liu, Y., 2023. Control and stability of large-scale power system with highly distributed renewable energy generation: Viewpoints from six aspects. *CSEE Journal of Power and Energy Systems*, 9(1), pp.8-14.
11. Hatziargyriou, N., Milanovic, J., Rahmann, C., Ajarapu, V., Canizares, C., Erlich, I., Hill, D., Hiskens, I., Kamwa, I., Pal, B. and Pourbeik, P., 2020. Definition and classification of power system stability–revisited & extended. *IEEE Transactions on Power Systems*, 36(4), pp.3271-3281.
12. Rekeraho, A., Cotfas, D.T., Cotfas, P.A., Bălan, T.C., Tuyishime, E. and Acheampong, R., 2024. Cybersecurity challenges in IoT-based smart renewable energy. *International Journal of Information Security*, 23(1), pp.101-117.
13. Bedi, G., Venayagamoorthy, G.K., Singh, R., Brooks, R.R. and Wang, K.C., 2018. Review of Internet of Things (IoT) in electric power and energy systems. *IEEE Internet of Things Journal*, 5(2), pp.847-870.
14. Salam, A. and Salam, A., 2020. Internet of things in sustainable energy systems. *Internet of Things for Sustainable Community Development: Wireless Communications, Sensing, and Systems*, pp.183-216.
15. Salama, R., Alturjman, S. and Al-Turjman, F., 2023. Internet of Things and AI in Smart Grid Applications. *NEU Journal for Artificial Intelligence and Internet of Things*, 1(1), pp.44-58.
16. Wu, Y., Wu, Y., Guerrero, J.M. and Vasquez, J.C., 2021. A comprehensive overview of framework for developing sustainable energy internet: From things-based energy network to services-based management system. *Renewable and Sustainable Energy Reviews*, 150, p.111409.

17. Nallagalva, S.K., Kirar, M.K. and Agnihotri, G., 2012. Transient stability analysis of the IEEE 9-bus electric power system. *International Journal of Scientific Engineering and Technology*, 1(3), pp.161-166.
18. Asija, D., Choudekar, P., Soni, K.M. and Sinha, S.K., 2015, March. Power flow study and contingency status of WSCC 9 Bus test system using MATLAB. In *2015 International Conference on Recent Developments in Control, Automation and Power Engineering (RDCAPE)* (pp. 338-342). IEEE.
19. Shaikh, S.A., Kumar, K., Solangi, A.R., Kumar, S. and Soomro, A.A., 2018, April. Short Circuit Analysis & Over current Relaying Coordination of IEEE 9-Bus System. In *2018 5th International Multi-Topic ICT Conference (IMTIC)* (pp. 1-6). IEEE.
20. Anwar, N., Hanif, A., Khan, H.F. and Ullah, M.F., 2020. Transient stability analysis of the IEEE-9 bus system under multiple contingencies. *Engineering, Technology & Applied Science Research*, 10(4), pp.5925-5932.
21. S. Al-Jufout, "Forming the differential-algebraic model of radial power systems for simulation of both transient and steady-state conditions," *International Conference on Computer, Electrical, and Systems Sciences, and Engineering*, vol. 68, pp. 2031-2034, 2012.
22. S. Al-Jufout, "Differential-algebraic model of ring electric power systems for simulation of both transient and steady-state conditions," *IEEE Mediterranean Electrotechnical Conference*, vol. 15, pp. 30-34, 2010.
23. S. Al-Jufout and E. Addasi, "Instantaneous- and time-overangle protection against three-phase faults on radial electrical power systems," *International Journal of Electrical & Power Engineering*, vol. 3, no. 1, pp. 69-75, 2009.
24. S. Al-Jufout, "Improved algorithm for fault simulation by hypothetical stub moving along medium-length transmission line," *European Journal of Scientific Research*, vol. 23, no. 3, pp. 400-405, 2008.

25. S. Al-Jufout, "Evaluating the error caused by load ignorance through simulation of short circuit in electrical power systems," *Quality and Reliability Engineering International*, vol. 24, no. 8, pp. 891-895, 2008.
26. S. Al-Jufout, "Evaluation of the error caused by load-ignorance through fault simulation in power systems," *International Conference on Quality, Reliability and Maintenance*, pp. 101-105, 2007.
27. S. Al-Jufout, "Fault simulation by hypothetical stub moving along medium-length transmission line," *IEEE Mediterranean Electrotechnical Conference*, vol. 13, no. 2, pp. 1098-1101, 2006.
28. Kumar, A. K., M. P. Selvan, and K. Rajapandiyan. "Grid stability analysis for high penetration solar photovoltaics." In *1st International Conference on Large-Scale Grid Integration of Renewable Energy in India*. 2017.
29. Omran, S. and Broadwater, R., 2020. Grid integration of a renewable energy system: modeling and analysis. *Int. Journal of Renewable Energy Research*, 10(3).
30. Acharya, S. and Ramezani, M., 2020, February. Transient stability assessment for generators and DER integration into the IEEE 9 Bus system. In *2020 IEEE Texas Power and Energy Conference (TPEC)* (pp. 1-6). IEEE.
31. Ramlochun, B., Vaithilingam, C.A., Alsakati, A.A. and Alnasseir, J., 2021, December. Transient stability analysis of IEEE 9-bus system integrated with DFIG and SCIG based wind turbines. In *Journal of Physics: Conference Series* (Vol. 2120, No. 1, p. 012023). IOP Publishing.

32. Alsakati, A.A., Vaithilingam, C.A. and Alnasseir, J., 2021. Transient stability assessment of IEEE 9-bus system integrated wind farm. In MATEC Web of Conferences (Vol. 335, p. 02006). EDP Sciences.
33. Kalyuzhny, A., B. Reshef, G. Yehuda, G. David, P. Koulbekov, and T. Day. "Design of capacitor bank in parallel to photovoltaic power plant." In Eurocon 2013, pp. 1362-1368. IEEE, 2013.
34. Mr. Piyush M. Desai, Mr. S. S. Khule. "Reactive Power Compensation Through Grid Connected PV System Using STATCOM. " International Journal for Research in Engineering Application & Management (IJREAM) ISSN : 2494-9150 Vol-02, Issue 05, Aug 2016.
35. Al-Adim, L., Aliasgari, M., Mozumdar, M. and Al Jufout, S., 2022, November. Reducing the number of central inverters of a photovoltaic plant using medium-voltage capacitor banks. In 2022 IEEE Green Energy and Smart System Systems (IGESSC) (pp. 1-6). IEEE.
36. Al-Adim, L., Aliasgari, M., Mozumdar, M. and Al Jufout, S., 2023, November. Harmonics Analysis of a Photovoltaic Plant with a Reduced Number of Solar Central Inverters. In 2023 IEEE Green Energy and Smart Systems Conference (IGESSC) (pp. 1-4). IEEE.
37. Stiger, A., Rivas, R.A. and Halonen, M., 2019, March. Synchronous condensers contribution to inertia and short circuit current in cooperation with STATCOM. In 2019 IEEE PES GTD Grand International Conference and Exposition Asia (GTD Asia) (pp. 955-959). IEEE.
38. de Oliveira, M.M. and Halonen, M., 2016, September. Dynamic reactive power compensation: Opportunities and challenges in the mexican grid. In 2016 IEEE PES Transmission & Distribution Conference and Exposition-Latin America (PES T&D-LA) (pp. 1-6). IEEE.
39. Gómez-González, J., D. Cañadillas-Ramallo, B. González-Díaz, J. Méndez-Pérez, J. Rodríguez, J. Sánchez, and R. Guerrero-Lemus. "Reactive power management in photovoltaic installations connected to low-voltage grids to avoid active power curtailment." Renewable Energy and Power Quality Journal 1 (2018): 7-8.

40. S. Balasubramanyan and M. Sasirekha. "Optimization Strategy for Reactive Power Compensation in Grid Connected PV Systems. " *Middle-East Journal of Scientific Research* 24 (3): 892-897, 2016, ISSN 1990-9233
41. IRENA Coalition for Action (2024), 100% renewable energy scenarios: Supporting ambitious policy targets, International Renewable Energy Agency, Abu Dhabi.
42. Bogdanov, D., Ram, M., Aghahosseini, A., Gulagi, A., Oyewo, A.S., Child, M., Caldera, U., Sadovskaia, K., Farfan, J., Barbosa, L.D.S.N.S. and Fasihi, M., 2021. Low-cost renewable electricity as the key driver of the global energy transition towards sustainability. *Energy*, 227, p.120467.
43. Jacobson, M.Z., von Krauland, A.K., Coughlin, S.J., Dukas, E., Nelson, A.J., Palmer, F.C. and Rasmussen, K.R., 2022. Low-cost solutions to global warming, air pollution, and energy insecurity for 145 countries. *Energy & Environmental Science*, 15(8), pp.3343-3359.
44. Teske, S., 2019. *Achieving the Paris climate agreement goals: Global and regional 100% renewable energy scenarios with non-energy GHG pathways for+ 1.5 C and+ 2 C* (p. 491). Springer Nature.
45. Strunz, K., Almunem, K., Wulkow, C., Kuschke, M., Valescudero, M. and Guillaud, X., 2022. Enabling 100% renewable power systems through power electronic grid-forming converter and control: System integration for security, stability, and application to Europe. *Proceedings of the IEEE*.
46. Jathunga, T.G., Wijethunga, A.H. and Ekanayake, J.B., 2021. Impact of inertia constant on frequency dynamics of a power system. *Ceylon Journal of Science*, 50(1), pp.3-10.
47. Aziz, T., Saha, T.K. and Mithulananthan, N., 2010, October. Distributed generators placement for loadability enhancement based on reactive power margin. In *2010 Conference Proceedings IPEC* (pp. 740-745). IEEE.
48. Khalili, S. and Breyer, C., 2022. Review on 100% renewable energy system analyses—A bibliometric perspective. *IEEE Access*, 10, pp.125792-125834.
49. Basso, T., 2014. *IEEE 1547 and 2030 standards for distributed energy resources interconnection and interoperability with the electricity grid* (No. NREL/TP-5D00-63157). National Renewable Energy Lab.(NREL), Golden, CO (United States).
50. ZERO, I.T., 2023. Interoperability of distributed energy resources: Benefits, challenges, and solutions.

51. Azzuni, A., Aghahosseini, A., Ram, M., Bogdanov, D., Caldera, U. and Breyer, C., 2020. Energy security analysis for a 100% renewable energy transition in Jordan by 2050. *Sustainability*, 12(12), p.4921.
52. Vythahavya Vadlamani, P.E. and Don Martin, P.E., Renewable energy design considerations, ABB.
53. MadhusudhanaRao, G. "REACTIVE POWER COMPENSATION IN A GRID CONNECTED PV SYSTEM WITH SOURCE SIDE CONTROL TECHNIQUES."
54. Jivrajani, Chirag. "International Journal of Advance Engineering and Research Development." Development 4, no. 2 (2017).
55. Bengourina, M. R., M. Rahli, and L. Hassaine. "Direct power control of a grid connected photovoltaic system, associated with an active power filter." *Revue des Energies Renouvelables* 20, no. 1 (2017): 99-109.
56. Albuquerque, Fabio L., Adélio J. Moraes, Geraldo C. Guimarães, Sérgio MR Sanhueza, and Alexandre R. Vaz. "Photovoltaic solar system connected to the electric power grid operating as active power generator and reactive power compensator." *Solar Energy* 84, no. 7 (2010): 1310-1317.

57. Alyyan, A., M. Lahham, M. Arni, A. Mohammed, and S. Al-Jufout. "Immittance matrix partition by hypothetical capacitor." *Lecture Series on Computers and Computational Sciences 4* (2005): 17-20.
  
58. S. Al-Jufout, "Fault simulation along short transmission line," *International Journal of Condition Monitoring & Diagnostic Engineering Management*, vol. 8, no. 1, pp. 32, 2005.
  
59. S. Al-Jufout, "Fault simulation by hypothetical stub moving along short transmission lines," *International Conference on Quality, Reliability and Maintenance*, pp. 283-286, 2004.
  
60. Romero-Cadaval, Enrique, Giovanni Spagnuolo, Leopoldo García Franquelo, Carlos-Andrès Ramos-Paja, Teuvo Suntio, and Weidong-Michael Xiao. "Grid Connected Photovoltaic Generation Plants. Components and Operation." *IEEE Industrial Electronics Magazine*, 7 (3), 6-20 (2013).
  
61. Hammad, Mahmoud, Munzer SY Ebaid, Ghassan Halaseh, and Baslan Erekat. "Large Scale Grid Connected (20MW) Photovoltaic System for Peak Load Shaving in Sahab Industrial District." *Jordan Journal of Mechanical & Industrial Engineering* 9, no. 1 (2015).
  
62. Biel, Domingo, and Jacquélien MA Scherpen. "Active and reactive power regulation in single-phase PV inverters." In *2018 European Control Conference (ECC)*, pp. 782-787. IEEE, 2018.
  
63. Hoseynpoor, Y., and T. PirzadehAshraf. "Maximum power point tracking and reactive power control of single stage grid connected photovoltaic system." *Research Journal of Applied Sciences, Engineering and Technology* 3, no. 12 (2011): 1430-1436.
  
64. NEPCO GRID REQUIREMENT, Intermittent Renewable Resources (IRR) Wind & PV, Transmission Interconnection Code (TIC)

65. Farivar, Masoud, Russell Neal, Christopher Clarke, and Steven Low. "Optimal inverter VAR control in distribution systems with high PV penetration." In 2012 IEEE Power and Energy Society general meeting, pp. 1-7. IEEE, 2012.
66. Hashemi, Seyedmostafa, Jacob Østergaard, and Guangya Yang. "Effect of reactive power management of PV inverters on need for energy storage." In 2013 IEEE 39th Photovoltaic Specialists Conference (PVSC), pp. 2304-2308. IEEE, 2013.
67. Krishna, Ravulapalli Rama, and Popavath Lakshman Naik. "A PV Solar Farm as PV-Statcom for Reactive Power Compensation and for Enhancement of Grid Power Transmission Limits." International Journal for Modern Trends in Science and Technology 4 (2018).
68. Das, Anubrata, Ankul Gupta, Saurav Roy Choudhury, and Sandeep Anand. "Adaptive reactive power injection by solar PV inverter to minimize tap changes and line losses." In 2016 National Power Systems Conference (NPSC), pp. 1-6. IEEE, 2016.
69. Ramonas, C., and V. Adomavicius. "Research of the reactive power control possibilities in the grid-tied PV power plant." Elektronika ir Elektrotechnika 19, no. 1 (2013): 31-34.
70. Al-Halalmeh, Mahmoud, and Saleh Al-Jufout. "Impact of Photovoltaic Penetration on the Distribution System Protection: A Case Study of 5-MW Plants of Mu'tah University and Kempinski Hotel." In 2019 IEEE Jordan International Joint Conference on Electrical Engineering and Information Technology (JEEIT), pp. 228-233. IEEE, 2019.

71. Farhoodnea, Masoud, Azah Mohamed, Hussain Shareef, and Hadi Zayandehroodi. "Power quality analysis of grid-connected photovoltaic systems in distribution networks." *Przeglad Elektrotechniczny (Electrical Review)* 2013 (2013): 208-213.
72. WEI, AGNES LIAU SIAU. "Stability Assessment of 132kV Sabah Grid-connected Solar PV System." PhD diss., Universiti Tun Hussein Onn Malaysia, 2014.
73. Gupta, B. R., and S. Chand. "Power system analysis and design." New Delhi, (2008).
74. Grainger, John J., William D. Stevenson, and William D. Stevenson. *Power system analysis.* 2003.
75. Lander, Cyril W. *Power electronics.* McGraw-Hill, Inc., 1987.
76. Yoro, K.O. and Daramola, M.O., 2020. CO2 emission sources, greenhouse gases, and the global warming effect. In *Advances in carbon capture* (pp. 3-28). Woodhead Publishing.
77. Bogdanov, D., Gulagi, A., Fasihi, M. and Breyer, C., 2021. Full energy sector transition towards 100% renewable energy supply: Integrating power, heat, transport and industry sectors including desalination. *Applied Energy*, 283, p.116273.
78. Chen, J.M., 2021. Carbon neutrality: toward a sustainable future. *The Innovation*, 2(3).
79. Kiwan, S. and Al-Gharibeh, E., 2020. Jordan toward a 100% renewable electricity system. *Renewable Energy*, 147, pp.423-436.

80. Alzboon, K.K., La'aly, A. and Alrawashdeh, K.A.B., 2021. Climate change indicators in Jordan: A new approach using area method. *Jordan Journal of Civil Engineering*, 15(1).
81. Wiedmann, T., Chen, G., Owen, A., Lenzen, M., Doust, M., Barrett, J. and Steele, K., 2021. Three-scope carbon emission inventories of global cities. *Journal of Industrial Ecology*, 25(3), pp.735-750
82. Hossein Motlagh, N., Mohammadrezaei, M., Hunt, J. and Zakeri, B., 2020. Internet of Things (IoT) and the energy sector. *Energies*, 13(2), p.494.
83. Esenogho, E., Djouani, K. and Kurien, A.M., 2022. Integrating artificial intelligence Internet of Things and 5G for next-generation smartgrid: A survey of trends challenges and prospect. *IEEE Access*, 10, pp.4794-4831.
84. Khatua, P.K., Ramachandaramurthy, V.K., Kasinathan, P., Yong, J.Y., Pasupuleti, J. and Rajagopalan, A., 2020. Application and assessment of internet of things toward the sustainability of energy systems: Challenges and issues. *Sustainable Cities and Society*, 53, p.101957.
85. Zohuri, B., Bowen, P.E., Kumar, A.A.D. and Moghaddam, M., 2022. Energy Driven by Internet of Things Analytics and Artificial Intelligence. *Journal of Energy and Power Engineering*, 16, pp.24-31.
86. Azzuni, A., Aghahosseini, A., Ram, M., Bogdanov, D., Caldera, U. and Breyer, C., 2020. Energy security analysis for a 100% renewable energy transition in Jordan by 2050. *Sustainability*, 12(12), p.4921.

87. Abu-Rumman, G., Khdair, A.I. and Khdair, S.I., 2020. Current status and future investment potential in renewable energy in Jordan: An overview. *Heliyon*, 6(2).
88. Al-Refaie, A. and Lepkova, N., 2022. Impacts of renewable energy policies on CO2 emissions reduction and energy security using system dynamics: The case of small-scale sector in Jordan. *Sustainability*, 14(9), p.5058.
89. Hussein, N., 2016. Greenhouse Gas Emissions Reduction Potential of Jordan's Utility Scale Wind and Solar Projects. *Jordan Journal of Mechanical & Industrial Engineering*, 10(3).
90. Jaber, J.O., Marahleh, G. and Dalabeeh, A., 2019. Emissions reduction resulting from renewable energy projects in Jordan. *Journal of Energy Technologies and Policy*, 9(6), pp.42-51.
91. Salah, A.A., Shalby, M.M. and Basim Ismail, F., 2023. The status and potential of renewable energy development in Jordan: exploring challenges and opportunities. *Sustainability: Science, Practice and Policy*, 19(1), p.2212517.
92. Shakerighadi, B., Anvari-Moghaddam, A., Vasquez, J.C. and Guerrero, J.M., 2018. Internet of things for modern energy systems: State-of-the-art, challenges, and open issues. *Energies*, 11(5), p.1252.
93. Abu Qdais, H., Wuensch, C., Dornack, C. and Nassour, A., 2019. The role of solid waste composting in mitigating climate change in Jordan. *Waste Management & Research*, 37(8), pp.833-842.
94. Kiwan, S. and Al-Gharibeh, E., 2020. Jordan toward a 100% renewable electricity system. *Renewable Energy*, 147, pp.423-436.

95. Hamed, T.A. and Bressler, L., 2019. Energy security in Israel and Jordan: The role of renewable energy sources. *Renewable energy*, 135, pp.378-389.
96. Yoro, K.O. and Daramola, M.O., 2020. CO2 emission sources, greenhouse gases, and the global warming effect. In *Advances in carbon capture* (pp. 3-28). Woodhead Publishing.
97. Asopa, P., Purohit, P., Nadikattu, R.R. and Whig, P., 2021, February. Reducing carbon footprint for sustainable development of smart cities using IoT. In *2021 Third International Conference on intelligent communication technologies and virtual mobile networks (ICICV)* (pp. 361-367). IEEE.
98. Song, W., 1 RESEARCH PHILOSOPHY AND METHODOLOGY.